AD-A121 105 NORTH PACIFIC OMEGA NAVIGATION SYSTEM VALIDATION(U) 1/4
MEGATEK CORP SAN DIEGO CA P LEVINE ET AL. 31 DEC 81
R2018-054-IF-5 ONSOD-01-81 N00123-78-C-0043

UNCLASSIFIED F/G 17/7 NL

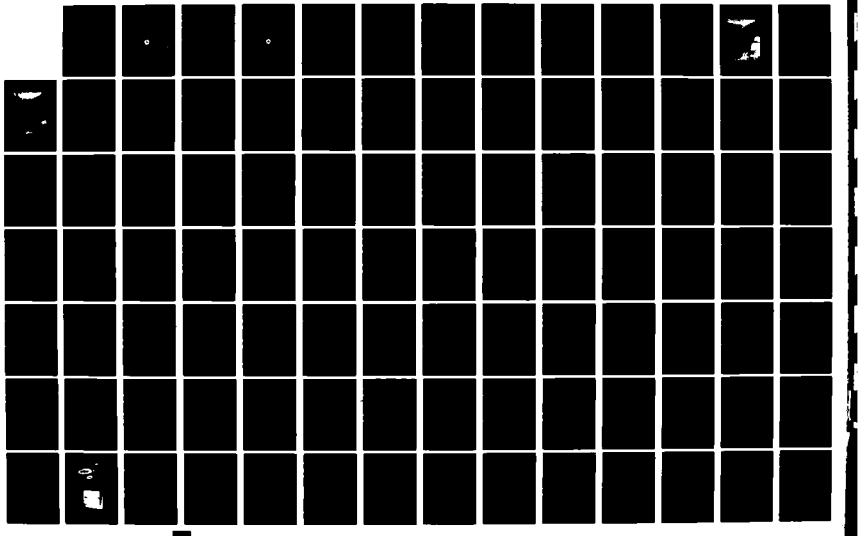

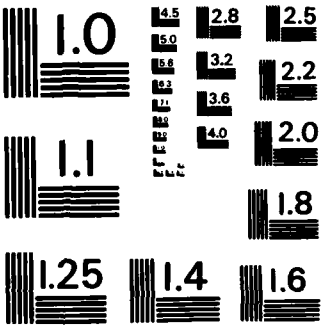

REPORT NO. CG-ONSOD-01-81

NORTH PACIFIC OMEGA NAVIGATION SYSTEM VALIDATION

FINAL REPORT

Dr. Paul H. Levine
Ronald E. Woods

Megatek Corporation
3931 Sorrento Valley Blvd.
San Diego, CA 92121

31 DECEMBER 1981

Prepared for
U.S. DEPARTMENT OF TRANSPORTATION
UNITED STATES COAST GUARD
OMEGA NAVIGATION SYSTEM OPERATIONS DETAIL
WASHINGTON, D.C. 20593

Technical Report Documentation Page

1. Report No.	2. Government Accession No.	3. Recipient's Catalog No.
CG-ONSOD-01-81	A121105	

4. Title and Subtitle
North Pacific OMEGA Navigation System Validation: Final Report

5. Report Date
31 December 1981

6. Performing Organization Code

7. Author(s)
Dr. Paul Levine, Ronald E. Woods

8. Performing Organization Report No.
R2018-054-IF-5

9. Performing Organization Name and Address
Megatek Corporation
3931 Sorrento Valley Blvd.
San Diego, CA 92121

10. Work Unit No. (TRAIS)

11. Contract or Grant No.
N00123-78-C-0043

12. Sponsoring Agency Name and Address
U.S. Dept. of Transportation
U.S. Coast Guard
OMEGA Navigation System Oper. Detail
Washington, D.C. 20593
Via: Naval Ocean Systems Center
San Diego, CA 92152

13. Type of Report and Period Covered
Final Report
1 Dec 1979 - 31 Dec 1981

14. Sponsoring Agency Code

15. Supplementary Notes

16. Abstract

OMEGA is a world-wide radio navigation system based on phase measurements of synchronized time-multiplexed continuous wave transmissions in the frequency band 10.2-13.6 kHz. Seven of the eight planned transmitting stations are already operational and are being utilized for enroute navigation by a large community of marine and aviation users. Commissioning of the final station is scheduled for 1982. A validation program, designed to assess system accuracy and coverage on a region by region basis, will be completed in 1985. The North Pacific, bounded by 100°W-165°E longitude and 10°S-70°N latitude, is the third such region to be validated in this program.

The validation procedure is to establish fixed and mobile monitor receivers to collect signal phase, amplitude and noise data and to supplement such data with controlled flight tests using specially fitted dedicated aircraft. The data thus obtained are then analyzed in the context of a well-developed theoretical propagation model in order to arrive at models of signal coverage and phase error statistics which are compatible with both the controlled measurements and operational experience of the user community. The coverage and phase statistics models thus derived then form the basis of the position-fix accuracy assessments which, in turn, are compared to navigational requirements in the region and to OMEGA system design objectives.

The results of this process show the North Pacific to be a region well-favored from the standpoint of OMEGA performance, with particularly good coverage and accuracy north of the Hawaiian Islands. In the fully implemented system, accuracy (2 drms) is expected to range between 1 and 4 nmi over most of the region, and is 1-2 nmi north of the Yokahama-Honolulu-Seattle axis. It is concluded that OMEGA will meet the enroute navigation requirements of both the marine and aviation user community in the North Pacific on a 24-hour full time basis.

17. Key Words	18. Distribution Statement
OMEGA Very Low Frequency Propagation Validation North Pacific	Document is available to the public through the National Technical Inst. Service, Springfield, VA 22151

19. Security Classif. (of this report)	20. Security Classif. (of this page)	21. No. of Pages	22. Price
UNCLASSIFIED	UNCLASSIFIED	372	

Form DOT F 1700.7 (8-72) Reproduction of completed page authorized

REPORT NO. CG-ONSOD-01-81

NORTH PACIFIC OMEGA NAVIGATION SYSTEM VALIDATION

FINAL REPORT

Dr. Paul H. Levine
Ronald E. Woods

Megatek Corporation
3931 Sorrento Valley Blvd.
San Diego, CA 92121

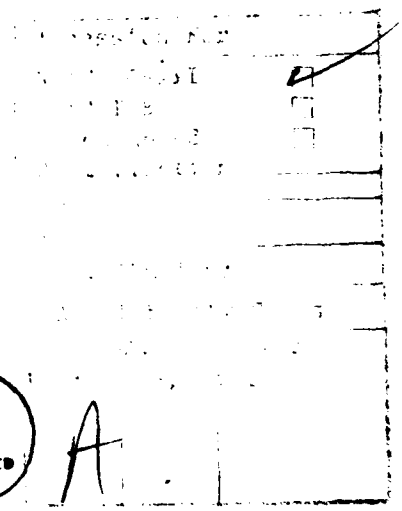

31 DECEMBER 1981

Prepared for
U.S. DEPARTMENT OF TRANSPORTATION
UNITED STATES COAST GUARD
OMEGA NAVIGATION SYSTEM OPERATIONS DETAIL
WASHINGTON, D.C. 20593

METRIC CONVERSION FACTORS

Approximate Conversions to Metric Measures

Symbol	When You Know	Multiply by	To Find	Symbol
		LENGTH		
in	inches	*2.5	centimeters	cm
ft	feet	30	centimeters	cm
yd	yards	0.9	meters	m
mi	miles	1.6	kilometers	km
		AREA		
in^2	square inches	6.5	square centimeters	cm^2
ft^2	square feet	0.09	square meters	m^2
yd^2	square yards	0.8	square meters	m^2
mi^2	square miles	2.6	square kilometers	km^2
	acres	0.4	hectares	ha
		MASS (weight)		
oz	ounces	28	grams	g
lb	pounds	0.45	kilograms	kg
	short tons (2000 lb)	0.9	tonnes	t
		VOLUME		
tsp	teaspoons	5	milliliters	ml
Tbsp	tablespoons	15	milliliters	ml
fl oz	fluid ounces	30	milliliters	ml
c	cups	0.24	liters	l
pt	pints	0.47	liters	l
qt	quarts	0.95	liters	l
gal	gallons	3.8	liters	l
ft^3	cubic feet	0.03	cubic meters	m^3
yd^3	cubic yards	0.76	cubic meters	m^3
		TEMPERATURE (exact)		
°F	Fahrenheit temperature	5/9 (after subtracting 32)	Celsius temperature	°C

*1 in = 2.54 (exactly). For other exact conversions and more detailed tables, see NBS Misc. Publ. 286, Units of Weights and Measures, Price $2.25, SD Catalog No. C13.10:286.

Approximate Conversions from Metric Measures

Symbol	When You Know	Multiply by	To Find	Symbol
		LENGTH		
mm	millimeters	0.04	inches	in
cm	centimeters	0.4	inches	in
m	meters	3.3	feet	ft
m	meters	1.1	yards	yd
km	kilometers	0.6	miles	mi
		AREA		
cm^2	square centimeters	0.16	square inches	in^2
m^2	square meters	1.2	square yards	yd^2
km^2	square kilometers	0.4	square miles	mi^2
ha	hectares (10,000 m^2)	2.5	acres	
		MASS (weight)		
g	grams	0.035	ounces	oz
kg	kilograms	2.2	pounds	lb
t	tonnes (1000 kg)	1.1	short tons	
		VOLUME		
ml	milliliters	0.03	fluid ounces	fl oz
l	liters	2.1	pints	pt
l	liters	1.06	quarts	qt
l	liters	0.26	gallons	gal
m^3	cubic meters	35	cubic feet	ft^3
m^3	cubic meters	1.3	cubic yards	yd^3
		TEMPERATURE (exact)		
°C	Celsius temperature	9/5 (then add 32)	Fahrenheit temperature	°F

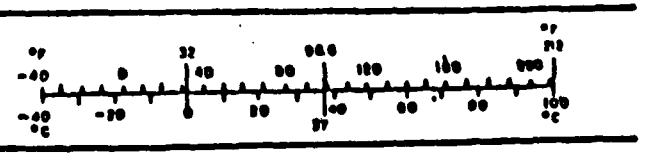

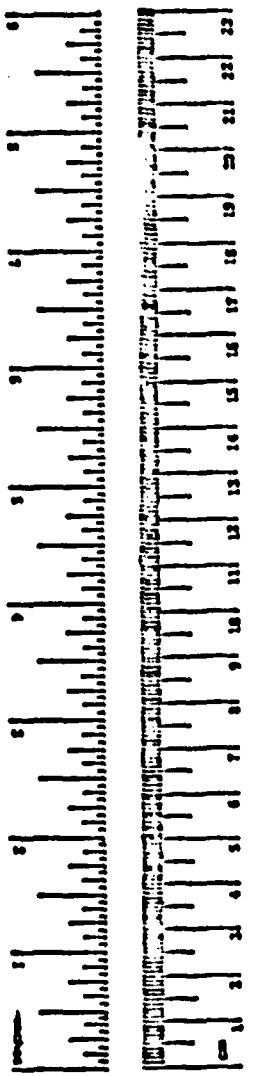

FIGURE 3. METRIC CONVERSION FACTORS

EXECUTIVE SUMMARY

A. PROBLEM STATEMENT

A validation study has been performed of the OMEGA navigation system in the North Pacific. For the purposes of the study, the principal validation region is bounded by 100°W and 165°E longitude, 10°S and 70°N latitude, although the analyses have also been extended westward to dovetail with the previously validated Western Pacific region. The validation region may also be described as comprising the oceanic areas centered on Hawaii and extending E-W from Acapulco to the end of the Aleutian chain and N-S from the top of Alaska to the Marquesas Islands.

The objectives of the validation study are to: i) characterize the inherent position-fixing accuracy of the OMEGA system in the North Pacific, as it will be when the eighth and final transmitting station is commissioned in Australia in 1982, and ii) to provide data on station coverage and signal characteristics which can enable OMEGA system users to navigate more effectively in the region.

The basic data resources available for meeting these objectives include:

- theoretical (10.2 kHz) boundaries of useful signal coverage
- a computer-based file of long-term OMEGA phase-difference data collected by ONSOD at fifteen fixed monitor sites in the region
- short-term signal amplitude and noise measurements taken with both fixed and airborne monitors for ONSOD by the Naval Ocean Systems Center (NOSC) cooperatively with the Federal Aviation Administration Technical Center (FAATC)
- shipboard phase, SNR and fix accuracy data from integrated satellite/OMEGA receivers
- operational fix accuracy and signal quality data from the marine and aviation user communities.

The North Pacific validation process must accommodate the circumstance that no experimental data is available for the Australia station. In addition, there are the following considerations which apply to all regional validations:

- signal coverage - and the associated fix accuracy - vary significantly as a function of frequency, location, time of day and season, thus complicating the task of arriving at a concise, omnibus characterization of system performance

- the available monitor data, being necessarily limited in the spatial and temporal coverage provided, must be extended with help of theoretical models in order to provide area-wide assessments.

B. OVERVIEW OF APPROACH

Intrinsic system accuracy can be defined in terms of the performance of a hypothetical optimum receiver. This receiver utilizes all four shared frequencies in the OMEGA signal format from all locally available stations, and optimally weights each signal in the position-fixing process according to signal quality and station geometry. A detailed statistical theory of the fix accuracy attainable with such a receiver is therefore first developed. Computer programs based on this theory are then generated, capable of producing contour maps of fix accuracy as a function of geographical position. Three of the commonly used measures of fix accuracy are thereby implemented:

- radial or r.m.s. error (also called d_{rms}), defined as the square root of the expected value of the square of the distance between a fix point and the true position.

- 50% CEP (radius of circle, centered on the true position,* containing 50% of the fixes).

- 95% CEP (radius of circle, centered on the true position,* containing 95% of the fixes).

---

* Bias errors are found to be insignificant for the statistical ensemble used (see below) hence the distinction between "CEP about the bias point" and "CEP about the true position" need not be made in the Northern Pacific validation region.

The position fix accuracy assessments are based upon a statistical ensemble in which all times of day and seasons are equally represented. No attempt is thus made to define fix accuracy for more restricted ensembles (e.g. "summer local noon" or "winter local midnight") as such assessments have been found (for the North Pacific*) to be of questionable value in bracketing the performance of an optimum receiver, especially when more than three stations are being used to derive the fix. Quoted fix accuracies are therefore a function of position alone.

The fix accuracy program requires two fundamental inputs to be derived from the available data base: a coverage model which specifies the usable signals at each geographical position, and a phase error model which characterizes the mean and standard deviation of the phase error (measured phase minus theoretical phase) for each OMEGA navigation signal.

The phase error model is derived from statistical analyses of the ONSOD long-term fixed monitor data base. Data for 10.2 kHz and 13.6 kHz are separately analyzed and lead to very similar results. This motivates the application of a single error model at all four of the shared OMEGA frequencies for each station. In the absence of experimental data, phase errors for the Australia station are conservatively approximated by those measured for the Argentina station which is located at a similar geomagnetic latitude and is about the same distance from the North Pacific region.

In the coverage model, an extremely conservative "worst-case" approach is adapted wherein at each geographical location, only those signals which are available at all times of day and all seasons with adequate SNR (>-20 dB @ 100 hz B.W.) and freedom from severe modal interference (<20 CEC) are used for position fixing. This "full-time" composite coverage model thus defines as a function of position the set of signals which can always be counted on to be available (barring station off-air periods). This model is obtained by first combining a set of theoretical coverage/modal interference boundaries generated for two times of day at four seasons of the year, and then validating the combined model by direct comparisons with all applicable experimental and operational data. Such boundaries are only presently available for

---

* Statistical analyses showed a difference of only 1/2 centicycle in the median 10.2 kHz phase errors measured at night (± 2 hours of local midnight) and during the day (± 2 hours of local noon).

10.2 kHz. While some improvements in coverage may be expected at the higher OMEGA frequencies, they are ignored - again in the spirit of conservatism - so that the 10.2 kHz coverage model is uniformly applied at all OMEGA frequencies.

Fix accuracy contour maps are generated both for the fully-implemented OMEGA system (i.e. Australia station on-the-air) and without this station. The latter results are validated by comparison with the operational and integrated satellite/OMEGA fix accuracy data. Accuracies for the fully implemented system are compared with navigational requirements and with OMEGA system design objectives.

C. FIX ACCURACY AND COVERAGE ASSESSMENTS FOR THE NORTH PACIFIC

• COVERAGE

The composite full-time signal coverage model is shown in Figure 1. Recall that the boundaries given for each station define regions where (four-frequency) OMEGA signals are expected to be available at all times with a signal-to-noise ratio in excess of -20 dB (in 100 Hz bandwidth) and with modal interference below 20 CEC*. As such, at any given time they may markedly understate the actual coverage which would apply.

The main conclusions to be emphasized regarding coverage are:

- With station G (Australia) on the air, the entire (oceanic) North Pacific validation region is covered by at least three stations - as required for hyperbolic navigation - at all times. Without station G, limited regions (shaded in Figure 1) will exist where three station, four-frequency coverage is not always available.

---

* Since predictions of modal interference zones were only available at 10.2 kHz, there is some degree of uncertainty in applying these zones at other frequencies. This situation will be ameliorated in future validation studies by the availability of 13.6 kHz predictions as well.

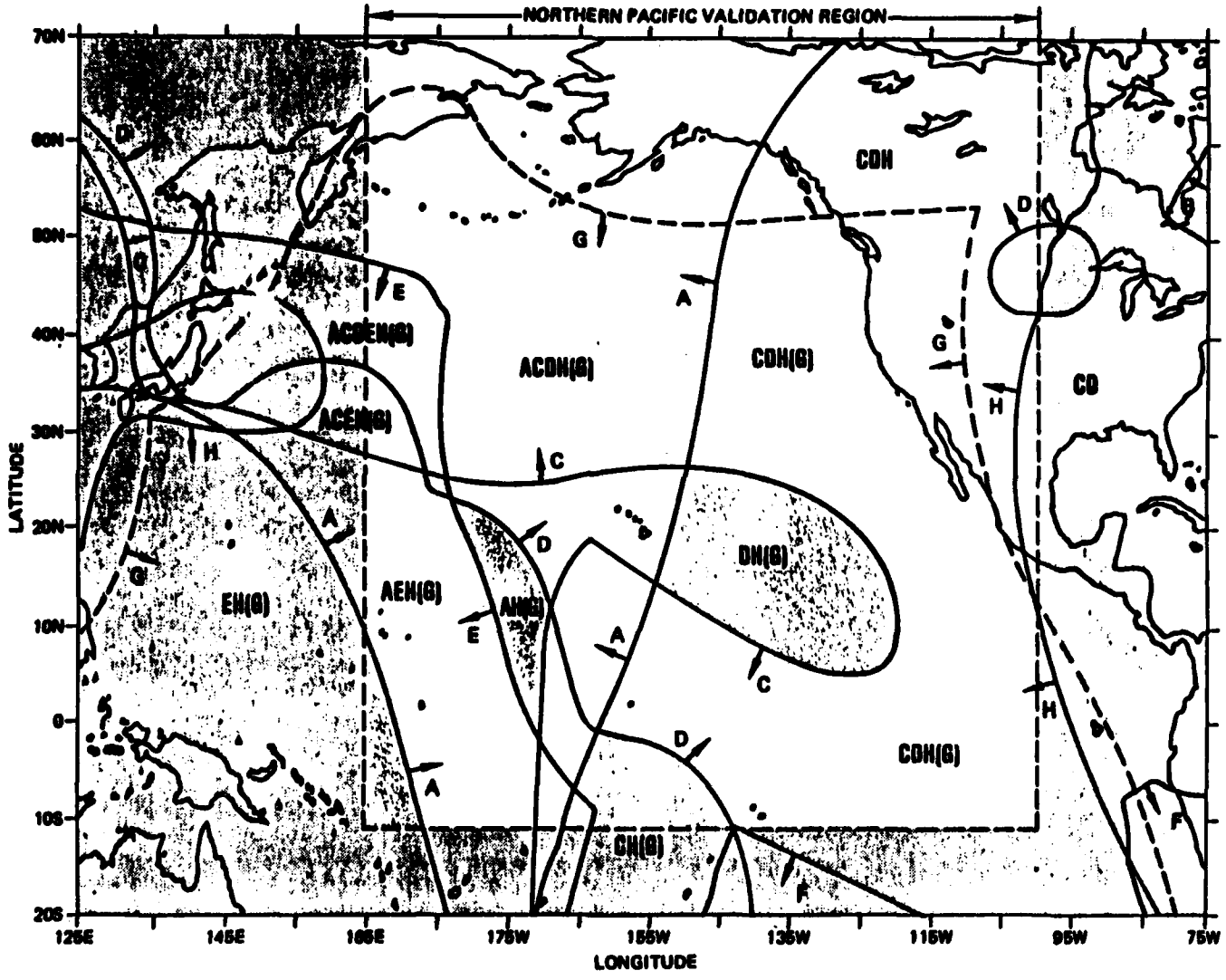

FIGURE 1. COMPOSITE DIAGRAM OF FULL-TIME SIGNAL COVERAGE CONTOURS

- The navigationally important routes between Japan and the West Coast U.S. ports are covered by from four to six stations (including G), thus providing adequate back-up capability for hyperbolic navigation in the event that one of the stations is off-air.

- Stations B (Liberia) and F (Argentina) are not expected to be available on a full-time basis anywhere in the North Pacific and hence will not enter into the fix accuracy assessments.

- ACCURACY

A map showing 95% CEP fix error contours in the North Pacific is given in Figure 2. The significance of the 95% CEP error in the present context is that if one chooses a day and time at random, and generates a fix by optimally combining the four OMEGA signals from each available station as specified by the coverage model, then (in the absence of ionospheric disturbances) the probability is 95% that the radial error of the fix will not exceed the 95% CEP value shown. Note that in the position fixing process, the standard tabulated propagation phase corrections (PPC's) are assumed to be applied so that PPC errors are included as a component of the 95% CEP error.

The main features of the fix accuracy contours may be summarized as follows:

- The best accuracies (95% CEP of 1 to 2 nmi) are obtained in the region north of an imaginary axis: Yokahama-Honolulu-Seattle. This is due to both the excellent coverage (4-6 stations) and the low geometrical dilution of precision (GDOP).

- Fix accuracies (95% CEP) are 2-3 nmi on the West Coast of the continental U.S. and in the environs of Hawaii.

- Over the whole (oceanic) North Pacific validation region, 95% CEP ranges between 1 and 4 nautical miles with the exception of two areas in the very south near the Solomon Islands and Samoa where the 95% CEP errors can grow to 6 nmi. (If propagation phase correction (PPC) biases are removed, errors in these two areas will be reduced to the order of 4 nmi).

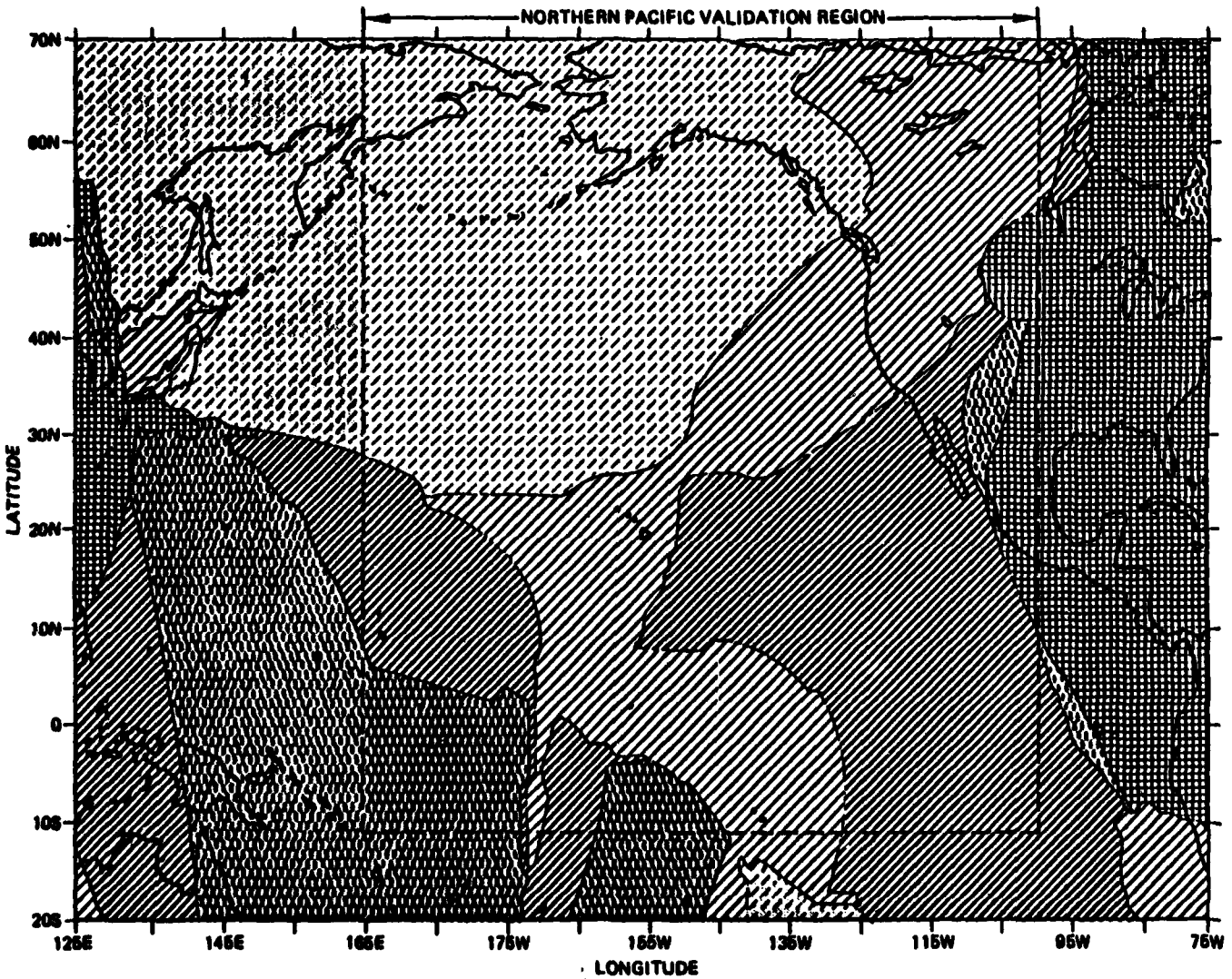

FIGURE 2. RADIUS OF CIRCLE CONTAINING 95% OF FIXES (4-FREQUENCY OMEGA -- WITH PPC BIASES)

LEGEND: 1 - 2 NMI; 2-3 NMI; 3-4 NMI; > 4 NMI; < 3 FULL TIME STATIONS

It is also instructive to display the 50% CEP (i.e. median) radial errors to provide a feel for the average accuracy as opposed to the extreme values represented by the 95% CEP. This is done in Figure 3. In terms of 50% CEP, accuracy in the sector north of Hawaii is better than 1 nmi and is 1-2 nmi practically everywhere else in the North Pacific validation region.

D. COMPARISON WITH GENERAL NAVIGATION REQUIREMENTS

The Federal Radionavigation Plan identifies OMEGA as the primary radionavigation system for oceanic enroute air users and oceanic marine users. For safety of marine navigation on the high seas, this plan specifies a minimum predictable accuracy (indicated position minus true position) of 2-4 nmi (2 drms) and a desirable predictable accuracy of 1-2 nmi (2 drms). Furthermore, the recommended maximum interval between fixes is two hours, with 15 minutes or less being the desired interval. With the exception of the two localized areas in the southernmost sector noted earlier, the accuracies shown in Figure 2 are generally consistent with 2-4 nmi (2 drms) requirement and those in the sector north of Hawaii are consistent with the 1-2 nmi desirable accuracy. (The 2 drms error measure exceeds 95% CEP by from 2 to 15% depending on the eccentricity of the error ellipse. This difference between 2 drms and 95% CEP is not considered significant in the present context). The OMEGA fix interval of 10 seconds is consistent with the desired interval of 15 minutes or less.

Of the various civil air oceanic routes in the North Pacific validation region, only the routes between Hawaii and West Coast U.S. and between Anchorage and Tokyo carry sufficient traffic to justify a formal track structure. By the end of 1981, it is expected that an airspace route configuration known as composite tracks will be implemented on these routes. Lateral separation between aircraft operating at the same altitude will be 100 nmi. The possibility has been suggested (by FAA sources) that in the future the International Civil Aviation Organization (ICAO) will implement a Minimum Navigational Performance Specification (MNPS) on these routes, similar to that adapted for the North Atlantic:

- The standard deviation of the lateral track errors shall be less than 6.3 nmi, i.e., 12.6 nmi (2 sigma).

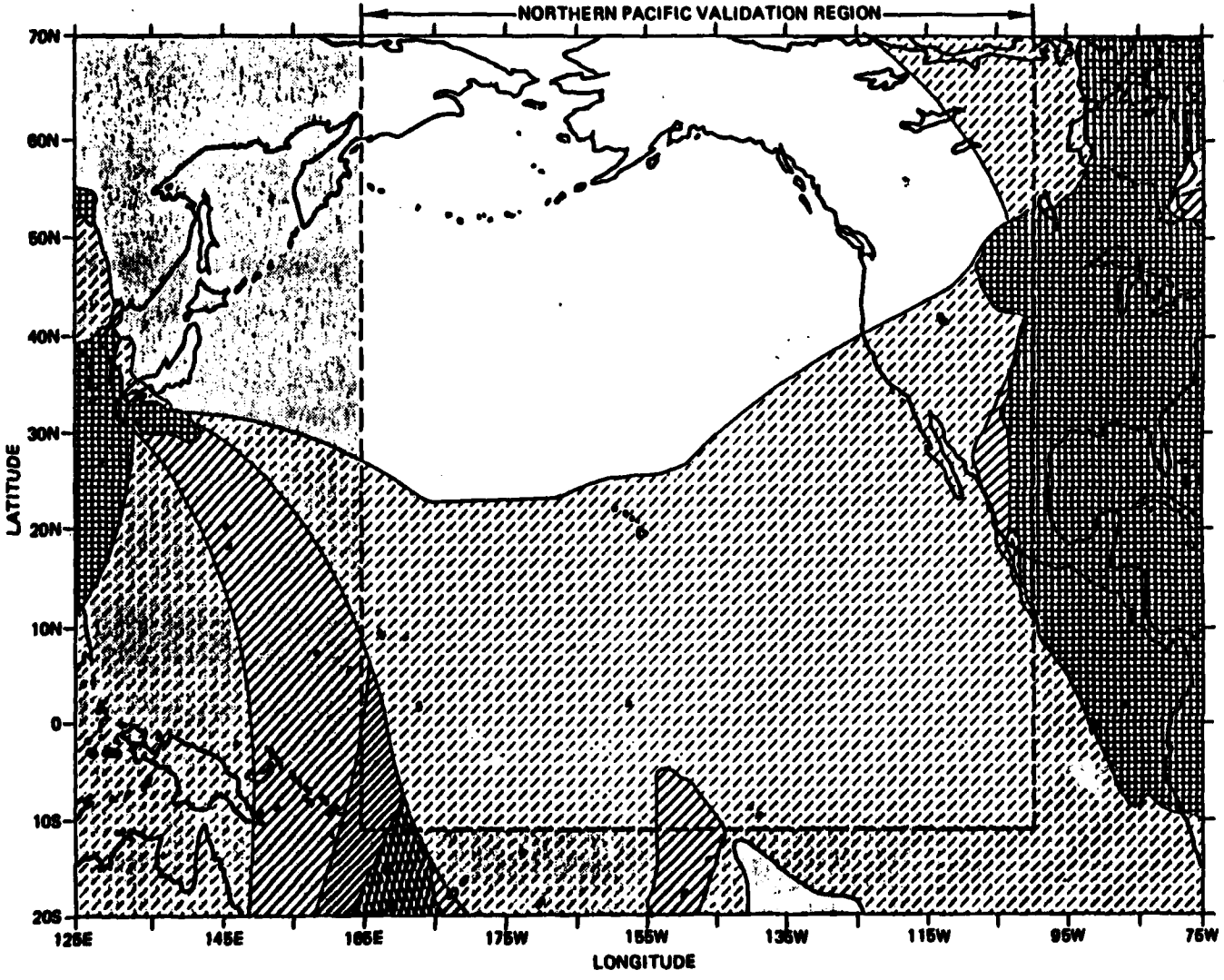

Figure 3. 50% CEP ERRORS IN NORTHERN PACIFIC (4-FREQUENCY OMEGA – WITH PPC BIASES)

- The proportion of the total flight time spent by aircraft 30 nmi or more off track shall be less than 5.3×10^{-4}, i.e. less than one hour in about 2,000 flight hours.

- The proportion of the total flight time spent by aircraft between 50 and 70 nmi off track shall be less than 1.3×10^{-4}, i.e. less than one hour in about 8,000 flight hours.

Again referring to Figure 2, and noting the approximate equivalence of the 95% CEP and 2 sigma error measures, it is seen that OMEGA accuracies over the two routes in question will be comfortably greater than that required to meet the 12.6 nmi (2 sigma) criterion. With regard to the second and third of the MNPS criteria it must be noted that such large cross track errors - or "blunders" - are difficult to assess quantitatively since they are largely specific to the particular receiver implementation, especially in regard to its human engineering aspects. One exception is the effect of an ionospheric disturbance, particularly the sudden ionospheric disturbance (SID) caused by a solar x-ray flare, for which error analyses are carried out in the report. It is found for the routes in question, flares (Class M1) with a nominal frequency of occurrence of one per day during the maximum of the sunspot cycle can cause a radial error (i.e. beyond that experienced in the absence of the flare) of at most 2-3 nmi. Rarer and stronger flares (Class X1), with a nominal frequency of occurrence of one per month during solar maximum, can induce errors of at most 5-6 nmi on these routes. Thus, OMEGA is not intrinsically susceptible to SID-induced blunders of 30 nmi or greater in those portions of the North Pacific which will be subject to an MNPS in the foreseeable future. Furthermore, redundent coverage in such areas permits Norway to be deselected during PCA events, thus mitigating the vulnerability to this (relatively rare) type of ionospheric distrubance as well.

E. OTHER RESULTS OF STUDY

• PHASE ERROR CHARACTERISTICS

Statistical analyses of the ONSOD long-term fixed monitor data show that - when averaged over all measurements taken in the North Pacific - the LOP phase error (measured phase minus theoretical phase) has a median absolute value of about 6 centicycles (CEC) at 10.2 kHz and 7 CEC at 13.6 kHz. (As a nominal rule of thumb, an LOP error of 10 CEC corresponds to an LOP displacement of 1 nmi at 10.2 kHz and .75 nmi at

13.6 kHz). At both frequencies, the median standard deviation of the LOP phase error is 11.5 CEC. The dominant source of phase errors is found to be complexities in the diurnal variation of the phase which are not fully modelled by the propagation phase correction (PPC) algorithm. Natural day-to-day phase variations due to changes in the earth-ionosphere waveguide are a less significant error source, averaging 4.8 CEC at 10.2 kHz and 5.7 CEC at 13.6 kHz.

- ERRORS ASSOCIATED WITH INDIVIDUAL LOP's

When averaged over monitor sites, time of day and season, significant variation is noted in the phase errors associated with individual LOP's. This is shown in Table 1, which lists for each of the major North Pacific LOP's, the total root-sum-squared (r.s.s.) phase errors* and the r.s.s. errors assuming removal of PPC bias errors (see below). It is seen that the total r.s.s. errors range over roughly a factor of two, from of the order of 10 CEC for LOP's corresponding to mid-latitude propagation paths (CD, CH, DH) to about 20 CEC for LOP's involving some propagation in equatorial regions (BD, BE). Indeed, it is thereby possible to rank the LOP pairs with respect to their associated r.s.s. errors in the North Pacific as (best to worst): CD, AC, DH, CH, AH, AD, CE and BD, although it must certainly be borne in mind that LOP crossing geometry will intervene to determine the optimum LOP combinations at a particular location.

---

* r.s.s. phase errors are defined as the square root of the sum of the squares of the errors due to: i) random propagation variations, ii) improper modelling of diurnal phase variations in the PPC's and iii) systematic PPC biases. In the absence of correlations among these error sources, the r.s.s. phase error provides a direct measure of the uncertainty associated with use of a given LOP.

TABLE 1. NORTH PACIFIC PHASE ERRORS BY LOP

	TOTAL R.S.S. ERRORS (CEC)		R.S.S. ERRORS WITH PPC BIASES REMOVED (CEC)	
LOP	10.2	13.6	10.2	13.6
AC	15.4 ± 4.0	14.8 ± 2.7	8.8 ± 1.7	8.3 ± 1.7
AD	14.5 ± 1.3	10.3 ± 1.8	10.3 ± 1.8	10.3 ± 4.9
AH	17.3 ± 3.4	16.5 ± 3.2	10.1 ± 3.4	9.0 ± 0.9
BD	21.6 ± 2.2	22.6 ± 0.9	18.6 ± 2.3	21.6 ± 0.9
CD	10.6 ± 4.0	11.5 ± 3.7	7.4 ± 1.7	7.5 ± 1.6
CE	20.1 ± 1.8	22.9 ± 0.5	17.8 ± 3.2	19.9 ± 2.7
CH	11.6 ± 2.6	12.1 ± 2.5	9.1 ± 2.7	9.8 ± 2.2
DH	13.2 ± 5.4	12.5 ± 3.6	9.1 ± 3.7	8.9 ± 2.1

- ERRORS ASSOCIATED WITH INDIVIDUAL STATIONS

The station-pair (LOP) phase error statistics can be further analyzed (under the assumption of approximate uncorrelation between the errors associated with each member of the station-pair) to break out the contributions of the individual OMEGA stations. The results of this procedure are shown in Table 2. The close similarity between the 10.2 kHz and 13.6 kHz data justifies averaging the two to arrive at a single error figure to be applied at all OMEGA frequencies. It is clearly seen that stations B, E and F (all of which involve propagation through equatorial regions into the North Pacific) cluster naturally into one group with phase errors roughly twice those of the "preferred" stations A, C, D and H. As with LOP's, the stations can again be ranked (best to worst):C, A, D, H, B, F and E.

TABLE 2. SINGLE-STATION PHASE ERRORS

	TOTAL R.S.S. PHASE ERROR (CEC)			R.S.S. PHASE ERROR WITH PPC BIASES REMOVED (CEC)		
STATION	10.2	AVG	13.6	10.2	AVG	13.6
A	11.6	11.5	11.4	6.1	5.0	3.9
B	21.3	21.0	20.5	16.1	17.1	18.1
C	9.2	9.0	8.7	4.3	4.4	4.5
D	12.9	12.5	12.1	9.8	9.4	9.0
E	21.0	21.3	21.6	19.0	19.3	19.5
F	23.0	22.7	22.4	16.5	17.5	18.4
H	13.4	13.2	13.0	9.6	10.0	10.4

- PPC MODEL EFFECTIVENESS

PPC "bias" errors refer to the failure of phase errors at a given monitor site to average out to zero over the full diurnal period. When examined on a case by case basis (where a "case" consists of a month's worth of data at a given monitor site for a given LOP), 13 cases of statistically significant bias errors in excess of 20 CEC are found out of a total of 544 cases at 10.2 kHz, and 15 out of 516 cases at 13.6 kHz. This indicates that in the vast majority of cases, bias errors are not a concern, and only exceed 20 CEC at a limited number of monitor sites during certain months of the year. Indeed, when averaged over season, only one case of seasonally-averaged PPC bias in excess of 20 CEC was found at either 10.2 or 13.6 kHz for receiving sites at which 12 or more semi-months of data were recorded, this one case being the 10.2 kHz BC LOP at Hokkaido, Japan. It is therefore concluded that in an average sense the existing PPC's are free of gross bias errors in the North Pacific. Such bias errors as do exist contribute roughly 1/2 nmi to the range error budget for an individual station.

In addition to PPC bias errors, the report also considers errors arising from complexities in the diurnal variation of the phase which are not fully modelled by the PPC algorithm. As noted earlier, these tend to be the dominant error source, particularly with stations

involving equatorial propagation (B, E, F and - presumably - G) where such "modelling" errors are in the range 15-18 CEC (rms). The "good" stations (A, C, D and H), involve PPC modelling errors less than half these values. Since from coverage considerations, these latter stations are by far the most important in the North Pacific, there would be relatively little impact on position fixing accuracy in the validation region (with the exception of the shaded areas in Figure 1) if the PPC modelling errors were improved for the "poor" stations (B, E, F and G). Thus, so far as the North Pacific is concerned, the existing PPC's are deemed adequate both with respect to the "bias" and "modelling" errors.

F. CONCLUSIONS AND RECOMMENDATIONS

It is concluded that when station G (Australia) is commissioned, the OMEGA navigation system under conditions of normal operation will meet the design predictable accuracy of 2-4 nmi (2-drms) and the enroute navigation requirements of the marine and aviation user communities in the North Pacific. On great circle routes between Japan and the West Coast of the U.S., the system is even now in a mature operational phase, with stable, demonstrable operating parameters. Of particular importance is the redundant coverage and low geometrical dilution of precision (GDOP) on these routes, which mitigates the effects of station off-air periods and ionospheric disturbances.

The emphasis in this study has been on the performance to be expected from a multifrequency, automatic receiver, since this gives proper recognition to the gains in position-fixing accuracy which will accrue from full utilization of the OMEGA signal format. It is recommended that this emphasis be continued in the remaining regional validations. To this end, the theoretical coverage/modal interference boundaries which proved so useful in the present study should be extended to the other shared OMEGA frequencies, at least to 13.6 kHz. Also, on a theoretical note, the analyses of PPC modelling errors have confirmed what has long been known, that propagation through equatorial regions is more difficult to model than on mid-latitude paths. While not of critical importance in the North Pacific, this will impact OMEGA performance in other validation regions. It is therefore recommended that attention be given to improving the PPC algorithm for paths with equatorial segments.

Finally, the present study has been based upon plausible estimates of coverage and phase error statistics for the Australia station. When this station has been commissioned, it would be worthwhile to validate these estimates experimentally. This could be most naturally accomplished in the reprise of the Western Pacific validation, currently scheduled later in the OMEGA regional validation program.

TABLE OF CONTENTS

LIST OF TABLES

LIST OF FIGURES

LIST OF FIGURES (Cont'd)

LIST OF FIGURES (Cont'd)

1.0 INTRODUCTION

1.1 Objectives Of Study

This is the third in a series of regional validations of the OMEGA navigation system conducted for the U.S. Coast Guard's OMEGA Navigation System Operations Detail (ONSOD), previous studies having addressed the Western Pacific[1] and North Atlantic[2]. The philosophy of the regional validation program has been elaborated by Scull[3] and Morris[4], and the role of validation in the broader context of OMEGA program management is discussed by McFarland et al[5].

Simply stated, the validation process is the assessment of OMEGA signal coverage and the attainable position-fixing accuracy using that mix of signals specified by the coverage diagrams (modified, if necessary) as usefully accessible in a given region, i.e. those signals which have an acceptable degree of phase regularity, signal-to-noise ratio, short-path/long-path signal ratio, and modal structure. Although system users are usually concerned only with a simple statement of fix accuracy, the unfortunate reality is that fix accuracy is a "soft" feature of performance since: (1) it normally is critically dependent on the quality of the available PPC's which can change substantially over a period of 2-5 years, and (2) can be characterized in so many different ways that virtually any accuracy criterion can be shown to be satisfied or not satisfied under appropriate scenarios. The "hard" features, on the other hand, are the signal characteristics themselves, such as phase stability (degraded by modal interference), signal amplitude, SNR, path dominance (short vs. long), mode dominance (mode 1 vs. higher modes) and anomalous conditions (vulnerability to SID's, PCA's, transequatorial behavior, etc.), which are usually independent of time (although they may depend on solar cycle). Thus, given that the signal properties are reasonably well validated, one can then discuss fix accuracy in the context of a carefully defined model with specified conditions.

A primary objective of the present study is therefore to characterize the inherent position-fixing accuracy of the OMEGA system in the North Pacific, as it will be when the eighth and final

transmitting station is commissioned in Australia in 1982. The form chosen for such characterization parallels that used by Thompson[6] in his global predictions of OMEGA system performance, viz. contour maps displaying as a function of geographical position the fix accuracy attainable with a hypothetical automatic receiver which makes optimal use in a least-squares sense of all locally available OMEGA signals. Coverage assessments are developed as one essential element of this fix accuracy model.

Secondary objectives of the study include: i) comparison of the attainable fix accuracies with user navigation requirements and system design objectives, ii) evaluation of the effectiveness of the ONSOD propagation phase corrections (PPC's) in the North Pacific, iii) determination of measures of signal quality for individual OMEGA stations which could be used to improve the combinational (i.e. position-fixing) filters in automatic receivers, and iv) assessment of OMEGA performance in the validation region under the abnormal conditions of station off-air periods and sudden ionospheric disturbances (SID's).

The North Pacific, for the purposes of this study, consists of the primary validation region bounded by 100°W and 165°E longitude, 10°S and 70°N latitude. In addition, to facilitate dovetailing with the Western Pacific and South Pacific regional validations, the analyses are extended to the broader domain bounded by 75°W and 125°E longitude, 20°S and 70°N latitude. These areas are shown in the map of Figure 1-1, on which are also indicated the ONSOD long-term monitor sites to be discussed presently.

1.2 Data Resources

Data from five principal sources have been integrated in the North Pacific OMEGA validation:

1. Long term (station-pair) phase difference data collected under controlled conditions by, or in cooperation with ONSOD, at the OMEGA ground monitor sites shown in Figure 1-1.

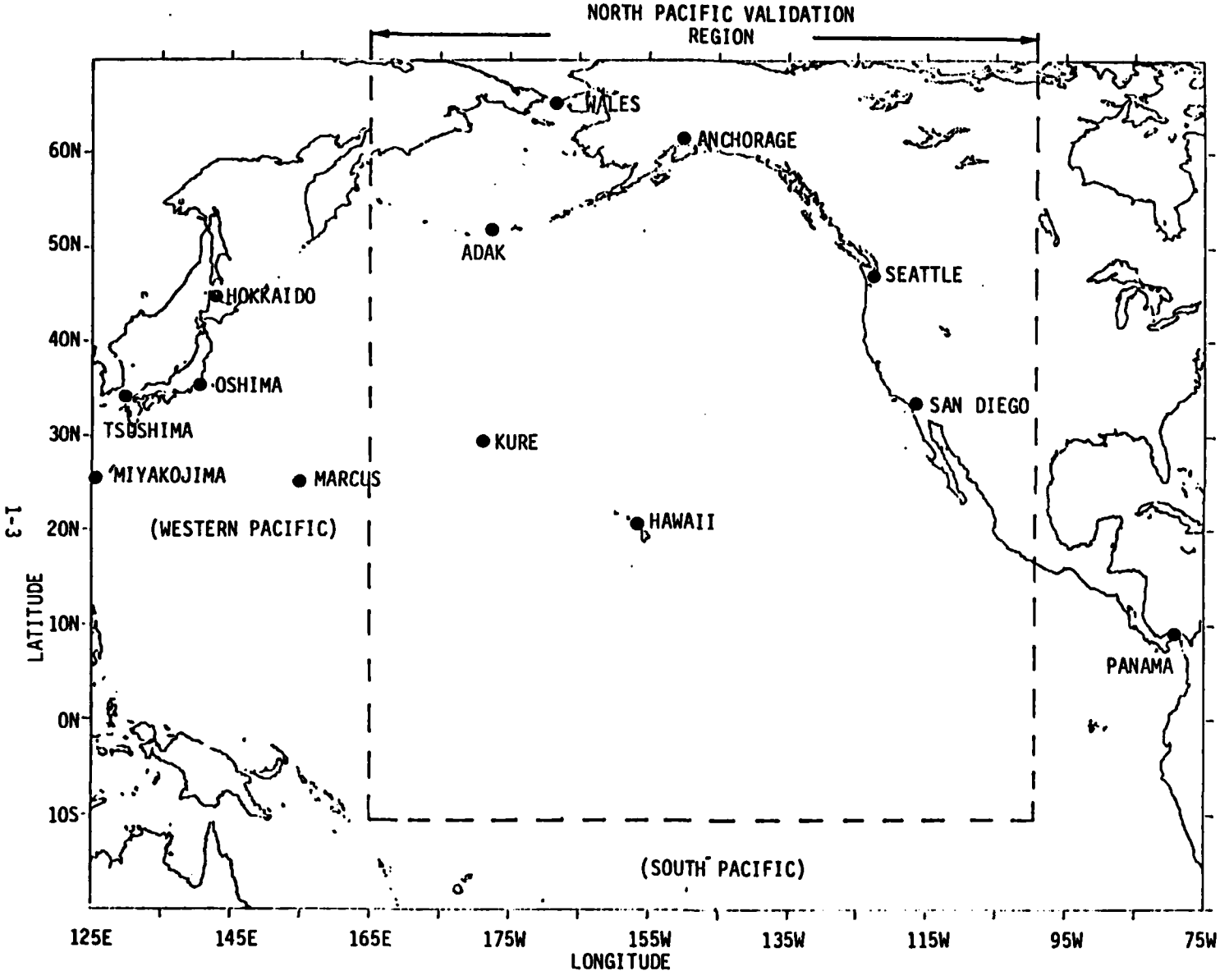

FIGURE 1-1. NORTH PACIFIC VALIDATION REGION INCLUDING FIXED MONITOR SITES

2. Calibrated signal amplitude and background noise measurements performed during the summer of 1979 by the Naval Ocean Systems Center (NOSC) cooperatively with the Federal Aviation Administration Technical Center (FAATC)[7]. These data were taken both at short-term fixed monitor ground sites and aboard a specially fitted aircraft following flight paths designed to probe specific coverage features, as shown in Figures 1-2 and 1-3.

3. Data taken with integrated OMEGA/satellite receivers[8] during voyages of four ships following the routes shown in Figure 1-4. Estimated phase (relative to a quartz oscillator) and SNR indices on an individual-station basis, as well as position-fix accuracy information is provided in these measurements at nominal 1-2 hour intervals.

4. Operational SNR and fix accuracy data of varying utility from three carriers (China Airlines, Pan American World Airways and Western Airlines) with trans-pacific routes and reports from five ships with voyages/patrols in the North Pacific.

5. 10.2 kHz OMEGA signal coverage/modal interference boundaries[9] computed for each station at two times of day and four months of the year using semi-empirical prediction models[10] supplemented with SNR data from ONSOD monitor sites.

Data from the ONSOD monitors and the integrated OMEGA/satellite receivers are available in digital form, thus considerably simplifying the reduction process. The NOSC test data is provided in formal technical reports containing both the fully processed data and interpretations. Operational data is contained in informal memoranda. The 10.2 kHz signal boundaries were provided in digital form by the U.S. Coast Guard.

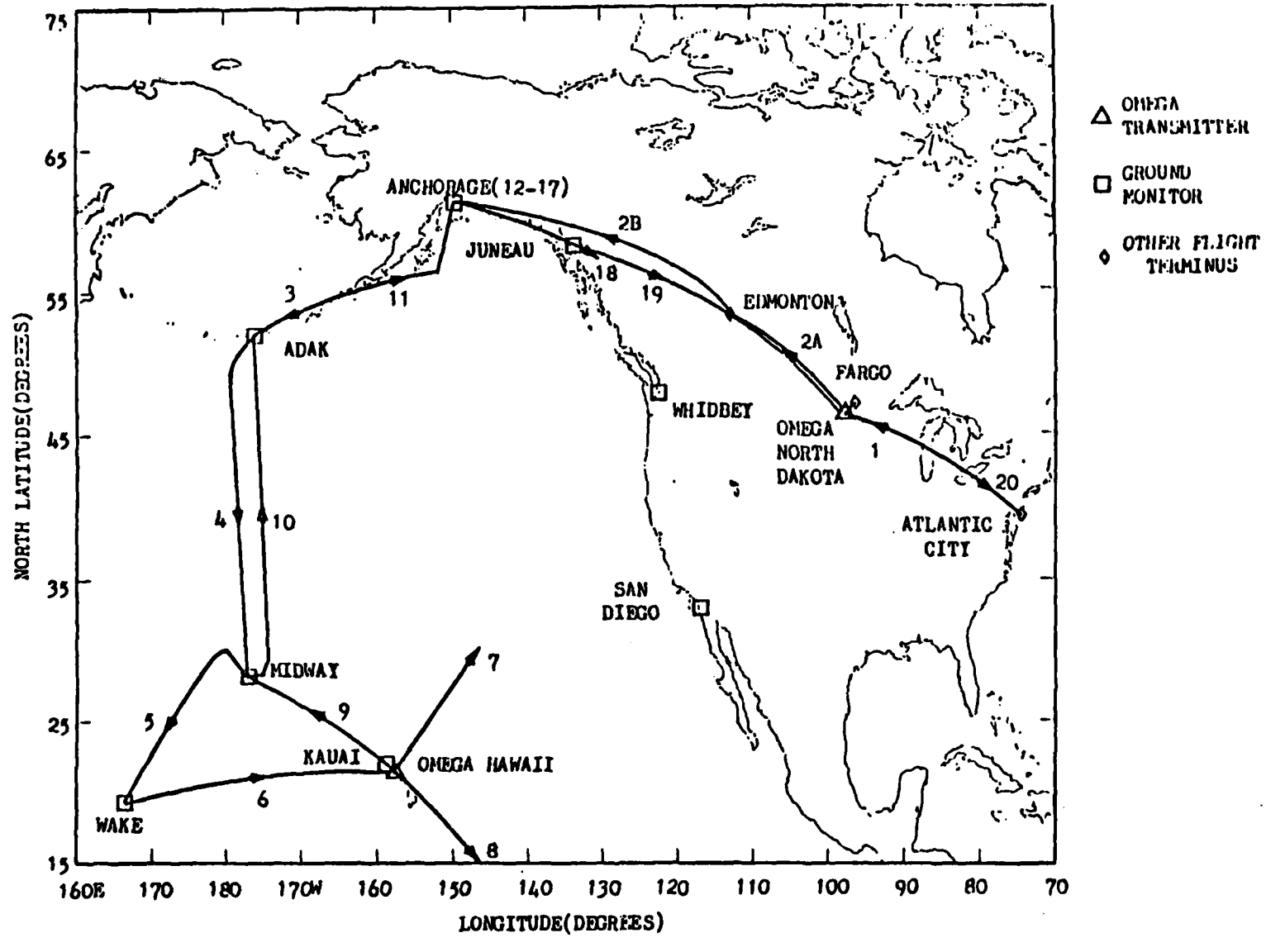

FIGURE 1-2. AIRCRAFT FLIGHT PATHS(FLTs 1-20) AND GROUND MONITOR LOCATIONS - NOSC TESTS

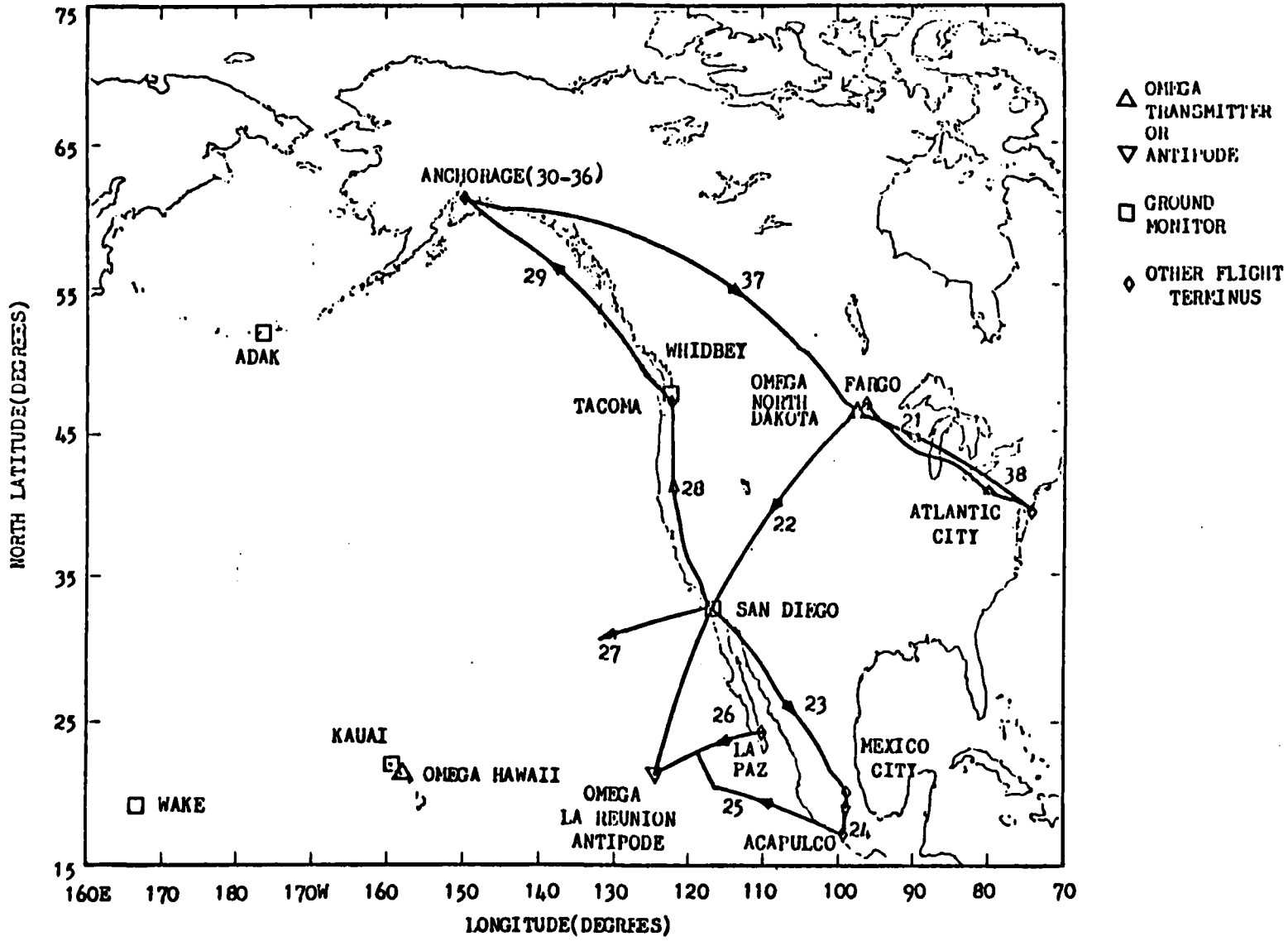

FIGURE 1-3. AIRCRAFT FLIGHT PATHS(FLTs 21-38) AND GROUND MONITOR LOCATIONS - NOSC TESTS

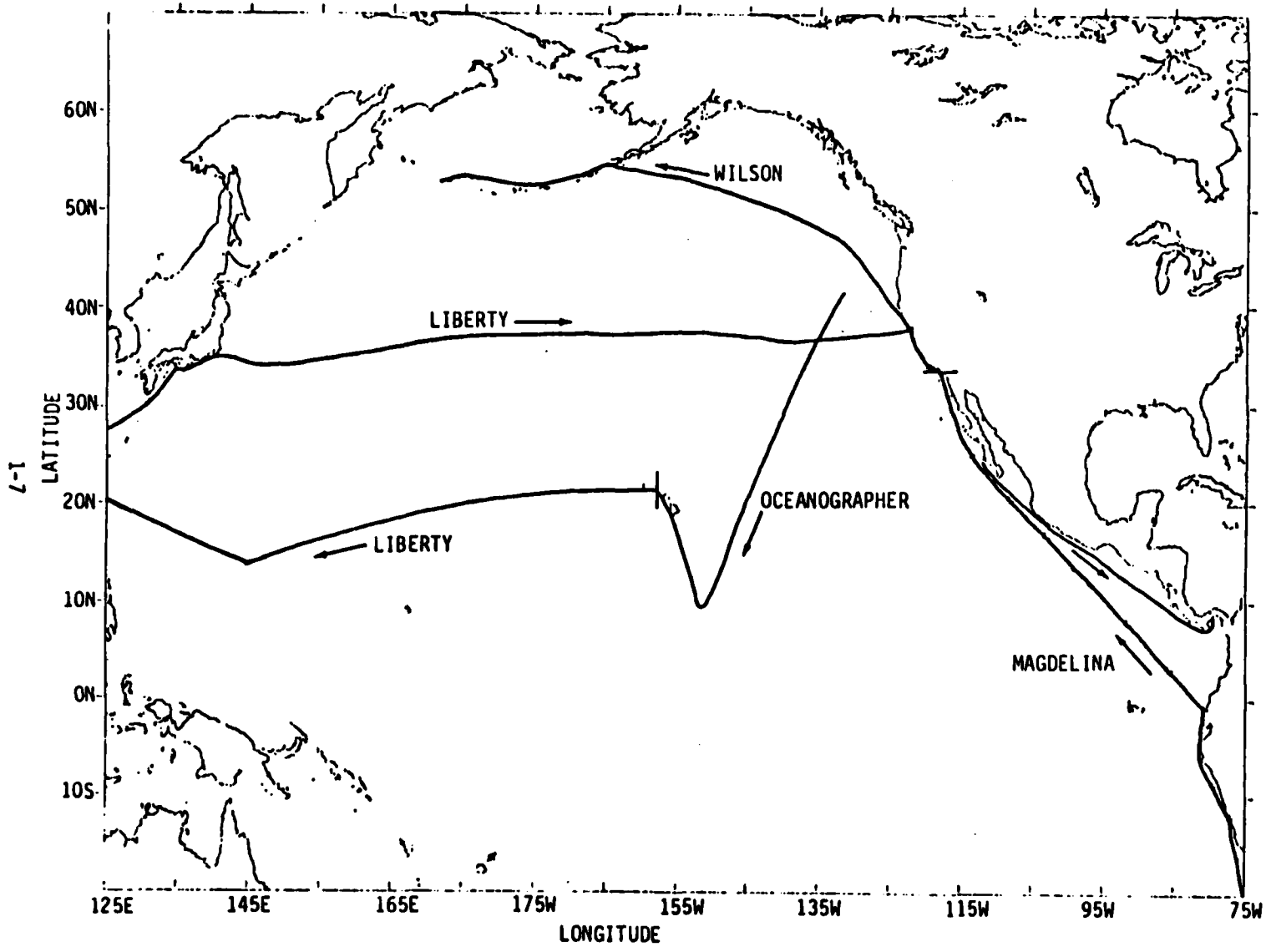

Figure 1-4. Voyages for Integrated Satellite/Omega Shipboard Data

In addition, unreduced phase measurements from the NOSC tests and SNR indices from some of the ONSOD long term monitors were available, if needed, to supplement the above data. As it turned out, however, the reduced data were deemed sufficient for the purposes at hand and these ancillary resources were not required.

1.3 Plan of Report

The methodology whereby the foregoing data are integrated to form coherent assessments of coverage and accuracy will be presently described in Section 2 as part of a general background discussion of the OMEGA system and the regional validation program. The essential feature of this methodology is that the desired accuracy assessments follow directly from a mathematical model of the performance of a hypothetical optimized automatic OMEGA receiver. The first item of business is therefore to develop this model, which is carried out in Section 3. As indicated earlier, this development is similar to that of Thompson[6], although the mathematical approach is quite different and the scope has been extended to include a more comprehensive characterization of the fix error statistics.

The fix error model requires two basic inputs: i) a model of the phase errors (i.e. measured phase minus theoretical phase) associated with each OMEGA signal received at a given position, and ii) a "coverage" model which specifies the actual mix of usable signals which are expected to be available at each position. Accordingly, Section 4 addresses the task of deriving the desired phase error model from the ONSOD long-term monitor data. Following this, the signal coverage model is developed in Section 5. Here, the approach is to derive the coverage model directly from the semi-empirical boundaries provided by the U.S. Coast Guard and then to validate this model by in-depth comparisons with the NOSC test data, the integrated OMEGA/satellite data and the operational data.

With the requisite input models now in place, the desired fix accuracy assessments are then generated in Section 6. First, to establish contact with existing fix accuracy data, results are obtained for the case of Station G off-air and those are then compared with operational experience and with the fix accuracies measured by the integrated OMEGA/satellite receivers. Following these comparisons, assessments are generated for the fully-implemented OMEGA system and are then measured against the requirements of the marine and aviation user communities.

Section 7 is devoted to a number of mutually unrelated peripheral issues which, while not essential to the fundamental question of whether OMEGA - under normal operation conditions - can provide adequate enroute navigational capabilities in the oceanic sectors of the North Pacific validation region, nervertheless are of interest to the OMEGA community and are therefore included under the general rubric of Operational Implications. A final section summarizes the conclusions and recommendations derived from the study.

Throughout the main body of the report, the emphasis is on the systematic presentation and discussion of results. The in-depth analyses from which such results were obtained are - in the interest of clarity - consigned to a series of Appendices.

2.0 BACKGROUND

2.1 Description and Status of the OMEGA System*

Any assessment of OMEGA performance must recognize at the outset that the system has been in a state of continuous evolution since 1966, when four developmental cesium-controlled transmitting stations first began operations on a 24-hour schedule. Over the subsequent years, stations have been added and subtracted, new frequencies have been implemented in the signal format, propagation phase corrections (PPC's) have been improved, techniques of station synchronization have matured, and receiver technology has progressed from the early manual single-frequency units to the microprocessor-controlled automatic multi-frequency receivers of today. Even further refinements are a possible outcome of the active ongoing dialogue between the U.S. Coast Guard and the user community[13]. It is therefore very important to clearly define the various elements of the OMEGA "system" whose performance is to be assessed. As a general guideline, the goal is to conservatively characterize the performance of the OMEGA system as it will be, in principle, when it is declared fully operational at the completion of the regional validation program.

TRANSMITTER NETWORK

Earlier validation studies[1,2] have tended to emphasize single frequency (10.2 kHz) operation with manually-applied PPC's, using the interim operational network consisting of the stations listed in

---

* It is difficult to improve upon the concise overview of OMEGA presented in the North Atlantic Validation report[2], to which the reader unfamiliar with OMEGA is therefore referred. A comprehensive bibliography[11] of OMEGA related publications is maintained by the International OMEGA Association (P.O. Box 2324, Arlington Va. 22202) and a general User Guide - soon to be updated - is also available[12].

Table 2-1, without including station G (Australia). While neglect of the Australia station was certainly appropriate in the North Atlantic where such coverage is expected to be minimal, the opposite is true in the Pacific where Australia will represent a primary resource. Thus, the fully-implemented transmitter network of Table 2-1 - including Australia - will be utilized.

SIGNAL FREQUENCIES AND RECEIVER TIMING

With regard to signal frequencies, it is noted that each of the four frequencies (10.2, 11.05, 11 1/3 and 13.6 kHz) shared among all stations are given equal weight in the OMEGA signal format shown in Figure 2-1. Although traditionally the 10.2 kHz signal has been viewed as the "primary" OMEGA frequency, the trend in design of modern sophisticated receivers is to utilize all of the shared frequencies for navigation, thereby exploiting the gains in position fixing accuracy which accrue from such redundancy. Accordingly, assessments of fix accuracy shall be based upon a four-frequency receiver. As a concession to economic realities, the receiver is not assumed to be equipped with a precision time standard and is thus incapable of pure rho-rho navigation. (In the spirit of conservatism, the unique frequencies are assumed to be used for format synchronization only, notwithstanding the fact that they can also in principle contribute additional gains in accuracy, even in the absence of a precise clock.)

RECEIVER SENSITIVITY

The SNR threshold for accurate phase tracking varies as a function of receiver design. The threshold value of -20dB (100 Hz bandwidth) appropriate to the early marine receivers has been used in the prior validation studies although it was noted in the North Atlantic validation[2] that -30dB would perhaps be more representative of modern receivers. In order to partially compensate for simplifying assumptions (regarding the statistical independence of phase errors on different

TABLE 2-1

OMEGA TRANSMITTING STATIONS

STATION LETTER DESIG.	SITE[3]	LATITUDE/LONGITUDE[1]	OPERATING AGENCY
A	Aldra, Norway	66.4202°N/13.1368°E	Norwegian Telecommunications Administration
B	Monrovia, Liberia	6.3053°N/10.6646°W	Liberian Ministry of Commerce, Industry and Transportation
C	Haiku, Oahu I, Hawaii	21.4047°N/157.8310°W	U.S. Coast Guard
D	La Moure, North Dakota	46.3659°N/98.3358°W	U.S. Coast Guard
E	La Reunion I, Indian Ocean	20.9742°S/55.2897°E	French Navy
F	Golfo Nuevo, Argentina	43.0536°S/65.1909°W	Argentine Navy
G	Woodside, Australia[2]	38.4813°S/146.9351°E	Australian Dept. of Transportation
H	Tsushima, Japan	34.6147°N/129.4535°E	Japanese Maritime Safety Agency

Notes: 1. Transmitter Position Datum: World Geodetic System 1972 (WGS-72)

2. A temporary station at Trinidad (10.6995°N/61.6383°W) transmitted in the G station segment until December 1980 when it was decommissioned. The Australia station is expected to be operational in 1982.

3. Stations A and D have been on-the-air since 1972-3, stations B,C,E,F and H since 1975-6.

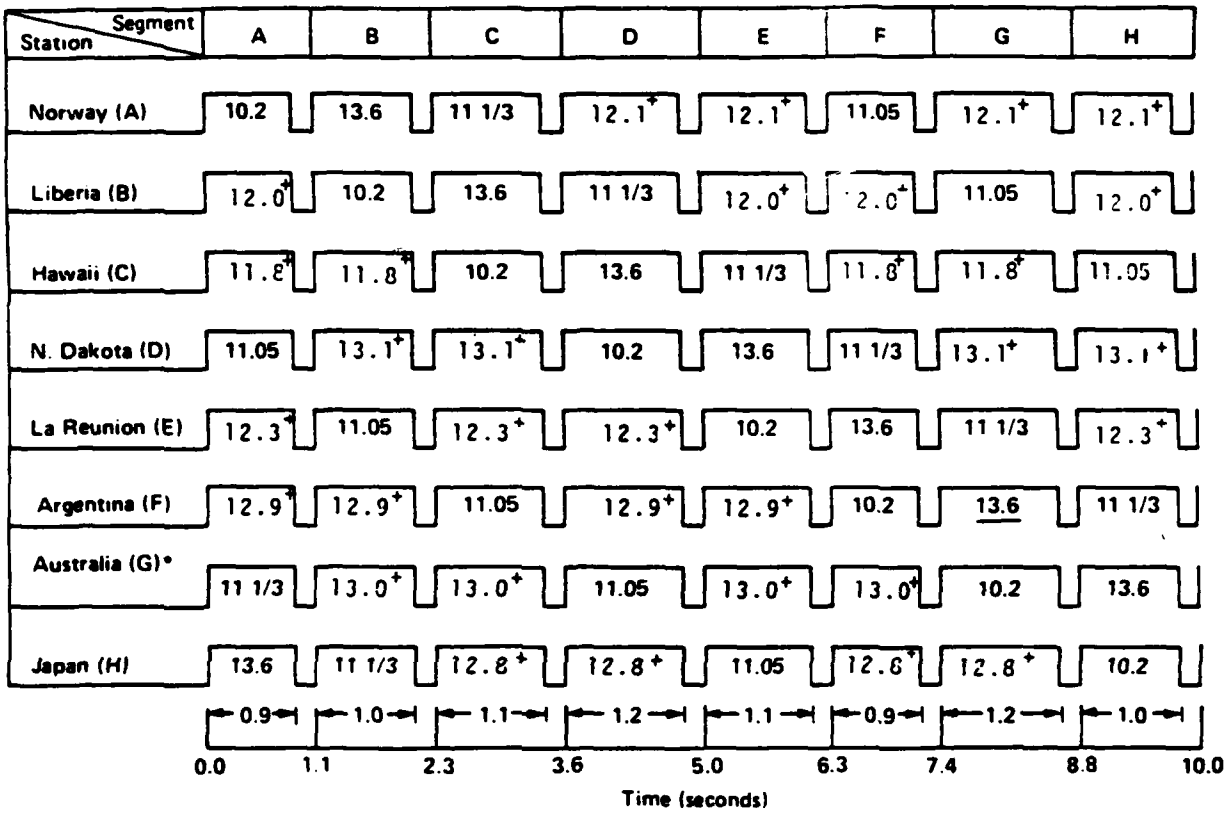

(+ denotes unique frequencies)

Figure 2-1
Omega Signal Transmission Format

OMEGA frequencies) which will be made later in the analysis and which tend to overestimate somewhat the gains in fix accuracies provided by signal redundancy, the more conservative -20dB sensitivity figure will be retained in the present study.

POSITION FIXING ALGORITHMS

By far the most significant determinants of position-fixing accuracy are the processing algorithms which are applied to the measured phase values of the different OMEGA signals in order to derive a position. These include algorithms for propagation phase corrections (PPC's), signal selection/deselection, and combinational filtering of multi-frequency/multi-station inputs. Performance of this (generally proprietary) software varies from one receiver manufacturer to the next, thus complicating the interpretation of operational data. For the purposes of the present system assessments, a least-squares optimized *combinational filter - derived in Section 3 -* is applied using signal quality factors based on measured phase variances in the North Pacific. Thus, the (hypothetical) receiver portion of the OMEGA "system" under evaluation has been optimized with respect to performance in the validation region. This is the multi-frequency/multi-station analog of the procedure followed in earlier validations, viz. basing accuracy assessments upon an empirically determined "best" pair of 10.2 kHz LOP's.

Propagation corrections in the hypothetical receiver are assumed to be derived from a software implementation of the ONSOD propagation prediction model[14], empirically modified as required to remove any gross biases*. Signal selection is based upon state-of-the-art a priori coverage and modal interference modelling[15].

---

* No such modification appears to be required in the North Pacific.

SOLAR/IONOSPHERIC DISTURBANCES

The final component of the OMEGA "system" to be specified is the state of the propagation medium, viz. the earth-ionosphere waveguide. The bulk of the accuracy assessments shall be based upon an assumed undisturbed ionosphere, i.e. in the absence of SID's and PCA's. The PCA affecting only the Norway transmissions in the North Pacific - is sufficiently rare (a few per year at solar maximum) to justify ignoring it in the present study, particularly since automatic deselection of the affected station is possible[16]. The SID, on the other hand occurs much more frequently and must be acknowledged in any evaluation of an ionospherically-dependent system. Accordingly, separate consideration will be given to accuracy degradations associated with SID's.

2.2 The Regional Validation Program

The OMEGA system is currently specified as "interim operational". Full operational status is expected to be declared in 1985 at the completion of a validation program designed to assess system accuracy and coverage on a region by region basis.

The validation reports are to "focus attention on overall system performance in a particular region, and act to suggest management emphasis with regard to the various technical endeavours underway at ONSOD", where "the overall performance measures are simply those of demonstrated system accuracy and signal availability"[15]. The accuracy goals of OMEGA are loosely specified in the proposed Federal Radionavigation Plan[17] as a 2 to 4 nmi 2-drms error of positioning with respect to geographical coordinates. A primary output of a validation study is thus to assess the degree to which this goal is being met in the region of interest.

Signal availability, or "coverage", is the specification - as a function of position and time - of the mix of OMEGA signals which are usable for navigation. Usability, in turn, translates into the dual requirements that the SNR exceed a standard threshold for phase tracking (-20 dB in 100Hz bandwidth as discussed earlier) and that the modal interference-induced phase deviation, relative to the reference signal phase, be less than a threshold value of 20 centicycles. Coverage is most conveniently specified by defining, for each OMEGA signal, geographical "boundaries" within which these usability criteria are met. Thus, a prerequisite to making accuracy assessments is the establishment of the location of such coverage boundaries.

Ideally, this latter process would take place by an iterative procedure whereby one: i) starts with boundaries determined from a theoretical (or semi-empirical) model, ii) tests these predictions by direct measurements of SNR and modal interference in the neighborhood of the presumed boundaries, and then iii) reconciles any discrepancies by empirical adjustments to the actual boundaries. Indeed, to a certain extent, this procedure has been followed (for 10.2 kHz boundaries) in the earlier validation studies[1,2]. The basic difficulty, however, is that the boundaries are expected to vary markedly as a function of time of day and season, are often highly irregular in shape, and thus are only incompletely verifiable by the spot checks in space and time which are afforded by a monitor program of feasible scope. Furthermore, theoretical boundaries are expensive to compute and have thus far been generated in any depth for only the 10.2 kHz OMEGA signal. Predicted coverages for the remaining three shared frequencies are thus not yet available.

With regard to "demonstrated system accuracy", operational results are very much dependent upon the specifics of receiver implementation, i.e. how the position fix was actually generated from the observed phase and it is difficult to extract the intrinsic

position-fixing capabilities of the OMEGA navigation system from such data. There are thus formidable methodological problems common to all of the regional validation studies. In addition, each validation region has unique propagation and operational features requiring particular attention. Before describing the methodology of approach which has been applied in the present study, it is therefore necessary to point out the distinguishing elements of the Northern Pacific validation.

2.3 Problems Specific to the N. Pacific Validation

The OMEGA stations of primary importance in the N. Pacific validation region are: Norway, Hawaii, N. Dakota, Japan and - to a lesser degree - La Reunion. Liberia and Argentina are of little navigational utility in the region. The Australia station, which is expected to provide coverage over virtually the entire validation region, must be included in any assessments of OMEGA performance yet will not be on the air until 1982 at the earliest. Thus the first problem specific to the N. Pacific validation is to devise a method for including the performance gains accruing from inclusion of the Australia transmissions in the OMEGA signal format in the absence of actual coverage and phase error statistical data for such signals.

The other special considerations derive from propagation features associated with some of the individual stations:

- Transmissions from Norway into the eastern half of the N. Pacific validation region must traverse the (low conductivity) Greenland ice cap. The consequent severe attenuation results in the expectation of a "Greenland shadow" region within which Norway signals are too weak to be usable for navigation.

- Hawaii lies in the center of the N. Pacific validation region and thus the near-field modal interference phenomena associated with this station will be important.

- The La Reunion antipode is expected to lie within the validation region (between Hawaii and Baja California - see Figure 2-3) so that long-path signals will be received in some parts of the validation region and short path signals in others.

The N. Dakota and Japan transmissions - in contrast - are expected to be relatively uncomplicated from a propagation standpoint since zones of anticipated modal interference (at least at 10.2 kHz where thay have been computed) do not intersect the validation region and ground conductivity variations - as a function of azimuth from the station - are not pronounced.

2.4 Methodology of Approach

In earlier validation studies[1,2], accuracy assessments have been carried out on a single frequency (10.2 kHz)/single LOP pair basis. After choosing a specific month for analysis, a scatter plot of fixes is generated for the given LOP-pair and the position errors associated with the mean fix and the scatter about the mean fix are thereby evaluated. The various possible LOP pairs are analyzed in this fashion and system accuracy - for the month in question - is identified with the fix errors found for the best LOP pair. While undeniably useful for the specification of performance to be expected using a single-frequency manual receiver, this procedure is inadequate for characterizing the fix accuracy attainable with a modern multi-frequency automatic receiver in which multiple lines of position contribute to the derived position fix. The clear trend among system users towards microprocessor based automatic receivers argues for a broadened characterization of fix accuracy, one which gives proper recognition to the improvements which follow from full utilization of the redundancy inherent in the OMEGA signal format.

As mentioned earlier, the approach followed in the present study parallels that of Thompson[6] in which fix accuracy is computed

for a hypothetical receiver which optimally combines - in a minimum least squared error sense - all available OMEGA signals to derive a fix. Modelling the performance of such a receiver - as carried out in Section 3 - is greatly facilitated if one makes the assumption that the phase errors (i.e. measured phase minus theoretical phase) associated with the individual OMEGA signals are uncorrelated, zero-mean random variables. Strictly speaking, of course, this is only an approximation to the actual situation, since phase errors on different signals are to some extent correlated (by virtue of propagating in a common earth-ionosphere waveguide and also since all PPC's are generated by the same computational algorithm) and residual "biases" (i.e. non-zero means) do in fact exist. The neglect of such correlations has the effect of overestimating somewhat the improvement in fix accuracy provided by use of an over-determined set of LOP's, so this will be partially compensated by a general policy of extreme conservatism in other estimates - particularly in signal coverage (see below). The zero-mean phase error approximation turns out to be justified in the N. Pacific validation region - as will be explicitly demonstrated in Section 4 - by virtue of choosing a sufficiently wide statistical ensemble in space and time that localized biases tend to average out.

Specifically, instead of attempting to characterize, say, the phase error associated with the 11 1/3 kHz N. Dakota signal at Adak, Alaska in the month of June during local night-time conditions, we broaden the basis of characterization to seek instead a single error measure for the 11 1/3 kHz N. Dakota signal representing an average over all times of day* and seasons and over all monitor sites (within the validation region) where this signal is usable. This programme - carried out in Section 4 - enables us to derive from the ONSOD

---

* Contrary to expectations, statistical analysis reveals (see Section 4) little difference between phase errors measured near local midnight as compared to local noon, thus justifying such diurnal averaging.

MASTERFILE fixed monitor data base an omnibus phase-error measure for each OMEGA signal which includes contributions due to random propagation effects as well as propagation prediction errors.

The fix accuracy attainable with the hypothetical optimized receiver is then a function only of these phase errors associated with each (usable) OMEGA signal, and the bearing angles to each station. While the former quantities are constant over the validation region (i.e. by virtue of the spatial averaging process used in deriving them), the bearing angles (and associated geometrical dilution of precision, GDOP) change continuously as a function of position, thus giving rise to a corresponding continuous variation of fix accuracy. Superimposed on this is a discontinuous variation in the mix of usable signals as coverage/modal interference boundaries are crossed. Thus, to obtain fix accuracy assessments at all locations within the validation region, it is necessary to specify these boundaries.

As mentioned earlier, one ideally arrives at the desired coverage/modal interference boundaries (i.e. the boundaries of the region within which each signal is usable by virtue of: i) freedom from modal interference in excess of 20 CEC, and ii) SNR (100 Hz BW) $\geq$ -20dB) by an iterative procedure of empirical refinement of theoretically-generated predictions. In practice, as was also noted, this is not possible since such predictions are thus far available only at 10.2 kHz and only at a limited sample of times-of-day and season. Furthermore, field measurements of feasible scope can only provide limited spot checks of such predictions in any event.

To surmount these difficulties, the following methodology has been devised:

1. Definition of "full-time" boundaries:

   Actual coverage boundaries and - more markedly - zones of modal interference vary with season and time of day. Rather than producing a corresponding compendium of fix accuracy assessments

(i.e. each associated with a given time of day and month of the year), it is more feasible to define "full-time" boundaries within which the given OMEGA signal is always expected to be usable for navigation (i.e. barring station off air periods and severe ionospheric disturbances). Fix accuracy assessments are then generated using these time-independent boundaries. This is a very conservative procedure since in general at any given time and place a wider mix of signals will be usable for navigation than those derived from the "full-time" boundaries. For example, modal interference zones which are predominantly a night-time phenomenon are in effect - applied at all times of day in deriving the full-time boundaries so that some regions of perfectly usable day time signals are not included. This conservatism, and the use of the -20 dB SNR threshold criterion are employed - as mentioned earlier - to offset the overestimated gains in fix accuracy which follow from the assumption of statistical independence of the phase errors associated with the various OMEGA signals.

2. Use of 10.2 kHz boundaries at all OMEGA frequencies:

Both SNR threshold and modal interference zone boundaries will vary with frequency to a certain degree. Ideally, one would determine individual full-time coverage boundaries for each of the four shared OMEGA frequencies. Practically speaking, however, this is not yet possible since theoretical predictions are only thus far available at 10.2 kHz[9,10]. As a practical expedient, therefore, the 10.2 kHz boundaries have been uniformly applied at all frequencies. From the standpoint of signal-to-noise this is probably a conservative approximation since the atmospheric noise background and signal attenuation rates tend to decrease with increasing frequency above 10.2 kHz. Modal interference on the other hand is too complex to similarly generalize and the application of 10.2 kHz modal interference zones at other frequencies can only be justified on the grounds of expediency. The net effect of this approximation, however, will probably primarily be felt on the full-time boundaries for OMEGA Hawaii since modal interference in the N. Pacific for the other important stations (Norway, N. Dakota, Australia and Japan) is not expected to be severe by virtue of the ranges and magnetic azimuths involved, although the 13.6 kHz near-field modal zone for N. Dakota and Japan probably extends somewhat into the N. Pacific region.

3. Validation of full-time boundaries:

The full-time boundaries for each station are initially generated by combining a series of 10.2 kHz theoretical* boundaries computed at two time of day and four seasons of the year. If correct, no

---

* These boundaries should more properly be called "semi-empirical" since they do embody corrections mandated by monitor data.

examples should be found in the available NOSC test data, non-test data or operational data of signals failing to meet the (SNR and modal interference) acceptability criteria within the boundaries. Thus, the procedure for validating the full-time boundaries is one of demonstrating their consistency with experimental observations, where consistency means simply that usable signals are always found where they are predicted to be available on a full time basis. The presence of usable signals beyond the full time boundaries - i.e. where they are not expected to be always available - is not in conflict with the boundaries since, as was pointed out earlier, the full-time boundaries intrinsically tend to underestimate coverage.

The final methodological question requiring background discussion is the treatment given to the Australia signals. In order to include Australia in the accuracy assessment, we must specify the phase errors which we expect will be associated with the Australia signals and the full-time boundaries within which these signals are expected to be usable for navigation. Fortunately, the theoretical (10.2 kHz) boundaries were in fact generated for Australia so full-time boundaries - albeit unvalidated by experimental data - can be constructed as with the other signals. The circumstance that the paths from Australia into the N. Pacific are of uniform (i.e. seawater) ground conductivity and the extended coverage from Argentina into the N. Atlantic (a path of similar range and magnetic azimuth) found in the earlier validation study lead to the expectation that the actual coverage which will be found in the N. Pacific when Australia is finally on the air will be consistent with theory. As regards the Australia phase errors, here we again shall adapt the most conservative procedure which is simply to determine the worst-case phase errors for the seven stations which are on the air and then to use these values for Australia. In other words, we assume Australia will be no worse from a phase error standpoint then the worst of the other signals. (In the North Pacific this turns out to be short-path Argentina signals).

Having thus discussed the principal methodological problems and the techniques devised for operating within such constraints, we are now ready to carry out this programme. The first step is to model the fix accuracy attainable with the hypothetical optimum receiver.

3.0 POSITION FIX ACCURACY MODEL

This Section develops the mathematical theory of the fix error statistics for a hypothetical receiver which optimally combines all available OMEGA signals. The phase errors associated with the individual OMEGA signals are assumed to be zero-mean uncorrelated random variables. Although the receiver is hyperbolic in that it is not assumed to contain a precision time standard, it is simpler to develop the theory in terms of single-station, rather than station-pair, phases. This pseudo-range implementation is a mathematical convenience only and the end results are the same as would have been obtained if the development had been carried through explicitly in terms of station-pair LOP's.

The performance of an optimum receiver has been considered earlier by Lee[19]. The present theory follows a more straightforward and physically transparent approach, and extends Lee's results to a more complete characterization of the fix error statistics. Since it has not appeared elsewhere in the literature, we carry out the development in full mathematical detail. (The reader wishing to bypass such details should skip to Section 4).

3.1 Problem Definition and Receiver Optimization

Consider the geometry shown in Figure 3-1, representing an area sufficiently close to the reference position that the Earth may be considered locally flat over this area. Great circles are straight lines in this approximation and a unit vector $\hat{u}_i$ in the direction of the station transmitting the ith navigation signal is drawn with bearing angle (measured from true North) given by θ_i. Let an optimum OMEGA receiver be located at position $\underset{\sim}{r}$ and let N navigation signals be received. Let ϕ_i be the measured phase of the i^{th} navigation signal (of frequency f_i). Let ϕ_i^0 be the (PPC-corrected) theoretical phase of i^{th} signal at the reference position. In terms of the relative phases δ_i:

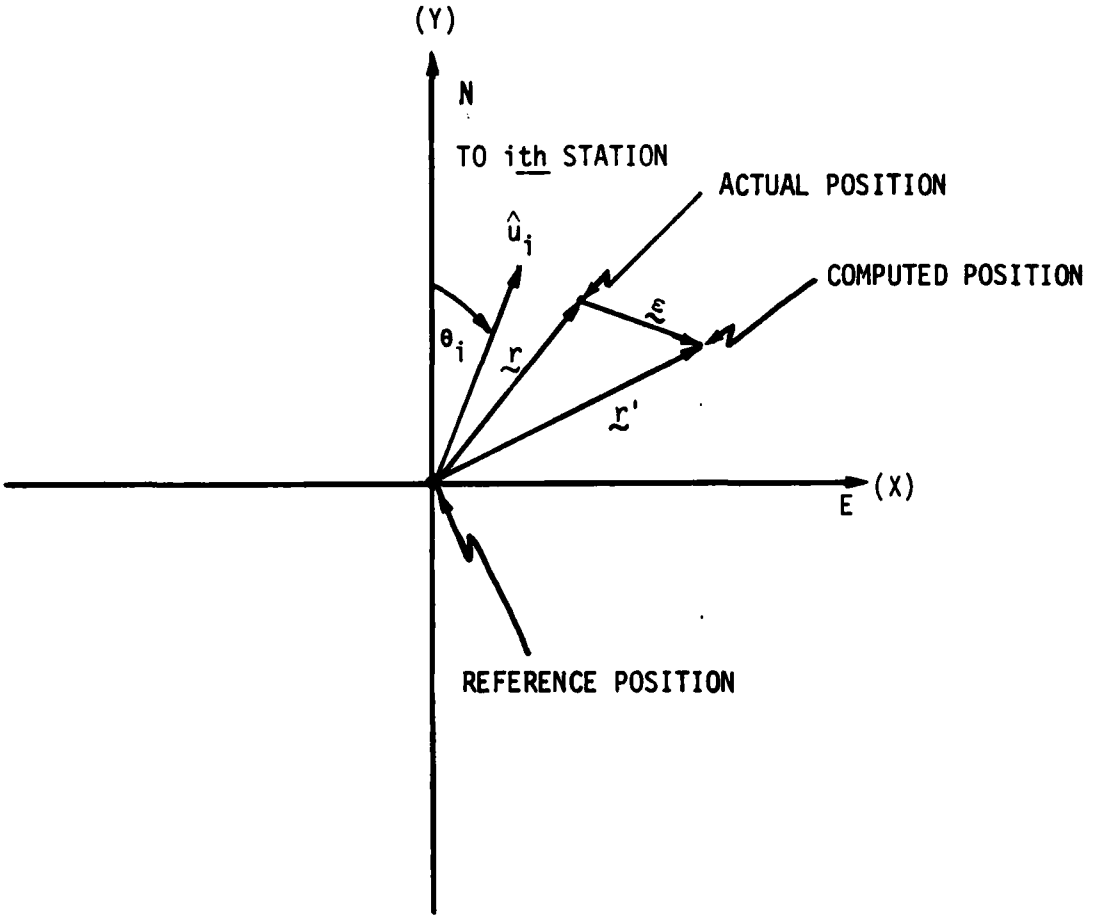

Figure 3-1

Fix Error Geometry

3-1) $$\delta_i \equiv \phi_i^{o} - \phi_i$$

The optimum receiver generates a position fix $\underset{\sim}{r}'$, whose E-W and N-S components (X',Y') are given by

3-2) $$X' = \sum \alpha_i \delta_i$$
$$Y' = \sum \beta_i \delta_i$$

In 3-2) and henceforth, the summation sign is understood to represent a sum over the index i from i=1 to N, unless otherwise noted. The weighting coefficients in 3-2), α_i and β_i, will be determined presently by an optimization procedure designed to minimize the fix error $\underset{\sim}{\varepsilon}$, defined by

3-3) $$\underset{\sim}{\varepsilon} = \underset{\sim}{r}' - \underset{\sim}{r}$$

The phase advances δ_i are modelled as follows

3-4) $$\delta_i = k_i \underset{\sim}{r} \cdot \hat{u}_i + 2\pi f_i \tau + n_i \qquad k_i = 2\pi f_i / c$$

where the first term is the phase advance due to the true displacement $\underset{\sim}{r}$ from the reference position, the second term arises from a timing error τ of the receiver relative to OMEGA system time, and the third term n_i is a phase error term arising from noise, random propagation variations and PPC errors. Letting angular brackets (<>) represent an expectation value taken by averaging over a yet-to-be-defined statistical ensemble, the fundamental assumptions regarding the n_i are

3-5) $\langle \eta_i \rangle = 0$

3-6) $\langle \eta_i \eta_j \rangle = \delta_{ij} \sigma_i^2$

where δ_{ij}, is the Kronecker symbol. In other words the phase errors are zero mean random variables with diagonal covariance matrix, i.e. which are uncorrelated from one navigation signal to another*. In terms of the probability density function for the random variable η_i, denoted by $\rho_i(\eta_i)$, we have

3-7) $$\int_{-\infty}^{\infty} d\eta_i \eta_i \rho_i(\eta_i) = 0$$

and

3-8) $$\int_{-\infty}^{\infty} d\eta_i \rho_i(\eta_i) \eta_i^2 = \sigma_i^2$$

Note that phase is <u>not</u> taken modulo 2π, which is tantamount to the assumption that a lane count is maintained by the optimum receiver. For now, we do <u>not</u> make the assumption that the ρ_i are normal distribution functions, but rather merely assume that the <u>set</u> of independent rand variables $\{\eta_i\}$ obeys the Central Limit Theorem in the sense described in Reference 18. In other words, any linear combination of N (different) η_i will tend to be normally distributed as N becomes large, and may in fact be expected to be adequately approximated by a normal distribution even for moderate N's of the order of 10.

Returning to 3-4), we first resolve the (true) displacement $\underline{r}$ into N-S and E-W components (X,Y):

---

* Note that the η_i refer to single station phases, <u>not</u> LOP's.

3-9) $$\underset{\sim}{r} = X\hat{i} + Y\hat{j}$$

in terms of which the dot product $\underset{\sim}{r}\cdot\hat{u}_i$ becomes

3-10) $$\underset{\sim}{r}\cdot\hat{u}_i = XS_i + YC_i$$

where we have introduced the shorthand notation

3-11) $$S_i = \sin(\theta_i)$$
$$C_i = \cos(\theta_i)$$

Using 3-10) and 3-4), 3-2) becomes

3-12) $$X' = X(\sum\alpha_i k_i S_i) + Y(\sum\alpha_i k_i C_i) + c\tau(\sum\alpha_i k_i) + \sum\alpha_i\eta_i$$
$$Y' = X(\sum\beta_i k_i S_i) + Y(\sum\beta_i k_i C_i) + c\tau(\sum\beta_i k_i) + \sum\beta_i\eta_i$$

Now it is desired that the fix (X',Y') be an unbiased estimator of the true position (X,Y), i.e. $\langle X'\rangle = X$ and $\langle Y'\rangle = Y$. From 3-12) we are therefore led to then following six <u>constraints</u> on the set of weighting coefficients $\{\alpha_i\}$ and $\{\beta_i\}$:

3-13) $$\sum\alpha_i k_i S_i = 1$$
$$\sum\alpha_i k_i C_i = 0$$
$$\sum\alpha_i k_i = 0$$
$$\sum\beta_i k_i S_i = 0$$
$$\sum\beta_i k_i C_i = 1$$
$$\sum\beta_i k_i = 0$$

(Note that the third and sixth constraints are consequences of the absence of a precise clock in the optimum receiver and thus would not be required if we had not assumed a hyperbolic optimum receiver as defined in the Introduction).

Optimization of the receiver now proceeds by minimizing the expected mean square fix error, $\langle \varepsilon^2 \rangle$ subject to the constraints 3-13). From 3-3) and 3-6) one finds

$$3\text{-}14) \qquad \langle \varepsilon^2 \rangle = \langle \underset{\sim}{\varepsilon} \cdot \underset{\sim}{\varepsilon} \rangle = \sum (\alpha_i^2 + \beta_i^2) \sigma_i^2$$

Introducing the usual device of the Lagrange multiplier, the minimization of 3-14), subject to the constraints 3-13) results in the set of requirements (j=1,...N)

$$3\text{-}15) \qquad \frac{\partial}{\partial \alpha_j} \left\{ \sum \left[\alpha_i^2 \sigma_i^2 - \lambda_1 \alpha_i k_i S_i - \lambda_2 \alpha_i k_i C_i - \lambda_3 \alpha_i k_i \right] \right\} = 0$$

and

$$3\text{-}16) \qquad \frac{\partial}{\partial \beta_j} \left\{ \sum \left[\beta_i^2 \sigma_i^2 - \lambda_4 \beta_i k_i S_i - \lambda_5 \beta_i k_i C_i - \lambda_6 \beta_i k_i \right] \right\} = 0$$

where λ_1 through λ_6 are the Lagrange multipliers. These equations are immediately solved to yield for the weighting coefficients α_i, β_i:

$$3\text{-}17) \qquad \alpha_i = \frac{\lambda_1 k_i S_i + \lambda_2 k_i C_i + \lambda_3 k_i}{2\sigma_i^2}$$

$$3\text{-}18) \qquad \beta_i = \frac{\lambda_4 k_i S_i + \lambda_5 k_i C_i + \lambda_6 k_i}{2\sigma_i^2}$$

Note that each navigation signal is weighted inversely proportional to its variance.

The 6 unknowns $\lambda_1,\ldots\lambda_6$ are now determined by substituting 3-17) and 3-18) back into the constraint equations 3-13). In matrix notation, one obtains the pair of equations

3-19) $$\begin{pmatrix} a & b & c \\ b & d & e \\ c & e & g \end{pmatrix}\begin{pmatrix} \lambda_1 \\ \lambda_2 \\ \lambda_3 \end{pmatrix}=\begin{pmatrix} 1 \\ 0 \\ 0 \end{pmatrix}$$

and

3-20) $$\begin{pmatrix} a & b & c \\ b & d & e \\ c & e & g \end{pmatrix}\begin{pmatrix} \lambda_4 \\ \lambda_5 \\ \lambda_6 \end{pmatrix}=\begin{pmatrix} 0 \\ 1 \\ 0 \end{pmatrix}$$

where we have defined

3-21)
$$a \equiv \sum\left(k_i^2 S_i^2/2\sigma_i^2\right) \qquad d = \sum\left(k_i^2 C_i^2/2\sigma_i^2\right)$$
$$b \equiv \sum\left(k_i^2 S_i C_i/2\sigma_i^2\right) \qquad e = \sum\left(k_i^2 C_i/2\sigma_i^2\right)$$
$$c \equiv \sum\left(k_i^2 S_i/2\sigma_i^2\right) \qquad g = \sum\left(k_i^2/2\sigma_i^2\right)$$

Solving 3-19) and 3-20) we obtain

3-22)
$$\lambda_1 = (dg-e^2)/\Delta \qquad \lambda_2 = (ec-bg)/\Delta \qquad \lambda_3 = (be-cd)/\Delta$$
$$\lambda_4 = (ec-bg)/\Delta \qquad \lambda_5 = (ag-c^2)/\Delta \qquad \lambda_6 = (bc-ae)/\Delta$$

where

3-23) $$\Delta \equiv adg + 2bec - c^2 d - e^2 a - b^2 g$$

The weighting coefficients α_i, β_i are now fully determined via 3-17), 3-18) and 3-22) in terms of the phase variances and station geometry. These results will be cast into more physically transparent forms later on; for now, we turn to the derivation of the fix error statistics.

3.2 Fix Error Distribution Function

Resolve the fix error vector $\underset{\sim}{\varepsilon}$ into E-W and N-S components $(\varepsilon_X, \varepsilon_Y)$ given by

3-24)
$$\varepsilon_X = X' - X = \sum \alpha_i \eta_i$$
$$\varepsilon_Y = Y' - Y = \sum \beta_i \eta_i$$

and let $P(\varepsilon_X, \varepsilon_Y)$ be the joint probability density, (or "distribution function") of ε_X and ε_Y. In terms of the distribution functions, $\rho_i(\eta_i)$, of the individual phase errors, one has by definition

3-25)
$$P(\varepsilon_X, \varepsilon_Y) = \int d\eta_1 \ldots d\eta_N \rho_1(\eta_1) \ldots \rho_N(\eta_N)\, \delta(\varepsilon_X - \sum \alpha_i \eta_i)\, \delta(\varepsilon_Y - \sum \beta_i \eta_i)$$

where δ is the Dirac delta function.

Introducing the Fourier integral representation of the delta function

3-26)
$$\delta(z) = \frac{1}{2\pi} \int_{-\infty}^{\infty} dk\, e^{jkz}$$

equation 3-25) can be cast into the form

3-27)
$$P(\varepsilon_X, \varepsilon_Y) = \frac{1}{(2\pi)^2} \int_{-\infty}^{\infty} dk_x \int_{-\infty}^{\infty} dk_y\, e^{j(k_X \varepsilon_X + k_Y \varepsilon_Y)} \left\{ \prod_{i=1}^{N} \int_{-\infty}^{\infty} d\eta_i \rho_i(\eta_i) e^{-j(k_X \alpha_i + k_Y \beta_i)\eta_i} \right\}$$

Now consider the random variable, R, defined by

$$3\text{-}28) \qquad R = \sum_{i=1}^{N} (k_x\alpha_i + k_y\beta_i)\eta_i$$

By the Central Limit Theorem, R tends with increasing N to be normally distributed with the distribution function

$$3\text{-}29) \qquad \phi(R) = \frac{1}{\sqrt{2\pi\sum(k_x\alpha_i + k_y\beta_i)^2\sigma_i^2}}\, e^{-R^2/2\sum(k_x\alpha_i + k_y\beta_i)^2\sigma_i^2}$$

for a broad class of phase error distribution functions $\{\rho_i(\eta_i)\}$ satisfying 3-7) and 3-8). (For Gaussian ρ_i, the distribution of R is <u>exactly</u> $\phi(R)$.) In view of the well known tendency of the normal distribution to represent a good approximation even for moderate N's (i.e. of order 10), we will henceforth use 3-29) as the distribution function for R even for non-Gaussian ρ_i.

Now, by definition,

$$3\text{-}30) \qquad \phi(R) = \int d\eta_1 \ldots d\eta_N \rho_1(\eta_1)\ldots\rho_N(\eta_N)\delta(R - \sum (k_x\alpha_i + k_y\beta_i)\eta_i)$$

which, using 3-26), can be cast into the form

$$3\text{-}31) \qquad \phi(R) = \frac{1}{2\pi}\int_{-\infty}^{\infty} dk e^{jkR}\left\{\prod_{i=1}^{N}\int_{-\infty}^{\infty} d\eta_i \rho_i(\eta_i) e^{-jk(k_x\alpha_i + k_y\beta_i)\eta_i}\right\}$$

But, from the Fourier integral representation of the Gaussian 3-29), we also have

$$3\text{-}32) \qquad \phi(R) = \frac{1}{2\pi}\int_{-\infty}^{\infty} dk e^{jkR}\, e^{-\frac{k^2}{2}\sum(k_x\alpha_i + k_y\beta_i)^2\sigma_i^2}$$

Comparing 3-31) and 3-32) we have

$$3\text{-}33) \qquad \prod_{i=1}^{N} \int d\eta_i \rho_i(\eta_i) e^{-jk(k_X\alpha_i+k_Y\beta_i)\eta_i} = e^{-\frac{k^2}{2}\sum(k_X\alpha_i+k_Y\beta_i)^2\sigma_i^2}$$

Now letting k=1, we obtain for 3-27):

3-34)

$$P(\varepsilon_X,\varepsilon_Y) = \frac{1}{(2\pi)^2}\int_{-\infty}^{\infty} dk_X \int_{-\infty}^{\infty} dk_Y e^{j(k_X\varepsilon_X+k_Y\varepsilon_Y)} e^{-\frac{1}{2}\sum(k_X\alpha_i+k_Y\beta_i)^2\sigma_i^2}$$

To proceed further, define:

$$3\text{-}35) \qquad \begin{aligned} c_1 &= \sum \alpha_i^2\sigma_i^2 \\ c_2 &= \sum \beta_i^2\sigma_i^2 \\ c_3 &= \sum 2\alpha_i\beta_i\sigma_i^2 \end{aligned}$$

and transform from the (k_X,k_Y) coordinate system to another (k_X',k_Y') formed by rotation through the angle θ:

$$3\text{-}36) \qquad \begin{aligned} k_X &= k_X'\cos\theta - k_Y'\sin\theta \\ k_Y &= k_X'\sin\theta + k_Y'\cos\theta \end{aligned}$$

Then we find

$$3\text{-}37) \qquad \sum(k_X\alpha_i+k_Y\beta_i)^2\sigma_i^2 = c_1k_X^2+c_2k_Y^2+c_3k_Xk_Y$$

$$= k_X'^2[c_1\cos^2\theta+c_2\cos^2\theta+c_3\sin\theta\cos\theta]$$

$$+ k_Y'^2[c_1\sin^2\theta+c_2\cos^2\theta-c_3\sin\theta\cos\theta]$$

$$+ k_X'k_Y'[(c_2-c_1)\sin2\theta + c_3\cos2\theta]$$

Thus, by choosing the rotation angle θ such that

3-38) $$\tan 2\theta \equiv \frac{c_3}{c_1 - c_2}$$

the $k_X'k_Y'$ cross term of 3-37) will vanish identically and

3-39) $$\sum (k_X\alpha_i + k_Y\beta_i)^2\sigma_i^2 = s_1^2 k_X'^2 + s_2^2 k_Y'^2$$

where

3-40) $$s_1^2 = c_1\cos^2\theta + c_2\sin^2\theta + c_3\sin\theta\cos\theta$$
$$s_2^2 = c_1\sin^2\theta + c_2\cos^2\theta - c_3\sin\theta\cos\theta$$

in terms of which 3-34) becomes

3-41) $$P(\varepsilon_X,\varepsilon_Y) = \left[\frac{1}{2\pi}\int_{-\infty}^{\infty} dk_X' e^{jk_X'(\varepsilon_X\cos\theta + \varepsilon_Y\sin\theta)} e^{-\frac{1}{2}s_1^2 k_X'^2}\right] \times \left[\frac{1}{2\pi}\int_{-\infty}^{\infty} dk_Y' e^{jk_Y'(\varepsilon_Y\cos\theta - \varepsilon_X\sin\theta)} e^{-\frac{1}{2}s_2^2 k_Y'^2}\right]$$

Finally, performing the indicated Fourier transforms, and introducing the rotated $(\varepsilon_X',\varepsilon_Y')$ coordinate system:

3-42) $$\varepsilon_X' = \varepsilon_X\cos\theta + \varepsilon_Y\sin\theta$$
$$\varepsilon_Y' = \varepsilon_Y\cos\theta - \varepsilon_X\sin\theta$$

we obtain the desired result:

$$3\text{-}43) \qquad P(\varepsilon_X', \varepsilon_Y') = \frac{1}{\sqrt{2\pi s_1^2}} e^{-\frac{\varepsilon_X'^2}{2s_1^2}} \cdot \frac{1}{\sqrt{2\pi s_2^2}} e^{-\frac{\varepsilon_Y'^2}{2s_2^2}}$$

Thus in the $(\varepsilon_X', \varepsilon_Y')$ system, the probability density is the product of two normal distributions in ε_X' and ε_Y', with variances s_1^2 and s_2^2 respectively (i.e. the socalled "bivariate normal distribution"). The zones of constant probability density are elliptical shells inclined at the angle θ as shown in Figure 3-2, with semi axes in the ratio s_1/s_2.

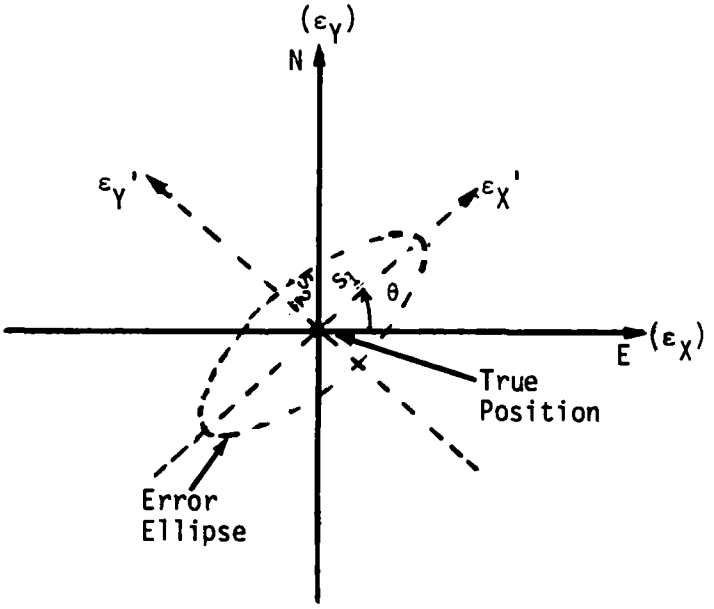

Figure 3-2: Geometry of Error Ellipse

Equation 3-43) fully characterizes the fix error statistics and various measures of circular error will presently be derived therefrom. First, however, it is worthwhile to derive from the definitions 3-38) and 3-40), more physically transparent expressions for the variances s_1^2 and s_2^2 and rotation angle θ, i.e. in terms of the station geometry and navigation signal variances σ_i^2directly.

To this end, from 3-35) and 3-17,18) we obtain

3-44) $$c_3 = 2\sum \alpha_i \beta_i \sigma_i^2 = 2\sum \frac{k_i^2}{4\sigma_i^2} [\lambda_1\lambda_4 S_i^2 + \lambda_2\lambda_5 C_i^2 + \lambda_3\lambda_6 + (\lambda_1\lambda_5+\lambda_2\lambda_4) S_i C_i + (\lambda_1\lambda_6+\lambda_3\lambda_4) S_i + (\lambda_5\lambda_3+\lambda_2\lambda_6) C_i]$$

which, using 3-21) can be rewritten in the form

3-45) $$c_3 = \{\lambda_1[\lambda_4 a+\lambda_5 b+\lambda_6 c] + \lambda_2[\lambda_4 b+\lambda_5 d+\lambda_6 e] + \lambda_3[\lambda_4 c+\lambda_5 e+\lambda_6 g]\}$$

But from 3-20), only the second term is non-zero and we obtain simply (using 3-22):

3-46) $$c_3 = \lambda_2 = (ec-bg)/\Delta$$

In a precisely similar fashion, we obtain after some algebra

3-47) $$c_1 = \lambda_{1/2} = (dg-e^2)/2\Delta$$
$$c_2 = \lambda_{5/2} = (ag-c^2)/2\Delta$$

Thus, from the definition 3-38) we have

3-48) $$\tan 2\theta = \frac{c_3}{c_1-c_2} = \frac{2\lambda_2}{\lambda_1-\lambda_5} = \frac{2(ec-bg)}{(dg+c^2-e^2-ag)}$$

Introducing the definitions 3-21), 3-48) becomes

3-49) $$\tan 2\theta = \frac{2\sum_i \sum_j \frac{k_i^2 k_j^2}{\sigma_i^2 \sigma_j^2} \{C_i S_j - C_i S_i\}}{\sum_i \sum_j \frac{k_i^2 k_j^2}{\sigma_i^2 \sigma_j^2} \{C_i^2 + S_i S_j - C_i C_j - S_i^2\}}$$

Now, exploiting the invariance of the double summations under the interchange of dummy indices ($i \leftrightarrow j$), the bracketed term in the numerator can be symmetrized as follows

3-50) $$\left\{C_i S_j - C_i S_i\right\} \longrightarrow \left\{1/2 C_i S_j + 1/2 C_j S_i - 1/2 C_i S_i - 1/2 C_j S_j\right\}$$

Then, from the definitions 3-11) and trigonometric identities 3-50) reduces to the simple form

3-51) $$\left\{C_i S_j - C_i S_i\right\} \longrightarrow -\sin(\theta_i+\theta_j) \cdot \sin^2\left(1/2(\theta_i-\theta_j)\right)$$

Similarly, by interchanging i and j in the S_i^2 term of the denominator of 3-49) and using the identity

3-52) $$C_i^2 - S_j^2 = (C_i+S_j)(C_i-S_j) = \cos(\theta_i+\theta_j) \cdot \cos(\theta_i-\theta_j)$$

we find the bracketed term in the denominator of 3-49) becomes

3-53) $$\left\{C_i^2+S_i S_j-C_i C_j-S_i^2\right\} \longrightarrow -2 \cos(\theta_i+\theta_j)\sin^2(1/2(\theta_i-\theta_j))$$

We thus obtain from 3-49) the desired result

3-54) $$\tan 2\theta = \frac{\sum_i \sum_{j>i} \frac{k_i^2 k_j^2}{\sigma_i^2 \sigma_j^2} \sin(\theta_i+\theta_j) \sin^2\left(1/2(\theta_i-\theta_j)\right)}{\sum_i \sum_{j>i} \frac{k_i^2 k_j^2}{\sigma_i^2 \sigma_j^2} \cos(\theta_i+\theta_j) \sin^2\left(1/2(\theta_i-\theta_j)\right)}$$

where we have again exploited the symmetry under $i \leftrightarrow j$, and the vanishing of $\sin^2(1/2\ (\theta_i - \theta_j))$ when $i=j$ to rewrite the double summations such that index $j > i$. Thus, the summations now include all possible pairs of stations (i,j) taken just once.

Turning now to the variances s_1^2 and s_2^2, we note that the defining equations 3-40) can be rewritten in the form

3-55)
$$s_1^2 = \frac{c_1+c_2}{2} + \frac{c_1-c_2}{2} \cos 2\theta + \frac{c_3}{2} \sin 2\theta$$

$$s_2^2 = \frac{c_1+c_2}{2} - \frac{c_1-c_2}{2} \cos 2\theta - \frac{c_3}{2} \sin 2\theta$$

which using 3-38) can be manipulated into

3-56)
$$s_1^2 = \frac{c_1+c_2}{2} + \frac{1}{2}\sqrt{c_3^2+(c_1-c_2)^2}$$

$$s_2^2 = \frac{c_1+c_2}{2} - \frac{1}{2}\sqrt{c_3^2+(c_1-c_2)^2}$$

Introducing the parameter γ defined by

3-57)
$$\gamma \equiv \frac{\sqrt{4c_1c_2-c_3^2}}{c_1+c_2} = \frac{2s_1s_2}{c_1+c_2}$$

and noting from 3-35) and 3-14) that

3-58)
$$c_1+c_2 = \langle \varepsilon^2 \rangle$$

we may write 3-56) as

3-59)
$$s_1^2 = \frac{\langle \varepsilon^2 \rangle}{2}\left[1 + \sqrt{1-\gamma^2}\right]$$

$$s_2^2 = \frac{\langle \varepsilon^2 \rangle}{2}\left[1 - \sqrt{1-\gamma^2}\right]$$

Thus the variances s_1^2 and s_2^2 have now been rewritten in terms of the mean square circular error $\langle\varepsilon^2\rangle$ and the parameter γ which is a measure of the eccentricity of the error ellipse*. We shall now derive relations analogous to 3-54) for $\langle\varepsilon^2\rangle$ and γ. Turning first to $\langle\varepsilon^2\rangle$, from 3-58) and 3-48) we have

$$3\text{-}60) \qquad \langle\varepsilon^2\rangle = \frac{dg-e^2+ag-c^2}{2\Delta} = \frac{g^2-e^2-c^2}{2\Delta}$$

where we have used the identity $d\equiv g-a$ which follows from the definitions 3-21). Writing out the numerator of 3-60) explicitly:

$$3\text{-}61) \qquad g^2-e^2-c^2 = \sum_i \sum_j \frac{k_i^2 k_j^2}{4\sigma_i^2\sigma_j^2}\left[1-(\cos\theta_i\cos\theta_j+\sin\theta_i\sin\theta_j)\right]$$

$$= \sum_i \sum_{j>i} \frac{k_i^2 k_j^2}{\sigma_i^2\sigma_j^2} \sin^2(1/2\ (\theta_i-\theta_j))$$

The denominator of 3-60) requires more involved manipulations. From the definitions 3-23) and 3-21), we have

---

* If $\gamma = 1$ the error ellipse becomes a circle. In general, one finds that γ is related to the eccentricity, e, of the error ellipse by

$$\gamma = \frac{2\sqrt{1-e2}}{2-e^2}$$

so that as the eccentricity varies from 0 to 1, γ varies from 1 to 0.

3-62) $$2\Delta = \frac{1}{4}\sum_i\sum_j\sum_\ell \frac{k_i^2 k_j^2 k_\ell^2}{\sigma_i^2\sigma_j^2\sigma_\ell^2}\Big[S_i^2C_j^2+S_jC_jC_\ell S_i + S_\ell S_i C_i C_j - S_iS_\ell C_j^2 - S_i^2C_jC_\ell - S_iC_iS_jC_j\Big]$$

Combining terms and using trigonometric identities, this reduces to

3-63) $$2\Delta = \frac{1}{4}\sum_i\sum_j\sum_\ell \frac{k_i^2 k_j^2 k_\ell^2}{\sigma_i^2\sigma_j^2\sigma_\ell^2}\sin\theta_i\cos\theta_j\Big[\sin(\theta_i-\theta_j) + \sin(\theta_j-\theta_\ell) + \sin(\theta_\ell-\theta_i)\Big]$$

Then by exploiting the antisymmetry of the square bracketed term under interchange of the dummy indices $i\leftrightarrow j$, this becomes

3-64) $$2\Delta = \frac{1}{8}\sum_i\sum_j\sum_\ell \frac{k_i^2 k_j^2 k_\ell^2}{\sigma_i^2\sigma_j^2\sigma_\ell^2}\sin(\theta_i-\theta_j)\Big[\sin(\theta_i-\theta_j) + \sin(\theta_j-\theta_\ell) + \sin(\theta_\ell-\theta_i)\Big]$$

Now, by cyclicly permuting the dummy indices i j ℓ, 3-64) can be cast into the symmetric form

3-65) $$2\Delta = \frac{1}{24}\sum_i\sum_j\sum_\ell \frac{k_i^2 k_j^2 k_\ell^2}{\sigma_i^2\sigma_j^2\sigma_\ell^2}\Big[\sin(\theta_i-\theta_j) + \sin(\theta_\ell-\theta_i) + \sin(\theta_j-\theta_\ell)\Big]^2$$

Finally, noting that the triple summation in the denominator has N(N-1)(N-2) non-zero terms of which N!/(N-3)!3! = N(N-1)(N-2)/6 are distinct, one may replace

$$\sum_i \sum_j \sum_\ell \rightarrow 6 \sum_j \sum_{j>i} \sum_{\ell>j}$$

in view of the symmetry of the summand. Then, using the triginometric identity

3-66) $$\sin(\theta_i-\theta_j) + \sin(\theta_\ell-\theta_i) + \sin(\theta_j-\theta_\ell) = -4 \sin \tfrac{1}{2}(\theta_i-\theta_j) \cdot \sin \tfrac{1}{2}(\theta_j-\theta_\ell) \cdot \sin \tfrac{1}{2}(\theta_\ell-\theta_i)$$

or obtains the compact result

3-67) $$\Delta = 2 \sum_i \sum_{j>i} \sum_{\ell>j} \frac{\sin^2(\frac{1}{2}(\theta_i-\theta_j)) \cdot \sin^2(\frac{1}{2}(\theta_j-\theta_\ell)) \cdot \sin^2(\frac{1}{2}(\theta_\ell-\theta_i))}{\sigma_i^2 \sigma_j^2 \sigma_\ell^2}$$

from which there follows finally

3-68)
$$\langle \varepsilon^2 \rangle = \frac{\frac{1}{4} \sum_i \sum_{j>i} \frac{k_i^2 k_j^2 \sin^2(\frac{1}{2}(\theta_i-\theta_j))}{\sigma_i^2 \sigma_j^2}}{\sum_i \sum_{j>i} \sum_{\ell>j} \frac{k_i^2 k_j^2 k_\ell^2 \sin^2(\frac{1}{2}(\theta_i-\theta_j)) \cdot \sin^2(\frac{1}{2}(\theta_j-\theta_\ell)) \cdot \sin^2(\frac{1}{2}(\theta_\ell-\theta_i))}{\sigma_i^2 \sigma_j^2 \sigma_\ell^2}}$$

Equation 3-68 represents the geometrical dilution of precision for optimally-combined navigation signals*. Before tackling the remaining problem of deriving an analogous explicit expression for the parameter γ, we digress to establish contact between 3-68) and the familiar GDOP equation[20] for a three station hyperbolic fix. Introducing Swanson's[20] notation:

$$3\text{-}69) \qquad |\theta_1-\theta_2| = \alpha \qquad |\theta_2-\theta_3| = \beta \qquad |\theta_3-\theta_1| = 2\gamma$$

(wherein the γ in 3-69) is not to be confused with the eccentricity parameter introduced in the present development), and specializing 3-68) to the case of N=3, we obtain

$$3\text{-}70) \qquad \langle\varepsilon^2\rangle_{N=3} = \frac{1}{4k^2\sin^2\gamma}\left[\frac{\sigma_3^2}{\sin^2\beta/2} + \frac{\sigma_1^2}{\sin^2\alpha/2} + \frac{\sigma_2^2\sin^2\gamma}{\sin^2\alpha/2\ \sin^2\beta/2}\right]$$

where all signals are of a common wavelength λ, and $k=2\pi/\lambda$. It is relatively simple to derive the trigonometric identity

$$3\text{-}71) \qquad \frac{\sin^2\gamma}{\sin(\frac{\beta}{2})\sin(\frac{\alpha}{2})} = \frac{\sin^2\alpha/2 + \sin^2\beta/2}{\sin\beta/2\ \sin\alpha/2} + 2\cos\gamma$$

which, when introduced into the third term of 3-70) gives

$$3\text{-}72) \qquad \langle\varepsilon^2\rangle = \frac{1}{4k^2\sin^2\gamma}\left[\frac{\sigma_3^2+\sigma_2^2}{\sin^2\beta/2} + \frac{\sigma_1^2+\sigma_2^2}{\sin^2\alpha/2} + \frac{2\sigma_2^2\cos\gamma}{\sin\alpha/2\ \sin\beta/2}\right]$$

which is Swanson's equation (8) when the σ's are equal.

---

* Apparently equivalent through less transparent results for $\langle\varepsilon^2\rangle$ have been obtained by matrix methods in Reference 19.

Returning now to the main thread of development, we note from the expression 3-57) for γ and 3-46) - 3-48) that

$$3\text{-}73) \qquad \gamma = \sqrt{\lambda_1\lambda_5 - \lambda_2^2} \; / \; \langle\varepsilon^2\rangle$$

But from 3-22),

$$3\text{-}74) \qquad \lambda_1\lambda_5 - \lambda_2^2 = \frac{g}{\Delta^2}\left[dag - e^2a - c^2d - b^2g + 2ecb\right] = \frac{g}{\Delta}$$

But from 3-60) and 3-61), we have

$$3\text{-}75) \qquad \frac{1}{\Delta} = \frac{2\langle\varepsilon^2\rangle}{\sum_i \sum_{j>i} \frac{k_i^2 k_j^2}{\sigma_i^2\sigma_j^2} \sin^2\left(\frac{1}{2}(\theta_i - \theta_j)\right)}$$

so, introducing the definiton 3-21)for g, we obtain finally

$$3\text{-}76) \qquad \boxed{\gamma = \sqrt{\frac{\sum_i k_i^2/\sigma_i^2}{\langle\varepsilon^2\rangle \sum_i \sum_{j>i} \frac{k_i^2 k_j^2}{\sigma_i^2\sigma_j^2} \sin^2\left(\frac{1}{2}(\theta_i - \theta_j)\right)}}}$$

Thus, equations 3-54), 3-68) and 3-76), provide the desired relationships between the parameters of the bivariate normal fix error distribution and the bearings and variances associated with the individual navigation signals as combined in an optimum receiver. As such, the fix error statistics are now fully characterized. We do not, however, require such complete characterization if we limit subsequent consideration to the radial (or "circular") errors which conventionally are used to describe navigation precision. Thus, in the next section we derive the radial error statistics by appropriate integrations over the distribution 3-43).

3.3 Radial Error Statistics

The radial error, ε_r, is defined by

3-77) $$\varepsilon_r = \sqrt{\varepsilon_x^2+\varepsilon_y^2} \quad = \sqrt{\varepsilon_{x'}^2+ \varepsilon_{y'}^2}$$

Its distribution function, $P(\varepsilon_r)$, is obtained from 3-43)by

3-78) $$P(\varepsilon_r) = \int_{-\infty}^{\infty} d\varepsilon_{x'} \int_{-\infty}^{\infty} d\varepsilon_{y'}\, P(\varepsilon_{x'},\varepsilon_{y'})\ \delta\ (\varepsilon_r - \sqrt{\varepsilon_{x'}^2+\varepsilon_{y'}^2})$$

Where δ is again the Dirac delta function. Introducing polar coordinates in $(\varepsilon'_x,\varepsilon'_y)$ space:

$$\varepsilon_x' = r\cos\phi$$

$$\varepsilon_y' = r\sin\phi$$

and carrying out the integration over r, we obtain

3-79) $$P(\varepsilon_r) = \frac{\varepsilon_r}{2\pi s_1 s_2} \int_0^{2\pi} d\phi e^{-\varepsilon_r^2 \left(\frac{\cos^2\phi}{2s_1^2} + \frac{\sin^2\phi}{2s_2^2}\right)}$$

Using 3-59) and half-angle trigonometric identities, 3-79) becomes

3-80) $$P(\varepsilon_r) = \frac{\varepsilon_r}{\pi<\varepsilon^2>\gamma} e^{-\frac{\varepsilon_r^2}{\gamma^2<\varepsilon^2>}} \int_0^{2\pi} d\phi \quad e^{\frac{\varepsilon_r^2}{<\varepsilon^2>\gamma^2}\cdot\cos 2\phi\ \cdot\sqrt{1-\gamma^2}}$$

Performing the integration, one obtains*

$$3\text{-}81) \qquad P(\varepsilon_r) = \frac{2\varepsilon_r}{\langle\varepsilon^2\rangle\gamma} e^{-\varepsilon_r^2/\gamma^2\langle\varepsilon^2\rangle} I_0\left(\frac{\varepsilon_r^2\sqrt{1-\gamma^2}}{\langle\varepsilon^2\rangle\gamma^2}\right)$$

where I_0 is the Bessel function. Following Lewis[21], we switch from ε_r to the dimensionless variable r, defined by

$$3\text{-}82) \qquad r \equiv \frac{\sqrt{2}\,\varepsilon_r}{\sqrt{\langle\varepsilon^2\rangle}}$$

and the corresponding distribution function $P_\gamma(r)$ satisfying

$$3\text{-}83) \qquad P(\varepsilon_r)d\varepsilon_r = P_\gamma(r)dr$$

Then for $P_\gamma(r)$ we obtain

$$3\text{-}84) \qquad \boxed{P_\gamma(r) = P(\varepsilon_r)\frac{d\varepsilon_r}{dr} = \frac{r}{\gamma} e^{-r^2/2\gamma^2} I_0\left(\frac{r^2}{2\gamma^2}\sqrt{1-\gamma^2}\right)}$$

in agreement with Lewis' result[21]. (Note that in the dimensionless units 3-82) the rms radial error is $\sqrt{2}$.) The properties of $P_\gamma(r)$ are discussed at length in Reference 21. Figure 3-3, taken from that document exhibits $P_\gamma(r)$ for γ=0, .5 and 1.0, and Table 3-1 gives values of $P_\gamma(r)$ for $0 \leq r \leq 4$ and $0 \leq \gamma \leq 1$.

---

* Note: In the special case γ=1 (error ellipse is a circle), if phase errors are not zero mean so that the error circle is centered about a bias point with radial error ε_b, the expression 3-81) is replaced by

$$P(\varepsilon_r) = \frac{2\varepsilon_r}{\langle\varepsilon^2\rangle} e^{-(\varepsilon_r^2+\varepsilon_b^2)/\langle\varepsilon^2\rangle} I_0\left(\frac{2\varepsilon_r\varepsilon_b}{\langle\varepsilon^2\rangle}\right)$$

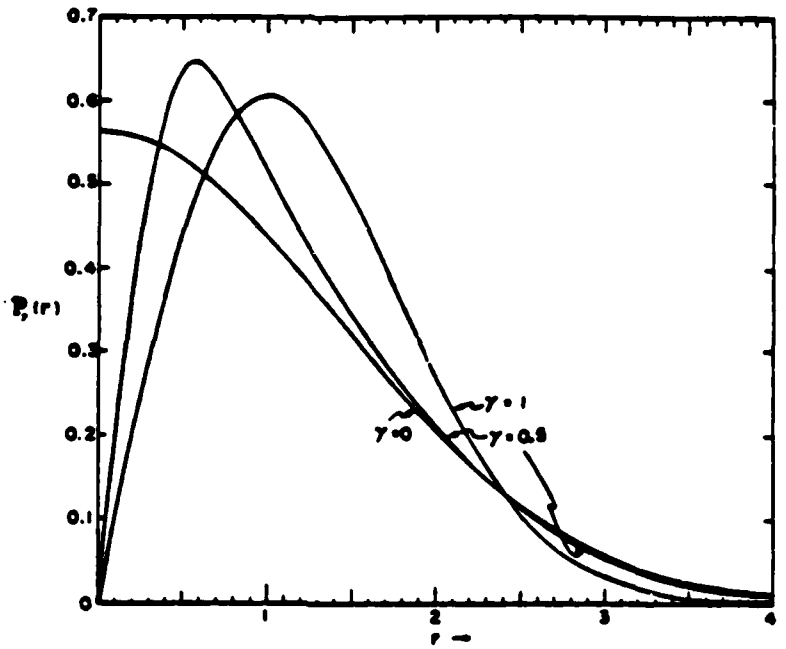

Figure 3-3

Radial Distribution Functions for γ=0, 0.5, and 1.0

Table 3-1. Values of $P_\gamma(r)$

	γ										
r	0	.1	.2	.3	.4	.5	.6	.7	.8	.9	1.0
0	(.56419)*	0	0	0	0	0	0	0	0	0	0
.1	.56278	.64464	.44290	.31554	.24236	.19605	.16437	.14141	.12403	.11043	.09950
.2	.55858	.61272	.64347	.53983	.44270	.36969	.31547	.27435	.24233	.21681	.19604
.3	.55164	.57114	.64651	.64152	.57557	.50421	.44235	.39139	.34969	.31537	.28680
.4	.54207	.55261	.59994	.65120	.63879	.59213	.53805	.48700	.44187	.40283	.36925
.5	.53001	.53686	.56374	.61898	.64803	.63530	.60029	.55806	.51588	.47665	.44125
.6	.51563	.52054	.53785	.57902	.62527	.64227	.63103	.60389	.57017	.53508	.50116
.7	.49914	.50287	.51535	.54362	.58905	.62440	.63532	.62602	.60459	.57727	.54789
.8	.48077	.48371	.49329	.51329	.55048	.59238	.61967	.62759	.62025	.60324	.58092
.9	.46077	.46314	.47078	.48574	.51408	.55428	.59070	.61266	.61921	.61375	.60028
1.0	.43939	.44134	.44751	.45924	.48058	.51506	.55410	.58559	.60416	.61024	.60653
1.1	.41692	.41853	.42358	.43298	.44931	.47712	.51415	.55044	.57811	.59457	.60068
1.2	.39362	.39495	.39910	.40672	.41947	.44124	.47367	.51068	.54405	.56892	.58410
1.3	.36977	.37086	.37427	.38045	.39053	.40739	.43429	.46900	.50476	.53556	.55842
1.4	.34564	.34653	.34929	.35428	.36229	.37530	.39677	.42734	.46264	.49675	.52544
1.5	.32147	.32218	.32440	.32838	.33469	.34471	.36136	.38696	.41964	.45455	.48698
1.6	.29749	.29806	.29980	.30292	.30782	.31546	.32808	.34859	.37724	.41082	.44486
1.7	.27393	.27437	.27570	.27807	.28179	.28750	.29684	.31260	.33650	.36709	.40077
1.8	.25098	.25130	.25228	.25401	.25672	.26086	.26754	.27914	.29810	.32459	.35622
1.9	.22881	.22903	.22969	.23088	.23274	.23556	.24011	.24822	.26247	.28425	.31250
2.0	.20755	.20768	.20809	.20881	.20995	.21169	.21453	.21977	.22979	.24668	.27067
2.1	.18733	.18739	.18758	.18791	.18844	.18929	.19075	.19370	.20009	.21229	.23153
2.2	.16824	.16824	.16824	.16824	.16828	.16841	.16877	.16993	.17332	.18126	.19563
2.3	.15034	.15029	.15014	.14988	.14952	.14906	.14857	.14834	.14935	.15361	.16331
2.4	.13367	.13358	.13331	.13285	.13217	.13126	.13011	.12883	.12803	.12926	.13472
2.5	.11826	.11814	.11778	.11715	.11623	.11498	.11334	.11131	.10907	.10802	.10984
2.6	.10410	.10396	.10353	.10279	.10170	.10020	.09821	.09565	.09259	.08968	.08852
2.7	.09119	.09103	.09055	.08973	.08852	.08686	.08465	.08175	.07809	.07397	.07053
2.8	.07947	.07930	.07880	.07793	.07665	.07490	.07256	.06949	.06550	.06062	.05556
2.9	.06892	.06875	.06823	.06734	.06603	.06425	.06187	.05874	.05462	.04936	.04327
3.0	.05947	.05930	.05878	.05789	.05659	.05482	.05247	.04937	.04529	.03995	.03333
3.1	.05105	.05089	.05038	.04952	.04825	.04653	.04425	.04126	.03733	.03211	.02538
3.2	.04362	.04345	.04297	.04214	.04093	.03928	.03711	.03429	.03059	.02565	.01912
3.3	.03717	.03692	.03646	.03567	.03453	.03299	.03096	.02834	.02491	.02036	.01432
3.4	.03136	.03121	.03078	.03005	.02899	.02756	.02569	.02328	.02017	.01606	.01050
3.5	.02645	.02626	.02586	.02518	.02421	.02290	.02119	.01902	.01623	.01258	.00770
3.6	.02209	.02198	.02161	.02100	.02011	.01892	.01739	.01545	.01298	.09794	.00552
3.7	.01845	.01830	.01798	.01742	.01662	.01556	.01419	.01247	.01032	.00757	.00396
3.8	.01526	.01517	.01487	.01437	.01366	.01272	.01152	.01002	.00815	.00582	.00278
3.9	.01262	.01250	.01224	.01180	.01117	.01035	.00930	.00800	.00640	.00444	.00195
4.0	.01034	.01026	.01003	.00964	.00909	.00837	.00746	.00635	.00500	.00336	.00134
$\hat{r}$**	0	$.12_6$	$.24_7$	$.36_2$	$.47_0$	$.57_8$	$.67_5$	$.76_0$	$.84_6$	$.92_5$	1.00_0

*This is a singular point; the value of the function depends on how the point is approached.
**See text.

Of more immediate interest is the probability of a fix being inside a circle of (dimensionless) radius R, $P_\gamma^{\,i}(R)$, defined by

$$3\text{-}85) \qquad P_\gamma^{\,i}(R) = \int_0^R P_\gamma(r)\,dr$$

Figure 3-4) shows $P_\gamma^{\,i}(R)$ for $\gamma = 0$, .5 and 1.0 while Table 3-2 tabulates $P_\gamma^{\,i}(R)$ for $0 \leq r \leq 4$ and $0 \leq \gamma \leq 1$.

As discussed by Burt et al[22], several different measures of error have been used to characterize two dimensional circular errors. In the present analysis we shall consider the three which appear to be of most common usage:

CIRCULAR ERROR PROBABLE (CEP) = radius of circle containing 50% of fixes:

$$3\text{-}86) \qquad P_\gamma^{\,i}(CEP) = .5$$

RADIUS OF 95% PROBABILITY CIRCLE (R(0.95)) = radius of circle containing 95% of fixes:

$$3\text{-}87) \qquad P_\gamma^{\,i}(R(0.95)) = .95$$

$$3\text{-}88) \qquad \text{RADIAL OR RMS ERROR } (d_{rms}) = \sqrt{\langle \varepsilon^2 \rangle}$$

Whereas d_{rms} is independent of γ and thus follows directly from 3-68), CEP and R(0.95) depend on both γ and $\langle \varepsilon^2 \rangle$ so that in general one must interpolate in Table 3-2 after determining γ from 3-76). However, analytical approximations for CEP and R(0.95) as functions of $\langle \varepsilon^2 \rangle$ and γ:

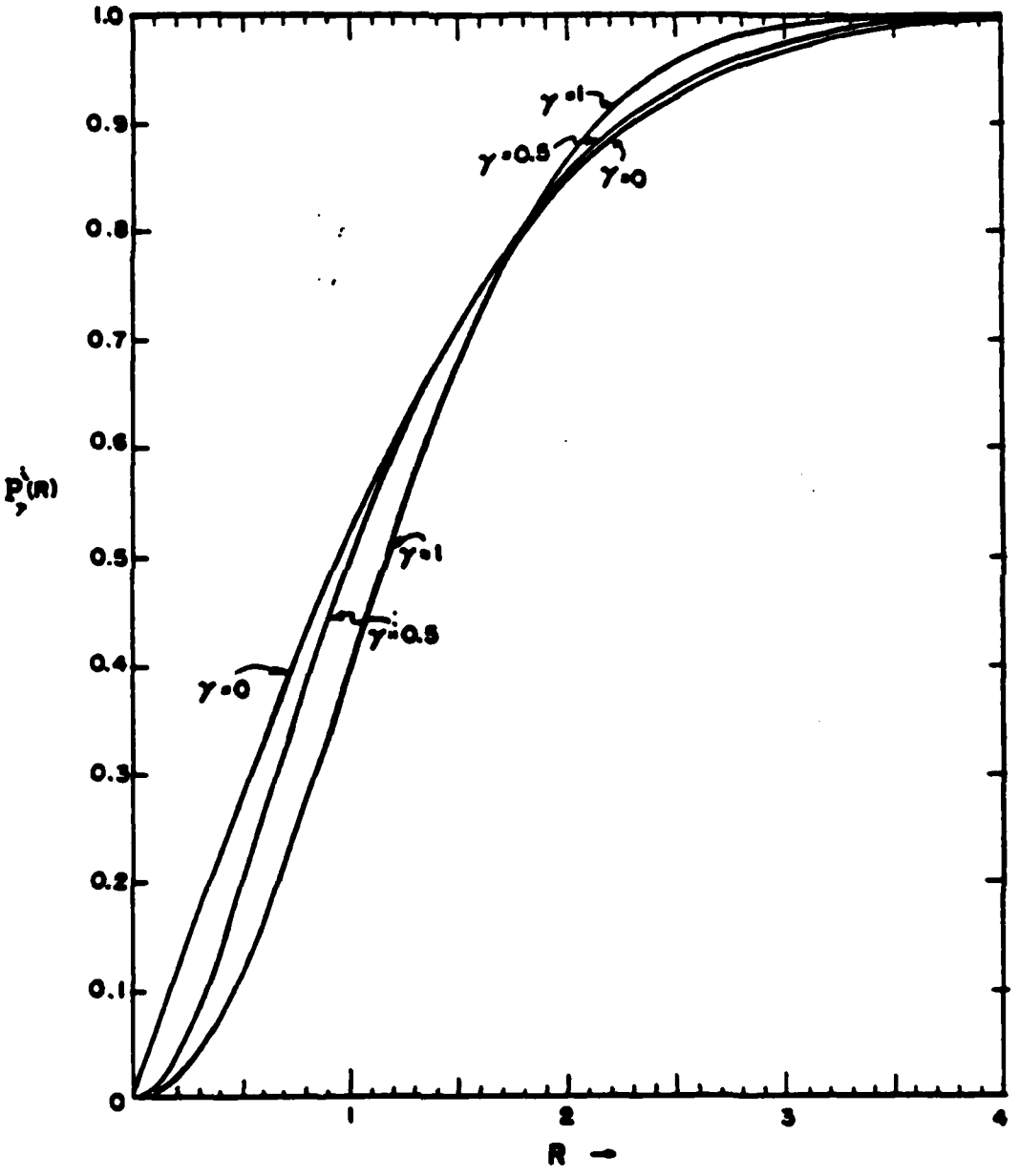

Figure 3-4

Probability of a Fix Being Inside of a Circle of Radius R

Table 3-2. Values of $P_\gamma^i(R) = \int_0^R P_\gamma(r)\,dr$

	γ										
R	0	.1	.2	.3	.4	.5	.6	.7	.8	.9	1.0
0	0	0	0	0	0	0	0	0	0	0	0
.1	.05637	.04004	.02353	.01621	.01231	.00990	.00828	.00711	.00623	.00554	.00499
.2	.11246	.10453	.08008	.05999	.04705	.03846	.03243	.02800	.02461	.02195	.01980
.3	.16800	.16333	.14553	.12001	.09857	.08252	.07056	.06144	.05433	.04864	.04400
.4	.22270	.21946	.20786	.18520	.15982	.13773	.11985	.10556	.09404	.08465	.07683
.5	.27633	.27393	.26593	.24888	.22452	.19945	.17705	.15802	.14209	.12875	.11750
.6	.32863	.32681	.32097	.30877	.28832	.26352	.23880	.21627	.19652	.17943	.16473
.7	.37938	.37799	.37362	.36486	.34907	.32697	.30226	.27791	.25538	.23515	.21730
.8	.42839	.42733	.42405	.41768	.40604	.38787	.36511	.34071	.31673	.29428	.27385
.9	.47548	.47468	.47226	.46762	.45925	.44522	.42569	.40281	.37880	.35522	.33302
1.0	.52050	.51991	.51818	.51487	.50897	.49869	.48297	.46278	.44005	.41650	.39347
1.1	.56332	.56291	.56174	.55948	.55545	.54828	.53639	.51962	.49922	.47681	.45393
1.2	.60386	.60358	.60287	.60147	.59888	.59419	.58578	.57270	.55537	.53504	.51325
1.3	.64203	.64188	.64154	.64082	.63938	.63661	.63116	.62169	.60784	.59031	.57044
1.4	.67780	.67777	.67772	.67756	.67702	.67573	.67270	.66650	.65622	.64195	.62469
1.5	.71116	.71118	.71141	.71169	.71186	.71172	.71060	.70720	.70033	.68953	.67535
1.6	.74210	.74219	.74261	.74325	.74398	.74472	.74506	.74397	.74017	.73280	.72196
1.7	.77067	.77081	.77138	.77230	.77346	.77486	.77629	.77701	.77584	.77169	.76425
1.8	.79691	.79709	.79778	.79890	.80038	.80227	.80450	.80658	.80756	.80627	.80210
1.9	.82089	.82110	.82187	.82313	.82484	.82709	.82987	.83293	.83557	.83669	.83553
2.0	.84270	.84293	.84375	.84511	.84697	.84944	.85259	.85632	.86016	.86322	.86466
2.1	.86244	.86267	.86353	.86494	.86688	.86948	.87284	.87698	.88164	.88615	.88975
2.2	.88021	.88045	.88131	.88274	.88471	.88735	.89081	.89514	.90029	.90581	.91108
2.3	.89612	.89637	.89722	.89864	.90059	.90322	.90666	.91104	.91641	.92253	.92899
2.4	.91031	.91055	.91139	.91277	.91466	.91722	.92059	.92489	.93026	.93665	.94387
2.5	.92290	.92313	.92393	.92526	.92707	.92953	.93275	.93688	.94210	.94850	.95606
2.6	.93401	.93423	.93499	.93625	.93796	.94028	.94332	.94722	.95218	.95836	.96595
2.7	.94376	.94397	.94469	.94586	.94747	.94962	.95245	.95608	.96070	.96653	.97388
2.8	.95229	.95248	.95315	.95424	.95592	.95770	.96030	.96363	.96787	.97325	.98016
2.9	.95970	.95988	.96049	.96150	.96284	.96465	.96702	.97004	.97386	.97873	.98508
3.0	.96611	.96627	.96684	.96775	.96897	.97060	.97272	.97543	.97885	.98319	.98889
3.1	.97162	.97177	.97229	.97311	.97420	.97566	.97752	.97996	.98297	.98678	.99181
3.2	.97635	.97649	.97695	.97769	.97866	.97994	.98161	.98373	.98636	.98966	.99402
3.3	.98038	.98050	.98092	.98158	.98242	.98355	.98501	.98685	.98913	.99196	.99567
3.4	.98379	.98390	.98427	.98486	.98559	.98657	.98784	.98943	.99138	.99377	.99691
3.5	.98667	.98677	.98710	.98761	.98825	.98909	.99018	.99154	.99319	.99520	.99780
3.6	.98909	.98918	.98947	.98992	.99046	.99118	.99210	.99326	.99465	.99631	.99847
3.7	.99111	.99119	.99145	.99184	.99229	.99290	.99368	.99465	.99581	.99718	.99893
3.8	.99279	.99286	.99308	.99342	.99381	.99431	.99496	.99577	.99673	.99785	.99927
3.9	.99418	.99424	.99444	.99473	.99505	.99546	.99600	.99667	.99748	.99836	.99950
4.0	.99532	.99537	.99554	.99580	.99606	.99639	.99683	.99739	.99803	.99874	.99967
R_γ^*	$.95_4$	$.95_9$	$.96_0$	$.96_8$	0.98_2	1.00_0	1.03_1	1.06_5	1.10_1	1.13_9	1.17_7

*See text.

3-89) $\quad CEP \approx 0.675 \sqrt{\langle \varepsilon^2 \rangle}$ sec (0.626γ)

3-90) $\quad R(0.95) \approx 1.96 \sqrt{\langle \varepsilon^2 \rangle} \cos (0.4784\gamma)$

may be obtained by curve fitting to interpolations from Table 3-2. The errors involved in using these approximations are at worst about 1% which is certainly adequate for our present purposes.

Thus, to summarize, the three measures of error: d_{rms}, CEP and R(0.95) for an optimum receiver are obtained at a given location by the following procedure:

a. Determine the bearing angles, $\{\theta_i\}$, to the OMEGA stations

b. For the statistical ensemble of interest (see Section 3.4) determine the variances, $\{\sigma_i^2\}$, for each navigation signal.

c. Compute $\langle \varepsilon^2 \rangle$ $(=d_{rms}^2)$ using 3-68)

d. Compute γ using 3-76)

e. Compute CEP and R(0.95) using 3-89) and 3-90).

The summations in 3-68) and 3-76) include all navigation signals available to the optimum receiver. Since several signals will in general be available from the same OMEGA station, it is convenient to perform the sums first over the signals common to each station since the geometrical factors are the same for all such terms. This is most directly accomplished by regarding the summation indices i,j,ℓ in 3-68) and 3-76) as labelling the OMEGA stations (e.g. $i=1,\ldots 8$) where the summations over signals common to each station have already been performed via

3-91) $$\frac{k_i^2}{\sigma_i^2} \equiv \sum_{\substack{\text{signals} \\ \text{common to} \\ \text{station } i}} \frac{(2\pi/\text{wavelength})^2}{\text{Phase variance (in radians}^2)}$$

Thus, the characterization of OMEGA fix accuracy has been reduced to the determination of (single-station) phase variances in the operational area of interest (i.e. Northern Pacific), and the mix of usable signals as a function of position within this region as determined from the coverage boundaries.

3.4 Requirements For Phase Error and Coverage Modelling

The primary application of the foregoing theory is to obtain an assessment of the attainable fix accuracy - relative to navigation requirements - as a function of position within the validation region. Complete characterization of fix accuracy would take account of the complex dependence upon time of day and season. However, as noted earlier, this would require an atlas of fix accuracies comparable in size to the PPC tables and would be of limited value in communicating to the system user a measure of the average performance of OMEGA in a given locale. For this reason, the validation methodology used in the present study is based upon averaging over both season and time of day so that fix accuracy becomes a function of position alone*.

---

* This is in contrast to the conventional procedure of separately specifying "day" and "night" accuracies, and thus requires some rationale: while one-way phases certainly can be diurnally segmented into "day", "night" (and "transition") periods, the segmentation times will differ for the various stations used in a fix. As a result, when three or more stations are combined to derive a fix, the resulting fix accuracy exhibits a complex dependence upon time of day (dominated, in fact, by the multiplicity of times of sunrise and sunset at each of the transmitters) which just does not fit into a simple binary (day vs night) classification. Thus, the fix accuracy measured at (Winter) local midnight and (Summer) local noon will not in general bracket the accuracies achieved at other times of day or seasons. Further justification for not segregating day and night will be given later (Section 4).

At a given position, the fix accuracy depends upon a number of factors:

a) which signals are available for use, i.e. with adequate SNR and acceptable levels of modal interference

b) the geometrical dilution of precision (GDOP) associated with the bearing angles to the Omega stations used

c) the statistical variability of the Omega phases themselves, i.e. due to the normally encountered day-to-day variations in propagation

d) PPC accuracy

e) how the various Omega signals are combined in the position-fixing process

Factors a), b) and c) determine the intrinsic accuracy of Omega, while d) and e) depend upon the specifics of system implementation. In order that the present validation analyses shall not be outdated by subsequent improvements in the PPC tables, two separate fix accuracy assessments will be performed, one which assumes that any PPC "bias" errors have been removed and one which takes approximate account of the bias errors associated with the PPC corrections (as of 1979.) Similarly, in order to fairly assess the intrinsic system accuracy, optimal combination is assumed in the position-fixing filter, the theory for which has already been developed in earlier in this section.

Recalling the development of Section 3.1, a pseudo-range implementation is applied and the fundamental statistical quantity is the one-way phase error, η_i, associated with the ith Omega signal:

3-92) $$\eta_i = LOP_i - PPC_i - \text{OBSERVED PHASE}_i$$

where LOP_i is the theoretical phase based on the geodetic distance and the reference phase velocity (c/.9974). In line with our intention to average over all time of day and seasons, η_i is a random variable drawn from the ensemble containing all possible phase measurements of the signal i at the given position, i.e. taken at any time during the year.

The fix accuracy will vary with position primarily through the spatial variation of factors a) and b) above. The spatial variation of a) is determined by associating with each OMEGA signal a "full-time" coverage region within which that signal is always available (excluding station off-air periods) with SNR >-20 dB (100 Hz bandwidth) and modal interference <20 CEC's. (The set of full-time coverage boundaries, called the Coverage Model, will be developed in Section 5). As such coverage boundaries are crossed, there is an abrupt change in the mix of signals used to derive the fix and the fix accuracy undergoes a corresponding discontinuity. The (smoothly varying) position dependence of GDOP, for a given set of signals, arises from the associated variation in the bearing angles to the stations.

Strictly speaking, of course, the statistical properties of η_i will also vary with position. However, it is difficult to model the mean and standard deviation of η_i as a continuous function of position based on the limited spatio-temporal sampling provided by monitor data. Our approach is therefore to suppress this spatial dependence and to derive instead from the monitor data an omnibus characterization of the η_i which is applicable uniformly throughout that part of the coverage region of the ith signal contained within the validation region. Specifically, the η_i are assumed to have zero mean and a standard deviation given by σ_i. Furthermore, the correlation between different η_i is zero. That is,

3-93) $$< \eta_i > = 0$$

3-94) $$< \eta_i \eta_j > = \sigma_i^2 \delta_{ij}$$

where the brackets denote averaging over all times of the year and all positions within the coverage region. The symbol $\delta_{ij}=1$ if i=j and zero otherwise.

It should be noted that the assumption of zero bias implied by Eq. 3-93) is not inconsistent with the observation of a PPC bias at a specific receiver site and during a specific day of the year. Rather we are merely assuming that when averaged over all sites and all time, these local biases tend to average out. Indeed, as will be seen in Section 4, the data supports this hypothesis in the N. Pacific.

PPC errors, although not contributing in the mean to $\langle\eta_i\rangle$, nevertheless will contribute to the mean squared phase error, σ_i^2. Since PPC errors are uncorrelated with the natural day to day phase variations due to propagation, we may write (cf. 3-92)

$$\sigma_i^2 = \sigma^2_{PPC_i} + \sigma^2_{PROP_i} \qquad 3\text{-}95)$$

where $\sigma^2_{PROP_i}$ is the contribution to σ_i^2 arising solely from random propagation[1] effects (exclusive of SID/PCA's). The PPC errors contributing to $\sigma^2_{PPC_i}$ are of two kinds, as shown schematically in Figure 3-5. Here is plotted a hypothetical diurnal variation of η_i as measured at a given site during a given half-month. η_i consists of a constant bias term, B_i, and a PPC modelling error M_i. B_i represents the error in the diurnally averaged LOP, whereas M_i represents the deviation of the diurnal phase variation from the simplified variation contained in the PPC model. M_i thus includes modal interference and sunrise/-sunset transition effects. Evidently, PPC refinements (see Ref 23) will tend to null out the B_i, whereas to eliminate the M_i, more structurally complex PPC models would be required. The M_i, being of mean zero when diurnally averaged are treated as "random PPC" errors*, which are uncor-

---

* Note that the word "random" is a bit misleading since these errors are strictly repeatable day to day.

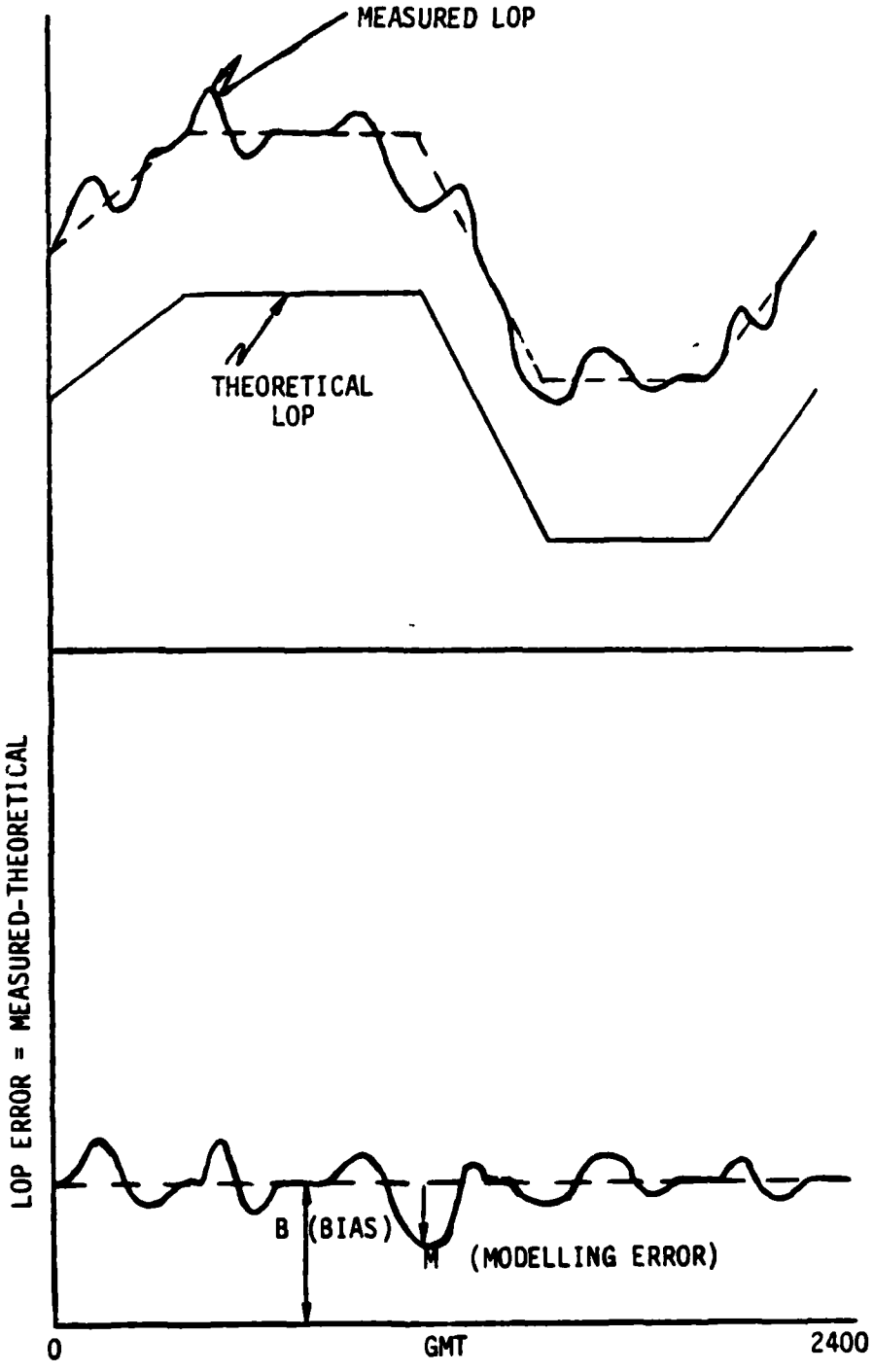

FIGURE 3-5. SCHEMATIC REPRESENTATION OF PHASE ERROR COMPONENTS

related from the "PPC bias" errors, B_i. We therefore write

3-96) $$\sigma^2_{PPC_i} = \sigma^2_{\substack{RAND \\ PPC_i}} + \sigma^2_{\substack{PPC \\ BIAS_i}}$$

where

3-97) $$\sigma^2_{\substack{RAND \\ PPC_i}} = \langle M_i^2 \rangle$$

$$\sigma^2_{\substack{PPC \\ BIAS_i}} = \langle B_i^2 \rangle = B_i^2$$

where the angular brackets here denote averaging over the diurnal period.

The net result is that the mean squared phase errors, σ_i^2, are simply the root-sum-square of their constituent error sources:

3-98) $$\sigma_i^2 = \sigma^2_{PROP_i} + \sigma^2_{\substack{PPC \\ BIAS_i}} + \sigma^2_{\substack{RAND \\ PPC_i}}$$

If PPC biases are assumed to have been removed by improved PPC's, then the second term on the right hand side of 3-98) would be set to zero.

The precise definitions of the three contrubutors to σ_i^2 will be given in the next section in terms of appropriate averages of monitor data. First, however we must note that because this data is structured on a <u>station-pair</u> basis, the single station σ_i^2 are not directly measurable. What <u>is</u> determinable is σ_{ij}^2 where i and j refer to the stations forming the recorded LOP, so in place of 3-98), we will be determining for each LOP

3-99) $$\sigma_{ij}^2 = \sigma^2_{PROP_{ij}} + \sigma^2_{\substack{PPC \\ BIAS_{ij}}} + \sigma^2_{\substack{RAND \\ PPC_{ij}}}$$

Once these are available, the single station squared phase errors, σ_i^2, are determined by assuming statistical independence of the errors on different stations, so that

3-100) $$\sigma_{ij}^2 \approx \sigma_i^2 + \sigma_j^2$$

A least squares procedure is then applied to determine the set $\{\sigma_i^2\}$ which minimizes the sum of squared residuals, R^2, where

3-101) $$R^2 = \sum_i \sum_j (\sigma_{ij}^2 - \sigma_i^2 - \sigma_j^2)^2$$

To summarize, the Omega validation methodology requires for each Omega signal, a single measure of squared phase error representing an average over all times and positions within the regions for which the signal is available. This measure is derived indirectly from station-pair squared phase errors which themselves arise from three sources: random propagation, PPC biases and irregularities in the diurnal phase variation not accommodated by the PPC model.

4.0 PHASE ERROR MODEL

The first essential component of the position fix accuracy model is the characterization of phase errors. A worldwide network of fixed OMEGA monitors has been established over the past decade and the phase data thereby obtained now covers a sufficient range of seasons, solar activity and geography to provide the basis for such characterization. The structured data base of phase measurements derived from the monitor network is called the MASTERFILE, and this section deals with the analysis of the MASTERFILE subset pertinent to the Northern Pacific region.

By way of background, Section 4.1 provides a description of the fixed OMEGA network and the structure of the MASTERFILE. In Section 4.2, the data analysis procedures which have been developed to distill the required information (see Section 3.4) from the MASTERFILE are described.

Section 4.3 presents the results of the analyses. First the cumulative phase error statistics taken over the entire data base are obtained. Next, by means of successive diurnal, monthly, seasonal and site averaging, one arrives at a series of reductions in the dimensionality of the data base, corresponding to a smoothing over the complex spatial and temporal fine-structure. This process culminates in a compact table (Table 4-14) of root-sum-squared single-station phase errors at 10.2 and 13.6 kHz both including PPC bias errors and with such biases removed. This table represents an average over season, site, and time of day and thus provides the omnibus characterization of phase variance required for fix accuracy assessments. The method of analysis also permits separate examination of the individual phase error components, viz. PPC biases (Section 4.4) and the natural day-to-day variability of VLF propagation. The final Section (4.5), presents an analysis of phase error statistics representing times near local noon

and local midnight, rather than diurnal averages. The absence of appreciable day/night differences in total phase errors justifies the diurnal averaging process.

4.1 Description of Fixed OMEGA Monitor Network and MASTERFILE Data Base

4.1.1 Fixed OMEGA Monitor Network

A world-wide network of land-based fixed OMEGA monitors is maintained by the Omega Navigation System Operations Detail (ONSOD) of the U.S. Coast Guard. The primary function of the network is to acquire OMEGA phase data over a sufficiently broad range of diurnal and seasonal conditions to confirm and - if necessary - upgrade propagation phase corrections (PPC's) and the underlying models from which they are derived. Analysis of such phase data also provides assessments of signal coverage, modal interference, phase stability and other signal characteristics required for system calibration and validation in the geographical area served by the monitor.

Since the inception of the monitoring program in 1966, the network has been systematically expanded to keep pace with the addition of new transmitters and the progress of OMEGA towards full implementation. Presently active monitor sites are listed in Table 4-1. The majority of sites are instrumented with a Magnavox MX-1104 receiver (see Figure 4-1) which outputs one-way phase (relative to an internal quartz oscillator) and a measure of SNR for three of the four common OMEGA frequencies (10.2, 11.3, 13.6 kHz) on a once per hour basis to a digital data logging device. Data is logged for a full month on a digital cassette which is then sent to ONSOD for processing. Since the receivers are generally not equipped with precision time standards, one-way phase measurements are not directly useful and must be combined into station-pair phase differences to remove effects of timing errors. The LITCOM receivers at the Omega transmitting sites measure phase difference but the path to the local transmitter is only 20-50 KM and hence the receiver provides "nearly" one-way phase measurements in strip-chart form.

TABLE 4-1. ACTIVE FIXED OMEGA MONITOR NETWORK SITES - JAN 1981

NAME	LAT	LON	DATE ESTABLISHED	RCVR EQUIPMENT
ADAK, ALASKA	51.99N	176.61W	JUNE 1979	MX-1104
AREQUIPA, PERU	16.47S	71.49W	JUNE 1978	MX-1104
ALEXANDRIA, EGYPT	-	-	DEC 1980	MX-1104
MANAMA, BAHRAIN	26.20N	50.60E	JUNE 1979	MX-1104
BERMUDA, ATLANTIC OCEAN	32.27N	64.88W	JUNE 1979	MX-1104
BRISBANE, AUSTRALIA	27.04S	153.17E	FEB 1980	MX-1104
BUENOS AIRES, ARG.	34.62S	58.36W	MAR 1978	MX-1104
CAMBRIDGE, MASS.	42.39N	71.14W	JULY 1977	MX-1104
CLARK AFB, PHILLIPINES	15.20N	120.52E	MAR 1977	MX-1104
KEFLAVIK, ICELAND	63.95N	22.72W	APR 1979	MX-1104
DARWIN, AUSTRALIA	12.38S	130.97E	JULY 1977	MX-1104
DIEGO GARCIA, INDIAN OCEAN	7.28S	72.36E	NOV 1977	MX-1104
BUTT OF LEWIS, U.K.	58.52N	6.26W	--	MX-1104
FROBISHER BAY, CANADA	63.76N	68.54W	NOV 1977	MX-1104
FARNBOROUGH, U.K.	51.29N	0.76W	JAN 1979	MX-1104
TRELEW, ARGENTINA	43.--S	63.--W	JUNE 1976	LITCOM
HESTMONA, NORWAY	66.53N	15.85E	1971	LITCOM
HOKKAIDO, JAPAN	45.52N	141.94E	SEPT 1977	MX-1104
INUVIK, CANADA	68.31N	133.50W	OCT 1978	MX-1104
KHARTOUM, SUDAN	15.61N	32.54E	APR 1980	MX-1104
KURE IS., HAWAII	28.39N	178.29W	OCT 1977	MX-1104
DICKEY, N. DAKOTA	46.--N	98.--W	1972	LITCOM
LA REUNION IS., INDIAN O.	21.--S	56.--E	MAR 1975	LITCOM
MAKAPUU PT., HAWAII	21.--N	158.--W	1972	LITCOM
MARCUS IS., PACIFIC OCEAN	24.29N	153.98E	FEB 1977	MX-1104
MIYAKOJIMA, JAPAN	24.73N	125.44E	--	FUJITSU
MONROVIA, LIBERIA	6.43N	10.81W	FEB 1977	LITCOM
MOMBASA, KENYA	4.07S	39.67E	SEPT 1979	MX-1104
NEA MAKRI, GREECE	38.10N	23.98E	JUNE 1977	MX-1104
SAN DIEGO, CALIFORNIA	32.70N	117.25W	OCT 1978	MX-1104
IBU-OSHIMA, JAPAN	34.80N	139.37E	--	FUJITSU
GALETA IS., PANAMA	9.40N	79.91W	AUG 1977	MX-1104
PERTH, AUSTRALIA	31.94S	115.98E	AUG 1979	MX-1104
RECIFE, BRAZIL	8.08S	34.90W	1977	599-R
NATAL, BRAZIL	5.93S	35.16W	JUNE 1978	MX-1104
RESOLUTE BAY, CANADA	74.71N	94.97W	JAN 1979	MX-1104
SAIPAN IS., PACIFIC OCEAN	15.13N	145.69E	APR 1979	MX-1104
SABANA SECA, PUERTO RICO	18.45N	66.23W	AUG 1977	MX-1104
PAGO PAGO, AMER. SAMOA	14.33S	170.72W	JULY 1977	MX-1104
SARDINIA, ITALY	40.86N	9.17E	JUNE 1978	MX-1104
ST. ANTHONY, CANADA	51.36N	55.63W	AUG 1977	MX-1104
ANCHORAGE, ALASKA	61.17N	149.97W	AUG 1977	MX-1104
KASUMGASEKI, JAPAN	35.68N	139.75E	1978	FUJITSU
TERCEIRA, AZORES	38.77N	27.16W	JUNE 1977	MX-1104
WASHINGTON, D.C.	38.86N	77.01W	OCT 1977	MX-1104
PORTSMOUTH, VIRGINIA	36.57N	76.26W	NOV 1977	MX-1104
RICHMOND, FLORIDA	25.63N	80.38W	AUG 1979	MX-1104
SOYA-MISAKI, JAPAN	45.52N	141.93E	1978	FUJITSU
RIO DE JANEIRO, BRAZIL	22.90S	43.22W	JAN 1978	MX-1104
SEATTLE, WASHINGTON	47.60N	122.33W	AUG 1977	MX-1104
COCOS IS., AUSTRALIA	12.19S	96.83E	JAN 1980	MX-1104

Figure 4-1. MX 1104 OMEGA Monitor System

In the Northern Pacific validation effort, the fifteen monitor sites listed in Table 4-2 and shown in Figure 4-2 were chosen for use. Two of these sites, Wales (Alaska) and Pyramid Rock (Hawaii) were active only in the early 1970's, and thus do not appear in Table 4-1.

TABLE 4-2. MONITOR SITES FOR N. PACIFIC VALIDATION

ADAK, ALASKA
ANCHORAGE, ALASKA
HOKKAIDO, JAPAN
KURE ISLAND, HAWAII
MAKAPUU PT., HAWAII
MARCUS ISLAND, JAPAN
MIYAKOJIMA, JAPAN
SAN DIEGO, CALIFORNIA
IBU-OSHIMA, JAPAN
GALETA ISLAND, PANAMA
PYRAMID ROCK, HAWAII
SEATTLE, WASHINGTON
TSUSHIMA, JAPAN
WAHIWA, HAWAII
WALES, ALASKA

Raw data from the monitor sites - either digital cassettes or strip charts as the case may be - are processed at ONSOD to obtain a structured data base of phase difference data called the MASTERFILE, as will be presently described. Primary emphasis is given to the 10.2 and 13.6 kHz data in constructing the MASTERFILE, as the 11 1/3 kHz data is of secondary importance in the validation program. The representation of each of the monitor sites listed in Table 4-2 in the 10.2 and 13.6 kHz MASTERFILES (i.e. as of Fall 1979) is shown in Tables 4-3 and 4-4 respectively. For each site, a dot under a given year, month or station indicates that at least one monthly data block is available for that year, month or station. An asterisk in the station section indicates close proximity of the receiver and transmitter sites.

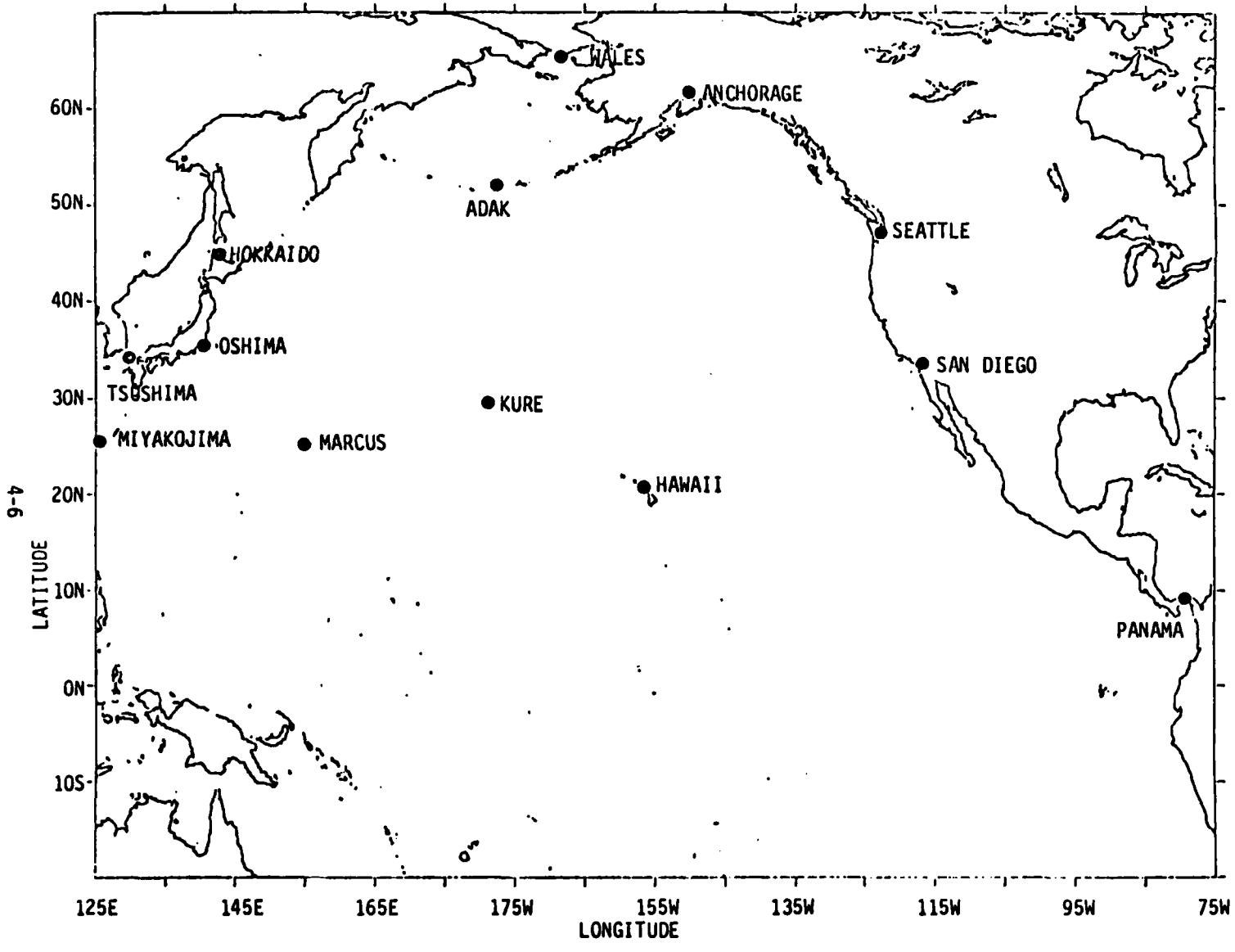

FIGURE 4-2. FIXED MONITOR SITES USED IN N. PACIFIC VALIDATION

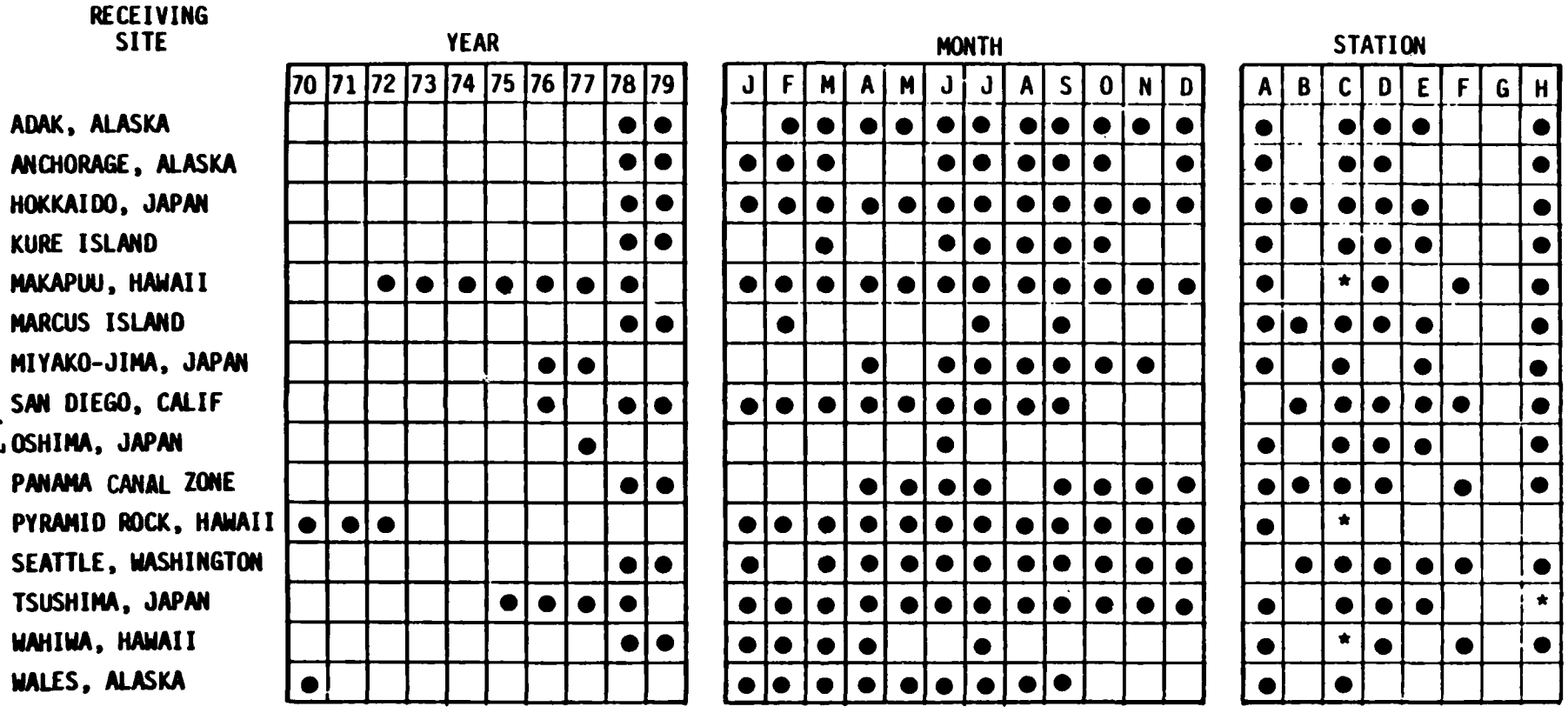

TABLE 4-3. ATTRIBUTES OF 10.2 kHz MASTERFILE DATA FOR N. PACIFIC VALIDATION

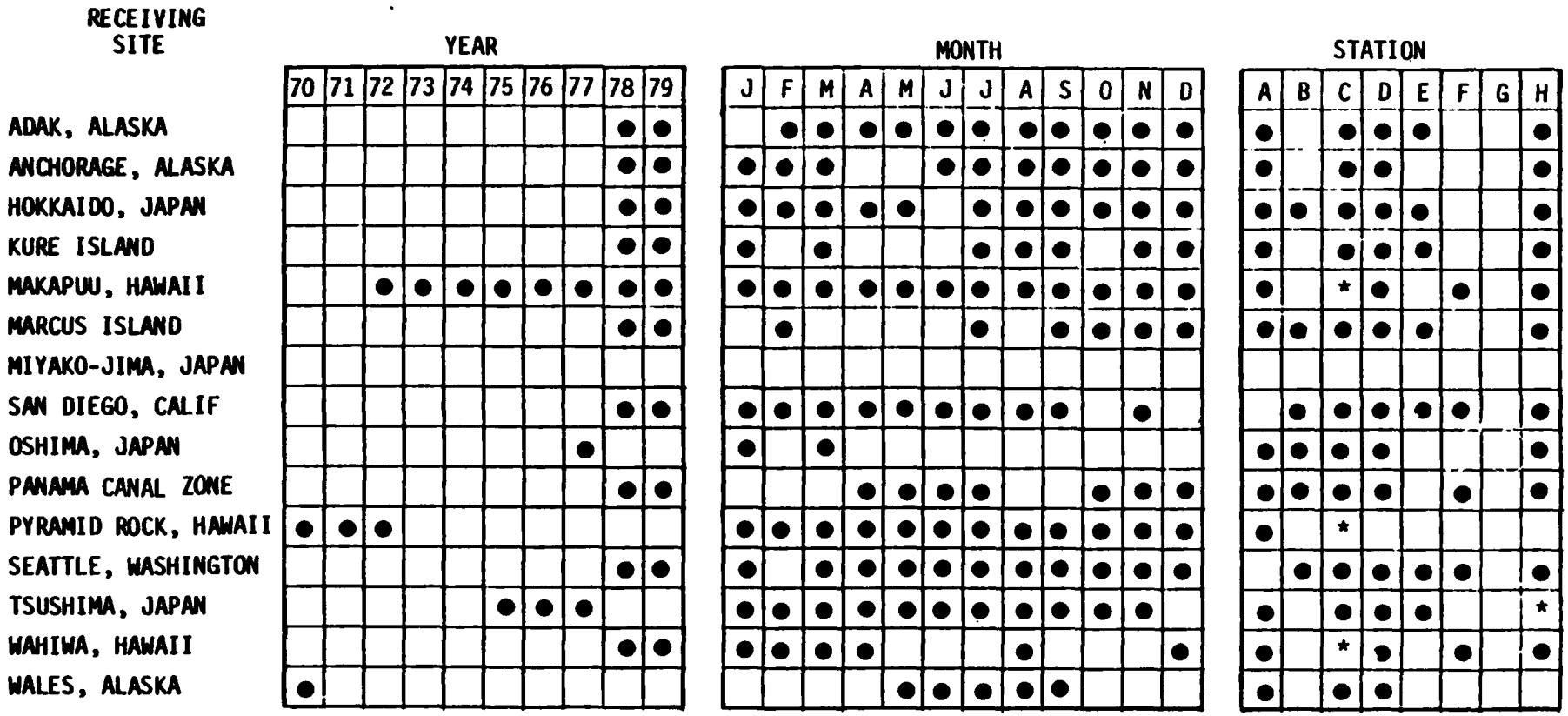

TABLE 4-4. ATTRIBUTES OF 13.6 kHz MASTERFILE DATA FOR NO. PACIFIC VALIDATION

4.1.2 MASTERFILE Data Base

The basic unit of the MASTERFILE data base is a record consisting of 40 lines of 120 characters each (see Figure 4-3) which corresponds to a given year, month, frequency, receiver site and LOP. The first line of the record is a header containing this and auxiliary information such as the receiver coordinates, nominal LOP, sunlit status of the paths at each hour, and day and night average phase error.

The next two lines contain PPC's computed for each hour for the first and second half months. Then follows 31 lines, corresponding to days 1 through 31, of hourly phase difference data. These data are constructed by subtracting the raw single-station phases (corresponding to the given LOP) which are recorded in integer centicyles, and resolving to the range of -49 to +50. Then, each such phase difference is flagged by appending an appropriate integer if one of the following anomalous conditions is detected:

data taken during recorded SID
data taken during recorded PCA
insufficient data for statistical analysis
data rejected as an outlier in a statistical analysis

If there is no monitor data, or if one of the transmitters was off-air at the hour and day in question, the phase difference is replaced by 400 or 300 respectively.

Each half-month is subjected to an independent statistical analysis which is first used to screen out outliers as indicated above. Within each half-month, those phase differences which are not flagged for any of the above reasons are combined to form a mean and standard deviation. Lines 35 and 36 (see Figure 4-3) contain the number of unflagged phase-difference data for each hour for the first and second semi-months respectively. Lines 39 and 40 are the corresponding standard deviations of the phase differences. Lines 37 and 38 are the

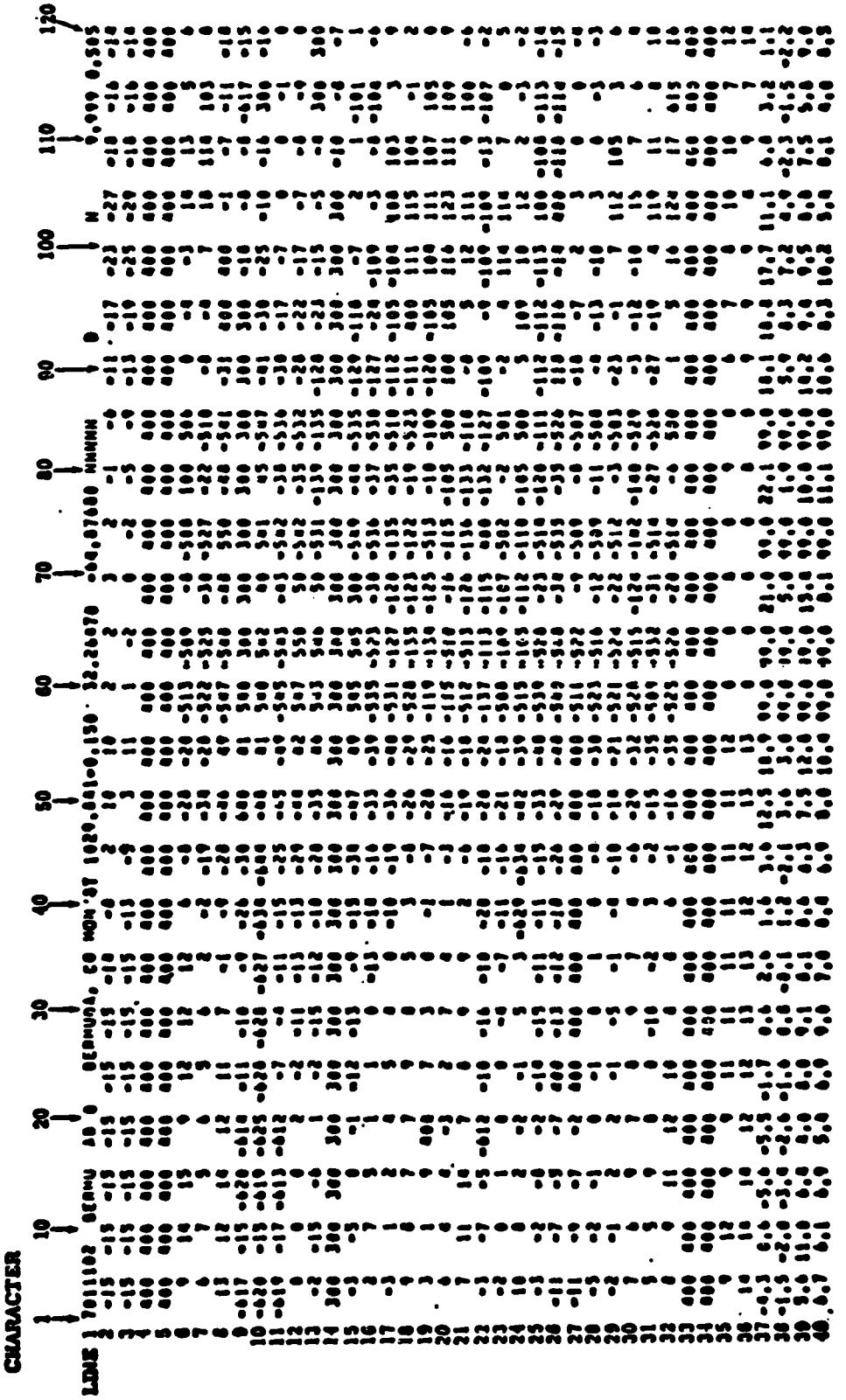

Figure 4-3. Sample Master File Record

mean phase-difference errors for the two semi-months, which are computed by subtracting the mean phase-differences from the PPC-corrected LOP:

Mean phase-difference error = LOP - PPC - mean phase-difference

and, if necessary, resolving to the range -49 to +50 CEC.

Thus, the last six lines of each MASTERFILE record contain the results of extensive preprocessing of the raw phase-differences for the purpose of screening out anomalies and deriving a characterization of the statistical properties of the phase-differences under nominal propagation conditions. Since there is little point in attempting to duplicate or improve upon this preprocessing, the present analysis is based upon a REDUCED MASTERFILE which is formed by deleting lines 2 through 34. The seven line record of the REDUCED MASTERFILE thus consists of the header line followed by (for each hour):

number of unflagged phase-differences - first half-month
number of unflagged phase-differences - second half-month
mean phase-difference error - first half-month
mean phase-difference error - second half-month
standard deviation of phase-difference - first half-month
standard deviation of phase-difference - second half-month

A procedure which permits a six to one compression of the MASTERFILE with corresponding reductions in disk-storage requirements.

4.2 Analysis Techniques

The sequence of operations involved in the reduction and processing of the MASTERFILE data is shown in Figure 4-4. The first two steps, culminating in the REDUCED MASTERFILE have already been described. At this point, for a given frequency, receiver site, month, year and LOP, three statistics are directly available from the MASTERFILE on a semi-monthly basis for each of the 24 hours in a day:

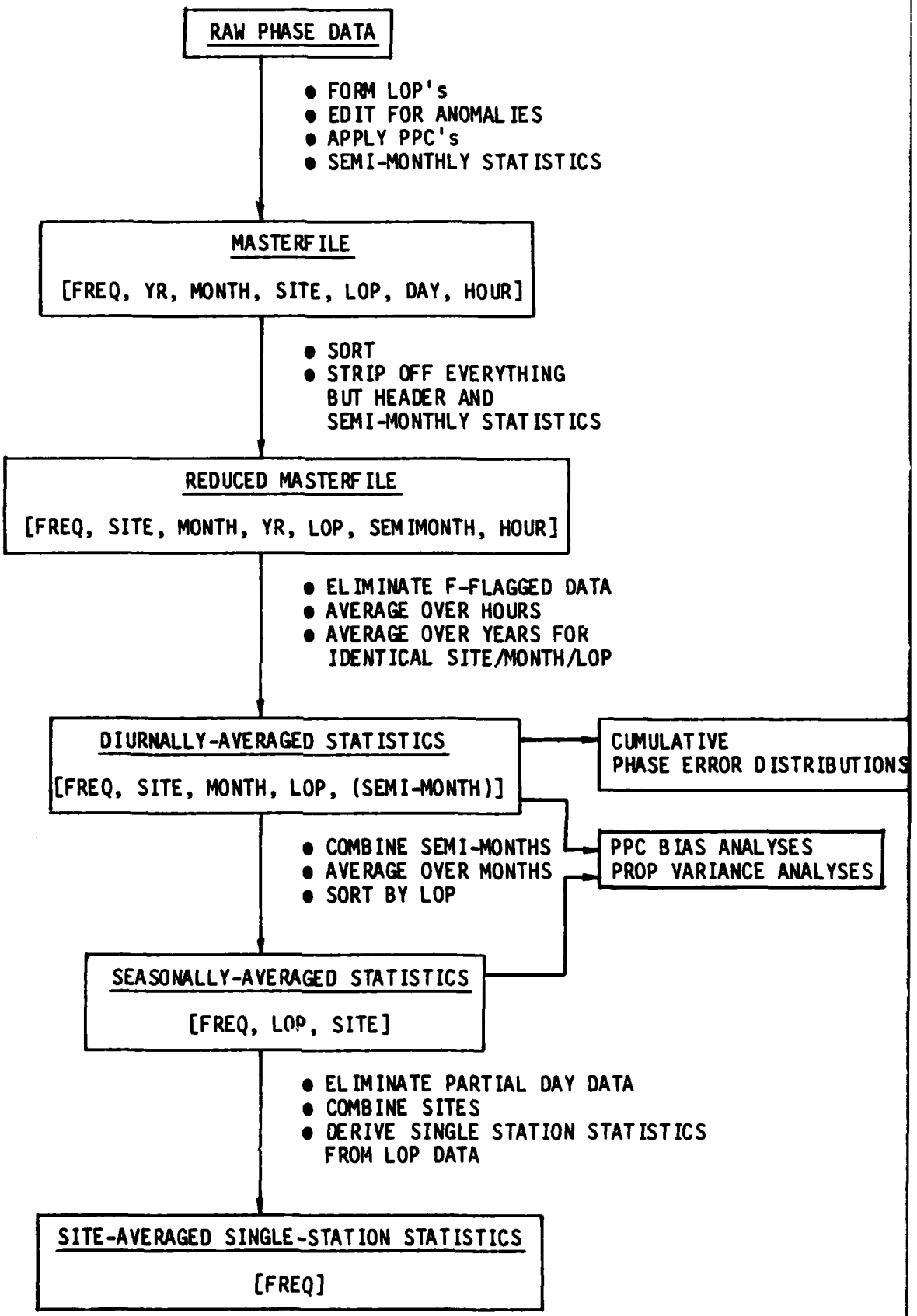

FIGURE 4-4. DATA ANALYSIS FLOWCHART

1) Mean phase error ($\bar{\phi}$)

2) Std. deviation of phase error (σ)

3) Number of error-free phase difference readings (N)

If (H,D) is the phase error (i.e. as given in the MASTERFILE and defined in Eq. 3-92) at hour H and day D within the given semi-monthly data block, then specifically:

$$\bar{\phi}(H) = \sum_D \eta(H,D)/N(H)$$

$$\sigma^2(H) = \sum_D \eta^2(H,D)/N(H) - \bar{\phi}^2(H) \qquad 4\text{-}1)$$

where the sum is over unflagged data only and where N(H) is the number of days contributing unflagged data for that hour and semi-month.

4.2.1 Diurnally-Averaged Statistics

In the next processing step, data blocks corresponding to the same frequency, site, month and LOP but differing in year are combined and an average is then performed over the 24 hour diurnal period. If $\bar{\phi}(H,Y)$, $\sigma(H,Y)$ and $N(H,Y)$ are the values obtained from 4-1) in a given year Y, then data from different years are combined according to:

$$N(H) = \sum_Y N(H,Y)$$

$$\bar{\phi}(H) = \left(\sum_Y N(H,Y)\bar{\phi}(H,Y)\right)/N(H) \qquad 4\text{-}2)$$

$$\sigma^2(H) = \left(\sum_Y N(H,Y)\sigma^2(H,Y)\right)/N(H)$$

The (diurnal) averages of the above quantities over H give equal weight to each hour for which unflagged data are available:

$$\bar{\phi} = \left(\sum_H \bar{\phi}(H)\cdot SGN\left(N(H)\right)\right)/N \qquad \text{[PPC BIAS]}$$

4-3) $$\sigma^2 = \left(\sum_H \sigma^2(H)\cdot SGN\left(N(H)\right)\right)/N \qquad [\sigma^2_{PROP}]$$

$$N = \sum_H SGN\left(N(H)\right) \qquad \text{[\# HOURS/DAY OF GOOD DATA]}$$

where SGN(X) is unity if X>0 and zero if X=0.

For each frequency, receiver site and LOP, one thus arrives directly at a set of up to 24 (i.e. one per semi-month) diurnally averaged quantities: $\bar{\phi}$ (mean phase error), σ (std deviation of phase error) and N (number of hours for which unflagged data are available). The mean phase error, $\bar{\phi}$, is identified with the PPC bias in cases where N is close to 24 since with unbiased PPC's, the phase error will - by definition - average out over the 24 hour period. Similarly, σ is identified with the rms phase variation due solely to propagation, since it arises from the day to day phase variation at the same hour within a *given semi-month*.

The "random" PPC error (or PPC modelling error, see Eq. 3-97)) can also be extracted from a particular diurnal average of the $\bar{\phi}$ (H) and $\sigma^2(H)$. To derive this, let us return to 4-1) and introduce the following explicit <u>model</u> for the phase error $\eta(H,D)$:

4-4) $$\eta(H,D) = B + M(H) + \rho(H,D)$$

In 4-4), B is the PPC bias error, M(H) is the PPC modelling error, both being *non-statistical*, i.e. *not random variables*. $\rho(H,D)$, *on the other hand*, <u>is</u> a random variable representing day-to-day phase variations due to propagation. $\rho(H,D)$ has an expected value of zero and a standard deviation of $\sigma^2(H)$. The quantity $\bar{\phi}(H)$, as computed from 4-1) and 4-4) is also a random variable, with expectation value B+M(H) and standard deviation $\sigma^2(H)/N(H)$. That is, $\bar{\phi}(H)$ may be written:

4-5) $\bar{\phi}(H) = B+M(H) + \tau(H)$

where $\tau(H)$ is a random variable for which

4-6)
$$<\tau(H) > = 0$$
$$<\tau^2(H) > = \sigma^2(H)/N(H)$$

where the brackets denote an expectation value taken over an ensemble representing different daily samples within a given semi-month.

Now, implicit in the separation of the PPC errors into a bias and a modelling component is the condition

4-7) $$\sum_H M(H) \text{ SGN } N(H) = 0$$

Thus, in computing the diurnally averaged quantity $\bar{\phi}$ in 4-3), we find that

4-8) $$\bar{\phi} = B + \frac{1}{N} \sum_H \tau(H) \cdot \text{SGN } N(H)$$

Let us now construct the statistic S^2 defined by

4-9) $$S^2 \equiv \frac{1}{N} \sum_H \left(\bar{\phi}(H)-\bar{\phi}\right)^2 \cdot \text{SGN}\left(N(H)\right)$$

From 4-5) and 4-9) we then have

4-10) $$S^2 = \frac{1}{N} \sum_H \left(M(H) + \tau(H) - \frac{1}{N} \sum_{H'} \tau(H') \cdot \text{SGN}\left(N(H')\right)\right)^2 \cdot \text{SGN}\left(N(H)\right)$$

Using 4-6) and 4-7), we then obtain for the expected value of the random variable S^2:

$$4\text{-}11) \qquad \langle S^2 \rangle = \frac{1}{N} \sum_H M^2(H) \cdot SGN\left(N(H)\right) + \frac{1}{N}\left(1 - \frac{1}{N}\right) \sum_H \frac{\sigma^2(H)}{N(H)} \cdot SGN\left(N(H)\right)$$

The first term on the right hand side is just $\sigma^2_{\substack{RAND \\ PPC}}$ as defined in Eq. 3-97), so using 4-9) we obtain the desired result

$$4\text{-}12) \qquad \sigma^2_{\substack{RAND \\ PPC}} = \left(\sum_H \left[\left(\bar{\phi}(H) - \bar{\phi} \right)^2 - \left(1 - \frac{1}{N}\right) \frac{\sigma^2(H)}{N(H)} \right] \cdot SGN\left(N(H)\right) \right) / N$$

The four diurnally-averaged statistics given in 4-3) and 4-12) are compiled for each semi-month, for a given frequency, receiver site and LOP. In addition, <u>all</u> of the unflagged phase error data for a given frequency-site-LOP-month are combined into three grand statistics: the mean phase error, its standard deviation and the number of unflagged phase measurements comprising the sample: (Y=year, D=day within month, H=hour)

$$4\text{-}13) \qquad \bar{\phi}_G = \sum_Y \sum_D \sum_H \eta(H,D,Y)/N_G \qquad \text{(mean phase error)}$$

$$\sigma_G = \sqrt{\sum_Y \sum_D \sum_H \eta^2(H,D,Y)/N_G - \bar{\phi}_g^{\,2}} \qquad \text{(standard deviation of phase error)}$$

$$N_G = \sum_Y \sum_D \sum_H \begin{Bmatrix} 1 \text{ if unflagged data} \\ 0 \text{ if flagged data} \end{Bmatrix} \qquad \text{(\# unflagged phase measurements)}$$

As indicated in Figure 4-4, certain cumulative phase error distributions are computed before proceeding further. Specifically, all receiver sites, months, and LOP's are combined (at each frequency) into a single data set and we then tabulate:

AD-A121 105 NORTH PACIFIC OMEGA NAVIGATION SYSTEM VALIDATION(U) 2/4
MEGATEK CORP SAN DIEGO CA P LEVINE ET AL. 31 DEC 81
R2018-054-IF-5 ONSOD-01-81 N00123-78-C-0043

UNCLASSIFIED F/G 17/7 NL

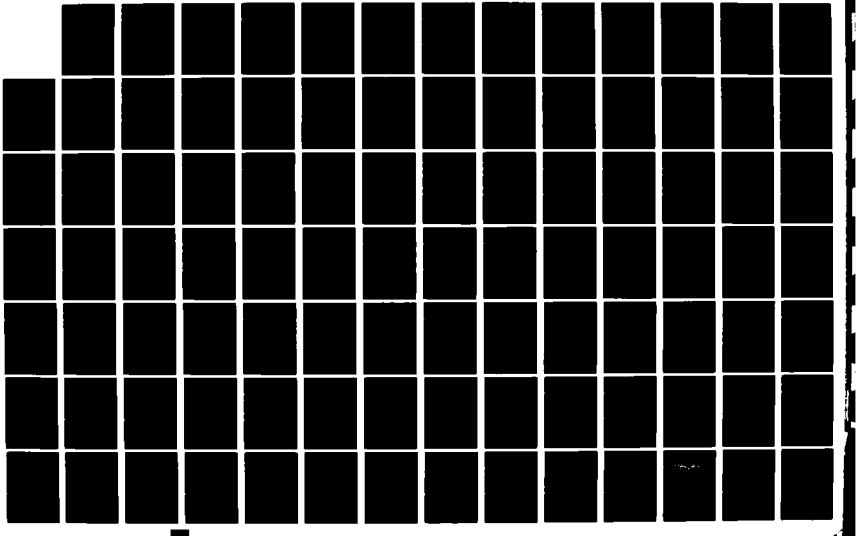

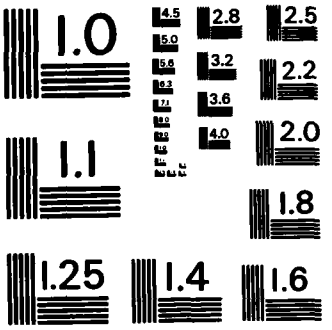

MICROCOPY RESOLUTION TEST CHART
NATIONAL BUREAU OF STANDARDS-1963-A

1) The fraction of cases* for which the absolute value of the mean phase error $|\bar{\phi}_G|$ exceeds a given value.

2) The fraction of cases for which the standard deviation, σ_G, of the phase error exceeds a given value.

3) The fraction of cases for which the r.m.s. phase variation due to propagation alone, (σ as given in 4-3), exceeds a given value.

4.2.2 Seasonally-Averaged Statistics

The next step is to average over semi-months to obtain seasonally-averaged data which now no longer depend on time, only on frequency, receiver site and LOP. We therefore compute the mean and standard deviation of the six quantities listed in Table 4-5, i.e. when averaged over all semi-months for which unflagged data were available. As indicated in Figure 4-4, these seasonally-averaged statistics can then be analyzed to uncover those combinations of receiver site and LOP for which significant PPC biases remain. ("Significant" in this sense means both large in magnitude and large compared to the standard deviation of the PPC bias). Similarly, the variation (i.e. as a function of receiver site and LOP) of the random propagation and "random" PPC (PPC modelling error) errors are also examined to spotlight typical cases. In the process, the spatial homogeneity of the errors for a given LOP within the validation region can also be quantitatively assessed.

---

* In this sense, a "case" corresponds to a specific receiver site, LOP and month.

STATISTIC	SYMBOL	DEFINING EQUATIONS
PPC BIAS	B	$\bar{\phi}$ as given in 4-3)
RANDOM PROPAGATION ERROR	P	$\sqrt{\sigma^2}$ as given in 4-3)
PPC MODELLING ERROR	M	$\sqrt{\sigma^2_{\substack{RAND \\ PPC}}}$ as given in 4-12)
HOURS/DAY OF GOOD DATA	N	N as given in 4-3)
TOTAL RSS ERROR	T	$\sqrt{B^2 + P^2 + M^2}$
RSS ERROR WITH BIASES REMOVED	C	$\sqrt{P^2 + M^2}$

TABLE 4-5: SEMI-MONTHLY STATISTICS TO BE SEASONALLY AVERAGED

4.2.3 Site-Averaged Single-Station Statistics

The final processing step is to average the total root-sum-squared error (T) and the r.s.s. error with biases removed (C) over receiving sites and to convert from an LOP (i.e. station-pair) basis to a single-station basis. The outputs of these procedures are the quantities σ_{T_i} and σ_{c_i}, which are respectively the r.s.s. phase error and r.s.s. phase error with PPC biases removed for Omega station #i. These quantities depend only upon frequency - being separately computed for the 10.2 and 13.6 kHz. MASTERFILES - and are applied uniformly throughout the coverage region of the ith signal at all times of the day and all seasons of the year.

As outlined earlier, a least-squares procedure is employed to accomplish the desired reduction. The specific procedure is as follows. After the seasonal averaging process, the MASTERFILE (at a

given frequency) has been reduced to a series of records, where each record corresponds to a specific receiver site and LOP and contains the total r.s.s. error and r.s.s. error with bias removed. Let the Kth record correspond to receiver site $R_{(K)}$ and transmitters $X_{1(K)}$ and $X_{2(K)}$ and let the r.s.s. errors be $T_{(K)}$ and $C_{(K)}$ respectively. We define the function

4-14)
$$W(R,X) = \begin{cases} 1 \text{ if distance between receiver site R and site X} > 100 \text{ NM} \\ 0 \text{ otherwise} \end{cases}$$

We seek to approximate the station-pair $T_{(K)}$ and $C_{(K)}$ by the quantities $\tilde{T}_{(K)}$ and $\tilde{C}_{(K)}$ which are constructed from single-station phase errors under the assumption of negligible path-path correlation:

4-15)
$$\tilde{T}^2_{(K)} \equiv \sigma^2_{T_{X_1(K)}} \cdot W\left(R_{(K)}, X_{1(K)}\right) + \sigma^2_{T_{X_2(K)}} \cdot W\left(R_{(K)}, X_{2(K)}\right)$$

$$\tilde{C}^2_{(K)} \equiv \sigma^2_{C_{X_1(K)}} W\left(R_{(K)}, X_{1(K)}\right) + \sigma^2_{C_{X_2(K)}} \cdot W\left(R_{(K)}, X_{2(K)}\right)$$

In particular, we seek to find the sets $\left\{\sigma_{T_i}{}^2\right\}$ and $\left\{\sigma_{C_i}{}^2\right\}$ (i=1,...8) which minimize the residuals:

4-16)
$$\rho_T \equiv \sum_K \left(T^2_{(K)} - \tilde{T}^2_{(K)}\right)^2$$

$$\rho_C \equiv \sum_K \left(C^2_{(K)} - \tilde{C}^2_{(K)}\right)^2$$

The algebra of minimization is identical for T and C so we can henceforth restrict consideration to T alone. Minimization of ρ_T leads to the set of 8 simultaneous equations

4-17) $$\frac{\partial \rho_T}{\partial \sigma_{T_j}^2} = 0 \qquad (j=1....8)$$

where the index j corresponds to a particular Omega station. The algebra is facilitated by writing 4-15) in the form

4-18) $$\tilde{T}_{(K)}^2 = \sum_i \sigma_{T_i}^2 \left[\delta_{iX_1(K)} + \delta_{iX_2(K)}\right] W\left(R_{(K)}, i\right)$$

Where $\delta_{iX_1(K)}$ is unity if the index i corresponds to the transmitter $X_{1(K)}$ and zero otherwise. Carrying out the differentiation 4-17) leads to the equation

4-19) $$\sum_K T_{(K)}^2 W\left(R_{(K)}, j\right)\left[\delta_{jX_1(K)} + \delta_{jX_2(K)}\right]$$

$$= \sum_K \sum_i \sigma_{T_i}^2 \cdot W\left(R_{(K)}, i\right) W\left(R_{(K)}, j\right)\left[\delta_{iX_1(K)}\right.$$

$$\left. + \delta_{iX_2(K)}\right]\left[\delta_{jX_1(K)} + \delta_{jX_2(K)}\right]$$

Defining the matrix elements

4-20) $$\alpha_{Ki} \equiv W\left(R_{(K)}, i\right)\left[\delta_{iX_1(K)} + \delta_{iX_2(K)}\right]$$

and

4-21) $$M_{ij} = \sum_K \alpha_{Ki} \cdot \alpha_{Kj} = M_{ji}$$

equation 4-19 becomes

4-22) $$\sum_K T_{(K)}^{2} \cdot \alpha_{Kj} = \sum_i \sigma_{T_i}^{2} \cdot M_{ij}$$

Finally, defining the row matrix, E, with elements

4-23) $$E_j \equiv \sum_K T_{(K)}^{2} \cdot \alpha_{Kj}$$

and the column matrix, S, :

4-24) $$S = \begin{bmatrix} \sigma_T^2{}_1 \\ \sigma_T^2{}_2 \\ \vdots \\ \sigma_T^2{}_8 \end{bmatrix}$$

equation 4-22) becomes the simple matrix equation

4-25 $$E = M \cdot S$$

Where the elements of M are given by 4-21).

The solution of 4-25) is just

4-26) $$S = M^{-1} \cdot E$$

Thus, the problem splits conveniently into the inversion of the matrix M (independent of the observed r.s.s. errors) and the evaluation of E (using 4-23)) in terms of the observed errors. (In practise, of course, one evaluates two E's, one based on the $T_{(K)}^2$ and one based on the $C_{(K)}^2$ errors.)

In carrying out the foregoing procedure, one refinement is introduced. Since many of the records correspond to seasonal averages involving too few semi-months to represent a true annual average, the Kth record is first screened to make sure that at least a threshold number of semi-months went into the seasonal averaging process. Only those records which pass this screening process enter into the K summations 4-21) and 4-23). The threshold value was chosen equal to 16 semi-months in the actual calculations.

4.3 Phase Variance Results

4.3.1 Cumulative Phase Error Statistics

The first-stage processing of the REDUCED MASTERFILE is an averaging over the diurnal period as shown in Figure 4-4 and described in the previous section. When this has been performed, the basic unit of the resulting data base is a record corresponding to a given frequency (10.2 or 13.6 kHz), receiver site, LOP, and month. Henceforth we shall refer to each such record as a "case".

For each such case a number of statistics are computed as will be exhibited in Section 4.3.2. Among these statistics are the

quantities defined in equation 4-13), viz. the mean phase error and the standard deviation of the phase error. The former arises, by definition, from PPC bias errors while the latter arises from phase measurement errors (i.e. noise), day to day phase variations due to propagation, and PPC modelling errors.

In order to obtain a gross characterization of these errors taken over the whole data base, cumulative distributions were compiled as shown in Figures 4-5 and 4-6. Figure 4-5 shows the cumulative distribution of the absolute value of mean phase error ($|\bar{\phi}_G|$ as defined in equation 4-13). The filled circles are derived from 544 cases at 10.2 kHz, while the open circles are from 516 cases at 13.6 kHz. The diurnally averaged mean phase error is a direct measure of PPC bias. Hence Figure 4-5 indicates that the median absolute values of PPC bias are 7 CEC at 10.2 kHz and 6 CEC at 13.6 kHz. Similarly, there is a 95% probability that the PPC bias is less than 24 CEC at 10.2 kHz and 22 CEC at 13.6 kHz.

Figure 4-6 shows the corresponding cumulative distributions for the diurnally averaged standard deviation of the phase error ($_G$ as defined in Eq. 4-13). Remarkably, the results are virtually identical at 10.2 and 13.6 kHz, with a median value of 11.5 CEC and a value of 25 CEC at the 95% level. The standard deviation of the phase error arises jointly from PPC modelling errors and from day to day phase variations due to propagation, as was discussed earlier. It thus is a reasonable measure of the irreducible average LOP phase error when biases are removed. The value of 11.5 CEC, which corresponds to an LOP position error of .91 nmi on the baseline at 10.2 kHz, is fully consistent with the nominal 1-2 nmi design accuracy of Omega.

In order to determine the relative importance of PPC modelling errors and day-to-day propagation variations, the cumulative distributions at 10.2 and 13.6 kHz were also generated for the

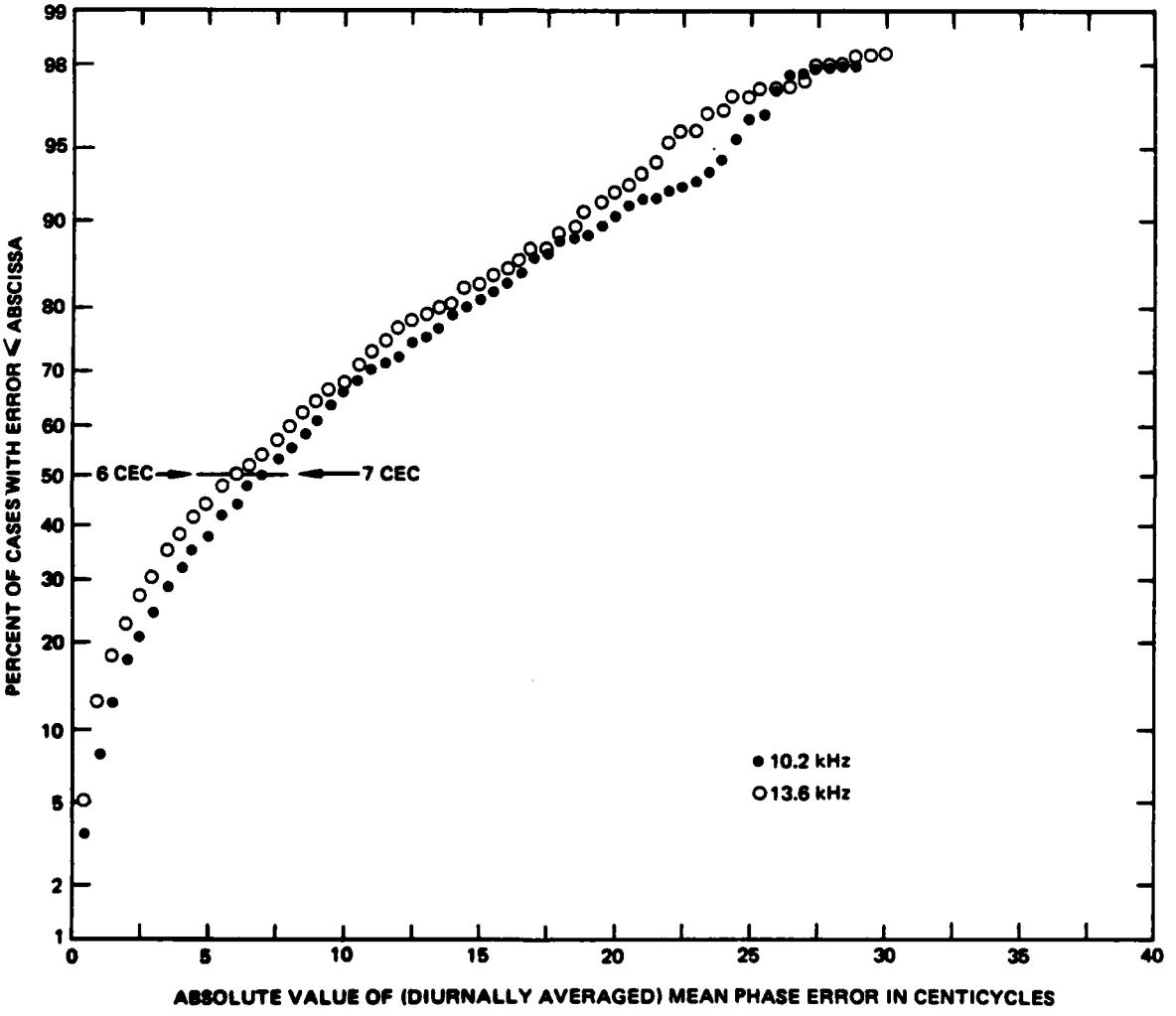

FIGURE 4-5

CUMULATIVE DISTRIBUTION OF MEAN PHASE ERRORS

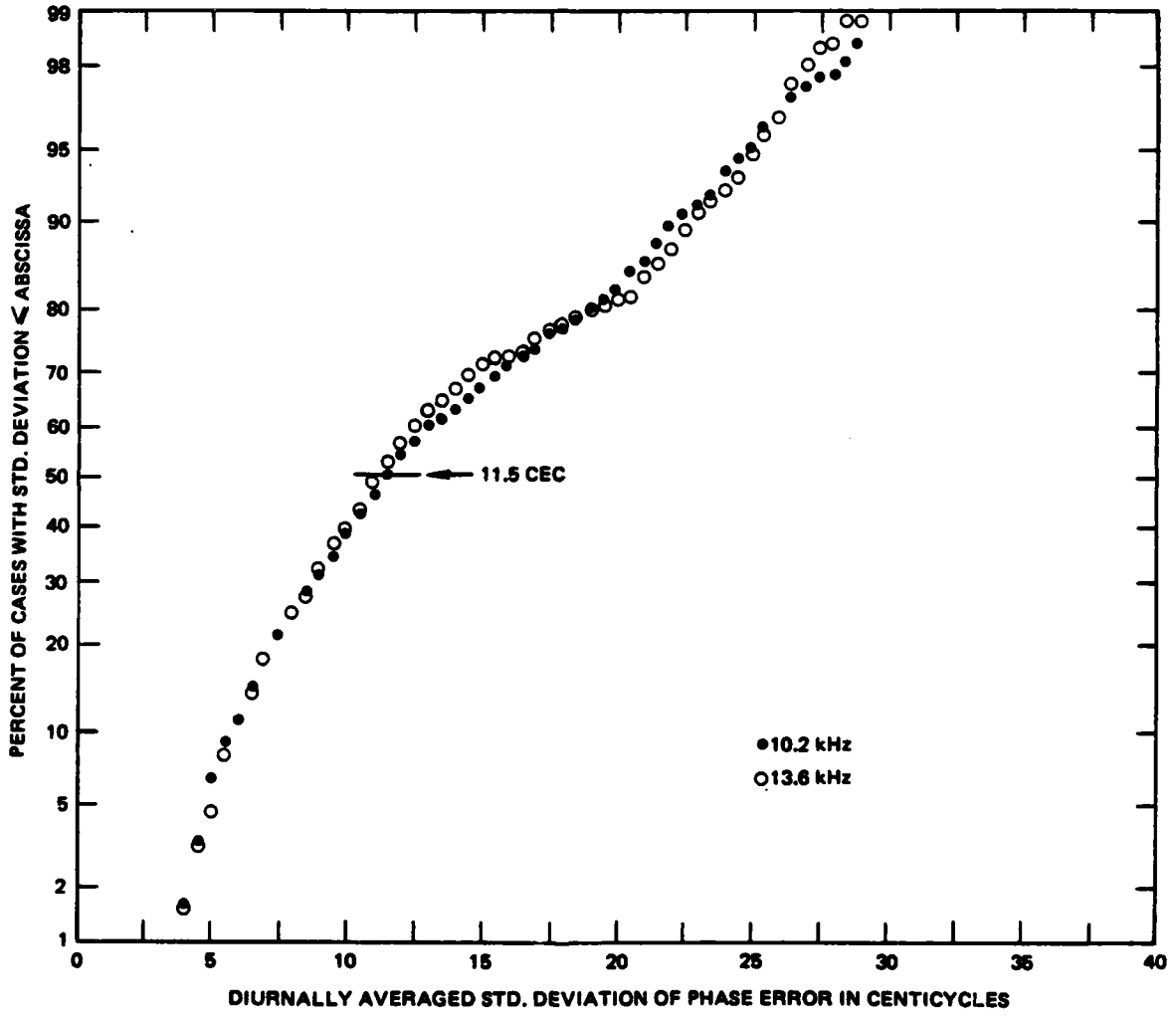

FIGURE 4-6

CUMULATIVE DISTRIBUTION OF PHASE ERROR STANDARD DEVIATION

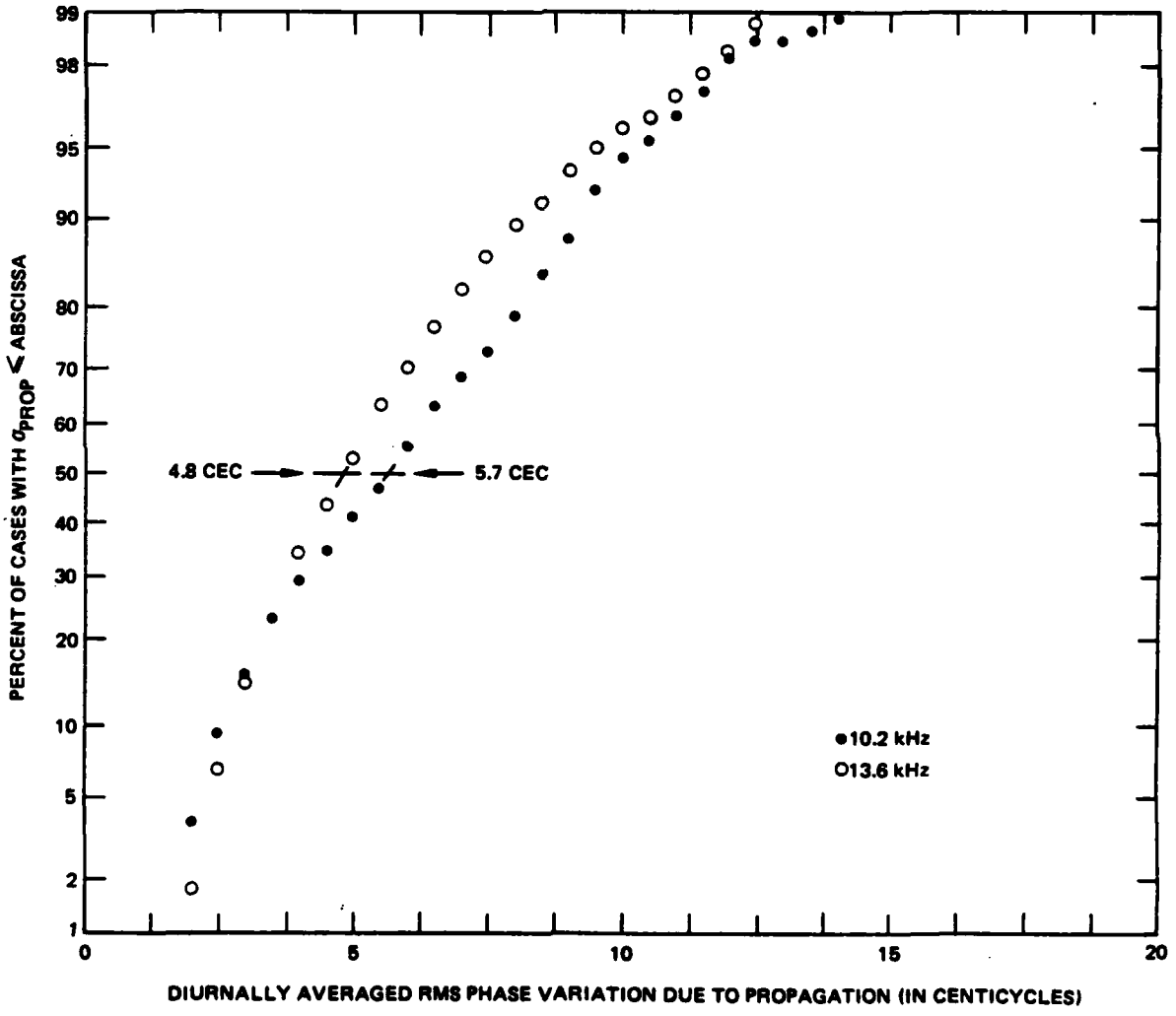

FIGURE 4-7

CUMULATIVE DISTRIBUTION OF PHASE ERRORS DUE TO RANDOM PROPAGATION

(diurnally averaged) r.m.s. phase variation due to propagation, i.e. σ_{PROP} as given in equation 4-3. The results are shown in Figure 4-7, indicating median phase errors of 5.7 and 4.8 CEC at 10.2 and 13.6 kHz respectively. It is therefore apparent that the major contribution (~10 CEC) to the observed 11.5 CEC standard deviation of the phase error arises from PPC modelling errors rather than propagation variations.

4.3.2 Diurnally Averaged Statistics

The individual "cases" from which the proceding cumulative statistics were derived are tabulated in Tables 4-6 (10.2 kHz) and 4-7 (13.6 kHz). Each entry in the tables corresponds to a given receiver site, month and LOP, which are identified in the first three columns. The corresponding diurnally-averaged statistics are grouped into three fields, the first of which represents grand monthly statistics formed from all available unflagged data for that case, and the second and third of which breakout more detailed statistics for the first and second half-months respectively.

The specific contents of each column in the tables are as follows:

Column #	Description
①	Four-letter abbreviation of receiver site. (Location is immediately evident from Table 4-2 with the exception of NELC and NOSC which are in San Diego).
②	Month designator: 1=Jan, 2=Feb, ...12=Dec.
③	LOP (Note: R denotes one-way phase)
④	Mean Phase error ($\bar{\phi}_G$ as defined in Eq. 4-13)
⑤	Standard deviation of phase error (σ_G as defined in Eq. 4-13)
⑥	Number of unflagged phase measurements (N_G as defined in Eq. 4-13)

⑦ Rms phase variation due to propagation (σ^2_{PROP} where σ^2_{PROP} is defined in Eq. 4-3) for first semi-month

⑧ PPC bias ($\bar{\phi}$ as defined in Eq. 2-13) for first semi-month

⑨ PPC modelling error (σ^2_{RAND} where σ^2_{RAND} is defined in Eq. 4-12) for first semi-month

⑩ Number of hours/day of good (i.e. unflagged) data (N as defined in Eq. 4-3) for first semi-month.

⑪-⑭ Same as 7-10, for second semi-month.

The primary value of the individual case data contained in Tables 4-6 and 4-7 is to spotlight those cases for which the PPC bias errors are atypically large. Accordingly, all cases which meet the following criteria have been flagged with an arrow at the left-hand margin:

i) Mean phase error (column 4) $\geq$20 CEC, and

ii) Mean phase error $\geq$ 2 times the standard deviation of the phase error (column 5), and

iii) at least 20 hours per day of good data (columns 10 and 14).

The 20 CEC criterion was chosen to parallel the 20 CEC criterion for "acceptable" modal interference errors. Criterion ii) was adopted to guarantee the statistical significance of the mean phase error, and the third criterion to guarantee the significance of the diurnal averaging process.

CASE ID			GRAND MONTHLY STATS			FIRST SEMI-MONTH				SECOND SEMI-MONTH			
①	②	③	④	⑤	⑥	⑦	⑧	⑨	⑩	⑪	⑫	⑬	⑭
ADAK	2	AD	-9.1	8.1	347	5.2	-10.3	4.5	24	6.7	-8	5.1	24
ADAK	2	AH	7.2	7.2	340	3.9	6.1	5.7	23	4.6	7.8	3.2	23
ADAK	2	CD	-10.7	9.8	453	6.2	-12.9	5.4	24	9.2	-10.1	6.7	24
ADAK	2	CE	-8.7	20.8	331	5.9	-8.6	19.4	21	6.7	-7.5	19.2	21
ADAK	2	CH	3.3	9.5	446	2.7	4.2	7.9	24	3.4	1.6	8.4	24
ADAK	2	EH	16.9	21.3	328	6.1	18.2	19.2	21	.7	15.2	20.9	21
ADAK	3	CD	-9.3	10.4	419	7.5	-10.6	5.2	24	8.8	-4.6	5.4	24
ADAK	3	CE	-1.3	21.4	245	5.6	-.3	20.3	17	7.9	-3.9	19.8	15
ADAK	3	CH	4.9	9.2	455	2.6	4.4	.9	24	2.3	5.8	7.9	24
ADAK	3	EH	8.8	18.8	218	5.8	.8	18.1	15	.7	11.9	15.9	12
ADAK	4	AD	-3.1	8.8	422	7.4	-4.1	4.1	24	7.9	-2.6	3.3	24
ADAK	4	AH	8.9	10.3	416	6.6	7.5	5.7	24	.9	9.1	2.9	24
ADAK	4	CD	-7.4	10.1	552	7.6	-8.2	5.8	24	9.2	-7.3	4.9	24
ADAK	4	CE	-13.2	17.7	333	7.6	-12	15.7	13	7.7	-13.8	14.3	13
ADAK	4	CH	6.2	7.4	589	2.3	6.3	7.5	24	.2	5.4	.7	24
ADAK	4	EH	14.5	18.5	270	7.5	14.4	17.2	15	7.3	15.5	16	15
ADAK	5	CD	13.5	7.9	285	0	0	0	0	.6	13.3	0	23
ADAK	5	CE	2.5	17	143	0	0	0	0	6.9	2.7	0	13
ADAK	5	CH	24.8	4.4	313	0	0	0	0	2.4	24.9	0	24
ADAK	5	EH	18.5	18	145	0	0	0	0	7.6	18.5	0	13
ADAK	6	AD	-6.1	12	54	0	0	0	0	10.9	-6	0	5
ADAK	6	AH	.4	7	72	0	0	0	0	6.6	.4	0	7
ADAK	6	CD	17.4	5.9	434	3.2	17	4.5	24	3.1	17.3	4	24
ADAK	6	CE	9.2	18.5	404	5.2	10.1	18.2	22	5.9	12.2	17.2	22
ADAK	6	CH	23.7	4.3	484	1.8	23.2	3.8	24	1.9	24.2	0	24
ADAK	6	EH	14.4	19.1	405	5.3	13.7	18.7	22	5.9	12.3	18.7	22
ADAK	7	AD	9.5	7.6	340	1.7	5.1	7.8	23	3.7	10.5	0	24
ADAK	7	AH	10.9	3.9	352	2.1	12.9	1.8	24	3.3	10.6	5	24
ADAK	7	CD	-1.9	7.7	458	4.6	-5.7	6.3	24	4.6	-.3	4.9	24
ADAK	7	CH	-.2	4.3	489	1.9	.1	3.7	24	2.4	-.3	3.4	24
ADAK	8	AD	-12	25.5	81	9.3	-13.8	26.8	6	8.2	-15.4	22.5	6
ADAK	8	AH	-24.3	21.8	107	4.8	-25.6	24.5	8	7.3	-22.4	22.9	8
ADAK	8	CD	19.9	12.4	61	9.5	23.3	2.1	4	11.5	18.5	9.7	4
ADAK	8	CE	3.1	9.5	12	6.6	-2.5	0	1	9.6	6	0	1
ADAK	8	CH	8.4	19.4	27	14.2	6.4	13.8	2	.9	10.7	13.6	2
ADAK	8	EH	-1.9	37.8	328	1.7	-2.1	38	19	2.3	-1.9	37.7	19
ADAK	9	AD	16.6	9.5	398	4.5	15.8	5.7	23	6.6	17.4	0	23
ADAK	9	AH	23.2	6.8	388	3.6	23.3	4.4	24	3.9	22.8	5.8	24
ADAK	9	CD	-6.8	10.1	519	6	-6	4.4	24	.9	-7	3.3	24
ADAK	9	CE	-19	14.9	470	4.4	-17.5	14.4	22	4.9	-19.6	12.6	22
ADAK	9	CH	1.8	4.8	583	2.4	1.4	3.9	24	2.5	2.1	3.6	24
ADAK	9	EH	23.1	16.8	516	4.2	21.6	16	24	5.1	23.2	14.7	24
ADAK	10	AD	1.8	13.5	166	8.8	4	8.8	14	4.9	-12	0	11
ADAK	10	AH	17	13.8	140	11.3	20.4	5.6	12	6.7	5.4	9.2	12
ADAK	10	CD	-10.7	11.6	284	9.1	-10	6.9	21	4.4	-14.5	0	21
ADAK	10	CE	-10.4	16.2	212	6.4	-11.2	13.8	18	5.7	-8.4	10.2	15
ADAK	10	CH	3	4.8	196	2.7	3	3.8	17	2.9	3.3	2.3	17
ADAK	10	EH	4.3	18.8	86	8.7	5.3	15.6	7	9.7	4.3	13.3	7
ADAK	11	AD	-10.8	9.8	493	7.3	-11.1	4.2	24	7.8	-10.9	4.9	24
ADAK	11	AH	9.7	10	500	8	7.2	6.5	24	5.7	11.1	3	24
ADAK	11	CD	-16.5	11.5	565	7.8	-15.4	7.3	24	8.8	-17.7	3.4	24
ADAK	11	CH	4.3	8.5	598	3.2	4.8	7.7	24	3.5	3.8	8	24
ADAK	11	EH	22.7	14.7	17	15.4	19.3	0	1	13.4	25.9	0	1
ADAK	12	AD	-6.6	11.9	457	8.4	-7.1	7.9	23	8.2	-6.7	7.6	23
ADAK	12	AH	10.1	10.5	514	8.6	10.7	5.5	24	8.4	9.4	6.3	24
ADAK	12	CD	-13.3	12.2	484	9.8	-11.3	7.4	21	9.1	-15.7	0	21
ADAK	12	CH	1.8	8.5	535	4	4.1	6.5	24	4.8	0	6.5	24
ANCH	1	AC	-4.4	7.5	484	4.3	-3	5.7	24	4.9	-5.3	4.4	24
ANCH	1	AD	-7.7	7.6	494	6	-7.8	5.2	24	5.9	-7.3	4.3	24
ANCH	1	AH	-10.4	7.5	476	4	-12.3	4.7	24	4.4	-9.7	7.1	24

TABLE 4-6: DIURNALLY-AVERAGED STATISTICS - 10.2 KHz

	ANCH	1	CD	-2.6	9.9	533	6.9	-3	6.7	24	7.8	-2.3	5.9	24
	ANCH	1	CH	-6	9.7	542	3.3	-9.4	8.8	24	4.2	-4.3	9.8	24
	ANCH	1	DH	-3	11.7	510	6.5	-6	9.2	24	6.8	-1.8	9	24
	ANCH	2	AC	-.8	7.5	282	3.4	-2.1	6.5	22	4	.2	4.6	22
	ANCH	2	AD	-6.3	9	253	6	-7.1	3.6	19	7.8	-5.5	3.7	19
	ANCH	2	AH	-5.2	11.4	291	3.9	-5.6	9.7	23	4.6	-5	9.5	23
	ANCH	2	CD	-4.3	10.3	371	6	-5.6	7	24	7.4	-3.6	7.3	24
	ANCH	2	CH	-3.6	11.7	353	3.2	-2.6	10.4	24	3.4	-4.1	10.4	24
	ANCH	2	DH	1.1	11	319	5.3	2.3	8.1	24	6.4	.2	8.3	24
	ANCH	3	AC	36.7	6.7	10	0	0	0	0	6.7	36.7	0	1
	ANCH	3	AD	37.9	7.7	10	0	0	0	0	7.8	37.9	0	1
	ANCH	3	AH	-32.3	9	10	0	0	0	0	9	-32.3	0	1
	ANCH	3	CD	2	7.6	178	0	0	0	0	6.2	2.1	0	15
	ANCH	3	CH	5.2	10.6	188	0	0	0	0	4.2	5.4	0	16
	ANCH	3	DH	3.2	9.8	143	0	0	0	0	6.5	2.9	0	13
	ANCH	6	AC	5.2	4.2	329	1.1	4.8	3.7	18	2.9	5.4	0	24
	ANCH	6	AD	9.8	5.4	261	3	9.9	5.3	17	3.6	9.7	0	21
	ANCH	6	AH	6.1	6.7	324	1.9	7.4	3.9	18	2.7	5.7	5.1	24
	ANCH	6	CD	3.9	5.1	293	3.1	4.7	4.6	17	3.4	3.7	3.2	23
	ANCH	6	CH	.9	7.9	348	2	2.6	5.7	18	1.6	.4	5.6	24
	ANCH	6	DH	-2.4	6.8	294	3.1	-2.8	6.1	17	3.2	-2.6	3.6	23
	ANCH	7	AC	4.9	4.6	519	3	5.4	3.3	24	2.9	4.7	3.7	24
	ANCH	7	AD	13.6	4.7	529	3.1	13.6	3.3	24	3	13.7	2.9	24
	ANCH	7	AH	6.4	6.1	533	3.3	7	5.4	24	3	5.8	5.7	24
	ANCH	7	CD	8.8	4.9	515	3.1	8.5	3.5	24	3.4	9	2.3	24
	ANCH	7	CH	1.4	7.4	528	1.6	1.5	7.8	24	2.1	.9	7.2	24
	ANCH	7	DH	-7.1	6.3	536	3.1	-6.6	5.7	24	3.4	-7.8	4	24
	ANCH	8	AC	19.9	6.1	588	4.9	22	2.6	24	5	18.1	8.5	24
→	ANCH	8	AD	26.4	6.4	566	4.8	28.9	2.7	23	5.3	24.1	10.8	23
→	ANCH	8	AH	20.3	7.9	598	5.2	23.6	3.6	24	6.4	17.5	10.9	24
	ANCH	8	CD	6.4	5.8	561	3.4	6.5	3.7	24	4.7	6.3	3.8	24
	ANCH	8	CH	.2	6	735	2.4	1.7	4.7	24	3	-.8	4.3	24
	ANCH	8	DH	-6.2	6	580	3	-4.7	4.3	24	4.2	-6.8	0	24
	ANCH	9	AC	19.5	9.2	663	7.3	20.6	4.4	24	7.6	19.7	6.1	24
	ANCH	9	AD	24	8	645	6.4	24.2	4.2	23	6.7	24.9	0	23
	ANCH	9	AH	17.3	10.6	676	8.5	18.3	4.4	24	8.4	16.7	7.1	24
	ANCH	9	CD	3.4	7.1	732	4.5	3.5	4.4	24	6	2.5	3.9	24
	ANCH	9	CH	-2.8	6.4	845	3.1	-2.3	5.3	24	3.5	-3.8	4.2	24
	ANCH	9	DH	-6.1	7.5	666	4.8	-5.6	3.8	24	6.4	-5.5	3.8	24
	ANCH	10	AC	.7	10.8	457	7.2	7.1	5	20	8.1	-3.9	0	20
	ANCH	10	AD	0	12.4	381	9.3	9.1	3.9	17	8.1	-6.3	0	17
	ANCH	10	AH	-.7	13.7	347	8.5	2.1	11.7	17	8.7	-4.6	7.2	17
	ANCH	10	CD	-1.9	8.6	564	5.2	1.7	4.4	24	6.2	-4.8	0	24
	ANCH	10	CH	-3.2	8.5	479	5.5	-4.1	5.9	24	4.6	-2.6	5.2	24
	ANCH	10	DH	-.4	11.7	440	8.1	-4.9	7.1	22	7.6	2.3	3.5	22
	ANCH	12	AC	1.4	7.3	446	5.4	-2.4	3.7	24	4.7	3	1.6	24
	ANCH	12	AD	-3.1	9.2	461	6	-4.5	7.6	24	5.6	-2.5	6.8	24
	ANCH	12	AH	-5.3	8	419	4.5	-8.2	5.2	24	4.6	-4.7	7	24
	ANCH	12	CD	-3.8	8.8	495	5.4	-2.8	6.4	24	5.8	-5.1	5	24
	ANCH	12	CH	-5.9	8.6	495	3.5	-3.9	7.6	24	3.7	-7.2	6.1	24
	ANCH	12	DH	-1.1	12.4	456	4.4	-1.9	11.2	24	5.2	-1.3	10.9	24
→	HOKK	1	AC	24.9	11.4	444	7.3	24	9.2	24	7.8	26	3.4	24
	HOKK	1	AD	-1	12.2	390	9.2	-3.6	6.4	21	8.8	1.6	5.1	21
	HOKK	1	AE	8.3	19.5	452	6.2	8.8	17.6	24	6.6	8.8	18.2	24
	HOKK	1	BC	1.3	33.2	206	9.1	4.2	32.4	12	9.8	3	31.3	12
	HOKK	1	CE	-5.1	20.1	395	5.1	-4.9	19	21	5.8	-7.3	17.8	21
	HOKK	1	CH	4.9	10.1	496	4.4	5	8.6	24	4.3	3.6	9.1	24
→	HOKK	2	AC	25.9	10.9	288	5.7	27.9	8	21	6.2	25.5	11.4	21
	HOKK	2	AD	4.8	12.6	343	8.6	4.7	7.1	23	9.3	5.3	6.6	23
	HOKK	2	AE	9.6	17.4	343	7.2	12.8	14.2	22	7.2	11.3	15.9	22

TABLE 4-6 : DIURNALLY-AVERAGED STATISTICS - 10.2 KHz CONT'D.

HOKK	2	BC	10.5	28.4	221	6.9	13.2	26.5	16	7.2	8.6	27.3	16
HOKK	2	CE	-4	20.5	332	3.5	-4.4	19.7	21	4.2	-3.5	19.7	21
HOKK	2	CH	1.5	11.6	432	3.9	-1.3	10.1	24	3.7	2.1	10	24
HOKK	3	AC	2.1	14.1	10	0	0	0	0	14.1	2.1	0	1
HOKK	3	BC	30.1	9.4	42	0	0	0	0	8.8	30	0	4
HOKK	3	CE	-.9	21.1	486	3.5	-.8	21.2	23	3.3	-2.2	20.9	23
HOKK	3	CH	.2	10.6	542	3.9	.4	10.8	24	3.4	-1	9.4	24
HOKK	4	AC	16.4	12.1	391	7.3	13	8.2	23	8.8	18.1	0	23
HOKK	4	AD	5	12	418	8.8	3.5	8.9	24	9.3	5.2	5.5	24
HOKK	4	AE	1	21	371	7.1	-.1	18.3	23	8.6	3	17.9	23
HOKK	4	BC	24.6	20.9	215	9.6	23.7	18.4	14	9.4	24.6	17.4	14
HOKK	4	CE	-.5	23.6	481	5.6	-.8	21.9	24	3.9	-.7	22.1	24
HOKK	4	CH	.9	9.3	532	4.9	1.2	7.8	24	3.4	-.2	7.7	24
HOKK	5	AC	15	10.8	586	5.7	13.7	8.3	24	6.3	16.7	4.8	24
HOKK	5	AD	4.2	12	525	6.5	5.6	9.1	22	6.6	3.4	9.6	22
HOKK	5	AE	.7	16.8	590	5.6	-1.3	15.7	24	6.4	2.7	14.8	24
HOKK	5	BC	25.6	12.5	281	8.3	23.7	9	13	8	27.6	0	13
HOKK	5	CE	-6.8	20.4	546	3.3	-6.6	20.1	22	3.5	-7.2	20.1	22
HOKK	5	CH	2.5	6.9	610	2.9	3	6.4	24	3.2	1.9	6	24
HOKK	6	AC	11.7	9	348	3	9.9	7.2	23	4.5	11.3	5.9	24
HOKK	6	AD	-1.3	12.4	305	4.5	-4	10.3	22	4.9	-1.8	10.3	23
HOKK	6	AE	-2.6	14.2	349	4.3	-4	13	20	5	-1.5	12	24
HOKK	6	BC	31.7	10.2	192	7.1	29.5	7.5	14	6.3	31	3.5	14
HOKK	6	CE	-9.9	16.7	479	3.9	-11	15.7	21	3.5	-8.2	16.8	21
HOKK	6	CH	1.1	5.5	580	2.8	.5	5.1	24	2.8	1.4	4.4	24
HOKK	7	AC	14.4	9.1	806	5.5	12.6	7.5	24	5.1	15.2	3.2	24
HOKK	7	AD	4.2	11.6	780	4.5	2	11.2	24	4.9	5.7	8.9	24
HOKK	7	BC	30.7	10.4	449	6.8	29.9	7.5	18	6.3	30.4	6.3	18
HOKK	7	CE	-7.9	15.8	516	7.1	-7.5	14.2	20	5.1	-8.4	13.8	20
HOKK	7	CH	.1	6.2	1045	3.2	.4	4.8	24	3.5	-.2	5	24
HOKK	7	AE	-1.2	14	365	5	-3.4	13.5	23	4.2	-.6	12.8	24
→ HOKK	8	AC	21.7	7.8	766	4.4	22.2	7	24	5.8	22.3	5.5	24
HOKK	8	AD	13	11	716	4.5	13.9	9.7	24	7.1	13.1	9	24
HOKK	8	AE	9.2	16.2	778	4.8	8.2	13.5	24	6.8	8.9	14.5	24
→ HOKK	8	BC	29.5	8.9	804	7.2	30.1	5.1	22	7.4	29.2	6.2	22
HOKK	8	CE	-7.2	17.7	981	3.9	-8.1	20.4	23	3.8	-7.6	20.5	23
HOKK	8	CH	.6	7.2	1135	3.9	0	6.1	24	3.7	1.5	5.8	24
→ HOKK	9	AC	24.1	11.3	294	7.7	21.1	5.5	24	5	31.2	0	24
HOKK	9	AD	8.3	12.8	290	7.5	7.7	8.3	24	3.8	10.7	8.2	24
HOKK	9	AE	11	22.8	275	7	9.3	20.6	23	3.8	19.6	15.1	23
HOKK	9	BC	31.6	8.4	200	7.6	31.3	2.6	17	6.5	32.4	0	17
HOKK	9	CE	-9.3	17.2	417	4	-8.7	16.8	21	3.9	-8.8	16.1	21
HOKK	9	CH	5.2	7.6	515	3.8	4.9	6.3	24	3.9	4.5	6.4	24
HOKK	10	AC	22.2	12.4	363	7.8	23.9	4.2	20	9.5	21.3	8.8	20
HOKK	10	AD	3.7	16.8	273	9.5	6.8	14.3	15	10.7	3	12.5	15
HOKK	10	AE	7.5	20	331	7.6	13.7	19.1	18	8.8	5.5	18.6	18
HOKK	10	BC	33.4	10.5	105	7.9	34.5	3.6	6	9.9	32.6	8.2	6
HOKK	10	CE	-2.1	16.4	344	4.8	.3	14.8	20	5.1	-4.5	13.7	20
HOKK	10	CH	2.6	9.9	435	4.3	3.8	7.1	24	4.4	1.9	7.9	24
HOKK	11	AC	23.3	11.7	348	10.9	20.4	4.6	20	7.6	25.3	0	20
HOKK	11	AD	-.1	13	416	9	.4	9.2	24	7.8	-.2	8.7	24
HOKK	11	AE	7.2	19.9	420	10.7	5.6	16.6	23	7.5	10.7	14.7	23
HOKK	11	BC	3.4	29.3	222	11.7	3.8	25.5	14	10.2	3.7	26.5	14
HOKK	11	CE	-.3	23.7	402	4.2	.4	23	23	4	.6	23.3	23
HOKK	11	CH	1	12.7	470	4.3	.7	11.9	24	4	0	11.4	24
HOKK	12	AC	23	11.9	365	0	20.2	6.5	20	9.2	25.5	0	20
HOKK	12	AD	2.3	12	336	8.6	3.9	7.5	19	9.5	1.6	3	19
HOKK	12	AE	7.6	18	430	7.3	5.2	14.1	22	7.9	12.9	10.8	22
HOKK	12	BC	10.4	30.5	227	9	5.1	30.3	14	10.1	15.3	26.5	14
HOKK	12	CE	-4.9	19.8	358	4.9	-7.3	17.7	20	5.8	-4.6	18.3	20

TABLE 4-6: DIURNALLY-AVERAGED STATISTICS - 10.2 KHz CONT'D.

HOKK	12	CH	3	8.9	490	4.1	2.8	7.2	24	4.6	2.2	7.4	24
KURE	3	CE	-3.1	21.8	245	7.4	-1.6	20.8	18	6.1	-3.6	18.5	17
KURE	3	CH	-8.7	15.6	297	2.6	-9.3	15	23	1.9	-8.5	15.5	23
KURE	3	DH	-24.3	14.4	13	13.9	-25.8	0	1	13	-16.5	6.3	1
KURE	3	EH	21.5	18.2	276	6.3	22.5	16.4	20	5.2	20.7	17.5	19
KURE	6	AD	-.1	19	345	6.6	-.5	18.1	20	6.3	-1.1	18.2	20
KURE	6	AE	-1.3	30.4	338	4.4	-1.9	30.4	21	4.9	-1.4	29.9	21
KURE	6	CE	-3.6	21.4	288	9.7	-3.2	19.9	16	9.9	-2.9	18.9	16
KURE	6	CH	-.4	11	353	6.6	.6	8.6	19	5.5	-.8	8.7	19
KURE	6	DH	2.5	22	255	10.3	1.8	18.7	13	8.7	1.3	19.8	13
KURE	6	EH	15.7	18.9	230	11.2	16.3	14.4	12	8.9	14.9	16.1	12
KURE	7	AD	1.6	21.6	330	4.9	1.1	20.5	23	6.3	2	20.4	23
KURE	7	CE	.1	23.9	154	10.5	.6	22.2	14	6.2	0	20.9	14
KURE	7	CH	-5	11.1	427	5.9	-4.2	9.1	22	6.1	-5.6	8.7	22
KURE	7	DH	-2.6	20.6	351	8.9	-3.6	17.8	18	8.4	-2.7	18	18
KURE	7	EH	14	18.6	137	9.1	13.2	17.1	12	8	13.4	14.3	12
KURE	8	AD	-1.7	20	153	5.3	-2.4	18.1	14	6.9	-.7	18.6	14
KURE	8	AE	-12.3	26.5	167	5.6	-14.8	25.8	15	7.5	-10.1	26.7	15
KURE	8	CE	4.5	19.8	347	9.6	6	17.7	20	8.8	5.7	16.9	20
KURE	8	CH	-5.7	12.9	393	8.1	-6.9	10.9	21	6.7	-5	10.3	21
KURE	8	DH	2.6	19.2	345	8.2	2.3	18.5	19	7.5	3	17.6	19
KURE	8	EH	13.8	20.2	321	9	14.1	18.1	17	9.2	15	17.1	17
KURE	9	AD	0	23.5	351	6.9	-1	21.1	21	9.4	-1.2	21	21
KURE	9	AE	-8.5	26	284	7.9	-11.6	24.3	18	8.2	-8.7	24.5	18
KURE	9	CE	-6.3	17.4	230	9.1	-7.2	13.6	13	10.9	-6.7	13.2	13
KURE	9	CH	-1.7	9.2	378	6.5	-3.9	6.9	21	6.4	-.8	5.7	21
KURE	9	DH	5.5	16.4	263	9.2	6.1	14.6	16	9.6	4.7	13.2	16
KURE	9	EH	16.3	16	242	6.4	18.7	14	15	7.1	17	15.1	15
KURE	10	CE	-19.1	14.2	10	14.2	-19.1	0	1	0	0	0	0
KURE	10	CH	-5	9.8	20	9.7	-5	0	2	0	0	0	0
KURE	10	DH	6	11.9	10	11.9	6	0	1	0	0	0	0
KURE	10	EH	7.9	9.7	10	9.7	7.9	0	1	0	0	0	0
MAKA	1	AC	-.6	11.6	1589	8.2	-4.4	9.3	24	6.5	1.8	8.6	24
MAKA	1	CD	1.8	10.1	937	5.7	2.9	9	24	5.1	1.4	9	24
MAKA	1	CF	2.5	26.4	447	8.5	2.5	25.6	19	6.7	2.1	25.2	19
MAKA	2	AC	1.5	11.6	1549	7.2	2.1	10.6	24	7.4	-2.8	9.6	24
MAKA	2	CD	.8	10.9	1969	5.4	1.7	9.3	24	5.9	.5	9.6	24
MAKA	2	CF	11.9	23.1	332	7.3	12.1	22.3	19	6.7	6.9	23.8	19
MAKA	2	CH	8.9	11.3	1132	7.6	11.4	10.6	24	4.4	7.8	10.9	24
MAKA	3	AC	-1.2	11.3	1926	9.7	-4.1	7.4	23	8.2	-.4	7.1	23
MAKA	3	CD	4	11.1	1650	6.5	4.9	10.2	24	5.1	3.7	9.8	24
MAKA	3	CH	13	11	1105	5.6	13.5	9.2	24	5.2	12.7	10.1	24
MAKA	4	AC	9.1	12.7	1581	9	7.1	9.5	24	6.8	11.4	6.1	24
MAKA	4	CD	3.7	6.3	581	3.9	5.4	5.7	24	2.5	2.4	5.8	24
MAKA	4	CH	10.6	8.1	593	2.9	12.5	7.6	24	2.6	9.1	9.1	24
MAKA	5	AC	12.2	10.6	1580	4.9	12.7	9.3	24	5.3	12.4	9.1	24
MAKA	5	CD	1.5	11.4	1137	2.4	1.3	11.1	24	3.2	.7	11.3	24
MAKA	5	CH	7.5	9.6	1153	5.3	7.8	7.2	24	6.1	7.3	7.6	24
MAKA	6	AC	10.4	9.8	2400	6.6	10.9	7.6	24	4.8	9.4	8.7	24
MAKA	6	CD	1.4	10.5	1957	5	1.6	9.4	24	4.7	.5	9.5	24
MAKA	6	CH	6.3	8.4	1972	5.6	6.9	6.2	24	5.5	5.6	6.7	24
MAKA	6	CF	3.9	22.3	445	6.4	5.3	21.9	23	6.5	3.6	22	23
MAKA	7	AC	14.1	13.2	1617	4.9	9.7	7.7	24	12.4	18	0	24
MAKA	7	CD	.1	11.6	1284	2.7	.1	11.5	24	2.5	.4	11.5	24
MAKA	7	CF	10.9	21.8	385	7.7	7.9	19.3	19	8.7	11.4	18.3	19
MAKA	7	CH	5.2	11.3	647	1.9	5	11.3	24	2.4	5.6	11	24
MAKA	8	AC	17.9	12.5	1282	5.7	15	10.5	24	7.3	20.2	0	24
MAKA	8	CD	.3	11.4	1245	2.4	.6	11.3	24	2.6	.3	11.3	24
MAKA	8	CF	13.5	20	400	8.1	11.4	16.1	20	9.2	14.4	16.2	20
MAKA	8	CH	6.9	12	679	2.8	6.4	11.7	24	2.5	7.2	11.3	24

TABLE 4-6: DIURNALLY-AVERAGED STATISTICS - 10.2 KHz CONT'D.

MAKA	9	AC	20	11.4	1549	6.1	21.2	9.6	24	8.2	20.1	10.2	24
MAKA	9	CH	5.5	11.1	863	3.7	4.8	11.9	24	5.2	5.8	9.9	24
MAKA	9	CD	-1.3	5.5	397	1.7	.2	5.7	23	2.5	-2.3	3.9	23
MAKA	9	CF	8.3	22.7	153	0	7.4	23.9	13	7.1	8.2	21.7	13
MAKA	10	AC	-1.7	11.7	1315	8.1	-.7	9.3	23	8.4	-3.3	6.5	23
MAKA	10	CD	-2.1	9.5	954	7	-2	7.4	24	6.5	-.7	7.5	24
MAKA	10	CH	2	5.9	615	2.6	2.3	4.8	24	2.9	3.7	4.5	24
MAKA	10	CF	8.1	19.3	344	6.1	9.8	17.4	17	6.8	7.2	17.7	17
MAKA	11	AC	-2.9	12	1621	7.7	-2.3	9.3	24	8.7	-3.7	8.6	24
MAKA	11	CD	.6	10.5	2142	5.3	0	9	24	6	2.1	8.9	24
MAKA	11	CH	11.4	11.9	779	5.7	10.7	8.8	24	6.7	12.8	7.5	24
MAKA	11	CF	-1.7	23.9	360	6.4	-5.7	23.4	19	6	.3	23	19
MAKA	12	AC	-.9	11.5	2260	8.7	-1.9	6	24	9.5	-.2	6.5	24
MAKA	12	CD	.1	8.3	2459	6	0	5.3	24	5.8	.9	5.9	24
MAKA	12	CF	16.3	21.2	247	5.6	12.9	21.1	14	7.5	16.5	15.7	16
MAKA	12	CH	9	10	1238	3	6.8	8.7	24	4	10.8	6.1	24
MARC	2	AC	14.7	17.6	65	6.7	16.7	12.2	5	9.3	14.5	14	5
MARC	2	AH	25	12.6	53	7.7	34.4	3.5	4	9.8	18.8	16.8	4
MARC	2	BE	18.8	25.3	50	8.2	22.7	22.7	4	8.7	19.6	23.2	4
MARC	2	BH	.8	24.6	38	11.1	-.4	23.1	3	7	-2.7	22.1	3
MARC	2	CD	7.2	18.4	89	11	8.1	15.3	6	10.5	8.4	14.4	6
MARC	2	EH	7.8	24.2	85	8	11.7	20.9	6	10.6	8.1	19.6	6
MARC	7	EH	23.5	12	18	12	23.5	0	1	0	0	0	0
MARC	9	AC	9	24	35	10.3	8.4	16.3	3	9.6	10.9	19	3
MARC	9	AH	19	14.9	37	10.7	19.7	9.1	3	11.8	20.5	6.3	3
MARC	9	BE	-3	21	46	10.4	-2.1	16.1	4	10.6	-2.4	16	4
MARC	9	BH	24.7	18.5	61	8.6	24.9	14.9	5	8.8	27.4	11.9	5
MARC	9	CD	4.6	13.8	112	9.9	5.7	8.6	9	9.2	5.1	8.5	9
MARC	9	EH	3.2	20.2	54	7.1	5.1	15.7	4	8.6	1.1	17.1	4
MIYA	4	AH	10.9	9.6	564	7.9	10.9	5.2	24	6.6	11.1	4.8	24
MIYA	4	CH	-15.8	8.7	573	5.5	-17.6	7.6	24	4.5	-14.7	9.3	24
MIYA	4	EH	6.7	17.6	599	4	4.9	16.4	24	3.4	7.4	16.4	24
MIYA	6	AH	9	9	1284	4.2	9.6	7.9	24	3.4	8.8	8.5	24
MIYA	6	CH	-16.3	12.1	1247	4.9	-16.4	11.3	24	4.6	-16.3	11.1	24
MIYA	6	EH	-1.6	15.9	1056	3.6	-.6	15.3	24	4.3	-1.6	15.4	24
MIYA	7	AH	10.7	7.8	591	3.3	11.5	6.7	24	3.3	10.3	7.6	24
MIYA	7	CH	-14.6	10.3	623	5.2	-16.3	9.9	24	5.3	-13.3	10.4	24
MIYA	7	EH	-.9	16.6	584	3.8	-2.2	15.3	24	4.4	.1	15.5	24
MIYA	8	AH	12.1	6.7	610	4.3	12.8	4.5	24	4.4	11.6	4	24
MIYA	8	CH	-12.6	9.2	629	5	-14	8	24	5.5	-11.4	8.7	24
MIYA	8	EH	1.4	18.1	614	4.5	1.4	17.2	24	4.3	1.2	17.4	24
MIYA	9	AH	14	6.2	526	4.4	14.1	4.4	24	4.5	14.1	3.3	24
MIYA	9	CH	-11.8	8.8	553	5.3	-11.7	6.7	24	5.8	-12.6	4.9	24
MIYA	9	EH	1.7	15.2	575	3.9	.3	13.8	24	3.8	2.5	14.2	24
MIYA	10	AH	14	9.5	552	6.4	13.5	3.7	24	9.7	14.5	8	24
MIYA	10	CH	-9.8	8.2	541	6.4	-9.8	4.9	24	5.7	-9.9	4.1	24
MIYA	10	EH	2.1	15.1	572	3.8	3.6	14.6	24	4.3	.6	14.4	24
MIYA	11	AH	16.6	10.7	640	7.9	16.7	5.3	24	7.5	16.3	6.8	24
MIYA	11	CH	-17.5	10.1	564	6.9	-17.5	6.7	23	6.7	-17.1	7	23
MIYA	11	EH	4.9	17.3	655	3.1	5.2	16	24	3.2	4.5	17.3	24
NELC	7	BF	-2.1	19.6	324	7.6	-1.1	18.4	14	7.8	-2.6	17.9	14
NELC	7	CD	.2	4.9	681	2.1	0	4.3	24	2.4	.4	4.2	24
NELC	7	DH	6.8	4.8	650	2	7.3	4	24	2.5	6.6	4.3	24
NELC	7	EF	-6.3	25.8	247	7.1	-6.7	25.4	11	7.2	-6.4	24.5	11
NELC	11	CD	7.5	12.5	224	4.2	16	8.5	10	2.9	-2	4.3	10
NOS2	7	BD	-9.9	19	304	4.7	-9.6	18.3	21	5	-8.1	18.5	21
NOS2	7	CD	-2.2	5.2	467	2.3	-1.4	4.6	24	2.1	-2.8	4.1	24
NOS2	7	CH	4.2	5.1	451	2.6	4.9	3.7	24	2.7	3.8	4.5	24
NOS2	7	DF	-11.6	13.9	183	5	-12.5	12.7	12	4.9	-9.7	13.9	12
NOS2	7	DH	6.5	3.7	451	2.1	6.4	2.5	24	2.3	6.5	2.4	24

TABLE 4-6: DIURNALLY-AVERAGED STATISTICS - 10.2 KHz CONT'D.

NOSC	1	BD	-13.5	18.8	505	4.7	-11.3	17.9	22	5.7	-12.8	17.8	22
NOSC	1	CD	-5	6	633	2.2	-5.3	5.2	24	2.4	-4.7	5.7	24
NOSC	1	CE	-3.5	24.2	353	7	-5.3	24.3	17	6.9	-3.6	24	17
NOSC	1	CH	-2	10.7	590	5.7	-5.7	6.8	24	6.9	.7	6.5	24
NOSC	1	DF	-8.2	14.7	349	5.8	-7.3	13.3	16	5.5	-8.5	12.5	16
NOSC	1	DH	2.3	8.5	572	4.9	-.5	4.8	24	6.8	4.7	0	24
NOSC	2	BD	-15.5	21.4	394	6.2	-14.3	20.7	22	6.4	-13.9	20.2	22
NOSC	2	CD	-2.7	6.4	499	1.9	-4.6	6.4	24	2	-1.9	6.6	24
NOSC	2	CE	-1.9	26.6	355	7.9	-4.2	24.9	22	8.5	-.1	25	22
NOSC	2	CH	10.7	7.5	461	2.5	9.7	7.1	24	3.2	11.2	5.1	24
NOSC	2	DF	-9.4	14.8	238	4.8	-8.2	12	14	6.3	-11	10.4	14
NOSC	2	DH	13.5	6.8	454	2.7	14.3	5.1	24	3.8	13.4	6.2	24
NOSC	3	BD	-11.6	20.5	376	5.7	-9.9	20.5	23	6	-10.9	19.2	23
NOSC	3	CD	-2.9	5.3	448	1.8	-3.1	5.4	24	1.8	-2.9	5.1	24
NOSC	3	CE	2.8	23.6	197	0	-.6	13.5	6	6.7	2.5	8	17
NOSC	3	CH	16.1	7.3	416	2.4	16.5	6.5	24	2.6	16	7.1	24
NOSC	3	DF	-13.8	10.8	142	5.5	-12.3	7	11	5.1	-13.1	7	11
NOSC	3	DH	19	7.1	413	2.6	19.5	5.7	24	2.8	18.9	6.9	24
NOSC	4	BD	-9.5	23.4	405	6.5	-9.3	22.3	20	4.9	-8.8	21.8	20
NOSC	4	CD	-3.3	5.5	634	1.7	-3.4	5.6	24	1.8	-3.4	5.1	24
NOSC	4	CE	-3.6	25.1	291	9.3	-4.9	24.3	16	9.4	-2.3	24.3	16
NOSC	4	CH	12.4	7.2	599	3.4	13.8	6.5	24	2.2	10.9	8.3	24
NOSC	4	DF	-13.1	8.8	320	3.2	-13.5	8	13	3	-12.6	8.6	13
NOSC	4	DH	15.7	6.8	595	3.7	17.3	5.9	24	2.4	14.3	8.6	24
NOSC	5	BD	-5.7	19.3	543	4.8	-3.4	19.2	23	5.2	-8.3	17.4	23
NOSC	5	CD	-3.1	4.4	620	2	-2.9	4	24	1.8	-3.3	3.6	24
NOSC	5	CE	.8	25.4	395	6.6	1.9	24.2	18	7.1	0	24.8	18
NOSC	5	CH	8	5	608	2.6	8.6	4.5	24	2.5	7.5	4.8	24
NOSC	5	DF	-5.6	20.1	401	4.9	-4.8	19.6	17	4.5	-4.5	20.3	17
NOSC	5	DH	11.2	4.4	613	2.6	11.5	4	24	2.6	10.9	4.1	24
NOSC	6	BD	-8.6	23.7	407	4.6	-7.4	23.4	22	5.3	-10.8	22.3	22
NOSC	6	CD	-1.9	4.7	483	1.7	-2.5	4.2	24	1.7	-1.9	4.5	24
NOSC	6	CE	1.1	22.8	259	4.3	-5.6	24.5	18	7.8	2.3	21.4	18
NOSC	6	CH	7.8	4.5	503	2	7.2	3.8	24	1.8	8	2.8	24
NOSC	6	DF	-13.7	8.8	250	4.1	-13.6	8.7	13	4.2	-13.2	7.7	13
NOSC	6	DH	9.7	3.4	469	1.7	9.7	2.8	24	2.1	9.9	2	24
NOSC	7	BD	-6.4	22.4	416	5.4	-6.6	21.5	21	5.9	-6.6	21.6	21
NOSC	7	CD	-.5	4.8	542	1.5	-.7	4.6	24	1.9	-.1	4.4	24
NOSC	7	CE	12.1	21.3	136	9.6	9	18.9	9	6.9	12.2	18.2	9
NOSC	7	CH	7.3	4.7	537	2.1	7.9	4	24	2.3	6.6	4.8	24
NOSC	7	DF	-12.2	8	259	4.1	-12.3	7.9	13	3.9	-11.2	6.8	13
NOSC	7	DH	7.9	3.6	533	1.7	8.7	2.7	24	2.2	6.8	4.5	24
NOSC	8	BD	-8.6	21.4	352	5.3	-7.6	20.6	21	7.8	-7.6	19.9	21
NOSC	8	CD	-.7	5.1	407	2.1	-.5	4	24	3.8	-1.3	3.2	24
NOSC	8	CE	-4	21.5	151	7.4	-.5	19.3	9	8.5	-7.1	18.2	9
NOSC	8	CH	6.3	5.6	567	2.1	6.9	4.7	24	2.2	6	5.5	24
NOSC	8	DF	-9.1	10.2	200	6.6	-8.6	6.2	12	6.7	-8.9	6.5	12
NOSC	8	DH	7.1	5.2	372	2.1	7.2	3.9	23	3.2	7.5	4	23
NOSC	9	BD	-7.3	21.9	371	5.8	-8.9	20.3	21	4.2	-5.3	21	21
NOSC	9	CD	-1.8	4.3	499	1.7	-1.8	4	24	1.9	-1.9	3.8	24
NOSC	9	CE	.7	27.4	56	6.3	4.3	25.5	5	4.8	-15.1	17.6	5
NOSC	9	CH	5.5	7.4	472	2.6	5.3	7.2	24	2.6	5.6	6.5	24
NOSC	9	DF	-8.6	12.5	252	5.9	-6.6	11.1	14	4.1	-9.2	10.1	14
NOSC	9	DH	7.4	7.2	463	2.6	7.4	6.8	24	2.5	7.6	6.1	24
OSHI	6	AH	14.6	8.2	604	3	14.5	7.5	24	3.2	14.9	7	24
OSHI	6	CH	-4	7.6	599	3.4	-3.3	6.6	24	4	-4.9	5.8	24
OSHI	6	DH	-6.3	6.8	597	3	-6.4	5.7	24	3	-6.1	5.7	24
OSHI	6	EH	4.9	19.1	387	3.3	5.4	18.3	24	2.9	7.2	16.8	24
PANA	4	AD	8	12.8	245	2.5	15	14.8	15	7.4	4.5	8.1	15
PANA	4	BD	11.4	18.4	233	6.4	9.4	17.6	12	7	13	12.4	12

TABLE 4-6: DIURNALLY-AVERAGED STATISTICS - 10.2 KHz CONT'D.

PANA	4	CD	-8.8	14	396	5.3	-8.9	18.4	18	5.3	-9.9	7.5	18
PANA	4	CF	-4.6	27	203	8	-5.3	23	11	8	-5.7	24.4	11
PANA	4	DH	25.5	11.8	16	12.3	28.1	0	1	10.9	23	10.1	1
PANA	5	AD	6.5	9.1	333	0	5.3	8	23	5.7	7	5.3	24
PANA	5	BD	12.7	17.3	200	0	16.2	10.1	13	6.8	12.2	16.2	15
PANA	5	CD	-11.9	7.1	356	0	-9.9	6.6	24	3.1	-11.9	4	24
PANA	5	CF	-25.9	9.7	209	0	-26.6	9.6	14	3.3	-26.1	7.6	15
PANA	6	AD	5.3	10.1	587	5	6.8	7.8	24	6.2	5.6	8.3	24
PANA	6	BD	11.1	20.4	578	7.7	9.4	19.7	18	7.2	11.7	18.5	18
PANA	6	CD	-13.4	6.5	980	2.5	-13.9	5.7	24	3	-13.1	6.6	24
PANA	6	CF	-24.9	9.8	538	2.5	-25.5	9.7	13	2.9	-25.2	10	13
PANA	6	CH	1.2	14.5	34	12.3	2.3	3.2	2	14.1	.5	3.3	2
PANA	7	AD	1.3	10.8	512	6.7	.2	8.1	20	6.2	1.7	8.1	20
PANA	7	BD	14.2	16	395	7.7	9.9	16.9	15	8.1	11.8	14.1	15
PANA	7	CD	-13.6	6.6	978	3.1	-13.3	5.9	24	3	-13.9	5.1	24
PANA	7	CF	-22.6	9.4	426	4.5	-22.5	8.3	13	4.8	-23.2	6.7	13
PANA	7	CH	-1.9	24	52	13	-2.1	20.5	3	9.9	-3.9	20.7	3
PANA	7	DH	-.3	28.2	104	13.3	-.6	24.9	6	9.7	0	25.3	6
PANA	9	AD	-12.7	21.8	139	8.7	-11.9	19.3	12	5.6	-12.1	20.5	12
PANA	9	BD	-19.7	14.7	255	5.3	-23.1	13.8	13	6.4	-17.2	16	13
PANA	9	CD	-15.4	15.9	487	4.3	-15.7	13.5	23	4.7	-15.6	15	23
PANA	9	CF	-5.1	23	339	7.8	-7.1	22	18	7.5	-2.7	21.7	18
PANA	10	AD	.9	17.3	130	0	-13.7	12.9	4	11.3	1.7	9.4	10
PANA	10	BD	-3.4	24.6	187	0	-19.9	20.7	6	8.2	-3.1	16.3	14
PANA	10	CD	-13.9	10.7	308	0	-13.4	8.2	9	4.4	-14.1	0	24
PANA	10	CF	-8.3	22.2	177	0	-18.9	5.5	2	8	-7.6	0	15
PANA	11	AD	5.3	10.6	490	7	5.3	6.8	24	6.4	5.7	7.5	24
PANA	11	BD	12.6	16.9	296	6.7	14.5	16	16	5.8	10.5	17.1	16
PANA	11	CD	-15.1	6.2	536	3.2	-13.2	4.8	24	3	-17.1	0	24
→ PANA	11	CF	-27.3	10.9	451	5.5	-28.2	9.4	23	4.6	-27.6	10.3	23
PANA	12	AD	.9	10.7	232	6.7	1.3	9	18	4.3	4.6	6.3	18
PANA	12	BD	-.9	28.9	161	5.7	1.1	28.4	14	3.1	-1.3	26	13
PANA	12	CD	-15.9	7.3	267	3.4	-14.6	5.2	21	1.2	-23.2	0	19
PANA	12	CF	-26.2	11.3	203	7.4	-26.3	8.1	17	2.9	-24.2	8.5	16
PANA	12	CH	8.7	25.7	53	13.4	8.6	21.5	5	2.7	12.9	19.5	5
PYRA	1	AC	2.8	8.8	888	5.8	-1.4	5	24	4.8	8.3	0	24
PYRA	2	AC	3.4	11.9	1390	9.2	4.9	8	24	7.5	-.2	8.8	24
PYRA	3	AC	-3.9	10.1	1501	7.7	-4.2	7.6	24	8.3	-4	4.7	24
PYRA	4	AC	6.6	10.8	912	8.1	8.2	6.9	24	7.8	5.2	7.5	24
PYRA	5	AC	8.5	6.4	514	3.9	8.8	5.9	24	2.8	7.7	5.7	24
PYRA	6	AC	6	4.8	983	3	6.7	3.6	24	2.9	5.2	4.5	24
PYRA	7	AC	9.7	5.3	1078	2.8	8	3.7	24	3.2	11.6	0	24
PYRA	8	AC	16.6	7	689	2.4	14.9	4.8	24	2.4	18.1	0	24
→ PYRA	9	AC	20.8	9.3	943	6.1	22.5	7.4	24	5.2	20.4	9.5	24
PYRA	10	AC	-3.7	10.5	1103	8.2	-2.3	9.4	23	6.2	-6.4	5.6	23
PYRA	11	AC	-3.3	10.5	915	7.5	-6.3	6.4	24	7.8	-1.1	6.8	24
PYRA	12	AC	5.3	8.9	1120	4.2	.9	5.4	24	6.8	8.7	0	24
SEAT	1	BD	-6.9	15	191	8.6	-7.3	10.4	11	9.6	-7.6	10.2	11
SEAT	1	CD	-4.2	6.3	533	3.5	-4.7	4.7	24	3.9	-3.7	5.3	24
SEAT	1	CE	-9	14	302	7.7	-11.5	9.4	16	9.9	-5.9	10.6	16
SEAT	1	CH	-9.6	11.8	511	5.7	-14.6	8.8	24	5.9	-4.7	10.8	24
SEAT	1	DF	20.8	14.2	324	7.5	18.8	11.9	17	8.5	19.7	10.7	17
SEAT	1	DH	-6	9.4	480	5.2	-10.2	7.1	24	5.1	-1.7	6.9	24
SEAT	3	BD	-10.2	16.4	517	7	-13.1	14.4	23	4.3	-8.4	15.9	23
SEAT	3	CD	-1.9	5.4	610	2.7	-2.6	4.9	24	2.8	-1.2	4.5	24
SEAT	3	CE	29	13.9	10	0	0	0	0	13.9	29	0	1
SEAT	3	CH	4.7	11.6	587	5.3	1.4	9.4	24	6.6	8.5	3.4	24
SEAT	3	DF	-3.6	9.1	21	7.6	-3.1	0	1	10.4	-4.2	0	1
SEAT	3	DH	6.4	9.5	574	4.5	4.1	7.9	24	5.2	9.4	1.4	24
SEAT	4	BD	-8.5	17.3	510	3.5	-9	17.4	22	3.4	-8.4	16.8	22

TABLE 4-6: DIURNALLY-AVERAGED STATISTICS - 10.2 KHz CONT'D.

SEAT	4	CD	1.1	5.9	592	3.4	-.1	4.5	24	3	2.4	3.8	24
SEAT	4	CE	1.6	24.1	61	8.5	-.1	22.6	4	14.6	3.2	20.2	4
SEAT	4	CH	6.4	10	540	6	4.4	7.9	24	6.2	7.9	4.1	24
SEAT	4	DF	-36	7.3	52	6.4	-32.8	0	3	6.4	-38.8	0	3
SEAT	4	DH	5.3	7.2	533	4.6	4.5	6.2	24	4	5.5	4.5	24
SEAT	5	BD	-5.2	20.8	634	2.9	-4.2	20.7	24	2.5	-5.7	20.1	24
SEAT	5	CD	5.5	6.7	645	2.2	4.9	6	24	2	5.9	5.7	24
SEAT	5	CE	19	14.5	46	15.3	18.1	0	2	13	20.6	0	2
SEAT	5	CH	11.6	6.4	588	3.4	11.2	5.5	24	3.4	11.7	4.6	24
SEAT	5	DF	-15.9	31.3	178	6.5	-17.8	30.5	8	7.5	-15.5	30	8
SEAT	5	DH	5.8	4.5	593	3.2	5.7	3.1	24	3.3	5.8	2.5	24
SEAT	6	BD	-5.1	20	592	2.2	-5.4	19.7	24	2.1	-5.4	19.7	24
SEAT	6	CD	9.2	9.6	611	1.4	8.7	8.5	24	2.1	10	8.6	24
SEAT	6	CH	17.9	9.8	494	6.3	16.5	5.9	22	6.4	19.5	0	22
SEAT	6	DF	-24.2	23.8	202	6.7	-24	23.7	9	7.3	-20.6	24.4	9
SEAT	6	DH	7.9	10	492	6.4	7.1	6	22	6.2	9	5.8	22
SEAT	7	BD	-5.3	20.1	749	6.3	-4.5	19.1	24	9.1	-5.6	18.9	24
SEAT	7	CD	5.7	9.9	1127	7.9	5.4	5.2	24	8.1	5.6	5.2	24
SEAT	7	CH	7.9	15.2	794	10.7	8.1	8.2	24	11.3	5.9	8.3	24
SEAT	7	DF	-8	28.6	460	20	-11.1	17.1	15	18.6	-12.2	17.1	15
SEAT	7	DH	3.5	6.4	826	4.4	3.5	2.9	24	5.3	3.1	2.6	24
SEAT	8	BD	-7.2	17.3	385	5	-6.7	13.8	21	7.1	-5.9	16.1	21
SEAT	8	CD	3.9	8.2	777	6.2	4	4.9	24	5.9	2.5	3.9	24
SEAT	8	CE	-6.5	11.8	90	8.8	-7.5	8.4	6	6.1	-4.3	7	6
SEAT	8	CH	1.4	6.7	673	4.7	2.3	4.9	24	3.3	1.3	4.2	24
SEAT	8	DF	4.6	29.1	258	11.5	6.5	25.8	16	11	4.7	25.8	16
SEAT	8	DH	1.5	6.8	497	4.1	2.3	4.5	24	3.2	-.2	3.5	24
SEAT	9	CH	-1.9	7.4	1049	4.6	-1.3	5.4	24	5.1	-2.2	5.2	24
SEAT	9	DF	24.4	12.7	326	10	23.8	9.1	10	10.2	22.4	8.2	10
SEAT	9	DH	-2.3	6.8	1035	3.7	-1.6	5.2	24	4.6	-2.4	4.9	24
SEAT	9	BD	-17.7	5	37	4	-19.7	0	2	3.6	-15.6	8.1	2
SEAT	9	CD	-.5	4.3	572	2.7	.3	2.6	24	3	-1.4	2.2	24
SEAT	10	BD	-12.5	7.8	123	6.5	-11.9	3.3	9	6.3	-13.9	0	9
SEAT	10	CD	-2	4.9	359	3.3	-2	3.3	24	3.4	-2.5	2.6	24
SEAT	10	CE	-1.2	12.6	108	9.7	-2	8.7	8	8	1.3	5.4	8
SEAT	10	CH	-5	13.4	222	10.6	-6.6	7.5	16	9	.3	0	16
SEAT	10	DF	17.8	15.1	193	9.7	16.4	10.9	13	7.6	18.7	9.6	13
SEAT	10	DH	-5.9	13.6	135	10.7	-6.9	7.4	10	11	-.5	0	10
SEAT	11	BD	3.2	17.3	216	8.7	1.2	14.8	12	8.7	3.3	13.7	12
SEAT	11	CD	-6.9	6.5	550	3.4	-5.5	4.9	24	3.8	-8.2	1.3	24
SEAT	11	CE	-12.1	15.9	344	10.8	-8.3	12.1	17	8.8	-15.7	4	17
SEAT	11	CH	-2.3	11.1	485	5.8	-1.2	9.5	24	5.7	-3.6	8	24
SEAT	11	DF	14.4	13.2	405	8.5	13.8	9.6	21	8.1	13.2	10.2	21
SEAT	11	DH	4.4	8.3	492	4.8	5	7	24	4.5	4	6.7	24
SEAT	12	BD	-2.3	19.2	136	4.9	-6.4	14.1	10	7.5	-4.1	15.4	10
SEAT	12	CD	-4.2	4.6	426	3.2	-1.1	3	23	2.9	-5.2	0	24
SEAT	12	CE	-15.2	14.6	259	7.5	-11.2	13.3	19	8.4	-16.6	7.3	19
SEAT	12	CH	-3.6	9.5	392	4.5	2.5	6	23	7.1	-5.6	0	24
SEAT	12	DF	16.1	15.2	183	5.5	11.5	13.2	12	8.3	14.9	9.8	12
SEAT	12	DH	.4	8.1	362	4.9	2.2	5.3	24	5.8	-.3	4.9	24
TSUS	1	AH	19.9	13.4	1039	6.2	21.4	12.1	24	6.6	20.6	12.6	24
TSUS	1	CH	-7.5	13.8	1110	6.5	-7.4	13.4	22	5.7	-9.3	12.6	22
TSUS	1	DH	17.7	14.3	977	9.1	19.3	10.7	24	9	17.3	12.5	24
TSUS	1	EH	15	21.7	603	3.6	15.1	20.9	24	3.5	15.5	20.9	24
TSUS	2	AH	21.6	12.6	440	5.4	22.9	9.7	19	6.3	19	13.6	19
TSUS	2	CH	-7.1	17.4	529	6.4	-6.7	16.6	22	6	-7.9	15.9	22
TSUS	2	DH	20.6	13.7	466	6.4	25.5	10	21	7.2	17.1	15.8	21
TSUS	3	AH	22.5	13.2	181	5.7	22	12	15	1.1	28.3	12.1	1
TSUS	3	CH	-5.2	18.1	442	5.9	-4	17.8	21	4.6	-5.8	17	21
TSUS	3	DH	18.4	15.9	311	7.9	23.7	10.8	17	6.9	11.1	15.9	17

TABLE 4-6: DIURNALLY-AVERAGED STATISTICS - 10.2 KHz CONT'D.

TSUS	4	AH	16.8	17.2	958	7.8	18.4	16	24	6.9	15.3	15.8	24
TSUS	4	CH	-8.4	16.2	985	10	-8.8	13.4	24	10.4	-9.4	12.9	24
TSUS	4	DH	9.2	19.7	944	9.1	15.5	16.2	24	8.2	5.7	18	24
TSUS	5	AH	16.1	11.4	1080	5.2	15.7	10.3	24	4.8	15.4	10.2	24
TSUS	5	CH	-8.3	16.2	1069	4.7	-7.3	14.2	23	6.2	-8.8	14	23
TSUS	5	DH	11.3	15.7	1040	5.9	10.7	14.1	24	6	12.5	12.6	24
TSUS	6	AH	13.3	10.3	1877	5.5	13.8	8.7	24	5.3	12.7	9.4	24
TSUS	6	CH	-7.1	15.4	1865	9.5	-6.5	12.9	24	9.3	-7.4	12.5	24
TSUS	6	DH	12.4	14.1	1797	6.6	12.8	12.6	24	6.2	12.2	12.8	24
TSUS	6	EH	5.1	19.1	392	3.4	5.8	18.6	24	2.8	6.2	19.1	24
TSUS	7	AH	12.4	10.3	1262	3.6	12.4	9.8	24	3.7	12.8	9.2	24
TSUS	7	CH	-8.2	15	1812	3.9	-8.9	14.7	23	4.3	-8	14.6	23
TSUS	7	DH	12.2	15.8	1798	5.6	12.9	14.8	24	6.2	11.9	14.8	24
TSUS	7	EH	4.8	25.2	1167	4.8	2.7	25	24	4.9	5.6	24.9	24
TSUS	8	AH	16.6	13.4	1475	4.8	17.5	10.3	24	5.1	16.8	11.6	24
TSUS	8	CH	-7.2	14.8	1831	4	-8.5	14.3	24	4.1	-7.1	14.8	24
TSUS	8	DH	9.4	17.3	1683	5.9	9.4	15.7	24	6.4	9.1	15.9	24
TSUS	8	EH	9.4	25	1198	4.3	10.2	25.4	24	4.4	9.4	25.7	24
TSUS	9	AH	15.5	16.3	603	5.2	15.5	15.5	23	4.9	16	14.9	23
TSUS	9	CH	-4.7	15.7	607	3.6	-4.9	15.5	24	3.4	-3.9	15.1	24
TSUS	10	AH	13.8	29.4	48	6.9	11.6	30.6	4	0	0	0	0
TSUS	10	CH	.4	7.2	85	6.1	.4	3	7	0	0	0	0
TSUS	10	DH	25.5	12.3	12	12.3	25.5	0	1	0	0	0	0
TSUS	11	AH	19	14.4	818	7.6	19.7	12.4	23	7.1	19.3	13	23
TSUS	11	CH	-7.7	14	789	5.4	-7.4	12.9	22	5.8	-8.5	12.5	22
TSUS	11	DH	12.8	15.6	831	8.8	13	12.6	24	9.8	13.4	11.9	24
TSUS	11	EH	17.9	20.3	612	3.3	18.1	19.3	22	3.4	17.9	20.1	22
TSUS	12	AH	23.9	11.3	1177	7.7	25	8.4	24	7.4	23.2	10.4	24
TSUS	12	CH	-9.6	14.2	1192	7.8	-10.2	11.4	24	8.1	-9.4	12	24
TSUS	12	DH	20.3	13.5	1167	10.8	22.6	8	24	10.3	19.3	11.4	24
TSUS	12	EH	10.3	21.7	563	3.1	11	22.2	24	3.8	11.7	21.6	24
WAHI	1	AC	9.6	5.9	348	2.8	11	4.9	24	3.9	8.7	6.3	24
WAHI	1	CD	-10.9	6.8	398	3.1	-10	6.5	24	3.6	-10.5	5.8	24
WAHI	1	CF	10.3	22.3	235	7.8	9.7	20.3	16	8.4	9.4	20.1	16
WAHI	1	CH	1.2	8	391	2.3	2.6	7.7	24	3.2	2	7.6	24
WAHI	2	AC	3.7	10.5	366	4.1	2.5	7.6	24	5.6	5.9	6.7	24
WAHI	2	CD	-4.8	7.4	481	3	-4.7	6.9	24	3.3	-3.4	7.2	24
WAHI	2	CF	-1	23	278	8.4	1.1	20.8	16	8.4	-4.7	19.8	16
WAHI	2	CH	3.3	8.9	481	2	4.3	8.6	24	2.3	4	8.4	24
WAHI	3	AC	15.3	19.4	177	0	0	0	0	9.9	15.2	0	15
WAHI	3	CD	1	4.8	312	0	1	4.2	22	2.9	1.1	3.4	22
WAHI	3	CF	-2.1	22.6	121	0	-3.9	18.7	6	7.8	-2.3	14	10
WAHI	3	CH	9	7.7	323	0	8	7.2	23	2.1	9.5	5.5	24
WAHI	4	AC	-7.2	7.5	322	4.9	-6.9	5.5	24	4.5	-7.3	4.7	24
WAHI	4	CD	1.8	5.3	428	2.9	.5	4.4	24	2.6	3	3.1	24
WAHI	4	CF	-4.6	23.7	278	8.1	-1	20.9	18	7.7	-6.7	20.6	18
WAHI	4	CH	9.6	7.5	428	2.2	9.4	7	24	1.3	9.6	6.8	24
WAHI	7	CH	-6.5	25	207	9.3	-6.3	22.8	14	7.5	-7.9	22.9	14
WALE	1	AR	1.6	5.3	510	3.5	-.2	2.5	24	3.9	3.8	0	24
WALE	1	CR	-4.1	6	582	2.8	-5.9	5.7	24	2	-3	6.1	24
WALE	2	AR	.6	6.1	222	3	2.5	2.9	18	5.4	-.6	0	18
WALE	2	CR	-6.4	6.1	434	3	-7.6	5.4	24	2.5	-7.2	6	24
WALE	3	AR	-3.4	10.1	70	4.2	5.4	3.3	7	3.6	-12.3	0	7
WALE	3	CR	-2.5	4.2	220	3	-1.1	1.8	15	3.5	-3.6	0	15
WALE	4	AR	8.2	5.7	273	6.1	8.3	3.1	22	3.5	7.8	2.5	22
WALE	4	CR	-5.4	7.2	440	2.7	-9.3	6.1	24	3.7	-8.2	6.1	24
WALE	5	AR	3.8	3.4	211	2.4	3.6	2.5	17	2.3	3.9	1.4	17
WALE	5	CR	-2.6	3.9	542	2.3	-2.6	3.2	24	1.9	-3	2.9	24
WALE	6	AR	2.2	3.5	183	2.4	1.3	1.7	16	2.4	3.1	0	16
WALE	6	CR	-2.5	3.3	427	2	-2.8	2.7	24	1.8	-2.6	2.4	24

TABLE 4-6: DIURNALLY-AVERAGED STATISTICS - 10.2 KHz CONT'D.

WALE	7 AR	2.6	4.3	377	3.8	3.1	1.9	24	2.8	1.6	2.2	24
WALE	7 CR	-2.6	3	442	1.7	-2.8	2	24	1.8	-2.3	2.2	24
WALE	8 CR	-4.1	4.8	539	2.3	-4.5	3.2	24	2.3	-3.4	4.1	24

TABLE 4-6: DIURNALLY-AVERAGED STATISTICS - 10.2 KHz CONT'D.

CASE ID			GRAND MONTHLY STATS			FIRST SEMI-MONTH				SECOND SEMI-MONTH			
①	②	③	④	⑤	⑥	⑦	⑧	⑨	⑩	⑪	⑫	⑬	⑭
ADAK	2	AD	-5.1	8.5	351	4.8	-6.6	4.8	24	5.9	-4	5.2	24
ADAK	2	AH	7.1	10.2	347	3.7	5	9.2	24	4.8	9.4	3.4	24
ADAK	2	CD	-10.8	9	461	5.8	-12	5.6	24	8.5	-10.4	5.9	24
ADAK	2	CE	-2	22.9	366	4.3	.1	21.9	22	4.7	-.7	21.9	22
ADAK	2	CH	-.8	12.8	442	2.7	-1	11.5	24	3.8	-.5	11.4	24
ADAK	2	EH	5.4	22.8	365	3.4	4.2	22.3	22	3.9	4.7	22.2	22
ADAK	3	CD	-9.6	9.3	431	6.9	-11.7	5.3	24	6.1	-3.8	4.9	24
ADAK	3	CE	3.2	23.6	407	3.7	2.9	23.8	23	3.6	5.7	22.8	23
ADAK	3	CH	.1	12.5	456	2.8	-.4	12.3	24	1.8	1.6	11.7	24
ADAK	3	EH	.4	22.6	388	3.6	.7	23.1	21	3.5	-.5	22.1	21
ADAK	4	AD	-.8	7.5	434	5.6	-2	4.5	24	6.5	0	3	24
ADAK	4	AH	8.3	11	428	5.3	6.6	8.4	24	7.2	8.9	6.6	24
ADAK	4	CD	-7.9	8.5	564	6.4	-8.6	5.1	24	7.6	-7.3	4.7	24
ADAK	4	CE	-3.8	22.9	512	2.7	-2.2	22 6	23	3.8	-2.9	22.5	23
ADAK	4	CH	2.2	9.7	388	2.4	2.6	10.3	24	2.8	2.1	8.7	24
ADAK	4	EH	4.5	23.4	477	2.6	3.4	22.7	22	3.1	3.1	22.8	22
ADAK	5	AD	-10.6	13.9	11	0	0	0	0	13.9	-10.6	0	1
ADAK	5	CD	18.7	6.7	285	0	0	0	0	4.3	18.6	0	23
ADAK	5	CE	8.1	24.6	192	0	0	0	0	3.6	8	0	17
ADAK	5	CH	31.9	6.7	301	0	0	0	0	3.5	31.8	0	24
ADAK	5	EH	10.2	24.8	200	0	0	0	0	5.9	9.7	0	18
ADAK	6	AD	-9.7	11.2	93	0	0	0	0	9.7	-9.7	0	9
ADAK	6	AH	-3	8.7	147	0	5.7	0	1	6.8	-3	0	14
ADAK	6	CD	23.6	7	445	2.9	22.9	6.1	24	3	24.1	3	24
ADAK	6	CE	14.2	25.6	364	2.9	12.7	26.4	19	3.1	16.6	25.1	19
ADAK	6	CH	30.9	5.9	488	2.4	30.4	5.5	24	2.6	31.3	0	24
ADAK	6	EH	1.5	22.7	472	3.5	2.1	22.5	24	3.5	-.5	22.3	24
ADAK	7	AD	11.7	6	312	1.6	8.9	6	20	2.2	12.5	0	24
ADAK	7	AH	11.8	5.4	315	2	14	4.7	23	2.9	11.5	6.4	23
ADAK	7	CD	-1.9	7	434	4.3	-4.6	5.3	24	3.7	-.7	5.1	24
ADAK	7	CH	-1.3	5.8	451	2.7	-.2	4.9	24	2.7	-1.6	4.7	24
ADAK	8	AD	-24.3	10.6	10	6.5	-27.5	0	1	11.5	-23.6	8.6	1
ADAK	8	CH	-25.2	13.8	13	14	-17.7	0	1	11.5	-29.9	0	1
ADAK	8	EH	5.1	31.3	420	2.4	3.5	31.5	24	2.1	4.9	31	24
ADAK	9	AD	17.7	8.9	366	4.3	15.4	4.7	21	5.8	19.1	0	21
ADAK	9	AH	18.6	8.3	400	3.2	18	7.2	24	3.6	18	7.2	24
ADAK	9	CD	-7.1	9.4	521	6.1	-6	3.1	24	9.4	-8.1	0	24
ADAK	9	CE	-9.2	19.6	536	3.8	-8.1	19.2	23	3.7	-9.5	18.7	23
ADAK	9	CH	-3	7.6	587	2.2	-3.1	7.3	24	2.4	-3.1	6 8	24
ADAK	9	EH	7.5	21.7	548	3.1	6.9	21.2	24	2.9	7.7	21.1	24
ADAK	10	AD	4.1	13.4	203	8.4	7.6	8	17	4	-9.8	0	16
ADAK	10	AH	14.1	13.9	182	10.8	17.2	6.7	15	5.3	4.1	9.5	15
ADAK	10	CD	-12.1	9.5	288	7.7	-10.7	4.7	21	5.8	-16.7	0	21
ADAK	10	CE	-.6	21.6	236	4.3	-1.4	21.2	21	3.8	-1.2	20.6	15
ADAK	10	CH	-5.5	9	239	5.1	-5.2	7	20	3	-4.5	6.5	20
ADAK	10	EH	-3.1	23.2	106	6.1	-1.8	21.9	10	7.9	-5.1	23.3	7
ADAK	11	AD	-7	9.1	490	6.3	-7.4	4.8	24	6.7	-6.8	5.7	24
ADAK	11	AH	10.6	11.4	483	6.4	8	10	24	4.8	11.7	6.7	24
ADAK	11	CD	-16.9	9.2	522	6.1	-16	5.4	24	6.9	-17.6	2	24
ADAK	11	CH	-.7	11.5	558	3.3	-.6	10.8	24	3	-.5	11	24
ADAK	11	EH	-10	15	20	15	-4.4	0	1	12.8	-15.6	0	1
ADAK	12	AD	-2.5	9.6	508	7.7	-3.4	6.8	24	6.3	-1.6	5.7	24
ADAK	12	AH	12.8	10.1	515	7.2	10.5	8	24	6.1	14.9	0	24
ADAK	12	CD	-13.3	9.2	570	7.5	-10.5	5.9	24	6.9	-15.6	0	24
ADAK	12	CH	0	10	541	3.6	.2	10.1	24	4.2	-.4	9.2	24
ANCH	1	AC	.3	7.4	495	3.3	1.4	6	24	4.3	-.4	5.9	24
ANCH	1	AD	2	5.7	482	4.3	2.1	3.8	24	4.2	2	3.5	24
ANCH	1	AH	-3.4	10.3	475	3.5	-5.5	8.9	24	4.3	-3.4	9.2	24
ANCH	1	CD	2.4	6.9	527	4.7	2.2	4.2	24	5.1	2.7	4.3	24
ANCH	1	CH	-4.3	11.8	517	2.8	-7	11.4	24	3.3	-3.1	11.7	24

TABLE 4-7: DIURNALLY-AVERAGED STATISTICS - 13.6 KHz

ANCH	1	DH	-6	11.1	490	4.6	-8.6	9.7	24	5.2	-5.3	10	24
ANCH	2	AC	1.8	8.2	290	3	.2	7.7	23	3.2	3.3	5.2	23
ANCH	2	AD	3.2	7.6	261	4.7	1.3	3.4	20	5.5	4.9	0	20
ANCH	2	AH	.1	14.3	279	3.8	-.4	11.9	22	4.3	.3	12.4	22
ANCH	2	CD	1.1	8	356	4.3	.2	6.3	24	5	2.2	5.4	24
ANCH	2	CH	-.7	13.6	353	3.4	.3	12.2	24	3.9	-1.2	12.3	24
ANCH	2	DH	-2.1	10.6	322	4.4	-.2	8.8	24	4.9	-3.5	8.2	24
ANCH	3	CD	7	6.7	210	0	0	0	0	5.3	7.1	0	18
ANCH	3	CH	7.5	10.9	204	0	0	0	0	4.6	7.7	0	17
ANCH	3	DH	1.6	9.8	132	0	0	0	0	5	1.3	0	12
ANCH	6	AC	8.5	3.7	333	.8	8	1.9	18	2.6	8.6	0	24
ANCH	6	AD	19	3.8	274	2.7	19.4	1.9	17	3	18.8	0	21
ANCH	6	AH	11.8	5.7	335	1.8	13.5	3.1	18	2.7	11.6	3.7	24
ANCH	6	CD	10.6	4.4	292	2.7	11.5	2.6	18	2.7	10.4	0	22
ANCH	6	CH	3.4	7.2	345	1.6	5.5	4.2	18	1.3	3	5.3	24
ANCH	6	DH	-6	5.2	293	1.9	-6	3.8	18	2.7	-6.1	0	22
ANCH	7	AC	7.2	3.5	522	2.2	7.3	2.6	24	2.3	7.1	2.7	24
ANCH	7	AD	21.4	3.7	536	2.4	21	2.2	24	2.4	21.6	0	24
ANCH	7	AH	11.1	5.2	528	2.6	11.5	4.8	24	2.5	10.7	5.2	24
ANCH	7	CD	14.4	4.6	528	2.4	13.8	3.4	24	2.7	14.7	0	24
ANCH	7	CH	4	6.8	531	1.7	4.2	7	24	2.2	3.7	6.5	24
ANCH	7	DH	-10.2	5.4	538	2.3	-9.4	4.8	24	2.7	-10.8	2.1	24
ANCH	8	AC	18.9	5.2	591	4.1	19.7	2.9	24	4.1	18.3	5.7	24
ANCH	8	AD	31.5	5.2	546	3.8	33.4	2.7	21	4.3	30	3.9	23
ANCH	8	AH	21.7	6.3	606	4.5	24	2.2	24	5.7	20.3	8.9	24
ANCH	8	CD	13.2	5.1	565	2.7	13.4	4	23	4.3	12.8	3.2	24
ANCH	8	CH	3	5.4	725	2.3	4.4	4.1	24	3.3	1.9	4.7	24
ANCH	8	DH	-10.2	4.8	566	2.7	-9	3.3	24	3.7	-10.9	0	24
ANCH	9	AC	20	6.9	681	5.3	20.2	3.8	24	5.4	20.5	2.5	24
ANCH	9	AD	30.7	6.4	615	5	30	2.8	23	5.8	32	0	23
ANCH	9	AH	20.1	8.8	681	6.5	20.5	4.8	24	6.3	19.9	6	24
ANCH	9	CD	9.8	6.9	747	3.8	10.2	4.8	24	5.7	9.4	5	24
ANCH	9	CH	-.1	6.6	846	3.2	.7	5.6	24	4	-1.4	4.5	24
ANCH	9	DH	-9.8	7.1	753	4.8	-9.6	3.2	24	7.2	-9.9	2	24
ANCH	10	AC	5.2	10.9	536	6.6	11.8	5.8	23	8	.2	2.4	23
ANCH	10	AD	10.3	12.9	437	7.9	19.7	6.2	19	8.1	3.1	8.2	19
ANCH	10	AH	5.1	13.4	344	8.9	8.7	8.8	16	8.9	1.6	8.5	16
ANCH	10	CD	4.7	6.5	560	4.1	8.2	3.5	24	4.8	2.2	3.9	24
ANCH	10	CH	-1.5	8.7	480	5.3	-2.3	6.1	24	5.4	-.7	4.9	24
ANCH	10	DH	-4.7	10.3	468	8.2	-9	4.2	24	7	-2.1	5.3	24
ANCH	12	AC	5.3	6.8	445	4.6	2	4.8	24	3.7	6.6	0	24
ANCH	12	AD	6	6.3	459	5.3	4.3	4.1	24	4.6	6.6	0	24
ANCH	12	AH	1.4	10.5	420	4.5	-1.2	7.6	24	4.2	1.3	8.4	24
ANCH	12	CD	1.5	5.8	474	3.9	2.7	4.5	24	4	.6	3.7	24
ANCH	12	CH	-2.9	10.7	492	3.2	-.7	9.1	24	3.9	-4.7	8.6	24
ANCH	12	DH	-3.5	11.2	458	3.5	-3.9	10.2	24	4.3	-4.5	9.9	24
HOKK	1	AC	23.2	11.4	445	7.6	22.1	8.2	24	8.1	24.5	0	24
HOKK	1	AD	-1.5	10.3	451	7.8	-4.4	5.4	24	7.3	.5	5.3	24
HOKK	1	AE	8.5	18.1	448	5.2	10.1	16.6	24	5	9	17.5	24
HOKK	1	BC	15.7	23.5	301	7.3	17.6	22.6	17	10.2	13.1	22.9	17
HOKK	1	CE	-11.6	22.3	443	5.4	-10.9	21.3	24	5.7	-13.1	20.4	24
HOKK	1	CH	-7.4	10.2	499	4.6	-7.7	9.1	24	5.5	-7.9	8.2	24
HOKK	2	AC	23.2	12.4	326	5.7	25.6	9.8	23	5.3	22.6	13.2	23
HOKK	2	AD	2.5	11.4	354	6.3	2.3	7.3	24	7.7	1.9	7.4	24
HOKK	2	AE	8.2	17.2	340	6.4	10.2	15.2	22	6.2	10.5	15.5	22
HOKK	2	BC	11.6	26.6	266	5.6	15.1	25.9	19	6.3	9	25.9	19
HOKK	2	CE	-2.5	21.7	327	4.3	-4.7	20.9	20	5	-1.3	21	20
HOKK	2	CH	-8.5	11.3	425	4.5	-10.3	9.4	24	4.3	-7.7	11	24
HOKK	3	BC	21.7	13.7	93	0	0	0	0	9.3	21.6	0	9
HOKK	3	CE	2.1	21.7	469	3.7	1.7	21.8	22	3.4	-.3	21.5	22

TABLE 4-7: DIURNALLY-AVERAGED STATISTICS - 13.6 KHz CONT'D.

HOKK	3	CH	-7.5	10.2	544	3.8	-7.7	9.9	24	3.8	-8.5	8.5	24
HOKK	4	AC	13.5	11.3	400	6.3	11.2	9.4	24	7.5	14.6	1.8	24
HOKK	4	AD	2.9	10.6	420	6.9	1.7	8.9	24	7.9	3.4	5.5	24
HOKK	4	AE	.5	22.3	386	6	-.5	19.7	24	7.1	2.6	19.7	24
HOKK	4	BC	21.1	14.2	282	8.7	19.8	11.7	18	8.6	19.8	11.1	18
HOKK	4	CE	-3.4	19.9	388	5.5	-3	19.5	20	4.3	-3.2	19.2	20
HOKK	4	CH	-5.4	9.2	520	4.7	-5.4	8.5	24	3.4	-6.7	7.3	24
HOKK	5	AC	11.7	7.6	579	4.8	10.7	6	24	5.1	12.8	0	24
HOKK	5	AD	1.7	8.1	556	4.8	3.5	5.2	23	5.6	0	3.9	23
HOKK	5	AE	.9	19.7	577	4.3	-.4	19.2	24	4.3	1.8	18.9	24
HOKK	5	BC	16.4	14.6	557	6.1	15.3	11.8	24	6.1	17.7	10.9	24
HOKK	5	CE	-5.1	19.5	503	3.3	-5	19.8	21	3.3	-6.2	19.5	21
HOKK	5	CH	-5.1	9.5	605	3.6	-4.5	7.7	24	3.3	-6.1	7.8	24
HOKK	7	AC	10.7	8.7	806	5.2	9.5	7.1	24	5.3	11.7	4.4	24
HOKK	7	AD	2.6	6.7	818	3.7	.5	6	24	4.1	3.5	3.4	24
HOKK	7	BC	18	11.5	658	7.7	16.7	8.7	22	6.9	18.6	6.1	22
HOKK	7	CE	-9.8	20.4	509	6.2	-10.1	21.7	23	4.9	-10.5	21	23
HOKK	7	CH	-7.5	10.4	1045	4.1	-7.2	9.8	24	4.7	-8.2	8.9	24
HOKK	7	AE	-1.4	17.2	346	4	-1.3	17.2	23	3.6	-1.2	16.7	23
HOKK	8	AC	17.7	8	792	4.6	17	6.1	24	5.5	18.6	1.7	24
HOKK	8	AD	10.1	8.1	712	3.6	10.5	6.5	24	6	10.3	5.5	24
HOKK	8	AE	8.6	18.6	780	3.5	7.1	17.3	24	5	7.7	17.9	24
HOKK	8	BC	18.5	10.7	1003	8.3	19.4	7.5	24	7.6	17.7	7.8	24
HOKK	8	CE	-7.4	20.6	1051	4.3	-9.7	21.1	24	4.2	-9.8	20.7	24
HOKK	8	CH	-6.4	8.8	1130	4.9	-7.5	7.9	24	4.2	-6	7.9	24
HOKK	9	AC	19.5	10.8	270	5.9	17.8	8	23	3.3	24.5	0	23
HOKK	9	AD	7.2	9	294	5	6.7	6.4	24	3.3	8.2	6.1	23
HOKK	9	AE	9.2	21.5	298	5.6	7.9	20.4	24	3.2	15.3	16.8	24
HOKK	9	BC	20.6	9.4	232	7.5	20	5.4	19	5.4	21.6	0	19
HOKK	9	CE	-6.6	20	475	3.6	-6.7	20.2	22	4.1	-6.5	19.5	22
HOKK	9	CH	-2.7	7.5	547	3.7	-2.9	5.9	24	4	-2.6	6.2	24
HOKK	10	AC	18.9	13.3	436	7.2	21.9	7.9	24	8.6	17.5	11.2	24
HOKK	10	AD	.1	12.7	385	9.9	3.1	8.7	22	7.9	-1.4	6.8	22
HOKK	10	AE	10.7	18.8	408	7.8	17.8	16.4	21	9.5	7.1	17.4	21
HOKK	10	BC	26.1	12.8	245	8.1	26.6	6.3	14	9.4	25.8	8.5	14
HOKK	10	CE	1.1	20.4	369	4.5	4.9	18.5	21	5.8	-1.4	18	21
HOKK	10	CH	-4.6	8.8	425	4.8	-4	6.6	23	5.4	-4.9	4.9	23
HOKK	11	AC	20.7	12	354	10.3	17.2	5.2	20	7.6	23.7	0	20
HOKK	11	AD	-.6	11.6	415	6.7	0	8.7	24	6.6	-1.2	8.6	24
HOKK	11	AE	4.3	20.6	427	8.9	3.7	18.4	24	6.6	7.8	17.4	24
HOKK	11	BC	16.9	15.3	227	10	16.8	11.8	14	9.5	16.8	10.7	14
HOKK	11	CE	-.8	23.1	368	4.8	.3	21.7	21	4.6	-.8	22	21
HOKK	11	CH	-8.6	10.5	457	4.2	-8.5	9.3	24	4	-9.5	8.8	24
HOKK	12	AC	21.9	12.1	401	7.2	17.4	6.5	22	8.7	25.9	0	22
HOKK	12	AD	-1.4	11.6	442	9.4	-.8	7	24	7.9	-1.2	4.1	24
HOKK	12	AE	8.3	20.1	479	6.7	4.9	17.6	24	6.7	14.4	12.6	24
HOKK	12	BC	24.1	12.7	249	8.9	19.8	7.1	15	7.5	27.2	0	15
HOKK	12	CE	-11	22.2	402	4.7	-13.2	19.6	23	6	-10.9	20.8	23
HOKK	12	CH	-7.3	9.7	487	5.4	-6.1	7.4	24	5	-9.4	4.8	24
KURE	3	CE	1.1	16	138	9.7	1.5	11	10	5.4	-5.7	9.5	10
KURE	3	CH	15.3	16.6	90	9.4	17.2	13.2	7	5.9	12.6	14.3	7
KURE	3	DH	10	14.9	142	8.9	11.6	11.7	10	5.1	5.7	13.2	10
KURE	3	EH	22.1	13.1	45	12.8	23.2	4.4	3	4.4	21.6	5.1	3
KURE	7	AD	6.7	6.3	380	2.8	6	6.1	24	2.5	7.1	4.5	24
KURE	7	CE	2.7	12.5	228	4.6	3.5	11.4	20	2.6	-.6	11.2	20
KURE	7	CH	9.5	9.6	459	3.8	11.1	9.3	22	3.9	9	9.7	22
KURE	7	DH	9.1	5.7	484	3.1	10.8	5.1	24	3.1	9	6.4	24
KURE	7	EH	5	14.4	232	3.6	5.7	14.5	20	2.3	4.8	13.8	20
KURE	8	AD	12.1	7.7	312	3.2	11.6	7.2	24	3.4	12.7	5.6	24
KURE	8	AE	9.9	16.7	300	3.8	8.1	15.1	24	4.7	8.9	15.7	24

TABLE 4-7: DIURNALLY-AVERAGED STATISTICS - 13.6 KHz CONT'D.

KURE	8	CE	3.6	14.3	521	6.4	2.8	14.3	24	5.6	2.9	13.2	24
KURE	8	CH	8.2	9.2	440	4.7	8.5	8.4	19	5.1	8.3	8	19
KURE	8	DH	1.7	11.6	457	4.2	0	12.1	21	6	-.1	12	21
KURE	8	EH	.7	12.7	432	4.1	1.3	12.4	20	4.4	1.8	12.4	20
KURE	9	AD	15.7	10.3	290	3.9	14.2	6.4	21	5.9	16.5	3.1	21
KURE	9	AE	14.8	16.5	336	4.3	15.7	13.3	24	5.7	14.4	14.8	24
KURE	9	CE	-.5	13.3	469	4.4	.8	9.9	24	5	-1.6	11	24
KURE	9	CH	6.5	10.7	413	4.2	7.4	8.9	21	5.8	6.2	9.5	21
KURE	9	DH	8.7	10.5	377	4.7	8.7	8.8	22	4.2	7.9	9.6	22
KURE	9	EH	6.5	14.9	411	4.8	6.5	13.3	22	5.3	7.6	13.2	22
MAKA	1	CD	4	6.7	583	4.1	5.2	6.2	24	3.3	3.9	6.4	24
MAKA	1	AC	1.6	7.9	572	4.6	.6	6.5	24	3.9	2.3	6.2	24
MAKA	1	CD	-.4	7.3	586	4.4	.8	6.5	24	3.6	-.7	6.1	24
MAKA	1	AC	.6	13	327	5.2	-1.7	12.1	22	4.3	2.5	11.5	22
MAKA	1	AC	7.6	11.2	869	6.4	8.5	9	24	6.1	6.5	9.7	24
MAKA	1	CD	-3.2	9.7	947	5.7	-2.6	8.6	24	4.7	-2.5	8.6	24
MAKA	1	CF	-7	21.3	452	5.2	-5.4	21.4	20	5.2	-7.5	20.5	20
MAKA	1	CH	1.6	10.9	607	3.4	1.8	10.1	24	4.1	1.7	10.2	24
MAKA	2	AC	4.6	13.3	1188	8.3	5	9.9	24	6.8	2.8	10.9	24
MAKA	2	CD	-.1	10.7	877	5.5	.5	8.8	24	3	-.1	10	24
MAKA	2	CF	-6.5	18.2	307	6.1	-4.5	17.1	19	5.5	-7.4	16.6	19
MAKA	2	CH	4.9	11.6	432	2.5	5.6	10.5	24	2.6	4.9	10.8	24
MAKA	3	AC	4.2	11.1	1079	9.8	1.1	6.7	24	7.7	5.7	2.8	24
MAKA	3	CD	-2.6	10.9	537	4.5	-1.5	11.7	24	3.4	-2.2	11.1	24
MAKA	4	AC	14.1	11.2	1072	7.4	11.4	8.4	24	5.9	16.5	0	24
MAKA	4	CD	1.2	11	532	2.4	1.5	11	24	2.3	.6	10.8	24
MAKA	5	AC	14.7	10.6	1915	5.8	15	8.2	24	5.6	14.2	9.3	24
MAKA	5	CD	1.2	12.3	1131	2.3	0	11.7	24	3.8	1.3	11.8	24
MAKA	5	CH	3	12.1	923	5.1	3.2	9.8	24	4.9	3.3	10.4	24
MAKA	6	AC	14.4	9.8	2176	5.7	15.4	8.3	24	5.3	13.2	9.7	24
MAKA	6	CD	.5	11.5	1921	6	.1	9.9	24	5.5	.5	9.9	24
MAKA	6	CF	-1.2	25.6	412	4.8	-1.3	25.7	23	5.2	-1.6	26.2	23
MAKA	6	CH	1.1	11.1	1301	5.8	.6	10	24	4.9	1.4	9.5	24
MAKA	7	AC	15.6	10.9	2476	5.5	13.7	6.6	24	10.3	17.1	0	24
MAKA	7	CD	0	9.4	2511	4.8	-.2	8.2	24	4.8	.3	8.1	24
MAKA	7	CF	-.6	22.9	382	5.6	-3.2	23	19	6.7	1.1	22.5	19
MAKA	7	CH	3.1	9.1	1879	5.4	2.9	7.6	24	5.5	3.3	7.2	24
MAKA	8	AC	19.8	10.9	1620	5.3	17.5	9.4	24	6.4	20.9	2.3	24
MAKA	8	CD	-.3	9.4	2436	5.4	-.1	7.8	24	5	-.1	8.1	24
MAKA	8	CF	-2.9	24.5	376	6.1	-7.5	23.3	21	5.8	-1.1	23.9	21
MAKA	8	CH	4.8	9.3	1865	6.6	4.8	6.3	24	6.3	5.3	6.5	24
MAKA	9	AC	20.2	11.5	1013	6.4	21.6	9.7	24	6.9	20.1	10.4	24
MAKA	9	CH	3.6	14	652	3	3.5	14.1	24	2.8	3.8	13.4	24
MAKA	10	AC	4.9	13.5	1875	12.1	8.3	9.3	23	9.7	1.7	7.1	23
MAKA	10	CD	-3.4	11.3	1583	5.6	-3.4	11.4	24	5.5	-2	10.9	24
MAKA	10	CH	.5	12	1089	6.1	.7	9.1	24	5.4	1.3	9.7	24
MAKA	10	CF	2.3	25.9	216	4.1	-.4	27.3	12	4.9	-.6	26.1	12
MAKA	11	AC	-1.2	8.3	298	3.9	-5.7	6.9	24	3.8	1.4	4.9	24
MAKA	11	CD	-.8	7.6	625	3.7	-1.4	7.2	24	3.8	.3	6.5	24
MAKA	11	AC	.5	11.3	478	5.4	1.2	9.4	23	5.7	0	9.7	23
MAKA	11	AC	4	14.8	839	7	4.9	13.4	24	7.4	2.5	13.2	24
MAKA	11	CD	-3.2	12.7	990	3.5	-3.4	12.7	24	4.1	-1.3	13.2	24
MAKA	11	CH	1	11.8	202	3.6	-2.5	9.3	14	6.3	2.5	8.4	16
MAKA	11	CF	-.3	18.7	406	6.7	-1.7	15.7	19	4	-.4	17	19
MAKA	12	AC	3.2	7.3	445	3.8	.2	3.3	24	3	6.9	0	24
MAKA	12	CD	-2.1	4.9	606	3.1	-1.3	3.5	24	3.2	-2.5	2.9	24
MAKA	12	CD	.7	10.6	564	3.2	1.8	10.6	23	4.1	.8	10.5	23
MAKA	12	AC	10.1	11.4	1091	6.7	8.1	8.9	24	6.8	10.9	7	24
MAKA	12	CD	-4.2	9.1	1171	4.6	-3.2	8.2	24	5.1	-3.7	8	24
MAKA	12	CF	-7.2	20.9	394	5.2	-10.8	18.4	19	5.3	-6.6	20.1	19

TABLE 4-7: DIURNALLY-AVERAGED STATISTICS - 13.6 KHz CONT'D.

MAKA	12	CH	2.9	9.3	545	3.1	3.1	8.3	24	3.5	3.4	8.5	24
MARC	2	AC	-4.3	21	215	7.3	-3.9	19	17	4.9	-6.4	18.4	17
MARC	2	AH	-9.7	27.2	88	10.3	-12.8	23.8	6	8.3	-5.6	25.8	6
MARC	2	BE	2	24.5	165	4.1	3.1	26.1	13	6.3	1.8	23	13
MARC	2	BH	-8.7	26.1	181	10.3	-13.7	23.7	13	9.5	-3.5	23.7	13
MARC	2	CD	-19.2	10.4	83	8.3	-15.8	7.9	5	5.4	-20.5	0	6
MARC	2	EH	-6.6	31.3	47	11.4	-14.8	26.6	3	10.8	-3	28.3	3
MARC	9	AC	-5.9	19.4	34	10	-6.3	12.3	3	9.7	-7.5	14.9	3
MARC	9	BE	-2.6	24.9	78	9.8	-2.9	22.4	6	13.9	.2	20.6	6
MARC	9	BH	-1.1	26	72	11.2	-1.3	22.8	6	8.9	-.5	23.3	6
MARC	9	CD	-23.4	13.4	35	8.6	-25.5	9.4	3	7.8	-24	11.4	3
MARC	9	EH	11.6	23.5	75	10.8	10.9	17.6	6	11.3	10.7	18.9	6
NOSC	1	BD	-2	21.9	347	4.8	-1.4	20.7	16	5.5	-4	20.6	16
NOSC	1	CD	-2.1	7.5	626	4	-2	6.1	24	3.7	-2.1	6.2	24
NOSC	1	CE	-1.8	25.3	471	5.9	-2.4	24.1	21	5.8	-.4	24.3	21
NOSC	1	CH	0	10.6	597	5.3	-3.1	8.1	24	6.3	2.1	6.6	24
NOSC	1	DF	-16.2	12.2	546	5.1	-14.7	11.2	23	4.9	-16.8	9	23
NOSC	1	DH	2.2	10.2	579	4.6	-1.3	7.9	24	6	4.2	5.7	24
NOSC	2	BD	4.3	21.7	292	5	3.9	20.8	18	5.9	5.9	20.1	18
NOSC	2	CD	0	7	471	2.9	-3	5.8	24	2.9	1.5	5.3	24
NOSC	2	CE	0	22.2	303	4.3	-2.2	21.4	19	5.1	2.6	20.3	19
NOSC	2	CH	8.3	10.1	426	3	6.7	9.2	24	3.4	9.2	7.4	24
NOSC	2	DF	-21.1	12.5	425	5.5	-18.6	10.2	23	5.9	-21.9	6	23
NOSC	2	DH	8.9	10.9	421	3.4	9.9	9.3	24	3.8	8	10.2	24
NOSC	3	BD	-2.4	26.4	335	5.4	-2.6	25.3	21	5.4	-3.7	25.1	21
NOSC	3	CD	-.6	5.8	437	2.5	-.3	5.7	24	2.4	-.9	5.2	24
NOSC	3	CE	-.5	24.3	174	0	-6.4	23.3	5	5.9	1.1	14.1	14
NOSC	3	CH	13.9	8.9	410	3.1	14	7.9	24	2.9	13.6	8.2	24
NOSC	3	DF	-18.6	17.4	206	6.1	-17.3	17.2	15	6.2	-18.6	14.9	15
NOSC	3	DH	14.6	8.6	407	2.7	14.4	8.2	24	3.1	14.4	7.7	24
NOSC	4	BD	-3.6	21.3	250	6.6	-4.3	20.5	13	3.7	-4.5	19.3	13
NOSC	4	CD	-.5	7.4	621	2.9	-1.3	6.2	24	3.1	.3	6.4	24
NOSC	4	CE	-7.3	21.4	289	7.9	-11.5	20.5	16	8.4	-5	20.2	16
NOSC	4	CH	10.3	8	592	3.7	11.4	7.2	24	2.9	9.2	8	24
NOSC	4	DF	-17.3	13.1	408	3.1	-17.6	12.5	16	3.4	-18.1	18.6	16
NOSC	4	DH	11.1	8.2	598	3.8	13.1	7.6	24	2.8	8.6	[illegible]	24
NOSC	5	BD	-7.9	17.9	429	4.7	-7.6	18.5	18	[illegible]	-11.5	15.7	18
NOSC	5	CD	1	8.4	615	3.1	1.4	8.1	24	2.9	.4	7.7	24
NOSC	5	CE	-.1	26.1	414	5.9	1.3	25	19	6.1	-1.4	25	19
NOSC	5	CH	8.9	7	608	3	9.5	6.7	24	3.2	8.3	6.8	24
NOSC	5	DF	-18.2	13.5	407	3.3	-18.7	13.3	17	2.9	-19.1	13.2	17
NOSC	5	DH	8	5.5	609	3	8	5	24	2.7	8.2	4.3	24
NOSC	6	BD	-1.5	20.2	295	4.4	-.3	20.8	16	5	-3	19.3	16
NOSC	6	CD	-.5	5.7	487	2.3	-.6	5.5	24	1.9	-.5	5.3	24
NOSC	6	CE	-1.6	25.4	287	4.7	-3.4	23.8	20	6.4	-1.3	23.9	20
NOSC	6	CH	5.6	5.1	502	2.2	5	4.6	24	2	5.6	3.9	24
NOSC	6	DF	-17.5	11.5	300	2.6	-18	11.4	15	3	-17.9	11.6	15
NOSC	6	DH	6.2	4.9	480	2.1	5.9	4.6	24	2.1	6.1	4.1	24
NOSC	7	BD	.4	19.5	317	4.5	.8	18.9	16	5.2	.8	18.6	16
NOSC	7	CD	.9	5.3	529	2.3	1	5	24	2.3	.6	4.5	24
NOSC	7	CE	-3	23.6	133	8	-1.7	21.2	10	5	-2.7	22.6	10
NOSC	7	CH	5.8	5.2	531	2.7	6.8	4.3	24	2.8	4.5	5.1	24
NOSC	7	DF	-19.8	18.4	425	4.2	-19.8	18.7	21	4.1	-21	18	21
NOSC	7	DH	4.9	4.6	532	1.9	5.8	3.7	24	2.4	3.8	4.6	24
NOSC	8	BD	4.6	22.6	316	6.1	3.9	20.8	18	7.7	5.7	20.7	18
NOSC	8	CD	1.8	6	407	3	1.9	4.8	23	3.9	.6	4.6	23
NOSC	8	CE	.3	24.9	240	5.6	7.6	22.2	12	9.8	-6.3	20.4	12
NOSC	8	CH	3	4.8	555	2.4	3.7	3.7	24	2.7	2.7	4.1	24
NOSC	8	DF	-17.6	13.9	282	4.1	-18	12.5	17	5.4	-17.8	12.6	17
NOSC	8	DH	1.5	5.8	403	2.9	1.9	4.1	24	3.6	2.2	4.5	24

TABLE 4-7: DIURNALLY-AVERAGED STATISTICS - 13.6 KHz CONT'D.

	NOSC	9	BD	8.6	21.1	334	4.3	5.6	20.4	18	4.9	7.9	20	18
	NOSC	9	CD	.7	5.4	511	2.6	.3	4.8	24	2.8	1	4.3	24
	NOSC	9	CE	8.1	22.8	147	8.8	14.2	18.2	12	6.2	-.7	19	12
	NOSC	9	CH	3.2	6.4	509	2.2	3.4	5.7	24	2.6	3.4	5.8	24
	NOSC	9	DF	-16.9	12.9	335	3.7	-16.3	12	17	3.6	-17.5	11.4	17
	NOSC	9	DH	2.1	7.1	503	2.9	2.8	6.4	24	3	1.5	6.2	24
	OSHI	1	CH	-6.3	13.7	582	8	-6.6	11.4	22	7.7	-6.4	10.5	22
	OSHI	1	DH	8.3	10.3	595	6.9	9.9	6.9	24	7.2	6.6	8	24
→	OSHI	3	AH	22.3	9.2	596	7.2	22.8	7.1	24	5.2	22	7.5	24
	OSHI	3	BH	5.3	16.1	597	5.1	8.9	14.5	24	5.5	3	14.8	24
	OSHI	3	CH	-.7	12.2	511	6	-7.8	11.1	20	5.9	-7.1	10.4	20
	OSHI	3	DH	1.9	8.5	577	7.9	2.6	3.4	24	6.2	1.3	4	24
	PANA	4	AD	11.5	14.9	265	2.7	21.4	17.2	16	6.8	6	14.3	16
	PANA	4	BD	1.7	26.2	232	4.5	-.4	28.9	12	5.8	2.8	23.9	12
	PANA	4	CD	-14.9	12.6	284	6.6	-13.7	13.7	13	5.5	-15.9	4.9	13
	PANA	4	CF	1.3	24.9	214	8.9	.9	24.9	11	4.7	-.3	22.7	11
	PANA	4	CH	-3.9	22	68	12.4	-5.7	17.3	4	12.3	-2.6	17.8	4
	PANA	4	DH	5.2	16.9	46	11.5	2	12.2	3	9.2	5.4	11.8	3
	PANA	5	AD	8.1	8.8	344	0	7.1	8.4	23	4.8	8.6	5.9	24
	PANA	5	BD	7.9	21.3	288	0	8.8	17.4	19	4.3	7.1	17.6	21
	PANA	5	CD	-14.1	7.7	362	0	-12.2	7.7	24	2.6	-14.2	4.9	24
	PANA	5	CF	2.3	25.7	349	0	1.7	24.9	22	3.8	2.6	23.6	24
	PANA	6	AD	5.7	8	330	2	3.7	8.3	23	3.8	5.6	6.3	24
	PANA	6	BD	5.3	22.4	434	5.2	6.1	20.3	21	4.9	5.3	21.4	21
	PANA	6	CD	-16.4	7.3	546	3.3	-16.6	6.8	24	3.2	-16.8	6.3	24
	PANA	6	CF	-4.5	24.8	562	3.7	-3.2	24.9	24	3.9	-5.1	24.2	24
	PANA	7	AD	4.8	8.6	715	4.9	4.5	7.1	24	4.9	5.3	6.4	24
	PANA	7	BD	16.6	19.4	526	7	12.6	20.3	17	7.1	13.6	19.4	17
	PANA	7	CD	-15.7	6.9	991	3.7	-14.9	5.9	24	3.9	-16.6	1.9	24
	PANA	7	CF	-3.3	24.2	959	4.9	-3.2	23.6	24	4.5	-3.7	23.7	24
	PANA	7	DH	-11.2	6.1	11	7	-9.9	0	1	3.4	-13.5	0	1
	PANA	10	AD	9.2	12	229	0	-2.8	9.5	6	8.2	9.3	0	18
	PANA	10	BD	10.2	17.2	243	0	-2.5	12.7	6	9.4	11.5	0	20
	PANA	10	CD	-15	11.5	269	0	-15.6	9.2	9	3.8	-14.9	0	21
	PANA	10	CF	-1	26.6	240	0	-4.7	24.2	6	5.1	.3	14.1	19
	PANA	11	AD	9.4	9.9	521	6.5	9.5	7.6	24	5.7	9.9	7.2	24
	PANA	11	BD	1.8	23.3	497	4.8	3.4	21.8	23	4.4	.2	22.5	23
	PANA	11	CD	-17.6	6.8	562	3.5	-16.1	5.3	24	3.6	-19	0	24
	PANA	11	CF	1.5	29.1	537	3.5	.5	28.7	24	3.6	-.1	28.6	24
	PANA	12	AD	5.5	10.4	257	6.8	5.5	8	20	3.3	9.8	3.4	20
	PANA	12	BD	-4.1	27.2	225	5.8	.2	25.4	18	3.4	-5.4	25.9	18
	PANA	12	CD	-18.9	7.5	243	3.6	-17.7	5.8	20	1.2	-24.8	0	15
	PANA	12	CF	4	28	247	4.1	3.8	28	20	1.4	-2.5	26.9	20
	PYRA	1	AC	7.4	9.3	1756	6.7	5.2	7.3	24	5.5	8.7	4.7	24
→	PYRA	1	CD	-32.9	8.5	635	3.9	-32	7.6	24	4.1	-34.6	0	24
	PYRA	1	AC	7.8	8.5	603	4.8	3.2	5.3	24	4	12.2	0	24
	PYRA	2	AC	4.1	11.4	1278	8.1	4.7	7.7	24	8.6	1.8	7.5	24
→	PYRA	2	CD	-31.1	9.8	553	3	-31.5	9.7	24	3.6	-32.1	8	24
	PYRA	2	AC	12.5	10.2	536	4.7	16.1	6.8	23	4.6	8.4	10.6	23
	PYRA	3	AC	-.1	9	1486	6.2	-.8	7.1	24	6.4	-.2	5.9	24
→	PYRA	3	CD	-30.6	10.7	705	3.2	-29.9	10	24	3.5	-31.1	7.8	24
	PYRA	3	AC	-2.5	10.1	697	6	-4	8.4	24	7.2	-1.1	6.9	24
	PYRA	4	AC	9.2	13.6	2391	14.5	7.4	5.9	24	8.8	11	0	24
	PYRA	5	AC	13.4	6.2	2419	4.1	13.3	5.4	24	3.4	13	5.3	24
	PYRA	6	AC	10	5.2	2174	3.4	11	3.8	24	2.6	9.1	5.7	24
	PYRA	7	AC	11.6	5.5	2742	3.5	10.5	4	24	4.1	12.3	0	24
	PYRA	8	AC	17.2	5.6	2529	3.8	16	3.8	24	3.3	18.1	0	24
	PYRA	9	AC	19.9	7.3	2560	4.2	19.9	6.2	24	4.4	20.1	5.1	24
	PYRA	10	AC	-.4	10	2387	8	1.3	9.2	24	6.2	-4.9	4.9	24
	PYRA	11	AC	5.2	8.8	1319	5.6	5.6	7.3	24	5.6	3.9	7.5	24

TABLE 4-7: DIURNALLY-AVERAGED STATISTICS - 13.6 KHz CONT'D.

→ PYRA	11	CD	-30.5	8.6	585	3.4	-30.6	8.5	23	4	-30.7	7.6	23
PYRA	11	AC	-3.1	8.6	558	4.4	-5	5.3	24	6.1	-1.4	6.2	24
PYRA	12	AC	6.8	9.3	2992	5.1	5.3	6.1	24	8.8	7.5	4	24
SEAT	1	BD	11	15.6	401	5.5	9.9	13.8	21	6.1	9.8	13.9	21
SEAT	1	CD	1	8.8	528	3	0	7.4	24	4	2.2	7.6	24
SEAT	1	CE	-14.2	19.4	376	5.2	-18.4	17.6	20	7.7	-9.8	19.6	20
SEAT	1	CH	-5.2	12.9	511	5.4	-9.6	10.9	24	5.5	-.9	10.7	24
SEAT	1	DF	10.6	20	411	5.2	10.1	18.8	21	6.3	8.5	19.1	21
SEAT	1	DH	-5.9	11.8	494	5.5	-9.4	10.4	24	5.3	-2.7	10.1	24
SEAT	3	BD	2.2	28.3	426	5.6	2.5	25.7	19	7.4	1.8	26.7	19
SEAT	3	CD	-1.1	7.1	619	3.1	-.7	6.4	24	3.5	-1.7	5.5	24
SEAT	3	CE	-12.8	23.5	34	0	0	0	0	12	-12.5	0	3
SEAT	3	CH	5.8	13.4	585	4.8	3.3	11.6	24	6	8.4	9.2	24
SEAT	3	DF	.6	17.3	111	6	2.3	16.8	6	9	2.2	15.5	6
SEAT	3	DH	7	12.3	584	5.4	3.9	9.9	24	7.8	10.8	0	24
SEAT	4	BD	.9	32.8	493	4.1	2.6	33.4	22	4.2	1.2	32.9	22
SEAT	4	CD	-1.1	8.4	583	4.1	-1.5	6.4	24	4.2	-1.2	6.8	24
SEAT	4	CE	-10.4	19.3	85	10.7	-16.4	14.6	6	10.8	-9.6	16.8	6
SEAT	4	CH	5.7	12.4	529	5.1	4.4	11.7	24	5.3	6	10.2	24
SEAT	4	DF	3.1	19.9	300	6.9	1.9	18.3	15	7.3	4.6	18	15
SEAT	4	DH	6.4	9.6	555	6	4.9	7.3	24	6.9	6.8	4.6	24
SEAT	5	BD	-1.6	32.5	551	3	-2.2	32.3	22	2.6	-3.3	32.4	22
SEAT	5	CD	3.8	11.7	610	3.2	3.1	10.1	24	3.1	4.6	10.6	24
SEAT	5	CE	-28.7	11.9	164	10.1	-29.8	6.4	8	9.1	-28.5	8	8
SEAT	5	CH	10.9	12.3	590	3.6	10.4	10.4	24	4.3	11.8	10.4	24
SEAT	5	DF	22.4	18.7	133	8.9	21.9	16.9	6	8.5	23.5	14.5	6
SEAT	5	DH	7	6.5	604	4.8	6.6	4.3	24	4.9	7	3.3	24
SEAT	6	BD	1.1	33.3	556	2.5	1.7	33.5	23	2.4	2.3	33.4	23
SEAT	6	CD	8	17.3	572	1.9	7	16.1	23	1.7	8.3	16.9	23
SEAT	6	CE	-21.7	14.4	175	7.4	-21.2	14.4	13	9.8	-21.6	10.3	13
SEAT	6	CH	14.2	16.3	518	2.5	13.6	15.3	23	2.5	14.3	15.8	23
SEAT	6	DF	-21.7	22.2	243	8.9	-20.8	19.2	12	9.8	-24.2	16.1	12
SEAT	6	DH	6.6	5.1	545	2.7	6.8	4.1	24	2.7	6.3	4.5	24
SEAT	7	BD	-3.5	26.5	810	14.6	-2.2	21.6	23	17.4	-4.4	19.3	23
SEAT	7	CD	6.5	18.4	1115	12.6	7.6	12.6	24	14.1	6	12.6	24
SEAT	7	CH	1.9	11.1	583	6.4	1.3	7.6	24	6.1	2.7	5.9	24
SEAT	7	DF	-18.7	24.4	501	12.9	-20.2	18.1	21	14.2	-15.9	20	21
SEAT	7	DH	9.1	12.7	613	8.3	6.9	7.9	24	8.6	6.8	6.3	24
SEAT	7	CE	-22.3	21.5	115	5.9	-23.7	19.1	7	5.9	-23.5	20.3	7
SEAT	8	BD	-5.3	22	632	13.2	-6.2	16.8	24	11.3	-5.9	15.3	24
SEAT	8	CD	.7	13.9	720	8.4	0	9.6	24	8	1.4	6.8	24
SEAT	8	CE	-19	15.5	355	6.3	-19.2	14.5	21	6.4	-18.8	14.4	21
SEAT	8	CH	3.1	6.6	742	5.5	2.9	3.3	24	4	2.7	3.4	24
SEAT	8	DF	-.2	18.5	346	7.3	.1	17.4	17	7.1	-1.3	14.8	17
SEAT	8	DH	1.9	6.2	504	3.6	3	4.4	24	3.4	0	4.2	24
SEAT	9	BD	-.7	15.5	683	8	-2.5	12.1	20	10.2	1	10.9	20
SEAT	9	CD	.7	4.8	1138	3.2	1	3.2	24	3.7	.3	3.2	24
SEAT	9	CE	-13.3	19.7	262	5.9	-12.1	20.1	14	7.1	-11.7	19.3	14
SEAT	9	CH	-.6	6.8	1109	4	.2	5	24	4	-1.2	5	24
SEAT	9	DF	4.1	17.8	693	6.8	3.8	17.7	20	5.9	4.1	17.9	20
SEAT	9	DH	-1.8	7.9	1090	5	-.8	5.7	24	5.8	-2.1	5	24
SEAT	10	BD	3.7	16.9	298	7.9	2.9	14.4	21	8.1	3.5	13	21
SEAT	10	CD	-1.1	5.2	358	3.5	-.6	3.3	24	3.6	-2.2	2.5	24
SEAT	10	CE	-8.1	12.9	190	9.3	-8.4	10.2	13	7.9	-8.8	6.5	13
SEAT	10	CH	-5.2	13.7	217	9.6	-5.5	8.4	16	9.1	-2.7	7.4	16
SEAT	10	DF	4.5	20.2	205	4.3	2.9	19.6	15	3.5	3.8	18.6	15
SEAT	10	DH	-3.7	16.5	171	11	-4.5	11.3	12	11.5	-.4	9.4	12
SEAT	11	BD	12.2	17.9	453	6.3	10.2	17	22	6.3	11.6	16.5	22
SEAT	11	CD	-3	7.9	555	3.6	-1.8	6.4	24	3.9	-4.4	5.7	24
SEAT	11	CE	-9.8	18.8	337	9.1	-7.4	18.1	17	5.9	-13.4	15	17

TABLE 4-7: DIURNALLY-AVERAGED STATISTICS - 13.6 KHz CONT'D.

SEAT	11	CH	.9	12.2	506	6	2.2	9.9	24	6.1	-.1	9.9	24
SEAT	11	DF	11.3	17.2	452	6.8	9.1	14.9	21	5.6	11.7	14.5	21
SEAT	11	DH	3.7	10.8	489	5	4.3	9.4	24	5.1	3.5	9.5	24
SEAT	12	BD	11.5	16.5	325	6.3	5.8	17.8	20	7	10.6	12.4	21
SEAT	12	CD	-.4	6.4	431	3.3	-1.2	5	24	4.6	-.1	3.2	24
SEAT	12	CE	-10.3	13.5	200	8.2	-3.5	12	14	7.5	-11.4	4.6	14
SEAT	12	CH	0	11.7	402	4.4	5.7	9.4	24	7.1	-1.7	8.2	24
SEAT	12	DF	1.8	16.8	238	4.7	1.3	11.8	16	5.3	.5	12.9	16
SEAT	12	DH	.3	11.8	372	4.2	6.8	7.6	24	7.4	-1.5	6.6	24
TSUS	1	AH	-27.3	9.4	424	6.8	-27.8	6.3	16	6.4	-27.6	6.9	16
TSUS	1	CH	-13	12.1	619	6.9	-14.2	10.1	22	6.2	-12.8	10.5	22
→ TSUS	1	DH	21.3	9.4	620	6.3	23.2	5.7	24	6.7	19.6	9.9	24
TSUS	1	EH	-.9	20.2	684	4.2	-.5	19.6	24	4.3	-.7	19.6	24
TSUS	2	AH	-26.9	10.8	341	7.1	-21.9	6.2	15	5.9	-31.7	0	15
TSUS	2	CH	-5.2	15	539	8.3	-6.5	12.5	23	6.5	-3.5	12.6	23
TSUS	2	DH	-.7	14.2	521	7.5	3.9	12.1	23	5.7	-3.8	10.1	23
TSUS	2	EH	-6.9	25.4	520	5.6	-8.4	24.3	24	6	-5.2	24.9	24
TSUS	3	AH	16.7	10.8	806	8	18.2	8.2	24	4.6	14.5	9.9	24
TSUS	3	CH	-12.7	12.2	613	6.8	-13.9	10.2	24	6.2	-12.5	10.7	24
TSUS	3	DH	15.7	8.7	562	7.7	16.7	4.9	23	5.8	15.4	6.4	23
TSUS	3	EH	4	23	636	3.4	5.8	22	24	3	4.3	23.1	24
TSUS	4	AH	16.9	14.6	1464	5.9	18.6	13.6	24	5.1	14.9	14.1	24
TSUS	4	CH	-8.3	.14	939	6.1	-10.4	15.2	24	6	-10.4	14.3	24
TSUS	4	DH	11.5	17.1	1416	7.5	16.5	14.4	24	6.4	7.8	16.7	24
TSUS	5	AH	14.6	9.2	1677	3.8	14.2	8.6	24	3.1	14.1	8.4	24
TSUS	5	CH	-2.1	15.3	1553	4.3	.5	17.9	24	5.3	.8	17.8	24
TSUS	5	DH	11.9	12.5	1615	5	11.3	11.3	24	4.8	13.1	9.4	24
TSUS	6	AH	12.4	8.9	2586	4.9	12.8	7.5	24	4.8	11.8	8.1	24
TSUS	6	CH	-1.2	16.5	2357	10.6	-.1	13.9	24	10.6	-2.2	13.6	24
TSUS	6	DH	13.5	11.6	2536	5.7	13.6	10.1	24	5.3	13.1	10.4	24
TSUS	6	EH	3.2	20.9	398	3	3.8	20.7	24	2.7	4.5	20.8	24
TSUS	7	AH	9.9	8.8	1295	3	9.9	8.3	24	3.1	10.4	7.7	24
TSUS	7	CH	-5.3	14.2	1692	4	-6.5	14.5	22	4.1	-5.7	14.3	22
TSUS	7	DH	10.9	12.3	1829	4.3	11.6	11.5	24	5.3	10.4	11.5	24
TSUS	7	EH	4.6	24.9	1117	4.1	2.1	25.1	23	4.1	5.4	24.8	23
TSUS	8	AH	15.2	12.1	892	3	14.2	9.6	24	4	15.9	9.2	24
TSUS	8	CH	-5.4	14.7	1084	4.6	-7	15.7	23	4.7	-6.6	15.3	23
TSUS	8	DH	8.7	16	1097	4.9	8.1	14.3	24	5.2	9.7	14.3	24
TSUS	8	EH	9.5	25.4	611	3.1	9.4	25.3	24	3.4	8.6	25.5	24
TSUS	9	AH	15.9	14.8	618	4.3	15.9	14	24	4.3	17	13	24
TSUS	9	CH	-1.3	14.7	542	3.6	-2.8	15	21	3.8	-.5	14.2	21
TSUS	10	AH	31.3	5.6	35	5.4	31.3	0	3	0	0	0	0
TSUS	10	CH	-2.6	4.3	85	4.1	-2.6	.5	7	0	0	0	0
TSUS	10	DH	27.4	11.7	32	11.2	27.7	.7	3	0	0	0	0
TSUS	11	AH	20.7	15.3	266	2	11.6	16	16	7.1	21.3	0	22
TSUS	11	CH	-7.3	11.5	179	.7	-15.1	11.4	12	7	-7.2	10.2	14
TSUS	11	DH	15.6	16.9	255	1.7	8.9	13.5	19	10.6	15.6	0	21
WAHI	1	AC	1.9	6.8	350	2.9	4.2	6.7	24	3.3	1.1	6.6	24
WAHI	1	CD	-3.4	6.5	402	2.4	-2.9	6.5	24	2.9	-2.7	6.5	24
WAHI	1	CF	-7.8	21.4	326	5.5	-7.5	20.8	21	6.9	-7.9	19.8	21
WAHI	1	CH	3.6	10.9	398	3	4.6	10.4	24	4.3	3.7	10.4	24
WAHI	2	AC	-3.6	10.7	365	3.5	-4.9	8.4	24	4.8	-1.7	9.1	24
WAHI	2	CD	.9	7.3	489	2.7	1	7.2	24	3.3	2.6	6.6	24
WAHI	2	CF	-8.1	18.6	351	5.7	-7.8	17	20	5.7	-9	17.3	20
WAHI	2	CH	6.7	11.1	473	2.7	7.9	10	24	2.7	7.6	10.5	24
WAHI	3	AC	-14.4	18.3	64	0	0	0	0	10.5	-13.9	0	6
WAHI	3	CD	-.5	4.4	312	0	-.4	4.5	22	2.8	-.3	3.4	22
WAHI	3	CF	-5.8	22	120	0	-7.8	20.9	8	8.8	-5.3	17	10
WAHI	3	CH	7.2	10.1	317	0	4.6	10.7	24	2.7	7.7	8.4	24
WAHI	4	AC	-3	7.8	326	4.6	-2.7	6.7	24	3.9	-3.1	5.9	24

TABLE 4-7: DIURNALLY-AVERAGED STATISTICS - 13.6 KHz CONT'D.

WAHI	4	CD	.5	4.9	430	2.4	-.2	4	24	2.2	1.4	3.7	24
WAHI	4	CF	-10	14.3	354	5	-8	14.3	22	3.9	-10.1	12.5	22
WAHI	4	CH	6.6	9	415	2.7	7	8.2	24	2.1	6.8	8.5	24
WAHI	7	CH	1.7	7.6	425	2.4	3	7	24	2.9	.4	7.1	24
WALE	1	AR	10.1	6	592	4.5	6.9	1.5	24	4.3	13.7	0	24
WALE	1	CR	-1	6	501	2.6	-2.8	5.5	24	2	0	5.4	24
WALE	1	DR	5.4	7.1	537	4.4	3.4	4.9	24	4.7	7.9	0	24
WALE	2	AR	9.9	6.8	294	3.6	12.3	3.6	20	5.8	7.8	6.3	20
WALE	2	CR	-2.4	5.6	436	2.9	-4.4	5.3	24	2.6	-2.7	5.4	24
WALE	2	DR	2.2	8.4	385	4.1	.7	5.1	24	5.8	2.1	5.4	24
WALE	3	AR	2.5	7.1	205	4.3	4.6	4.3	16	6.2	.4	0	16
WALE	3	CR	.9	4.4	224	3.7	1.9	2.1	15	3.5	.3	1.7	15
WALE	3	DR	-2.2	11	194	6	4.4	7.9	14	5.1	-7.5	0	14
WALE	4	AR	14.2	4	416	3.9	15.5	1.4	24	2.9	13.2	5.5	24
WALE	4	CR	.2	6.3	437	2.5	-3.1	5.8	24	3.5	2.4	3.1	24
WALE	4	DR	.8	10.1	392	6	-2.2	7.2	23	5	2.7	5.4	23
WALE	5	AR	13	3.8	1013	.3	13.1	1.5	24	3.7	12.8	2.2	24
WALE	5	CR	3.2	5.1	1014	2.7	1.9	3.8	24	3.6	3.8	2.3	24
WALE	5	DR	5.6	10.7	940	6.3	2.6	7.3	24	6.6	7.4	3.9	24
WALE	6	AR	13.3	3.9	943	4.4	14	0	24	3.2	12.9	3.6	24
WALE	6	CR	4.1	4.4	1005	3.3	3.5	3.1	24	2.7	4.6	2.1	24
WALE	6	DR	9.4	8.2	893	4.5	9.2	7	24	3.7	9.5	6.6	24
WALE	7	AR	11.3	3.4	1088	3.6	10.7	.4	24	2.5	11.9	0	24
WALE	7	CR	3.1	4.2	1120	2.7	3.4	3	24	2.1	2.8	3.5	24
WALE	7	DR	9.3	8.6	1025	3.7	9.1	7.5	24	3.7	9	7.3	24
WALE	8	AR	17.4	3	650	1.5	16.2	1.5	24	2.9	18.6	0	24
WALE	8	CR	2	5.5	1177	2.8	2.2	4.7	24	2.5	1.6	4.9	24
WALE	8	DR	7.9	8.7	1110	4.3	8.6	7.4	24	5.2	7.4	6.3	24
WALE	9	AR	17.7	5	834	4	15.9	1.6	24	3.5	20.3	0	24
WALE	9	CR	.8	6.7	1048	2.5	.8	6.3	24	2.5	.7	6.4	24
WALE	9	DR	5.7	8.3	940	4.8	5.1	6.5	24	4.9	7.4	4.7	24
WALE	10	AR	.9	7.5	443	4.1	4.5	6.1	23	4	-2.3	0	23
WALE	10	CR	.4	6.4	519	3.3	2.9	5.8	24	3	-1.7	4.3	24
WALE	10	DR	6.6	9.4	452	4.7	11.8	6.7	24	6.1	2.7	6.8	24
WALE	11	CR	1.2	4.1	161	1.8	-.5	2.4	15	2.8	2.5	0	15

TABLE 4-7: DIURNALLY-AVERAGED STATISTICS - 13.6 KHz CONT'D.

Thirteen cases meeting these criteria were found at 10.2 kHz, and 15 cases at 13.6 kHz. They are listed in Tables 4-8 and 4-9 respectively, and their implications will be discussed in Section 4.4.

TABLE 4-8. LARGE PPC BIAS ERRORS AT 10.2 kHz

RCVR SITE	MONTH	LOP	MEAN PHASE ERROR (CEC)	STD. DEVIATION (CEC)
ADAK	5	CH	24.8	4.4
ADAK	6	CH	23.7	4.3
ADAK	9	AH	23.2	6.8
ANCH	8	AD	26.4	6.4
ANCH	8	AH	20.3	7.9
HOKK	1	AC	24.9	11.4
HOKK	2	AC	25.9	10.9
HOKK	8	AC	21.7	7.8
HOKK	8	BC	29.5	8.9
HOKK	9	AC	24.1	11.3
PANA	11	CF	-27.3	10.9
PYRA	9	AC	20.8	9.3
TSUS	12	AH	23.9	11.3

TABLE 4-9. LARGE PPC BIAS ERRORS AT 13.6 kHz

RCVR SITE	MONTH	LOP	MEAN PHASE ERROR (CEC)	STD. DEVIATION (CEC)
ADAK	5	CH	31.9	6.7
ADAK	6	CD	23.6	7.0
ADAK	6	CH	30.9	5.9
ANCH	7	AD	21.4	3.7
ANCH	8	AD	31.5	5.2
ANCH	8	AH	21.7	6.3
ANCH	9	AD	30.7	6.4
ANCH	9	AH	20.1	8.8
HOKK	1	AC	23.2	11.4
OSHI	3	AH	22.3	9.2
PYRA	1	CD	-32.9	8.5
PYRA	2	CD	-21.1	9.8
PYRA	3	CD	-30.6	10.7
PYRA	11	CD	-30.5	8.6
TSUS	1	DH	21.3	9.4

4.3.3 Seasonally-Averaged Statistics

As described in Section 4.2, the next step is to average over semi-months to obtain seasonally averaged data which now no longer depend on time, only on frequency, receiver site and LOP. The results are given in Tables 4-10 (10.2 kHz) and 4-11 (13.6 kHz).

Tabulated are the means and standard deviations of the averages over semi-month of the quantities defined in Table 4-5. (Note: the PPC modelling error is labelled "RAND. PPC" and the RSS error with biases removed is labelled "CORR. RSS" in the Tables). Additionally, the number of semi-months for which data was available is tabulated in the column headed "#SM". The data are organized according to LOP so that homogeneity across the N. Pacific validation region can be assessed by inspection.

In order to obtain a gross characterization of the errors associated with each LOP in the validation region, the total r.s.s. error and r.s.s. error with biases removed have been averaged over receiving sites with the results shown in Table 4-12. Only those LOP's for which at least 16 semi-months of data had been recorded at 3 or more receiving sites were processed. In the table, the standard deviations refer to the averaging over receiver sites and thus measure the spatial homogeneity of the mean values. Several conclusions follow immediately from inspection of Table 4-12.

LOP	SITE	PPC BIAS MEAN	PPC BIAS STDV	RAND. PPC MEAN	RAND. PPC STDV	RAND PROP MEAN	RAND PROP STDV	TOTAL RSS MEAN	TOTAL RSS STDV	CORR. RSS MEAN	CORR. RSS STDV	HOURS/DAY MEAN	HOURS/DAY STDV	#SM
AC	ANCH	7.7	11.3	3.7	2.3	4.9	1.9	12.5	8.5	6.5	1.9	21.5	5.4	17
AC	HOKK	19.5	6.6	5.1	2.6	7.5	1.3	22.1		11.2	1.3	21.5		23
AC	MAKA	6.1	8.6	7.7	2.6	8.5	1.1	14.9		11.2	1.3	23.0		24
AC	MARC	12.6	3.1	15.3	2.5	8.5	1.2	22.2		17.0	1.3			4
AC	PYRA	5.5	7.9	5.3	2.2	5.3	1.2	12.1	4.2			2.3		24
AC	WAHI	4.1		5.1	2.1	7.2	1.2	11.1				22.1		7
AD	ADAK	-3.2	9.0	6.6	2.6	7.2	1.1	14.4		10.1	1.4	19.1		17
AD	ANCH	9.1	14.4	3.7	2.2	5.3	1.2	16.5		7.7	1.3	20.0		17
AD	HOKK	4.4	4.5	8.6	2.4	7.4	1.2	13.0		11.6	1.3	22.0		22
AD	KURE	-.4	1.3	19.3	1.2	6.6	1.2	20.8		20.0	1.4	19.0		8
AD	PANA	1.6	7.5	10.0	4.3	6.6	1.2	17.6		11.9	1.6	17.0		16
AE	HOKK	6.1	6.1	15.5	2.2	6.6	1.2	22.1		16.9	1.6	22.0		22
AE	KURE	-.8	4.9	26.9	2.2	6.4	1.2	29.3		27.9	1.7	18.0		6
AH	ADAK	6.8	12.7	6.7	2.6	6.3	1.2	16.8		9.8	1.7	19.0		17
AH	ANCH	1.2	13.4	6.3	2.2	6.3	1.2	14.4		8.0	1.6	21.1		17
AH	MARC	23.3	6.4	8.9	4.9	10.3	1.2	27.1	15.4	13.8	1.6	3.0		4
AH	MIYA	12.3	2.3	5.1	2.1	5.3	1.2					24.0		14
AH	OSHI	14.7		7.2		5.3	1.2					24.0		2
AH	TSUS	18.0	4.2	12.3	4.4	6.3	1.2	16.6	4.0	13.7	1.7	21.1	6.4	23
BC	HOKK	21.6	11.2	13.9	11.4	8.3	1.1	23.1		17.3	1.9			23
BD	NOS2	-8.8	.7	16.4		4.3	1.4	31.1				21.4		4
BD	NOSC	-.9	2.8	20.4	1.6	5.3	1.4	20.2		19.1	1.9	21.0		2
BD	PANA	3.4	12.4	17.9		5.3	1.4	23.1		21.1	1.9	21.0		16
BD	SEAT	-7.4	5.0	13.8		5.5	1.4	18.2		15.0	1.8	16.5		22
BE	MARC	9.4	11.7	19.5	3.4	9.5	1.1	25.6	6.1	21.0	1.8	2.0		4
BF	NELC	-1.8	.7	18.1		7.8	1.1	19.7		19.2	1.8	14.4		2
BH	MARC	12.3	13.9	18.0	4.7	8.3	1.1	27.1		20.0	1.8	4.2		4
CD	ADAK	-3.2	12.5	4.6	2.4	7.5	1.2	15.8				21.4		21
CD	ANCH	1.2	4.7	4.2	2.2	5.5	1.1	8.6				23.0		17
CD	MAKA	1.1	1.7	8.7	2.2	4.4	1.1	10.0				23.0		24
CD	MARC	6.8	1.4	11.7	3.1	10.1	1.1	17.8		15.0	2.1	7.0		4
CD	NELC	3.6	7.2	5.3	1.8	2.2	1.1	9.2				1.0		4
CD	NOS2	-2.1	.7	4.3		2.2	1.1	5.3						2
CD	NOSC	-2.5	1.4	4.7		2.1	1.1	5.5				24.0		18
CD	PANA	-13.8	3.2	6.6		3.3	1.1	16.7				21.0		16
CD	SEAT	.5	4.7	4.3	2.1	3.6	1.1	7.4				23.0		22
CD	WAHI	-2.8	4.8	5.1	1.5	3.7	1.1	7.7				23.0		8
CE	ADAK	-4.9	9.3	13.0		6.4	1.2	18.0				16.0		15
CE	HOKK	-.5	3.4	18.6	2.9	6.4	1.2	20.0		15.0		21.0		24
CE	KURE	-2.9	6.5	16.6	5.4	6.3	1.2	21.3		19.2	1.9	21.0		11
CE	NOSC	-.9	5.9	21.1	4.6	6.9	1.2	23.0		22.0	1.8	14.0		18
CE	SEAT	-.7	13.8	8.6	6.4	10.3	1.2	18.0		14.2	1.8	13.0		15
CF	MAKA	7.4	5.3	20.9	3.9	6.7	1.2	24.1		22.1	1.9	9.0		18
CF	PANA	-18.9	9.2	11.5	6.9	4.8	1.1	21.5	4.2	12.0	1.9	18.0		16
CF	WAHI	.2	5.8	19.4	2.2	7.8	1.1	21.1		20.2	1.9	14.0		8
CH	ADAK	6.6	7.5	6.1	3.3	5.3	1.2	11.8	2.2	4.0	1.2	21.1		21
CH	ANCH	-1.9	3.6	6.4	2.5	5.3	1.2	8.8				23.1		17
CH	HOKK	1.6	1.7	7.6	2.1	5.3	1.2	8.8				24.0		24
CH	KURE	-4.4	3.9			6.3	1.2	12.1	4.2	2.2	1.2	19.4		11
CH	MAKA	.8	3.1	8.7	2.1	4.5	1.2	12.2	4.3	2.2	1.2	2.0		22
CH	MIYA	-14.1	2.6	7.9	2.2	4.5	1.2	17.6	5.2	9.0	1.8	23.8		14
CH	NOS2	4.3		4.1		4.2	1.2	6.3		4.0	1.2	24.0		2
CH	NOSC	7.9	5.5	5.6	1.4	4.2	1.2	8.8	1.2	6.7	1.2	24.0		18
CH	OSHI	-4.1	.8	6.2		3.3	1.2	8.8				24.0		2
CH	PANA	.3	5.9	14.7	8.1	10.0	1.2	20.0	3.3	19.0	1.9	3.0		6
CH	SEAT	2.8	7.8	5.8		6.6	1.2	11.9	2.2	6.6	1.2	2.3		22
CH	TSUS	-7.2	2.3	13.6	2.6	6.3	1.2	16.9	3.1	15.0	1.8	22.1		23
CH	WAHI	3.5	5.9	10.4	6.4	6.3	1.2	13.0	2.6	10.1	1.9	21.1		18
DF	NOS2	-11.1	1.4	13.3		4.3	1.2	18.7		14.1	1.8	12.0		2
DF	NOSC	-9.9	2.8	10.2		4.4	1.2	15.7	2.7	11.4	1.8	13.6		18
DF	SEAT	.1	18.6	13.5	9.3	9.2	1.2	22.5		17.5	1.9	11.3		22
DH	ANCH	-2.9	3.3	15.8	3.2	8.1	1.2	19.3	3.3	17.0	1.9	22.1		17
DH	KURE	-2.1	9.6	13.1	7.1	10.1	1.2	20.0		17.2	1.9	12.2		11
DH	NELC	6.9	.3	4.1		2.2	1.2	8.7		4.3	1.2	24.0		2
DH	NOS2	6.4	.8	2.4		2.2	1.2	8.7		4.3	1.2	24.0		2
DH	NOSC	10.3	4.9	4.6	1.9	2.2	1.2	12.2		5.3	1.2	23.0		18
DH	OSHI	-6.2	.1	5.7		3.3	1.2	8.8		6.6	1.2	24.0		2
DH	PANA	12.6	13.1	15.8	10.6	11.5	1.2	20.8		20.2	1.9	3.0		4
DH	SEAT	2.1	4.7	4.8		5.7	1.2	8.8		7.2	1.2	22.5		22
DH	TSUS	15.2	5.4	12.7	3.7	7.7	1.2	22.0		15.0	1.9	21.0		21
EF	NELC	-6.5	1.1	24.9		7.2	1.1	26.6		25.0	1.9	11.0		2
EH	ADAK	13.1	7.9	16.4	10.2	7.1	1.1	23.3		19.7	1.9	15.0		17
EH	KURE	15.7	3.7	14.5	4.7	8.3	1.1	23.3		17.0	1.9	13.0		11
EH	MARC	9.9	7.6	14.6	7.3	8.3	1.1	22.0		18.1	1.9	4.0		5
EH	MIYA	1.9	2.7	15.6	1.1	8.3	1.1	23.6		16.1	1.8	24.0		14
EH	OSHI	6.3		18.5		8.3	1.1	19.0		18.0	1.8	24.0		2
EH	TSUS	18.7	4.8	21.9	2.5	8.3	1.1	25.0		22.0	1.8	23.0		12
AR	WALE	2.2	4.7	1.7	1.7	3.3	1.1	6.1				10.0		14
CR	WALE	-3.9	2.1	3.7	1.7	3.3	1.1	6.1				23.0		18
CR	WALE	-3.9	2.1	3.7	1.7	3.3	1.1	6.1				23.0		18

TABLE 4-10: SEASONALLY-AVERAGED STATISTICS AT 10.2 KHz

LOP	SITE	PPC BIAS MEAN	PPC BIAS STDV	RAND. MEAN	PPC STDV	RAND MEAN	PROP STDV	TOTAL MEAN	RSS STDV	CORR. MEAN	RSS STDV	HOURS/DAY MEAN	HOURS/DAY STDV	#SM
AC	ANCH	8.4	7.3	3.7	2.1	3.9	1.7	11.4	5.6	5.7	2	23.3	1.4	16
AC	HOKK	18.3	5.1	5.3	4	6.3	1.6	20.7	4.9	9	2.7	23.2	1.2	20
AC	MAKA	7.9	7.1	7.6	3.4	6.3	1.9	14.3	4.7	10.3	2.8	23.7	.	34
AC	MARC	-.6	1.3	16.1	2.7	7.9	2	19.2	1.3	18.2	1.6	10	7	4
AC	PYRA	7.1	6.9	5.4	2.5	7.7	2.3	12.7	3.5	8.1	2.6	23.9	2	32
AC	WAHI	-.3	5.2	6.7	2.2	5.4	10	10	3.1	8.5	1.3	21.4	6.2	7
AD	ADAK	-2.7	11.9	3.7	2.3	6.5	2.9	13.6	6			17.9	8.4	18
AD	ANCH	13.6	11.6	2.2	1.3	4.6	1.6	17.7	10	5.5	2.3	21.8	2.2	16
AD	HOKK	2.3	3.8	6.3	1.3	6.4	1.8	10.1	1.9	9.1	1.9	23.6	.6	20
AD	KURE	11.3	3.7	5.7	1.3	6.6	1.4	13.3	3.3	6.7	.8	23	1.4	6
AD	PANA	7.3	5.9	7.4	1.9	4.3	2.4	12.6	4.6	9.5	3.1	20.4	4.9	14
AE	HOKK	6.7	5.4	17.4	1.7	5.7	1.7	20.3	1.7	18.4	1.6	23.4	1	20
AE	KURE	11.7	3.5	14.7	3	4.6	1.6	19.6	1.6	15.4	.8	24	0	4
AH	ADAK	10	5.5	5.8	3.2	6.5	2.4	13.8	4	8.1	3	20.6	.6	16
AH	ANCH	8.3	9.2	7.1	2.9	4.6	2	14.7	4.9	8.7	3	22.3	2.8	16
AH	MARC	-9.2	3.6	24.8	.6	9.3	.9	28.2	.6	26.5	.5	6	0	2
AH	OSHI	22.4	3.4	7.3	1.3	6.2	1.5	24.3	.5	9.6	.4	24	0	2
AH	TSUS	7.5	17.3	8.3	4.7	6.8	1.5	21.1	5.5	10.3	2.8	20.9	5.3	21
BC	HOKK	18.8	4.2	18.6	4.7	7.8	1.3	24.4	3.3	14	.6	18.1	.4	21
BD	NOSC	-.4	5.3	20.3	2.1	5.2	1.9	21.6	1.7	21	2.1	17.1	.2	18
BD	PANA	4.5	5.3	19.8	6.8	4.7	2.4	22.3	4.3	20.9	5.1	17.7	4.6	14
BD	SEAT	2.3	5.3	21.1	2	7.2	3.8	23.8	6.7	22.9	7.3	21.5	1.4	22
BE	MARC	.	2.5	23	1.9	8.5	3.7	24.9	.9	24.8	.9	9.5	3.5	4
BH	MARC	-4.7	5.2	23.3	.	9.3	.8	26.3	1.6	25.4	.5	9.5	3.5	4
BH	OSHI	5.9	2.9	14.6	.	5.3	.2	16.9	.8	15.5	.2	24	0	2
CD	ADAK	-4.9	12.4	3.4	2.8	6.1	1.7	14.6	4.8	7.5	1.6	23.6	.9	19
CD	ANCH	7.3	4.9	3.4	1.4	10	1	10.8	3.1	5.4	1.6	23.1	1.1	17
CD	MAKA	-.4	8.9	2.4	1.3	4.1	1	10.2	2.1	9.9	2.2	23.9	1.2	32
CD	MARC	-21.4	3.7	7.1	1.2	7.5	1.2	24.2	3.9	10.8	3.2	4.2	1.1	4
CD	NOSC	8	1.1	5.8	.5	2.5	5	6.4	1	6.3	.9	23.8	.3	18
CD	PANA	-16.3	2.8	5.7	1.4	3.1	1.7	17.9	2.4	6.6	3.1	20.2	.5	14
CD	PYRA	-31.5	1.3	7.4	1.4	3.2	1.3	32.7	.9	8.5	1.8	23.7	.	8
CD	SEAT	1.1	1.3	7.6	3.9	4.2	3.1	9.7	4.8	9.3	4.4	23.9	.2	22
CD	WAHI	-.1	1.2	5.3	1.3	3.6	.9	6.1	1.4	5.8	1.4	23.5	21	8
CE	ADAK	1.5	7.2	20.3	6.4	3.6	1.4	22.4	4.8	21	5.4	21	2.8	13
CE	HOKK	-5.4	2.5	20.4	1.4	4.6	1.7	22.2	1.7	20.9	1	21.9	1.5	22
CE	KURE	.4	2.3	11.4	1.4	5.1	1.9	13.1	1.6	12.7	1.7	19.5	.5	8
CE	NOSC	-1.4	2.5	21.6	1.2	6.1	.8	23.2	1.4	22.6	1.4	15.3	.5	18
CE	SEAT	-15.6	7.3	13.4	3.6	7.6	1.8	23.3	5.2	16.2	3.7	12.8	.5	21
CF	MAKA	-3.6	3.3	21.5	3.6	5.4	.7	22.8	3.2	22.2	3.5	19	.2	16
CF	PANA	-.9	2.6	24.5	4.2	5.3	2.1	25	3.2	24.8	3.5	19.7	.8	14
CF	WAHI	-7.9	1.4	17.4	1.4	5.5	2.3	20.1	2.8	18.3	2.3	18	.6	8
CH	ADAK	1.4	14	7.1	1.9	3.5	2.9	14.6	6.8	7.9	2.2	21.4	.2	21
CH	ANCH	.6	3.7	6.9	2.3	3.4	1.1	8.9	2.5	7.9	2.8	23.2	.2	17
CH	HOKK	-6.7	2.3	7.2	3.3	4.5	.6	11.4	1.9	9.1	2.5	23.9	.2	22
CH	KURE	10	3.8	10.1	2.1	5.3	1.7	15.3	3.9	11.5	2.5	17.2	.6	8
CH	MAKA	2.7	1.8	9.4	1.9	4.5	1.3	11.1	1.3	10.6	1.4	23.1	.2	20
CH	NOSC	6.4	4.4	6.2	1.6	4.3	10	10	3.2	7.4	1.7	24	0	18
CH	OSHI	-6.9	2.5	10.8	.5	3.6	.5	14.6	.5	12.8	.7	21	1.8	4
CH	PANA	-4.1	1.5	17.5	.9	12.3	.8	21.9	.4	21.4	.1	4	0	2
CH	SEAT	3.1	5.2	5.3	1.7	5.7	1.7	12.3	.3	10.7	.2	23.1	.2	22
CH	TSUS	-6.6	3.5	12.8	3.1	5.7	2.2	16.6	1.3	14.3	.3	21.2	.4	21
CH	WAHI	5.3	2.1	9.1	1.1	5.2	1.1	11.1	1.7	9.5	.4	24	0	18
DF	NOSC	-18.2	2.1	12.6	3.3	4.2	1.1	22.7	2.2	13.4	.7	18.2	.3	18
DF	SEAT	1.3	11.9	16.8	2.1	7.4	2.3	21.6	5.3	18.5	2.2	15.4	.5	22
DH	ANCH	-6.3	3.6	5.8	2.2	4.9	1.7	10.4	2.2	7.2	2.9	22.8	.3	17
DH	KURE	6.7	4.3	9.8	2.2	4.9	1.7	13.7	2.1	11	.7	19.2	.5	8
DH	NOSC	6.5	4.3	6.2	1.9	3.1	.9	10.1	3.6	7	.2	24	0	18
DH	OSHI	3.1	3.8	5.5	1.2	3.1	.6	10.7	2.6	9.1	1.2	24	0	4
DH	PANA	-.4	7.8	7.6	2.9	7.7	.9	14.7	1.8	10.5	2.5	2	1.4	4
DH	SEAT	2.8	4.7	6.6	2.4	5.9	2.3	10.7	2.7	9.1	2.8	22.9	3.4	22
DH	TSUS	12.7	6.7	9.8	2.4	6.1	2.3	18.7	3.8	12.3	2.9	22.2	3.4	19
EH	ADAK	1.3	5.7	19.4	9.4	7.3	2.3	22.7	4.5	21.6	5.8	18.2	.8	17
EH	KURE	9	7.9	11.1	3.7	5.2	2.9	17.2	4.3	12.9	4.1	16.2	.7	8
EH	MARC	.9	10.6	22.8	4.2	11	2	27.6	3.8	25.4	4.1	4.8	.1	4
EH	TSUS	2.4	6.5	22.9	2.2	3.9	.9	23.9	2.5	23.3	2.5	23.8	.2	12
AR	WALE	11.1	5.6	1.9	2.1	3.9	1	12.8	.8	4.6	1.5	22.7	.3	20
CR	WALE	.9	2.3	3.7	1.8	3.7	.5	5.4	1.2	4.8	1.2	21.7	.8	24
CR	WALE	.9	2.3	3.7	1.8	3.7	.5	5.4	1.2	4.8	1.2	21.7	.8	24

TABLE 4-11: SEASONALLY-AVERAGED STATISTICS AT 13.6 KHz

TABLE 4-12. SPATIALLY AVERAGED PHASE ERRORS

	TOTAL R.S.S. ERRORS (CEC)		R.S.S. ERRORS WITH PPC BIASES REMOVED (CEC)	
LOP	10.2	13.6	10.2	13.6
AC	15.4 ± 4.0	14.8 ± 2.7	8.8 ± 1.7	8.3 ± 1.7
AD	14.5 ± 1.3	13.5 ± 2.7	10.3 ± 1.8	10.3 ± 4.9
AH	17.3 ± 3.4	16.5 ± 3.2	10.1 ± 3.4	9.0 ± 0.9
BD	21.6 ± 2.2	22.6 ± 0.9	18.6 ± 2.3	21.6 ± 0.9
CD	10.6 ± 4.0	11.5 ± 3.7	7.4 ± 1.7	7.5 ± 1.6
CE	20.2 ± 1.8	22.9 ± 0.5	17.8 ± 3.2	19.9 ± 2.7
CH	11.6 ± 2.6	12.1 ± 2.5	9.1 ± 2.7	9.8 ± 2.2
DH	13.2 ± 5.4	12.5 ± 3.6	9.1 ± 3.7	8.9 ± 2.1

First it is seen from the standard deviations that in general it is in fact sensible to average over receiving sites to obtain single data characterizing the validation region as a whole. Second, there is no significant difference between the 10.2 and 13.6 kHz results, thereby suggesting that 10.2 kHz phase error data can generally be taken to be representative of the entire Omega band. Third, it is seen that the total r.s.s. errors range over roughly a factor of two, from of the order of 10 CEC for LOP's corresponding to mid-latitude propagation paths (CD, CH, DH) to about 20 CEC's for LOP's involving some propagation in equatorial regions (BD, CE). LOP's involving transpolar propagation (AC, AD, AH) lie somewhere in between. (These characteristics will show up more clearly in the single-station analyses of Section 4.4). Finally, the effect of PPC bias removal is seen to be much more significant for mid-latitude LOP's (30% reduction in phase error) than for the LOP's involving equatorial propagation. Indeed, close examination of Tables 4-10 and 4-11 for this latter category of LOP shows that it is the large PPC modelling errors that are primarily

responsible for the larger r.s.s. errors. Further implications of these results will be discussed presently.

4.3.4 Single-Station Phase Variances

The final processing step is the extraction of single-station phase errors from the LOP data, as described in Section 4.2. The results of this procedure are given in Table 4-13. For each station, at 10.2 and 13.6 kHz, are tabulated the total r.s.s. phase error and r.s.s. phase error with PPC biases removed. The column labelled "avg" represents the average of the 10.2 and 13.6 kHz results.

TABLE 4-13. SINGLE-STATION PHASE ERRORS

	TOTAL R.S.S. PHASE ERROR (CEC)			R.S.S. PHASE ERROR WITH PPC BIASES REMOVED (CEC)		
STATION	10.2	AVG	13.6	10.2	AVG	13.6
A	11.6	11.5	11.4	6.1	5.0	3.9
B	21.3	21.0	20.5	16.1	17.1	18.1
C	9.2	9.0	8.7	4.3	4.4	4.5
D	12.9	12.5	12.1	9.8	9.4	9.0
E	21.0	21.3	21.6	19.0	19.3	19.5
F	23.0	22.7	22.4	16.5	17.5	18.4
H	13.4	13.2	13.0	9.6	10.0	10.4

As in the LOP data, it is again seen that 10.2 and 13.6 kHz results are very close, and for this reason the average of the two will henceforth be uniformly employed at all Omega frequencies in the fix error model*. Also it is evident that in the Northern Pacific region, the stations divide naturally into two classes: "good" stations (A, C, D

* As discussed earlier in the spirit of conservatism the phase errors for the "worst" station in the N. Pacific, station F, will be used for the Australia station.

and H) with total r.s.s. phase errors in the range 9-13 CEC, and "poor" stations (B, E and F) with errors of 21-23 CEC. The "poor" stations, again, are those involving propagation in the equatorial region, while the "good" stations do not.

To anticipate somewhat the results of the fix error analyses, the average phase errors of Table 4-13 can be converted into range errors at each of the four shared Omega frequencies as shown in Table 4-14.

TABLE 4-14. AVERAGE OMEGA R.S.S. RANGE ERRORS IN N. PACIFIC (NMI)

	WITH PPC BIASES				WITHOUT PPC BIASES			
STATION	10.2	11.05	11.33	13.6	10.2	11.05	11.33	13.6
A	1.83	1.69	1.64	1.37	0.79	0.73	0.71	0.60
B	3.34	3.08	3.00	2.50	2.72	2.51	2.45	2.04
C	1.43	1.32	1.29	1.07	0.70	0.65	0.63	0.52
D	1.99	1.83	1.79	1.49	1.49	1.38	1.34	1.12
E	3.38	3.12	3.05	2.54	3.07	2.83	2.76	2.30
F	3.61	3.33	3.25	2.70	2.78	2.57	2.50	2.08
H	2.10	1.94	1.89	1.57	1.59	1.47	1.43	1.19

Since the effects of geometrical dilution of precision (GDOP) will be largely offset by the error reduction from exploiting the redundancy provided by use of multifrequencies, Table 4-13 suggests that even with existing PPC biases, use of the "good" stations (A, C, D and H) will support navigation to the 1-2 nmi design accuracy of Omega, while elimination of bias errors should provide roughly half a nautical mile improvement in fix accuracy.

4.3.5 Propagation Variance Analysis

It has already been shown that of the various error sources, the day-to-day variability of propagation is generally the least significant. In Figure 4-7, for example, it was found that the median LOP variation due to propagation is of the order of 5 CEC. From a fundamental standpoint, one would expect the phase variance due to propagation to increase with increasing path length and to be greater for the propagationally more complex paths (transequatorial, mixed land-sea, etc.). To explore this, a reduction to single-station variances precisely parallel to that of Section 4.3.4 has been performed, where the input (LOP) phase errors are the "random propagation" errors tabulated in Section 4.3.3.

The results, given in Table 4-15, validate these expectations. Rms (10.2 kHz) phase errors due to propagation vary from 2.5 CEC for Hawaii to 6.6 CEC for Argentina. At 13.6 kHz, the corresponding variation is 3.1 CEC to 5.8 CEC. It should be recalled that these errors represent averages over time of day, season and receiver site.

TABLE 4-15. R.M.S. PHASE VARIATION DUE TO PROPAGATION (CEC)

STATION	10.2 kHz	13.6 kHz
A	4.8	4.0
B	4.6	5.4
C	2.5	3.1
D	4.9	4.5
E	5.8	5.7
F	6.6	5.8
H	4.8	4.4

4.4 PPC Errors

In Section 4-2 we have distinguished two types of PPC errors (see Figure 3-5): PPC "bias" errors and PPC "modelling" errors. Over the whole data base, median (absolute) values for the PPC bias error of 6-7 CEC were found (Figure 4-5). When examined on a case by case basis, 13 cases of statistically significant bias errors in excess of 20 CEC were found out of a total of 544 cases at 10.2 kHz, and 15 out of 516 cases at 13.6 kHz (see Tables 4-8 and 4-9). Clearly this indicates that in the vast majority of cases, bias errors are not a concern, and only exceed 20 CEC at a limited number of monitor sites during certain months of the year. Indeed, when averaged over season - as in Tables 4-11 and 4-12 - only one case of seasonally-averaged PPC bias in excess of 20 CEC was found at either 10.2 or 13.6 kHz for receiving sites at which 12 or more semi-months of data were recorded, this one case being the 10.2 kHz BC LOP at Hokkaido. It is therefore concluded that the existing PPC's are free of gross bias errors in the Northern Pacific. Those bias errors which do exist have the effects on single-station range accuracy shown in Table 4-14 from which it was noted that elimination of the residual PPC biases would result in roughly a 1/2 nmi improvement in range accuracy. Thus, the PPC bias situation may be summarized by stating that there are no glaring errors requiring immediate attention but that there is justification for improving the PPC's at a point in the future.

PPC modelling errors (or "random PPC" errors as they are called in Tables 4-10 and 4-11 are generally the dominant error source, particularly for the propagationally more complex LOP's, as shown in these tables. Physically, such errors arise from modal interference and from the sunrise/sunset transition dynamics of the ionosphere. In an attempt to quantify the difference between "good" and "poor" propagation paths as far as the PPC modelling errors are concerned, we have (as in Section 4.3.5) derived single-station errors from the (LOP) "RAND. PPC"

errors of Tables 4-10 and 4-11. The results of this admittedly approximate procedure are given in Table 4-16. It is seen that the paths involving equatorial propagation have PPC modelling errors in the range 15-18 CEC, while the "good" paths involve errors less than half these values. (It is naturally not possible to conclusively ascribe the difficulty to equatorial propagation per se since the "poor" paths tend also to be longer and involve marked ground conductivity variations). Since from coverage considerations, the "good" stations (A, C, D and H) are by far the most important in the Northern Pacific, there would be very little impact on position fixing accuracy in the validation region if the PPC modelling errors were improved for the "poor" stations (B, E and F). Thus, so far as the Northern Pacific is concerned, the existing PPC's are deemed adequate both with respect to "bias" and "modelling" errors.

TABLE 4-16. SINGLE-STATION PPC MODELLING ERRORS (CEC)

STATION	10.2 kHz	13.6 kHz
A	3.3	2.9
B	15.1	16.6
C	4.9	2.3
D	6.9	8.4
E	17.6	18.2
F	15.5	14.8
H	7.7	9.2

4.5 Day vs. Night Phase Error Statistics

In the present study, averages are taken over the full 24-hour diurnal period so that quoted accuracies will apply to fixes generated at totally random times of day. Since it has been customary to quote OMEGA system accuracy as "2 nmi at night, 1 nmi by day", one can legitimately question the utility of such diurnal averaging if night and

day accuracies are in fact so radically different. Accordingly, an analysis was performed of the phase error statistics for two separate data sets, one representing MASTERFILE data taken within ±2 hours of local noon and the other within ±2 hours of local midnight. Each data set was processed identically, using the same procedures described in Section 4.2.

The results, for the North Pacific at least, are in conflict with conventional wisdom in that relatively little difference is found between day and night phase errors. Figure 4-8, for example, displays the cumulative distribution of the absolute value of mean phase error for day and night 10.2 kHz data. As in Figure 4-5, the cumulative distribution is taken over all North Pacific MASTERFILE (unflagged) data approximately 500 cases in all, where each case represents a site-month for a given LOP. The median error is only slightly larger at night than during the day (8.5 vs 8.0 CEC). Similarly, the cumulative distribution of the standard deviation of the phase error (which measures both random propagation and PPC modelling errors) is shown in Figure 4-9 for 10.2 kHz data. Here, the day and night data sets have identical medians (7.5 CEC). Day/night differences do appear, however, in the phase variation due to random propagation as shown in Figure 4-10. It is seen that - as one would expect - nighttime propagation is less repeatable (day-to-day) than during daytime, with a median r.m.s. variation (at 10.2 kHz) of 5.6 CEC at night vs 4.0 CEC during the day. Since such random propagation effects do not appear to be the dominant source of phase error in the N. Pacific, it is understandable that the overall phase errors can be similar day and night despite this difference in stability of propagation. Similar results are found in the 13.6 kHz data.

Summary tables of seasonally averaged data (analogous to Tables 4- and 4-) for the day and night data sets at 10.2 and 13.6 kHz are given in Appendix B. Also of interest are the results for the one-way (i.e. single station) r.s.s. phase errors deduced from these data.

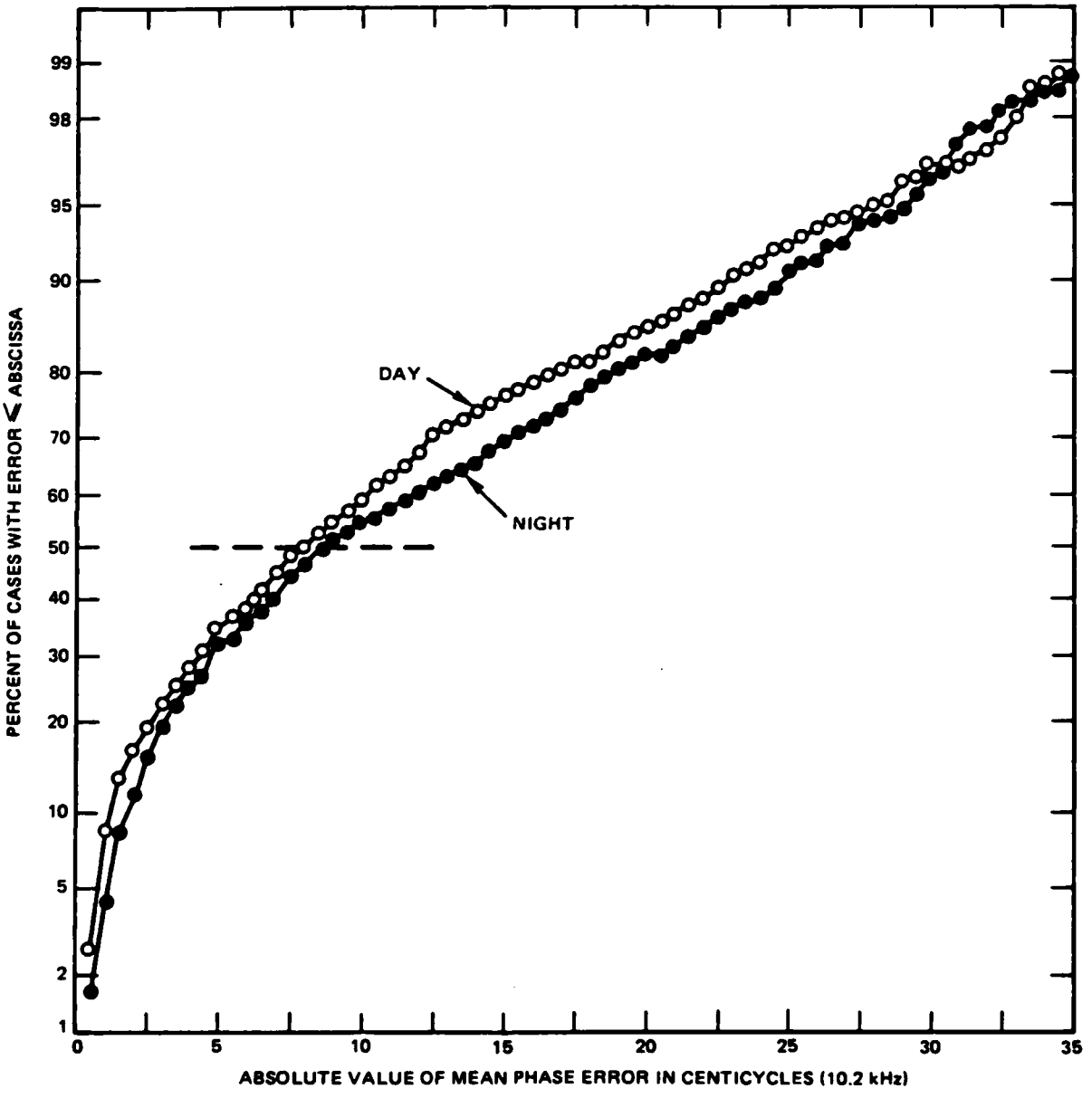

FIGURE 4-8. CUMULATIVE DISTRIBUTION OF NIGHT AND DAY MEAN PHASE ERRORS (10.2 kHz)

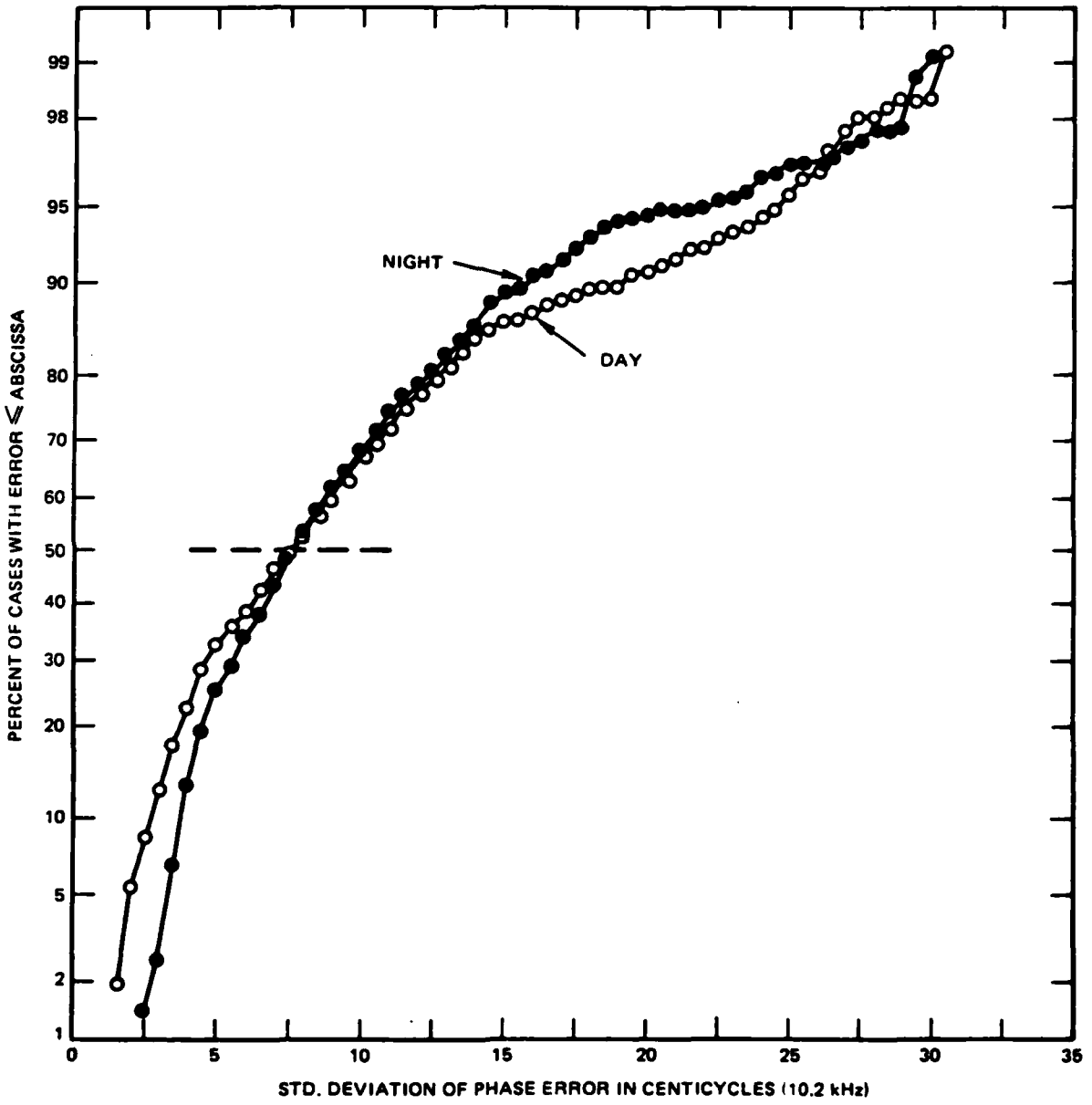

FIGURE 4-9. CUMULATIVE DISTRIBUTION OF NIGHT AND DAY PHASE ERROR STANDARD DEVIATION (10.2 kHz)

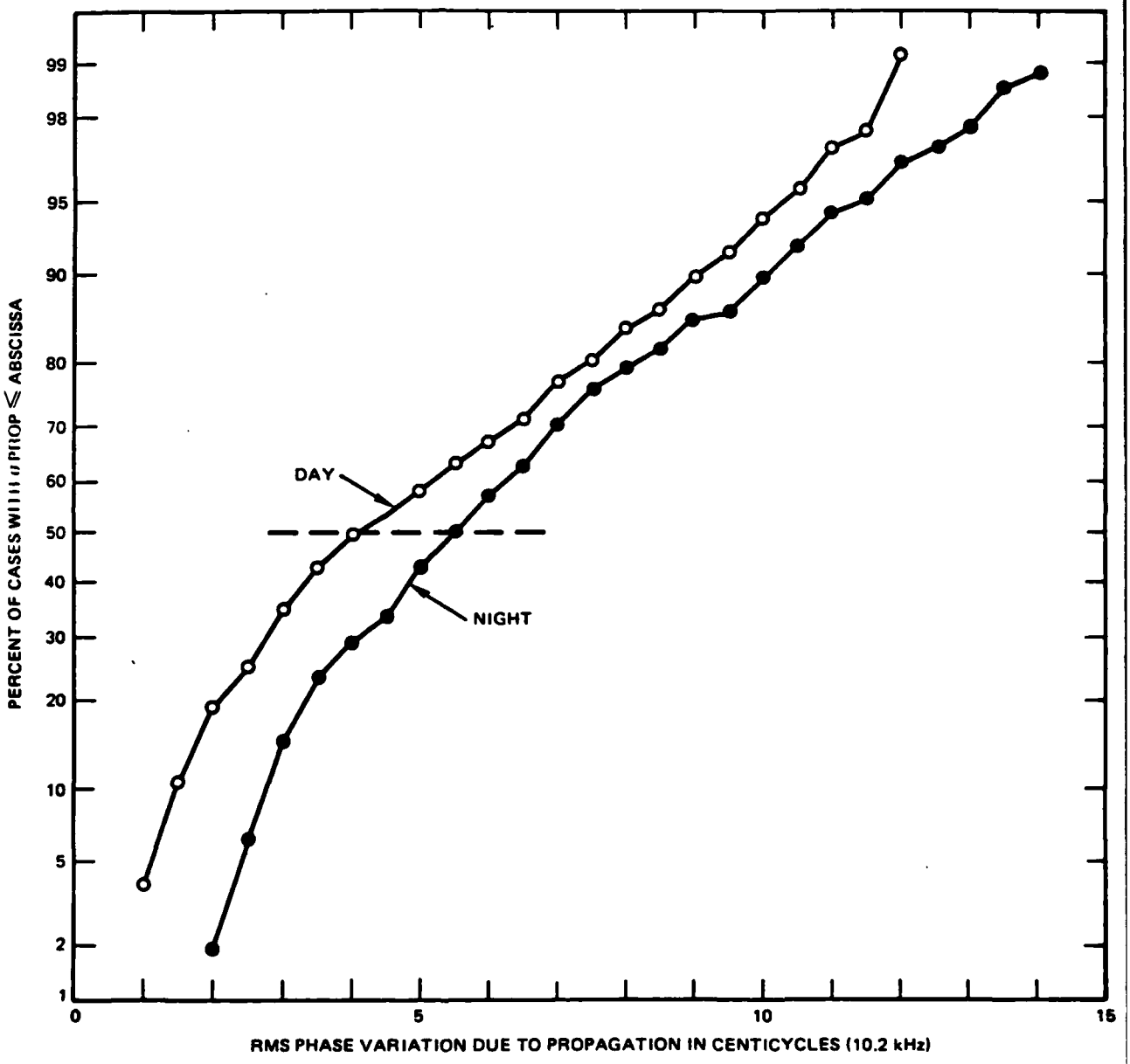

FIGURE 4-10. CUMULATIVE DISTRIBUTION OF NIGHT AND DAY PHASE ERRORS DUE TO RANDOM PROPAGATION (10.2 kHz)

These are displayed in Table 4-17 for 10.2, 13.6 and the average of 10.2 and 13.6 kHz. For comparison purposes, the corresponding values (from Table 4-13) obtained from the full 24 hour data set are also shown. Appreciable day/night differences are found only for stations B and F, the former worse during the day and the latter worse at night. (Neither B nor F is navigationally significant in the N. Pacific). Stations A and C are 10-20% worse at night compared to day at both 10.2 and 13.6 kHz. Station H is worse during the day at both frequencies. E is virtually identical day and night while D is worse at night at 10.2 and worse during the day at 13.6. Overall, as shown in the last three comumns of the table, the day/night differences in phase errors were not felt to be significant enough to warrant separate calculations of fix accuracies for day and night*.

Table 4-17. Day and Night Single Station R.S.S. Phase Errors in CEC

	10.2 KHZ			13.6 KHZ			(10.2 + 13.6)/2		
STATION	NITE	DAY	24 HR	NITE	DAY	24 HR	NITE	DAY	24 HR
A	12.5	11.5	11.6	12.0	10.8	11.4	12.3	11.2	11.5
B	17.3	23.9	21.3	14.5	23.4	20.5	15.9	23.7	20.5
C	10.2	7.6	9.2	9.1	7.1	8.7	9.7	7.4	9.0
D	11.3	13.9	12.9	12.2	11.4	12.1	11.8	12.7	12.5
E	22.3	22.6	21.0	21.5	22.6	21.6	21.9	22.6	21.3
F	28.2	20.0	23.0	30.8	17.1	22.4	29.5	18.6	22.7
H	11.5	12.4	13.4	10.2	14.5	13.0	10.9	13.5	13.2

* It should be noted that the mix of usable signals used will generally be the same day and night over most of the N. Pacific validation region with the exception of portions of the Hawaii modal interference region (see Section 5) which disallow use of station C at night only

5.0 COVERAGE MODEL

The position fix accuracy model derived in Section 3 requires two basic inputs: i) the expected r.s.s. phase errors associated with each navigation signal, and ii) the specification of which signals are usable for navigation at the given location where an accuracy assessment is sought. The Phase Error Model, item i) above, was obtained in Section 4 and is summarized in Table 4-13. The present section deals with item ii), the Coverage Model.

The methodology for obtaining a Coverage Model has already been discussed at some length in Section 2. One starts with a set of semi-empirically derived SNR threshold (-20 dB in 100 Hz BW @ 10.2 kHz) boundaries and modal interference zones (>20 CEC @ 10.2 kHz) computed for each station at two times of day and 4 days of the year by The Analytic Sciences Corporation[9,10]. These were substantially modified by ONSOD to be consistent with observational results and other criteria. Then as was done in Ref. 15, the geometrical union of these contours are generated in order to derive regions within which the signals are expected to be usable for navigation (i.e. SNR $\geq$ -20 dB and < 20 CEC modal interference) at all times of day and all seasons. This combining process was actually carried out as a two step process. First, as discussed in Section 5.1, the -20 dB contours are combined and then (Section 5.2) the modal interference zones are introduced. The resulting full-time Coverage Model is introduced in Section 5.3.

Next, this Coverage Model is validated by comparisons with NOSC test data (Section 5.4), ONSOD fixed monitor data (Section 5.5) and operational data (including integrated satellite/OMEGA data) in Section 5.6. The in-depth analyses of operational data upon which Section 5.6 is based are reported in full detail in Appendix A. Appendices C, D and E contain material documenting intermediate steps in the process of deriving and validating the Coverage Model.

5.1 Predicted Signal Threshold Boundaries

The most recent Omega signal coverage diagrams for 10.2 kHz were obtained from the Analytic Sciences Corporation in printed form and on digital magnetic tape. This data included -20 dB and -30 dB contours and 20 CEC modal interference contours for 2 times of day (0600 and 1800 GMT) for each season (Feb., May, Aug., Nov.) for each transmitter. The -20 dB contours were selected as the thresholds for usable signals from each Omega station.

A combined contour was derived by choosing from these 8 contours for each station the minimum range at a given bearing at which the signal fell below -20 dB at any time of day in any season. The resulting contour is used to approximate the signal threshold boundary for that station for all times - day or night, year round. These all-time contours encompass the regions within which the signal from a given Omega transmitter should always be available. Figure 5-1 presents these all-time signal threshold boundaries for Omega stations A, C, D, E, F and H in a composite diagram. In Appendix C these all-time signal threshold boundaries are presented individually for these stations in Figures C-1 to C-6. Because Liberia is out-of-range in the North Pacific the contour for station B is not included in the figures. Since Australia is not yet operating, its contour is shown by a dashed line in Figure 5-1 and is shown individually in Figure C-17.

5.2 Predicted Modal Interference Regions

The 20 CEC modal interference contours received from the Analytic Sciences Corporation were surveyed to identify regions in the North Pacific where the Omega signals were likely to be affected by modal interference. The near-fields of Omega Hawaii and Japan were found to be such regions in this area. The boundaries for these modal interference regions were plotted for winter night and summer day at the transmitter to show the extent of this effect when it is most likely to

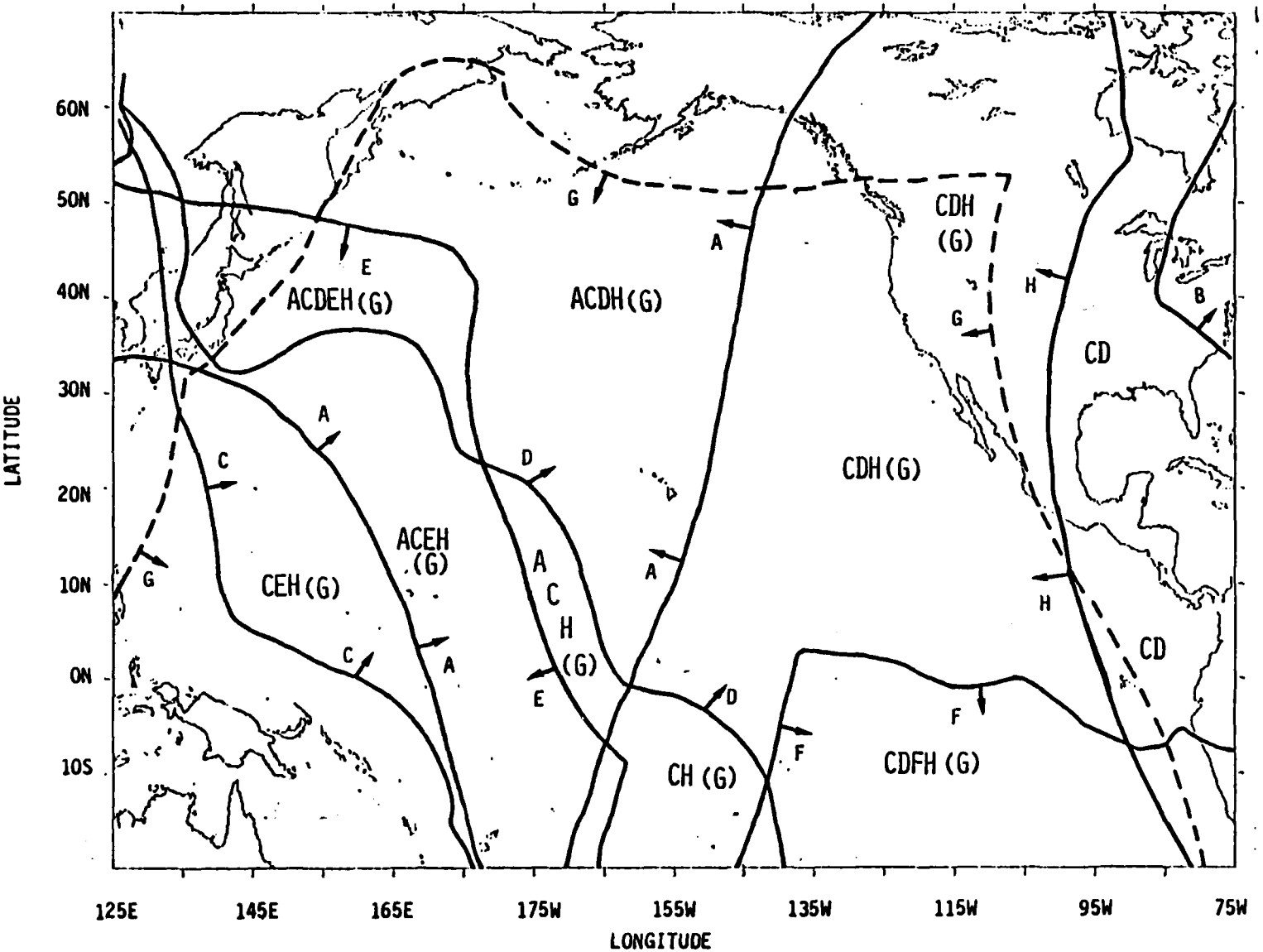

FIGURE 5-1. Composite Diagram of Predicted Signal Threshold Boundaries (-20 dB)

be prevalent. These maps are presented in Appendix C in Figures C-7 to C-10. Note that during the night the predicted modal interference region for Hawaii extends well to the east and all the way west/southwest of the transmitter. The area northwest of the Argentina station is extensively affected by modal interference during the night as shown in Figure C-11 for winter night. This effect makes station F virtually unusable in the North Pacific, although it is often available off the coast of Central America. Indeed, over virtually all of the North Pacific, the 10.2 kHz signals are usually long-path, especially during short-path day (i.e. centered at about 2000 Z).[30]

5.3 Composite Coverage Model

The predicted modal interference regions were subtracted from the area enclosed by the -20 dB signal threshold boundaries to define the regions within which the Omega signals are not only available but also usuable without modal interference effects. These combined contours were derived for all-times, i.e. any region likely to be affected by modal interference at any time during any season was subtracted from the signal threshold area for the Omega transmitter. Thus, the resultant all-time contours are for "worst-case" signal coverage. At certain times of day and season the signal may be available and usuable outside the enclosed region; but, the signal should always be available and usuable within the region defined by the predicted contour. Figure 5-2 displays the predicted all-time signal coverage contours for Omega Norway, Hawaii, North Dakota, La Reunion, and Japan in a composite diagram. These contours are given individually in Figures C-12 to C-16 of Appendix C. Liberia is out-of-range; and Argentina is affected by modal interference in the small southeast area where it is available. Hence, the figures for these stations are not included individually in the Appendix. Since Australia is not yet operating, its contour is shown by the dashed line in Figure 5-2. Because there is no modal interference region for Australia in this area the all-time contour is the same as the signal threshold boundary given in Figure C-17. Figure 5.2 represents the desired Coverage Model to be used in the fix accuracy assessments.

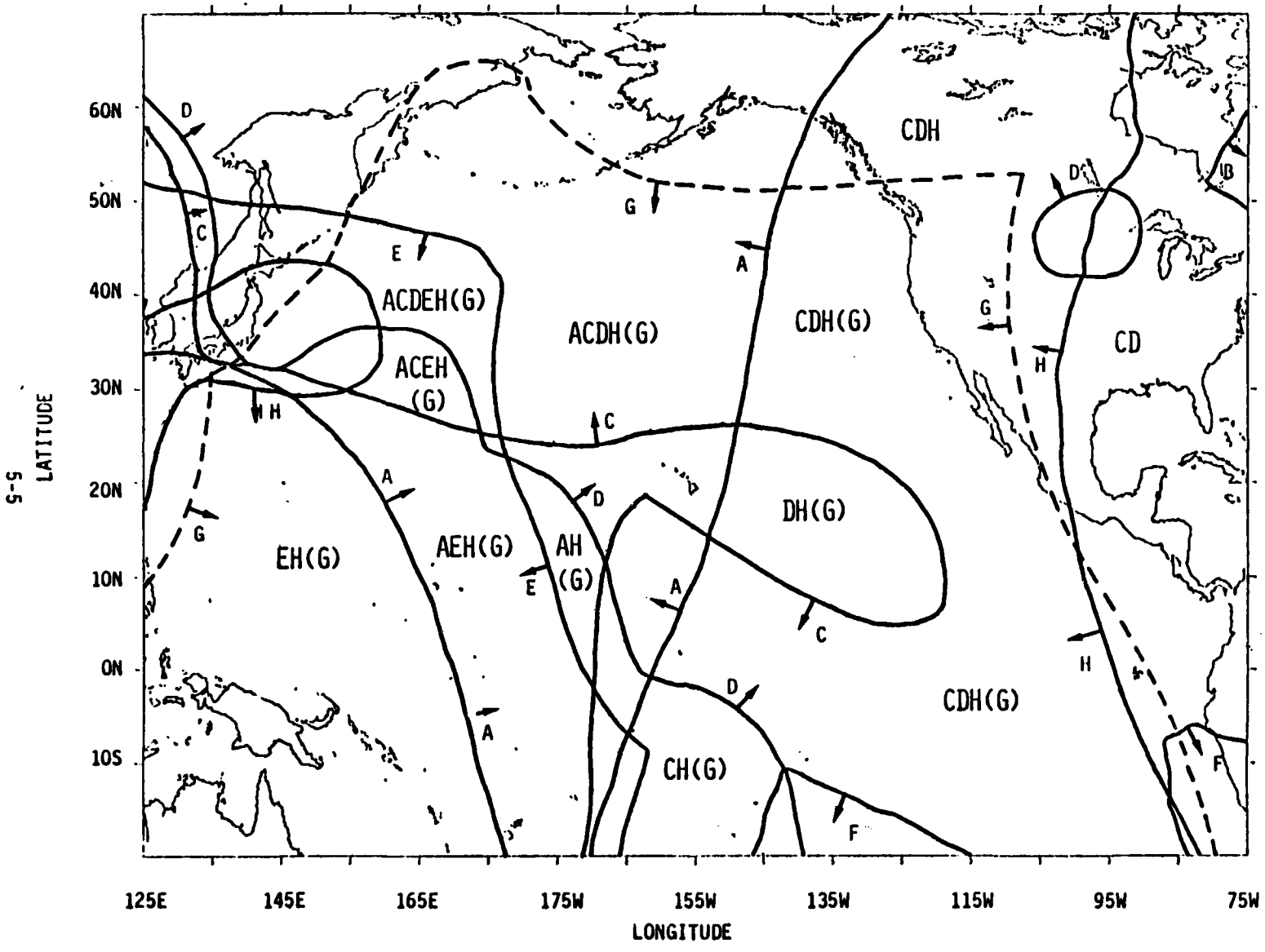

FIGURE 5-2. Composite Diagram of Predicted All-time Signal Coverage Contours

5.4 Comparison With NOSC Test Data

The Naval Ocean Systems Center conducted both airborne and ground-based tests of Omega performance during 1979 in the North Pacific. The results of processing the data from these tests were received in a preliminary report[7]. Although Volume I of the Data Supplement to the NOSC report was unpublished at the time of this review of the test results, the necessary aircraft data was obtained from NOSC for comparison with the predicted all-time signal coverage contours. Volume II of the Data Supplement was reviewed for verification of these contours from the ground data. This section presents the comparisons with the NOSC test data. It should be recalled that the "theoretical" all-time contours which are to be compared with the Test Data represent "worst-case" coverage and thus are expected to be almost always conservative relative to spot observations.

5.4.1 Comparisons With NOSC Aircraft Test Data

Although many flights were made during the NOSC tests of 1979, few of the flights traversed predicted signal boundaries. These flight data were reveiwed for indications of changes in signal coverage. The test data, however, can only be considered a marginal indicator of signal boundaries for 2 reasons: 1) the tracking response of the receivers deteriorates when SNRs are near the -20 dB to -30 dB range and 2) the noise measurements are possibly contaminated by aircraft noise and do not reveal true atmospheric noise. Derivation of SNRs from the observed signal amplitude and the observed noise is, hence, a rough approximation to the actual SNR variations. Therefore, where marginal signal levels have been observed, it may not be reasonable to assume that the signal was indeed fading or below -20 dB. The receivers are not sensitive enough to monitor signal behavior in this range.

Nevertheless, flights within areas where the contours indicate good signal coverage confirmed the predictions. The flight data in support of predicted signal coverage is too extensive to be concisely presented in this report. This data will be published in Volume I of

the Data Supplement to the NOSC preliminary report[7]. Of particular interest here are those areas where the data revealed minimal to non-existent signal coverage in the vicinity of the predicted boundaries or those areas likely to be affected by modal interference.

The observed noise listings for the test flights were used to determine the -20 dB SNR level on the relevant time plots of observed signal amplitude. The time where the SNR dropped below this level was marked and the position found in the listing of the navigation data. The position where the flight was predicted to find the signal boundary was read from the contour plot and the approximate time found in the navigation data listing. Thus, the comparison of observed and predicted boundaries was clearly evident on the time plot. Figure D-1 of Appendix D is an example of a time plot marked in this way. A listing of observed and predicted locations for contour crossings is given in Table D-2 of Appendix D for the flights shown in the figures of this section.

Without reviewing observed phase behavior one can not confidently locate boundaries of regions affected by modal interference. The observed phase data was not processed; however, a rough estimate of the distance from the transmitter at which the signal amplitude stabilizes can be made from the dB-vs.-distance plots for radials from the transmitter. For example, the radial flights from Hawaii confirmed the near-field modal interference of that transmitter. Figure D-2 of Appendix D is one of the radial plots marked where the signal amplitude appeared to stabilize.

Table D-1 of Appendix D lists the flights that traversed predicted signal boundaries. The signal coverage characteristics identified by these flights are discussed below. The relevant figure for the station is noted to the right of the station name. In these figures, an asterisk indicates the boundary location deduced from the test data. Flight numbers are contained in boxes, and the SNR values given in parentheses are discussed in the next section.

A) NORWAY Figure 5-3

Flights 18 and 29 located the eastern signal boundary for Norway about 100-150 miles southeast of Anchorage, about 5^{o} east of the predicted boundary. The Hawaii radial probes, Flights 7 and 8, noted marginal coverage northeast and southeast of Hawaii out to the predicted boundary.

C) HAWAII Figure 5-4

From Wake to Honolulu on Flight 6 the signal was very unstable and most likely affected by modal interference. Flight 7 noted signal instability to the predicted boundary. Flight 8 did not go as far as the boundary but the signal stabilized at approximately the same distance from the transmitter as Flight 7. About 700 km out toward Midway the signal stabilized on Flight 9.

D) NORTH DAKOTA Figure 5-5

Marginal signal coverage faded out near Wake Island on Flight 5, just a little south of the boundary. Modal interference apparently affected the signal until 300 km southwest of FARGO on Flight 22, little more than halfway to the predicted boundary.

E) LA REUNION No figure

Although the predicted boundary indicated that the signal may fade east of the dateline, Flight 6 observed good coverage from Wake to Honolulu with the signal even slightly stronger near Hawaii. (Summer day coverage is much better than coverage at night: however, all-time contour shows "worst-case" coverage, i.e. night-time coverage.)

H) JAPAN Figure 5-6

Flight 22 noted the only discrepancy between observed and predicted coverage. The signal was minimal until almost 10^{o} West of the predicted boundary. Evidently, attenuation due to a partial ice path over the Bering Sea is greater than expected. With the slightly more southern sea path to the transmitter Flight 23 observed good coverage at least as far as Mexico City.

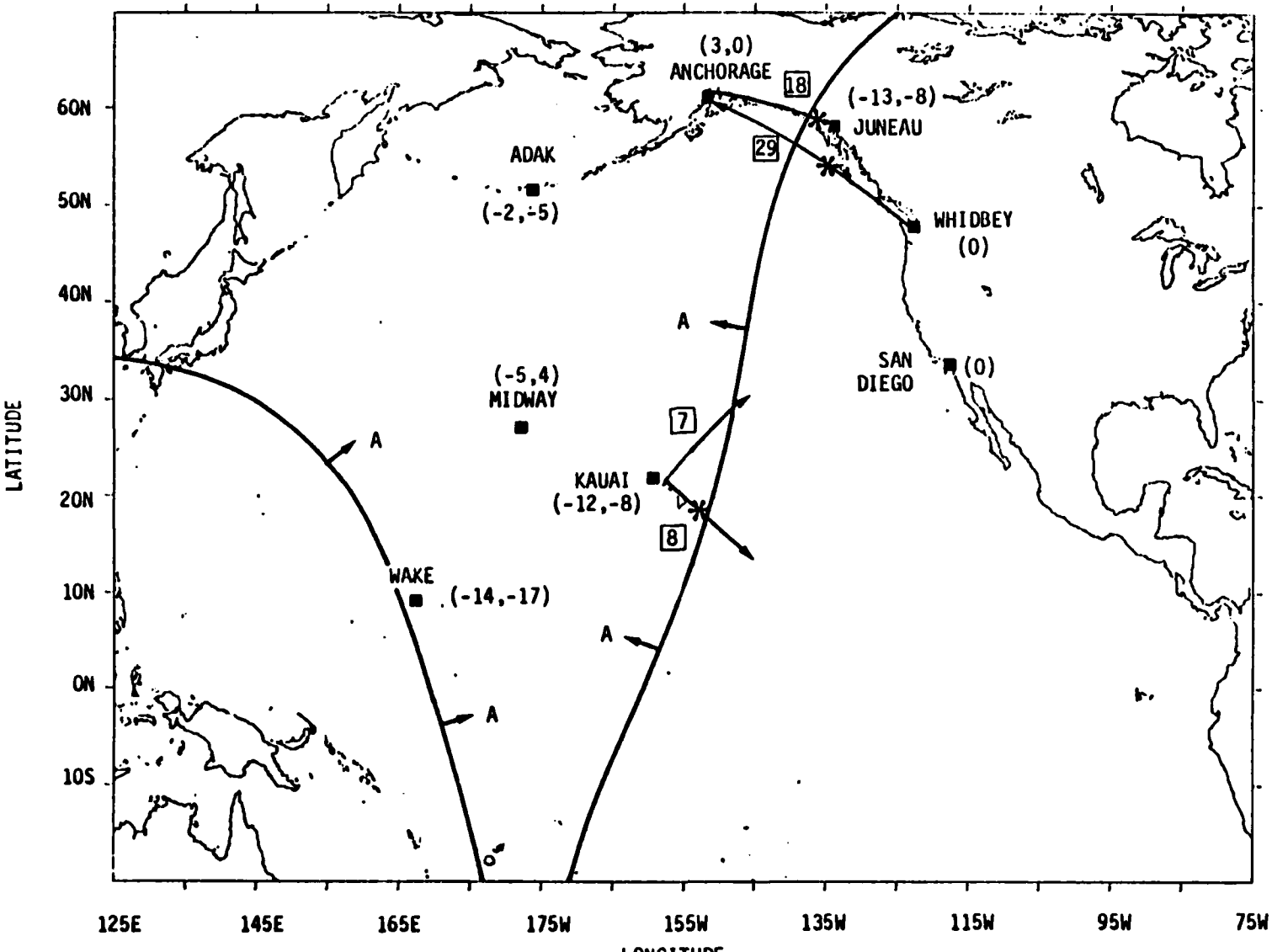

FIGURE 5-3. Comparison of Omega Norway Predicted All-time Signal Coverage Contour with NOSC Test Data

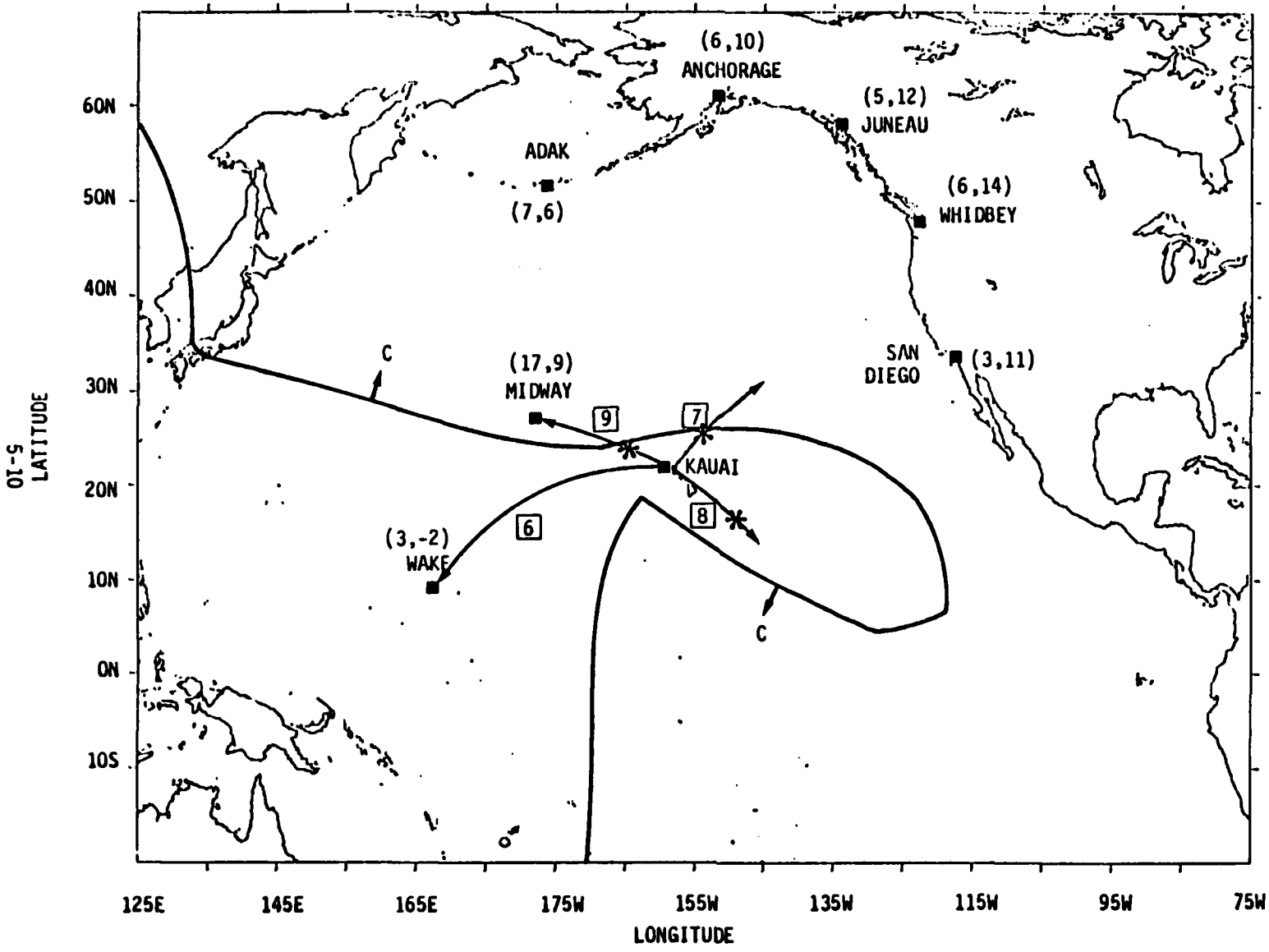

FIGURE 5-4. Comparison of Omega Hawaii Predicted All-time Signal Coverage Contour with NOSC Test Data

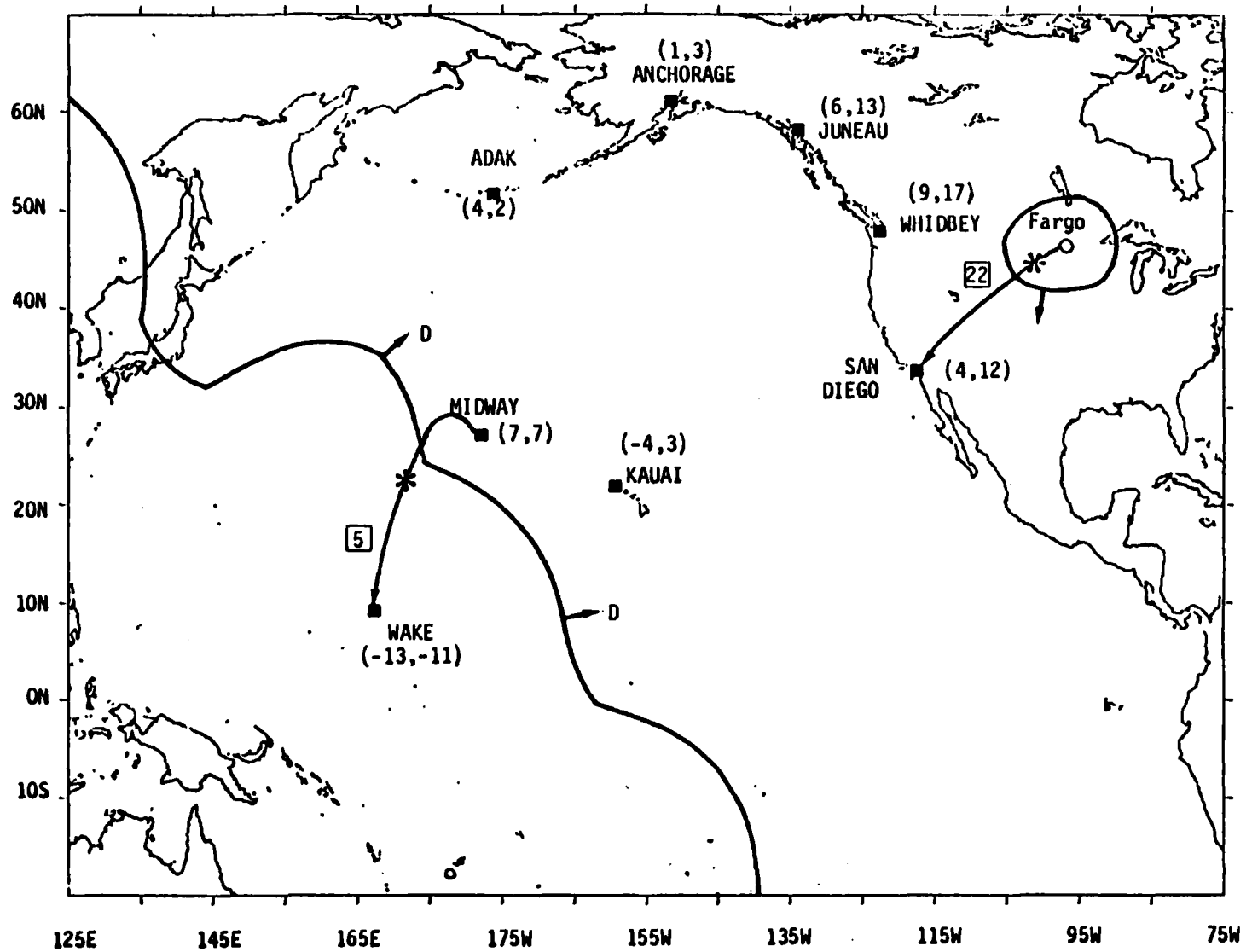

FIGURE 5-5. Comparison of Omega North Dakota Predicted All-time Signal Coverage Contour with NOSC Test Data

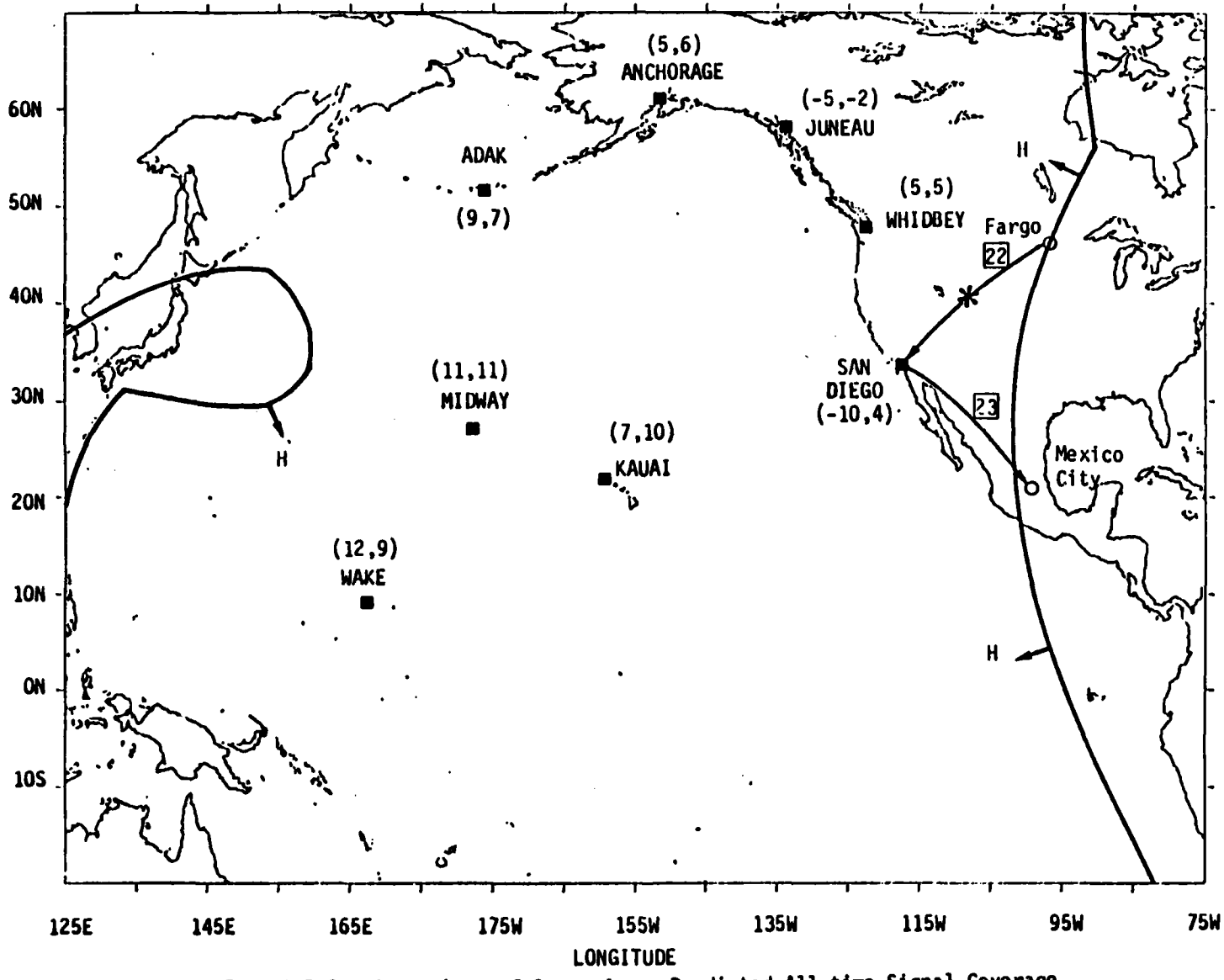

FIGURE 5-6. Comparison of Omega Japan Predicted All-time Signal Coverage Contour with NOSC Test Data

5.4.2 Comparisons With NOSC Fixed-Site Test

The fixed-site data were available in Volume II of the Data Supplement of the NOSC report[7] as weekly plots of mean and standard deviation of calibrated signal amplitude recorded over 24 hrs. To compare this data with the -20 dB SNR contours, the CCIR predicted noise values listed in Table E-1 of the North Pacific Omega Validation Test Plan[24] were used to convert the absolute signal amplitudes to SNR estimates. This conversion was done for 6 times during the day for sample weeks during the summer (June-July-August) each site. These data were tabulated in Table D-3 of Appendix D. The SNR values for day and night (2200 and 1000 GMT) in the region were entered as ordered pairs next to the fixed-site on the contour maps for a quick visual comparison with the predicted contours. The results of this comparison are evident in Figures 5-3 to 5-6 and need not be discussed individually. (The "(0)" next to Whidbey and San Diego in Figure 5-3 indicates that the signal was indistinguishable from noise.) The fixed-site data confirms signal coverage predicted by the contours and some coverage slightly beyond the boundaries, as in the case of Norway at Juneau. Though not shown in a figure, the La Reunion signal was observed at moderate levels at Kauai as well as at Wake; but at the other sites it was mostly noise. Coverage as far east as Kauai is not unusual because there is a wide seasonal variation in the range of La Reunion's signal and the all-time contour depicts "worst-case" coverage.

5.5 Comparisons with Non-Test Data

The Omega MASTERFILE data received from ONSOD were analyzed for station usage in the region. The various monitor sites were plotted on the composite diagram of the predicted all-time signal coverage contours. Next to each site shown in the resulting Figure 5-7 are the Omega stations observed at the site at any time from 1970-1979. Station letters in parenthesis indicate that although data were collected for that station, the data were flagged as being in error in some way. For example, stations B, E, and F were monitored at Seattle and San Diego

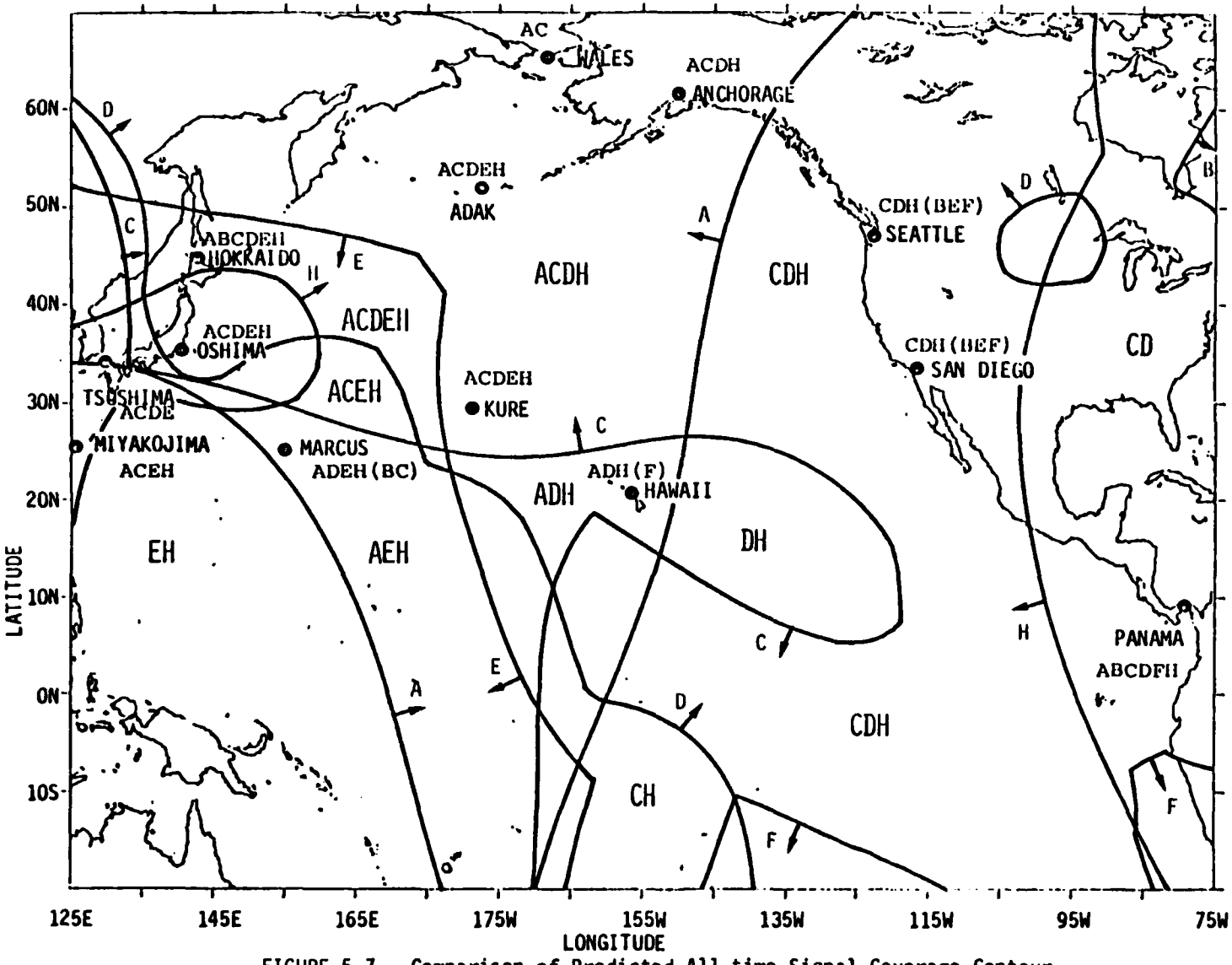

FIGURE 5-7. Comparison of Predicted All-time Signal Coverage Contour with Non-test Data from Omega MASTERFILE

but the data were error flagged. This is as expected because these sites are located where these stations are either out-of-range or subject to modal interference. A survey of the figure shows general agreement between actual station usage and predicted coverage. The conservative nature of the contours is, however, evident in that stations are often available slightly beyond the contour. La Reunion was observed at Adak and Kure, for instance, to the east of the predicted boundary; and North Dakota was observed at Marcus and Tsushima, just west of the contour.

5.6 Comparisons With Operational Data

The predicted all-time signal coverage contours for each Omega station are compared in this section with the results of the analysis of operational data collected in the North Pacific. Appendix A contains the description of this data, the methods of analysis applied to the data, and the results in tabular or graphical formats. For ease of comparison three types of figures were constructed for each station using figures from Appendix A with the all-time contour for that station superposed.

The first type of figure, exemplified in Figure 5-8, is a cylindrical projection of the North Pacific region with the ships' paths noted by dotted lines and the Pan-American flight routes noted by solid lines. (Note that 165°E and 10°S were the limits for processing the Pan-Am data.) Waypoints for the China Airlines flights are noted by small triangles. This figure is essentially Figure A6-1 of Appendix A with the labeling omitted for clarity. Reference to that figure easily identifies any given path or route. The signal boundary is shown by a heavy solid line with arrows next to the station letter pointing toward increasing signal strength. Asterisks accompanied by an arrow on the ships' paths or flight routes note positions where station usage began or ended; the arrow points to the portion of path along which that station was used to obtain location. If the station was off-the-air for a voyage or flight, the path is not shown in the figure. If the station was not used at all for a voyage or flight, the path is not shown.

The second type of figure is the azimuthal equidistant projection of the world centered on the given transmitter which displays the "OK" data from the MAGOEXEC station data file as described in Section A2.2.3 of Appendix A. The appropriate "all-time" contour was superposed on Figures A2-20 to A2-26 of Appendix A to compare these contours with the shipboard observations of station coverage. These figures are referred to as OK plots in the discussion and are given in Appendix E. Figure E-1 is an example of this type of plot.

The third type of figure is the azimuthal equidistant projection of the world centered on the given transmitter which displays the positions of possible modal interference noted in the MAGOEXEC station data file as described in Section A2.2.3 of Appendix A. The "all-time" contour for the appropriate transmitter was superposed on Figures A2-27 to A2-33 of Appendix A. The resulting figures, referred to as MI plots in the discussion, provide an easy comparison of potential problem areas with the predicted contours and are given in Appendix E. Figure E-2 is an example of this type of plot.

A survey of the three figures generated for each station shows that the "all-time" contours are conservative estimates of signal boundaries. Because of seasonal and daily variations in signal coverage, station usage beyond the noted boundary is to be expected; however, this extended coverage was generally within 5-10 degrees of the boundary. Only in the case of La Reunion did the boundary seem too conservative an estimate. (See notes below.) Signal coverage within the contours is confirmed by the operational data, though the shipboard data indicates modal interference to be a potential source of error throughout the region but most likely in the near-field of the transmitters. Specific comments regarding the comparison of the operational data with the predicted contours are as follows:

A) NORWAY Figures 5-8, E-1, E-2

The western edge of the "Greenland Shadow" was noted clearly by both ships and aircraft. The LIBERTY on its return voyage to San Franscisco found station A available beyond this edge (see OK plot) but stopped using A in computing best fix about 8 degrees west of the noted boundary, indicating that the signal fades near the boundary. The WILSON and the OCEANOGRAPHER both began picking up A just prior to exiting the shadow, which further suggests that the boundary would be more accurately depicted by a narrow strip about 10 degrees wide. Pan-Am flight E900, however, bound for San Francisco, found the edge crisp and clear at 145 W. The MAGDELENA observed the eastern edge of the "Greenland Shadow", even though the contour does not show coverage in this region. The OK plot further shows this more Southeast Pacific coverage. Also note that coverage extends well beyond the more western boundary shown; no evidence from the operational data confirms this predicted limit. Occassionally, A is available at a minimal level within the shadow, as was observed by Pan-Am flight B953. Modal interference is most likely within 10 degrees east of the Japan and within 15 degrees west of the Hawaii transmitters. (See MI plot.)

B) LIBERIA No figures

The LIBERIA transmitter is out-of-range within the North Pacific; so, the signal coverage boundary does not traverse the region. Therefore, this station was omitted from consideration. Minimal availability of station B was observed west of 155E on the fringe of its range.

C) HAWAII Figures 5-9, E-3, E-4

Both the Canadian Marconi CMA-740 and the Magnovox MX-1104(5) automatically deselect the Omega station within 300 nmi of the transmitter; therefore, the operational data neither confirms nor invalidates the shape of the signal boundary in the near-field of Hawaii. The OCEANOGRAPHER data displayed in the OK and MI plots, however, does seem to verify that the near-field effect extends further east than a 300 nmi-radius circle would indicate. Positions of possible modal interference were much more prevalent than OK data points through the eastern lobe of the signal boundary. The LIBERTY voyage west of the station also shows modal interference a likely occurrence in that direction, although the signal provides good results in that area.

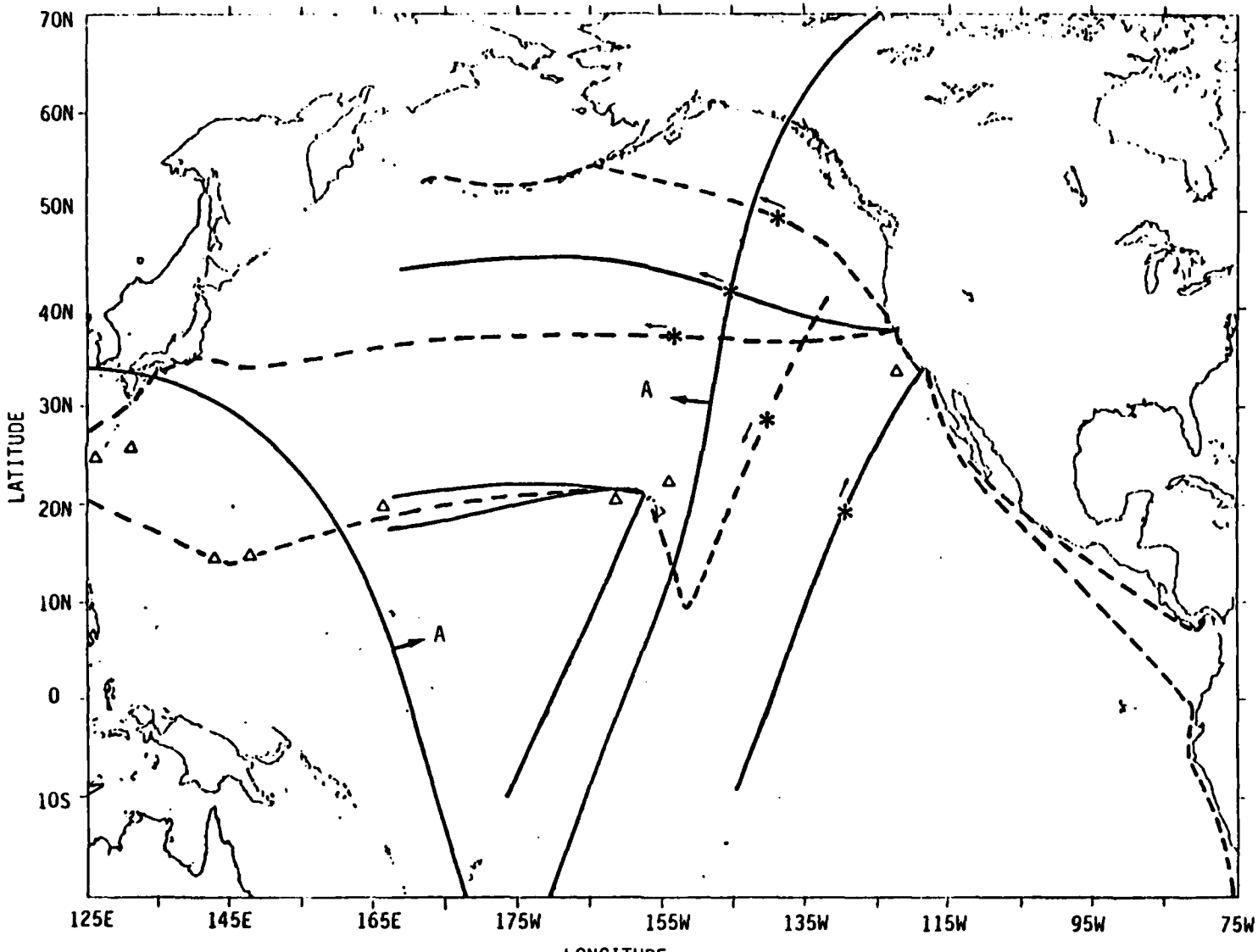

FIGURE 5-8. Comparison of Omega Norway Predicted All-time Signal Coverage Contour with Operational Data

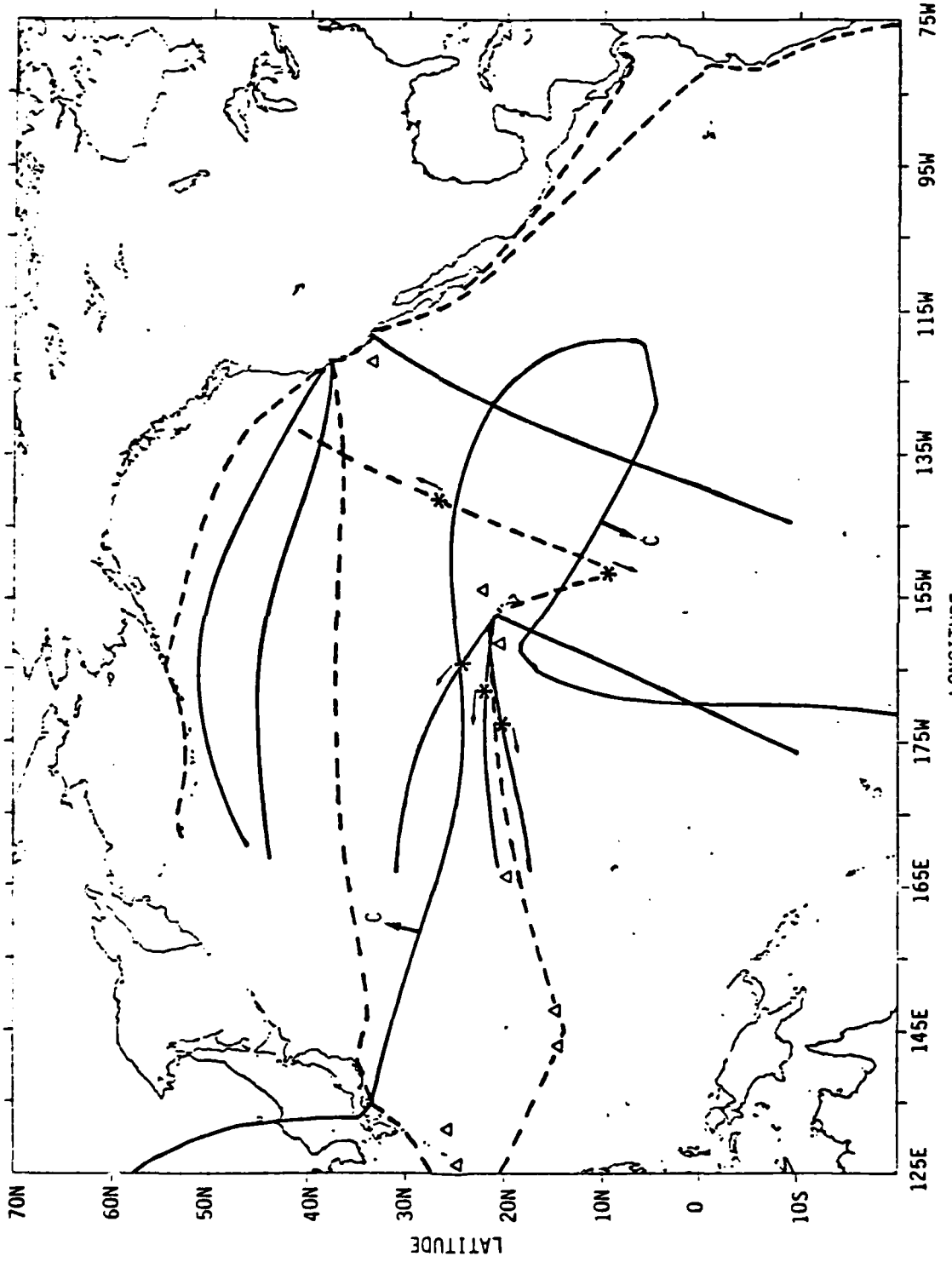

FIGURE 5-9. Comparison of Omega Hawaii Predicted All-time Signal Coverage Contour with Operational Data

D) NORTH DAKOTA — Figures 5-10, E-5, E-6

Even beyond the predicted limit of signal coverage, station D was used effectively for navigation. The operational data confirms the strength and availability of the North Dakota signal throughout the North Pacific. To the west of Hawaii and Japan are small areas of possible modal interference. No evidence was found in the operational data to confirm the location of the predicted signal boundary.

E) LA REUNION — Figures 5-11, E-7, E-8

A glance at Figure 5-11 indicates that station E is usable further east than the predicted boundary and suggests that, perhaps, the boundary is too conservative an estimate of signal coverage. The TASC contours indicate a wide-seasonal variation in the range of La Reunion's signal. The all-time contour shows "worst-case" coverage; so, coverage east of the contour is likely at certain times of year, (e.g. in May and November at 1800 GMT the TASC contours show coverage to the California coast). Pan-Am flight X935 experienced some problem with station E just east of the boundary; but the MI plot shows that the LIBERTY found this position an area of potential modal interference. LIBERTY also noted this problem 10 degrees south and east of the northern limit of signal coverage - perhaps in support of fading signal strength.

F) ARGENTINA — No figures

Except for the southeastern area of the North Pacific off the coast of Central America, station F is out-of-range for most of the region. The predicted signal boundary barely enters the region; and only the MAGDELINA traversed this area using the Argentina signal south of Mexico. Pan-Am flights B953 and FB951 observed signal coverage southeast of Hawaii. Other studies[30] indicate that the 10.2 kHz signal is long-path over most of the N. Pacific, especially during short-path day (circa 2000Z).

G) TRINIDAD — No figures

Operational data for the temporary station at Trinidad is not relevant to validation of the permanent Omega system; therefore, it is not considered here. Furthermore, no operational data is yet available for comparison with the predicted Australia coverage boundary, because that station is not operable at this time.

H) JAPAN — Figures 5-12, E-9, E-10

Strong signal coverage for Japan was verified by the operational data for the whole of the North Pacific. The MAGDELINA observed station H all the way down the coast of central and South America. The LIBERTY noted the near-field of the transmitter as an area most likely affected by modal interference. The predicted eastern boundary is probably a conservative estimate of JAPAN's coverage.

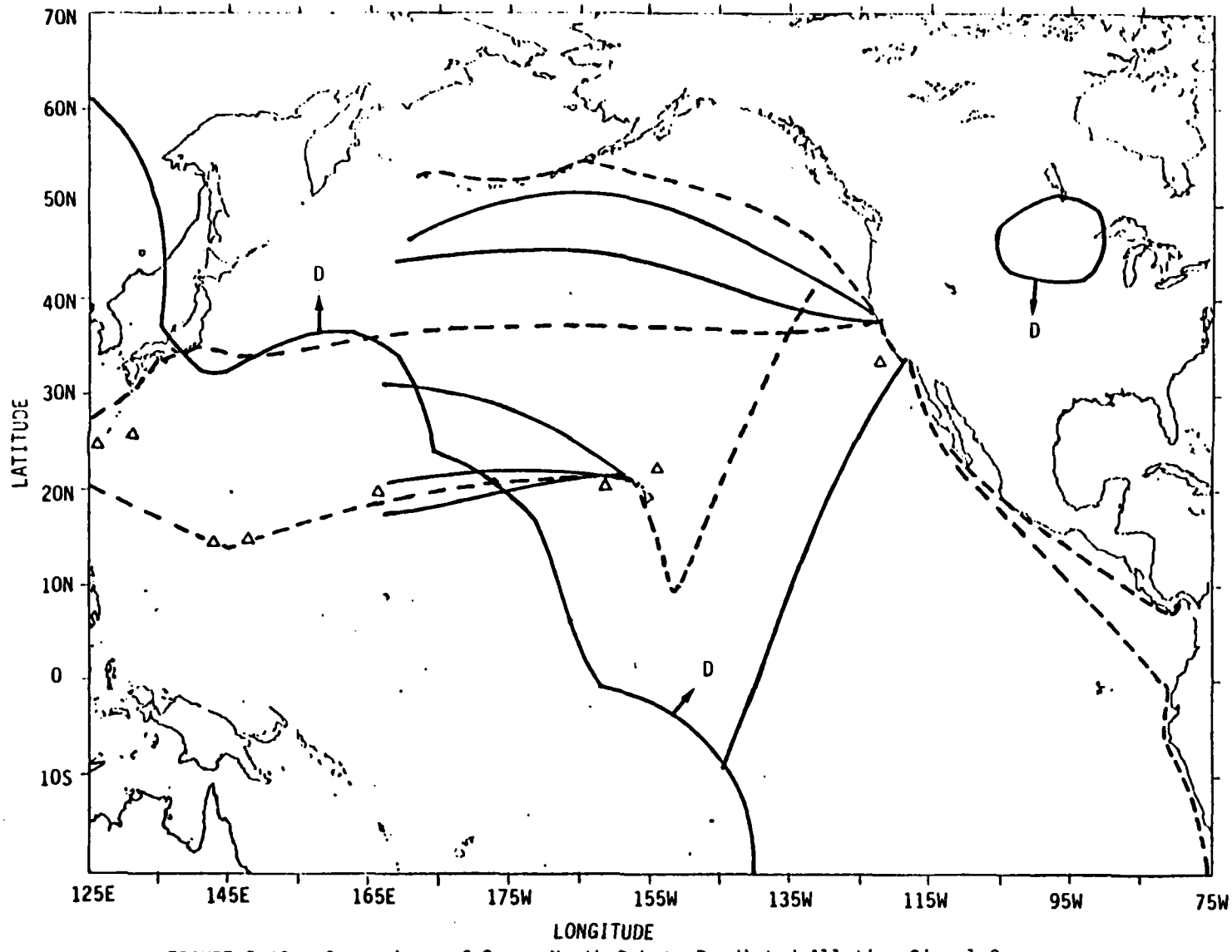

FIGURE 5-10. Comparison of Omega North Dakota Predicted All-time Signal Coverage Contour with Operational Data

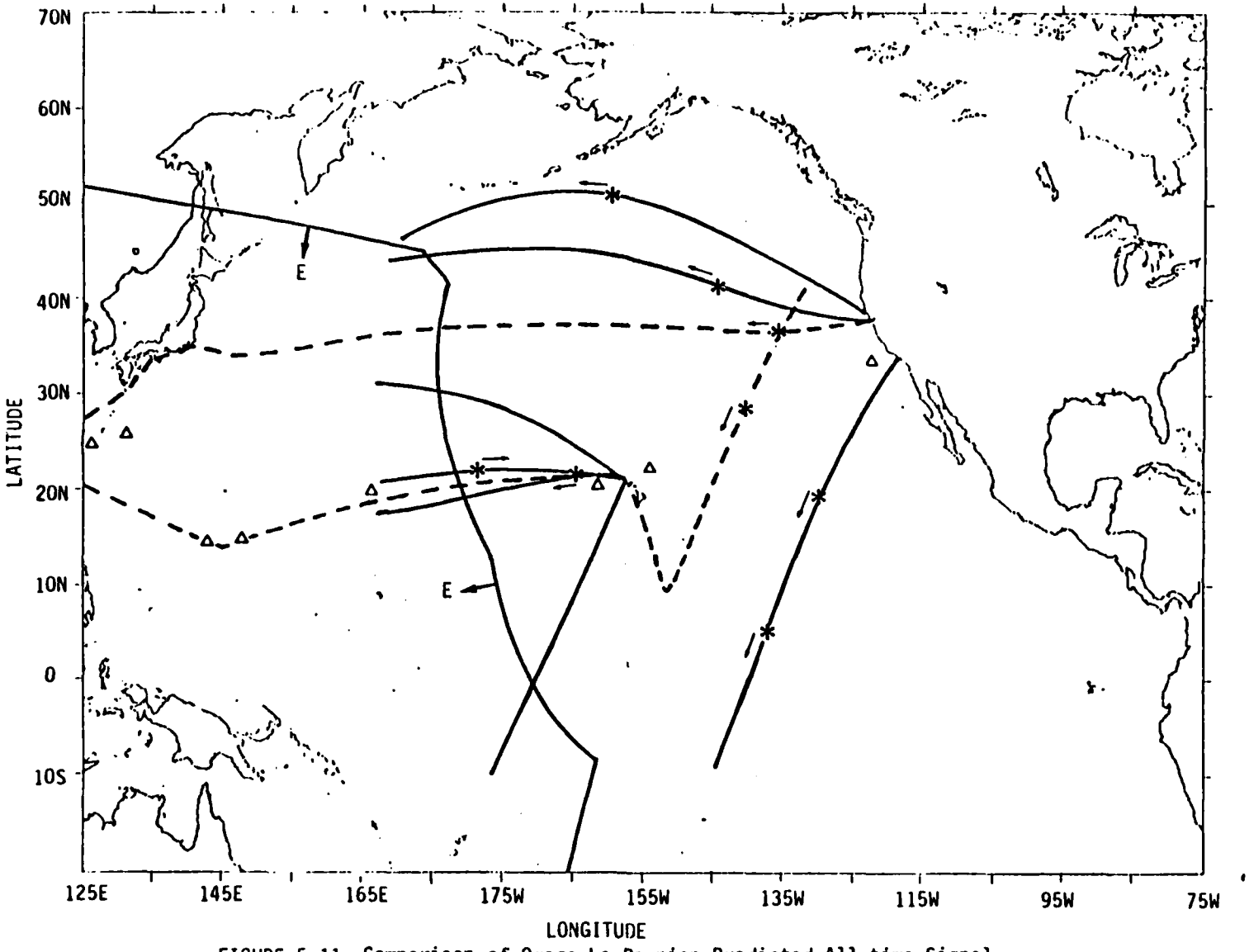

FIGURE 5-11. Comparison of Omega La Reunion Predicted All-time Signal Coverage Contour with Operational Data

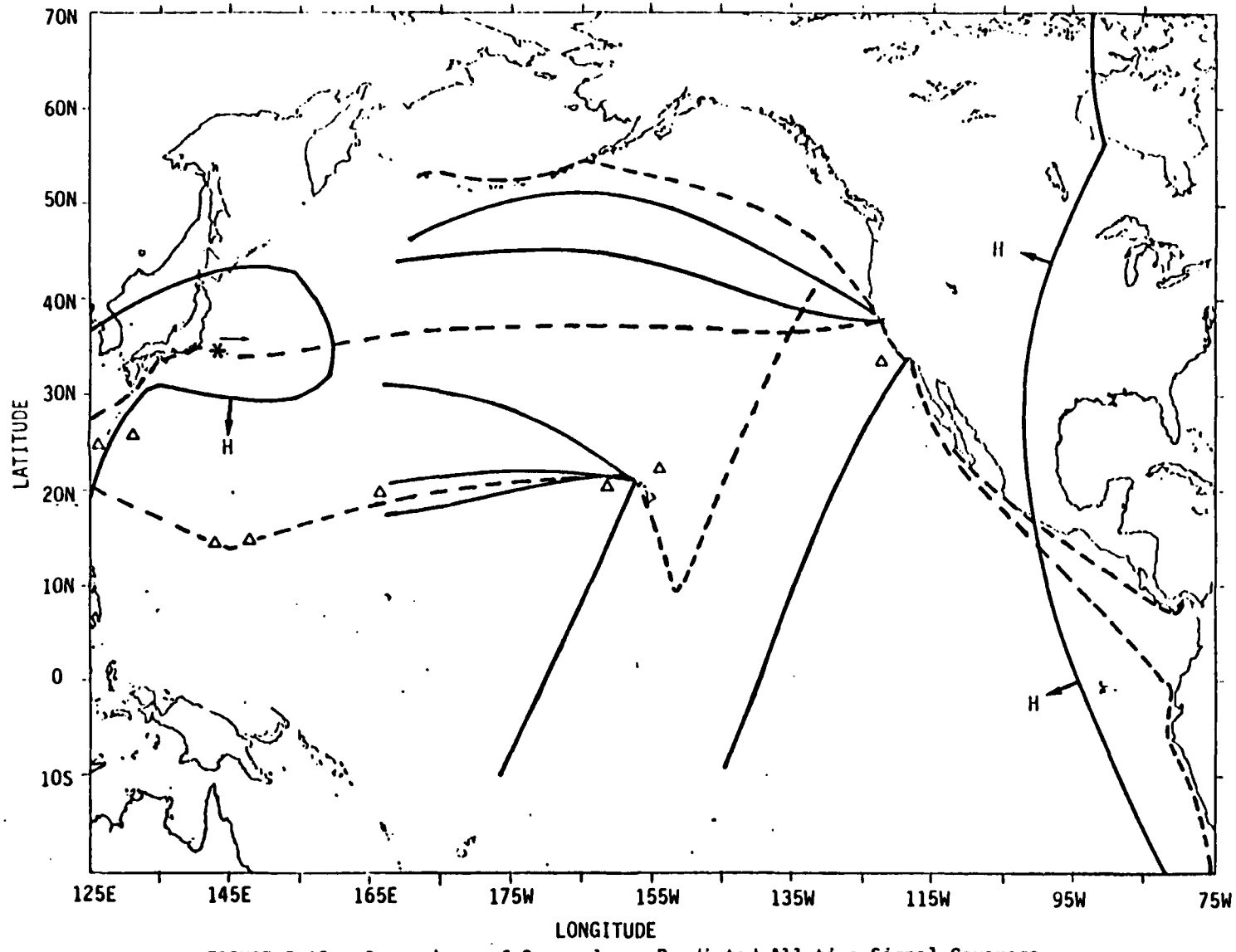

FIGURE 5-12. Comparison of Omega Japan Predicted All-time Signal Coverage Contour with Operational Data

6.0 NORTHERN PACIFIC FIX ACCURACY AND COVERAGE MAPS

The essential elements - a Phase Error Model and a Coverage Model - are now in hand to apply the position fix accuracy model developed in Section 3 to the N. Pacific validation region. The phase errors, $\{\sigma_i\}$, associated with OMEGA navigation signals from each transmitter site were obtained in Table 4-14 and are collected in Table 6-1. Recall that the slight degree of variation observed in these errors between 10.2 and 13.6 kHz motivated their application uniformly to all four signals from each site.

Table 6-1. Summary of Phase Error Model (R.S.S. Phase Error in CEC)

STATION	INCLUDING PPC BIASES	WITH PPC BIASES REMOVED
A	11.5	5.0
B	21.0	17.1
C	9.0	4.4
D	12.5	9.4
E	21.3	19.3
F	22.7	17.5
G	22.7	17.5
H	13.2	10.0

The full-time Coverage Model, derived and conservatively validated (at 10.2 kHz) in Section 5, is shown in Figure 6-1. Here, the area outside the primary validation region has been shaded to emphasize that the coverage boundaries are intended for application only to this region. Within the validation region, four areas are shaded to identify zones which depend on the Australia station to provide the three station coverage required for hyperbolic navigation. (As will be seen in Section 6.5 these zones are - relatively speaking - less significant from the standpoint of traffic density and user requirements). Note that the navigationally important great circle routes between Japan and the West Coast U.S. ports are covered by at least four stations (including Australia).

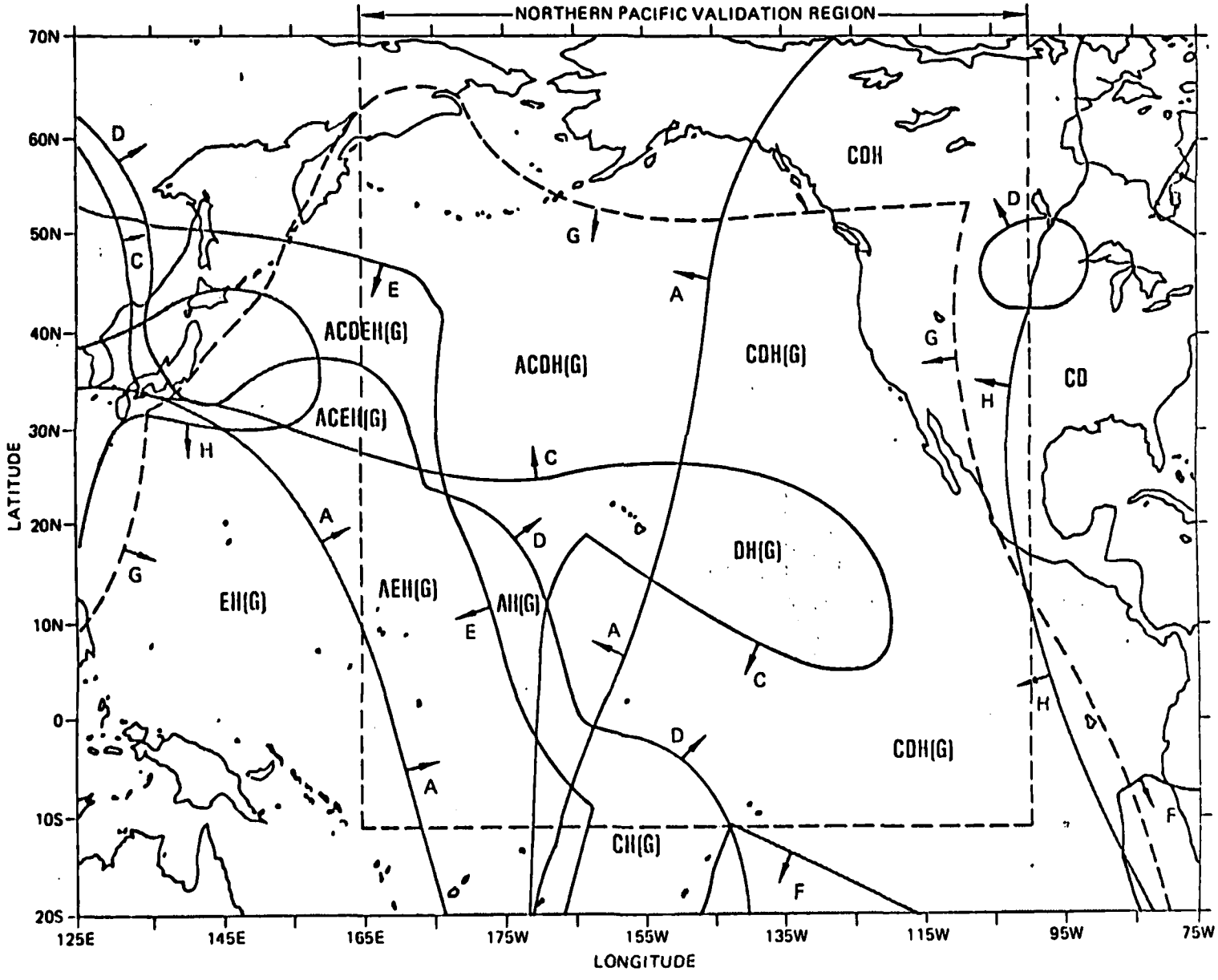

FIGURE 6-1. COMPOSITE DIAGRAM OF FULL-TIME SIGNAL COVERAGE CONTOURS

The coverage boundaries of Figure 6-1 were generated in the form of a (1 degree resolution) range-azimuth table for each station. A computer program was written in which the total area of Figure 6-1 is scanned in a grid of (nominally) 1.3^{o} resolution in longitude and 1.1^{o} resolution in latitude. At each grid point, range and bearing to all OMEGA stations are computed and - using these coverage tables - the mix of usable signals is thereby obtained. Applying the phase errors of Table 6-1, and summing over this mix of usable signals as indicated by the theory of Section 3, the program then computes the three fix error measures of interest: r.m.s. (circular) error, 50% CEP and 95% CEP at each grid point. Finally, a line-printer map is generated in which the integer part of the given fix error measure is printed at each grid point, super-imposed upon a map of major coastal boundaries. In selected cases of particular interest, contour maps of fix accuracy were also generated - using a digital plotter - by applying standard contouring routines to the grid of computed fix error values.

In the first applications of these techniques (Section 6-1), the Australia station is not used. This is in order to establish contact with past experience under the partially implemented OMEGA system. In Sections 6-2 and 6-3, these assessments are then respectively compared with the integrated satellite/OMEGA shipboard data and the other operational data analyzed in Appendix A.

The fix accuracy maps for the fully-implemented OMEGA system are presented in Section 6.4. While primary emphasis is given to four-frequency operation using PPC's as they were in 1979, maps are also generated for single-frequency OMEGA and for the case where PPC bias errors have been removed. (The latter case may be viewed as an assessment of OMEGA under fully ideal conditions, viz. optimum combinational filtering of the multiple signals and PPC's refined to the point of being bias-free). The accuracy assessments are discussed in the context of user requirements of the marine and aviation communities in Section 6.5.

6.1 Partially Implemented System

The line-printer map of r.m.s. (circular) errors obtained without station G is shown in Figure 6-2. Each integer printed is the integer part of the r.m.s. error (nmi) at the indicated grid point. If the r.m.s. error is less than 1 nmi, the grid point is left blank. Errors in excess of 10 nmi are indicated by a ">", and the symbol "#" means that fewer than 3 stations are usable at the grid point on a full-time basis. Major coastlines and islands are indicated by a semicolon. (These conventions will be follwed in all such plots).

Figure 6-2 predicts that without station G, r.m.s. errors should be less that 2 nmi in the northern half of the N. Pacific validation region. Accuracy degrades south of Hawaii, particularly to the southeast. The zones of inadequate (<3 station) coverage to the east, west and south of Hawaii which were noted earlier are also apparent. The figure also predicts degradation in accuracy as one proceeds south along the west coast of Mexico towards the Panama Canal. At the other extreme, excellent accuracy (<1 nmi rms) is predicted near the Aleutian chain.

Similar plots for the (50%) CEP and (95%) CEP errors are given in Figures 6-3 and 6-4 respectively. Differences in the shape of the error contours are a manifestation of the different dependences of the various error measures on the eccentricity of the error ellipse. The general structual complexity of these plots illustrates the interplay of GDOP and coverage. Figure 6-5 is a contour plot generated from the data grid of Figure 6-3. Here, the type of cross-hatching encodes the fix error range for the contour, as indicated in the legend.

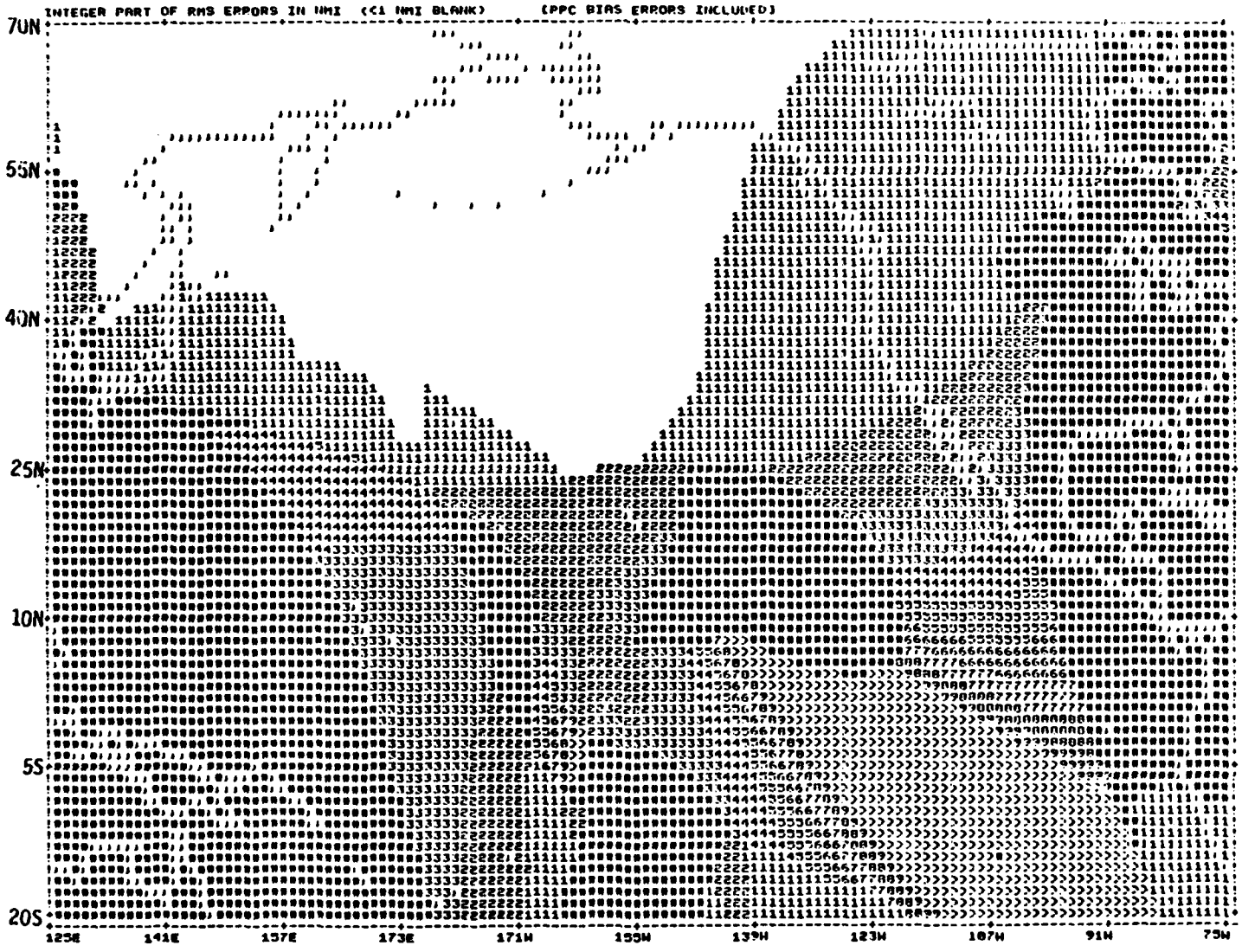

FIGURE 6-2. RMS CIRCULAR ERRORS IN N. PACIFIC (WITHOUT STATION G)

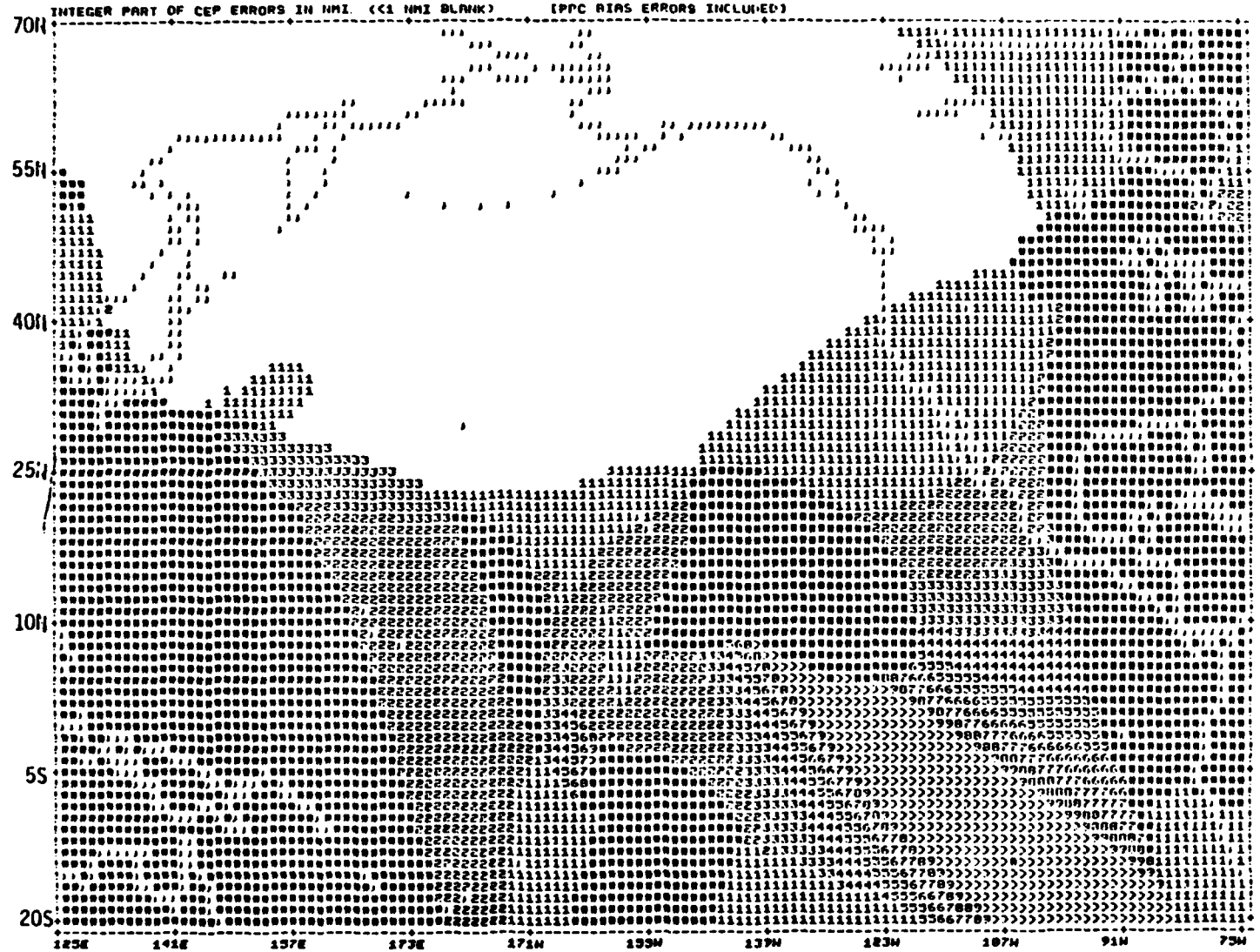

FIGURE 6-3. 50% CEP ERRORS IN N. PACIFIC (WITHOUT STATION G)

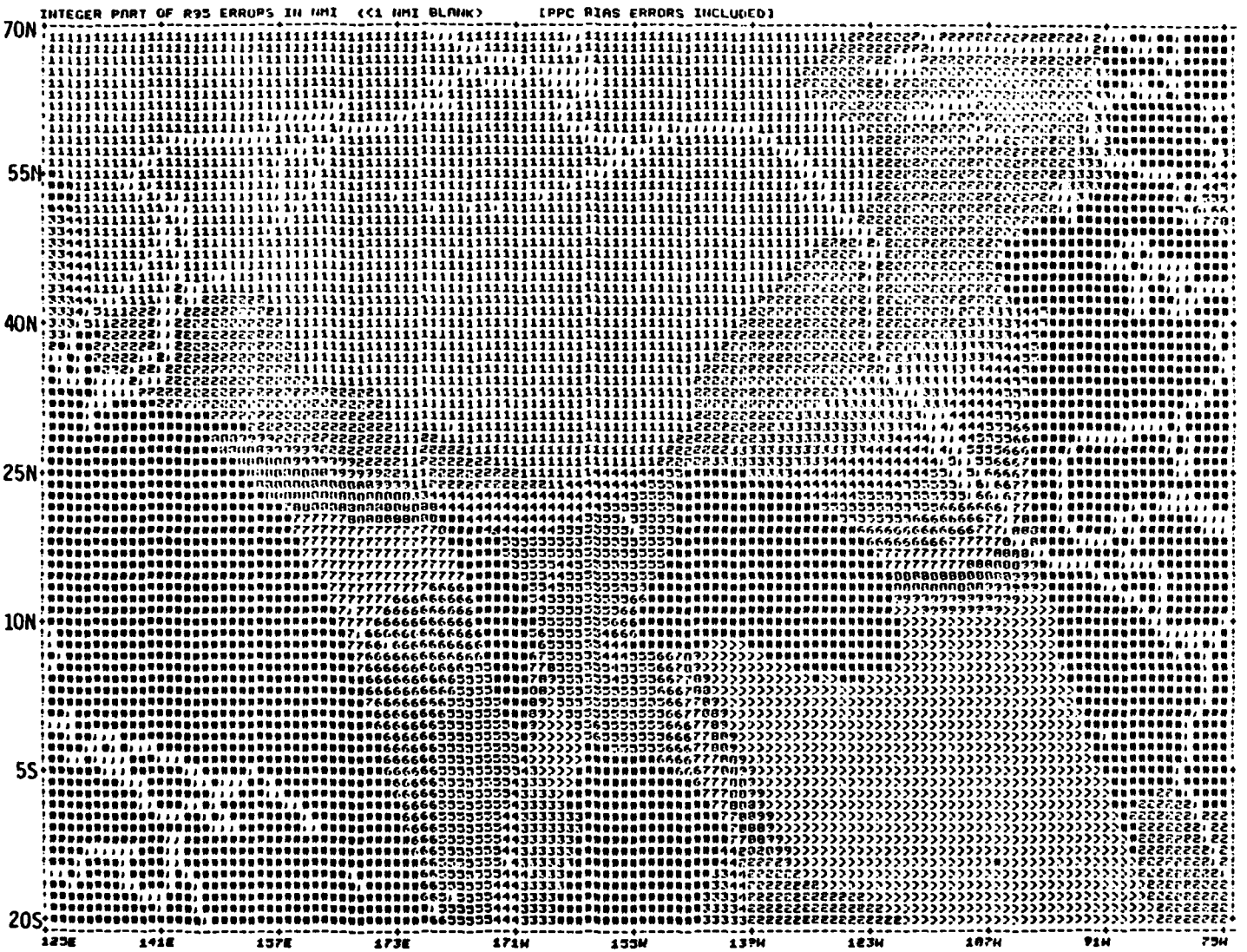

FIGURE G-4. 95% CEP ERRORS IN N. PACIFIC (WITHOUT STATION G)

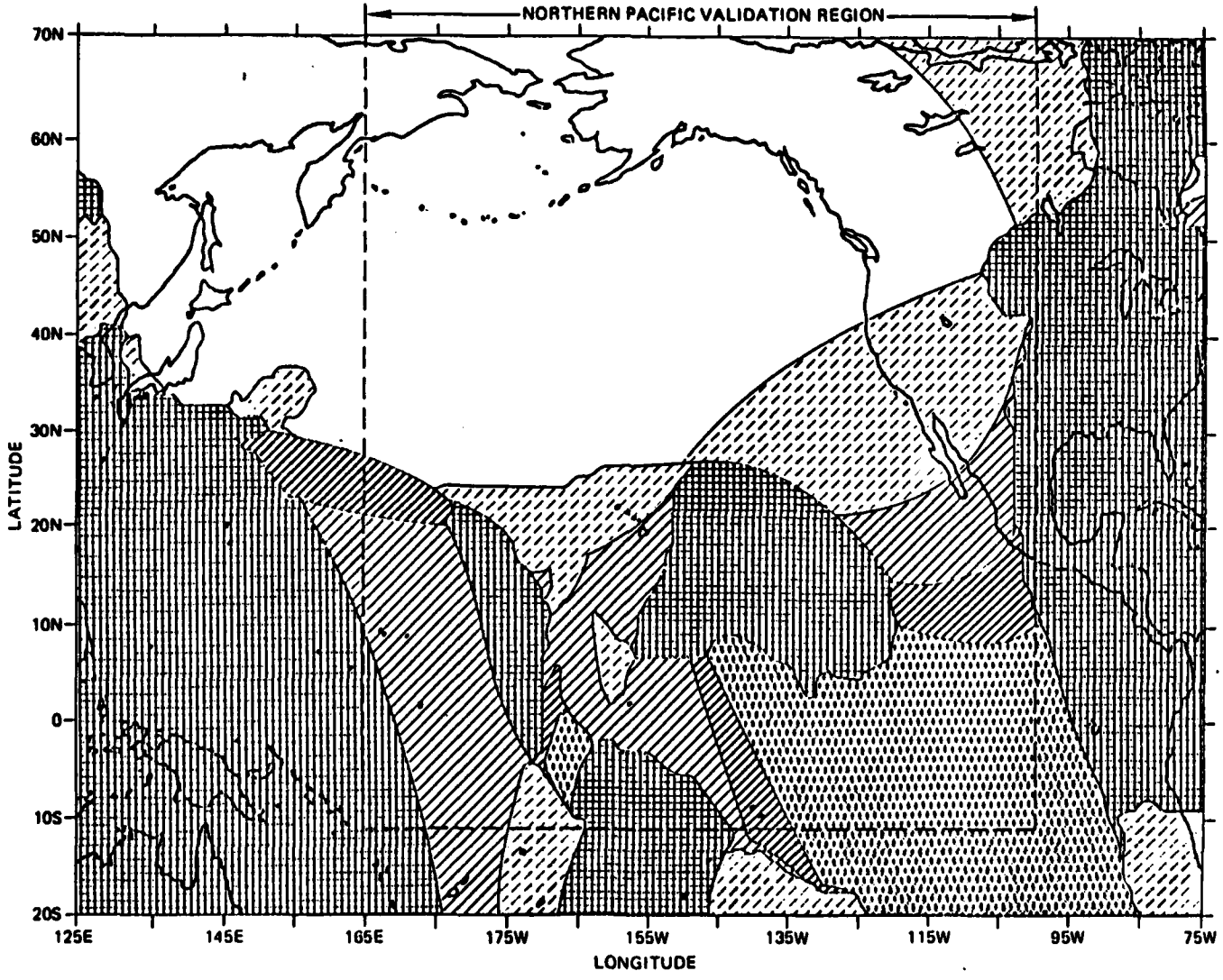

FIGURE 6-5. 50% CEP ERRORS WITH STATION G OFF-AIR (4-FREQUENCY OMEGA – WITH PPC BIASES)

LEGEND: < 1 NMI | 1-2 NMI | 2-3 NMI | 3-4 NMI | > 4 NMI | < 3 FULL TIME STATIONS

6.2 Comparison with Integrated Satellite/OMEGA Shipboard Data

The integrated satellite/OMEGA shipboard data, presented in depth in Section A-2 of Appendix A, represents the best quality data for comparisons with our model since the satellite fixes - accurate to a few hundred meters - allow relatively precise determination of radial errors. Also, recording actual measured phases permits ex post facto fix generation using accurate PPC's, thereby avoiding dependence upon receiver-specific fix algorithms.

The data of Section A.2.3.1 were examined and seven voyage segments were identified which lay within the primary N. Pacific validation region, as indicated in Table 6-2. For each such segment, the experimentally observed error measures (50% CEC, 95% CEP, RMS) were each averaged over the three frequencies for which data were available. This was necessary since fix accuracies had been generated on a single-frequency basis, i.e. rather than combining data from different frequencies. The theoretical predictions were obtained directly from the appropriate regions of Figures 6-2 through 6-4.

As seen in Table 6-2, the measured data are generally in very good agreement with the theoretical predictions, both with respect to error magnitudes and the variation of system accuracies from one region to another. (Indeed, comparisons of the fine structure of the geographical variation of measured fix accuracies shown in Appendix A with corresponding details of the theoretical contours indicate very similar morphologies). Also gratifying is the agreement, within each case, of the relative magnitudes of the three error measures. It is therefore concluded that the integrated satellite/OMEGA shipboard data are generally consistent with the fix accuracy model upon which will be based assessments for the fully-implemented OMEGA system.

TABLE 6-2. COMPARISON OF PREDICTED ACCURACIES WITH INTEGRATED SATELLITE/OMEGA DATA

SHIP (VOYAGE SEGMENT)	GEOGRAPHICAL REGION PROBED	DATA REFERENCES (APPENDIX A)	CIRCULAR ERROR MEASURES (NMI) 50% CEP		95% CEP		RMS	
			EXP*	THEOR	EXP*	THEOR	EXP*	THEOR
OCEANOGRAPHER (II)	ENVIRONS EAST, SOUTHEAST OF HAWAII	FIGS A2-2, A2-3, A2-4 TABLE A2-2	2.1	2-3	6.7	5-6	3.4	2-3
WILSON (II)	ALEUTIANS, GULF OF ALASKA	FIGS A2-5, A2-6, A2-7 TABLE A2-3	0.6	<1	1.6	1-2	.95	<1
MAGDELINA (AI)	W. COAST OF MEXICO	FIGS A2-8, A2-9, A2-10 TABLE A2-4	1.4	1-3	5.6	4-6	2.5	2-3
MAGDELINA (BI)	W. COAST OF MEXICO	FIGS A2-11, A2-12, A2-13 TABLE A2-4	1.4	1-3	5.6	4-6	2.6	2-3
LIBERTY (AI)	ENVIRONS WEST OF HAWAII	FIGS A2-14, A2-15, A2-16 TABLE A2-5	1.3	1-2	3.6	4-6	1.9	1-2
LIBERTY (BII)	NORTH CENTRAL PACIFIC (JAPAN-SAN FRANCISCO)	FIGS A2-17. A2-18, A2-19 TABLE A2-5	0.6	<1	1.9	1-2	0.9	<1
LIBERTY (BIII)	W. COAST U.S. (SAN FRANCISCO)	FIGS A2-17, A2-18, A2-19 TABLE A2-5	1.8	1-2	4.0	2-3	2.5	1-2

* NOTE: "EXP" is average of 10.2, 11.3 and 13.6 kHz single-frequency measured fix accuracies.

6.3 Comparison With Operational Data

Less clear-cut are comparisons with the operational data described in-depth in Sections A-3, A-4 and A-5 of Appendix A. Here we must contend with idiosyncracies of (the generally sup-optimal) receiver position-fixing algorithms, smaller statistical samples, less precise reference positions (e.g. INS), inappropriate station selection, and an over-all lesser degree of documentation relative to what was available with the integrated satellite/OMEGA data.

The China Airlines data (see Table A3-1, Appendix A) avoids the reference position problem since it is based upon fixes at well-defined waypoints. The results (waypoint 1 through 4) show a fairly uniform mean radial error of 2.8-2.9 nmi along the nominal track: Los Angeles-Hawaii-Taipei. This is generally consistent with the 1-3 nmi (50%) CEP errors shown in Figure 6-3 for this track, expecially when one considers that the standard deviations of the measured radial errors range from 1.4-2.2 nmi.

The Pan American data is summarized in Table A4-2 of Appendix A. Flights with questionable INS references, with critical OMEGA stations off-air, or which used (temporary) station G are not applicable in comparisons with the theoretical model. Of the remainder, Flight X935/29 (segments I and III) which probed the environs west of Hawaii, experienced rms errors of 1.3-1.5 nmi - somewhat better than the 2-3 nmi predicted in Figure 6-2. Flight E901/17 July (Segment II)*, probing the region northwest of Hawaii, experienced an r.m.s. error of 1.03 nmi, despite the fact that Norway was off-air. This is consistent with the 1-2 nmi predicted in Figure 6-2. Similarly, Flight E901/17 Sept (Segment II) covering a region south west of Hawaii, experienced an

---

* Segment I of this flight (r.m.s. error of 2.56 nmi) is not usable since Norway off-air is critical in this region.

r.m.s. error of 1.96 nmi, close to the 2-3 nmi predicted in Figure 6-2. Here the stations actually used were ACEH (D was off-air) while the theoretical values were based on ACDH. Larger errors (3.8-9.6 nmi rms) were experienced on Flights B953/13 and FB951/15 which traversed the shaded region ESE of Hawaii shown in Figure 6-1 and for which theoretical error forecasts (in the absence of G) were not generated. These large errors may be due to use of stations C and F which can be of poor navigational quality in this region.

In the other operational data (see Section A-5 of Appendix A), the USCGC Jarvis reported that in the Aleutians, LOPs A-H, D-H and A-D consistently provided accuracy within 2 nmi and often as close as 0.5 nmi. Similar results were reported in the Bering Sea. This is in general accord with the model's prediction of exceptional system performance in the Aleutian region. Somewhat worse results (1-4 nmi error) were reported by the USCGC Mellon in the same geographical area, although this was based upon comparisons with "Loran-C, radar and visual" whose absolute accuracy as references could not be assessed. Similarly, the M/S Nopal Lane data (Table A5-1) is with respect to a reference position of unknown absolute accuracy, so it is difficult to assess the significance (if any) of the reported 4.5 nmi errors at a latitude ($\sim 40^{o}$ N) where errors closer to one nmi were expected. Finally, the Western Airlines data (Table A5-2) could not be utilized for the present comparison purposes since (temporary) station G had been used in the fix.

6.4 Fully Implemented System

The fully-implemented OMEGA system includes station G (Australia), which provides the third station required for hyperbolic navigation in the shaded regions of Figure 6-1 and generally improves navigation accuracy in the southern half of the N. Pacific validation region. Applying the fix accuracy model to the fully-implemented system

leads to the line-printer maps in Figures 6-6 through 6-8, which repsectively display the r.m.s., 50% CEP and 95% CEP errors. These calculations are based upon phase errors which include PPC bias errors (as of 1979).

Note that in contrast to the corresponding (No G) results in Figures 6-2 through 6-4, good performance is now predicted throughout the primary N. Pacific validation region (50% CEP <2 nmi, 95% CEP <4 nmi). As before, excellent accuracy (50% CEP and d-rms <1 nmi, 95% CEP <2 nmi) is predicted in the Central Pacific north of about the 25th parallel.

Contour plots have been generated for the 50% CEP and 95% CEP cases as shown in Figures 6-9 and 6-10. It is now seen quite clearly, from Figure 6-9 for example, that three or more stations are available on a full-time basis (barring off-air periods) over virtually the entire N. Pacific validation region, the one exception being a very small region near Acapulco. This is also shown in the line printer map of Figure 6-11, which displays the number of stations expected on a full-time basis at each grid point.

EFFECT OF PPC BIAS REMOVAL

Similar calculations have also been performed using the phase error model given by the third column of Table 6-1, i.e. with PPC bias errors removed, in order to assess the improvements in performance which could conceivably result from refinements* in future PPC's. The resulting line printer plots are shown in Figures 6-12 through 6-14. To facilitate comparisons with and without biases, a contour plot of 50% CEP is given in Figure 6-15, which can be directly compared with Figure 6-9. Note that in the absence of PPC biases, 95% CEP (which is approxi-

---

* We only consider refinements which remove "bias" errors, not PPC "modelling" errors as defined in Section 3.4.

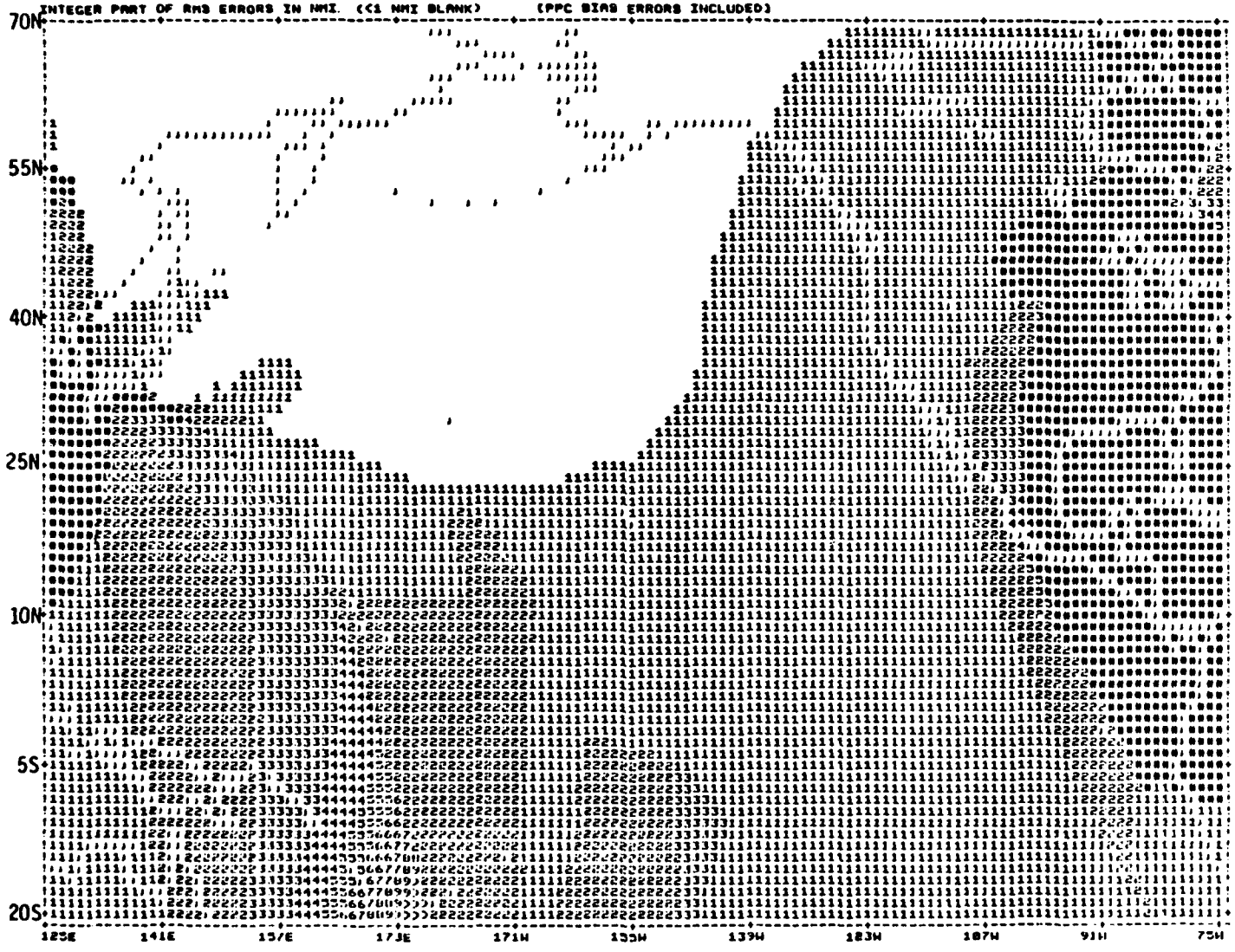

FIGURE 6-6. RMS CIRCULAR ERRORS IN N. PACIFIC (FULLY IMPLEMENTED SYSTEM)

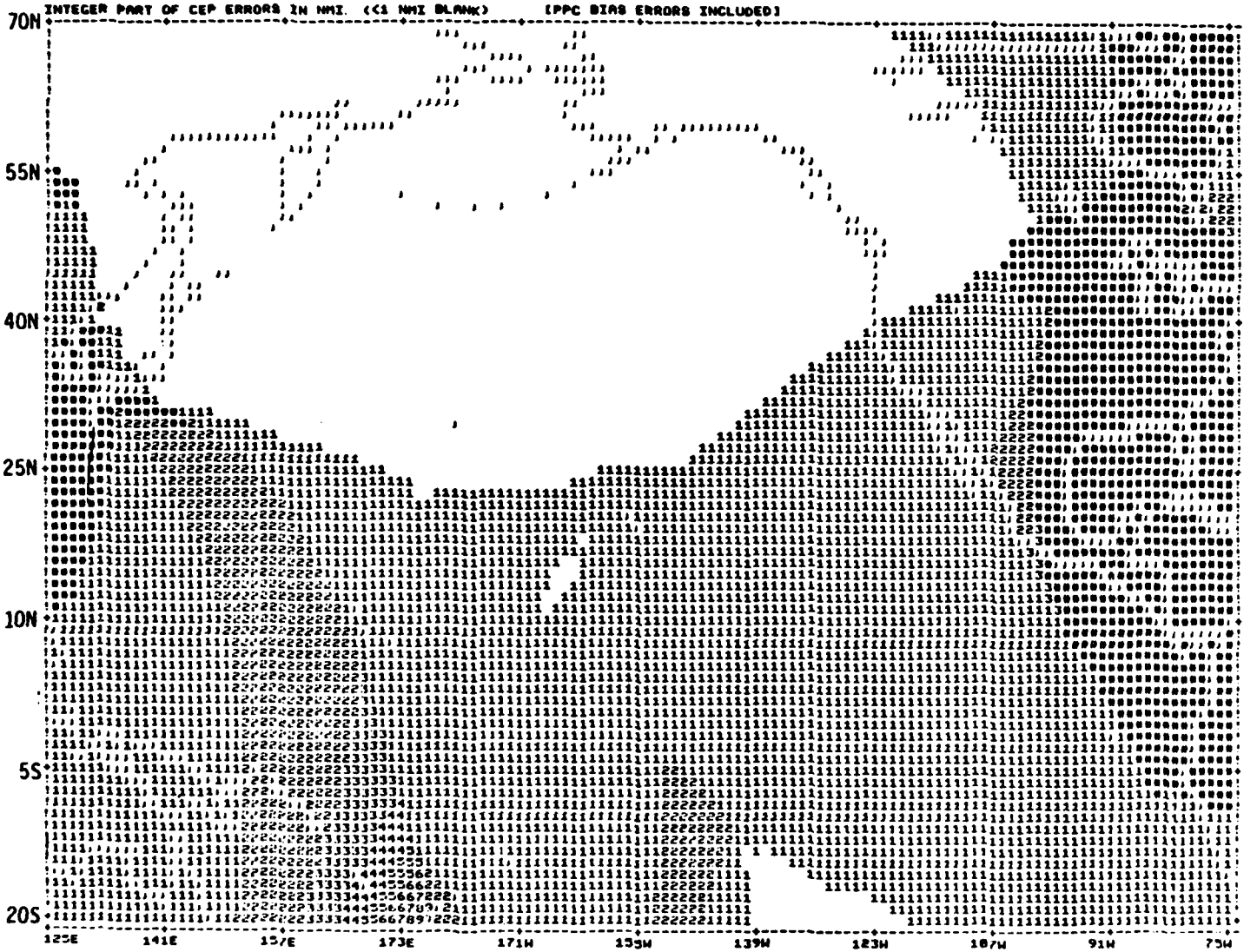

FIGURE 6-7. 50% CEP ERRORS IN N. PACIFIC (FULLY IMPLEMENTED SYSTEM)

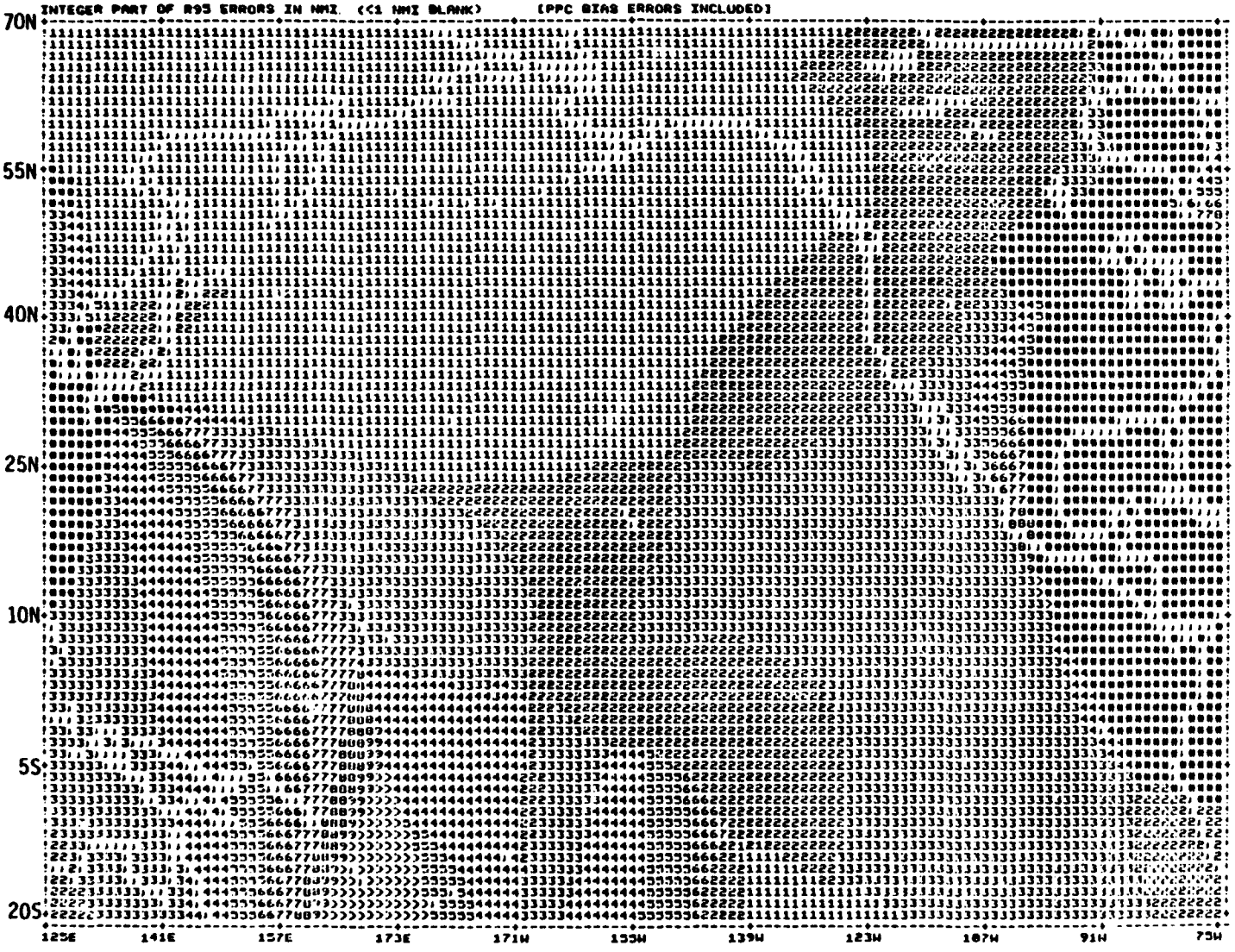

FIGURE 6-8. 95% CEP ERRORS IN N. PACIFIC (FULLY IMPLEMENTED SYSTEM)

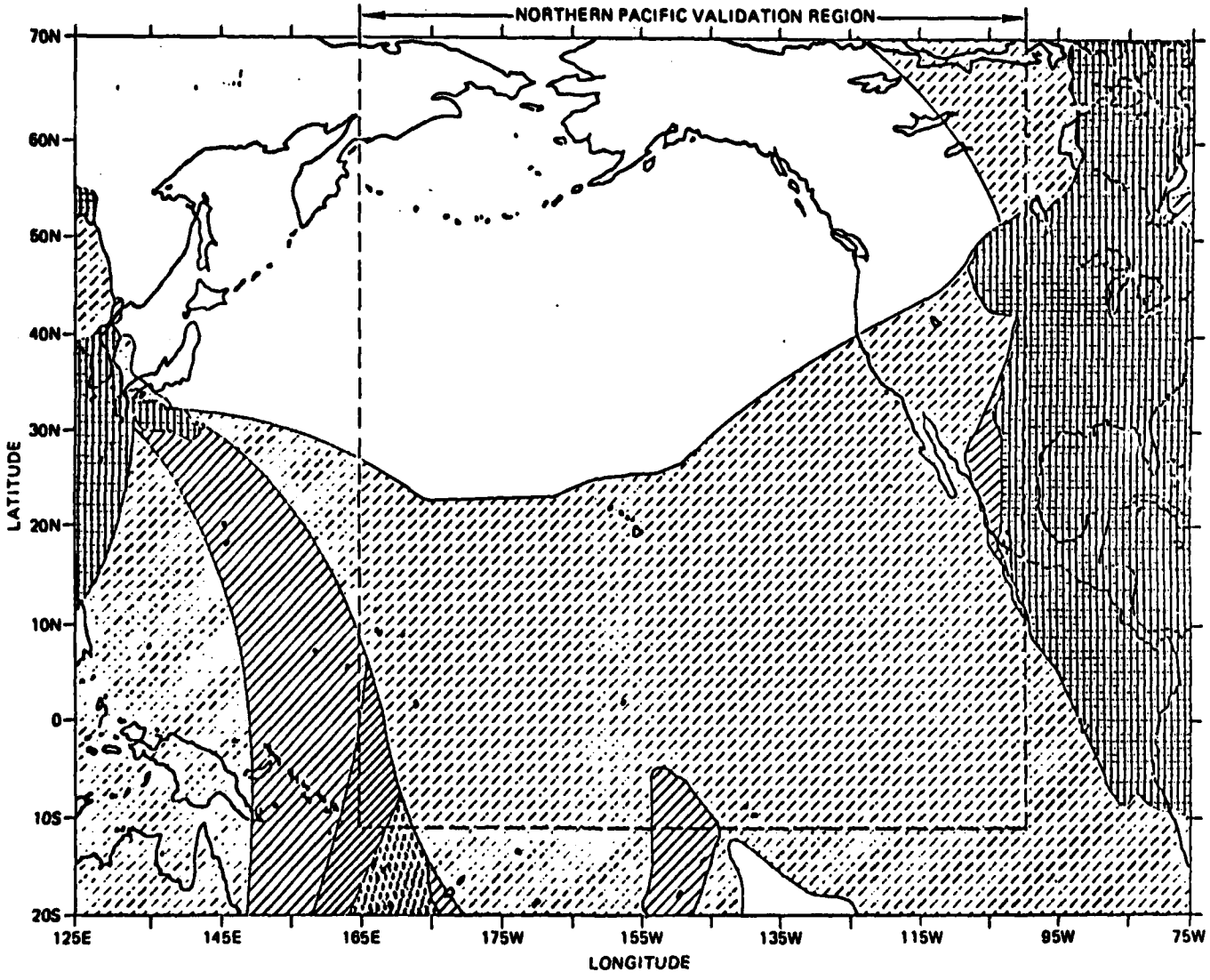

Figure 6-9. 50% CEP ERRORS IN NORTHERN PACIFIC (4-FREQUENCY OMEGA – WITH PPC BIASES)

LEGEND: < 1 NMI | 1-2 NMI | 2-3 NMI | 3-4 NMI | > 4 NMI | < 3 FULL TIME STATIONS

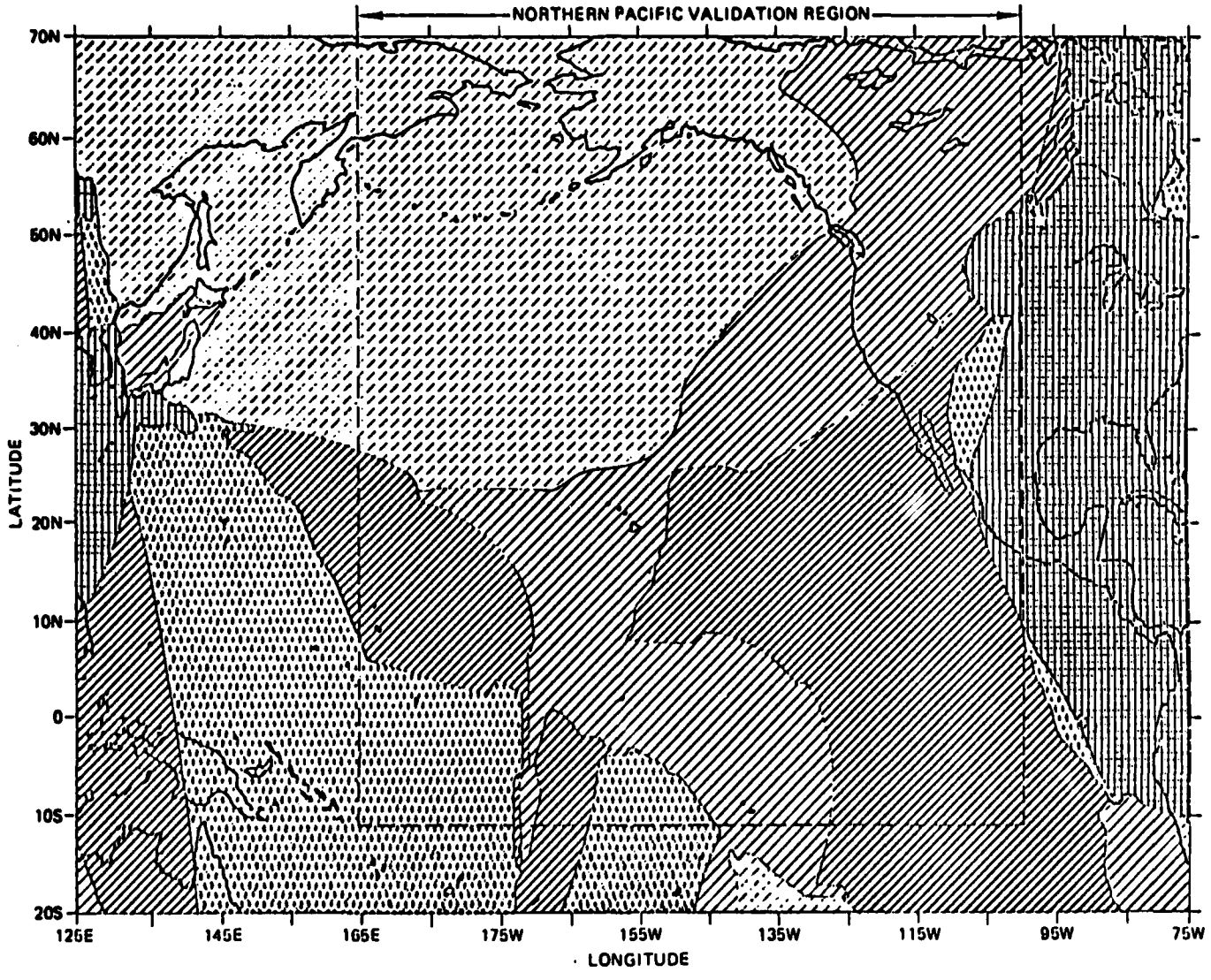

FIGURE 6-10. RADIUS OF CIRCLE CONTAINING 95% OF FIXES (4-FREQUENCY OMEGA – WITH PPC BIASES)

LEGEND: 1 - 2 NMI; 2 - 3 NMI; 3 - 4 NMI; > 4 NMI; < 3 FULL TIME STATIONS

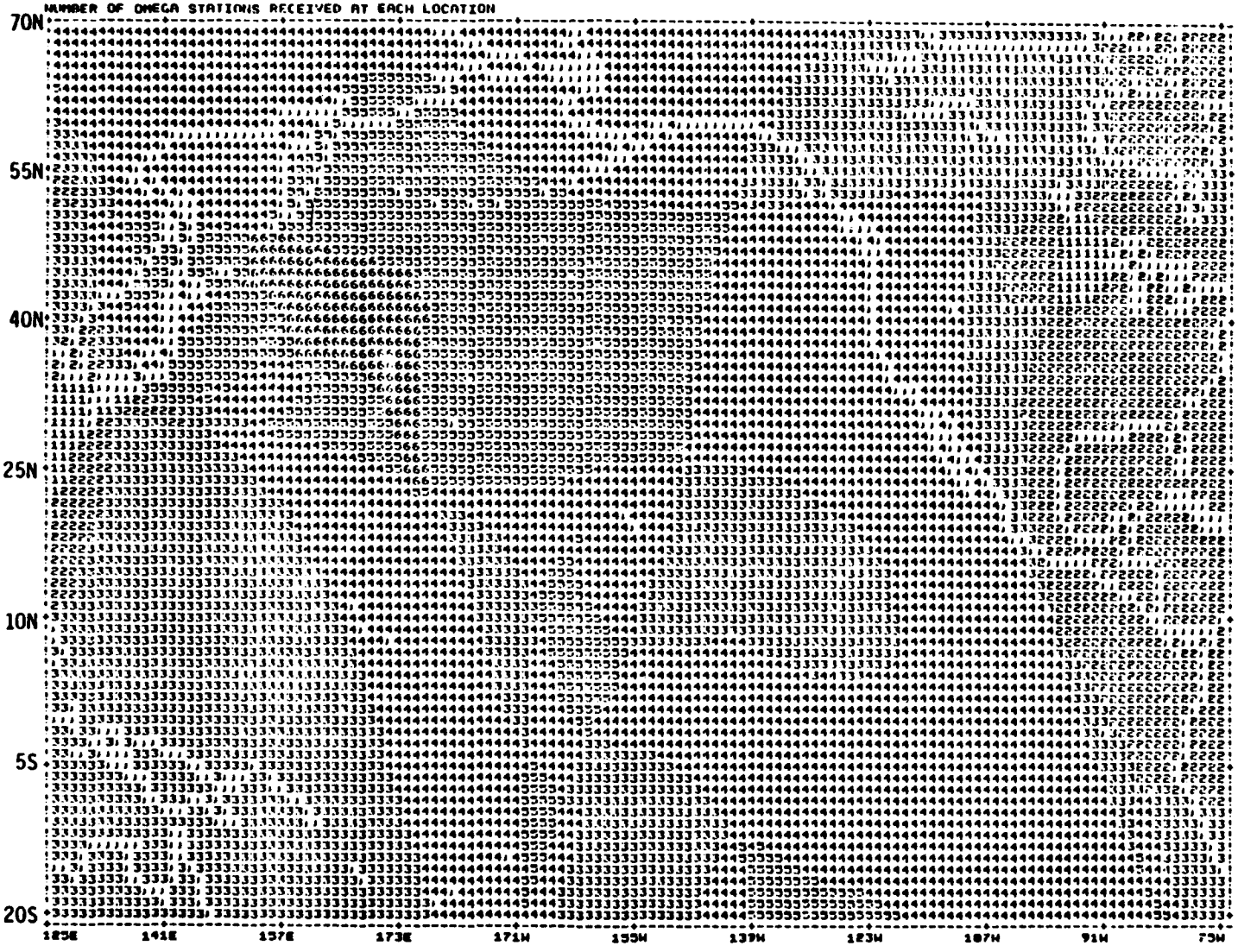

FIGURE 6-11. NUMBER OF STATIONS USABLE ON A FULL-TIME BASIS (FULLY IMPLEMENTED SYSTEM)

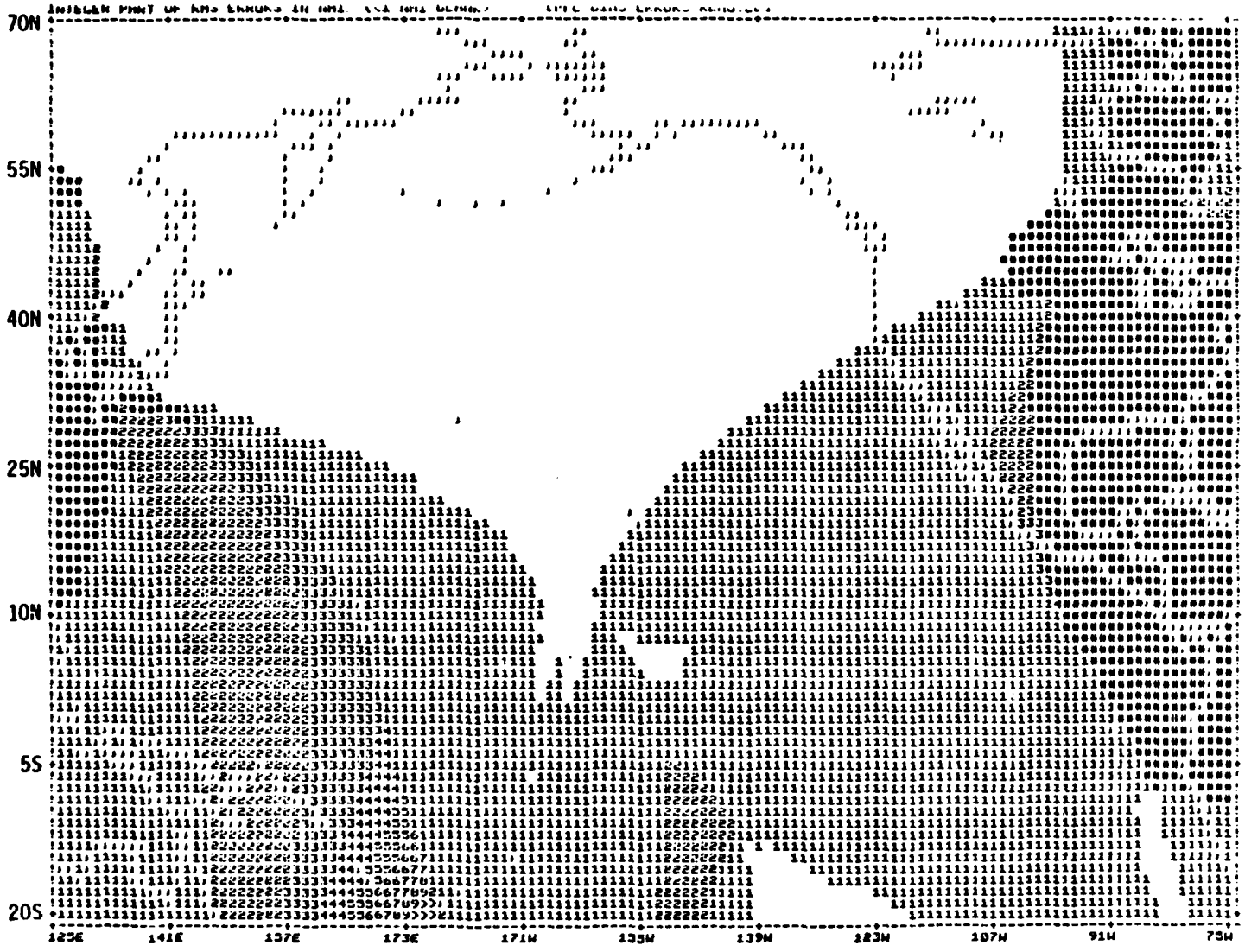

FIGURE 6-12. RMS CIRCULAR ERRORS IN N. PACIFIC (PPC BIAS ERRORS REMOVED)

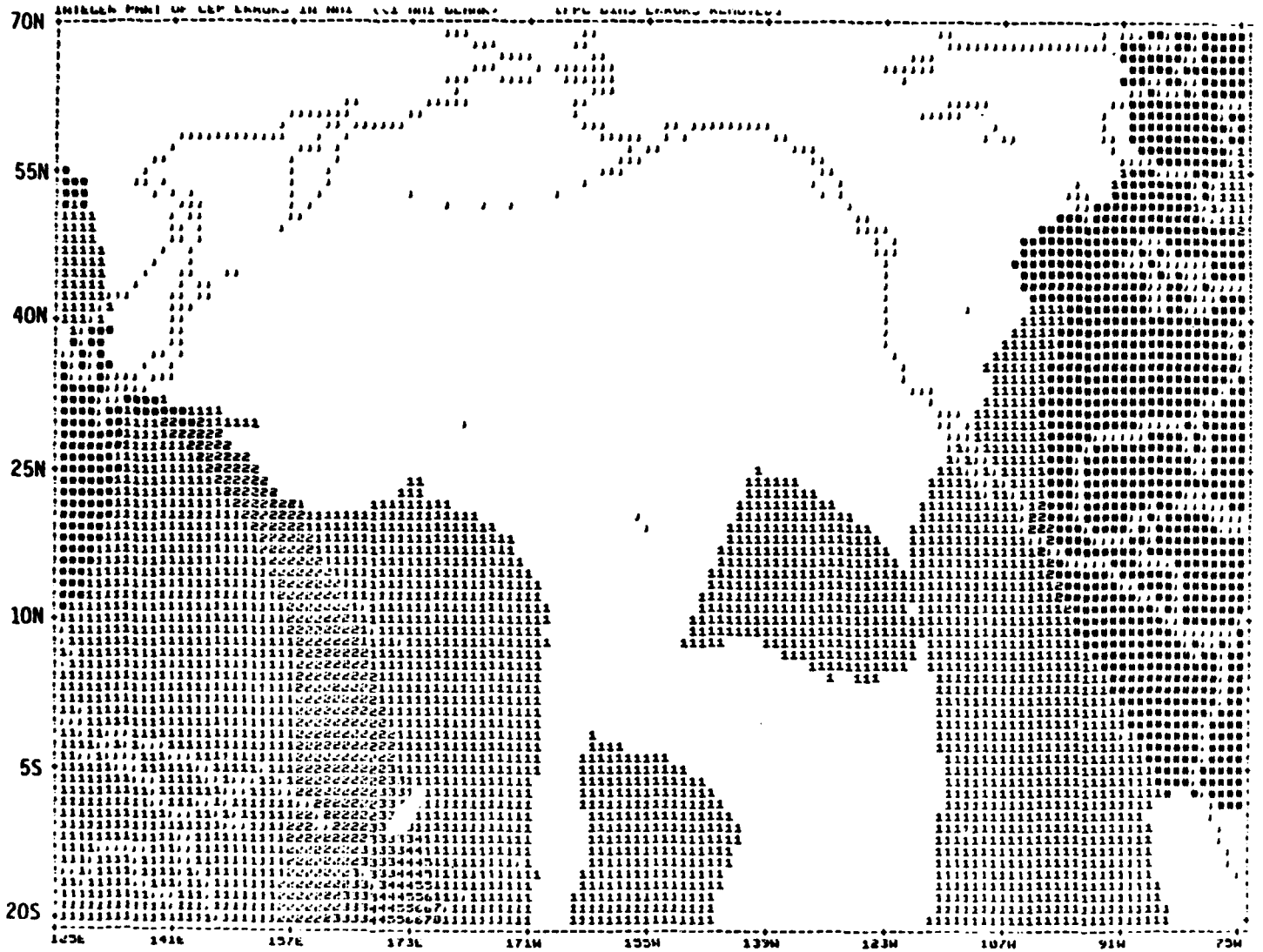

FIGURE 6-13. 50% CEP ERRORS IN N. PACIFIC (PPC BIAS ERRORS REMOVED)

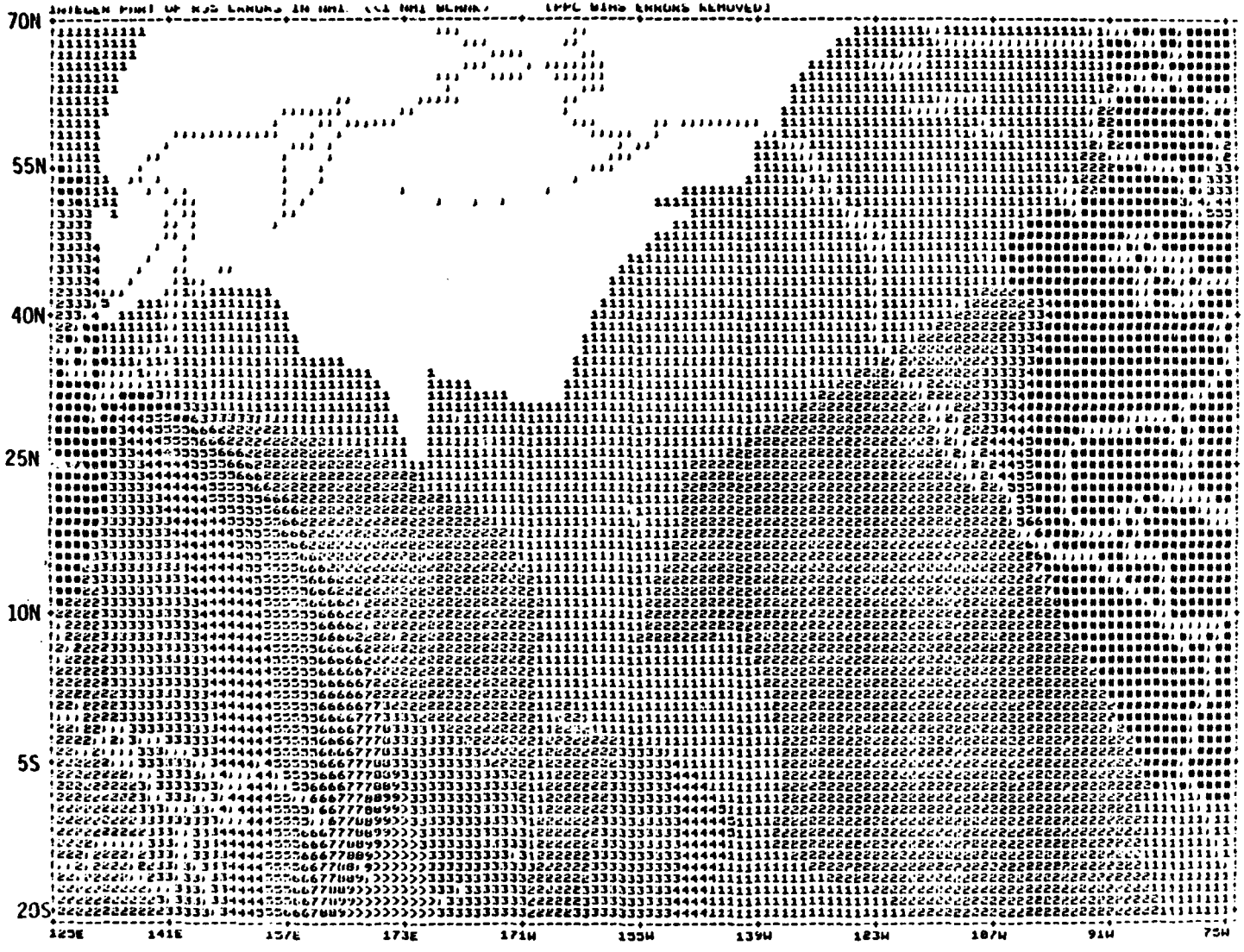

FIGURE 6-14. 95% CEP ERRORS IN N. PACIFIC (PPC BIAS ERRORS REMOVED)

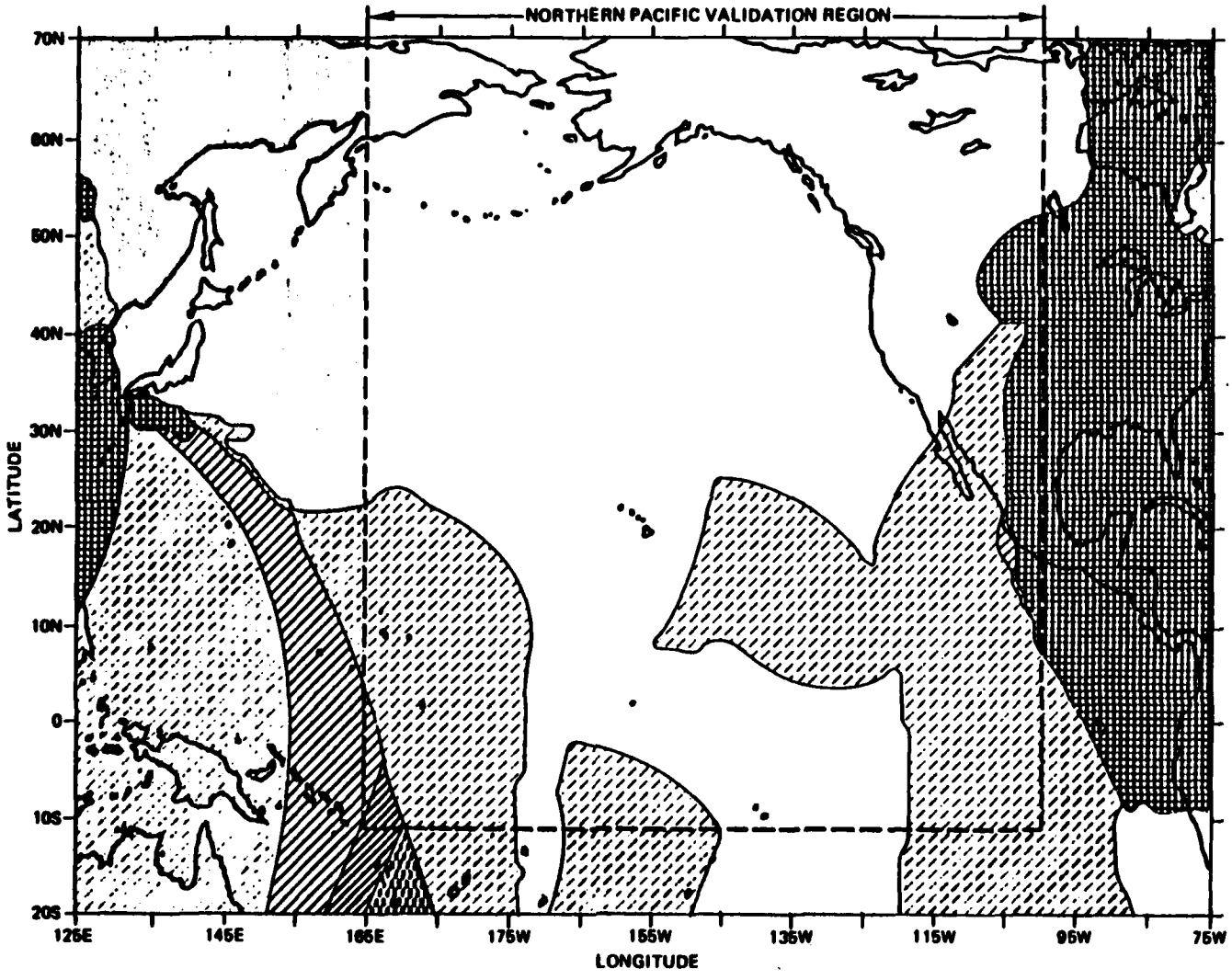

FIGURE 6-15. 50% CEP ERRORS IN NORTHERN PACIFIC (4-FREQUENCY OMEGA – PPC BIASES REMOVED)

LEGEND: < 1 NMI | 1-2 NMI | 2-3 NMI | 3-4 NMI | > 4 NMI | < 3 FULL TIME STATIONS

mately equivalent to the frequently used 2 d-rms measure) is below 3 nmi throughout most of the primary validation region. Also, improvements in accuracy are particularly apparent in the region south of Hawaii.

EFFECT OF SINGLE FREQUENCY OPERATION

In the fix accuracy model, the assumed statistical independence of phase errors at different frequencies results in a scaling of fix errors $\sim 1/\sqrt{N}$ where N is the number of frequencies used. Accordingly, the predicted errors for single-frequency OMEGA may be obtained from the four-frequency results given thru far simply by multiplying by two*. This has been carried out for the 50% CEP contours (with PPC biases included), leading to the results shown in Figure 6-16. It is seen that under this conservative assumption of two-fold degradation, 50% CEP errors range 1-2 nmi north of Hawaii 2-3 nmi in most areas south and east of Hawaii.

6.5 Comparison With Navigational Requirements

Having completed the assessments of intrinsic navigational accuracy available through OMEGA, it now remains to match this accuracy with the requirements of the marine and aviation user communities. In doing so it must be borne in mind that all areas of the N. Pacific validation region are not of equal navigational importance since traffic density is markedly inhomogeneous. Figure 6-17, for example, shows an estimate [25] of merchant ship distribution (including fishing vessels). It is seen that for marine users, the primary areas in the N. Pacific are: i) above the 40th parallel, ii) west coast of U.S. and Mexico, and iii) routes from Japan-via Hawaii-to the fishing area west of Peru. Note in particular the relative lack of traffic in the quadrant south of Hawaii.

---

* It is recognized, however, that since such statistical independence is questionable, the difference between single-frequency and four-frequency operation will probably not be this great. Thus the factor of two should be viewed as an upper limit.

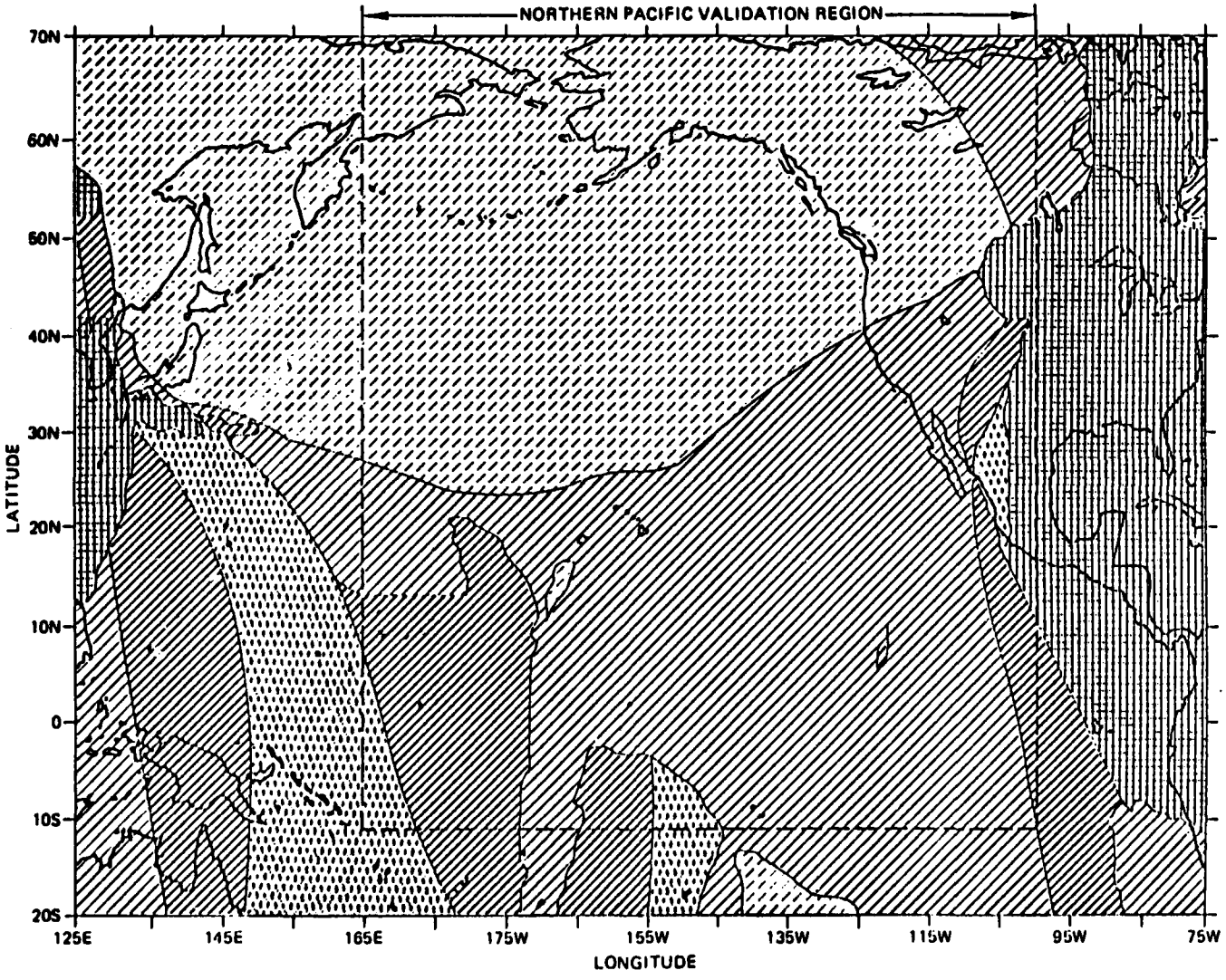

FIGURE 6-16. 50% CEP ERRORS IN NORTHERN PACIFIC (SINGLE FREQUENCY OMEGA – WITH PPC BIASES)

LEGEND: 1 - 2 NMI | 2 - 3 NMI | 3 - 4 NMI | > 4 NMI | < 3 FULL TIME STATIONS

AD-A121 105 NORTH PACIFIC OMEGA NAVIGATION SYSTEM VALIDATION(U) 3/4
MEGATEK CORP SAN DIEGO CA P LEVINE ET AL. 31 DEC 81
R2018-054-IF-5 ONSOD-01-81 N00123-78-C-0043

UNCLASSIFIED F/G 17/7 NL

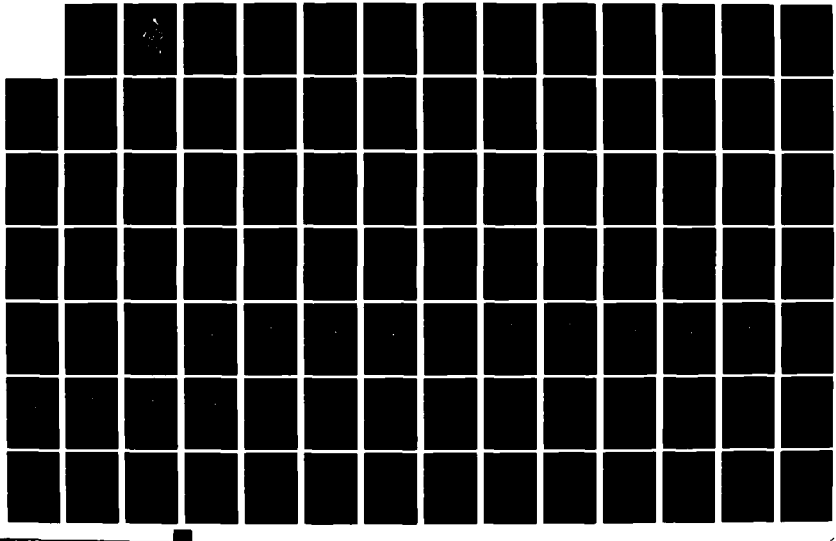

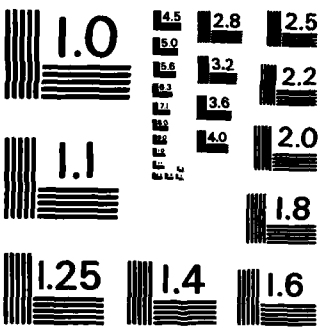

MICROCOPY RESOLUTION TEST CHART
NATIONAL BUREAU OF STANDARDS-1963-A

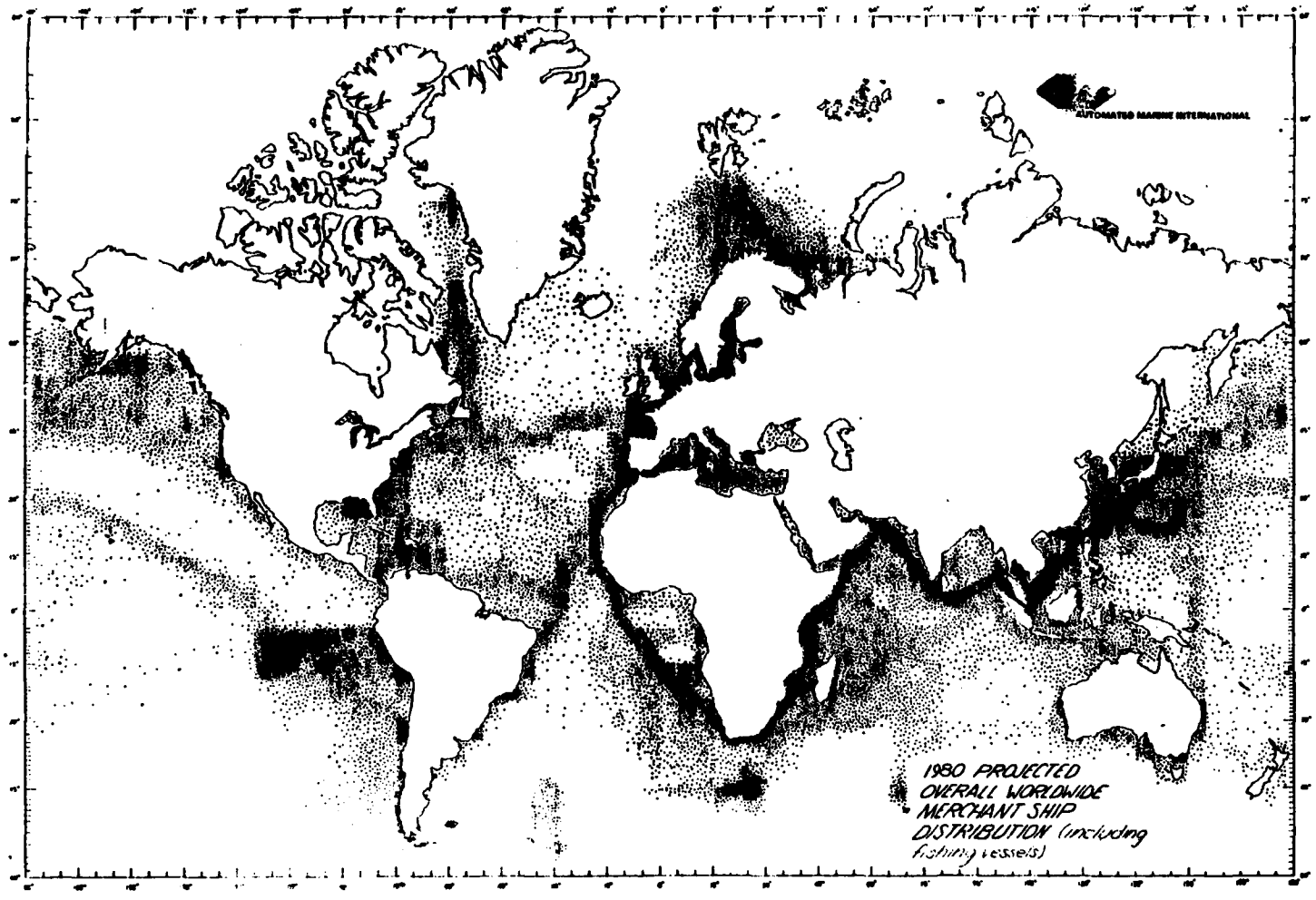

FIGURE 6-17. 1980 PROJECTED OVERALL WORLDWIDE MERCHANT SHIP DISTRIBUTION (INCLUDING FISHING VESSELS)

For safety of marine navigation on the high seas, the proposed Federal Radionavigation Plan[26] specifies a minimum predictable accuracy (indicated position minus true position) of 2-4 nmi (2drms)* and a desirable predictable accuracy of 1-2 nmi (2drms). Furthermore, the recommended maximum interval between fixes is two hours, with 15 minutes or less being the desired interval. Referring to Figure 6-10 and reading off the 95% CEP values for the above-delineated regions of significant traffic density, one finds a 95% CEP of 1-2 nmi in North-Central Pacific above the 40th parallel, and a 2-4 nmi 95% CEP along the West Coast of U.S. and Mexico and between Hawaii and the fishing areas off Peru. Thus in the navigationally important regions of the North Pacific accuracy requirements of the proposed Federal Radionavigation Plan are met by OMEGA. The OMEGA fix interval of 10 seconds is consistent with the desired interval of 15 minutes or less.

Of the various civil air oceanic routes in the North Pacific validation region, only the routes between Hawaii and West Coast U.S. and between Anchorage and Tokyo carry sufficient traffic to justify a formal track structure. By the end of 1981, it is expected that an airspace route configuration known as composite tracks will be implemented on these routes. Lateral separation between aircraft operating at the same altitude will be 100 nmi. The possibility has been suggested (by FAA sources)[27] that in the future the International Civil Aviation Organization (ICAO) will implement a Minimum Navigational Performance Specification (MNPS) on these routes, similar to that adapted for the North Atlantic:

- The standard deviation of the lateral track errors shall be less than 6.3 nmi, i.e., 12.6 nmi (2 sigma).

---

* The 2drms error measure exceeds 95% CEP by from 2 to 15% depending on the eccentricity of the error ellipse. This difference between 2drms and 95% CEP is not considered significant in the present context of approximate "broad brush" requirements specifications. Hence 95% CEP contours will be used in the comparisons.

- The proportion of the total flight time spent by aircraft 30 nmi or more off track shall be less than 5.3×10^{-4}, i.e. less than one hour in about 2,000 flight hours.

- The proportion of the total flight time spent by aircraft between 50 and 70 nmi off track shall be less than 1.3×10^{-4}, i.e. less than one hour in about 8,000 flight hours.

Again referring to Figure 6-10, and noting the approximate equivalence of the 95% CEP and 2 sigma error measures, it is seen that OMEGA accuracies over the two routes in question will be comfortably greater than that required to meet the 12.6 nmi (2 sigma) criterion. With regard to the second and third of the MNPS criteria it must be noted that such large cross track errors - or "blunders" - are difficult to assess quantitatively since they are largely specific to the particular receiver implementation, especially in regard to its human engineering aspects. One exception is the effect of an ionospheric distrubance, particularly the sudden ionospheric disturbance (SID) caused by a solar x-ray flare, for which error analyses are carried out later in the report (Section 7.3). It is found for the routes in question, flares (Class M1) with a nominal frequency of occurrence of one per day during the maximum of the sunspot cycle can cause a radial error (i.e. beyond that experienced in the absence of the flare) of at most 2-3 nmi. Rarer and stronger flares (Class X1), with a nominal frequency of occurrence of one per month during solar maximum, can induce errors of at most 5-6 nmi on these routes. Thus, OMEGA is not intrinsically susceptible to SID-induced blunders of 30 nmi or greater in those portions of the North Pacific which will be subject to an MNPS in the foreseeable future. Furthermore, redundent coverage in such areas permits Norway to be deselected during PCA events, thus mitigating the vulnerability to this (relatively rare) type of ionospheric disturbance as well. It is concluded that OMEGA, when fully implemented, will meet enroute navigation requirements of both the marine and aviation user community in the North Pacific on a 24-hour full time basis.

7.0 OPERATIONAL IMPLICATIONS

In addition to providing assessments of coverage and accuracy under normal conditions, secondary objectives of the present study are to provide recommendations on how OMEGA can be more effectively used in the North Pacific and to investigate the performance impact of non-standard conditions such as ionospheric disturbances and station off-air periods. With regard to the first of these objectives, the optimum receiver implementation derived in Section 3 should prove of general utility in the combinational filtering of multiple OMEGA signals. (For the North Pacific, optimization is achieved by using the single station phase error model given in Table 4-14). Even with such optimal filtering, however, the user must still apply the best available PPC's and, more critically, should avoid use of propagationally unstable signals. Our conclusions regarding PPC effectiveness* are therefore summarized in Section 7.1 and Section 7.2 presents in capsule form the recommendations regarding station selection.

System operation under non-standard conditions is then analyzed. Section 7.3 deals with the impact of solar/ionospheric disturbances while the operational implications of station off-air periods are discussed in Section 7.4.

7.1 PPC Model Effectiveness

It has proven useful to distinguish two types of PPC errors. PPC "bias" errors refer to the failure of phase errors at a given site to average out to zero over the full diurnal period. PPC "modelling"

---

* The PPC's used in the present study were those extant in 1979. The effect of the newer coefficients, as reported in Ref. 23, has not been evaluated although it is reasonable to expect that they will lead to improved PPC accuracy in the N. Pacific and in particular, that the difficulties noted with transequatorial propagation will be ameliorated.

errors, on the other hand, arise from complexities in the diurnal variation of the phase which are not fully modelled by the PPC algorithm (see Figure 3-5). The analyses of Section 4 have shown that in a vast majority of cases (where a "case" consists of a month's worth of data at a given monitor site for a given LOP), bias errors are not a concern, and only exceed 20 CEC at a limited number of monitor sites during certain months of the year. At 10.2 kHz, 13 cases of statistically significant bias errors in excess of 20 CEC are found out of a total of 544 cases and 15 out of 516 cases at 13.6 kHz. When averaged over month, only one case of such seasonally-averaged PPC bias in excess of 20 CEC was found at either 10.2 or 13.6 kHz for receiving sites at which 12 or more semi-months of data were recorded (this one case being the 10.2 kHz BC LOP at Hokkaido, Japan).

The foregoing conclusions apply only to diurnally-averaged phase errors. It is conceivable that although the diurnally-averaged bias is small, significant errors could occur for extended periods during day or night yet be offset by smaller or opposite-signed errors at other times. The day/night analyses of Section 4.5 are therefore of interest in this regard. Appendix B contains the day and night phase error statistics for each LOP and site. Cases for which statistically significant* large biases were found are listed in Table 7-1.

The 33.9 CEC night-time error at 10.2 kHz on La Reunion observed at OMEGA Japan (Tsushima) has been noted before in the literature[28]. The Hokkaido 10.2 kHz and 13.6 kHz data suggest that large night-time bias errors are associated with the Hawaii signal in Northern Japan. These and the other examples of Table 7-1 serve to focus attention on isolated problem areas and provide good test cases for assessing improvements with upgraded PPC algorithms.

---

* Mean bias $\geq$ 20 CEC and $\geq$ twice the standard deviation of the phase error; # semi-months of data $\geq$ 12.

TABLE 7-1. DAY/NIGHT BIAS ERRORS

CONDITION	MONITOR SITE	LOP	MEAN	STD. DEV.	#SEMI-MONTHS OF DATA
10.2kHz-NIGHT:	HOKKAIDO	AC	20.6	3.8	22
	HOKKAIDO	BC	26.9	3.3	22
	HOKKAIDO	CE	-23.8	5.5	24
	TSUSHIMA	AH	29.5	3.0	20
	TSUSHIMA	EH	33.9	3.4	12
	MIYAJIMA	EH	23.4	4.1	14
13.6 kHz-NIGHT:	HOKKAIDO	AC	21.2	4.0	20
	HOKKAIDO	CE	-26.9	4.4	22
	TSUSHIMA	EH	25.5	8.7	12
	NOSC	DF	-34.6	6.6	12
	PANAMA	CF	24.7	6.1	13
10.2 kHz-DAY:	HOKKAIDO	AE	23.2	7.8	22
	TSUSHIMA	DH	26.3	8.6	20
	PANAMA	BD	21.7	2.9	14
13.6 kHz-DAY:	HOKKAIDO	AE	21.2	7.4	20
	HOKKAIDO	BC	28.5	8.4	18
	PANAMA	BD	24.5	1.4	14
	PANAMA	CD	-21.4	6.5	14
	PANAMA	CF	-21.3	3.0	14
	SEATTLE	CE	-33.7	8.2	13

The PPC "modelling" errors have been found to be the dominant error source, particularly for stations involving equatorial propagation into the N. Pacific (B, E, F and - presumably - G), where such errors are in the range 15-18 CEC (rms). The "good" stations (A, C, D, H) involve PPC modelling errors less than half these values. Stations B and F are of little navigational utility in the N. Pacific so there is correspondingly little impact of PPC errors for these stations. Station E is useful in the western sector of the N. Pacific so some benefit

would accrue from PPC modelling improvements for this station*. Assessment of PPC errors for Australia must obviously wait until such data are available.

7.2 Station Selection

The general conclusions reached regarding usability in the N. Pacific Validation region of the various OMEGA stations are:

STATION A (NORWAY):	May be used everywhere it is received with adequate SNR (i.e. west of Greenland shadow).
STATION B (LIBERIA):	Not generally usable in N. Pacific validation region.
STATION C (HAWAII):	A primary station in N. Pacific. (Night-time) modal interference zones to east and southwest of Hawaii.
STATION D (N. DAKOTA):	A primary station usable without restriction throughout N. Pacific validation region.
STATION E (LA REUNION):	Usable only in western part of N. Pacific validation region (i.e. west of Hawaii). Possibility of long path propagation into eastern Pacific.
STATION F (ARGENTINA):	Generally not usable in N. Pacific validation region.
STATION G (AUSTRALIA):	(will be) a primary station usable everywhere in N. Pacific it is received with adequate SNR (i.e. south of Alaska).
STATION H (JAPAN)	A primary station usable without restriction everywhere in N. Pacific validation region.

Thus the general guidelines for manual deselection of stations in the N. Pacific are:

F and B to be deselected everywhere

E deselected east of Hawaii

C deselected at night in zones to east and southwest of Hawaii (see Figure 6-1)

---

* As indicated in Ref. 23, recent improvements in the PPC algorithm significantly reduce errors on transequatorial paths.

Phase error analyses performed in Section 4.3 have led to the following ranking of LOP pairs in the N. Pacific (best to worst): CD, AC, DH, CH, AH, AD, CE. On a (usable) single station phase error basis, the corresponding best to worst ranking is C, A, D, H and E.

7.3 Impact of Solar/Ionospheric Disturbances

In addition to assessing OMEGA performance in the N. Pacific under normal conditions, it is also of interest to investigate the vulnerability of OMEGA to solar/ionospheric disturbances, viz. the Polar Cap Absorption (PCA) and Sudden Ionospheric Disturbance (SID) events. PCA's, whose frequency of occurrence ranges from about 20 per year at solar maximum to none at solar minimum, affect only the Norway signals in the N. Pacific. If three stations - other than Norway - are available at a given location, simple deselection of Norway permits navigation to proceed in the presence of a PCA, albeit at somewhat reduced accuracy because one fewer station is being used to derive the fix. Such deselection is routine via radio advisories once the event has been detected by monitors and is even possible in near-real time by sophisticated algorithms which detect that use of Norway is "pulling" the position away from that indicated by the other stations. Thus, it can be said that OMEGA is PCA vulnerable in the N. Pacific only at locations where Norway must be used for hyperbolic navigation. Reference to Figure 6-1 shows only one such region, the small shaded area WSW of Hawaii. In reality, however, the measurements discussed in Section 5 and Appendix A have indicated that the North Dakota boundary of Figure 6-1 is quite conservative so it is almost certain that this small area showing full time availability of only A, H and G also will have D available full-time. Thus, unless a station other than Norway happens to be off-air during a PCA, the N. Pacific does not appear to be intrinsically vulnerable to such events. Even in such event however, referring again to Figure 6-17, Figure 6-1 shows that in the navigationally important areas of the N. Pacific where Norway is

received, there are usually at least four stations besides Norway available so that in such areas even a single station off-air will still allow Norway to be deselected.

SID events, caused by solar x-ray flares, affect signals from all stations which have some sunlit path component. Since the effect of an SID is always a phase advance(for mode 1 signals), there is some vectorial cancellation as the fix point tries to move simultaneously closer to all stations with sunlit paths. Thus the quantitative net effect of an SID is complex function of season, time of day, station bearing angles, flare strength, etc. The frequency of occurrence of SID's, as a function of flare strength, is shown in Table 7-2 for the year 1980 - near solar maximum. (Generally speaking, flares weaker than Class M1 do not produce significant effects on navigation). As a convenient rule of thumb, it is seen that M class flares occurred about once per day on the average while X class flares occured about once per month in 1980.

TABLE 7-2. FREQUENCY OF OCCURRENCE OF SID'S DURING 1980

FLARE CLASS	1-8A PEAK SOLAR FLUX ($ergs/cm^2$-sec)	NUMBER OF EVENTS
M1	1×10^{-3}	165
M2	2×10^{-3}	77
M3	3×10^{-3}	32
M4	4×10^{-3}	22
M5	5×10^{-3}	11
M6	6×10^{-3}	5
M7	7×10^{-3}	6
M8	8×10^{-3}	8
M9	9×10^{-3}	2
X1	1×10^{-2}	6
X2	2×10^{-2}	5
X3	3×10^{-2}	2
X4	4×10^{-2}	1
X9	9×10^{-2}	1

In order to quantitatively assess the effects of SID's on navigation, we have utilized on approximate model[29] according to which the phase advance $\Delta\phi$(in CEC) at frequency f(kHz) is given by

$$7\text{-}1) \qquad \Delta\phi = \frac{130}{f} \int_{XMTR}^{RCVR} g(s)\, ds$$

$$\text{where } g(s) = \begin{cases} 0 \text{ if } F_X \cos \chi(s) < F_C \\ \log \left[F_X \cos \chi(s)/F_C\right] \text{otherwise} \end{cases}$$

where the integration is over the path length (expressed in radians), F_X is the solar 1-8A flux in ergs/cm^2-sec, χ is the local solar zenith angle along the path, and $F_C = 1.5 \times 10^{-3}$. By means of 7-1), the SID-induced phase errors can be determined at any given location for all navigation signals. Then, since the theory of Section 3 specifies the weighting coefficients which are applied to each navigation signal it is thereby possible to determine the net SID-induced position displacement that results when all of the available signals are combined in the optimum receiver to derive the fix.

A number of such calculations were performed for Class M1 and Class X1 flares. The date chosen for calculation was June 21, and the times studied were 0000, 0600, 1200 and 1800 (local time) as well as 0000Z and 0600Z. The resulting line-printer plots are given in Appendix F. Here the integer part of the SID-induced position displacement (i.e. above and beyond whatever position error may have existed prior to the flare) is printed out at each grid point. The dependence of SID-induced errors on location and time is complex and difficult to summarize. However, for the navigationally important areas indicated in Figure 6-17, it is seen that for Class M1 flares, the SID-induced errors are at most 2-3 nmi (i.e. for the times studied), while for Class X1 flares, they are at most 5-6 nmi. In other locations (where the vectorial

cancellation is not so effective) larger errors can be experienced. Figure F-4, for example, shows errors in excess of 10 nmi in a region southwest of Hawaii for a Class X1 flare occurring at 0600 local time. This is a worst-case situation since at dawn the sunlit paths are all to the east. However, the apriori probability of a Class X flare occurring within ±1 hour of dawn at a given location is only about once per year at solar maximum so this need not be viewed as a significant system vulnerability.

7.4 Effect of Station Off-Air Periods

The number of OMEGA stations usable on a full-time basis (i.e. in the absence of station off-air periods) was shown in Figure 6-11. The Japan-to-U.S. and west coastwise US routes are seen to be covered by at least four stations so such routes are not vulnerable to loss of hyperbolic navigation in the event of a single off-air station. The Hawaii (night-time) modal interference zone ESE of Hawaii, however, is a potential trouble slot since only three station full-time coverage (D, G & H) will be available and this zone lies on the route between Japan and the fishing region west of Peru. When D, G or H goes down for annual maintenance, navigators will attempt to use C, E and/or F, each of which presents difficulties. It is possible however that since modal interference is frequency dependent, one or more of the Hawaii signals may be usable at a given location in this region, despite that fact that the other Hawaii signals are modally distrubed. Thus, appropriate alerts and special guidance regarding night-time use of Hawaii signals may be required in this zone during annual maintenance of D, G and H.

8.0 CONCLUSIONS AND RECOMMENDATIONS

The foregoing assessments of coverage and accuracy attainable with OMEGA in the N. Pacific lead to the conclusion that under conditions of normal operation, OMEGA - when fully implemented - will meet the design predictable accuracy of 2-4 nmi (2drms) and the enroute navigation requirements of the marine and aviation user communities. On the particularly important routes between Japan and the U.S. and along the U.S. West Coast, these same conclusions apply even without Australia on-air, and are well supported by existing operational data. The one potential problem area with the partially implemented system - a night-time modal interference zone (station C) ESE of Hawaii - should be normalized when Australia is on-air to provide a third station to combine with D and H in this zone.

The methodology of the study has been based upon performance assessments for a four frequency automatic reciever since this gives recognition to the gains in position-fixing accuracy which will accrue from full utilization of the OMEGA signal format. Admittedly such gains are difficult to accurately quantify in the absence of data on the statistical correlation of phase errors on different frequencies. It is felt, however, that the clear trend towards future use of microprocessor-based receivers, in place of the older single-frequency manual units, mandates this approach and it is recommended this be continued in future validation studies. To facilitate this, test measurements should be extended to all four of shared frequencies and the 11-1/3 kHz fixed monitor data should also be processed and stored in the MASTERFILE.

On the theoretical front, since predicted coverage/modal interference boundaries are absolutely essential in providing a framework for the interpretation of test and operational data (as well as experiment design), it is recommended that such boundaries be

generated at the other shared OMEGA frequencies, at least at 13.6 kHz. With regard to the PPC's, the study has shown that with the PPC algorithm circa 1979, no glaring biases exist in the N. Pacific after averaging over time of day and season. However, a clear reduction in accuracy was found in the diurnal phase variation of transequatorial signals (~20 CEC r.m.s. error), in agreement with well-recognized shortcomings of the 1971 coefficients used by the algorithm. New coefficients for the Swanson propagation correction model, made available in 1980[23] - too late for use in the present study - promise to improve this situation. It would therefore be of interest to repeat the analyses of Section 4 for newly-generated MASTERFILE data based on the latest PPC algorithm. Since the software for such analyses is already in place, this could be achieved at a relatively modest level of effort.

Finally, it has been necessary to rely exclusively on theoretical predictions of coverage and modal interference for the Australia station. When Station G is finally commissioned, it will be important to validate through measurements that indeed it provides usable signals in those area where Australia will constitute the third station required for hyperbolic navigation.

REFERENCES

1. Karkalik, F.G., Sage, G.F., and Vincent, W.R., "Western Pacific OMEGA Validation," Systems Control, Inc. (vt), ONSOD Report No. CG-ONSOD-01-78, April 1978.

2. Campbell, L.W., Servaes, T.M., and Grassler, E.R., "North Atlantic OMEGA Navigation System Validation," Analytical Systems Engineering Corp., ONSOD Report No. CG-ONSOD-01-80, July 1980.

3. Scull, D.C., "OMEGA Worldwide Calibration and Validation," Proc. of Conference on Navigation in Transportation, DOT-TSC-RSPA 78-22, September 1978.

4. Morris, P.B., "The Determination of Regional OMEGA Signal Characteristics Through Prediction, Validation and Calibration," Proc. of the Third Annual Meeting of the International OMEGA Association, London, England, 26-28 September 1978.

5. McFarland, R.C., Haislip, D.T., and Scull, D.C., U.S. Coast Guard-OMEGA Program Management," Proc. of the Fifth Annual Meeting of the International OMEGA Association, Bergen, Norway, 5-7 August 1980.

6. Thompson, A.D., "OMEGA System Performance Predictions," Navigation-Journal of the Institute of Navigation, Vol 24, No. 4, pp. 304-311, Winter 1977-1978.

7. Kugel, C.P., Ferguson, J.A., Rider, K.B., Pieper, W.A., Bradford, W.R. and Bickel, J.E., "North Pacific OMEGA Validation (Preliminary Report)," Naval Ocean Systems Center.

8. Maenpa, J.E., "Hybrid Satellite/OMEGA Navigation in the MX1105," Proc. of the Third Annual Meeting of the International OMEGA Association, London, England, 26-28 September 1978.

9. Gupta, R.R., Donnelly, S.F., Creamer, P.M. and Sayer, S., "OMEGA Signal Coverage Prediction Diagrams for 10.2 kHz, Vol. II: Individual Station Diagrams," The Analytical Sciences Corporation, Report No. ADA 092742, October 1980.

10. Gupta, R.R., Donnelly, S.F., Creamer, P.M. and Sayer, S., "OMEGA Signal Coverage Prediction Diagrams for 10.2 kHz, Vol. I: Technical Approach," The Analytical Sciences Corporation, Report No. ADA 092741, October 1980.

11. "Biblography of Omega Publications," International Omega Association, Second Ed., January 1981.

12. "OMEGA Navigation System: User Guide," Dept. of the Navy, Navy Electronic Systems Command, 1 March 1978.

13. Swanson, E.R., Britt, J.E., Smith, A.N., "OMEGA Possibilities: Limitations, Options, and Opportunities," Tech. Rept. 283, Naval Ocean Systems Center, 23 June 1978.

14. Morris, P.B. and Cha, M.Y., "OMEGA Propagation Corrections: Background and Computational Algorithm," ONSOD Report 01-74, December 1974.

15. Gupta, R.R. and Warren, R.S., "OMEGA Station 10.2 kHz Signal Selection Made Easy," Proc. I.O.N. National Aerospace Meeting, 8-10 April 1981.

16. Healy, R.D., Gupta, R.R. and Morris, P.B., "Updated Station Selection Procedures to Support Automatic OMEGA Receiver Operation," unpublished paper to appear in Proceedings of NAECON '81 (Dayton) May 1981.

17. "Federal Radionavigation Plan," Dept. of Defense and Dept. of Transportation, November 1979 - Draft.

18. Feller, W., "An Introduction to Probability Theory and its Application," Vol I, p238, (2nd Edition), Wiley (N.Y.), 1957.

19. Lee, H.B., "A Novel Procedure for Assessing the Accuracy of Hyperbolic Multilateration Systems," IEEE Trans. Aerospace and Electronic Systems, Vol. AES-11, No. 1, January 1975.

20. Swanson, E.R., "Geometrical Dilution of Precision," Navigation, Vol. 25, No. 4, pp 425-429, Winter 1978.

21. Lewis, E.A., "Geometry and First-Order Error Statistics for Three- and Four-Station Hyperbolic Fixes on a Spherical Earth," AFCRL Physical Sciences Research Paper No. 29, June 1964.

22. Burt, W.A., et al, "Mathematical Considerations Pertaining to the Accuracy of Position Location and Navigation Systems, "Research Memorandum NWRC-RM 34, Stanford Research Institute, November 1965.

23. Morris, P.B., and Swanson, E.R., "New Coefficients for the Swanson Propagation Correction Model", Proc. Fifth Ann. Mtg, Int'l Omega Assn, 5-7 August 1980.

24. Kugel, C.P., Ferguson, J.A., Rider, K.B., Pieper, W.A. and Bickel, J.E., "North Pacific OMEGA Validation Test Plan (working paper)", Naval Ocean Systems Center, 1 June 1979.

25. Thompson, R.P., "Size and Ocean Distribution of the World Merchant Fleet: Present and Future", Navigation, Vol. 18, No. 2, Summer 1971, pp 176-187.

26. "Federal Radionavigation Plan", Rept. of Defense and Dept. of Transportation", November 1979 - Draft.

27. Private Communication from Mr. Jerry Davis, Federal Aviation Administration.

28. Swanson, E.R., "OMEGA Errors Observed at Various Locations", Naval Ocean Systems Center Technical Note TN629, 23 February 1979.

29. Levine, P.H., "Tests of a Simple OMEGA Phase Model Including Solar Flare Effects", Proc. of the Fifth Annual Mtg. of the International OMEGA Association, 5-7 August 1980, Bergen Norway.

30 Morris, P.B., private communication

ACKNOWLEDGMENTS

This study has been based upon data collected by groups at the U.S. Coast Guard OMEGA Navigation System Operations Detail (ONSOD) and at the Naval Ocean Systems Center (NOSC). In addition to supplying such data, these groups also provided valuable guidance in critical discussions at various points in the study. It is therefore a pleasure to acknowledge the contributions of Mr. Peter B. Morris and Cdr. Robert L. Vence of ONSOD, Mr. David C. Scull of DOT/RSPA, and Msrs. Carl P. Kugel, Jerry A Ferguson and John E. Bickel of NOSC.

The Authors are especially indebted to Dr. Radha R. Gupta of The Analytic Sciences Corporation for providing 10.2 kHz coverage/modal interference boundaries in digital form and to Mr. C.C. Yu of China Airlines for performing extensive analyses of operational data in response to our request.

APPENDIX A: ANALYSIS OF OPERATIONAL DATA

TABLE OF CONTENTS

LIST OF FIGURES

LIST OF TABLES

A1.0 Introduction and Overview

This Appendix surveys the operational data collected by the U.S. Coast Guard's Omega Navigation System Operations Detail (ONSOD). These data are organized in this report according to the comprehensiveness and orderliness of the information, and its suitability for statistical analysis.

The integrated satellite and Omega data collected on US Coast Guard and US Navy ships are thus presented first in Section A2.0. These digital tapes were easily processed by minicomputer. China Airlines International and Pan-American World Airways, provided data from their Omega logs in tabular form, which data had to be digitized before analysis and display. Sections A3.0 and A4.0 present the results of this processing. Comments and user evaluation of Omega performance from marine users are summarized in Section A5.1. Data from two of Western Airlines flights are listed in Section A5.2. An overall summary of Omega fix accuracy and signal coverage is given in the final section.

> NOTE: Omega Trinidad ceased operation in December 1980. Analysis of operational experience in using Trinidad is, therefore, no longer relevant to the validation of the permanent Omega network. Data regarding Trinidad were not considered for this report.

A2.0 INTEGRATED SATELLITE/OMEGA SHIPBOARD DATA

A2.1 Description of Data

Satellite and Omega data were collected on several ships that traversed the Pacific Ocean in 1979 and 1980. The data were recorded onto cassettes from a Magnavox MX 1102/4 or MX 1105 Omega Monitor. These cassettes were sent to the US Coast Guard's Omega Navigation Systems Operations Detail (ONSOD) for preliminary processing. The raw data are separated into 3 ASCII formats using programs developed at ONSOD. Separating the data into single-station, line-of-position (LOP) and fix files facilitates subsequent analysis of Omega fix accuracy and signal coverage.

ONSOD provided integrated satellite and Omega data from the 4 ships listed in Table A2-1. The data were on magtapes with 4 files for each ship: the raw data, the single-station, LOP and fix data files. The dates and paths listed in Table A2-1 are for those portions of the voyages within the Northern Pacific region (10^{o}S to 70^{o}N, 125E to 75W). Figure A2-1 displays a map of these voyages.

Table A2-1. Integrated Satellite/Omega Data - Ships, Dates, and Path Descriptions

Ship Name	Dates	Path Description	Monitor
Oceanographer	04-15 Feb 79	Off coast of Wash. to Honolulu	MX 1102/4
Wilson	15-25 Apr 79	San Diego to Aleutian Islands	MX 1102/4
Magdelina	06-12 Nov 79 14-26 Dec 79	Baja, Mexico to Panama Canal Off coast of Chile to San Diego	MX 1105
Liberty	14-24 Mar 80 26 Mar-8 Apr 80	Honolulu to Guam to Southeast Asia Japan to San Francisco	MX 1102/4

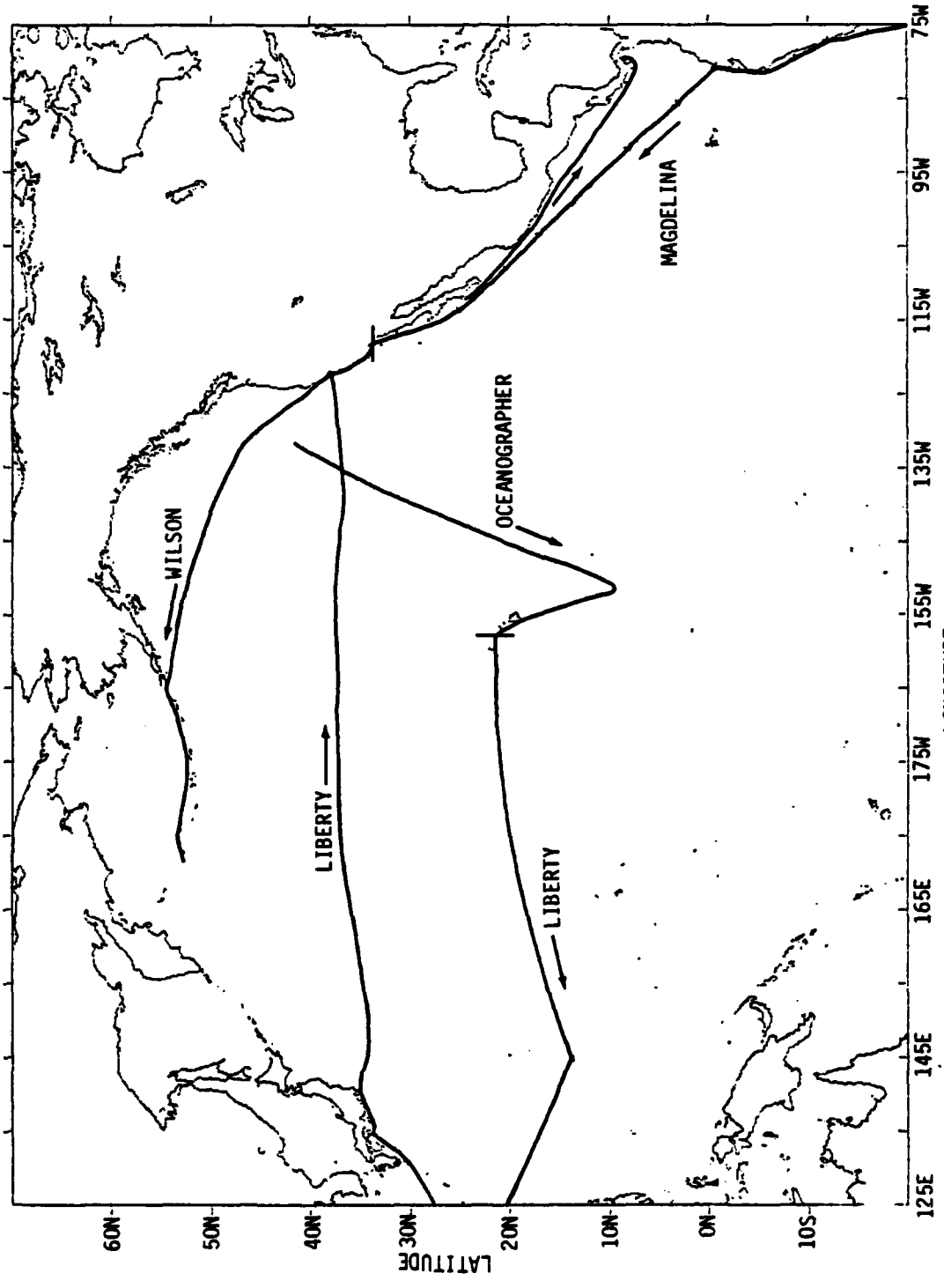

Figure A2-1. Integrated Satellite/Omega Shipboard Data

A2.2 Methods of Analysis

A2.2.1 Processing the Raw Data

The MAGOEXEC program running on the Data General ECLIPSE S-200 minicomputer at ONSOD processes the raw data into 3 files: 1) single-station, 2) line-of-position, and 3) fix data files. The raw data, however, often contains unnecessary, incorrect, or "scrambled" data blocks. Prior to running the MAGOEXEC program, these data should be removed or corrected. A program called PREFIX2 was developed for this purpose. PREFIX2 screens out data that are not co-incident with a satellite fix or that contain errors and "unscrambles" data jumbled by a loss of synchronization between the MX 1102/4 and the Omega stations. The primary output is a reduced raw data file to be processed by MAGOEXEC.

A2.2.2 Analyzing Omega Fix Accuracy

The fix data file output by MAGOEXEC contains fix error information for all possible 3- and 4- station fixes for each of the 3 Omega frequencies. Although each line of this ASCII file contains a multitude of information for each observation, the radial error, the stations used for the fix, and the position (lat., long., date & GMT) are the pertinent data for assessing Omega fix accuracy. A program was developed to select from the fix data file those fixes with the minimum radial error. Three files are output, one for each frequency (10.2, 11-1/2, & 13.6 kHz), for each ship. Each of these files contains the elapsed time (in dec. hrs.) since the beginning of the voyage, the radial error from the satellite fix, the Omega stations used to compute the fix, and the latitude and longitude. Only the data for the "best" fix at each date and time are written to the file: from the fixes listed for each 3- or 4- station combination of available Omega signals, the fix with the minimum radial error is passed to the output file. Thus, the best fix file for each frequency contains the best possible estimates of Omega fix accuracy and station usage for each time and position.

A graphical format was designed to display this history of fix errors and Omega station usage. Figure A2-2 is the first of these graphs which are discussed in detail in Section A2.3.1. The bottom portion of the graph is a plot of the radial errors (nmi) vs. time. Those points marked with the delta symbol correspond to fixes obtained within ±4 hours of local midnight; all other points are marked with the plus sign. Thus, nightime accuracy can easily be distinguished. Errors in excess of 7 nmi. are plotted as 7 nmi. The middle portion of the graph displays the history of station usage. Those Omega stations used to compute the fix are marked by a plus sign. In those instances when the fix data file contained flags indicating best stations among the stations used, the delta symbol was used to mark the best stations. The upper portion of the graph is a map of the part of the ship voyage corresponding to the data plotted below the map. The beginning of each day is marked with a plus sign along the path. Those voyages lasting longer than a couple of weeks were split into 2 parts for greater clarity in the figures.

Visual inspection of the figures for each ship determined which segments of the voyages had similar station usage and fix accuracy. The data for these segments were analyzed statistically for the mean and rms of the radial errors, for the 50% and 90% CEPs, and for the predominant stations, i.e. those stations used in computing at least 1/2 of the fixes for that segment. This information is tabulated for each Omega frequency for each segment and for each ship. The segments are separated in the figures by a dotted line in the fix-error summary and by Roman numerals next to the ship's path. The summary tables and the figures together give a complete picture of Omega station usage and fix accuracy related to the geography of the Northern Pacific area.

A2.2.3 Analyzing Omega Coverage

The single-station data file output by MAGOEXEC contains information on each Omega station receivable at each observation time and position. The signal-to-noise ratio (SNR) for the signal on each frequency and a "note" flag indicating signal quality are listed for each observation. These data were sorted into 3 files for each Omega station in the following way:

1) The latitude and longitude were transferred to the "OK" file for the Omega station if:

   a) the SNRs for all 3 frequencies were greater than or equal to 8 (linear scale) and

   b) the "note" flag indicated the signal was "OK" or for a different lane.

2) The latitude and longitude were transferred to the "LP" file for the Omega station if:

   a) the SNRs for all 3 frequencies were greater than or equal to 8 and

   b) the "note" flag indicated the signal probably came from the wrong way, i.e. the long path.

3) The latitude and longitude were transferred to the "MI" file for the Omega station if:

   a) the SNRs for all three frequencies were greater than or equal to 8 and

   b) the "note" flag indicated the signal was possibly affected by modal interference.

The data from all 4 ships were processed in this way for the entire voyage of each ship. The 24 resultant files (3 types x 8 Omega stations) contain geographic locations at which the Omega signal was of a particular quality. To best display this information a program was developed to plot azimuthal equidistant projections of the world centered on a given Omega station. The latitudes and longitudes from the various files are then plotted as small squares on the appropriate

map. Figure A2-20. is the first of these world maps. The circles are drawn at 1000 nmi intervals, so that range can be easily estimated from the plot. These maps display valuable information on Omega signal coverage. For example, the first map shows those positions at which Omega Norway signals were usable by at least one of the ships. The results are discussed in Section 2.3.2 in detail. The "LP" files were not plotted because the criteria used for flagging data as affected by "wrong way" signals were considered insufficient for identifying long-path signals.

A2.3 Results

A2.3.1 Fix Accuracy and Coverage from MAGOEXEC Fix Data File

Each of the 4 ships are discussed below in terms of observed availability and fix accuracy attainable from "best" station selection. Station G, Trinidad was not included in these assessments, because it was not a perminent OMEGA station. Data outside of the map displayed were not processed, thus there are gaps in continuity of the voyage. Other gaps are times for which there was no data. Errors in excess of 7 nmi were plotted in the figures as 7 nmi.; "outliers" in excess of 10 nmi. were excluded from the statistics. Predominant stations were those used in obtaining at least half of the fixes for that segment of the voyage.

OCEANOGRAPHER

Figures A2-2, 3, and 4
Table A2-2

Coverage: A - obscured by "Greenland Shadow" for first segment; moderate past 140W

B - out-of-range

C - strong till (21N, 145W) when near-field encountered; strong while sitting at (10N, 152W); not used within near-field again, (9N, 153W) to Hawaii.

D - strong

E - strong west of 140W

F - out-of-range

H - strong

Accuracy: For first segment, accuracy was excellent with rms of errors about 1.5 nmi. using stations C, D, and H (and G). For second segment, accuracy was good with rms of 3-3.5 nmi. using stations A, D, E, and H. Stations A and E, though less dominant than C, compensated for the intermittent use of C within the near-field of that transmitter.

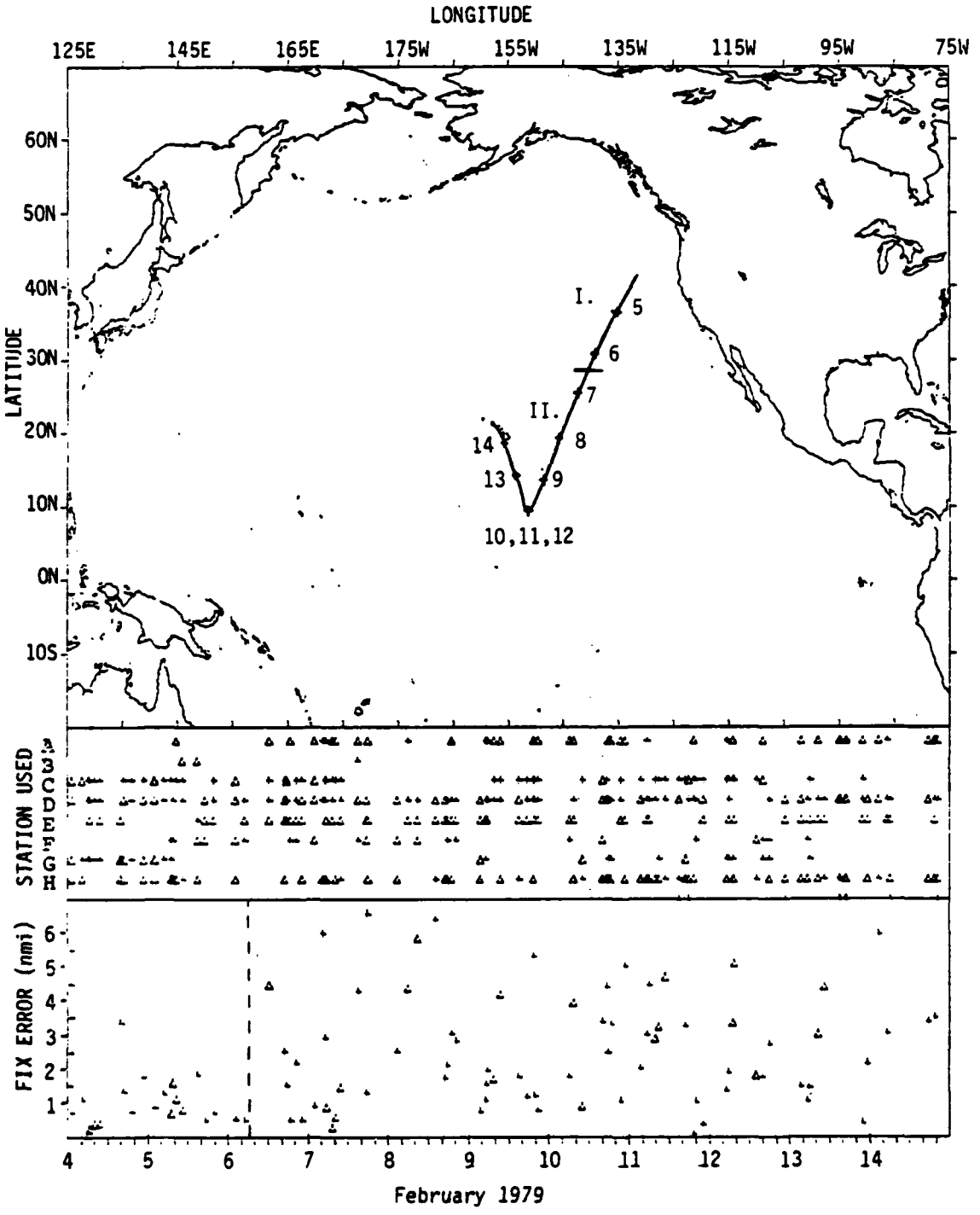

Figure A2-2. Oceanographer - 10.2 kHz

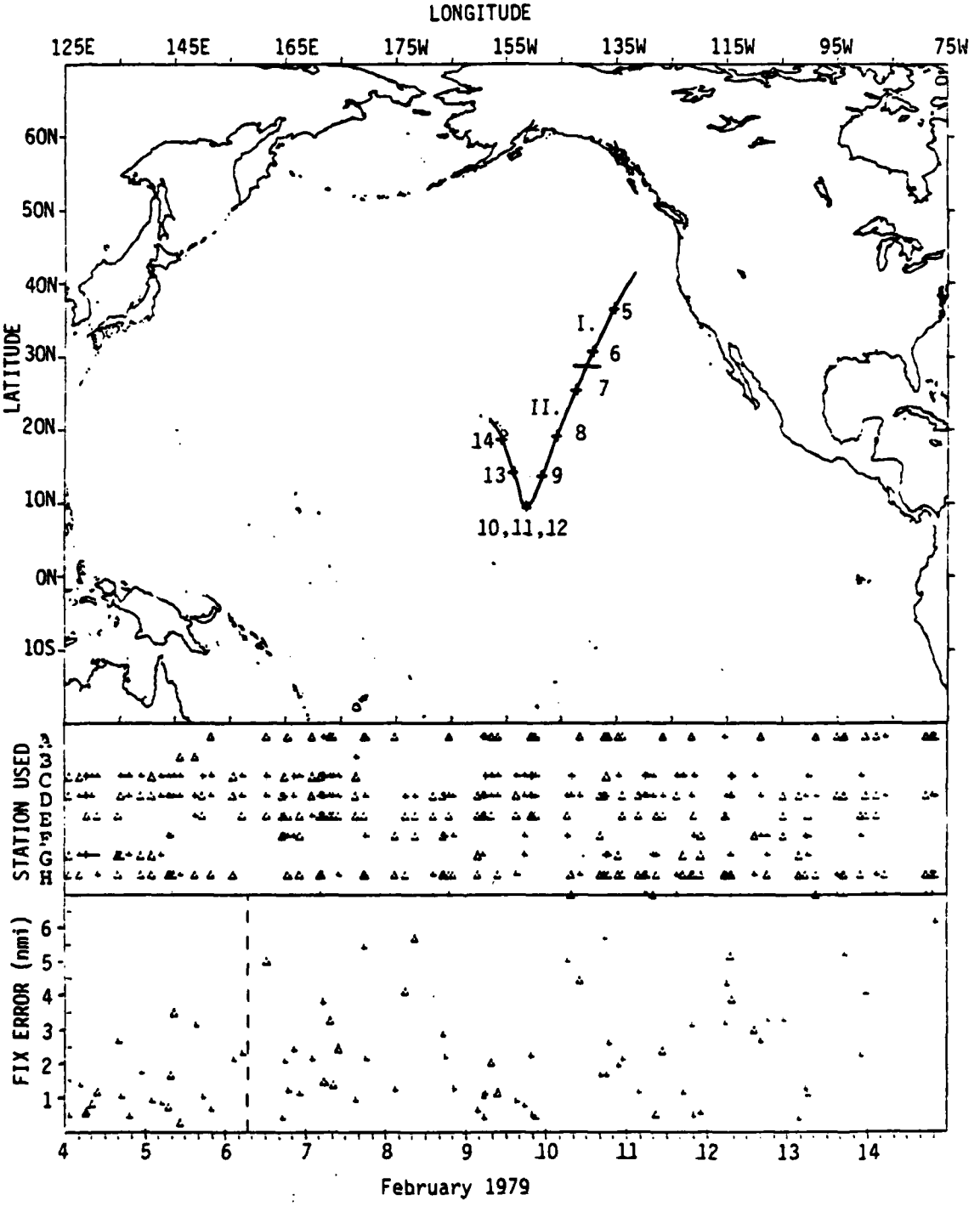

Figure A2-3. Oceanographer - 11-1/3 kHz.

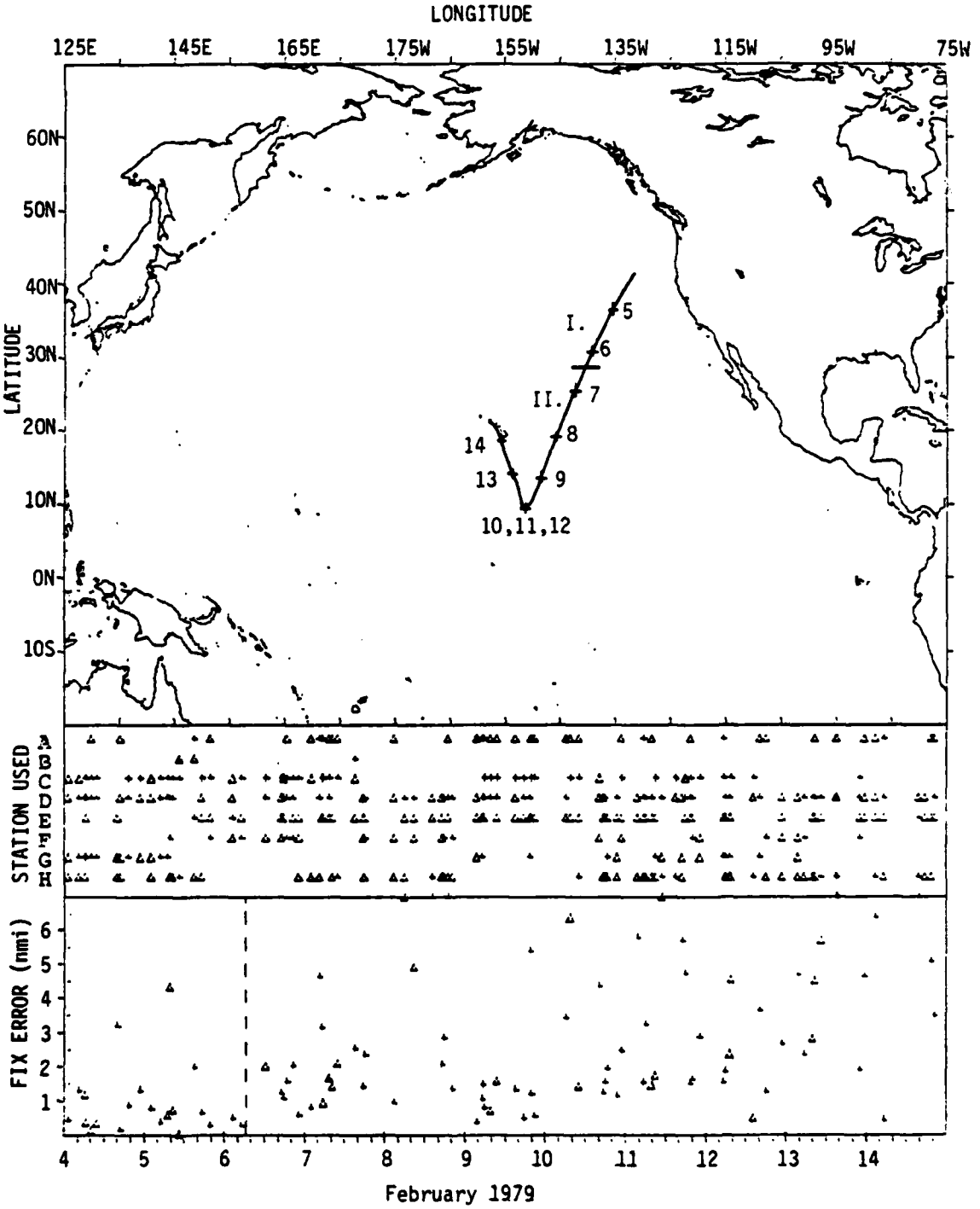

Figure A2-4. Oceanographer - 13.6 kHz.

OCEANOGRAPHER

Segment	Start	End	Predominant Stations	Freq.	Total Fixes	No. of Outliers	Radial Error Mean	Radial Error rms	CEP 50%	CEP 95%
I.	04 Feb 79	06 Feb 79	CD GH	10.2	21	0	0.98	1.21	0.72	1.76
	0000Z	0700Z	CD GH	11 1/3	21	0	1.34	1.61	0.90	2.64
			CD GH	13.6	21	0	0.95	1.41	0.50	1.98
II.	06 Feb 79	15 Feb 79	A CDE H	10.2	81	8	2.66	3.16	2.16	5.98
	0700Z	0000Z	A DE H	11 1/3	77	10	2.76	3.43	2.16	7.01
			DE H	13.6	79	4	2.85	3.57	1.97	7.21

Table A2-2. Summary of Omega Fix Accuracy - OCEANOGRAPHER

WILSON

Figures A2-5, 6, and 7
Table A2-3

Coverage: A - Absent while hidden by "Greenland Shadow" off west coast; moderate to strong past 140W and into Aleutian Chain.

B - out-of-range

C - strong

D - strong

E - out-of-range

F - available just off San Diego then out-of-range

H - strong

Accuracy: During the first day, using station F as well as the primary triad, C, D, and H, Omega was less than 2 nmi. off on the average. Accuracy was excellent - less than 1 nmi - for the other 9 days of the voyage. Stations C, D, and H are best in this area, with A an extra guarantee to the north of the Greenland Shadow.

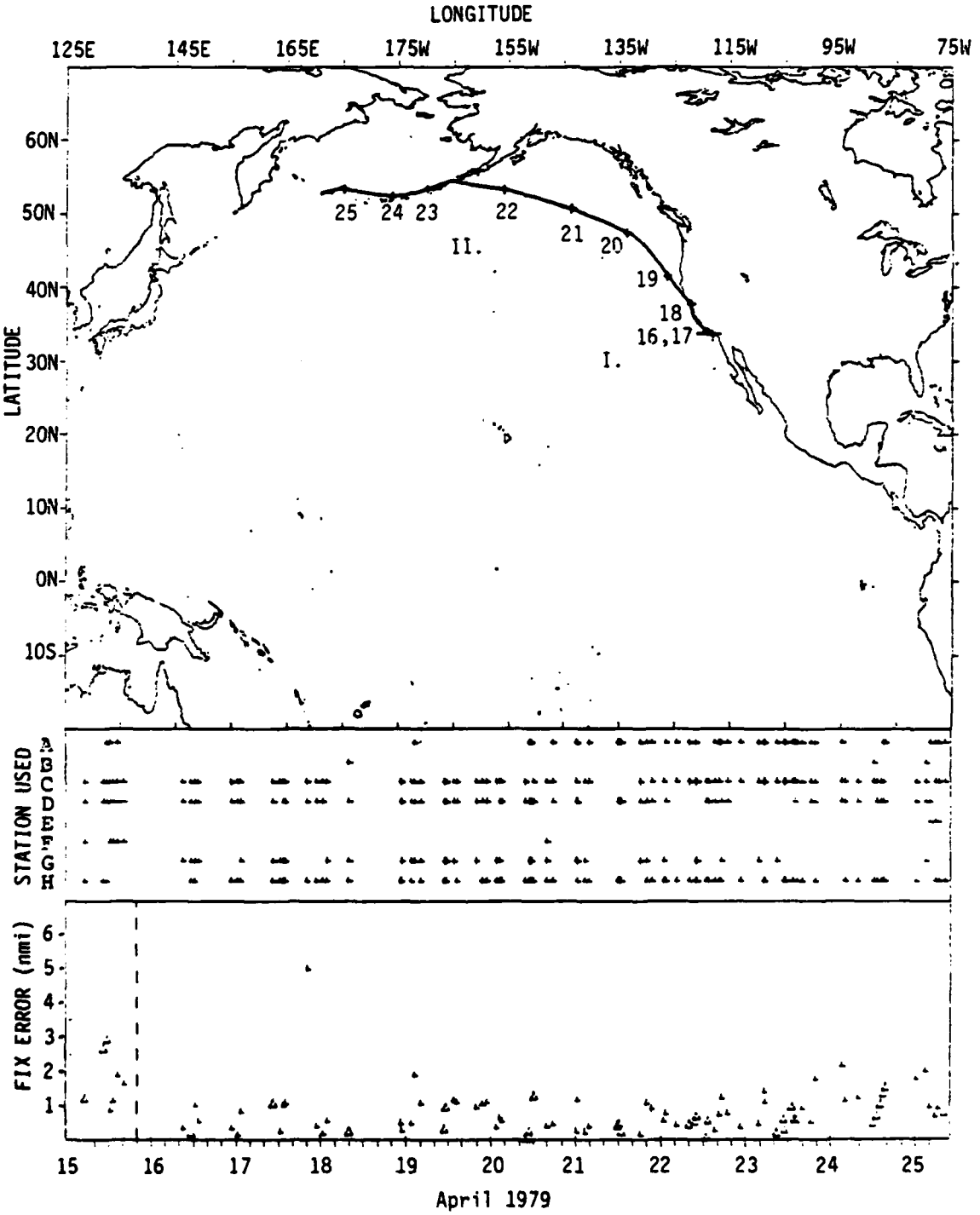

Figure A2-5. Wilson - 10.2 kHz.

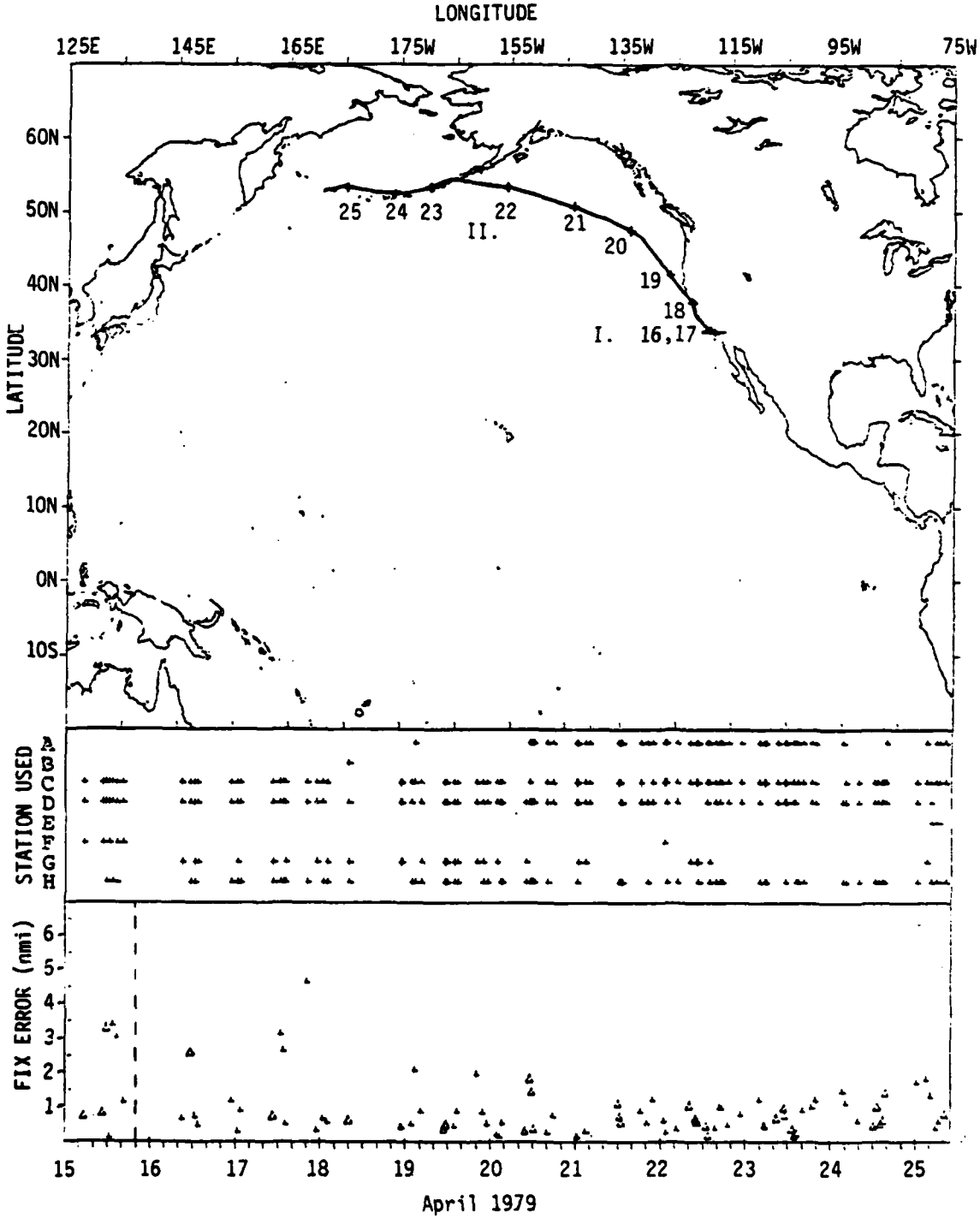

Figure A2-6. Wilson - 11-1/3 kHz.

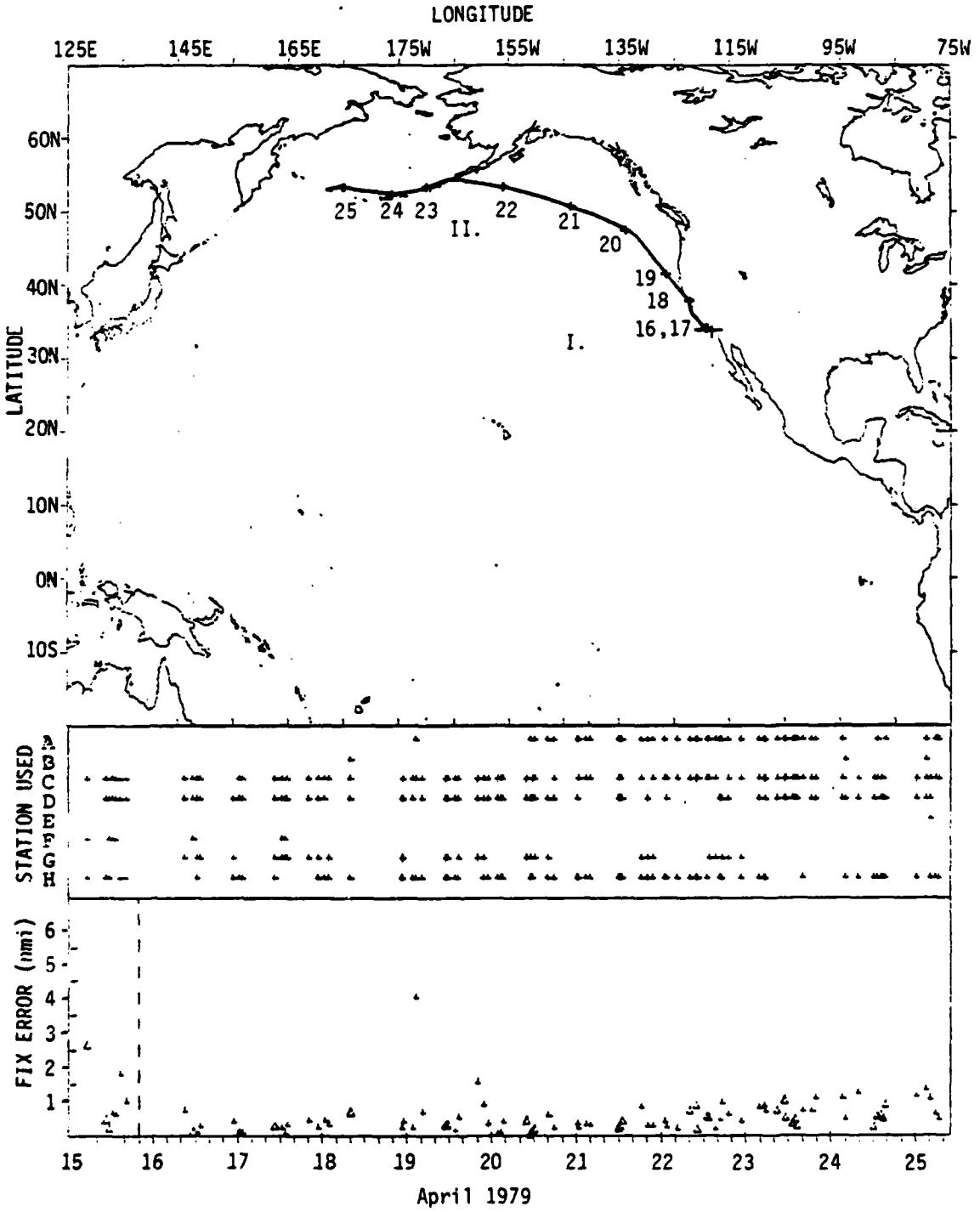

Figure A2-7. Wilson - 13.6 kHz.

WILSON

Segment	Start	End	Predominant Stations	Freq.	Total Fixes	No. of Outliers	Radial Error Mean	Radial Error rms	CEP 50%	CEP 95%
I.	15 Apr 79	15 Apr 79	A CD F H	10.2	7	0	1.76	1.91	1.23	2.69
	0000Z	2000Z	CD F H	11 1/3	7	0	1.80	2.21	0.83	3.31
			CD F H	13.6	7	0	1.07	1.34	0.62	1.82
II.	16 Apr 79	25 Apr 79	CD H	10.2	86	0	0.77	1.01	0.59	1.77
	0600Z	1000Z	A CD H	11 1/3	86	0	0.84	1.10	0.64	1.96
			A CD H	13.6	85	0	0.53	0.73	0.41	1.10

Table A2-3. Summary of Omega Fix Accuracy - WILSON

MAGDELINA - PART A

Figures A2-8, 9, and 10
Table A2-4

Coverage:
- A - absent while signal path across Greenland; strong south *and east of* (12N, 93W)
- B - out-of-range
- C - strong
- D - strong
- E - out-of-range
- F - strong
- H - strong but fading out for second segment to the southeast as range increases.

Accuracy: About 2 nmi. for first 4 days off coast of Mexico. With A obscured by Greenland, C, D, F, and H were predominant. After the Norway signal cleared Greenland, accuracy was even better - less than 1 nmi. - even though Japan was fading out-of-range.

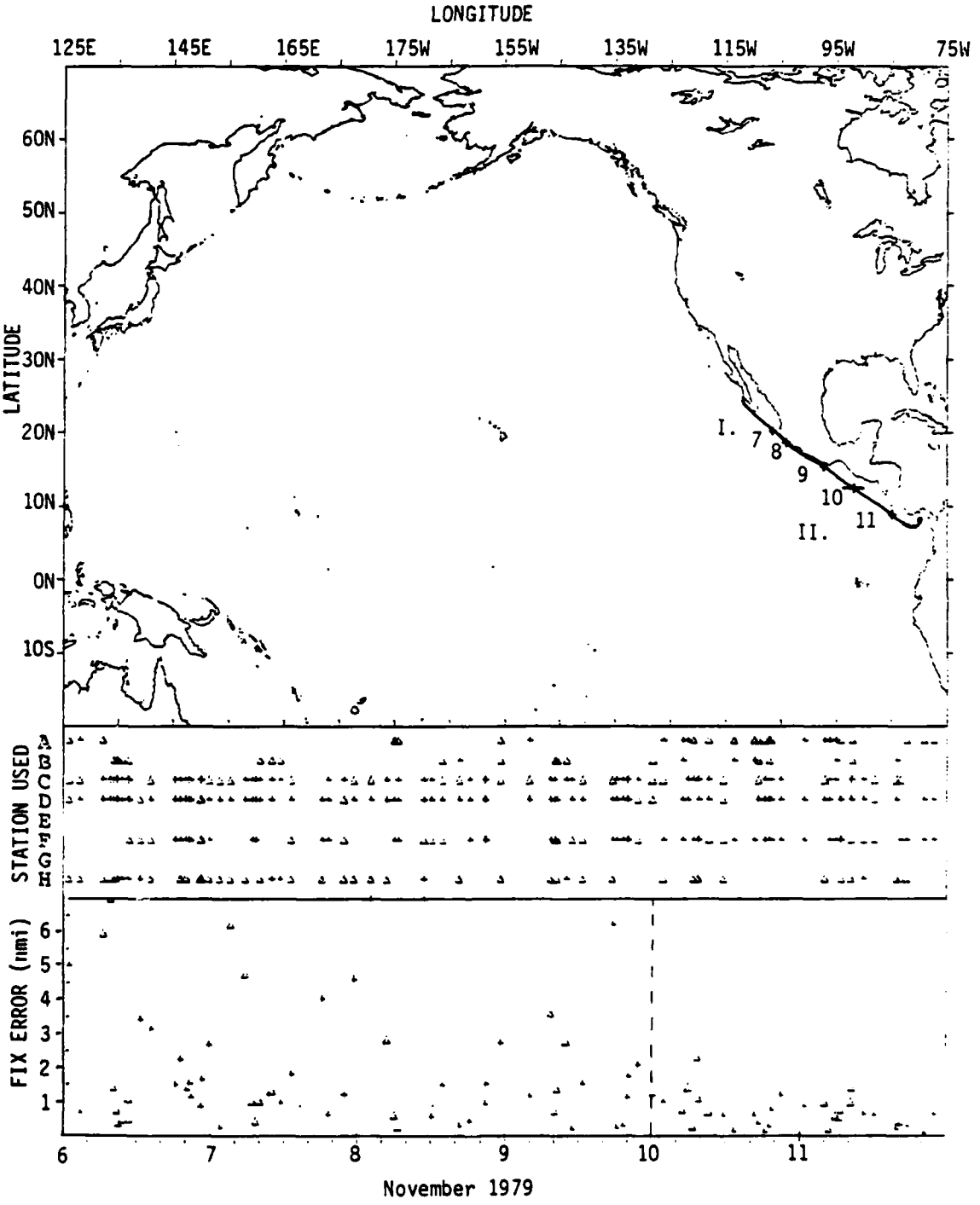

Figure A2-8. Magdelina - Part A - 10.2 kHz.

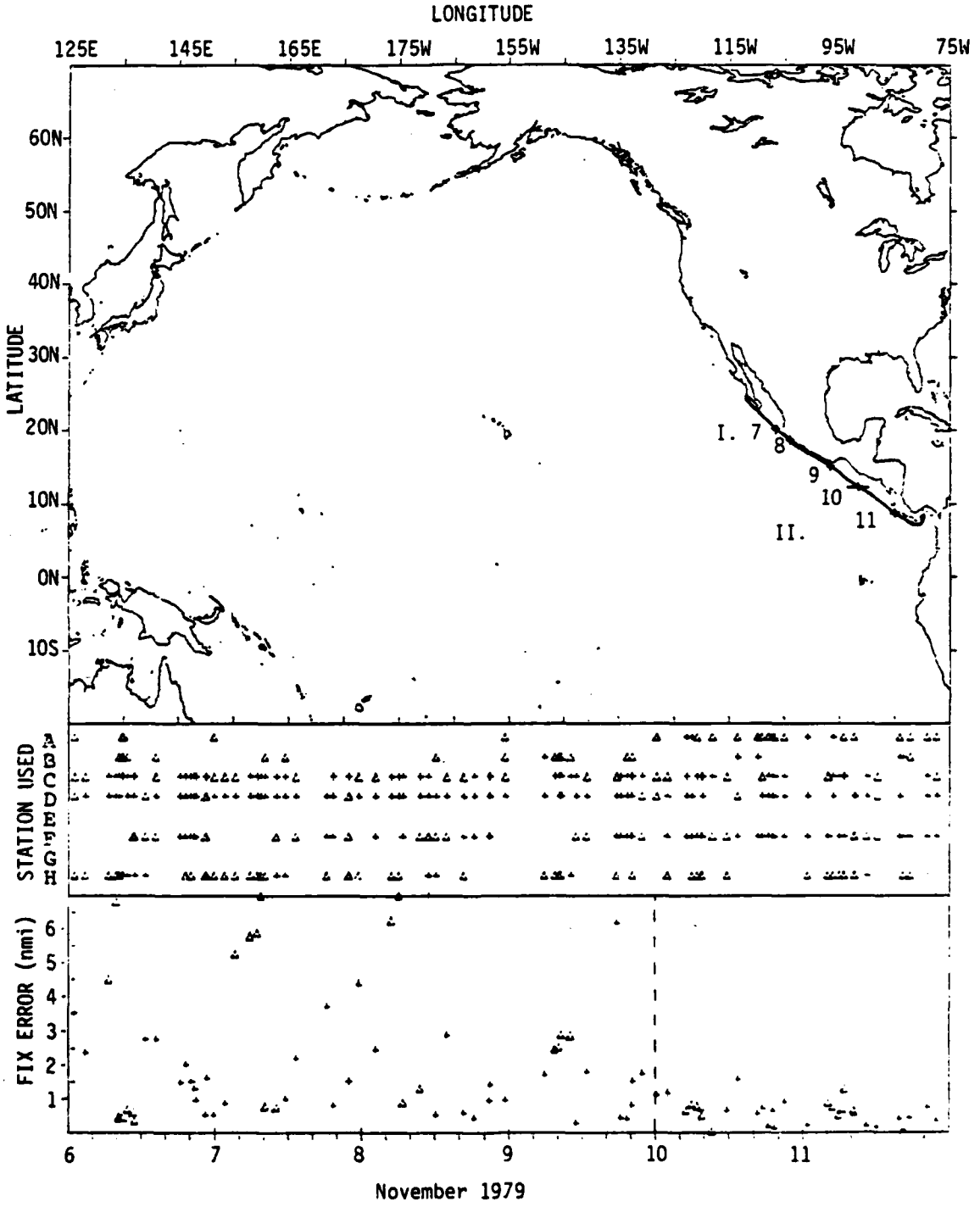

Figure A2-9. Magdelina - Part A - 11-1/3 kHz.

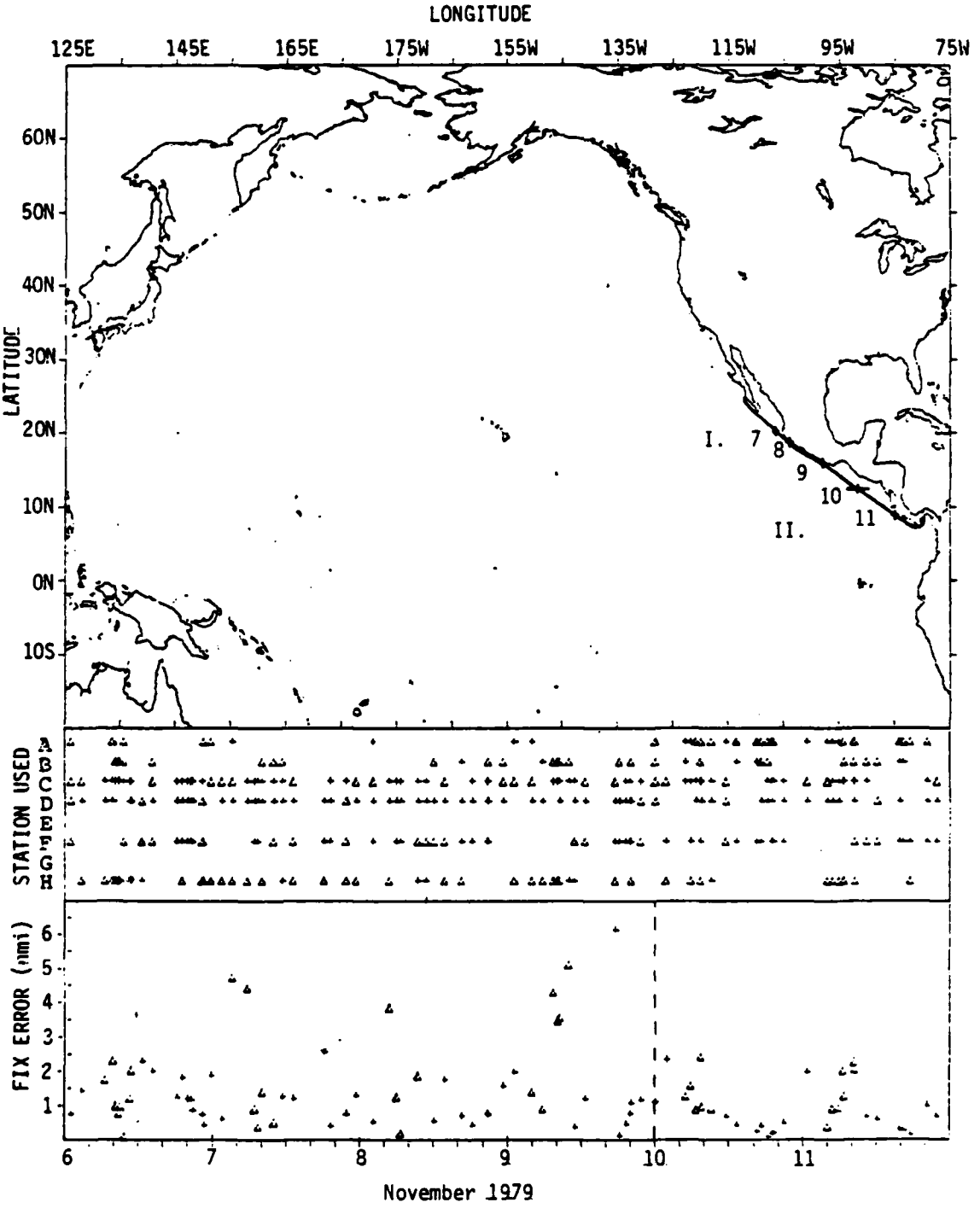

Figure A2-10. Magdelina - Part A - 13.6 kHz.

MAGDELINA - PART A

Segment	Start	End	Predominant Stations	Freq.	Total Fixes	No. of Outliers	Radial Error Mean	Radial Error rms	CEP 50%	CEP 95%
I.	06 Nov 79	10 Nov 79	CD F H	10.2	58	2	1.93	2.62	1.35	5.99
	0000Z	0000Z	CD F H	11 1/3	59	2	2.12	2.82	1.50	6.20
			CD F H	13.6	61	1	1.55	2.03	1.20	4.45
II.	10 Nov 79	12 Nov 79	A CD F	10.2	31	0	0.72	0.87	0.62	1.44
	0000Z	0000Z	A CD F H	11 1/3	31	0	0.62	0.72	0.64	1.17
			A CD F	13.6	31	0	0.96	1.19	0.69	2.29

MAGDELINA - PART B

Segment	Start	End	Predominant Stations	Freq.	Total Fixes	No. of Outliers	Radial Error Mean	Radial Error rms	CEP 50%	CEP 95%
I.	14 Dec 79	22 Dec 79	A CD F H	10.2	98	1	1.03	1.31	0.84	2.45
	1200Z	0000Z	A CD F H	11 1/3	98	0	0.88	1.19	0.62	2.62
			A CD F H	13.6	98	0	0.82	1.11	0.52	1.98
II.	22 Dec 79	26 Dec 79	CD F H	10.2	114	3	2.01	2.66	1.37	5.37
	0000Z	1800Z	CD F H	11.3	112	7	2.06	2.59	1.62	4.92
			CD F H	13.6	115	0	1.84	2.65	1.24	6.63

Table A2-4. Summary of Omega Fix Accuracy - MAGDELINA

MAGDELINA - PART B

Figures A2-11, 12, and 13
Table A2-4

Coverage: A - strong until signal encounters Greenland ice path northwest of (10N, 94W) then it was absent
B - out-of-range
C - strong
D - strong
E - out-of-range
F - strong
H - strong

Accuracy: Around 1 nmi. for first segment with A, C, D, F, and H providing redundant coverage. With A lost behind Greenland accuracy shifted to 2 nmi. - still excellent and within expected limits. Stations C, D, F, and H cover this area with strong, reliable signals.

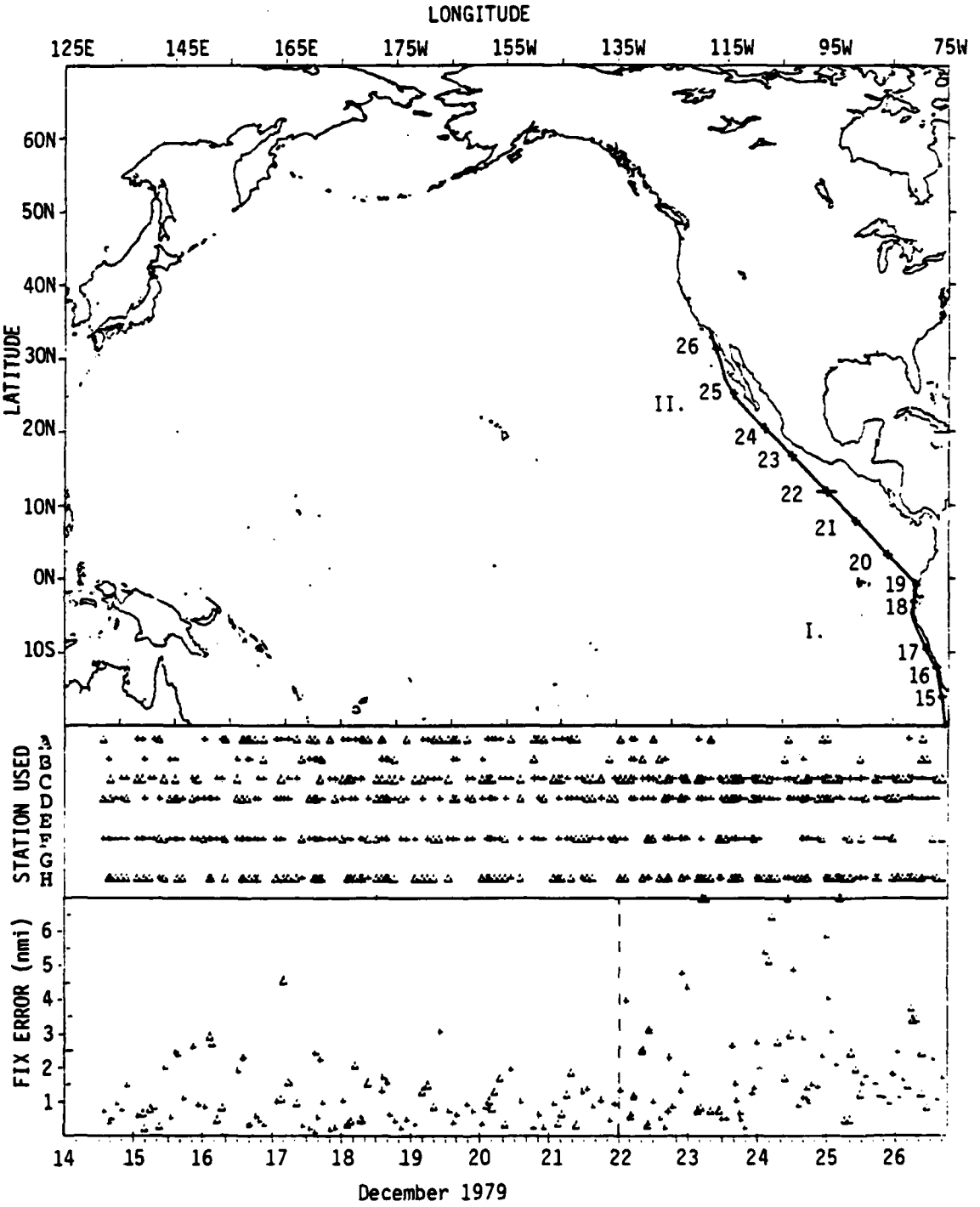

Figure A2-11. Magdelina - Part B - 10.2 kHz.

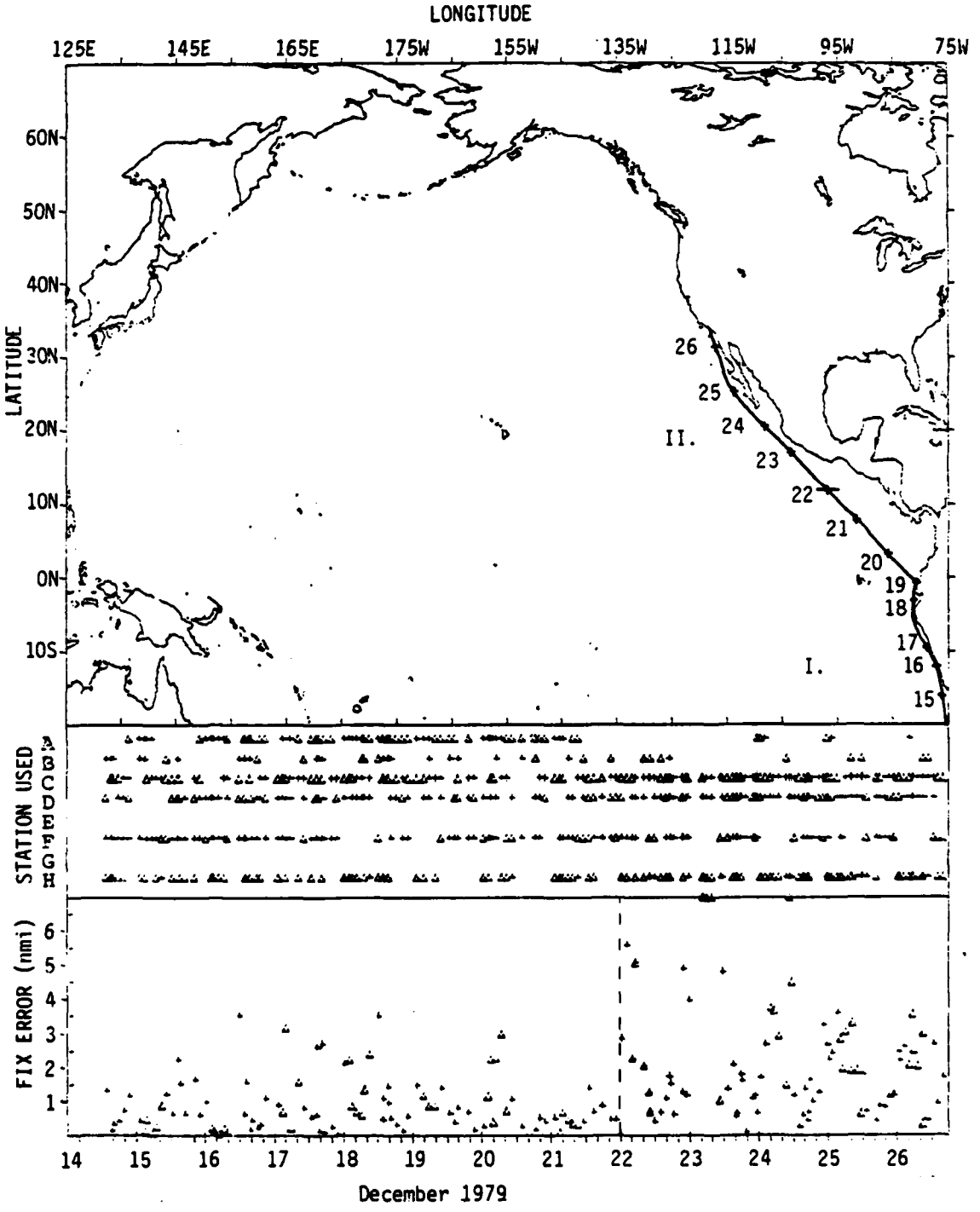

Figure A2-12. Magdelina - Part B - 11-1/3 kHz.

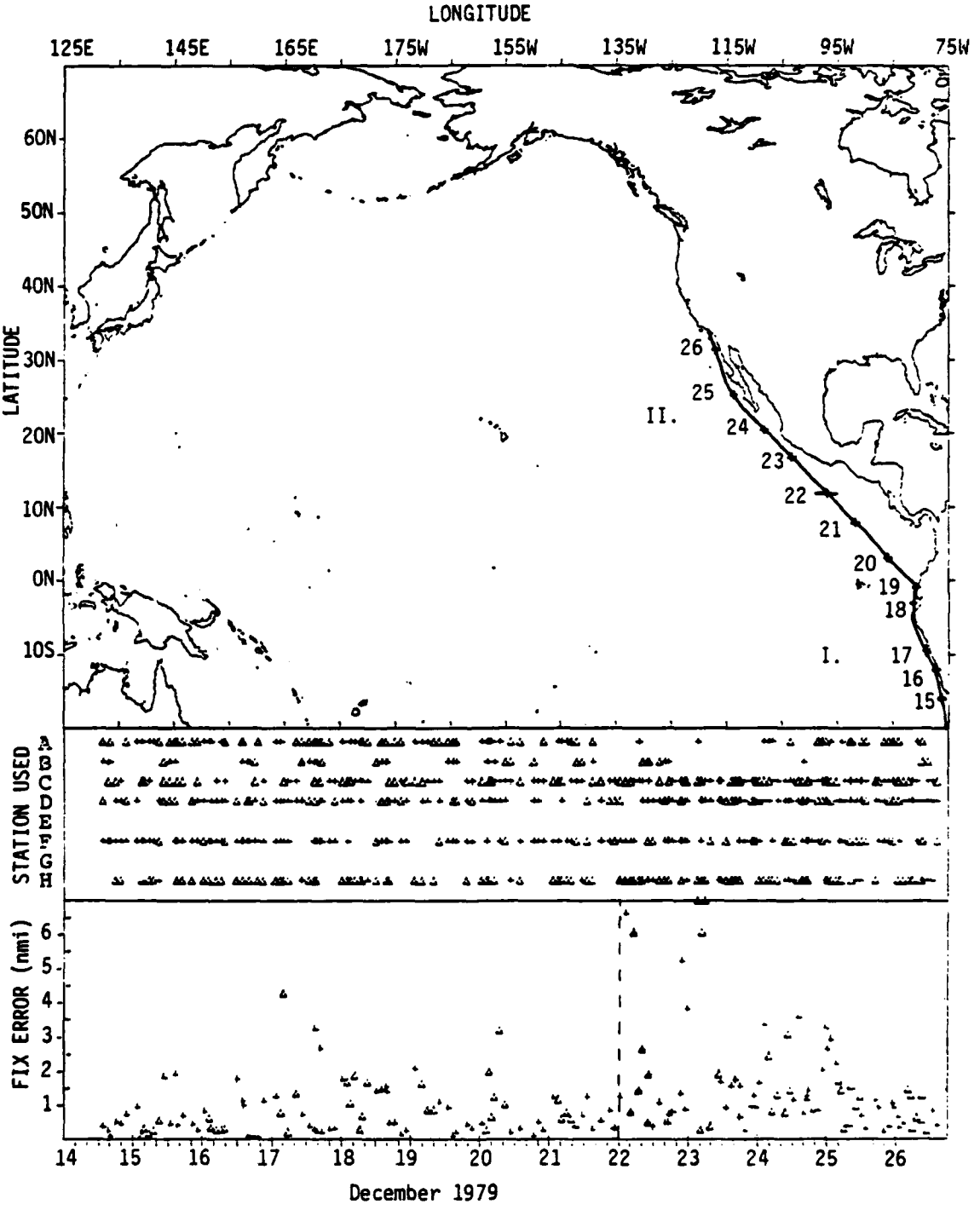

Figure A2-13. Magdelina - Part B - 13.6 kHz.

LIBERTY - PART A

Figures A2-14, 15, and 16
Table A2-5

Coverage:
- A - strong
- B - out-of-range until west of (19N, 167E) then moderate
- C - strong west of 163W, once out of near-field; moderate west of 145E.
- D - strong
- E - strong
- F - out-of-range
- H - strong

Accuracy: Excellent throughout this part of voyage with average and rms about 1-2 nmi. Stations A, C, D, E, and H provided more than adequate coverage. Some variation in station usage is noted for different frequencies; but this did not affect fix accuracy, because at least 4 stations were available all the time.

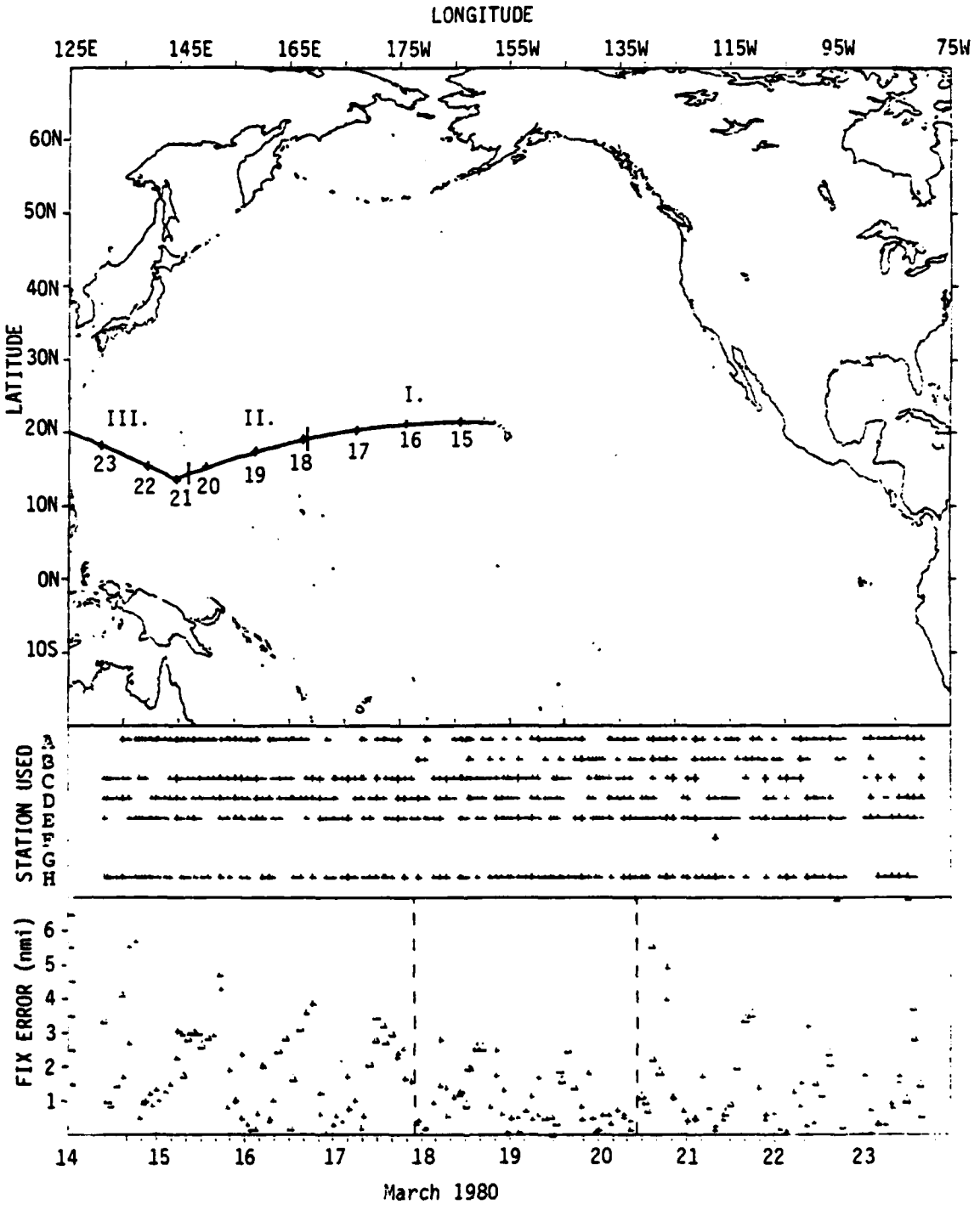

Figure A2-14. Liberty - Part A - 10.2 kHz.

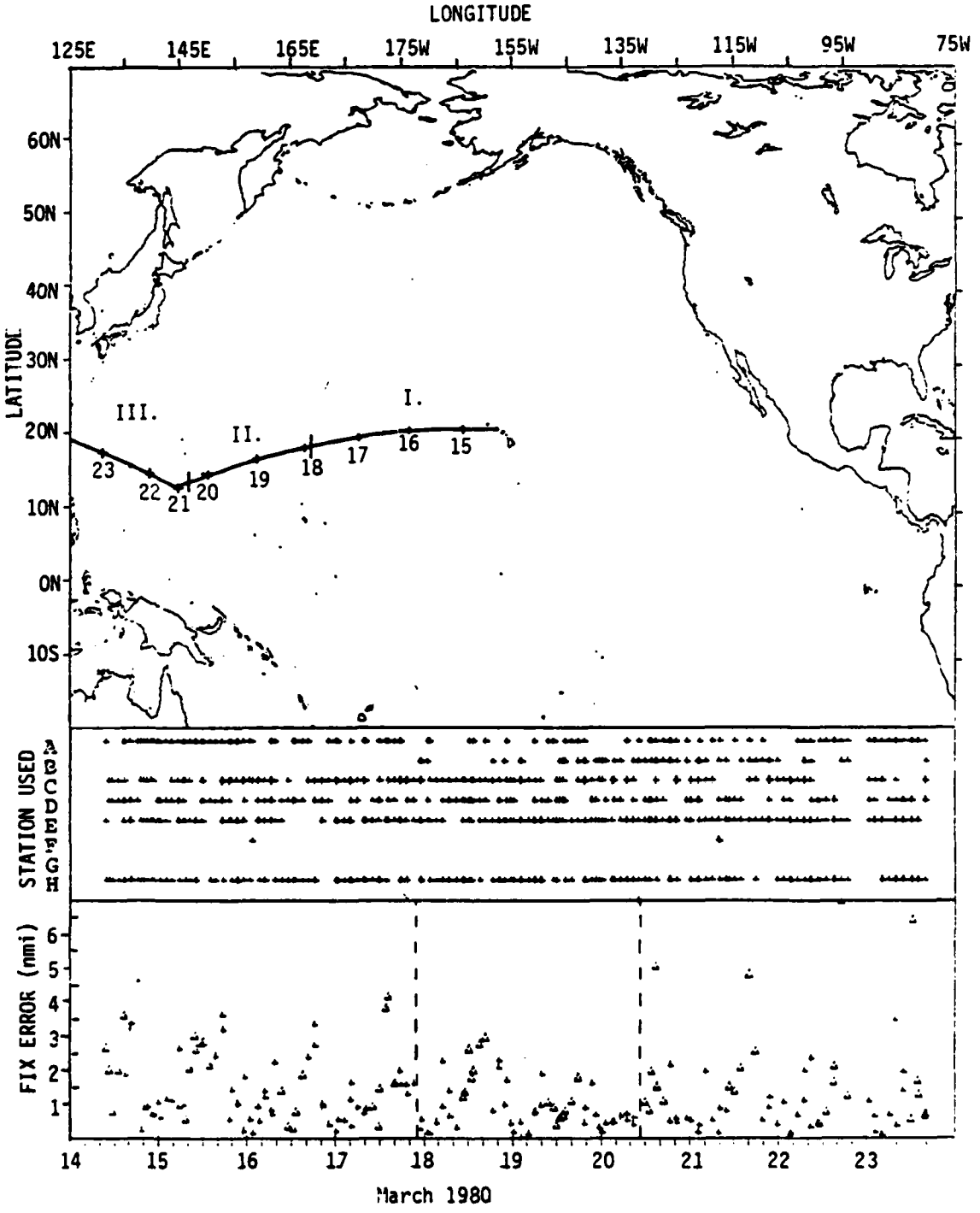

Figure A2-15. Liberty - Part A - 11-1/3 kHz.

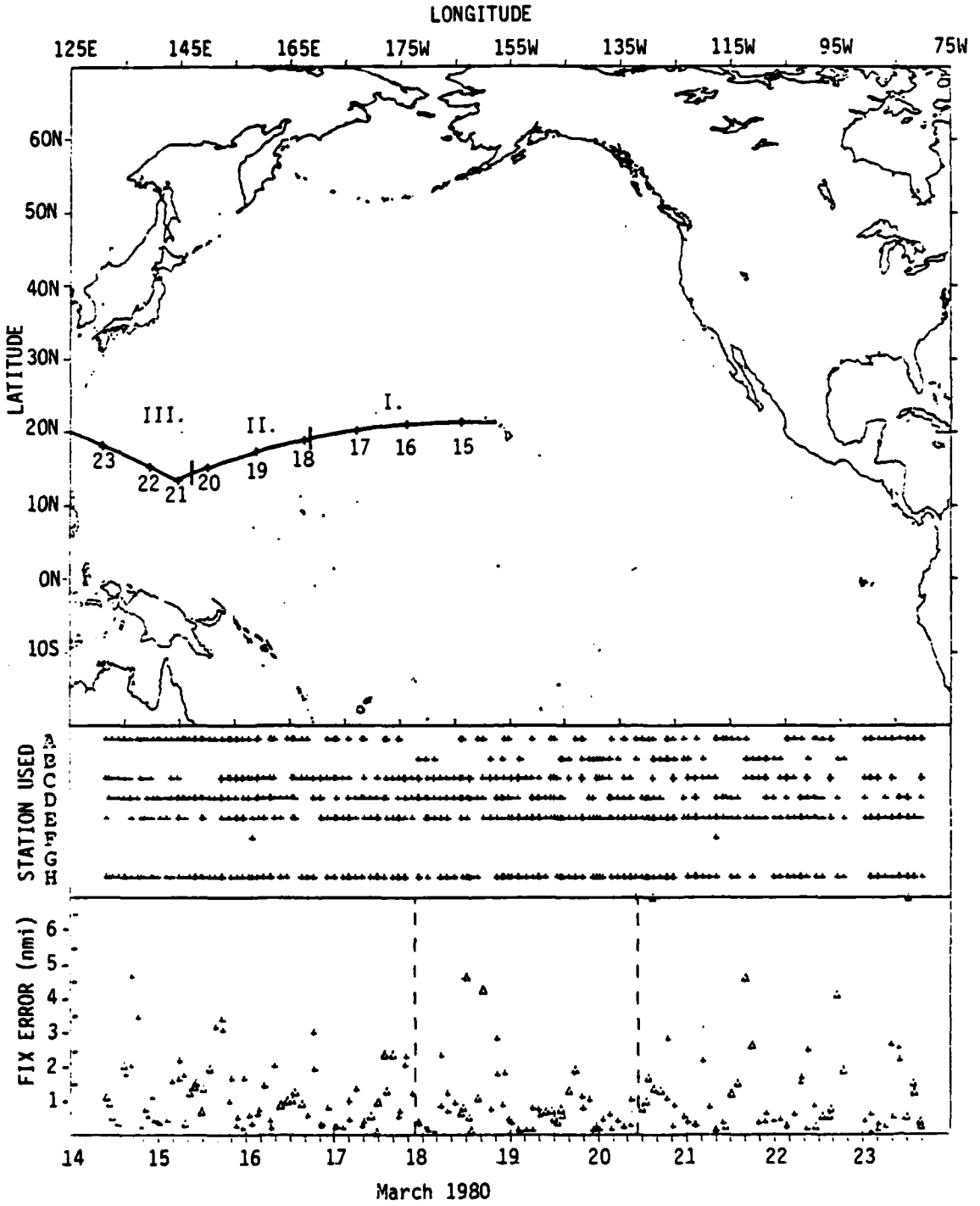

Figure A2-16. Liberty - Part A - 13.6 kHz.

LIBERTY - PART A

Segment	Start	End	Predominant Stations	Freq.	Total Fixes	No. of Outliers	Radial Error Mean	Radial Error rms	CEP 50%	CEP 95%
I	14 Mar 80 0000Z	17 Mar 80 2200Z	A CDE H	10.2	77	0	1.92	2.33	1.67	4.18
			A CDE H	11 1/3	77	0	1.56	1.89	1.14	3.65
			A CDE H	13.6	76	0	1.18	1.50	0.95	3.07
II.	17 Mar 80 2200Z	20 Mar 80 1100Z	A CDE H	10.2	54	1	0.96	1.22	0.58	2.51
			CDE H	11 1/3	54	1	0.98	1.22	0.70	2.29
			CDE H	13.6	54	1	0.84	1.25	0.59	2.33
III.	20 Mar 80 1100Z	23 Mar 80 1800Z	A DE H	10.2	61	1	1.42	2.09	0.90	3.97
			A DE H	11 1/3	61	0	1.34	1.99	0.81	3.47
			A CDE H	13.6	61	0	1.20	1.90	0.56	2.82

LIBERTY - PART B

Segment	Start	End	Predominant Stations	Freq.	Total Fixes	No. of Outliers	Radial Error Mean	Radial Error rms	CEP 50%	CEP 95%
I.	26 Mar 80 2000Z	30 Mar 80 2000Z	ABCDE	10.2	90	1	1.22	1.60	0.85	2.76
			ABCDE	11 1/3	90	2	0.99	1.25	0.76	2.23
			ABCDE	13.6	90	0	0.96	1.21	0.73	2.38
II.	30 Mar 80 2000Z	06 Apr 80 1400Z	CD H	10.2	148	0	0.78	0.98	0.61	1.86
			A CD H	11 1/3	148	0	0.71	0.93	0.53	1.76
			A CDE H	13.6	148	0	0.69	0.91	0.50	1.98
III.	06 Apr 80 1400Z	08 Apr 80 0400Z	CD H	10.2	27	0	2.38	2.72	2.56	3.82
			CD H	11 1/3	33	1	2.10	2.59	1.57	4.59
			CD H	13.6	32	1	1.78	2.17	1.37	3.57

Table A2-5. Summary of Omega Fix Accuracy - LIBERTY

LIBERTY - PART B

Figures A2-17, 18, and 19
Table A2-5

Coverage:
- A - strong then absent east of (28N, 155N) as signal path traverses Greenland
- B - moderate then out-of-range east of (33N, 147E)
- C - strong
- D - strong
- E - strong then moderate east of (33N, 147E)
- F - out-of-range
- H - strong east of 145E, once out of near-field of transmitter.

Accuracy: Continued to be excellent (1-2 nmi.) throughout return voyage. Stations A, C, D, and H were used for more than half the journey. Stations B and E provided redundancy within the near-field of Japan for first segment. As ship entered the western edge of Greenland shadow, accuracy shifted to 2 nmi., though C, D, and H give excellent results here as well.

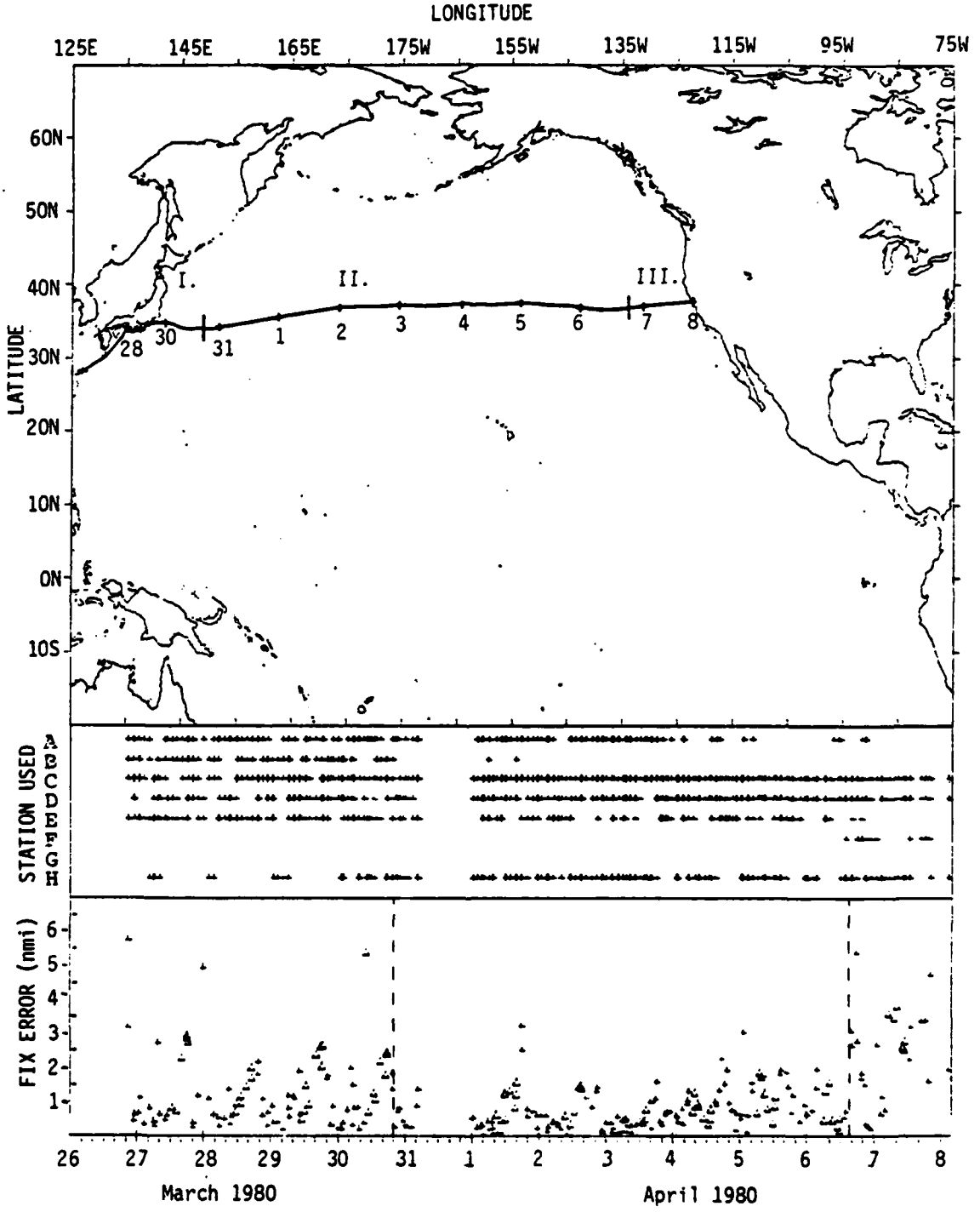

Figure A2-17. Liberty - Part B - 10.2 kHz.

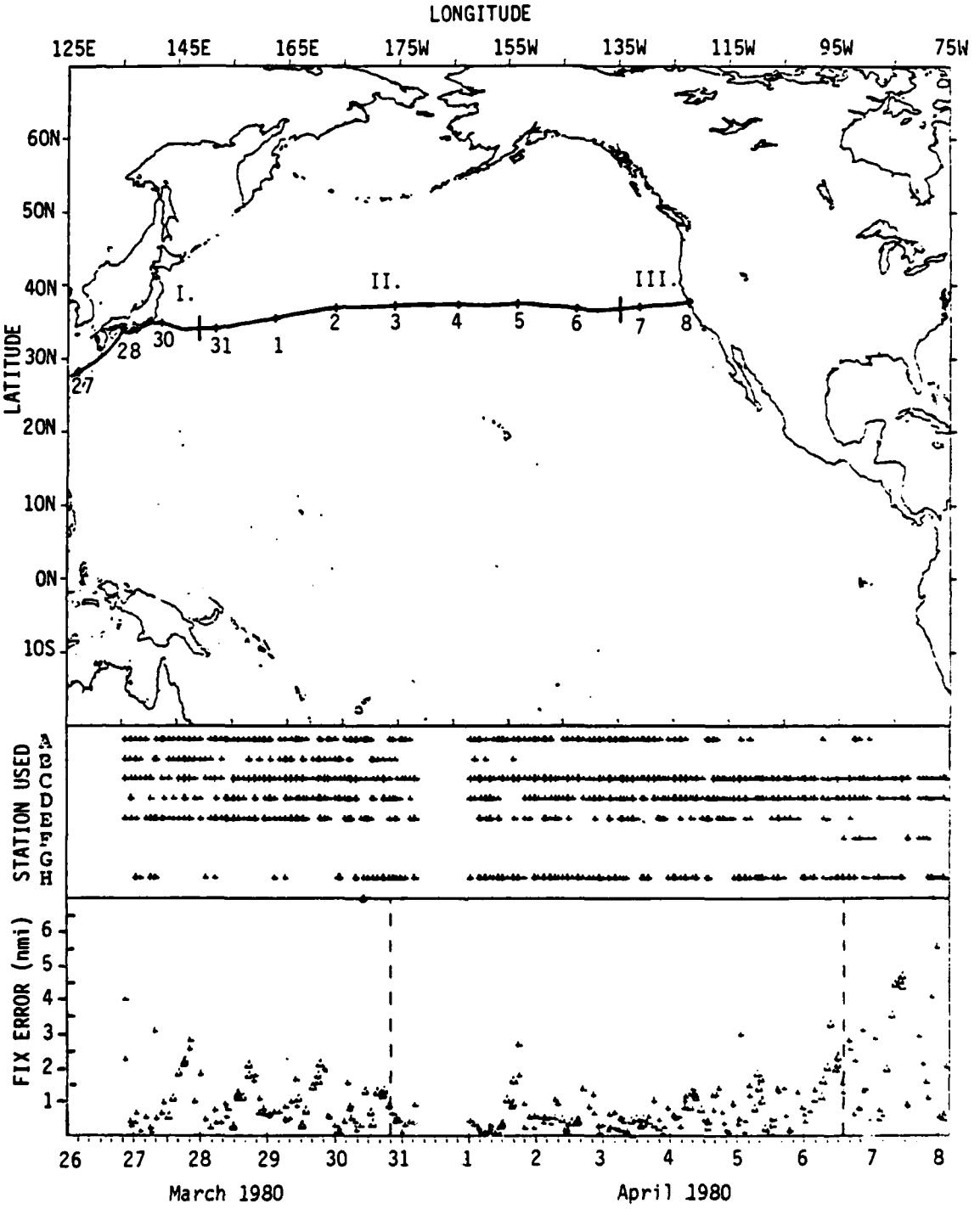

Figure A2-18. Liberty - Part B - 11-1/3 kHz.

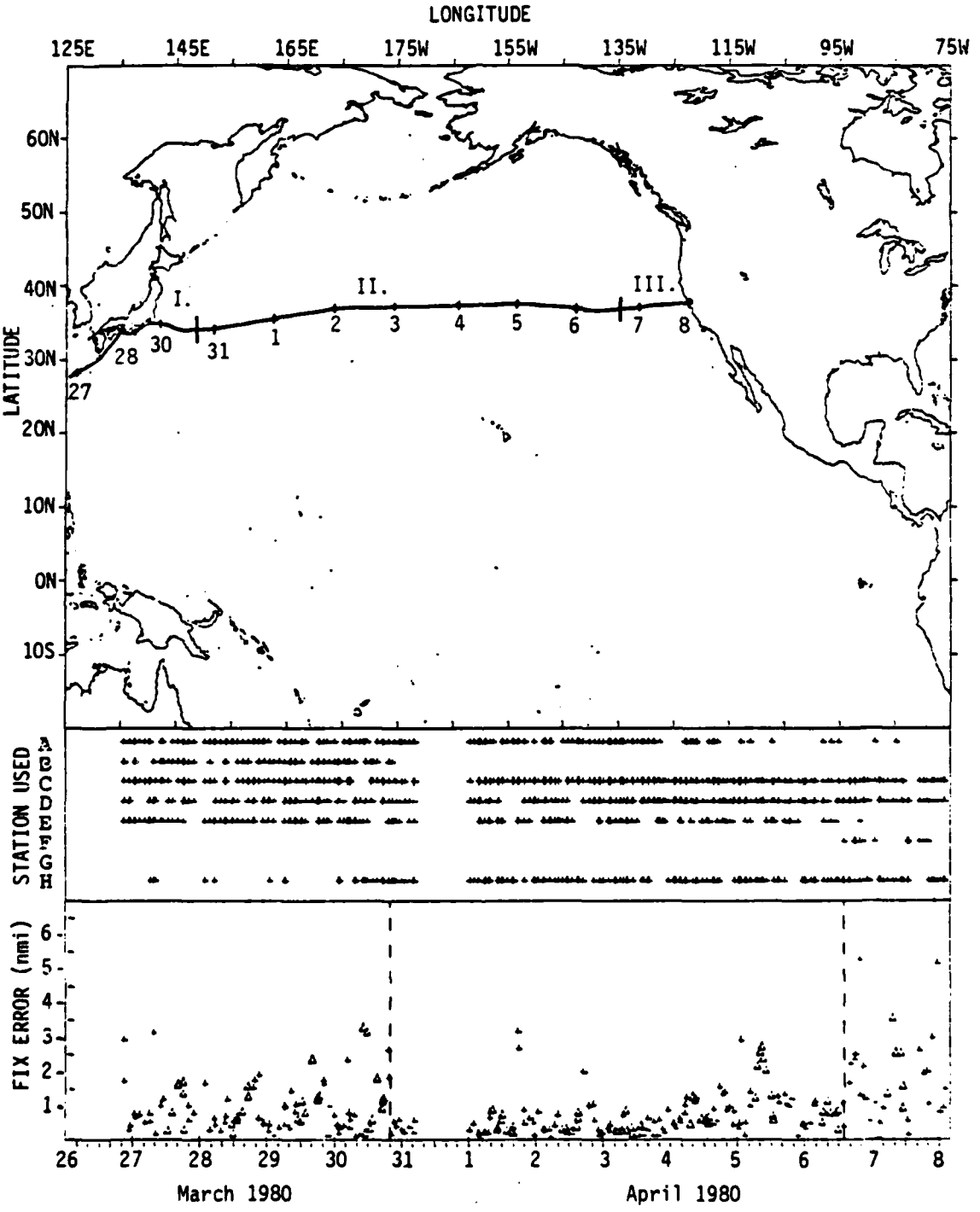

Figure A2-19. Liberty - Part B - 13.6 kHz.

2.3.2 Signal Coverage from MAGOEXEC Station Data File

2.3.2.1 "OK" Data

As explained in Section A2.2.3, the single-station files for each ship were sorted according to transmitter and signal quality. The data flagged as "OK" are displayed for each Omega station in Figures A2-20 through A2-26. These figures give an overview of Omega coverage. Because no restriction was placed on the positions reported from each ship, some of the data are outside the Northern Pacific region; however, these data provide useful information. Noteworthy results from these figures are as follows:

A) Norway — Figure A2-20

Although all of the ships traversed some part of US coastal waters, the Norway signal was unusable in this area, because of severe attenuation in crossing the Greenland ice mass. This "Greenland Shadow" is clearly noticed in the figure by the absence of data points between bearings 285 and 335. Coverage extends to 6500 nmi.

B) Liberia — Figure A2-21

Except the northwestern Pacific near Japan where the LIBERTY cruised, Liberia is out-of-range for most of the Northern Pacific. The area off the Japanese coast and somewhat south is 7000-9000 nmi. from the transmitter, near the far-field limit for reliable signals, yet coverage is good in that area.

C) Hawaii — Figure A2-22

Signals from this transmitter are strong and reliable throughout the region. Only within the near-field of the transmitter are signals suspect because of possible modal interference. The near-field radius is about 300-500 nmi. Signals were noted strong to 6500 nmi.

D) North Dakota — Figure A2-23

Like Hawaii, North Dakota signals are strong throughout the region to 6500 nmi. Omega D gives excellent coverage in the Pacific.

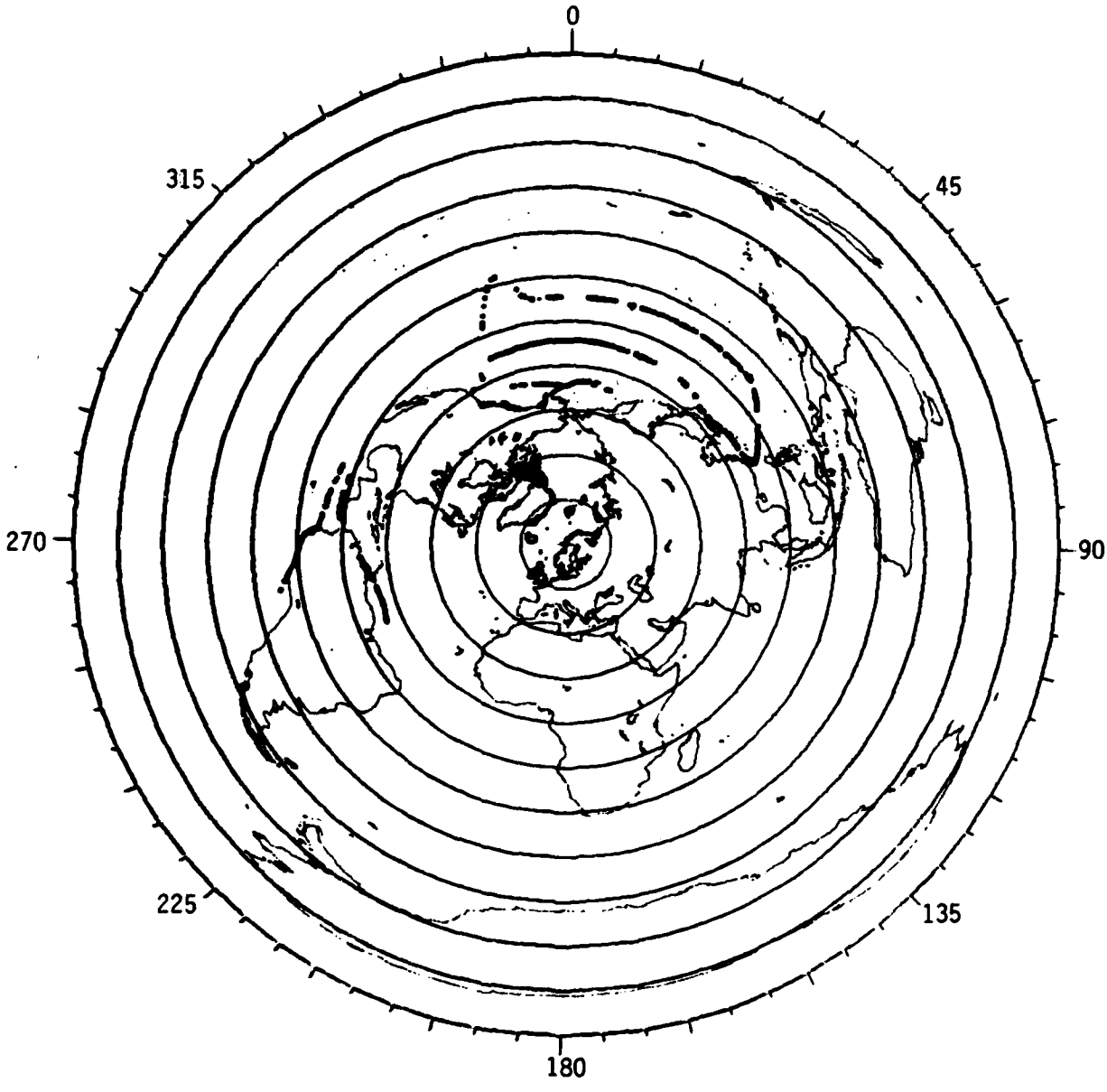

Figure A2-20. Omega Norway Signal Coverage
Integrated Satellite/Omega Data

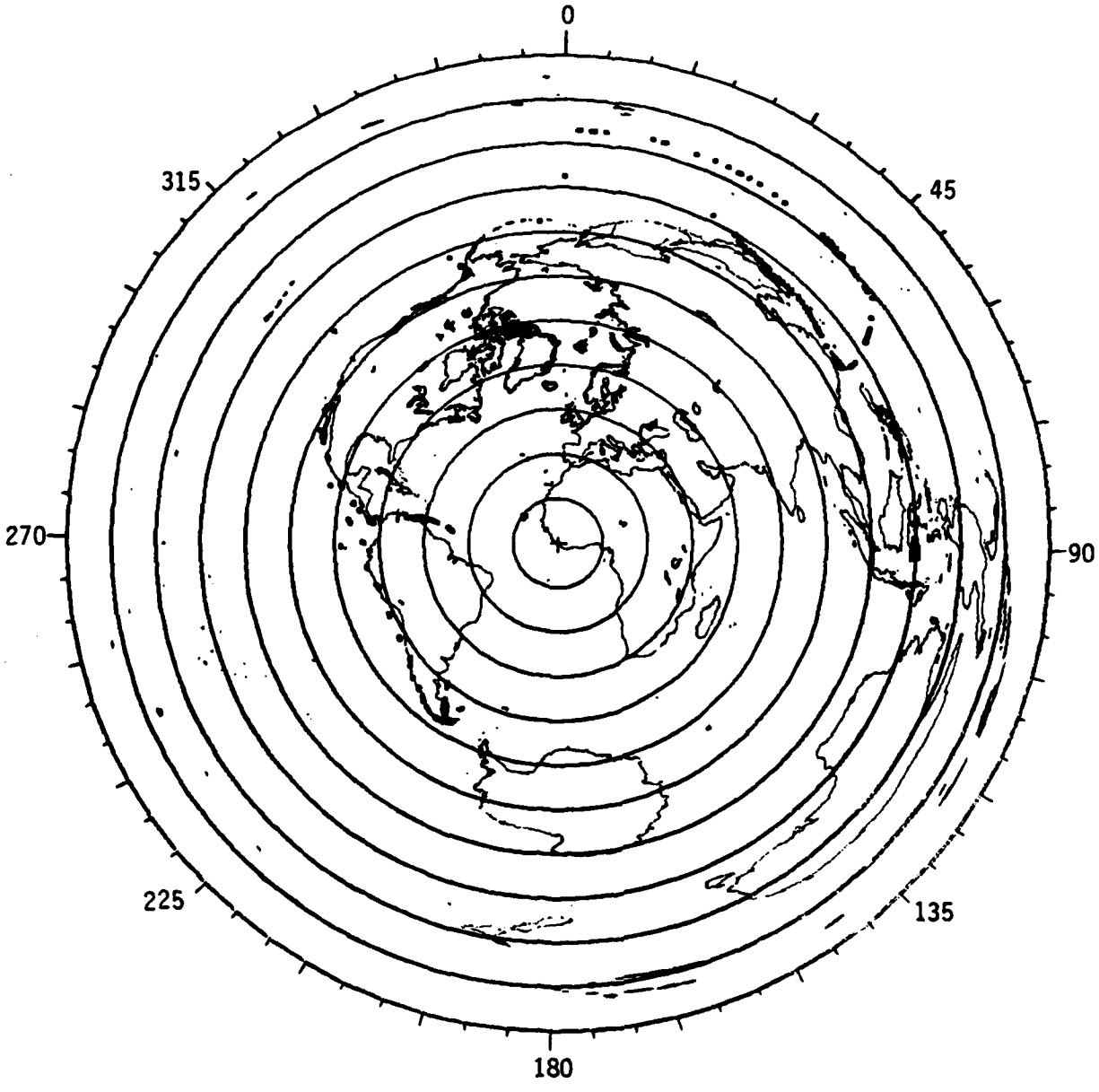

Figure A2-21. Omega Liberia Signal Coverage - Integrated Satellite/Omega Data

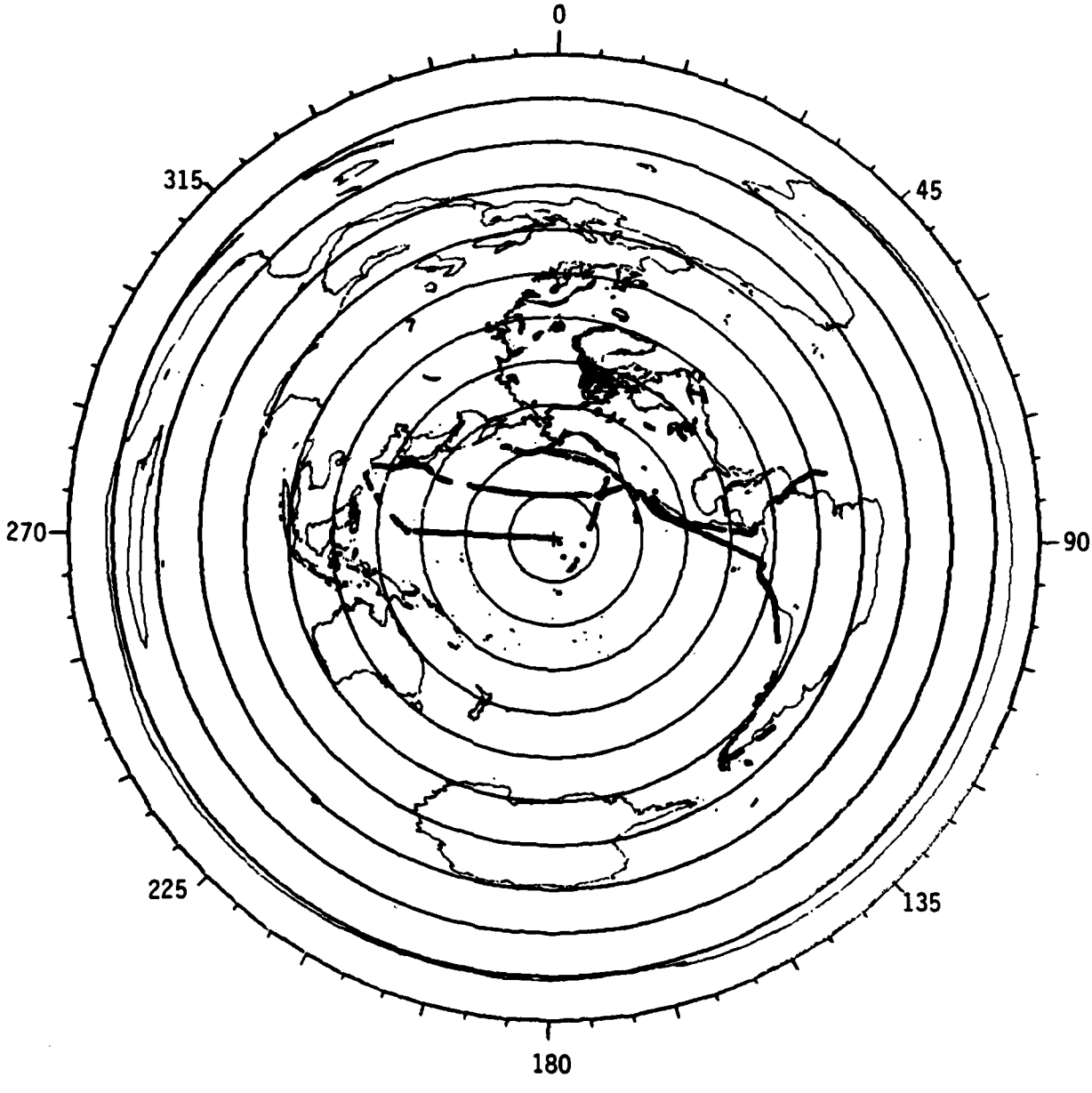

Figure A2-22. Omega Hawaii Signal Coverage - Integrated Satellite/Omega Data

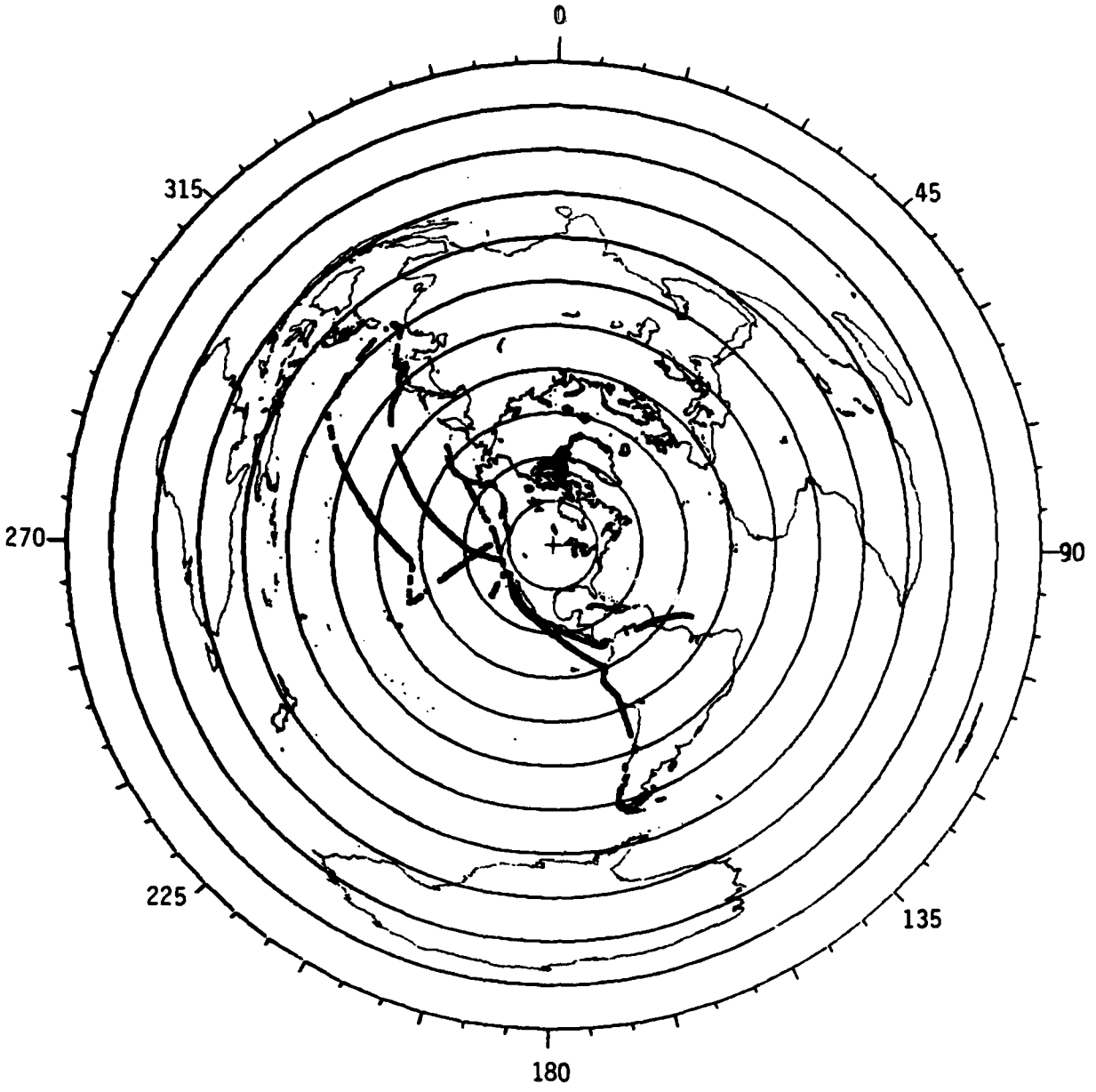

Figure A2-23. Omega North Dakota Signal Coverage - Integrated Satellite/Omega Data

E) La Reunion — Figure A2-24

La Reunion is out-of-range except in the western Pacific where signals are comparable to those of Liberia. The LIBERTY reported signals to a range of 9000 nmi. for La Reunion.

F) Argentina — Figure A2-25

Signals from Argentina were reported by the MAGDELINA from south California to the tip of South America. For the North Pacific, Argentina is out-of-range and generally its signals are not usable.

H) Japan — Figure A2-26

Omega Japan's signals are excellent throughout the region. Near-field modal interference is probable within a 300-500 nmi. as with Hawaii. Signals were still good out beyond the 9000 nmi range, down the coast of South America.

A2.3.2.2 Modal Interference Data

Data in the MAGODEXEC single-station files that were possibly affected by modal interference were sorted into "MI" files for the Omega stations as described in Section A2.2.3. These files were plotted for each station on azimuthal equidistant projections of the world centered on the transmitter. Figures A2-27 through A2-33 are these maps with the data points marked with small triangles. A glance through these figures reveals that the possibility of modal interference is widespread throughout the region for all the Omega transmitters. The near-field regions of the transmitters are areas where this effect was more likely to occur, as evidenced by the concentration of data points. The strongest stations, A, C, D, and H were less likely to be affected by modal interference in the region. The relative percentage of "MI" points to "OK" points was 35% for A, C, and H and only 20% for D. The weaker stations, B, E, and F were more likely to be affected: relative percentage was 75% for E and F and 90% for B.

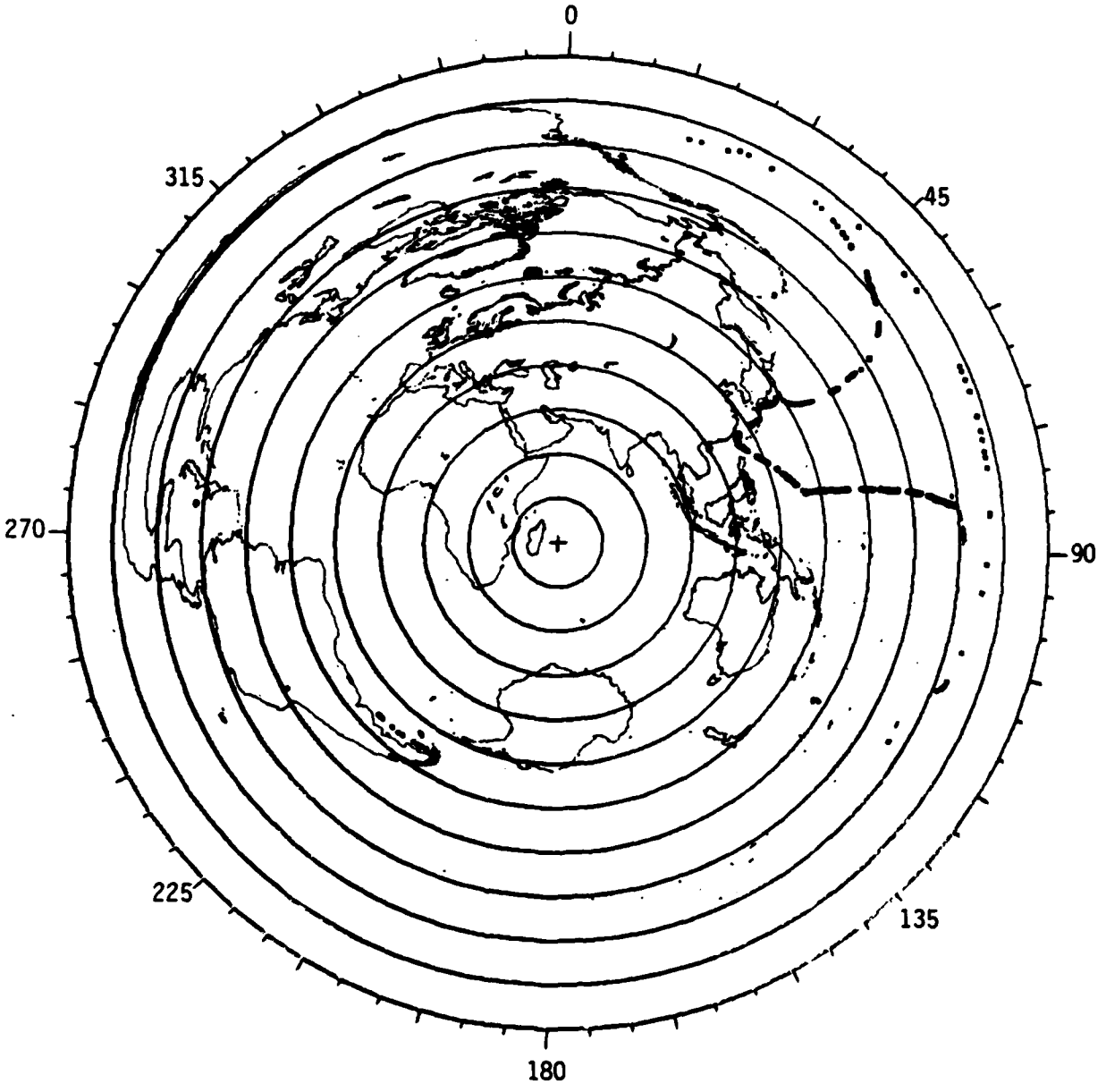

Figure A2-24. Omega La Reunion Signal Coverage - Integrated Satellite/Omega Data

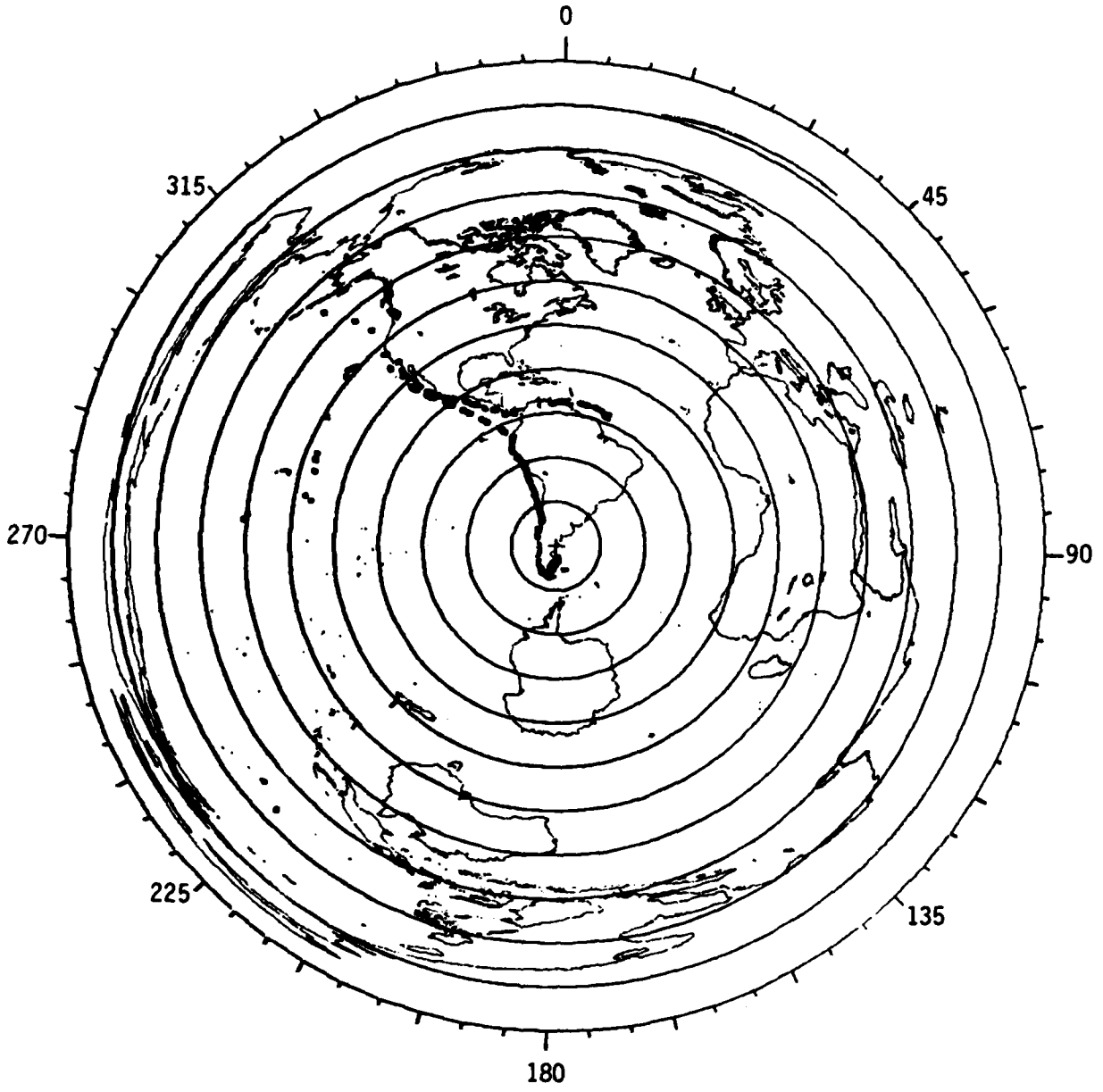

Figure A2-25. Omega Argentina Signal Coverage - Integrated Satellite/Omega Data

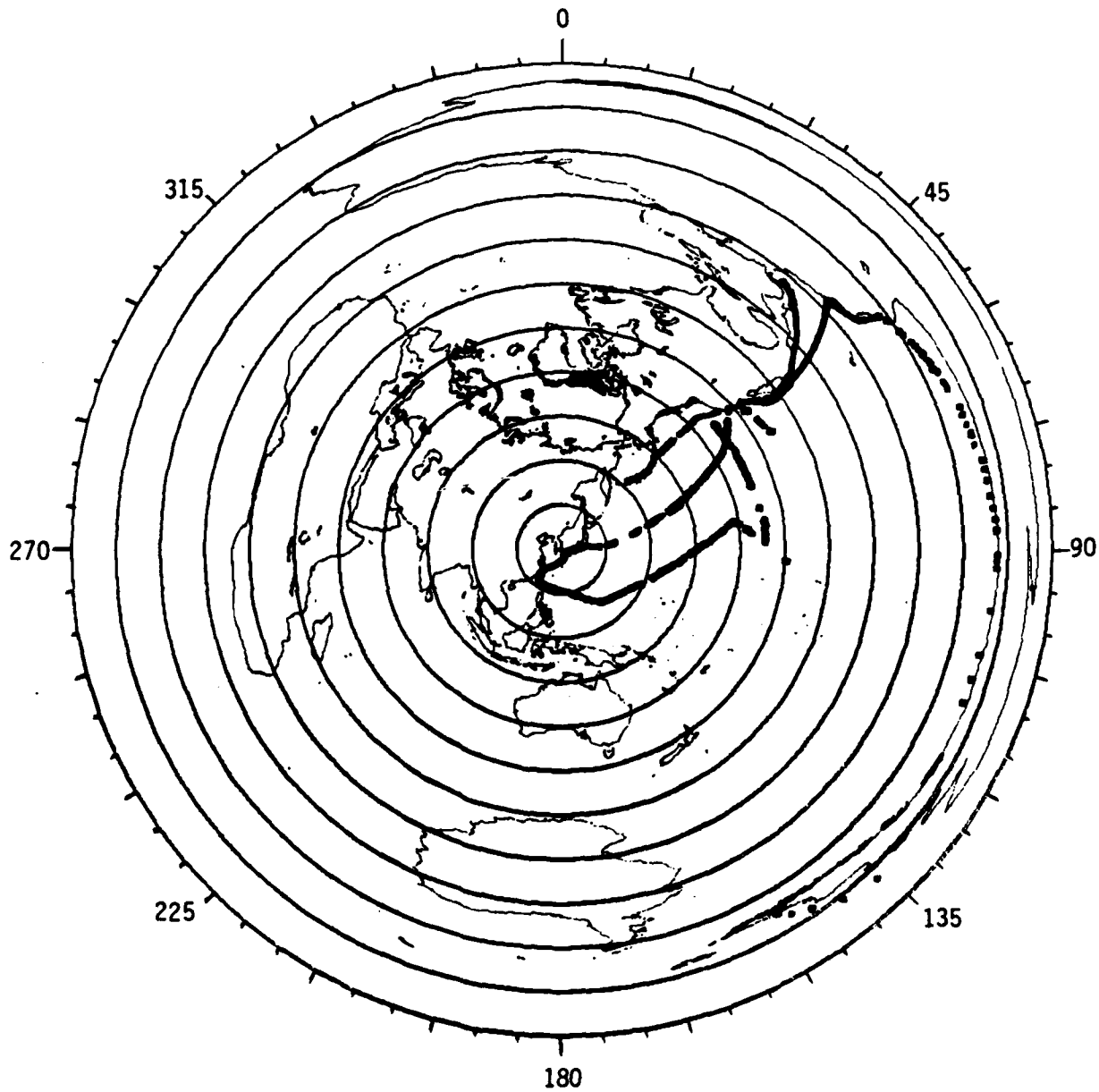

Figure A2-26. Omega Japan Signal Coverage - Integrated Satellite/Omega Data

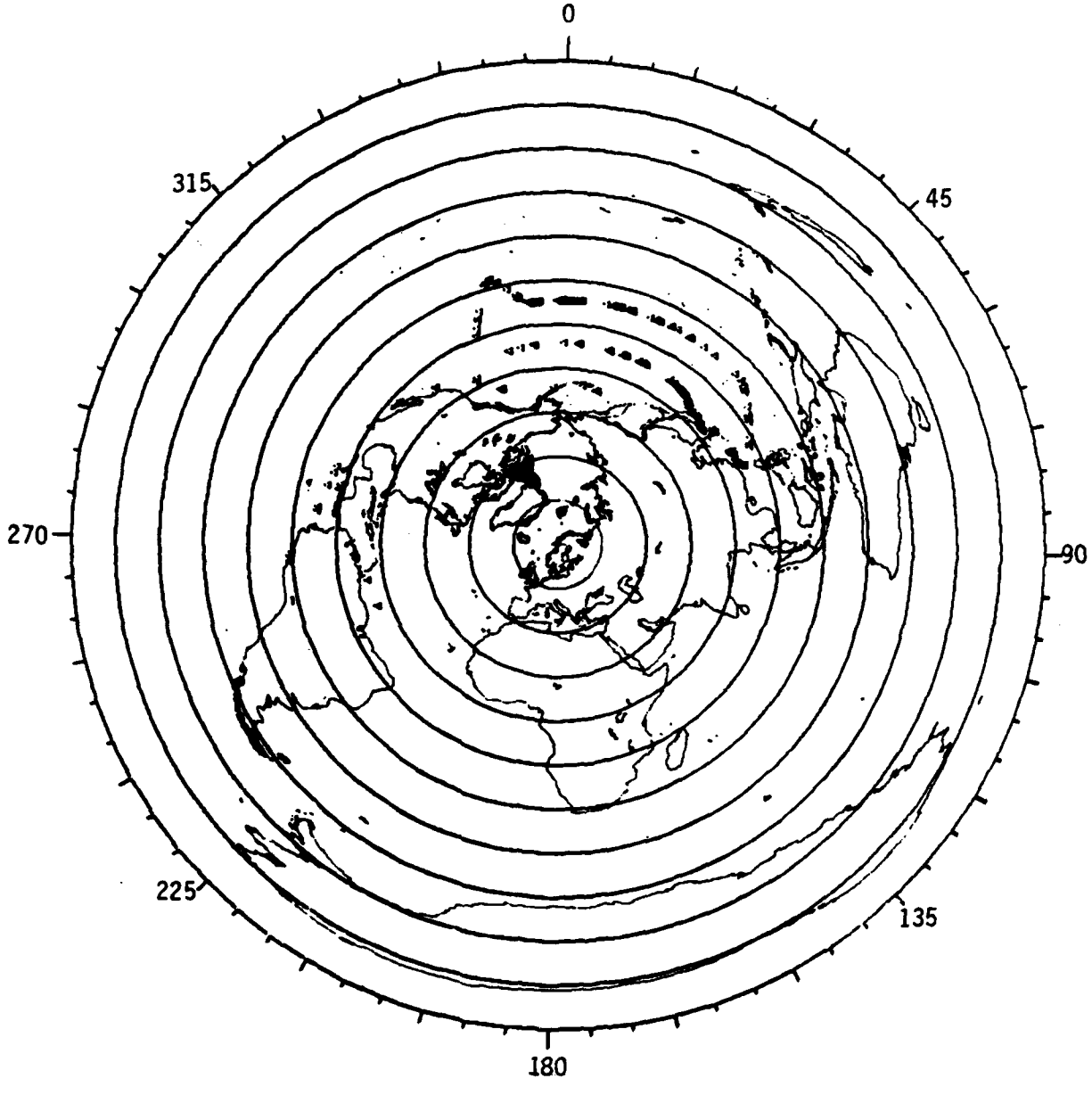

Figure A2-27. Positions of Possible Modal Interference for Omega Norway From Integrated Satellite/Omega Data

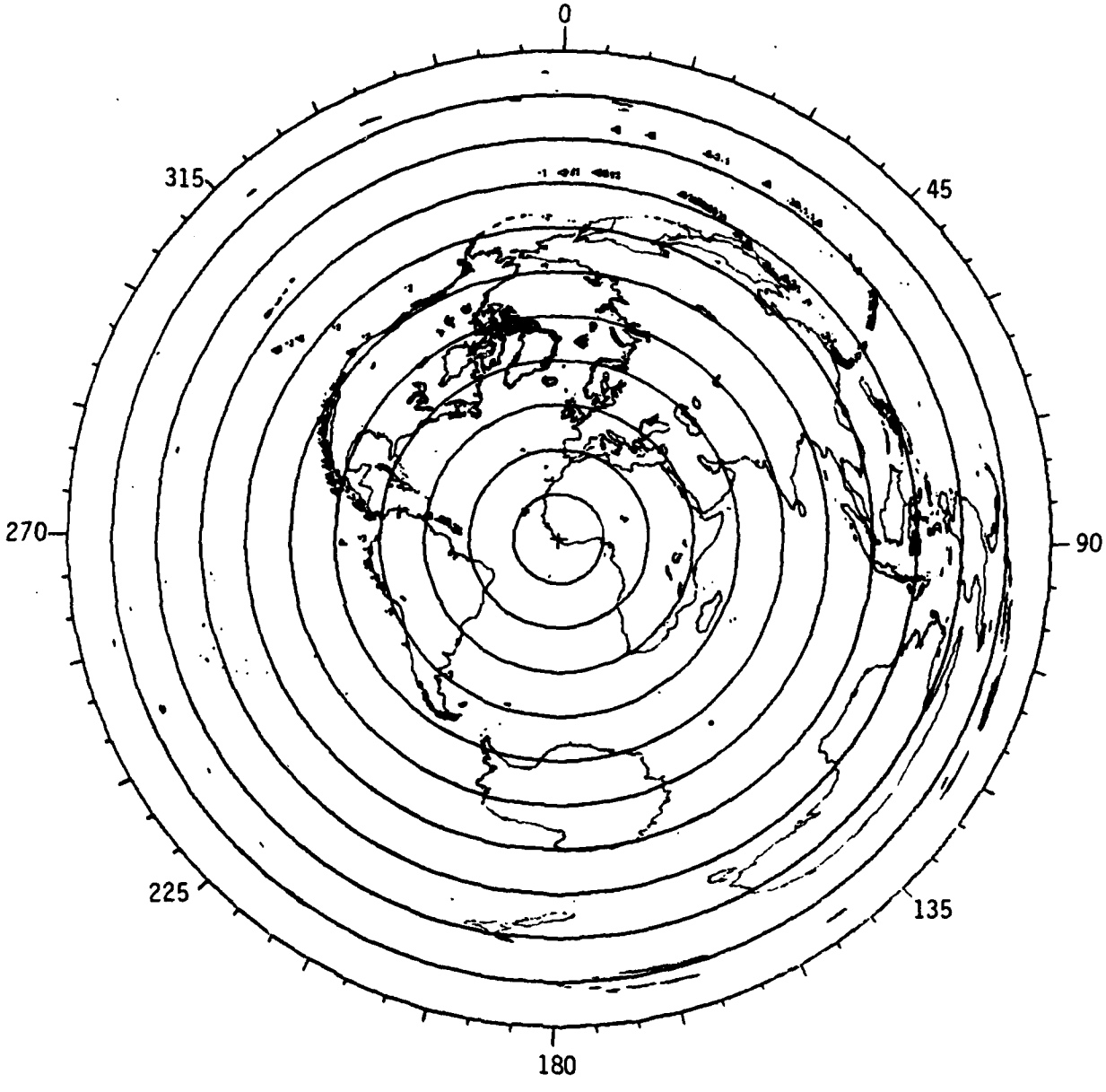

Figure A2-28. Positions of Possible Modal Interference for Omega Liberia From Integrated Satellite/Omega Data

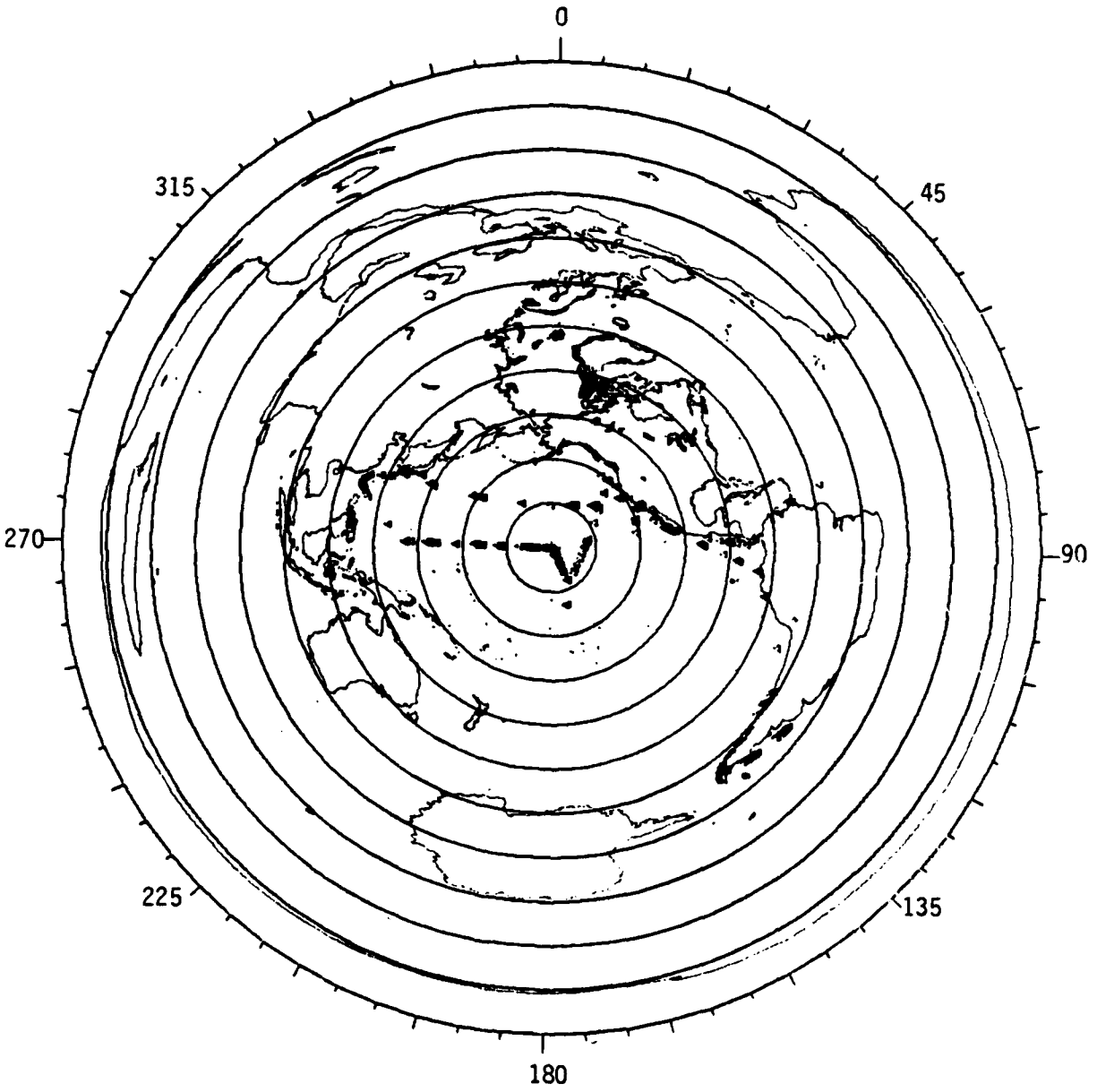

Figure A2-29. Positions of Possible Modal Interference for Omega Hawaii From Integrated Satellite/Omega Data

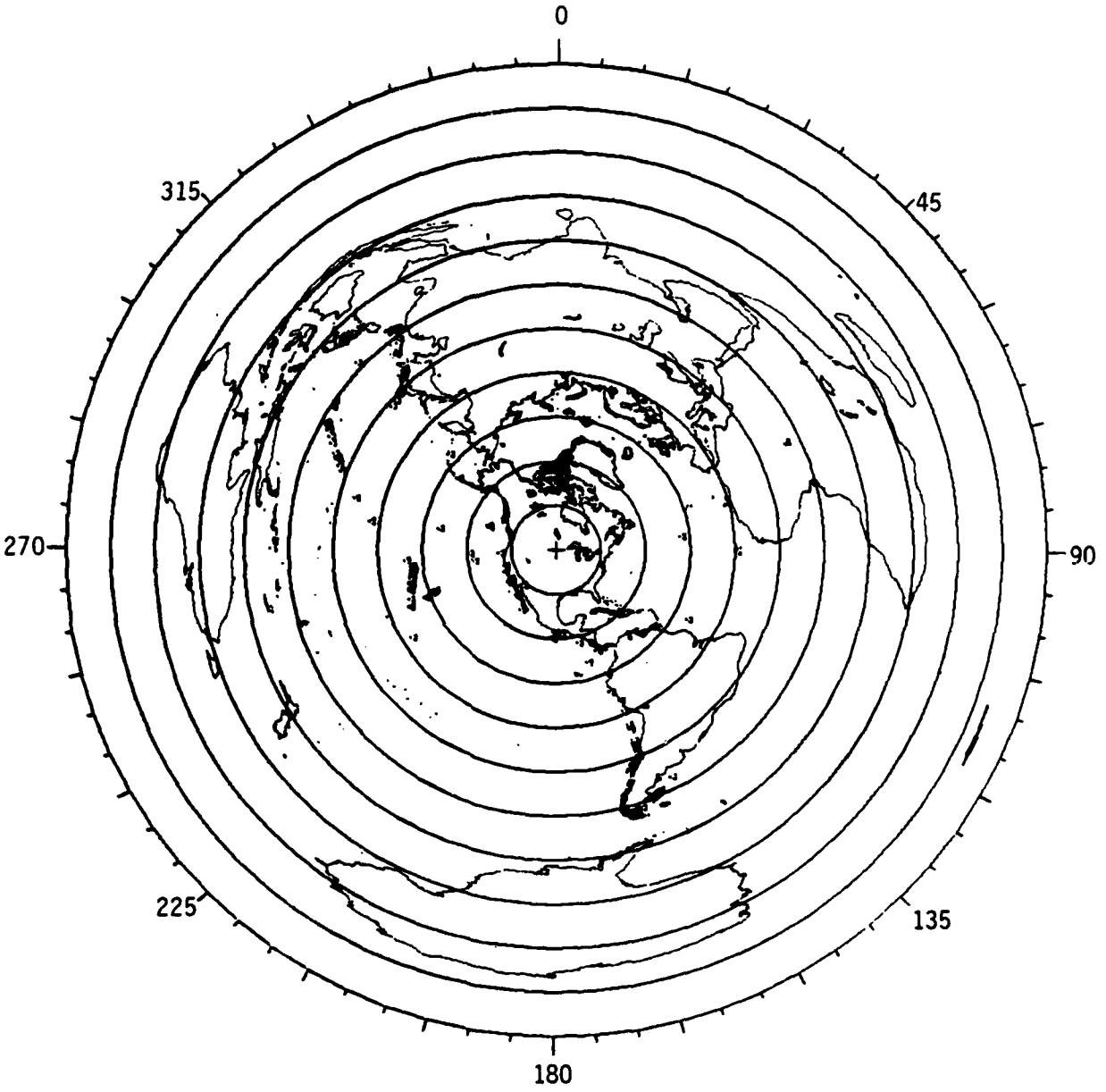

Figure A2-30. Positions of Possible Modal Interference for Omega North Dakota From Integrated Satellite/Omega Data

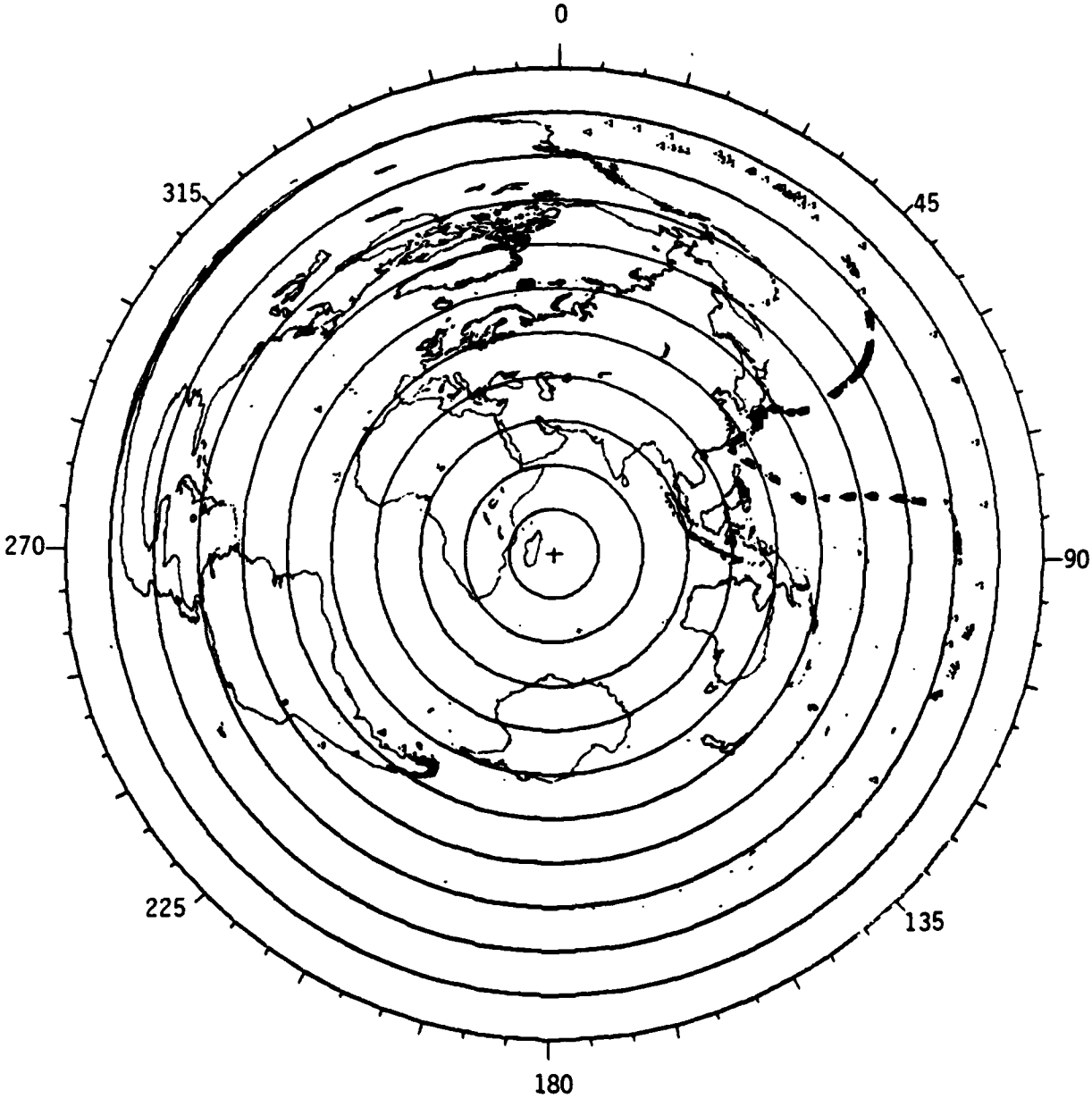

Figure A2-31. Positions of Possible Modal Interference for Omega La Reunion From Integrated Satellite/Omega Data

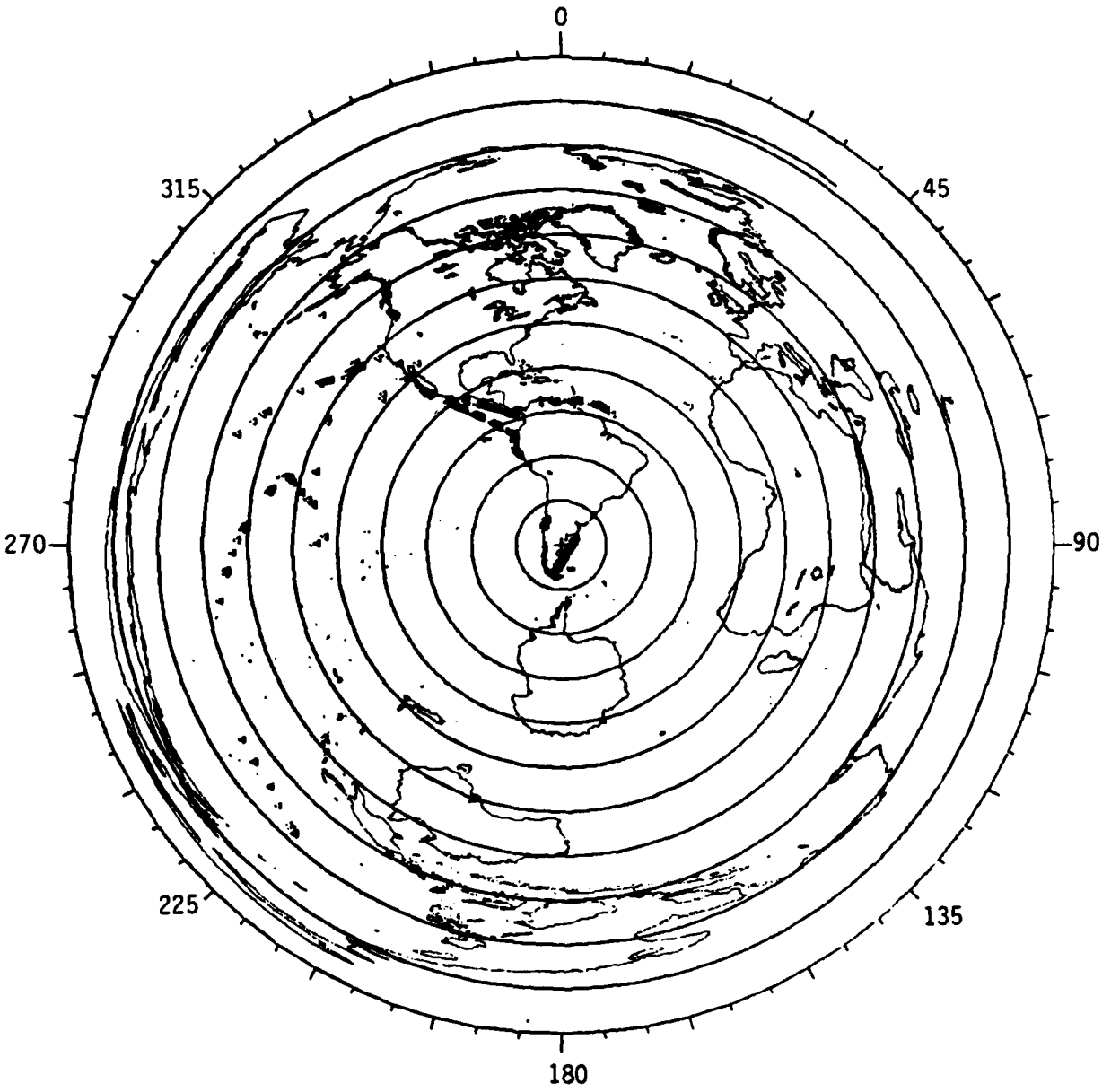

Figure A2-32. Positions of Possible Modal Interference for Omega Argentina From Integrated Satellite/Omega Data

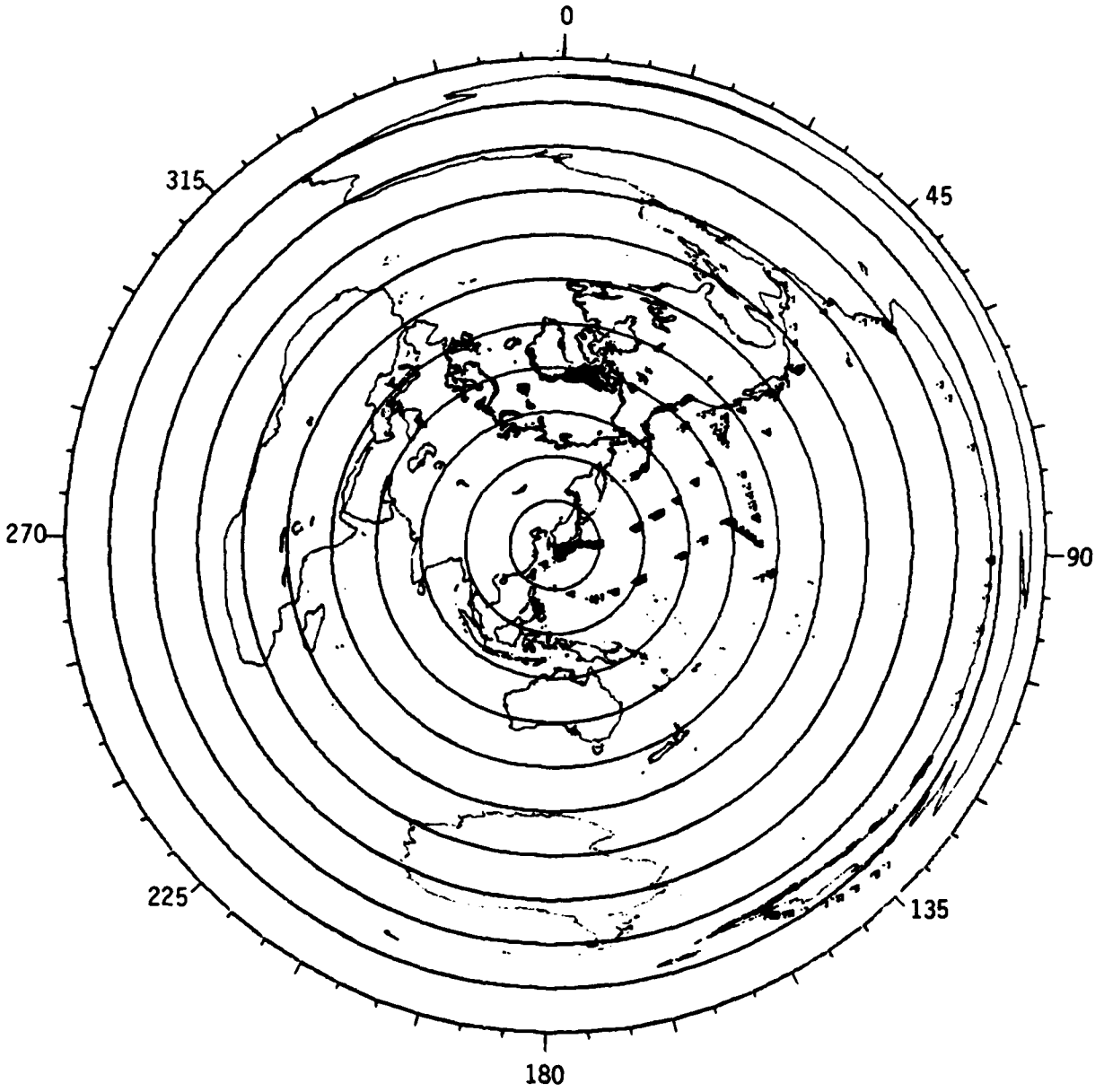

Figure A2-33. Positions of Possible Modal Interference for Omega Japan From Integrated Satellite/Omega Data

A3.0 CHINA AIRLINES DATA

A3.1 Description of Data

China Airlines International reported over 700 observations from twin ONS CMA 740 units on several cargo flights over the Pacific during 6 June to 30 September 1978. These observations compared the Omega positions with the actual positions of waypoints along the flight routes.

The listing of each observation in this report included date and GMT, position id code, course, ONS unit number, latitude and longitude errors, radial and lateral errors, accumulated radial and lateral errors, and Omega stations used to obtain the fix. Observations taken on the flights from Taipei/Kua Hsien/Guam/Honolulu/Los Angeles and on the return flights on this route provided data within the Northern Pacific region.

A3.2 Methods of Analysis

Of the two ONS observations listed for each date/time and waypoint in the report, the best fix was selected for calculation of statistics. After waypoints outside the area of interest and those with an insignificant number of observations (less than 5) were excluded from consideration, the data for 8 waypoints along the Los Angeles-to-Taipei route were analyzed. The mean and standard deviation of the radial errors were computed. "Outliers", or errors more than 3 times the standard deviation from the mean, were excluded from these calculations.

A3.3 Results

Table A3-1 lists the mean and standard deviation of the radial errors reported for each waypoint. The associated map shows the location of these waypoints. The sun condition listed in the table

indicates whether at least half of the observations at that waypoint were made during the day, at night, or during transition. The predominant stations listed are those Omega stations used to obtain the fix for more than half of the observations. On the average the radial error was less than 3 nmi. with a standard deviation within 2.5 nmi. of the mean. Norway signals are attenuated below threshold in crossing Greenland and so are not usable at waypoint 1. Also La Reunion and Liberia are out-of-range. Hawaii signals were not used within the near-field of the transmitter at waypoints 2 and 3. Stations A and E, however, compensate for deselection of C. West of 150E Liberia's signals become usable and add to station redundancy for waypoints 5-8. Overall coverage was excellent.

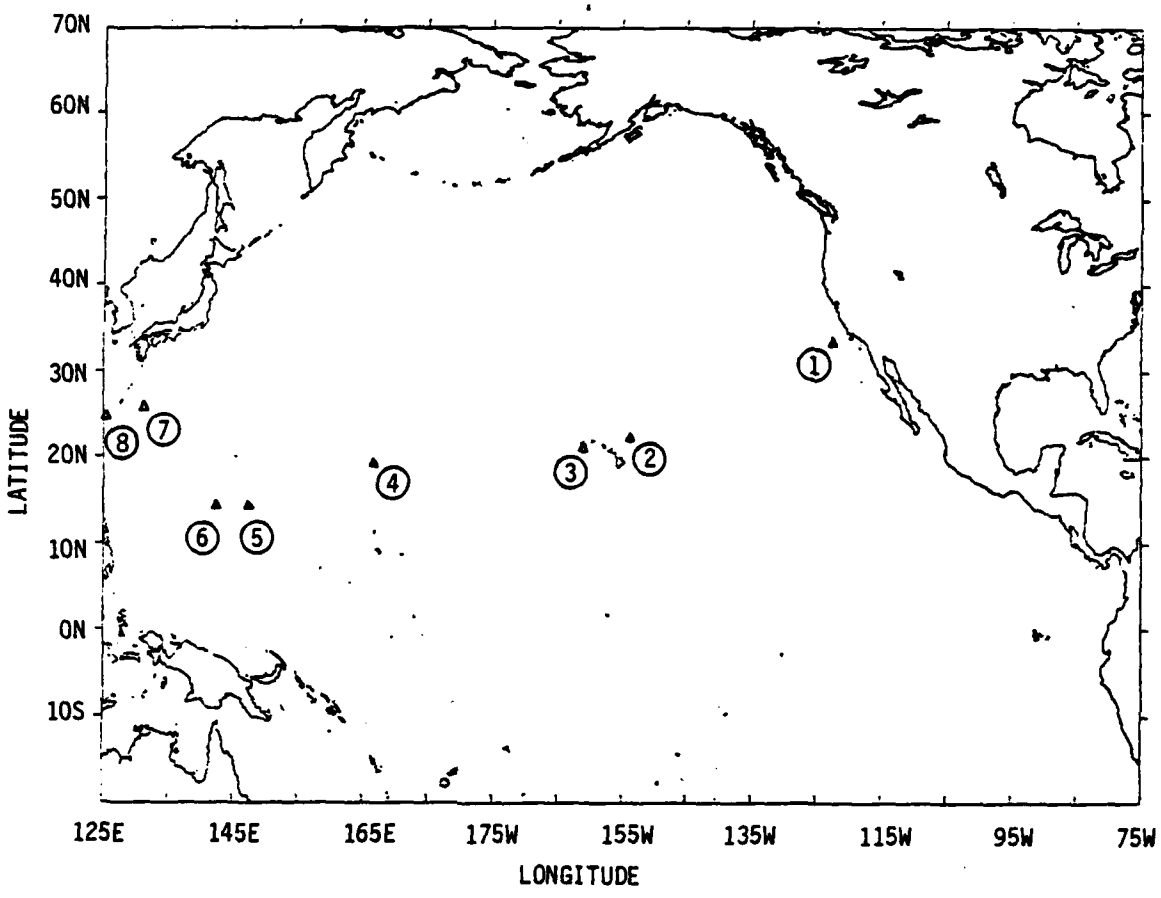

Way-point	Position Lat.	Lon.	Predominant Stations	Total Fixes	Sun*	Radial Error Mean	SDev	No. of ** Outliers
1.	N33.48	W122.58	CD H	42	D	2.9	1.8	4
2.	N22.37	W153.88	A DE H	41	T	2.8	1.4	2
3.	N21.25	W161.07	A DE H	24	N	2.9	2.1	5
4.	N19.30	E166.60	A CDE H	23	N	2.9	2.2	3
5.	N14.47	E147.63	ABCDE H	31	N	2.7	1.7	3
6.	N14.45	E142.42	ABCDE H	35	T	2.7	2.4	3
7.	N25.83	E131.25	ABCDE H	5	N	1.5	0.9	0
8.	N24.78	E125.30	ABCDE H	21	T	2.0	1.4	2

* - predominant sun condition at position for at least half of fixes: D - ±4 hrs. from local noon
N - ±4 hrs. from local midnight
T - all other times (transition)

** - outliers were excluded in calculation of statistics

Table A3-1. CHINA AIRLINES DATA - 6 June to 30 Sept 1978

A4.0 PAN-AMERICAN AIRLINES DATA

A4.1 Description of Data

Pan-American World Airways collected the most data on airborne OMEGA performance. C.J. Gibbs of Canadian Marconi Company compiled data from several flights traversing the Pacific region in 1977.[A1] The report contains notes on Omega performance from the flight logs, log sheets listing Omega and INS positions along with Omega stations used, and log sheets listing observed signal strengths. Twin ONS CMA-740 pre-production units were evaluated during these flights. A Carousel IV Inertial Navigation System (INS) was the primary reference; however, occassional comparisons with Doppler and actual position are included in the flight notes.

The Appendices of this report contained brief notes on signal availability and data on positional accuracy from several flights in 1976 when a prototype CMA-740 was being evaluated. Table A4-1 lists the flight numbers, dates and itineraries for the Pan-Am flights of 1976 and 1977. Only those portions of the routes traversing the Northern Pacific region (70^{o}N to 10^{o}S, 165^{o}E to 110^{o}W) were analyzed for this study. Figure A4-1 displays the routes for the Pan-Am flights of 1977.

Three types of data were compiled in the report of the Canadian Marconi Company:

1. Chronological notes written during the flight giving the differences between INS and Omega, Doppler and Omega, and Omega and actual, and other pertinent comments on signal strengths and stations monitored.

2. Latitude and longitude tabulated at 10-30 min. intervals for the two Omega systems and the INS.

3. Omega signal strengths recorded at 1/2 hr. intervals for all 3 frequencies (10.2, 11-1/3, 13.6 kHz) for both Omega systems.

Pan-American World Airways Flights - 1977

Flight No.	Flight Itinerary	Date	No. of Fixes
B953	Los Angeles to Papeete	13 March 1977	28
FB951	Papeete to Los Angeles	15 March 1977	24
X935	Honolulu to Guam	29 June 1977	19
X904	Guam to Honolulu	01 July 1977	14
E901	Honolulu to Tokyo	17 July 1977	17
E902	Tokyo to San Francisco	18 July 1977	26
E901	Honolulu to Nandi	17 Sept. 1977	19
E900	Tokyo to San Franscisco	27 Sept. 1977	30

Pan-American World Airways Flights - 1976

Flight No.	Flight Itinerary	Date
825	N.Y. to Honolulu via Dallas	08 April 1976
818	Honolulu to San Francisco	10 April 1976
815	San Francisco to Tahiti	11 April 1976
816	Tahiti to San Francisco	13 April 1976
815	San Francisco to Auckland	25 April 1976
812	Sydney to Honolulu via Pago Pago	20 May 1976

Table A4-1. Pan-American Flights

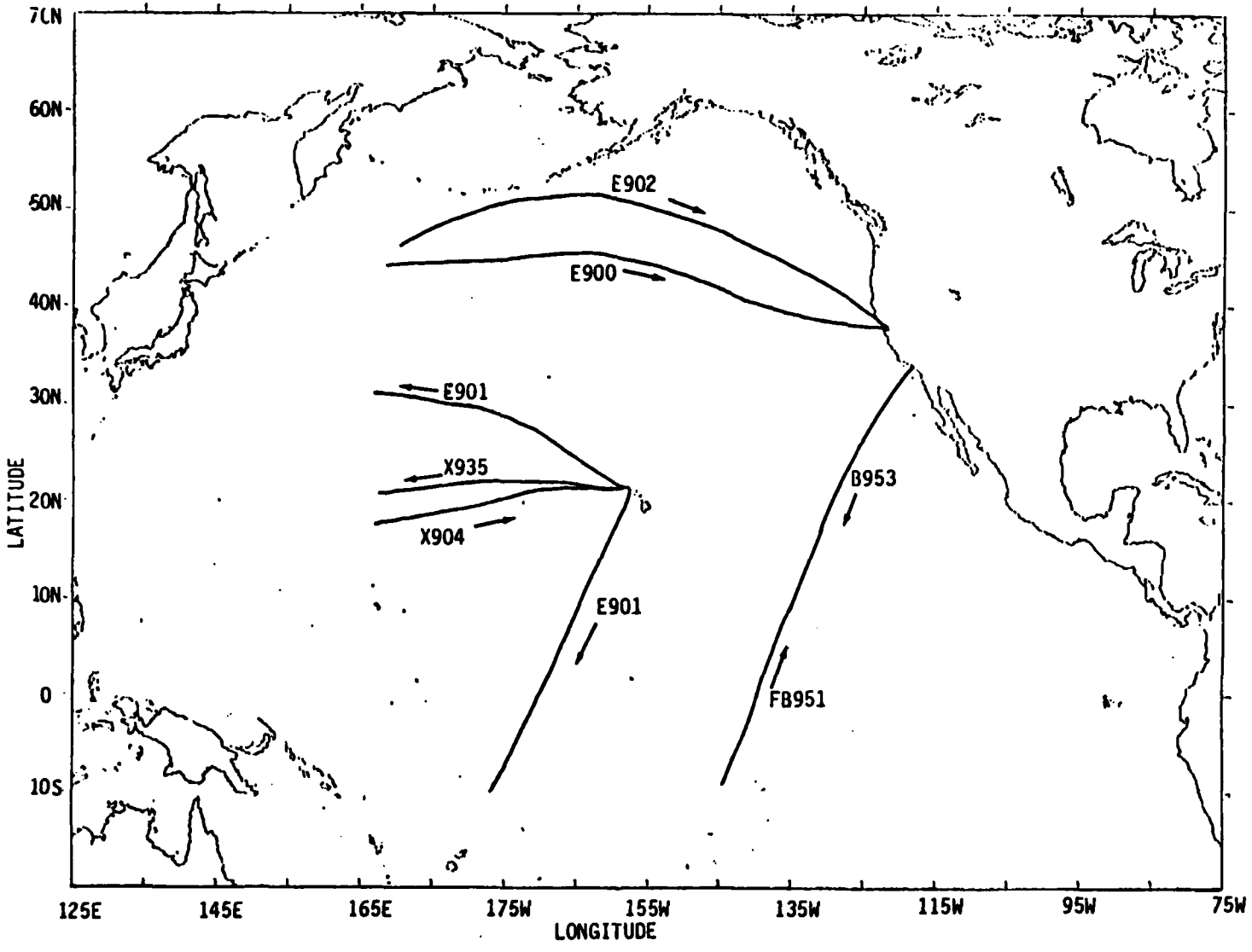

Figure A4-1. Pan-American Flights 1977 - Overview

A4.2 Methods of Analysis

A4.2.1 Pan-Am Flights - 1977: Analysis

The observed positions were first tabulated from the log sheets for one of the Omega systems and for the INS. Although two Omega systems were operated on each flight, only the data for the ONS not using VLF mode was considered. For all but 2 of the 8 flights this was ONS #2; for the other 2 flights the positions from ONS #1 were evaluated. The Omega stations used to obtain the fix were also listed for each position. Observed signal strengths for each Omega station were listed separately.

Initial analysis of the radial error between ONS and INS positions revealed an almost linear increase in the error over the duration of the flight. Comparison of the INS with actual position, typically at the beginning and end of a flight, confirmed a drift of the INS from actual position. To obtain a more accurate reference for evaluating ONS performance, a corrected INS position was calculated by subtracting an interpolated drift for that time in the flight. The rate of drift was obtained by assuming INS and actual positions to be the same at the start of the flight (because the INS is usually initialized before takeoff) and by using the final INS-vs-actual observation from the flight notes. (In Appendix AA, Table AA-1 lists differences between INS and actual at the end of each flight.) Although comparison of the ONS and the corrected INS positions seems to result in a more representative error distribution, the assumption of a linear drift in the INS may not adequately depict the variation in INS errors, as has been noted in reference A2. Therefore, such reference errors may lead to a somewhat inaccurate evaluation of Omega performance. Nevertheless, the radial error between the ONS and corrected INS position was computed for each observation and tabulated along with the input data. (Appendix AA contains the table of Omega-vs-INS positions, radial errors, and station usage for each flight.) The formula used for computing the radial error in nmi. is

$$r_e = 60 \sqrt{\left[(\phi_\Omega - \phi_{INS}) \cos(\phi_{INS})\right]^2 + (\theta_\Omega - \theta_{INS})^2}$$

where

ϕ_Ω, θ_Ω denote latitude and longitude of ONS position in degrees
ϕ_{INS}, θ_{INS} denote latitude and longitude of INS position in degrees

To display the results of this analysis the same graphical format used for the integrated shipboard data was chosen to evaluate Omega coverage and accuracy for each flight. The mean and standard deviation of the radial errors were then computed for the segments of the flight routes with similar station usage and error distribution, as was done for the integrated shipboard data.

Notes on signal availability and strength were collated from the flight notes to complement the SNR data from the log sheets. The maximum and minimum SNR values were converted from the linear scale of the receiver to dB values, using the calibration curve for the CMA 740 display. The maximum and minimum SNR values for each station were tabulated for each flight. (Appendix AB contains the linear-scale SNR table for each flight for 10.2 and 13.6 kHz.)

A4.2.2 Pan-American Flights - 1976: Analysis

The Appendix of the Canadian Marconi report on the 1977 Pan-American flights included background information on some early evaluation flights in 1976. Because not all of this data is pertinent to the Northern Pacific region, this Appendix was edited for relevant information. The qualitative nature of this data precluded detailed analysis; and so, the assessments of coverage and accuracy are only summarized in Section A4.3.2.

A4.3 Results from Pan-American Flights

A4.3.1 Pan-American Flights - 1977: Results

The statistics summarizing Omega fix accuracy observed on the Pan-American Flights of 1977 are listed in Table A4-2. The mean, standard deviation, 50% CEP, and 95% CEP were computed for flight segments using the same program developed for the integrated satellite/Omega shipboard data. (See Section A2.2.2.) For some flight segments the mean and rms of the radial errors are outside the expected range of Omega accuracy. In some of these instances, however, Omega station selection or coverage was abnormal in some way as indicated under "Remarks". Nevertheless, for most flights, stations C, D, and H provided good, strong, reliable signals throughout the Northern Pacific region, yielding average fix accuracy within 1-3 nmi during normal operation.

The maximum and minimum SNR values for each station are listed for each flight in Table A4-3. These SNR ranges for each Omega station give a clearer idea of the observed signal coverage on these flights. The SNR tables are included in Appendix AB. Figures A4-2 through A4-9 display the history of fix errors and station usage and the map of the flight route for each flight in the same graphical format described in Section A2.2.2. Again note that errors in excess of 7 nmi are plotted as 7 nmi. The actual data values can be read from the tables in Appendix AA. In the plot of fix errors, points marked with the delta are observations made within ±4 hours of local midnight. Flight segments are separated by a dotted line and by Roman numerals next to the flight route. Although these tables and figures provide a compact, comprehensive picture of Omega performance for these flights, the following discussion of observed Omega fix accuracy and signal coverage on a flight-by-flight basis highlights important aspects of these results and clarifies station usage with comments from the flight notes.

Flight No./Date	Geographic Area	Direction	Segment	Total No. Fixes	No. of Outliers	Radial Mean	Error rms	Predominant Stations	CEP 50%	CEP 95%	Remarks
E902/18 July	N	W E	I.	10	1	6.50	6.63	CDE H	6.05	7.52	A off-the-air
			II.	16	0	3.39	4.01	CD H	2.38	6.32	E out of range INS not good on this flight
E900/27 Sept.	N	W E		30	0	3.07	3.20	A CDE GH	2.91	4.17	Possible PCA effects
X904/01 July	W	W E		14	0	4.64	4.84	A CDE H	5.04	6.03	INS possibly degrading
X935/29 June	W	E W	I.	9	0	1.18	1.28	A CDE H	1.18	1.81	
			II.	3	0	4.12	4.24	A CDE H	--	--	E causing errors
			III.	7	0	1.43	1.48	A CD H	1.19	1.86	E deselected
E901/17 July	NW	E W	I.	3	0	2.49	2.56	DE H	--	--	C near-field and
			II.	14	0	0.96	1.03	CDE H	0.98	1.35	A off-the air
E901/17 Sept.	WS	N S	I.	3	0	7.30	7.34	A E GH	--	--	D off-the-air; C near-field
			II.	16	0	1.83	1.96	A C E H	1.81	2.70	
B953/13 March	E	N S	I.	12	0	5.02	5.07	ABCD F H	4.94	5.89	A and B weak
FB951/15 March	E	S N	II.	12	2	9.28	9.61	CD FGH	8.50	12.12	E lost; G gained; slipped lane
B953/13 March	SE	N S	II.	16	0	8.90	9.37	BCDEF H	8.30	12.97	F lost for some min; VLF used till F regained
FB951/15 March	SE	S N	I.	12	0	3.34	3.81	CDEF H	2.87	5.92	

Summary of Omega Fix Accuracy and Coverage: Pan-American Flights - 1977

Table A4-2

Pan-Am Flight No.	OMEGA Stations A	B	C	D	E	F	H
E902	OFF	0/0	3/5	- 2/7	0/-1	0/-15	-5/7
E900	0/4	0/-14	6/9	6/8	0/-4	0/-6	5/8
X904	0/-2	0/-17	1/10	-11/1	0/6	0/-7	-12/6
X935	0/-2	0/-17	5/12	-17/1	-10/1	0/-18	-3/6
E901	OFF	0/-6	7/10	-5/2	2/5	0/-6	4/7
E901	-10-2	-6/1	8/15	OFF	- 1/4	0/-13	3/7
B953	0/-20	0/-4	7/12	0/9	0/4	0/-7	1/6
FB951	0/0	0/0	8/15	-6/9	0/7	0/-3	-1/7

Note: 0 indicates below -20 dB

Table A4-3. 10.2 kHz Min/Max SNR value (dB scale)

From Pan-Am Flights 1977

Flight E902/18 July 1977
Tokyo to San Francisco

Figure A4-2.
Tables AA-2, AB-2.

Note. The flight notes were preceded by the following comment on INS performance: "The eastbound accuracy of the INS unit had been worsening over previous flights, although it remained excellent on the westbound flights such as the immediately previous Flight E901. Except for the first few hours, the INS did not constitute a meaningful reference of Omega accuracy for this flight."

Coverage:

A - Off-the-air, 11-25 July
B - Deselected
C - Strong
D - Strong
E - Out-of-range (> 8483 nmi) @ 1900Z (51N, 157W)
F - Deselected
G - Deselected
H - Strong

Accuracy: Even after a corrected INS was computed, the errors still seemed somewhat scattered, perhaps indicating the INS was indeed not a good reference. Nevertheless, some tentative remarks can be made: Accuracy probably would have been better for the first segment if A had been on the air. (Addition of Australia will most likely help compensate for loss of E because of range.) Deselection of E earlier or even for the whole flight may have given better results. Judging from the second segment C, D, and H LOPs should be sufficient.

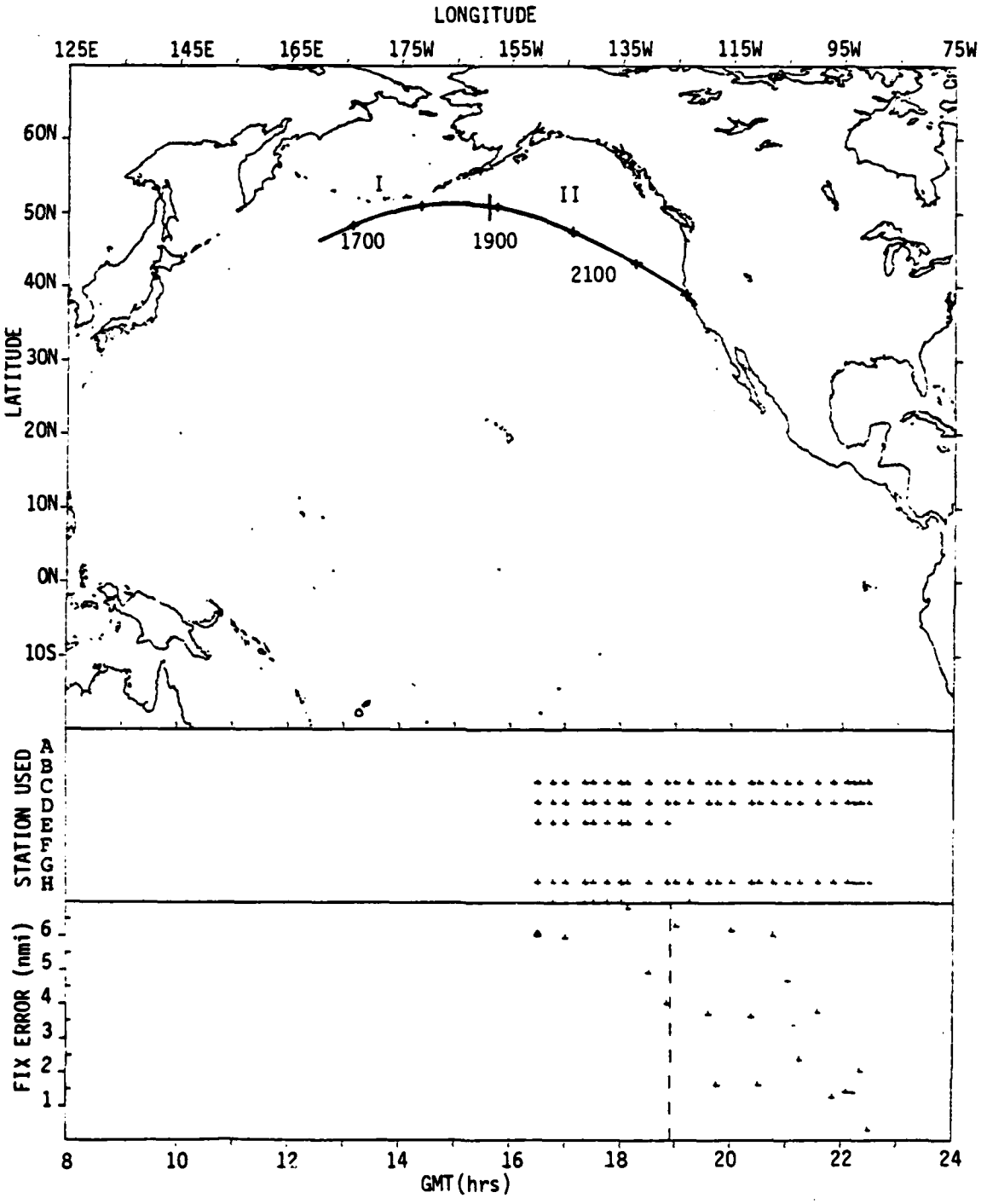

Figure A4-2. Pan-American Flight E902/18 July 1977
Tokyo to San Francisco

Flight E900/27 September 1977 — Figure A4-3.
Tokyo to San Francisco — Tables AA-3, AB-3.

Coverage:

A - Good until 150W where signal path encounters "Greenland Shadow".
B - Minimal
C - Strong
D - Strong
E - Out-of-range (> 9300 nmi) @ 0945Z (41N, 144W)
F - Deselected
G - Moderate signal
H - Strong

Accuracy: Acceptable; around 3 nmi. Selection of E may not be necessary, because its signal is moderate at the outset and tapers off rapidly as range increases. Again, C, D, and H LOPs seem to be sufficient, although with A available its selection will be useful; its signal did not seem to be affected by PCA activity, which was reported as likely by a NOTAMS forecast for this period. Note that this flight took place at night in contrast to the previous daytime summer flight E902.

Flight X904/01 July 1977 — Figure A4-4.
Guam to Honolulu — Tables AA-4, AB-4.

Coverage:

A - Moderate signal
B - Deselected
C - Strong; deselected @ 1500Z (21N, 162W) because of near-field effect.
D - Strong
E - Initially off-the-air; returned @ 1130Z
F - Deselected: out-of-range
H - Strong

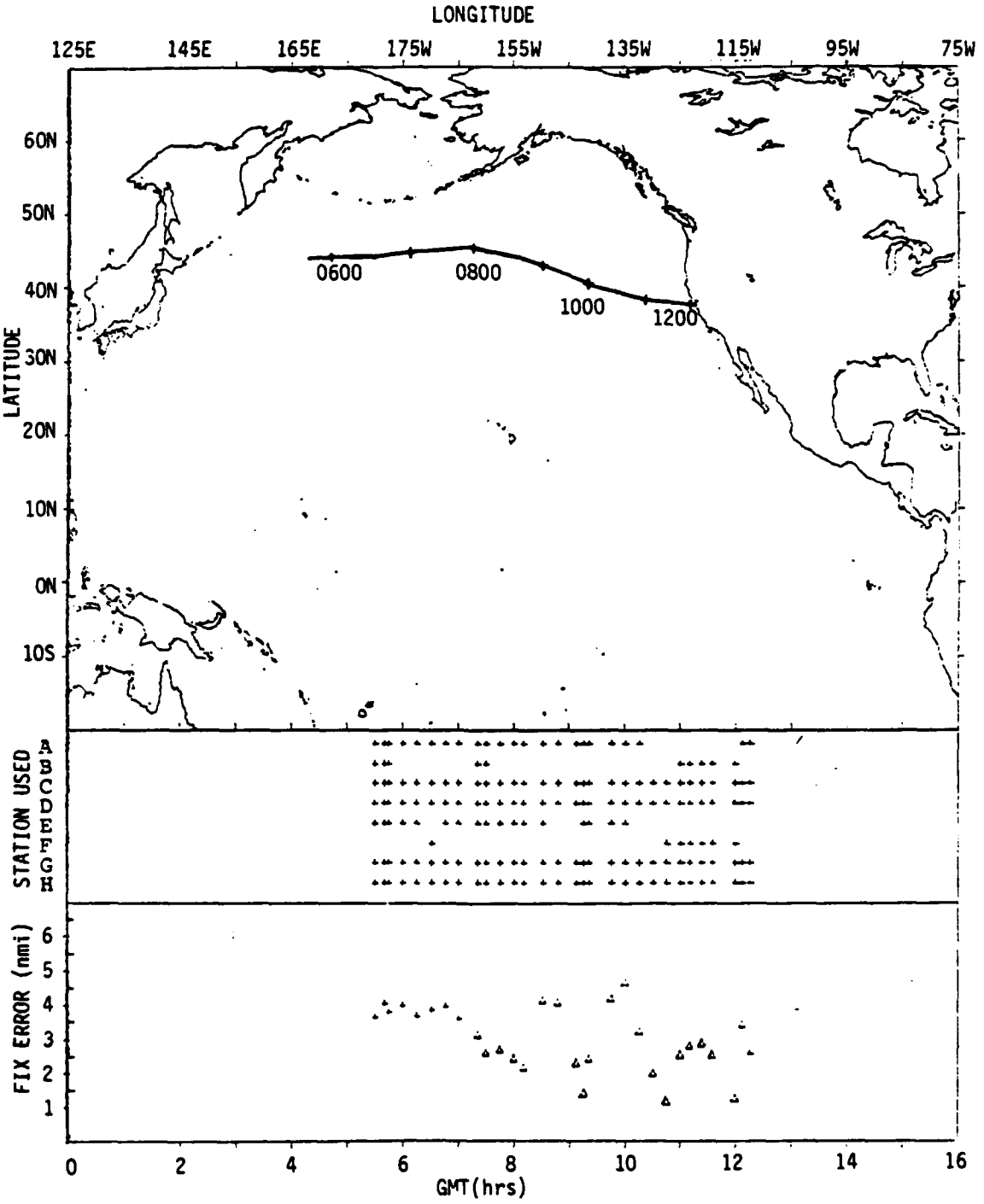

Figure A4-3. Pan-American Flight E900/27 Sept 1977
Tokyo to San Francisco

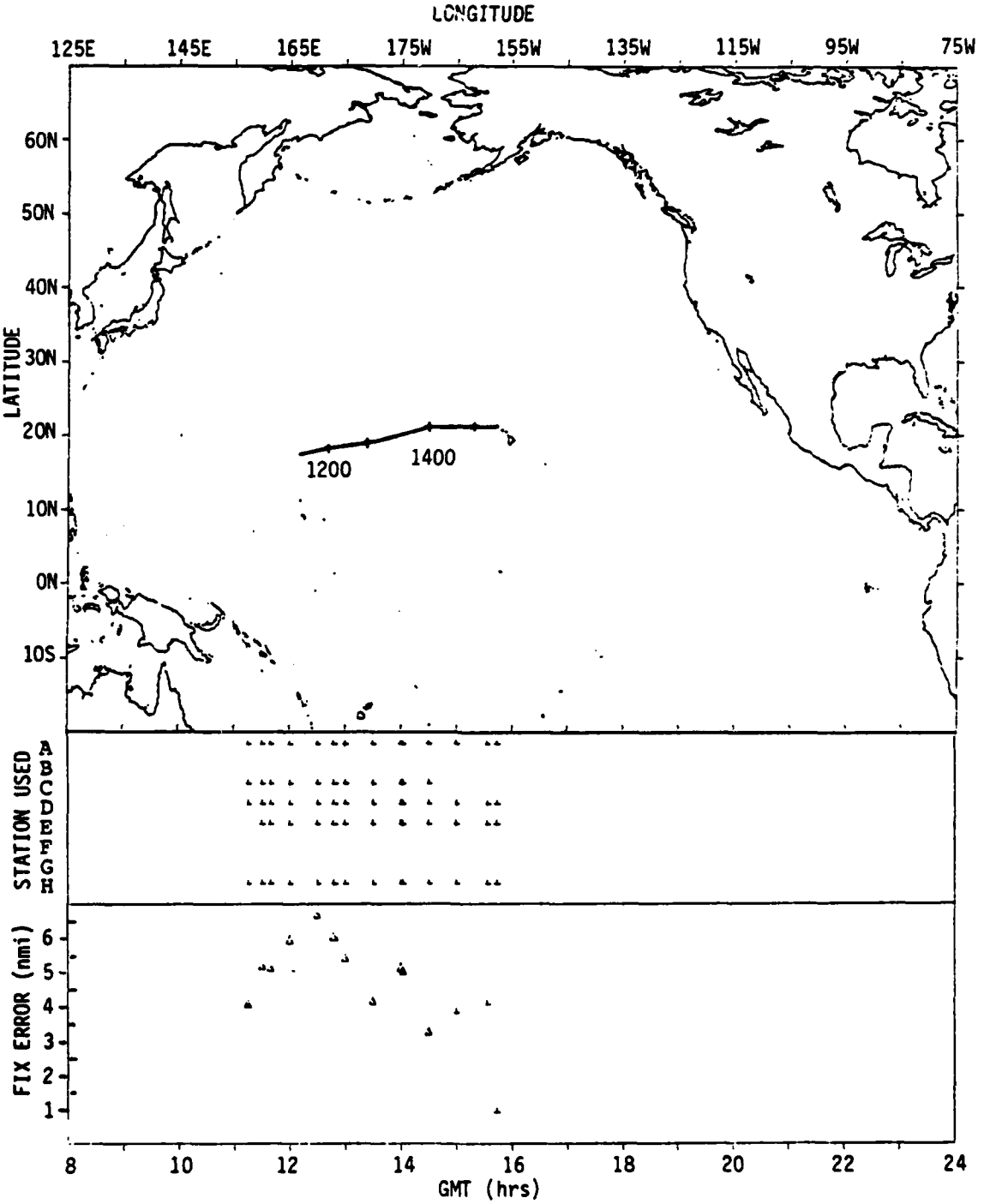

Figure A4-4. Pan-American Flight X904/01 July 1977
Guam to Honolulu

Accuracy: The eastbound accuracy of the INS unit was noticably degrading on flights prior to E902. The visible variation in the ONS errors relative to the INS suggests that the INS may not have been a stable reference for comparison. Thus, the mean and rms of the radial errors are outside the expected limit for Omega accuracy, although fair for safe navigation. Within the near-field of C, stations A, D, E, and H provided adequate signals.

Flight X935/30 June 1977 — Figure A4-5.
Honolulu to Guam — Tables AA-5, AB-5.

Coverage:

A - Moderate signal
B - Deselected
C - Deselected because of near-field effect until 1235Z (21N, 165W); then strong
D - Strong
E - Moderate but seemed to be causing problems @ 1430Z (22N, 180E); deselected at 1430Z
F - Deselected
G - Deselected
H - Strong

Accuracy: Except for the interval where E seemed to be causing problems, accuracy was excellent for this flight - within 1.5 nmi. Again, deselection of E may have been acceptable for the whole flight. As this was a nightime flight, modal interference may have been the problem with E. Deselection of C until approx. 300 nmi from Hawaii was appropriate. A, C, D, and H are best in this area.

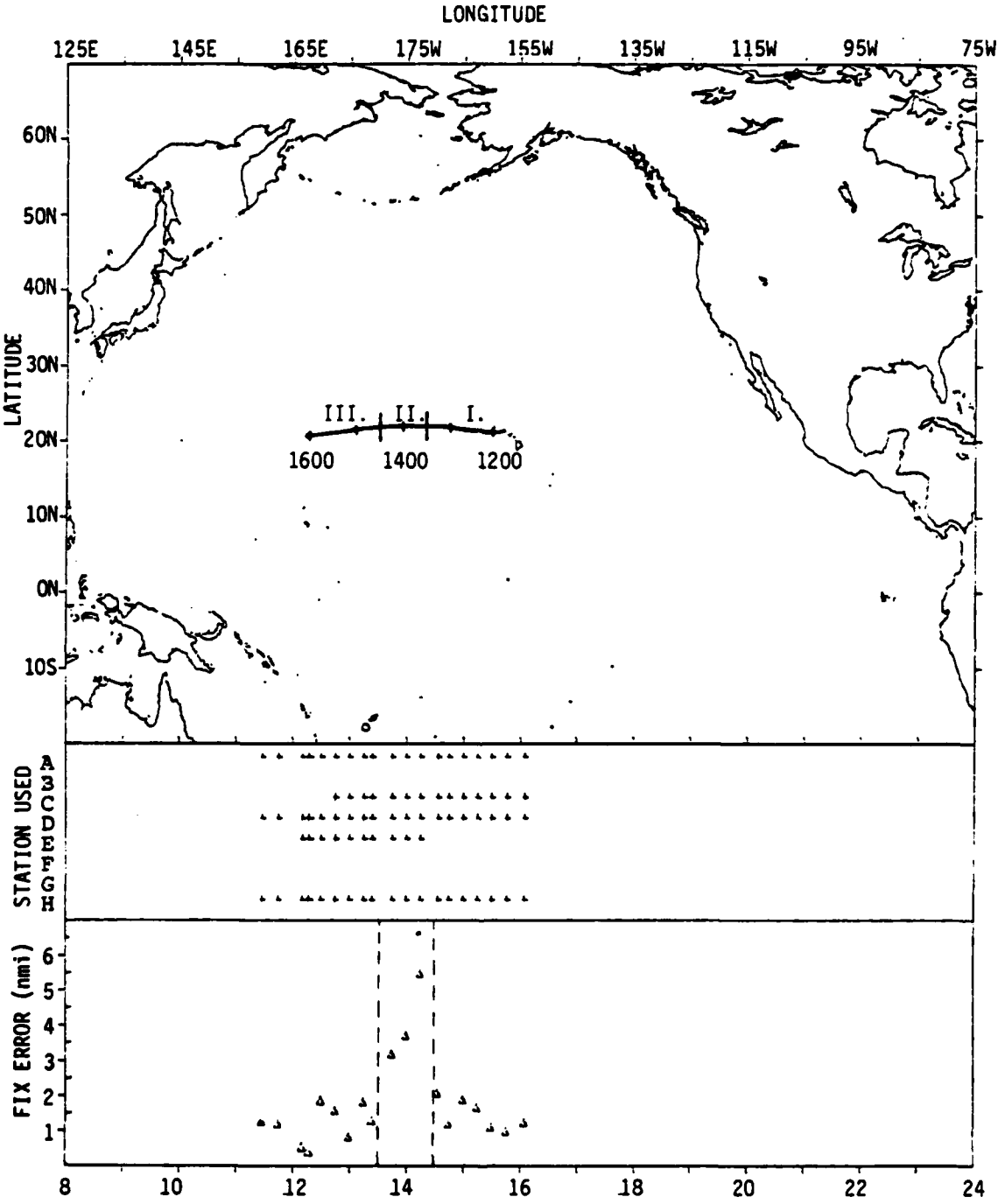

Figure A4-5. Pan-American Flight X935/30 June 1977
Honolulu to Guam

Flight E901/17 July 1977 — Figure A4-6. Tables AB-6, AB-6.

Coverage:

A - Off-the-air 11-25 July for annual maintenance
B - Deselected
C - Deselected because of near-field effect until 2008Z (24N, 164W); then strong
D - Strong till 2300Z then moderate
E - Strong
F - Deselected
G - Deselected
H - Strong

Accuracy: With A off-the-air, accuracy within the near-field of C was good (2.5 nmi.) but might have been better with A. Omega accuracy was exceptional for this flight - around 2 nmi. C, D, E and H provided excellent coverage.

Flight E901/17 September 1977 — Figure A4-7.
Honolulu to Nandi — Tables AA-7, AB-7.

Coverage:

A - Moderate signal
B - Deselected
C - Deselected because of near-field effect until 2003Z (16N, 160W); then strong
D - Off-the-air for annual maintenance
E - Strong
F - Deselected
G - Minimal
H - Strong

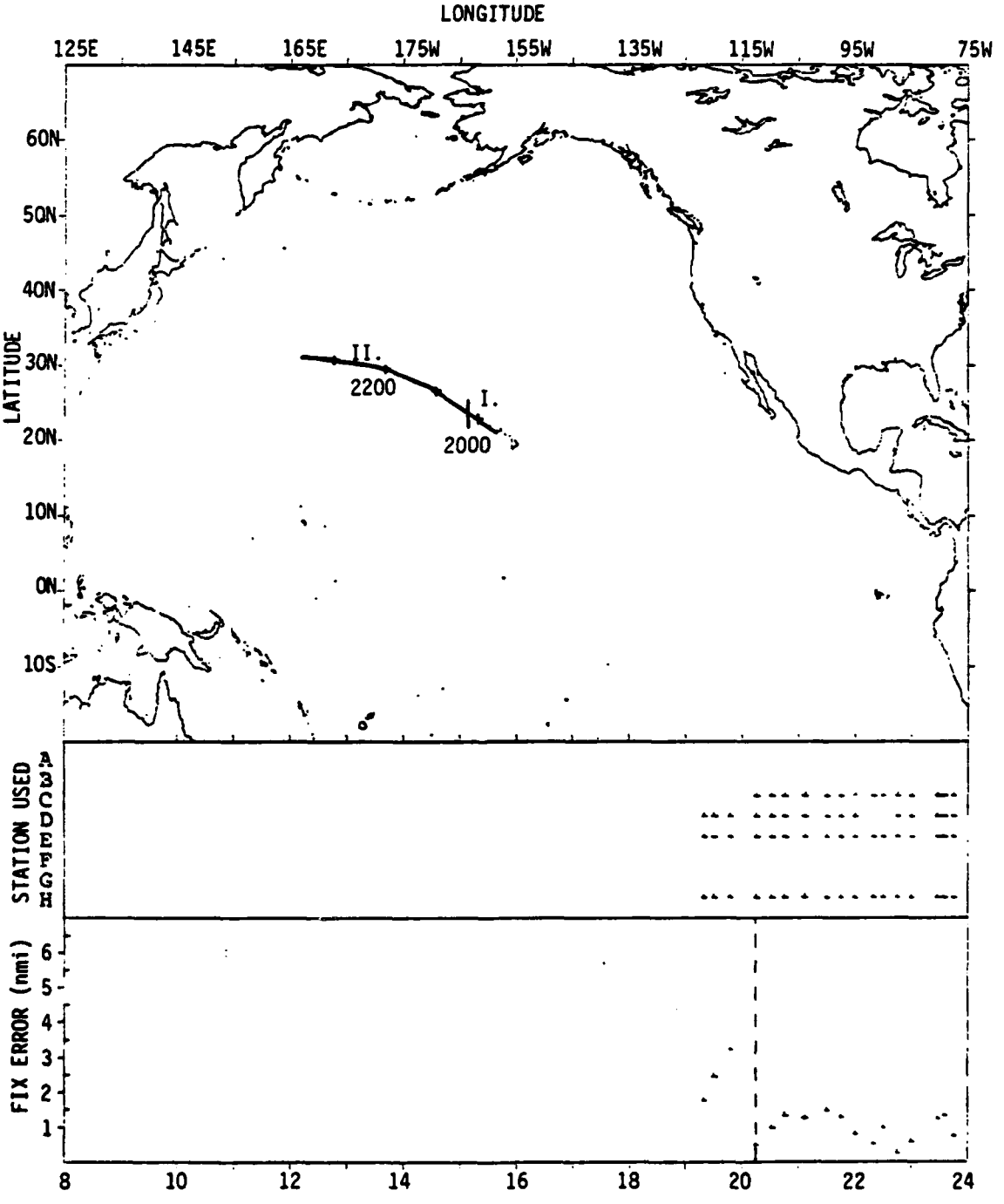

Figure A4-6. Pan-American Flight E901/17 July 1977
Honolulu to Tokyo

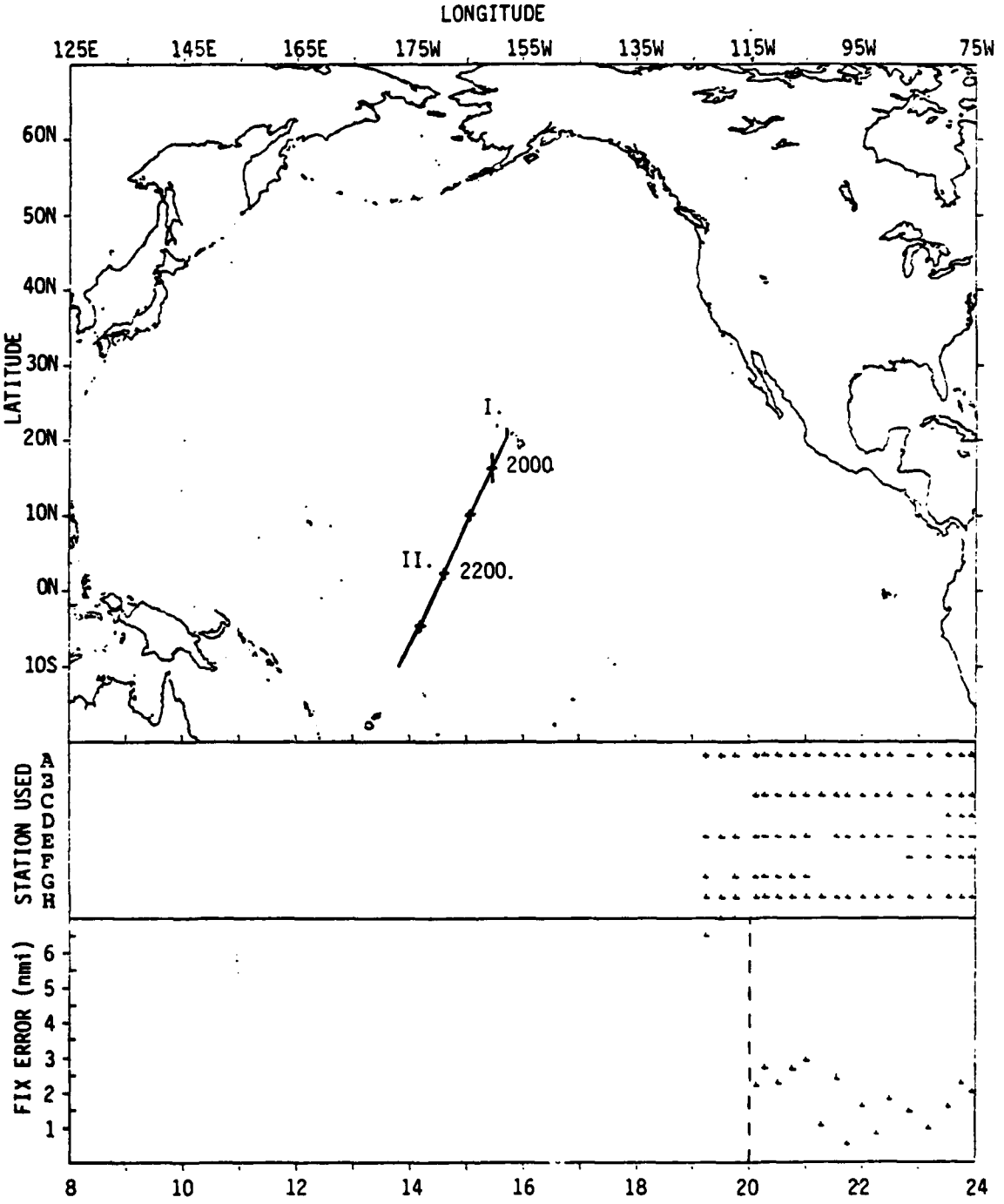

Figure A4-7. Pan-American Flight E901/17 Sept 1977
Honolulu to Nandi

Accuracy: Without D, accuracy was poor within the near-field of Hawaii; initialization with only A, E, G, and H was probably inadequate. Once C was reselected, however, accuracy was excellent - within 2 nmi. on the average.

Flight B953/13 March 1977
Los Angeles to Papeete

Figure A4-8.
Tables AA-8, AB-8.

Coverage:

A - Minimal
B - Minimal (out-of-range)
C - Strong
D - Strong then fading to moderate after 0930Z
E - Out-of-range until 0950Z (4N, 137W) then moderate
F - Moderate then dropped out about 0800Z and came back on after 0815Z
G - Deselected
H - Strong

Accuracy: Omega accuracy was fair to poor (5-9 nmi) for both segments of this flight. Because A and B had weak signals if at all, both should have been deselected. F had mid-range signals but briefly went off-the-air and was intermittent after that. VLF mode was used when F dropped out; and the ONS seemed to have slipped a lane which probably went uncorrected for the second segment of the flight. Forewarning of this outage on F would have avoided the difficulty by deselection and reselection at appropriate times. Gaining E did not help, although it might have had good results, if the lane slip had been corrected properly.

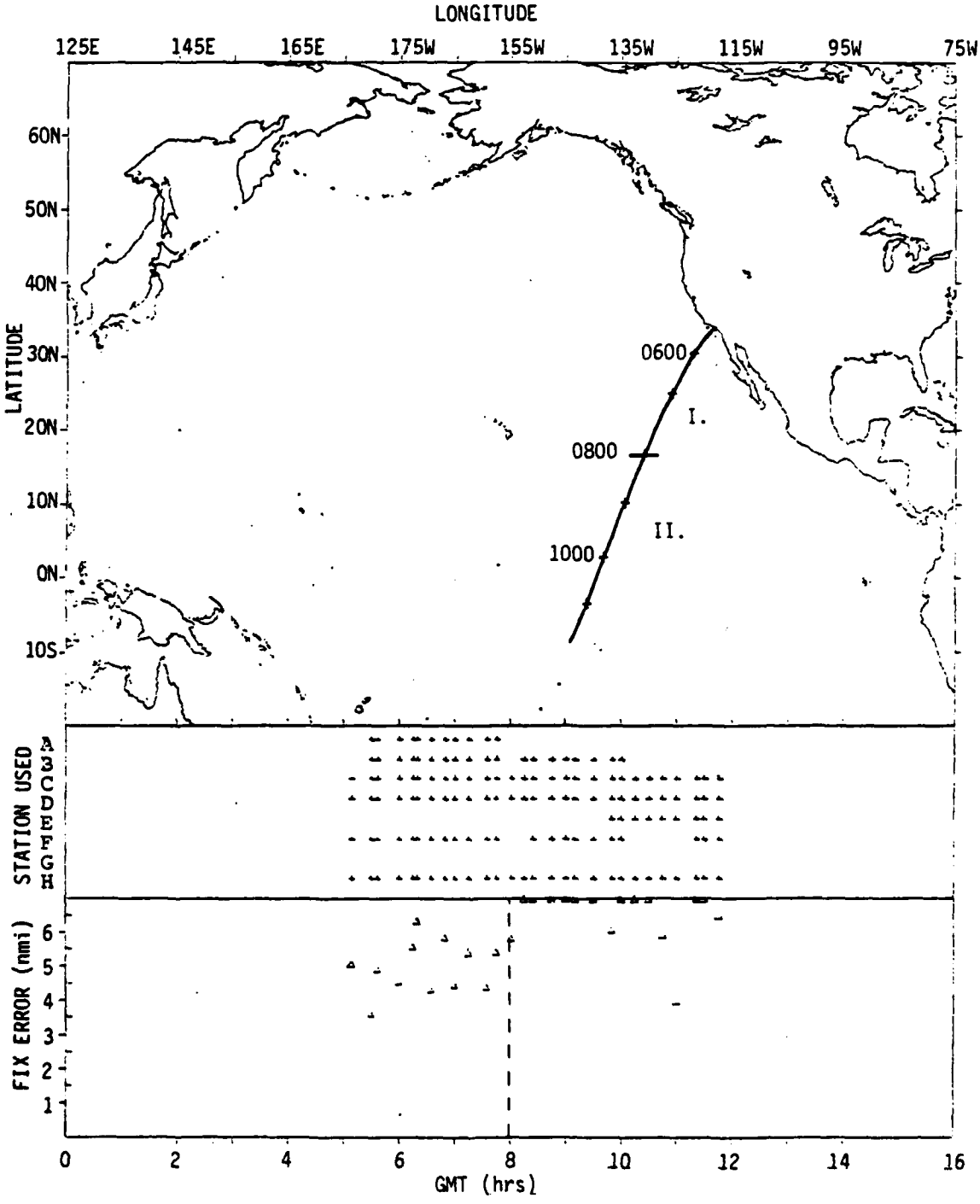

Figure A4-8. Pan-American Flight B953/13 March 1977
Los Angeles to Papeete

Flight FB951/15 March 1977 — Figure A4-9.
Papeete to Los Angeles — Tables AA-9, AB-9.

Coverage:

A - Deselected (Greenland shadow)
B - Deselected
C - Strong
D - Strong
E - Moderate until dropped @ 0930Z (11N, 134W)
F - Moderate until dropped @ 1100 (23N, 127W)
G - Minimal till 0915Z
H - Strong

Accuracy: For the first segment of this flight accuracy of approximately 3.5 nmi was within limits for Omega After 0930Z the monitor seemed to have trouble with station selection. Station E was steady though moderate throughout, but the receiver dropped it for some reason @ 0930Z and picked up G instead. The flight notes mention turbulence at this time, and the motion may have resulted in the observed lane slip. The notes also mention that the slip was corrected; however, the data do not support that statement. Most likely the ONS was not re-initialized to the proper lane. Argentina (F) faded after 1100Z without explanation. The effect of such an unscheduled outage can be avoided by appropriate deselection.

A4.3.2 Par-American Flights - 1976: Results

Though the interim report included in the Appendix of Gibbs' report[A3] discussed several flights, only the few listed in Table A4-1 were within the Northern Pacific region. Of those flights only flight PA812/20 May 1976 was discussed in some detail. The flight departed Sydney at 0601Z, arrived in Pago Pago at 1128Z, departed at 1213Z, and arrived in Honolulu at 1723Z. Omega evaluation on this flight is summarized below in the same format as for the 1977 flights.

AD-A121 105 NORTH PACIFIC OMEGA NAVIGATION SYSTEM VALIDATION(U) 4/4
MEGATEK CORP SAN DIEGO CA P LEVINE ET AL. 31 DEC 81
R2018-054-IF-5 ONSOD-01-81 N00123-78-C-0043

UNCLASSIFIED F/G 17/7 NL

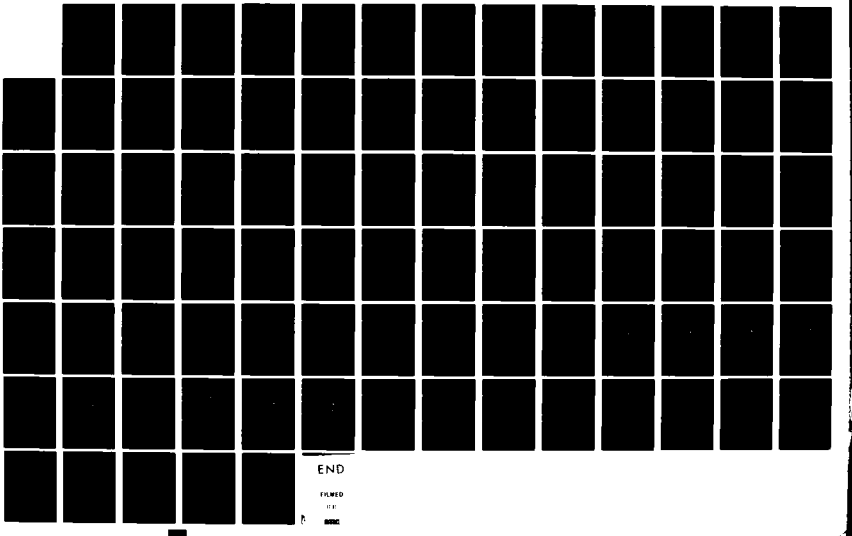

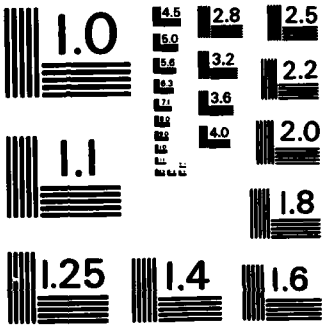

MICROCOPY RESOLUTION TEST CHART
NATIONAL BUREAU OF STANDARDS - 1963 - A

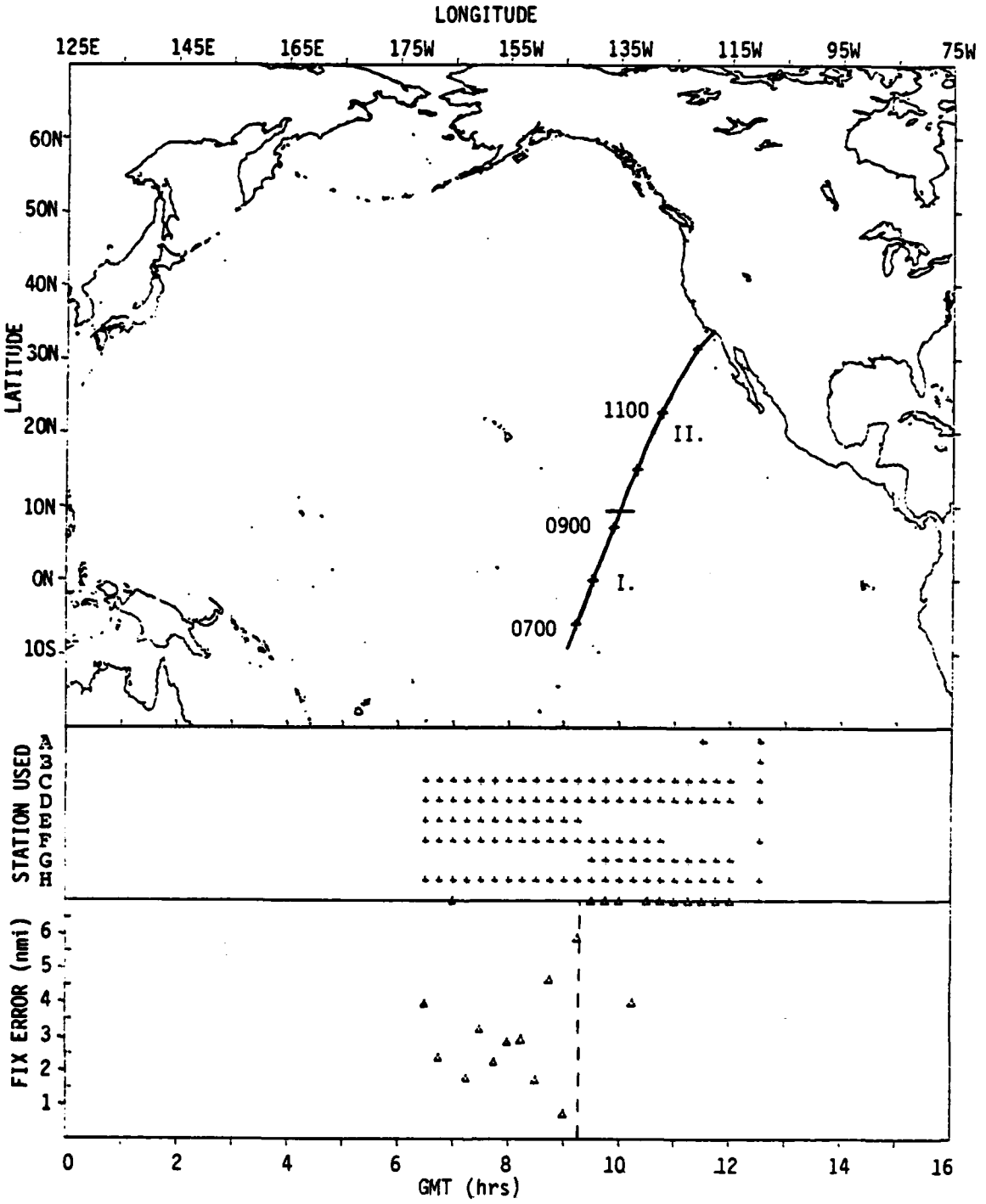

Figure A4-9. Pan-American Flight FB951/15 March 1977
Papeete to Los Angeles

FLT 13/76 PA812/20 May 76 Sydney-Honolulu via Pago Pago

Coverage:

A - Strong
B - Deselected
C - Strong until deselected because of near-field effect (17N, 160W)
D - Strong
E - Strong
F - Deselected
G - Deselected
H - Strong

Accuracy: Stations A, C, D, E and H provided fix accuracy within 1-2 nmi, as was noted for all of the flights discussed together with this flight. The general comment on Omega accuracy was as follows: "...it is believed safe to say the airborne accuracy potential of Omega ha been defined, as predicted, to be one to two nautical miles at about the two sigma (95%) level."

Data from other Omega evaluation flights were appended to the interim report, and the data for segments of flight routes over the Northern Pacific as listed in Table A4-1 are included in Appendix AC. These data were mostly just checks of the ONS over the initial and terminal airports and not observations for waypoints en route. As such the data were not sufficient for statistical analysis; however, the errors are generally within 1-3 nmi. The primary stations were C, D, E, and H for these flights.

A4.3.3 Summary of Pan-American Experience

P.R.J. Reynolds, manager of Pan-American's Navigation Services, summarized their operational experience with Omega in a

presentation[A5] to the Fourth Annual Meeting of the International Omega Association in September 1979. He makes no specific mention of mean errors for the Northern Pacific region; but the analysis of the data for 1976 and 1977 flights indicates that the errors are within 1-3 nmi. during normal operation. His consideration of the availability of Omega signals does include the Northern Pacific and his comments on each Omega station are summarized as follows:

A) Norway - Strong and reliable over Northern Pacific, except in areas where the signal path crosses Greenland. In the "Greenland Shadow" as it is called, signals are severely attenuated. The western edge of this shadow falls midway between San Francisco and Hawaii (See data on Flights E900, B953, and FB951 of 1977.)

B) Liberia - Reliably available some distance eastward of Japan and Australia but generally out of range for most of Northern Pacific.

C) Hawaii - Prime station over the entire Pacific with strong, reliable signals. Within 300 nmi. of its transmitter, the CMA 740 ONS automatically deselects C; this deselection usually ensures that ONS does not slip lanes because of modal interference.

D) North Dakota - Prime station over the Northern Pacific with SNR levels comparable to Omega Hawaii. No problems noted with its availability.

E) La Reunion - Good signal over western part of the Northern Pacific but drops out of range east of Hawaii. (Refer to data on Flights E902 and E900 of 1977.)

F) Argentina - Range-constrained west of the San Francisco - Christmas Island line in the Northern Pacific, and often not available somewhat east of that line because of the large amount of land entering the signal path. Some coverage is noted south of the equator on flights to and from Tahiti in 1977 (Refer to data on Flights B953 and FB951.)

G) Trinidad - Will cease operation in December of this year, so its coverage is not relevant to validation of the permanent Omega system.

H) Japan - Prime station for the Northern Pacific with near-saturation SNRs throughout the area. Omega Hawaii, North Dakota, and Japan are the major triad for reliable signals in this region.

A5.0 OTHER OPERATIONAL DATA

A5.1 Shipboard Data

The US Coast Guard Omega Navigation Systems Operations Detail (ONSOD) maintains files of marine users' comments on Omega signal availability, accuracy and performance. Such operational data were received from the following ships which traversed the Northern Pacific region:

- USS Buttonwood
- USCGC Jarvis
- USCGC Mallow
- USCGC Mellon
- M/S Nopal Lane

The non-systematic nature of this data precluded any quantitative evaluation except for the data from the Nopal Lane which included error information. The user comments, therefore, are either summarized or reprinted in the following paragraphs. Note that except for the propagation anomalies associated with the near-field of Omega Hawaii and with polar cap absorption of Omega Norway signals, Omega performance is considered by these users to be at least satisfactory, if not excellent.

A quote regarding submarine use of Omega from reference A4 has also been included in this section. (See Section A5.1.6).

A5.1.1 USS Buttonwood

A copy of 3 pages from the Omega navigation log of the USS Buttonwood's voyage from Honolulu to American Samoa and back, 13 Oct-17 Nov 1978, noted LOPs, PPCs and resulting fixes for irregular times during the journey. Stations A, C, D, E, F, and H were used in various LOP pairs. Because reference information was not provided and no

comments were included with the data, Omega accuracy could not be evaluated for this voyage.

A5.1.2 USCGC Jarvis

The US Coast Guard Cutter Jarvis reported excellent overall Omega system performance, usually within 2 NM accuracy, during voyages in the North Pacific from 15 May-29 July 1978. Comments on Omega accuracy from this report are summarized below for each patrol segment.

A) During the transit to Kodiak, 15-25 May, three problem areas were noted as responsible for errors of up to 17 NM:

(1) Operator unfamiliarity with the Navidine ESZ-1000 Omega receiver and ESZ-2001 navigational computer and inordinate stabilization times after entering new station or LOP.

(2) Difficulty in properly initializing the receiver and computer in the proximity of Omega station Hawaii and lack of subsequent reference to update the Omega system once beyond the near-field limit (600 NM from Oahu).

(3) Signal propagation: Within the near-field radius of Omega station Hawaii, only LOPs A-D, D-H and A-H could be used with A-D being less than satisfactory, perhaps because some PCA activity was noted during this time. For the rest of the voyage, LOPs A-C, C-H, C-D and D-H provided adequate positional accuracy.

B) During 2 patrol segments in the Aleutian chain usually within 10 NM of land, Omega and Loran C were used as backup to radar and visual navigation with excellent results. LOPs A-H, D-H and A-D consistently provided accuracy within 2NM and often as close as 0.5 NM. Omega Hawaii was off-the-air from 2-7 June and again on 12 June and could not be used. The computer was updated periodically to radar and visual fixes; celestial fixes were not available due to constant cloud cover.

C) In the Bering Sea west of the Pribilof Islands, Omega accuracy was again excellent, within 2 NM, even though the cloud cover and lack of nearby land masses prevented updating the computer. Loran C agreed with Omega for this period.

D) On the transit south to Hawaii, Omega was used to locate the scene of the collision between the Star K and Taiwan Phoenix on 19 July 1978. Throughout the search-and-recovery operation Omega and Loran C were within 5NM of each other. Within 800 NM of Oahu, celestial fixes and Loran C complemented Omega coverage for accurate navigation within the near-field of Omega Hawaii.

A5.1.3 USCGC Mallow

During 3 patrols in the vicinity of Hawaii in March 1977, the Mallow noted fair to excellent results with Omega navigation, as reprinted below from a letter to ONSOD from the Mallow:

"a. During MALLOW's ELT patrol from 1-4 March, fair results were obtained from rate CD in the vicinity of Lanai.

"b. From 10-11 March fair to excellent results were obtained with rate BH. The increase in accuracy was apparent when MALLOW was 55 nm from the OMSTA, in the vicinity of Kahoolawe. BD plotted well near Molokini Island, although it was up to 100 nm NW of the visual position in the Kaiwi Channel near Oahu. AB and AC plotted poorly throughout the trip (up to 90 nm away from the OMSTA).

"c. Omega fixes were fair in the Kauai Channel and improved to an accuracy of 2 miles off visual position near Makahuena Pt., Kauai."

Standard Omega coding forms for a voyage of the Mallow in November 1977 from near the Marshall Islands to the vicinity of Hawaii were also received by ONSOD. As with the coding forms from the Buttonwood, no reference positions were provided to judge the accuracy of the Omega fixes. The Omega stations used were A, C, D, E, and H in various LOP pairs.

A5.1.4 USCGC Mellon

Two reports from the Mellon were received regarding Omega coverage and accuracy during patrols evidently following an itinerary similar to that of the USCGC Jarvis.

The first report, received 17 July 1978, commented on Omega performance probably observed during the voyage north from Hawaii to Alaska in Feb 1978. LOPs C-D, C-H, D-H, A-H, and A-C were used. Though atmospheric conditions were good, signals from Omega Norway were unreliable. During periods of PCA activity, station A could not be used. LOPs using station C were unreliable because Omega Hawaii signals were intermittent for approximately 13 days. Stations D and H, however, were reliable for this period. As compared with LORAN-A, LORAN-C and visual systems, Omega consistently plotted to the north approx. 1-3 nmi.

The second report, received 3 August 1978, refered to Omega accuracy in the Bering Sea and Aleutian chain area. LOPs C-D, A-C, C-H, and A-C were used. No PCA activity was noted during this voyage. The report included the following comments on Omega accuracy:

"As compared to LORAN "C" radar and visual the following is noted.

A. In north and northeast Bering Sea Omega plotted constantly to the southwest 1-4 miles.

B. In mid and south Bering Sea Omega plotted to the southeast 1-4 miles.

C. During last weeks operations in Aleutian chain area, Omega not receiving signals from C,D, and H which are the only useable stations for this region."

A5.1.5 M/S Nopal Lane

The Norwegian merchant ship Nopal Lane provided data for 17-18 June 1976 from its Omega log, comparing the Omega fix with a reference position approximately once each hour. This data is listed in Table A5-1, including the error in nautical miles recorded on the log sheets. The LOPs used were C-D, A-C and C-H. The mean radial error was 4.5 nmi. with standard deviation of 1.2 nmi.

A5.1.6 Submarine Omega Performance

In an article in reference A4, LCDR B.A. Pinz commented on the potential of the Omega system for submarine use: "The data indicates an average fix spread of 3-5 NM. While this is satisfactory for open ocean transits (less passages thru restricted waters), the typical operating scenario of a submarine requires fix resolutions of substantially less than that. The value of Omega as a submarine navigational aid is exponential relative to fix resolution. It is recognized that on going programs are developing refinements in programming propagation anomaly correction factors into the system to account for the many variables associated with signal transmission disturbance phenomena. Significant improvements in this area could enhance Omega Navigational Aid data to primary status which would be an invaluable asset supporting Submarine Force navigational requirements."

A5.2 Aircraft Data

On two Western Airlines flights in 1978 to and from Hawaii, W.M. Molesworth of the FAA compared the Litton ONS and the INS. The flight numbers dates, itineraries and stations used are listed in Table A5-2. The time for each observation was not included on the copies of the log sheets; and so, it is not listed. The radial error was computed for each position according to the formula given in Section A4.2.1. The

OMEGA LOG FROM "NOPAL LANE" 17-18 JUNE 1976

17 JUNE 1976

GMT	OMEGA		REFERENCE		ERROR
0000	40-18.	163-46.	40-18.	163-45.	2.
0100	40-15.	164-12.	40-13.	164-02.	2.5
0200	40-08.	164-34.	40-09.	164-34.	4.5
0300	40-10.	164-53.	40-07.	164-55.	4.
0400	40-07.	165-20.	40-04.	165-22.	3.5
0500	40-04.	165-48.	40-01.5	165-51.	3.
0600	40-01.	166-15.	39-59.	166-17.	4.
0715	39-58.	166-49.	39-55.	166-52.	4.
0800	39-55.	167-10.	39-53.	167-13.	3.
0900	39-52.	167-36.	39-50.	167-40.	4.2
1000	39-50.	168-02.	39-48.	168-09.	6.
1100	39-47.	168-32.	39-45.	168-35.	3.
1200	39-46.	168-59.	39-43.	169-02.	4.
1300	39-45.	169-25.	39-40.	169-29.	5.5
1400	39-42.	169-55.	39-38.	169-56.	4.5
1500	39-41.	170-20.	39-35.	170-21.	5.5
1600	39-38.	170-45.	39-32.5	170-47.	5.5
1700	39-35.	171-11.	39-30.	171-13.	5.
1800	39-32.	171-34.	39-27.5	171-39.	6.
1900	39-28.	172-04.	39-25.	172-01.	4.
2000	39-25.	172-31.	39-23.	172-27.	4.
2300	39-18.	173-50.	39-15.	173-47.	4.

18 JUNE 1976

GMT	OMEGA		REFERENCE		ERROR
0000	39-15.	174-16.	39-17.	174-11.	5.
0200	39-12.	175-08.	39-12.	175-03.	4.
0300	39-09.	175-36.	39-10.	175-27.	7.
0400	39-07.	176-00.	39-07.5	175-52.	6.
0600	39-03.	176-49.	39-05.	176-42.	5.5
0700	39-01.	177-15.	39-00.	177-08.	5.5

Table A5-1. Data from Omega Log of M/S NOPAL LANE

WESTERN AIRLINES FLIGHT 584/28 NOV 1978 HONOLULU TO SAN JOSE

OMEGA LAT	OMEGA LON	INS LAT	INS LON	STATIONS USED	RADIAL ERROR
21-20.0	157-56.3	21-19.7	157-56.7	A CD FGH	0.48
25-22.6	154-13.4	25-22.1	154-14.2	A CD FGH	0.92
29-52.4	146-13.2	29-53.2	146-14.9	A CD FGH	1.84
32-32.5	140-32.6	32-35.4	140-35.5	A CD FGH	3.79
34-28.8	135-55.2	34-29.8	135-59.3	A CD FGH	4.18
36-16.5	130-55.9	36-17.8	130-57.3	A CD FGH	1.75
37-32.8	126-39.7	37-34.4	126-44.2	A CD FGH	4.65
37-20.9	121-54.0	37-24.2	122-00.3	A CD FGH	6.82*

NO. OF FIXES = 7 NO. OF OUTLIERS = 1
RADIAL ERROR AVERAGE = 2.52 STN DEV = 1.67

WESTERN AIRLINES FLIGHT 551/20 NOV 1978 SAN DIEGO TO HONOLULU

OMEGA LAT	OMEGA LON	INS LAT	INS LON	STATIONS USED	RADIAL ERROR
32-05.8	120-57.4	32-06.5	120-58.5	A CD FGH	1.25
30-25.3	126-31.5	30-25.5	126-34.0	A CD FGH	2.51
28-46.0	132-41.2	28-45.1	132-41.4	A CD FGH	0.81
27-21.8	136-59.7	27-23.4	137-01.5	A CD FGH	2.29
25-08.2	143-07.4	25-07.9	143-10.3	A CD FGH	2.91
23-42.2	146-37.1	23-42.0	146-39.0	A CD FGH	1.91
21-08.4	152-20.9	21-04.6	152-22.9	A CD FGH	4.07
21-19.1	157-54.9	21-20.6	157-57.1	A CD FGH	2.61

NO. OF FIXES = 8 NO. OF OUTLIERS = 0
RADIAL ERROR AVERAGE = 2.30 STN DEV = 1.01

* - DENOTES OUTLIER

Table A5-2. Western Airlines Flights - 1978

mean and standard deviation are also listed in Table A5-2. Although these values are within acceptable limits for Omega accuracy, in using the INS as the reference the same reservations apply as mentioned in Section A4.2.1. A corrected INS could not be computed for a better comparison, because the observation times were not known.

A6.0 SUMMARY OF SIGNAL COVERAGE AND FIX ACCURACY

A6.1 Signal Coverage

A composite diagram of observed signal coverage is given in Figure A6-1. The Pan-Am flight routes, the ships' paths and China Airlines waypoints have all been plotted on the same map. The predominant stations used for each segment are indicated by the station letters next to the routes. Positions where stations become unavailable (because of excessive range, for example) were identified by review of the station usage history associated with each route. From this information rough estimates of coverage boundaries were drawn as an overlay. Thus, Figure A6-1 displays the overall picture of signal availability for the Northern Pacific as deduced from operational data.

It is easy to see at a glance that the operational data confirms aspects of Omega's coverage predicted by theory. The "Greenland Shadow" of Omega Norway is immediately evident and extends well into the coastal waters of the US and Mexico. Liberia's signal is only available in the southwest quadrant. The near-field of the Hawaii transmitter has a 300-500 nmi. radius and extends somewhat more eastward than westward. Hawaii has strong usable signals outside of this circle. North Dakota's signals are available throughout the region; and so, no boundary is shown. La Reunion's signal covers most of the area but drops out of range east of approximately 140W. Argentina's signal is only available in the southeast quadrant of the Pacific. Except for its near-field circle, Japan's signals provide strong coverage in the area.

Stations C, D, and H provide primary coverage, and stations A and E give strong secondary coverage for redundancy or back-up in the event that one of the major stations is not available. Stations B and F also complement C, D, and H for redundancy in the southern part of the region.

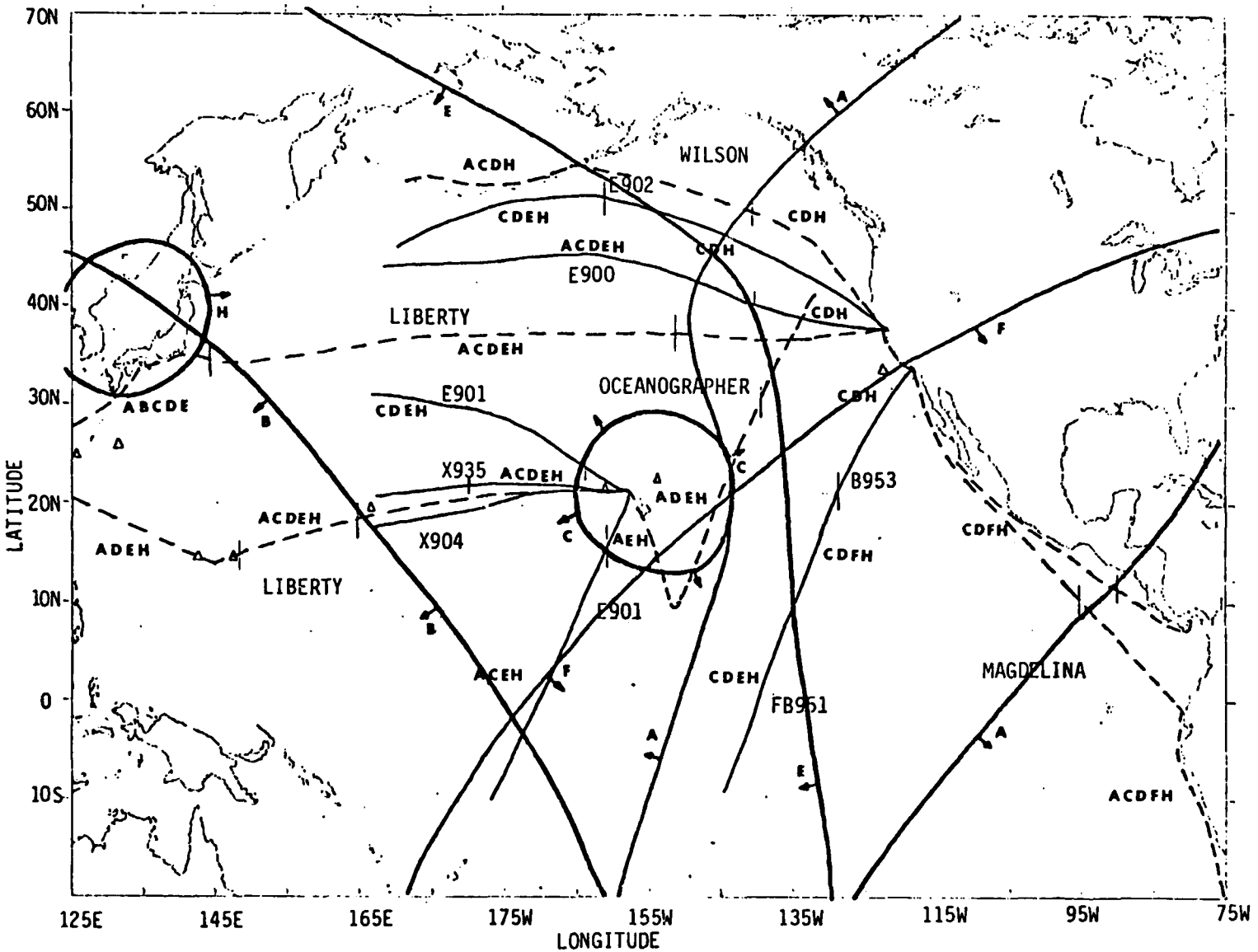

Figure A6-1. Composite Omega Signal Coverage From Operational Data

A6.2 Fix Accuracy

Compared with satellite fixes, Omega gives excellent results, within 1-2 nmi., and often less than 1 nmi., for marine navigation. Comapred with INS fixes, Omega gives accuracy during normal operation within 1-3 nmi. for aircraft navigation. Because the INS is a less stable reference than satellite reference, airborne Omega accuracy may actually be better than the observed results. Station selection plays a key role in determining fix accuracy. This is especially evident from the Pan-American data, in which abnormal signal conditions degraded fix accuracy, because station selection may not have been the best. In such situations manual deselection may be required to improve performance.

REFERENCES

A1. C.J. Gibbs, Canadian Marconi Company, "CMA-740 Omega Navigation System Pacific Region As Collected by Pan-American World Airways", 27 October 1977.

A2. T. Palsson and A. Thorhallson, "Certification of Omega for Navigation in the MNPS Area - Icelandiar's Experience", Proceedings of the Fourth Annual Meeting, International Omega Association, 10-12 Sept. 1979, San Diego, CA.

A3. "Pacific Flights (Prototype CMA-740) Interim Omega Evaluation Report, June 24, 1976", Appendix to reference 1.

A4. LCDR B.A. Pinz, COMSUBPAC, Code 402, "Submarine Force Pacific Performance Analysis for Omega Receiver Set AN/BRN-7", Proceedings of the Fourth Annual Meeting, International Omega Association, 10-12 Sept. 1979, San Diego, CA.

A5. P.R.J. Reynolds, "Pan-American World Airways Omega Experience", Proceedings of the Fourth Annual Meeting, International Omega Association, 10-12 Sept. 1979, San Diego, CA

APPENDIX AA

Pan-Am Flights - 1977: Fix Accuracy Data

Flight No.	GMT START	GMT END	DIFF. LAT.	DIFF. LON.
B953	0450	1320	1.7S	6.1E
FB951	0450	1232	12.4N	0.2E
X935	1050	1923	2.4N	4.0E
X904	0750	1544	15.4S	4.7W
E901	1830	2713	2.8N	1.0E
E902	1230	2229	2.4N	26.8E
E901	1815	2712	1.6S	2.8W
E900	0118	1215	1.3N	17.0E

Table AA-1. Difference Between INS and Actual Positions at End of Pan-American Flights-1977

PAN-AM FLIGHT E902/18 JULY 1977 TOKYO TO SAN FRANCISCO

GMT	CORRECTED INS LAT	CORRECTED INS LON	RADIAL ERROR	STATIONS USED	OMEGA LAT	OMEGA LON	INS LAT	INS LON
1630	N 46- 8.6	E169-47.4	6.85	CDE	H N 46- 4.7	E169-53.0	N 46- 9.6	E169-58.1
1646	N 47-13.9	E173- 5.6	7.20	CDE	H N 47- 9.8	E173-11.6	N 47-14.9	E173-17.1
1700	N 48- 6.0	E175-44.7	5.98	CDE	H N 48- 2.2	E175-50.3	N 48- 7.1	E175-56.8
1721	N 49-18.3	E180- 8.0	10.75	CDE	H N 49-13.7	E179-57.6	N 49-19.5	E179-55.0
1730	N 49-47.8	W178- 6.6	7.50	CDE	H N 49-42.5	W178- 0.8	N 49-49.0	W177-53.2
1745	N 50-25.2	W174-50.2	8.39	CDE	H N 50-19.1	W174-44.4	N 50-26.5	W174-36.1
1800	N 50-58.0	W171-25.1	7.52	CDE	H N 50-51.5	W171-19.4	N 50-59.3	W171-10.3
1807	N 51- 8.8	W169-57.9	6.84	CDE	H N 51- 2.2	W169-52.5	N 51-10.2	W169-42.8
1830	N 51-20.6	W164-31.7	4.96	CDE	H N 51-14.1	W164-27.8	N 51-22.0	W164-15.6
1850	N 51-12.5	W159-52.5	4.05	CDE	H N 51- 6.3	W159-50.7	N 51-14.0	W159-33.5
1900	N 50-49.7	W157-36.2	6.32	CD	H N 50-42.9	W157-33.7	N 50-51.3	W157-18.8
1915	N 50-10.6	W154-12.9	7.55	CD	H N 50- 3.3	W154-10.8	N 50-12.2	W153-54.8
1935	N 49-12.5	W149-51.2	3.73	CD	H N 49- 5.0	W149-50.6	N 49-14.2	W149-32.2
1945	N 48-28.2	W147-38.1	1.65	CD	H N 48-20.8	W147-38.2	N 48-29.9	W147-18.6
2000	N 47-30.0	W144-18.8	6.20	CD	H N 47-23.4	W144-19.7	N 47-31.8	W143-58.7
2021	N 46-11.1	W139-53.4	3.68	CD	H N 46- 5.3	W139-54.7	N 46-13.0	W139-32.3
2030	N 45-30.1	W138-11.5	1.65	CD	H N 45-25.0	W138-13.1	N 45-32.0	W137-50.0
2045	N 44-17.7	W135-22.1	6.05	CD	H N 44-11.6	W135-23.8	N 44-19.7	W135- 0.0
2100	N 43-12.2	W132-34.8	4.74	CD	H N 43- 6.1	W132-36.8	N 43-14.2	W132-12.0
2114	N 42-10.7	W129-55.2	2.38	CD	H N 42- 5.5	W129-57.3	N 42-12.8	W129-31.8
2133	N 40-43.6	W126-52.7	3.80	CD	H N 40-39.8	W126-52.8	N 40-45.8	W126-28.4
2150	N 39-28.4	W124-21.6	1.29	CD	H N 39-26.6	W124-22.8	N 39-30.6	W123-56.5
2205	N 38- 5.1	W122-50.1	1.42	CD	H N 38- 4.1	W122-51.2	N 38- 7.4	W122-24.4
2212	N 37-37.5	W122-21.6	1.44	CD	H N 37-36.1	W122-22.1	N 37-39.8	W121-55.6
2220	N 37-37.3	W122-21.4	2.05	CD	H N 37-35.4	W122-20.7	N 37-39.7	W121-55.0
2229	N 37-36.8	W122-23.2	0.30	CD	H N 37-36.5	W122-23.2	N 37-39.2	W121-56.4

Table AA-2. Data For Pan-Am Flight E902

PAN-AM FLIGHT E900/27 SEPT 1977 TOKYO TO SAN FRANCISCO

GMT	CORRECTED INS LAT	CORRECTED INS LON	RADIAL ERROR	STATIONS USED	OMEGA LAT	OMEGA LON	INS LAT	INS LON
530	N 43-53.2	E167-36.3	3.68	ABCDE GH	N 43-55.9	E167-38.8	N 43-53.7	E167-42.8
541	N 44- 5.9	E169-58.2	4.08	ABCDE GH	N 44- 7.6	E170- 1.9	N 44- 6.4	E170- 5.0
545	N 44- 7.7	E170-48.9	3.82	ABCDE GH	N 44- 9.2	E170-52.4	N 44- 8.2	E170-55.8
600	N 44-12.6	E173-44.7	4.02	A CDE GH	N 44-13.1	E173-48.7	N 44-13.2	E173-52.0
615	N 44- 3.9	E176-45.7	3.70	A CDE GH	N 44- 4.2	E176-49.4	N 44- 4.5	E176-53.4
631	N 44- 8.2	E179-59.3	3.90	A CD FGH	N 44- 8.4	E179-55.4	N 44- 8.8	E179-51.2
647	N 44-33.7	W176-49.0	3.99	A CDE GH	N 44-32.8	W176-45.1	N 44-34.4	W176-40.5
700	N 44-44.6	W174-16.8	3.63	A CDE GH	N 44-42.7	W174-13.5	N 44-45.3	W174- 8.0
721	N 45- 9.0	W169-52.6	3.17	ABCDE GH	N 45- 5.7	W169-49.7	N 45- 9.7	W169-43.2
730	N 45-11.8	W168- 7.5	2.64	ABCDE GH	N 45- 8.2	W168- 5.2	N 45-12.5	W167-57.9
745	N 45-14.3	W165-10.1	2.73	A CDE GH	N 45-10.9	W165- 7.6	N 45-15.1	W165- 0.1
800	N 45-14.4	W162-11.1	2.47	A CDE GH	N 45-11.5	W162- 8.8	N 45-15.2	W162- 0.7
811	N 45-13.3	W159-59.3	2.20	A CDE GH	N 45- 9.8	W159-57.4	N 45-14.1	W159-48.6
831	N 44-35.6	W156-20.3	4.17	A CDE GH	N 44-31.0	W156-18.6	N 44-36.5	W156- 9.1
848	N 43-58.8	W153-12.7	4.11	A CD GH	N 43-54.9	W153-14.0	N 43-59.7	W153- 1.1
907	N 43- 8.3	W149-57.2	2.35	A CD GH	N 43- 5.2	W149-58.4	N 43- 9.2	W149-45.1
915	N 42-45.0	W148-42.2	1.45	A CDE GH	N 42-42.3	W148-43.4	N 42-45.9	W148-29.9
921	N 42- 0.8	W146-19.3	2.45	A CDE GH	N 41-58.1	W146-21.5	N 42- 1.8	W146- 6.8
945	N 41-19.8	W144- 9.7	4.22	A CDE GH	N 41-17.1	W144-13.2	N 41-20.8	W143-56.6
1000	N 40-32.8	W141-41.3	4.69	A CDE GH	N 40-29.5	W141-44.8	N 40-33.8	W141-27.8
1015	N 39-51.3	W139-20.8	3.26	A CD GH	N 39-47.0	W139-23.0	N 39-52.4	W139- 6.9
1030	N 39-19.2	W136-52.3	2.02	CD GH	N 39-16.5	W136-54.3	N 39-20.3	W136-38.0
1045	N 38-46.9	W134-19.7	1.20	CD FGH	N 38-44.7	W134-20.3	N 38-48.0	W134- 5.0
1100	N 38-19.8	W131-19.4	2.57	BCD FGH	N 38-17.3	W131-20.9	N 38-21.0	W131- 4.3
1110	N 38- 4.6	W130- 1.4	2.82	BCD FGH	N 38- 2.7	W130- 3.6	N 38- 5.8	W129-46.1
1122	N 37-56.7	W126-49.0	2.91	BCD FGH	N 37-55.8	W126-51.8	N 37-57.9	W126-33.4
1134	N 37-54.2	W125-51.1	2.57	BCD FGH	N 37-54.0	W125-53.7	N 37-55.4	W125-35.2
1159	N 37-23.6	W122-13.6	1.28	BCD FGH	N 37-24.9	W122-14.0	N 37-24.9	W121-57.0
1206	N 37-34.6	W122-21.8	3.46	A CD GH	N 37-38.1	W122-22.0	N 37-35.9	W122- 5.0
1215	N 37-34.2	W122-23.1	2.58	A CD GH	N 37-36.6	W122-22.1	N 37-35.5	W122- 6.1

Table AA-3. Data For Pan-Am Flight E900

PAN-AM FLIGHT X904/01 JULY 1977 GUAM TO HONOLULU (OMEGA #1)

GMT	CORRECTED INS LAT	CORRECTED INS LON	RADIAL ERROR	STATIONS USED	OMEGA LAT	OMEGA LON	INS LAT	INS LON
1115	N 17-31.3	E166-40.9	4.07	A CD H	N 17-29.1	E166-36.9	N 17-24.6	E166-38.9
1130	N 17-48.6	E168-42.7	5.19	A CDE H	N 17-46.6	E168-37.6	N 17-41.5	E168-40.5
1139	N 18- 0.5	E170- 4.4	5.14	A CDE H	N 17-57.0	E169-59.8	N 17-53.1	E170- 2.1
1200	N 18-24.0	E173- 6.2	5.96	A CDE H	N 18-21.7	E173- 0.6	N 18-15.9	E173- 3.7
1230	N 18-51.9	E177-30.4	6.70	A CDE H	N 18-46.0	E177-27.2	N 18-42.8	E177-27.6
1248	N 19- 6.0	E179-55.0	6.03	A CDE H	N 19- 1.2	E179-58.9	N 18-56.3	E179-58.0
1300	N 19-22.9	W178-16.8	5.42	A CDE H	N 19-19.5	W178-21.4	N 19-12.8	W178-19.9
1330	N 20-12.3	W174-17.0	4.17	A CDE H	N 20- 8.1	W174-21.1	N 20- 1.3	W174-20.4
1400	N 21- 5.8	W170-27.5	5.15	A CDE H	N 21- 2.7	W170-32.3	N 20-53.8	W170-31.2
1403	N 21-11.1	W170- 5.1	5.04	A CDE H	N 21- 8.5	W170- 9.8	N 20-59.0	W170- 8.8
1430	N 21- 7.4	W166-21.2	3.27	A CDE H	N 21- 4.7	W166-24.0	N 20-54.4	W166-25.2
1500	N 21-15.2	W162- 4.3	3.83	A DE H	N 21-10.2	W162- 5.4	N 21- 1.2	W162- 8.6
1534	N 21-19.5	W157-55.3	4.07	A DE H	N 21-14.3	W157-55.4	N 21- 4.4	W157-59.9
1544	N 21-20.0	W157-55.2	0.92	A DE H	N 21-18.9	W157-55.5	N 21- 4.6	W157-59.9

Table AA-4. Data For Pan-Am Flight X904

PAN-AM FLIGHT X935/30 JUNE 1977 HONOLULU TO GUAM (OMEGA #1)

	CORRECTED INS		RADIAL	STATIONS		OMEGA		INS	
GMT	LAT	LON	ERROR	USED		LAT	LON	LAT	LON
1128	N 21-19.7	W157-55.2	1.24	A D	H	N 21-18.2	W157-55.5	N 21-19.9	W157-54.9
1145	N 21-19.4	W157-56.6	1.18	A D	H	N 21-18.3	W157-57.4	N 21-19.7	W157-56.2
1210	N 21- 3.6	W160- 3.4	0.51	A DE	H	N 21- 3.3	W160- 3.9	N 21- 4.0	W160- 2.8
1218	N 21- 6.2	W161- 7.7	0.38	A DE	H	N 21- 5.7	W161- 7.9	N 21- 6.6	W161- 7.0
1230	N 21-15.5	W162-38.0	1.85	A DE	H	N 21-13.1	W162-37.6	N 21-16.0	W162-37.2
1245	N 21-24.0	W164-42.7	1.55	A CDE	H	N 21-22.1	W164-42.6	N 21-24.5	W164-41.8
1300	N 21-39.9	W166-45.2	0.80	A CDE	H	N 21-39.1	W166-45.5	N 21-40.5	W166-44.2
1315	N 21-53.1	W168-52.8	1.81	A CDE	H	N 21-51.3	W168-52.8	N 21-53.8	W168-51.7
1324	N 21-57.8	W170- 2.0	1.28	A CDE	H	N 21-56.5	W170- 2.1	N 21-58.5	W170- 0.8
1345	N 21-57.1	W173- 5.4	3.18	A CDE	H	N 21-53.9	W173- 5.4	N 21-57.9	W173- 4.0
1400	N 21-56.3	W175-14.8	3.71	A CDE	H	N 21-52.6	W175-15.0	N 21-57.2	W175-13.3
1415	N 21-56.8	W177-30.4	5.48	A CDE	H	N 21-52.7	W177-26.8	N 21-57.8	W177-28.8
1434	N 21-52.9	E179-55.1	2.06	A CD	H	N 21-52.6	E179-57.1	N 21-53.9	E179-56.8
1445	N 21-43.9	E178-12.4	1.19	A CD	H	N 21-42.8	E178-12.9	N 21-45.0	E178-14.2
1500	N 21-32.8	E176-14.2	1.86	A CD	H	N 21-30.9	E176-14.8	N 21-34.0	E176-16.1
1515	N 21-23.4	E174-21.3	1.64	A CD	H	N 21-22.1	E174-22.6	N 21-24.6	E174-23.4
1530	N 21- 7.8	E172-13.2	1.10	A CD	H	N 21- 6.6	E172-14.0	N 21- 9.1	E172-15.4
1547	N 20-54.1	E169-56.9	0.97	A CD	H	N 20-52.5	E169-57.5	N 20-55.5	E169-59.2
1605	N 20-36.3	E167-28.2	1.21	A CD	H	N 20-34.3	E167-29.4	N 20-37.8	E167-30.7

Table AA-5. Data For Pan-Am Flight X935

PAN-AM FLIGHT E901/17 JULY 1977 HONOLULU TO TOKYO

GMT	CORRECTED INS LAT	CORRECTED INS LON	RADIAL ERROR	STATIONS USED	OMEGA LAT	OMEGA LON	INS LAT	INS LON
1919	N 21-19.4	W157-56.5	1.78	DE H	N 21-17.9	W157-55.2	N 21-19.7	W157-56.6
1930	N 21- 6.7	W158-35.0	2.45	DE H	N 21- 3.4	W158-33.7	N 21- 7.0	W158-35.1
1947	N 21-59.8	W160-29.2	3.25	DE H	N 21-56.6	W160-28.5	N 22- 0.2	W160-29.3
2015	N 23-45.4	W163-50.3	0.50	CDE H	N 23-45.2	W163-50.8	N 23-46.0	W163-50.5
2031	N 24-47.0	W165-46.8	1.00	CDE H	N 24-45.9	W165-46.9	N 24-47.6	W165-47.0
2045	N 25-39.9	W167-30.8	1.35	CDE H	N 25-38.4	W167-31.3	N 25-40.6	W167-31.1
2106	N 26-59.7	W170- 0.8	1.28	CDE H	N 26-58.1	W170- 2.0	N 27- 0.5	W170- 1.1
2130	N 27-53.5	W173-16.7	1.50	CDE H	N 27-52.2	W173-17.5	N 27-54.5	W173-17.0
2145	N 28-41.0	W175-17.9	1.31	CDE H	N 28-39.8	W175-18.7	N 28-42.0	W175-18.3
2200	N 29-16.4	W177-23.0	0.82	CDE H	N 29-15.6	W177-23.7	N 29-17.5	W177-23.4
2219	N 29-51.3	W179-53.5	0.54	CDE H	N 29-50.7	W179-54.0	N 29-52.5	W179-53.9
2230	N 30- 3.7	E178-11.0	0.98	CDE H	N 30- 2.8	E178-10.0	N 30- 5.0	E178-10.5
2245	N 30-16.0	E175-57.4	0.25	CDE H	N 30-15.5	E175-57.5	N 30-17.4	E175-56.9
2300	N 30-30.6	E173-44.5	0.59	CDE H	N 30-30.0	E173-45.0	N 30-32.0	E173-44.0
2327	N 30-59.0	E169-50.2	1.24	CDE H	N 30-57.7	E169-49.8	N 31- 0.6	E169-49.6
2335	N 31- 0.8	E168-33.3	1.35	CDE H	N 30-59.4	E168-32.8	N 31- 2.4	E168-32.7
2345	N 31- 1.0	E167- 1.8	0.76	CDE H	N 31- 0.2	E167- 1.7	N 31- 2.7	E167- 1.2

Table AA-6. Data For Pan-Am Flight E901

PAN-AM FLIGHT E901/17 SEPT 1977 HONOLULU TO NANDI

GMT	CORRECTED INS LAT	CORRECTED INS LON	RADIAL ERROR	STATIONS USED	OMEGA LAT	OMEGA LON	INS LAT	INS LON
1913	N 21-20.1	W157-56.4	6.50	A E GH	N 21-20.3	W157-49.9	N 21-19.9	W157-56.7
1930	N 20-23.3	W157-52.3	8.31	A E H	N 20-22.5	W157-44.0	N 20-23.1	W157-52.7
1945	N 18-30.4	W158-48.5	7.09	A E GH	N 18-31.3	W158-41.5	N 18-30.1	W158-49.0
2006	N 16- 2.7	W160-26.7	2.20	A C E GH	N 16- 4.6	W160-25.4	N 16- 2.4	W160-27.3
2016	N 14-58.5	W161- 8.5	2.70	A C E GH	N 15- 1.9	W161- 7.6	N 14-58.1	W161- 9.1
2030	N 13-23.6	W162- 9.0	2.28	A C E GH	N 13-26.7	W162- 8.1	N 13-23.2	W162- 9.7
2045	N 11-39.4	W163-13.5	2.68	A C E GH	N 11-41.9	W163-11.3	N 11-39.0	W163-14.3
2100	N 9-55.7	W164-15.8	2.92	A C E GH	N 9-59.0	W164-15.5	N 9-55.2	W164-16.7
2116	N 8- 2.1	W165-27.4	1.06	A C H	N 8- 2.3	W165-26.3	N 8- 1.6	W165-28.3
2132	N 6-11.3	W166-32.6	2.41	A C E H	N 6-13.7	W166-32.4	N 6-10.7	W166-33.6
2143	N 4-55.4	W167-18.6	0.54	A C E H	N 4-57.8	W167-18.4	N 4-54.8	W167-19.7
2200	N 3- 2.1	W168-25.4	1.61	A C E H	N 3- 3.6	W168-24.9	N 3- 1.4	W168-26.6
2215	N 1-13.2	W169-29.3	0.80	A C E H	N 1-14.6	W169-28.7	N 1-12.5	W169-30.6
2228	S 0- 6.4	W170-16.1	1.81	A C E H	S 0- 4.8	W170-15.3	S 0- 7.2	W170-17.4
2250	S 2-50.3	W171-46.7	1.46	A C EF H	S 2-48.8	W171-46.3	S 2-51.1	W171-48.1
2310	S 5- 0.7	W173-23.3	0.97	A C EF H	S 4-59.2	W173-22.4	S 5- 1.6	W173-24.8
2331	S 7-19.4	W174-55.0	1.59	A CDEF H	S 7-17.7	W174-53.6	S 7-20.3	W174-56.6
2345	S 8-53.8	W176- 2.5	2.27	A CDEF H	S 8-51.5	W176- 1.4	S 8-54.8	W176- 4.2
2356	S 10- 7.9	W176-54.7	2.02	A CDEF H	S 10- 5.4	W176-54.0	S 10- 8.9	W176-56.5

Table AA-7. Data For Pan-Am Flight E901

PAN-AM FLIGHT B953/13 MARCH 1977 LOS ANGELES TO PAPEETE

GMT	CORRECTED INS LAT	CORRECTED INS LON	RADIAL ERROR	STATIONS USED	OMEGA LAT	OMEGA LON	INS LAT	INS LON
509	N 33-56.5	W118-22.8	5.11	CD F H	N 33-51.6	W118-19.6	N 33-56.4	W118-22.6
530	N 32-51.2	W119-43.7	3.65	ABCD F H	N 32-45.9	W119-40.1	N 32-51.1	W119-43.2
537	N 32-21.9	W120-27.4	4.94	ABCD F H	N 32-16.8	W120-23.4	N 32-21.7	W120-26.8
600	N 30-23.2	W122-13.5	4.58	ABCD F H	N 30-18.7	W122- 9.6	N 30-23.0	W122-12.7
615	N 28-49.6	W123-22.7	5.60	ABCD F H	N 28-45.0	W123-18.7	N 28-49.3	W123-21.7
620	N 28-12.5	W123-48.8	6.35	ABCD F H	N 28- 7.8	W123-44.5	N 28-12.2	W123-47.7
635	N 26-41.7	W124-51.7	4.36	ABCD F H	N 26-37.4	W124-47.3	N 26-41.3	W124-50.4
650	N 25- 4.5	W125-56.7	5.89	ABCD F H	N 25- 0.4	W125-52.5	N 25- 4.1	W125-55.3
700	N 24- 0.2	W126-38.4	4.48	ABCD F H	N 23-56.3	W126-34.2	N 23-59.8	W126-36.8
715	N 22-18.6	W127-42.1	5.43	ABCD F H	N 22-15.0	W127-37.9	N 22-18.1	W127-40.4
735	N 20- 4.4	W129- 4.9	4.41	ABCD F H	N 20- 0.2	W129- 0.7	N 20- 3.8	W129- 2.9
745	N 18-50.9	W129-49.1	5.45	ABCD F H	N 18-47.4	W129-44.9	N 18-50.3	W129-47.0
801	N 17- 9.9	W130-48.6	5.85	CD H	N 17- 2.3	W130-42.8	N 17- 9.3	W130-46.3
815	N 15-37.6	W131-40.5	10.74	BCD H	N 15-28.3	W131-35.0	N 15-36.9	W131-38.0
825	N 14-30.4	W132-19.3	8.30	BCD F H	N 14-16.4	W132-12.7	N 14-29.7	W132-16.7
845	N 12-17.8	W133-32.6	12.97	BCD F H	N 12- 5.6	W133-27.1	N 12-17.0	W133-29.8
900	N 10-37.1	W134-27.4	7.56	BCD F H	N 10-23.0	W134-21.9	N 10-36.3	W134-24.4
910	N 9-27.4	W135- 5.1	15.38	BCD F H	N 9-13.0	W134-59.6	N 9-26.5	W135- 2.0
930	N 7- 9.3	W136-18.5	10.54	BCD F H	N 6-55.3	W136-13.1	N 7- 8.4	W136-15.2
950	N 4-44.1	W137-14.6	6.10	BCDEF H	N 4-31.1	W137- 8.5	N 4-43.1	W137-11.0
1000	N 3-40.7	W137-59.4	11.97	BCDEF H	N 3-28.3	W137-54.0	N 3-39.7	W137-55.7
1015	N 2-18.1	W138-41.9	9.37	CDE H	N 2- 6.3	W138-36.8	N 2-17.0	W138-38.0
1030	N 0-30.8	W139-42.0	10.76	CDE H	N 0-19.4	W139-37.9	N 0-29.7	W139-37.9
1045	S 1-18.5	W140-36.6	5.94	CDE H	S 1-30.0	W140-31.5	S 1-19.7	W140-32.4
1100	S 3-23.8	W141-19.1	4.03	CDE H	S 3-23.8	W141-15.1	S 3-25.0	W141-14.7
1121	S 5-42.0	W142-47.5	8.82	CDEF H	S 5-51.6	W142-43.8	S 5-43.3	W142-42.8
1130	S 6-58.4	W143-25.7	7.58	CDEF H	S 7- 7.4	W143-22.7	S 6-59.7	W143-20.9
1146	S 8-38.3	W144-16.7	6.50	CDEF H	S 8-46.0	W144-13.1	S 8-39.7	W144-11.7

Table AA-8. Data For Pan-Am Flight B953

PAN-AM FLIGHT FB951/15 MARCH 1977 PAPEETE TO LOS ANGELES

GMT	CORRECTED INS LAT	CORRECTED INS LON	RADIAL ERROR	STATIONS USED	OMEGA LAT	OMEGA LON	INS LAT	INS LON
630 S	9-24.4	W144-44.9	3.99	CDEF H S	9-21.4	W144-42.3 S	9-21.7	W144-44.9
645 S	7-41.4	W143-50.5	2.40	CDEF H S	7-38.3	W143-48.2 S	7-38.3	W143-50.5
700 S	5-57.8	W142-59.0	7.46	CDEF H S	5-50.1	W142-57.4 S	5-54.3	W142-58.9
715 S	4-10.0	W142- 4.2	1.81	CDEF H S	4- 6.6	W142- 4.6 S	4- 6.1	W142- 4.1
730 S	2-35.2	W141-17.9	3.23	CDEF H S	2-31.4	W141-18.1 S	2-30.9	W141-17.8
745 S	0-53.1	W140-28.5	2.28	CDEF H S	0-49.6	W140-29.0 S	0-48.4	W140-28.4
800 N	0-48.2	W139-36.8	2.87	CDEF H N	0-52.3	W139-36.4 N	0-53.3	W139-36.7
815 N	2-32.2	W138-43.2	2.94	CDEF H N	2-35.6	W138-42.3 N	2-37.7	W138-43.1
830 N	4-17.0	W137-49.2	1.75	CDEF H N	4-21.2	W137-49.3 N	4-22.9	W137-49.1
845 N	6- 1.0	W136-53.0	4.70	CDEF H N	6- 5.7	W136-54.2 N	6- 7.3	W136-52.9
900 N	7-46.2	W135-55.4	0.75	CDEF H N	7-51.4	W135-54.8 N	7-52.9	W135-55.3
915 N	9-32.8	W134-56.9	5.92	CDEF H N	9-38.7	W134-57.7 N	9-39.9	W134-56.8
930 N	11-24.1	W134- 2.3	7.12	CD FGH N	11-40.9	W134- 4.9 N	11-31.6	W134- 2.2
945 N	13-19.2	W132-56.9	8.50	CD FGH N	13-30.2	W132-59.7 N	13-27.1	W132-56.8
1000 N	15-10.2	W131-50.4	10.11	CD FGH N	15-21.4	W131-53.5 N	15-18.5	W131-50.3
1015 N	17- 5.3	W130-43.4	4.01	CD FGH N	17-17.6	W130-46.7 N	17-14.0	W130-43.3
1030 N	19- 3.9	W129-34.9	12.64	CD FGH N	19-16.5	W129-37.7 N	19-13.0	W129-34.8
1045 N	21- 2.0	W128-22.3	8.23	CD FGH N	21-16.0	W128-23.9 N	21-11.5	W128-22.1
1100 N	23- 3.1	W127- 4.3	8.19	CD GH N	23-19.6	W127- 5.6 N	23-13.0	W127- 4.1
1115 N	25- 3.9	W125-42.4	19.78	CD GH N	25-23.5	W125-45.1 N	25-14.2	W125-42.2
1130 N	27-13.4	W124-11.7	10.29	A CD GH N	27-33.3	W124-14.5 N	27-24.1	W124-11.5
1145 N	29-12.4	W122-45.4	11.58	CD GH N	29-31.7	W122-46.4 N	29-23.5	W122-45.2
1200 N	31-15.1	W121-26.0	20.27	CD GH N	31-35.6	W121-26.5 N	31-26.6	W121-25.8
1232 N	33-32.0	W118-25.7	12.12	ABCD F H N	33-55.0	W118-23.7 N	33-44.4	W118-25.5

Table AA-9. Data For Pan-Am Flight FB951

APPENDIX AB

Pan-Am Flights - 1977: SNR Data

Pan-Am Flight No.	OMEGA Stations A	B	C	D	E	F	H
E902	OFF	0-0	86-96	63-95	0-73	0-17	51-95
E900	3-87	0-21	94-97	94-96	0-58	0-47	93-96
X904	5-67	0-14	80-99	27-79	2-94	0-40	23-94
X935	0-63	0-14	91-98	14-77	31-76	0-12	60-94
E901	OFF	0-43	95-98	51-82	64-91	0-46	89-95
E901	33-65	47-80	97-100	OFF	71-88	1-21	85-95
B053	0-11	0-52	95-98	0-97	0-89	0-40	76-94
FB951	0-0	0-0	96-100	44-97	0-95	0-59	71-95

Table AB-1

10.2 kHz SNR Values (Linear Scale) From Pan-Am Flights - 1977

GMT	A	B	C	D	E	F	H
1646	0	0	86	63	73	17	95
1730	0	0	94	84	55	0	93
1800	0	0	96	86	64	0	94
1830	0	0	94	92	0	0	92
1900	0	0	94	90	0	0	91
1945	0	0	93	92	0	0	81
2030	0	0	96	92	0	0	70
2100	0	0	91	90	0	0	68
2150	0	0	91	95	0	0	51

Table AB-2

10.2 kHz SNR Values - Pan Am Flight E902/18 July 1977

GMT	A	B	C	D	E	F	H
0545	54	4	95	94	58	28	96
0615	66	0	96	95	57	47	95
0647	80	0	96	95	27	13	93
0730	87	0	96	94	25	0	94
0831	87	1	97	94	16	24	93
0915	79	7	96	94	18	19	95
0945	70	4	96	95	0	27	94
1015	39	3	96	95	11	8	94
1045	14	0	95	95	10	0	94
1100	3	4	96	95	0	0	94
1122	8	21	94	96	2	12	93

Table AB-3

10.2 kHz SNR Values - Pan-Am Flight E900/27 Sept 1977

GMT	A	B	C	D	E	F	H
1115	5	9	84	62	2	6	69
1130	38	6	95	63	23	40	91
1200	58	14	93	68	62	30	91
1230	53	0	90	65	51	9	86
1300	67	0	80	78	82	0	92
1330	65	8	98	79	83	0	94
1400	67	0	98	66	76	12	91
1430	58	6	93	54	91	0	79
1500	9	1	99	27	94	0	23

Table AB-4

10.2 Khz SNR Values - Pan Am Flight X904/1 July 1977

GMT	A	B	C	D	E	F	H
1210	12	2	97	61	74	2	60
1300	63	14	98	73	81	0	84
1345	57	13	96	77	76	0	94
1415	65	0	96	66	64	12	84
1445	50	14	96	63	60	6	96
1515	56	0	96	51	45	6	90
1605	0	0	91	14	31	0	72

Table AB-5

10.2 kHz SNR Values - Pan Am Flight X935/30 June 1977

GMT	A	B	C	D	E	F	H
1930	0	43	98	82	84	0	89
2015	0	37	98	81	90	0	94
2045	0	19	98	75	80	27	94
2130	0	0	97	75	64	0	94
2200	0	0	96	61	80	14	95
2230	0	0	96	55	77	46	95
2300	0	0	96	56	89	29	94
2335	0	0	95	51	91	33	95

Table AB-6

10.2 kHz SNR Values - Pan-Am Flight E901/17 July 1977

GMT	A	B	C	D	E	F	H
1930	45	80	100	0	79	12	87
2006	53	70	98	0	87	11	92
2030	48	62	98	0	86	2	85
2116	65	72	99	0	71	1	92
2200	50	67	98	5	88	17	94
2331	33	47	97	56	75	21	95

Table AB-7

10.2 kHz SNR Values - Pan Am Flight E901/17 Sept 1977

GMT	A	B	C	D	E	F	H
0537	0	38	97	84	84	0	76
0620	0	52	96	87	0	0	84
0700	0	0	97	97	12	0	92
0745	0	0	95	63	89	0	93
0815	11	0	95	54	34	31	94
0900	0	0	97	32	26	38	84
0930	0	0	96	30	42	40	86
1000	0	0	96	0	0	30	87
1030	0	0	98	0	46	0	87
1030	0	0	98	0	46	0	87
1100	0	0	97	0	47	25	88
1130	0	0	98	0	80	0	83

Table AB-8

10.2 kHz SNR Values - Pan-Am Flight B953/12 Ma 1977

GMT	A	B	C	D	E	F	H
0645	0	0	97	44	40	59	85
0715	0	0	98	79	47	57	95
0745	0	0	100	84	44	28	80
0815	0	0	99	90	42	35	76
0845	0	0	99	93	47	47	78
0915	0	0	98	96	47	44	80
0945	0	0	99	96	76	27	71
1015	0	0	96	97	86	17	83
1045	0	0	97	97	95	0	81
1115	0	0	96	97	39	14	92
1145	0	0	96	97	0	0	90

Table AB-9

10.2 kHz SNR Values - Pan-Am Flight FB951/15 Mar 1977

APPENDIX AC

Pan-Am Flights - 1976: Fix Accuracy and Station Usage

Appendix AC

Pan-American Flights-1976: Fix Accuracy and Station Usage

DATA FLT. 4/76 PA825/08APR NEW YORK-HONOLULU via DALLAS

Dallas-Honolulu

GMT	DATE	PLACE NAME	LAT. DIFF.	LONG. DIFF.	STATIONS	REMARKS
0254	04/09/76	Oakland VOR	0.4N	1.8W	CD GH	Overhead
0741	04/09/76	Agate Intx.	0.5N	2.6E	A DE H	Overhead
0824	04/09/76	Honolulu Airport	2.1N	1.3E	A DE H	Touchdown, Rwy 04
0830	04/09/76	Honolulu Airport	1.1N	1.5E	A DE H	At Gate 20

DATA FLT. 5/76 PA818/10APR HONOLULU-SAN FRANCISCO

1937	04/10/76	Honolulu Airport	0.6N	2.1E	A DE H	In posn. Rwy 08
0008	04/11/76	San Francisco Airport	0.3S	0.9W	CD GH	Touchdown Twy 28R
0014	04/11/76	San Francisco Airport	0.4N	0.7W	CD GH	At Gate 2
0017	04/11/76	San Francisco Airport	0.1S	0.1E	CD GH	After resynching

DATA FLT. 6/76 PA815/11APR SAN FRANCISCO-TAHITI

0515	04/12/76	San Francisco Airport	1.2S	0.2E	CD GH	At Gate 4A
0536	04/12/76	San Francisco Airport	0.1N	0.6E	CD FGH	In posn. Twy 10L
0606	04/12/76	Avenel VOR	1.3S	2.1E	CD GH	Overhead
0635	04/12/76	Los Angeles Airport	0.8S	0.4E	CD FGH	Touchdown
?	04/12/76	Los Angeles Airport	0.2S	0.9E	CD FGH	At Gate 27
					VOR off air	
?	04/12/76	Rangiroa NDB	2.3N	5.8W	CDE H	a beam to west
1601	04/12/76	Tahiti Airport	3.0N	1.6W	CDE H	Touchdown
1605	04/12/76	Tahiti Airport	2.7N	2.3W	CDE H	At Terminal
1607	04/12/76	Tahiti Airport	2.1N	3.3W	CDE H	After resynch.

DATA FLT. 7/76 PA816/13APR TAHITI-SAN FRANCISCO
(TAS rate aid inop.)

0700	04/13/76	Tahiti Airport	0.2N	0.2E	CDEF H	At Terminal
0705	04/13/76	Tahiti Airport	0.7N	0.6E	CDE H	In posn. Rwy 4
0900	04/13/76	$4^{o}S/142^{o}W$ - noted divergence to left of Doppler/Loran				
0943	04/13/76	$00^{o}.140^{o}W$ - updated Longitude 16'E viz Doppler/Loran				
1250	04/13/76	$22^{o}N/129^{o}W$ - removed 16'E 0943Z update				
1440	04/13/76	Los Angeles Airport	0.7N	12.0W	CD GH	Touchdown
1459	04/13/76	Los Angeles Airport	5.3N	5.0W	At Terminal	
1501	04/13/76	Los Angeles Airport	0.0	0.3W	After Resynching	

LOS ANGELES-SAN FRANCISCO

GMT	DATE	PLACE NAME	LAT. DIFF.	LONG. DIFF.	STATIONS	REMARKS
1535	04/13/76	Los Angeles Airport	0.0	0.2W	CD GH	At Gate 27
1541	04/13/76	Los Angeles Airport	0.5N	0.6W	CD GH	At Gate 27
1614	04/13/76	Los Angeles Airport	1.4S	1.3W	CD FGH	In posn. Rwy 24L
1653	04/13/76	Big Sur VOR	0.7S	0.8E	CD FGH	Overhead
1713	04/13/76	San Francisco Airport	1.4S	1.0W		Touchdown, Rwy 28L
?	04/13/76	San Francisco Airport	1.1S	1.3W	CD FGH	At Gate 4A

DATA FLT. 8/76 PA815/25APR SAN FRANCISCO-AUCKLAND

San Francisco-Los Angeles (TAS rate aid operative)

0211	04/25/76	San Francisco Airport	1.7S	1.5W	CD GH	At Terminal
0219	04/25/76	San Francisco Airport	0.7N	1.7W	CD GH	End Rwy 28R
0248	04/25/76	Avenal VOR	0.4S	0.7W	CD GH	Overhead
0313	04/25/76	Los Angeles Airport	0.3N	1.8E	CD GH	Touchdown
0318	04/25/76	Los Angeles Airport	0.2N	1.1E	CD GH	At Gate 24

LOS ANGELES-TAHITI

0404	04/25/76	Los Angeles Airport	0.5S	1.2E	CD GH	At Gate 24
0430	04/25/76	Los Angeles Airport	0.9S	0.9E	CD GH	Departing Gate 24
0503	04/25/76	Turning Point	1.8N	3.5E	CD GH	Right on STA DME
1214	04/25/76	Rangiroa VOR	1.9S	4.0E	CDE H	Overhead
1253	04/25/76	Tahiti Airport	2.9N	8.2W	CDE H	Touchdown Rwy4 update
1259	04/25/76	Tahiti Airport	2.9N	1.8W	CDE H	At Terminal

TAHITI-LOS ANGELES

0555	04/30/76	Tahiti Airport	0.7N	3.9E	CDEF H	At end Twy 04
0625	04/30/76	Rangiroa VOR	1.0S	1.7E	CDEF H	Overhead
1300	04/30/76	Sta. Catalina DME	156/156			Omega/DME Comparison
1337	04/30/76	Los Angeles Airport	1.8S	2.3E	CD GH	Touchdown Rwy 25R
1346	04/30/76	Los Angeles Airport	1.0S	0.5W	CD GH	At Gate 29
1348	04/30 76	Los Angeles Airport	0.5N	0.0	CD FGH	At Gate 29

LOS ANGELES-SAN FRANCISCO

?	04/30/76	Los Angeles Airport	0.6N	0.4W	CD FGH	On ground
1600	04/30/76	San Francisco Airport	1.4S	0.7W	CD FGH	At Gate 4B

APPENDIX B: SEASONALLY-AVERAGED PHASE ERROR STATISTICS - NIGHT AND DAY

LOP	SITE	PPC BIAS MEAN	PPC BIAS STDV	RAND. MEAN	PPC STDV	RAND MEAN	PROP STDV	TOTAL MEAN	RSS STDV	CORR. MEAN	RSS STDV	HOURS/DAY MEAN	HOURS/DAY STDV	#SM
AC	ANCH	4.6	10.9	1.8	2.5	5.1	2.2	12.2	5.7	5.9	2.4	4.6	.5	16
AC	HOKK	20.6	3.8	4.4	3.8	6.8	2.3	22.6	3.2	9	2.2	5	0	22
AC	MAKA	5.5	7.8	.9	1.1	6.5	1.8	11.1	4	6.7	1.7	5	0	24
AC	PYRA	4.6	6.3	1.1	1.3	5.1	1.7	9.3	2.6	5.4	1.8	5	0	24
AC	WAHI	3.3	6	1.1	2.1	5.4	3.4	9.2	3.1	6	3.4	4.8	.3	7
AD	ADAK	1.9	10.4	1	1.6	5.4	2.3	11.6	4.1	5.8	2.2	4.3	1.3	15
AD	ANCH	7.5	13.6	2.1	2.6	4.9	1.9	15.1	7.2	5.7	2.5	4.3	1	16
AD	HOKK	7.2	6.5	3.5	2.8	7	2.5	12.4	4.2	6.5	1.9	4.5	.8	22
AD	KURE	-15.3	2.6	15.8	2	4.1	2.6	22.6	2.6	16.6	1.6	4.5	.5	8
AD	PANA	3.2	5.1	4.9	9	5.4	2.6	18.4	8.3	8.9	7.9	4.4	.8	15
AE	HOKK	-8.8	7.1	3.1	2.4	6.1	1.5	12.6	4.9	7.2	1.5	4.6	.6	22
AE	KURE	-3.3	7.5	27.5	2	3	1.7	20.9	2	27.7	1.9	4	.8	6
AH	ADAK	3.7	13.8	3.4	4.7	7.2	3.3	16	10.2	8.6	4.7	4	1.5	17
AH	ANCH	-1.5	12.2	3.2	4	5.3	2.6	13.6	5.3	6.8	3.9	4.6	.5	16
AH	MARC	31.7	7	8.9	8.9	11.6	2.8	36.7	3	13.8	7	1	0	2
AH	MIYA	14.3	2.2	2.1	2.1	4.9	1.5	15.5	2	5.7	1.6	5	0	14
AH	OSHI	21.3	.2	1.4	1.4	2.8	.2	21.5	0	3.3	.7	5	0	2
AH	TSUS	29.5	3	3.5	3	5.5	1.4	30.4	3	6.9	2.3	4.9	.3	20
BC	HOKK	26.9	3.3	4.2	3.5	8.3	2.1	28.9	2.7	9.9	2.6	4	1.2	22
BD	NOS2	-10.8	0	10.2	.1	3.9	.1	15.3	0	10.9	0	5	0	2
BD	NOSC	-13.8	2.6	8.6	1.9	5.3	1.4	17.3	2.8	10.2	2.1	5	0	18
BD	PANA	-11.3	10.1	6.5	5.4	6.8	3.4	17.4	7.4	10.7	3.9	3	1.2	16
BD	SEAT	-10.2	4.9	7.9	5.5	5.4	3.1	15.9	3.1	10.4	5	4.3	.8	22
BF	NELC	-24.7	4.3	6.3	6.3	13.2	1.4	29.7	1.6	15.5	3.7	1	0	2
CD	ADAK	0	10.1	.7	1.2	6.8	2.2	11.3	5.4	7	2.1	5	0	19
CD	ANCH	2.6	3.3	.6	1.1	4.7	1.1	6.5	1.3	5	.9	4.8	.4	17
CD	MAKA	1.6	5.1	2.4	2.3	4.1	.9	7.2	2.6	5.2	1.2	4.9	.2	24
CD	MARC	13.7	8.6	0	0	9.9	1.8	17.7	7	9.9	1.8	1.5	.5	4
CD	NELC	-1.3	.6	.2	.2	3.2	.2	3.5	0	3.2	.2	5	0	2
CD	NOS2	-2.4	1.4	1.1	1.1	3.2	0	4.5	.4	3.6	.4	5	0	2
CD	NOSC	-2.6	1.1	1.1	1.2	2.2	.4	3.9	1	2.7	.8	5	0	18
CD	PANA	-12.4	4.3	2.3	2.8	3	1.4	13.5	3.6	4.4	2.3	4.6	1	16
CD	SEAT	3	7.2	.7	1.6	4.6	3.2	8.5	4.9	4.8	3.4	5	0	22
CD	WAHI	-7.3	6	2.5	1.7	3	1.2	9	5.3	4.3	1.3	5	0	8
CE	ADAK	-3.9	9.4	7.4	4.7	6.2	2.3	14.6	3.8	10.9	2.2	3.6	1.3	15
CE	HOKK	-23.8	5.5	8.5	10	5.5	1.6	20	4.1	11.5	8.6	4.5	.5	24
CE	KURE	1.9	14.9	18.8	5.5	9	2.5	26.4	1	21.2	4.7	2.6	.4	10
CE	NOSC	-4.4	13.2	15.3	9.2	6.7	2.8	23.3	5.2	17.5	8.1	3.4	1.1	16
CE	SEAT	2.4	11.3	1.4	1.9	10.3	3	14.3	7.2	10.6	2.9	3.6	1.5	13
CF	MAKA	14.1	8.7	15.1	9.3	7	2.6	24.8	5.6	17.8	7.5	3.6	1	18
CF	PANA	-3.4	20.7	9.8	8.6	8.8	2.6	26.1	3.7	15	5.4	3.7	1.3	9
CF	WAHI	3.8	12.7	5.2	5	9.6	1.6	17.6	3.7	11.7	3.2	3.5	.4	7
CH	ADAK	8.1	8.4	1.3	1.2	4.4	3	10.5	7.6	4.8	2.9	4.5	1.1	21
CH	ANCH	-3.7	2	2.1	1.8	3.4	.9	7.4	1.5	4.4	1	4.7	.8	17
CH	HOKK	10.1	2.9	4.8	2.7	4.9	.5	12.7	2.2	7.2	1.6	5	0	24
CH	KURE	-15.5	6.2	1.5	2.1	7.6	3.4	18.2	4.8	8	3.5	3.9	1.3	11
CH	MAKA	1.6	2.5	1.2	1.1	3.9	1.5	5.2	1.6	4.3	1.3	5	0	22
CH	MIYA	-17	4.7	4.1	3.3	8.1	1.6	19.9	3.7	9.5	2.2	5	0	14
CH	NOS2	6.1	.1	3	.4	3.4	.1	7.6	0	4.5	.3	5	0	2
CH	NOSC	10.3	5.7	2.6	1.8	3.1	1.1	12	3.9	4.4	1.3	5	0	18
CH	OSHI	-8.3	.3	1.4	.8	4.5	.5	9.6	.4	4.8	.2	5	0	2
CH	PANA	6.9	1.1	0	0	11.5	1	13.5	.3	11.5	1	1	0	2
CH	SEAT	2.3	9.5	1.8	2.6	7.5	3.5	12.5	4.3	8.2	3.4	4.8	.5	22
CH	TSUS	-7.4	8.2	6.2	4.9	8.4	2.3	15.1	5.7	11.4	3.3	4.6	.5	23
CH	WAHI	-4.2	10.1	4.7	4.3	3	3.2	9.7	9.3	5.7	5.3	4.8	.3	18
DF	NOSC	23.3	14	1.2	2.2	8.8	2.8	27	10	9.1	3	2	1	4
DF	SEAT	0	23	14.2	14.5	8.6	5.9	31.2	8.8	19.2	12.3	4.1	1.2	20
DH	ANCH	-7.9	3.6	1.9	1.7	4.9	1.7	10.2	2.1	5.5	1.7	4.7	.6	17
DH	KURE	-1.8	2.1	13.4	1.8	7.8	1.3	15.8	2	15.6	1.8	5	0	8
DH	NELC	8.8	.8	3.4	1.2	2.7	.2	9.9	.3	4.3	1	5	0	2
DH	NOS2	8.3	.9	0	0	2.4	.1	8.6	.9	2.4	.1	5	0	2
DH	NOSC	12.8	5.6	2.2	1.9	3.2	1	14	4.6	4.2	1.4	5	0	18
DH	OSHI	-1	.1	6.3	0	2.7	.2	6.9	0	6.8	0	5	0	2
DH	PANA	11.7	13.9	15.8	11.3	11.6	1.1	29.1	1.2	21.3	7.8	1.5	.5	4
DH	SEAT	-.1	3.9	1.4	1.9	5.7	2.4	7.2	2.8	6.2	2.4	4.8	.5	22
DH	TSUS	7.4	7.7	5.3	3.5	7.3	1.6	13.8	4.4	9.5	2.2	4.9	.3	20
EH	ADAK	16	5.5	12	8.5	6.9	3.4	22.8	6.6	15.6	5.8	3.8	1.3	15
EH	KURE	8.5	6	16.7	3.8	10.3	1.5	22.6	1.7	19.8	3.6	3.2	.4	10
EH	MARC	20	3.4	0	0	12.3	1.3	30.6	3.4	12.3	1.3	1	0	5
EH	MIYA	23.4	4.1	2.3	2.5	6	.9	24.5	3.6	6.8	1.6	5	0	14
EH	OSHI	32.9	3.6	2.5	2.5	4.1	.7	33.3	3.3	5.2	1.8	5	0	2
EH	TSUS	33.9	3.4	1.8	2.1	4.4	.8	34.3	3.3	5.1	1.3	5	0	12
AR	WALE	2	5	.5	.9	3.3	1.3	6	2.6	3.5	1.3	4.2	1	14
CR	WALE	-4.1	2.6	1	1.1	2.6	.3	5.3	2.1	2.9	.6	5	0	18
CR	WALE	-4.1	2.6	1	1.1	2.6	.3	5.3	2.1	2.9	.6	5	0	18

Table B-1. Seasonally-Averaged Statistics: 10.2 kHz - Night

LOP	SITE	PPC BIAS MEAN	PPC BIAS STDV	RAND. MEAN	PPC STDV	RAND MEAN	PROP STDV	TOTAL MEAN	RSS STDV	CORR. MEAN	RSS STDV	HOURS/DAY MEAN	HOURS/DAY STDV	#SM
RC	ANCH	5.7	9.4	1.3	1.6	3.8	1.8	10.6	3.3	4.3	1.9	4.7	.5	16
RC	HOKK	21.2		1.4		7.2		23.1	3.6	8.6	3.3	4.9	.3	28
RC	KURE	9.1		1.1		5.8		12		5.3	2.1		.8	34
RC	NORC	-14	15.	1.1		3.3		19.3	6.2	6.3	2.1	4.9	.1	4
RC	PYRR	8.	6.	1.1		5.1		11.4	4.7	3.7	2.1	5	.8	32
RC	WAHI	2.		1.1		3.4		5.4	3.6		1.1	5	.8	6
RD	ADAK	15.	10.	1.1		6.1		11.3	4.9	5.7	2.1	4.2	.7	14
RD	ANCH	13.	13.	2.2		6.2		17.3	6.4	5.7	2.2	4.2	1.1	16
RD	HOKK			2.2		6.4		11	4.3	5.7	2.2	4.9	.3	28
RD	KURE	16.	1.	2.2		6.4		17.3	6.6	5.7	2.2	4.6	.4	6
RD	PANS	-7.	7.	1.1		4.4		11.3	4.5	5.7	2.1	4.	.1	14
RE	HOKK	-7.	7.	1.1		5.1		12.4	4.7	5.7	2.1	4.6	.8	28
RE	KURE	4.		1.1		5.1		10.3	4.3	5.7	2.1	4.6	.8	4
RE	ADAK	4.	6.	2.2		6.1		10.3	3.9	7.4	2.2	4.4	.1	13
RH	ANCH	2.	3.	2.2		6.5		14	5.3	5.7	2.2	4.3	.1	16
RH	HARC	-31.	3.	1.1		4.4		9.6	3.1	3.5	1.1		.8	2
RH	OSHI	26.		1.1		3.3		9.6	3.2	3.5	1.1		.8	2
RH	TSUS	13.	2.	1.1		4.3		9.6	3.2	3.5	1.1		.8	20
RC	HOKK	15		1.1		4.3		9.6	3.2	3.5	1.1		.8	28
RD	NORC	-1.	3.	1.1		4.4		9.6	3.2	3.5	1.1		.8	18
RD	PANS	-10.	11.	1.1		4.4		9.6	3.2	3.5	1.1		.8	14
RD	SEAT		11.	1.1		4.4		9.6	3.2	3.5	1.1		.8	22
RE	HARC	-27.	4.	1.1		4.4		9.6	3.2	3.5	1.1		.8	4
RH	HARC	-34.	2.	1.1		4.4		9.6	3.2	3.5	1.1		.8	4
RH	OSHI	-2.	2.	1.1		4.4		9.6	3.2	3.5	1.1		.8	2
CD	ADAK		14.	1.1		4.4		9.6	3.2	3.5	1.1		.8	19
CD	ANCH	7.	4.	1.1		4.4		9.6	3.2	3.5	1.1		.8	17
CD	HARC	-1.	3.	1.1		4.4		9.6	3.2	3.5	1.1		.8	32
CD	HARC	-30.	9.	1.1		4.4		9.6	3.2	3.5	1.1		.8	4
CD	NORC	4.	3.	1.1		4.4		9.6	3.2	3.5	1.1		.8	18
CD	PANS	-16.	6.	1.1		4.4		9.6	3.2	3.5	1.1		.8	14
CD	PYRR	-32.	6.	1.1		4.4		9.6	3.2	3.5	1.1		.8	8
CD	SEAT	-4.	6.	1.1		4.4		9.6	3.2	3.5	1.1		.8	22
CD	WAHI	-4.	6.	1.1		4.4		9.6	3.2	3.5	1.1		.8	8
CE	ADAK	8.	14.	1.1		4.4		9.6	3.2	3.5	1.1		.8	13
CE	HOKK	-26.	4.	1.1		4.4		9.6	3.2	3.5	1.1		.8	22
CE	KURE	-1.	6.	1.1		4.4		9.6	3.2	3.5	1.1		.8	8
CE	NORC	-1.	12.	1.1		4.4		9.6	3.2	3.5	1.1		.8	18
CE	SEAT	-17.	13.	1.1		4.4		9.6	3.2	3.5	1.1		.8	18
CF	HAKS	5.	7.	1.1		4.4		9.6	3.2	3.5	1.1		.8	16
CF	PANS	24.	6.	1.1		4.4		9.6	3.2	3.5	1.1		.8	13
CF	WAHI	13.	10.	1.1		4.4		9.6	3.2	3.5	1.1		.8	8
CH	ADAK	1.	13.	1.1		4.4		9.6	3.2	3.5	1.1		.8	19
CH	ANCH	-1.	8.	1.1		4.4		9.6	3.2	3.5	1.1		.8	17
CH	HOKK	-8.	9.	1.1		4.4		9.6	3.2	3.5	1.1		.8	22
CH	KURE	19.	4.	1.1		4.4		9.6	3.2	3.5	1.1		.8	6
CH	MAKS	-3.	2.	1.1		4.4		9.6	3.2	3.5	1.1		.8	20
CH	NOSC	-7.	5.	1.1		4.4		9.6	3.2	3.5	1.1		.8	18
CH	OSHI	-9.	3.	1.1		4.4		9.6	3.2	3.5	1.1		.8	4
CH	PANS	12.	2.	1.1		4.4		9.6	3.2	3.5	1.1		.8	2
CH	SEAT	1.	4.	1.1		4.4		9.6	3.2	3.5	1.1		.8	22
CH	TSUS	-11.	9.	1.1		4.4		9.6	3.2	3.5	1.1		.8	21
CH	WAHI	-2.	2.	1.1		4.4		9.6	3.2	3.5	1.1		.8	10
DF	NORC	-34.	6.	2.2		6.4		13.3	5.3	7.1	2.2	4.9	.3	12
DF	SEAT	17.	2.	1.1		4.4		9.6	3.2	3.5	1.1	4.9	.3	16
DH	ANCH	-9.	2.	1.1		4.4		9.6	3.2	3.5	1.1	4.9	.3	17
DH	KURE	6.	12.	1.1		4.4		9.6	3.2	3.5	1.1	4.9	.3	8
DH	NORC	2.	4.	1.1		4.4		9.6	3.2	3.5	1.1	4.9	.3	18
DH	OSHI	7.		1.1		4.4		9.6	3.2	3.5	1.1	4.9	.3	4
DH	PANS	18		1.1		4.4		9.6	3.2	3.5	1.1	4.9	.3	2
DH	SEAT	3.	7.	1.1		4.4		9.6	3.2	3.5	1.1	4.9	.3	22
DH	TSUS	9.	3.	1.1		4.4		9.6	3.2	3.5	1.1	4.9	.3	18
EH	ADAK	-1.	3.	1.1		4.4		9.6	3.2	3.5	1.1	4.9	.3	15
EH	KURE	12.		1.1		4.4		9.6	3.2	3.5	1.1	4.9	.3	6
EH	HARC	8.		1.1		4.4		9.6	3.2	3.5	1.1	4.9	.3	2
EH	TSUS	25.		1.1		4.4		9.6	3.2	3.5	1.1	4.9	.3	12
AR	WALE	11.		1.1		4.4		9.6	3.2	3.5	1.1	4.9	.3	20
CR	WALE	1.		1.1		4.4		9.6	3.2	3.5	1.1	4.9	.3	24
CR	WALE	1.	2.	1.1		4.4		9.6	3.2	3.5	1.1	4.9	.3	24

Table B-2. Seasonally-Averaged Statistics: 13.6 kHz - Night

LOP	SITE	PPC BIAS MEAN	PPC BIAS STDV	RAND. MEAN	PPC STDV	RAND MEAN	PROP STDV	TOTAL RSS MEAN	TOTAL RSS STDV	CORR. MEAN	RSS STDV	HOURS/DAY MEAN	HOURS/DAY STDV	#SM
AC	ANCH	7.1	10.7	1.2	1.6	5.2	2.2	11.7	8.1	5.6	2.1	4.7	.9	17
AC	HOKK	10.6	8.2	2.9	4	6.3	2	20.4	8.2	7.6	3.2	4.0	.5	22
AC	MAKA	9.1	7.7	1.0	1.0	6.3	2.1	12.9	5.3	6.8	2.1	5	0	24
AC	PYRA	8.8	7	1.6	1.7	5.6	2.3	12.1	4.9	6.1	2.3	5	0	24
AC	WAHI	7	8.2	.5	.9	4.7	1.6	10.9	4.8	4.8	1.5	5	0	7
AD	ADAK	-5.7	10.9	5.8	8.8	7.2	3.1	16.6	7.1	10.2	8.2	4.3	1.3	16
AD	ANCH	8.3	17.1	2.9	3.3	6.6	2.6	19.4	7.4	7.8	3.1	4.4	1	17
AD	HOKK	-2.5	4.5	4.0	2.6	7.4	2.2	10.4	3.2	9.1	2.6	4.0	.3	22
AD	KURE	6.7	3.7	2.3	4	9.1	1.4	12.6	2.5	10.1	2.2	4.5	.8	8
AD	PANA	2.7	12.4	1.7	1.9	4.6	2.1	12	7.1	5.4	1.9	4.4	1	14
• AE	HOKK	23.2	7.8	7	8.4	6.1	2	26.5	7.5	10.6	6.9	4.4	.7	22
AE	KURE	-.6	8.2	23.5	2.4	10	1.9	27	1.5	23.6	2.4	3	.8	6
AH	ADAK	6.9	14.7	3.2	3.4	5.7	2.4	16.5	7.2	7.3	2.7	4.7	.7	17
AH	ANCH	7.7	12.8	4.9	3.6	5.8	2.6	16.1	6.5	8.1	3.5	4.7	.9	17
AH	MARC	30.3	9.3	4.7	8.1	7.9	.9	33.5	5.4	11.1	5.3	1	0	4
AH	MIYA	10.2	4.9	1.6	1.7	5.2	1.9	12.1	4.5	5.7	1.9	5	0	14
AH	OSHI	12.1	.1	1.5	.7	3.3	.3	12.6	.1	3.7	0	5	0	2
AH	TSUS	7.9	3.1	3.1	1.9	5.8	1.8	10.6	3.4	6.7	2.3	4.9	.2	21
BC	HOKK	6.7	30.2	3.5	5.4	7.8	2.1	32.1	5.6	9.4	4.2	2.9	1.6	23
BD	NOS2	8.8	.7	13.7	.2	5.2	.7	17.1	0	14.7	.4	4	0	2
BD	NOSC	4.2	5.3	23.3	3.2	4.6	1.1	24.8	3.1	23.8	3	4.6	.4	10
• BD	PANA	21.7	2.9	3.5	3.9	2.6	1.6	22.6	2.6	5	3.5	4	1	14
BD	SEAT	-1.3	6.1	17.8	12.4	5.7	4.1	22.7	6.6	21.4	7.9	3.3	1.6	18
BE	MARC	34.1	3.5	10.1	5.2	3	1.2	36.2	1.7	10.5	5.3	2	0	2
BF	NELC	1.4	1.3	20.3	0	7.1	.2	21.6	0	21.5	.1	5	0	2
BH	MARC	-17.3	.3	1.4	1.4	7.3	.5	18.9	0	7.6	.8	2	0	2
CD	ADAK	-6.9	14.8	2.3	2.7	7.6	3.3	17.4	6.9	8.2	3.6	4.7	.8	21
CD	ANCH	1.6	8.6	1.5	1.6	5.7	2.7	10.8	2.4	6.1	2.8	4.9	.2	17
CD	MAKA	-2.5	2.1	1.1	1	2.9	1.8	4.6	2	3.3	1.8	5	0	24
CD	MARC	-4.5	2.8	0	0	9.2	5.5	10.4	6	9.2	5.5	1	0	4
CD	NELC	7.8	7.8	1.2	1	1.9	1	8.7	7.3	2.3	1.3	5	0	4
CD	NOS2	2.2	.6	.8	.6	1.1	.2	2.7	.3	1.4	.1	5	0	2
CD	NOSC	1.1	1.8	1.1	1.1	1.1	.5	2.7	1.2	1.7	1.1	5	0	10
CD	PANA	-13.6	9.1	3.5	2.7	2.1	1.3	16.6	4.1	4.7	2	4.3	1.1	16
CD	SEAT	1.3	2.4	.9	1	1.9	.8	3.6	1.2	2.3	1.1	5	0	22
CD	WAHI	-4.2	5.5	.4	.4	2	1	5.9	4.3	2.1	1	5	0	8
CE	ADAK	3.6	9	14.3	4.6	5	1.4	18.1	4.3	15.6	2.9	4.8	.5	13
CE	HOKK	7.4	3	11.7	5.6	2.9	1.1	14.0	4.8	12.2	5.5	5	0	24
CE	KURE	.7	7	9.3	4.3	9	2	14.9	4.1	13.3	3.5	3.8	.9	10
CE	NOSC	1.9	12.8	10.1	11.1	6.8	2.1	24.8	7.7	20.7	8.6	3.3	1.4	17
CE	SEAT	-13.6	10	5.6	8	11.1	2.5	22.3	3.6	14.1	4.9	1.7	.8	8
CF	MAKA	-.2	13.7	18.9	7.7	5.1	1.9	24.0	4.6	19.8	7.2	3.9	1.1	10
CF	PANA	-17.8	6.3	6.9	9.2	2.4	2.1	21.9	4.6	8	8.8	4	1.5	16
CF	WAHI	-2.5	10.6	21.4	2.3	5.9	2.3	24.9	2.1	22.3	1.9	3.3	.9	8
CH	ADAK	8.4	7.6	3.8	3.4	1.6	.8	10.1	7.5	4.4	3.3	4.8	.3	19
CH	ANCH	5.9	4	4.9	3.3	2.[illegible]	1.3	9.2	3.4	5.9	3.2	5	0	17
CH	HOKK	-2.0	3.3	2.5	2.5	2.3	.8	5.2	3.3	3.8	2.1	5	0	24
CH	KURE	1.6	1.1	.5	.4	2.4	.3	3.1	.8	2.4	.4	5	0	10
CH	MAKA	9.5	5.6	5.3	3.6	2.9	2	11.7	6.2	6.4	3.6	5	0	22
CH	MIYA	-8.2	4	3.7	2.2	2.9	.8	9.8	3.8	5.1	1.3	5	0	14
CH	NOS2	7.9	.8	3	.7	2.1	.3	8.7	.5	3.7	.4	5	0	2
CH	NOSC	13.5	6.9	3.6	2.7	2.5	1.6	14.8	6.3	4.9	2.4	5	0	10
CH	OSHI	4.3	.8	1.8	.6	1.2	.3	4.9	.3	2.2	.7	5	0	2
CH	SEAT	8.3	7.5	4.4	3.7	5	2.6	12.8	5.1	7.4	3.3	4.6	.6	22
CH	TSUS	-1.2	3.3	2.4	1	2.9	2.4	5.1	2.6	4	2.1	5	0	22
CH	WAHI	7.3	2.7	10.3	5.2	3.3	2.5	13.9	4.5	10.9	5.6	4.8	.3	10
DF	NOS2	-13.4	1.5	6.7	1.1	3.2	0	15.4	.8	7.5	1	5	0	2
DF	NOSC	-9.2	1.7	2.6	1.6	3	.5	10.1	1.9	4.2	1	5	0	10
DF	SEAT	7.6	13.6	2.7	2.7	9.9	2.2	18.5	4.5	10.7	1.6	2.8	1.2	12
DH	ANCH	4.5	8.6	3.7	4	5.4	2.7	11.2	6	7.1	4	4.8	.3	17
DH	KURE	4.3	3.8	1.4	2.1	10.4	1.1	12.1	1.9	10.7	.9	4.2	1.2	8
DH	NELC	4.6	.5	2.1	.4	1.7	.2	5.4	.2	2.7	.4	5	0	2
DH	NOS2	5.6	.1	2.3	.1	2	.1	6.4	.1	3.1	0	5	0	2
DH	NOSC	12.3	7.2	3.3	2.2	2.7	1.4	13.5	6.9	4.6	1.9	5	0	18
DH	OSHI	-2.7	.8	1.7	.7	3.1	.3	4.6	0	3.5	.6	5	0	2
DH	SEAT	6.8	7.5	3.9	3.2	3.7	2.2	10.9	5.3	5.8	3.1	4.5	1.1	22
• DH	TSUS	26.3	8.6	5.6	5.2	7.1	1.7	28.4	8.4	9.8	3.9	4.5	1	20
EF	NELC	-8.6	2	21.9	.1	7.0	0	24.8	.8	23.2	.1	4	0	2
EH	ADAK	.7	6.7	17.2	8.6	4.6	2.4	20.2	5.8	18.7	6.9	4.1	.7	15
EH	KURE	-.8	5.3	8.2	3.6	7	2	12.5	2.8	11.3	2.6	2.8	.4	10
EH	MARC	-8.8	9.8	0	0	2.4	1	11.1	7.5	2.4	1	1	0	4
EH	MIYA	-9.3	3.1	4	1.6	1.5	.3	10.5	2.8	4.5	1.3	5	0	14
EH	OSHI	-9.5	.2	7.3	0	1	.2	12	.1	7.4	0	5	0	2
EH	TSUS	-11.1	10.3	18.5	7.7	2.1	.6	24.3	6.9	18.6	7.7	4.8	.3	12
AR	WALE	3.8	2.9	.5	.9	3.5	1.2	6.1	1.3	3.7	1.2	4.1	1.2	12
CR	WALE	-2.6	1.8	.6	1	1.7	.6	3.6	1.4	1.9	.9	4.5	1.2	18
CR	WALE	-2.6	1.8	.6	1	1.7	.6	3.6	1.4	1.9	.9	4.5	1.2	18

Table B-3. Seasonally-Averaged Statistics: 10.2 kHz - Day

LOP	SITE	PPC MEAN	PPC STDV	BIAS MEAN	BIAS STDV	RAND. MEAN	RAND. STDV	PPC MEAN	PPC STDV	RAND MEAN	RAND STDV	PROP MEAN	PROP STDV	TOTAL MEAN	TOTAL STDV	RSS MEAN	RSS STDV	CORR. MEAN	CORR. STDV	RSS MEAN	RSS STDV	HOURS/DAY MEAN	HOURS/DAY STDV	#SM
AC	ANCH	8.1	6.7			1.4								18.3		5.		4.7				3	0	16
AC	HOKK	13.3	6.7			2.								15.1				6.4				4.9	.3	28
AC	MAKA	9.4	7.5											12.5									0	34
AC	MARC	4.2	9.4			1.								16.5									1	4
AC	PYRA	8.6	6.8											11.6									1	32
AC	WAHI	-3.2	8.9											7.								4.3	0	7
AD	ADAK	-3.5	9.1											11.7								4.6	0	13
AD	ANCH	17.1	12.4			1.								18.9								4.6	.5	16
AD	HOKK	-2.3	4.3			1.								8.									0	28
AD	KURE	8.3	2.6																				0	6
AD	PANA	10.7	6.9			1.								12.								4.7	.7	14
AE	HOKK	21.2	7.2			11.																4.6	0	28
AE	KURE	30.9	9.3											31.										4
AH	ADAK	11.5	6.3			6.								13.								4.4	0	16
AH	ANCH	13.8	5.1											18.									0	16
AH	OSHI	14.4	6.1											15.									0	2
AH	TSUS	7.7	5.6											10.									1	16
BC	HOKK	20.5	8.3											29.								4.3	.5	21
BD	NOSC	-.6																				4.4	.6	18
BD	PANA	24.3	1.8											25.								4.4	.3	14
BD	SEAT	6.1	8.4											1.								4.	.7	22
BE	MARC	12.8	10.2											21.									0	4
BH	MARC	-11.9	17.2											31.									0	4
BH	OSHI	11.3	8.1											15.									0	2
CD	ADAK	-6.2	12.1											14.									0	19
CD	ANCH	9.6												11.									0	17
CD	MAKA	-3.8	2.2											5.									0	32
CD	MARC	-24.8												25.								1.	.5	4
CD	NOSC	.2	1.6											2.									0	18
CD	PANA	-21.4	6.7			5.								22.								4.	.5	14
CD	PYRA	-36.5	2.8			4.								37.									0	8
CD	SEAT	6.5	8.1			1.								9.									0	22
CD	WAHI	-1.7	1.5											3.									0	8
CE	ADAK					21.								23.								4.	.5	13
CE	HOKK	10.7				14.								20.								4.	.5	22
CE	KURE	13.9				6.								16.								4.	.2	8
CE	NOSC	-3.8	9.8			10.								22.								4.	.7	17
CE	SEAT	-33.7	9.3			3.								35.								4.	.7	13
CF	MAKA	-18.9	3.			13.								24.								4.	.4	16
CF	PANA	-21.3				4.								22.								4.	.5	14
CF	WAHI	-16.8	8.			12.								23.								4.	.5	8
CH	ADAK	8.8	10.4			4.								11.								4.	.5	19
CH	ANCH	8.9	4.											11.										17
CH	HOKK	-1.3												4.										22
CH	KURE	.5												3.								4.	.5	8
CH	MAKA	5.2	1.3			4.								8.								4.	.5	20
CH	NOSC	13.2				4.								14.										18
CH	OSHI	-4.5	2.			6.								8.										4
CH	SEAT	13.4	10.			5.								17.								4.	.5	22
CH	TSUS	-.4				2.								7.								4.	.5	28
CH	WAHI	.8	4.			6.								11.										18
DF	NOSC	-13.1	1.7			1.								13.										18
DF	SEAT	-8.3	7.1			2.								10.								4.	.5	28
DH	ANCH	-.3	8.2			4.								11.										17
DH	KURE	.6	2.											6.										6
DH	NOSC	13.7	7.4			2.								14.										18
DH	OSHI	3.4	1.6			1.								8.										4
DH	SEAT	8.3	6.			3.								12.								4.8	.5	22
DH	TSUS	17.2	10.			3.								20.								4.8	.5	18
EH	ADAK	-6.5	5.			20.								24.								4.7	.5	17
EH	KURE	-12.6	2.1			6.								14.								4.5	.3	6
EH	MARC	-9.4	21.			14.								30.										4
EH	TSUS	-12.	10.			21.								28.								4.8	.5	12
AR	WALE	11.4	5.											12.								4.5	.5	28
CR	WALE	1.9	3.											4.								4	1.7	24
CR	WALE	1.9	3.											4.								4	1.7	24

Table B-4. Seasonally-Averaged Statistics: 13.6 kHz - Day

APPENDIX C: PREDICTED (10.2 kHz) SIGNAL THRESHOLD AND MODAL INTERFERENCE BOUNDARIES IN THE NORTH PACIFIC

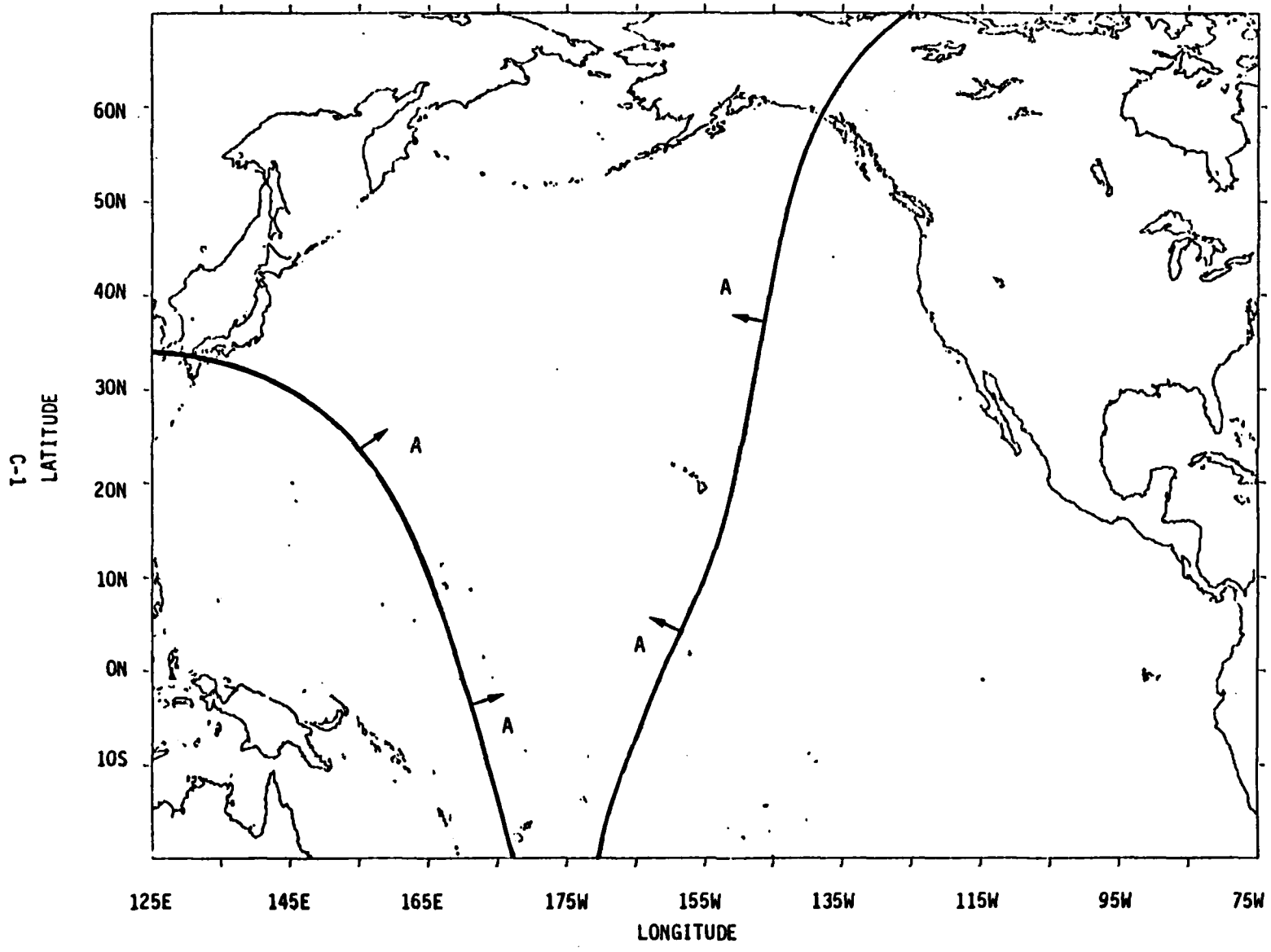

FIGURE C-1. Omega Norway Predicted Signal Threshold Boundary (-20 dB)

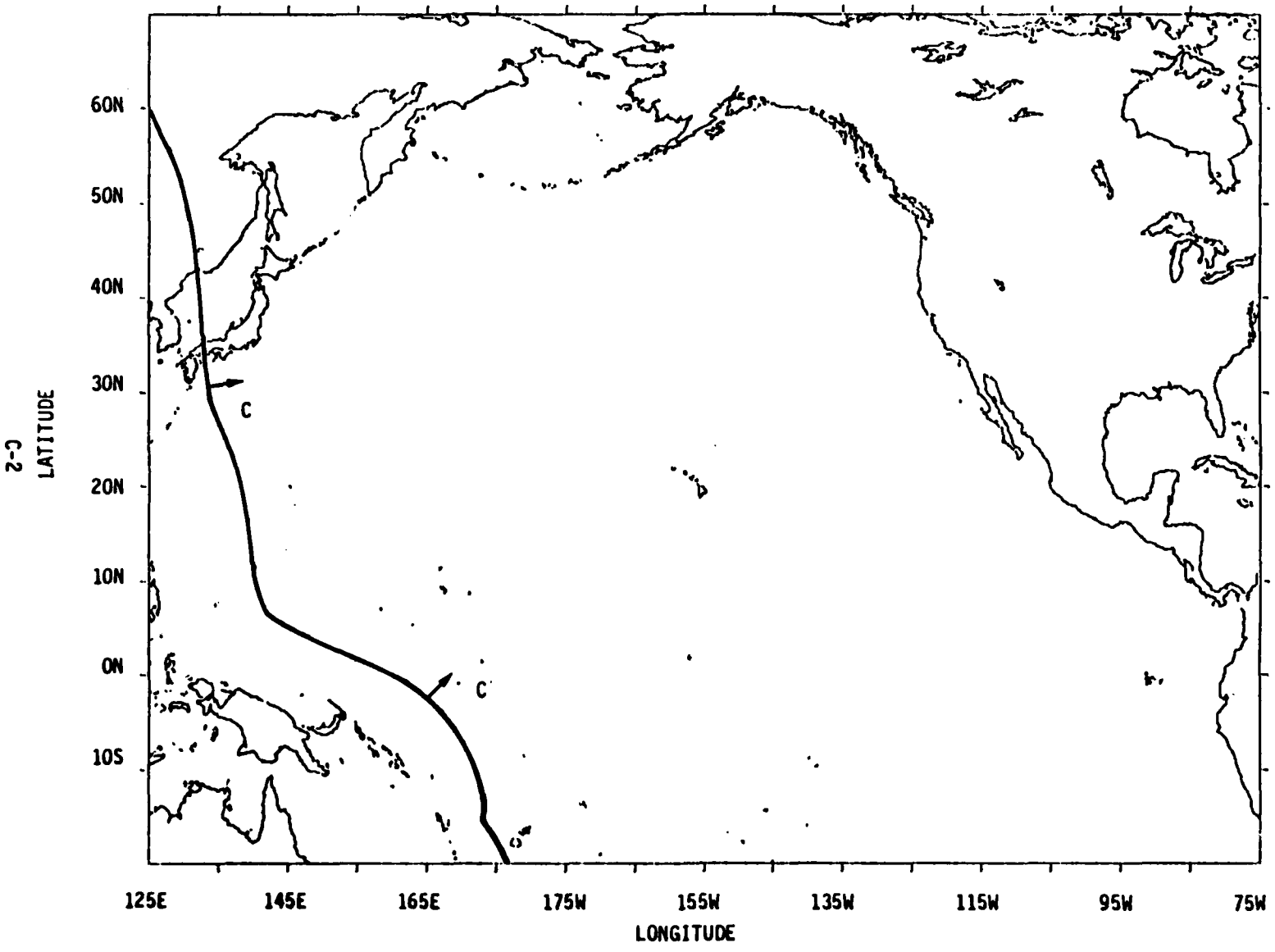

FIGURE C-2. Omega Hawaii Predicted Signal Threshold Boundary (-20dB)

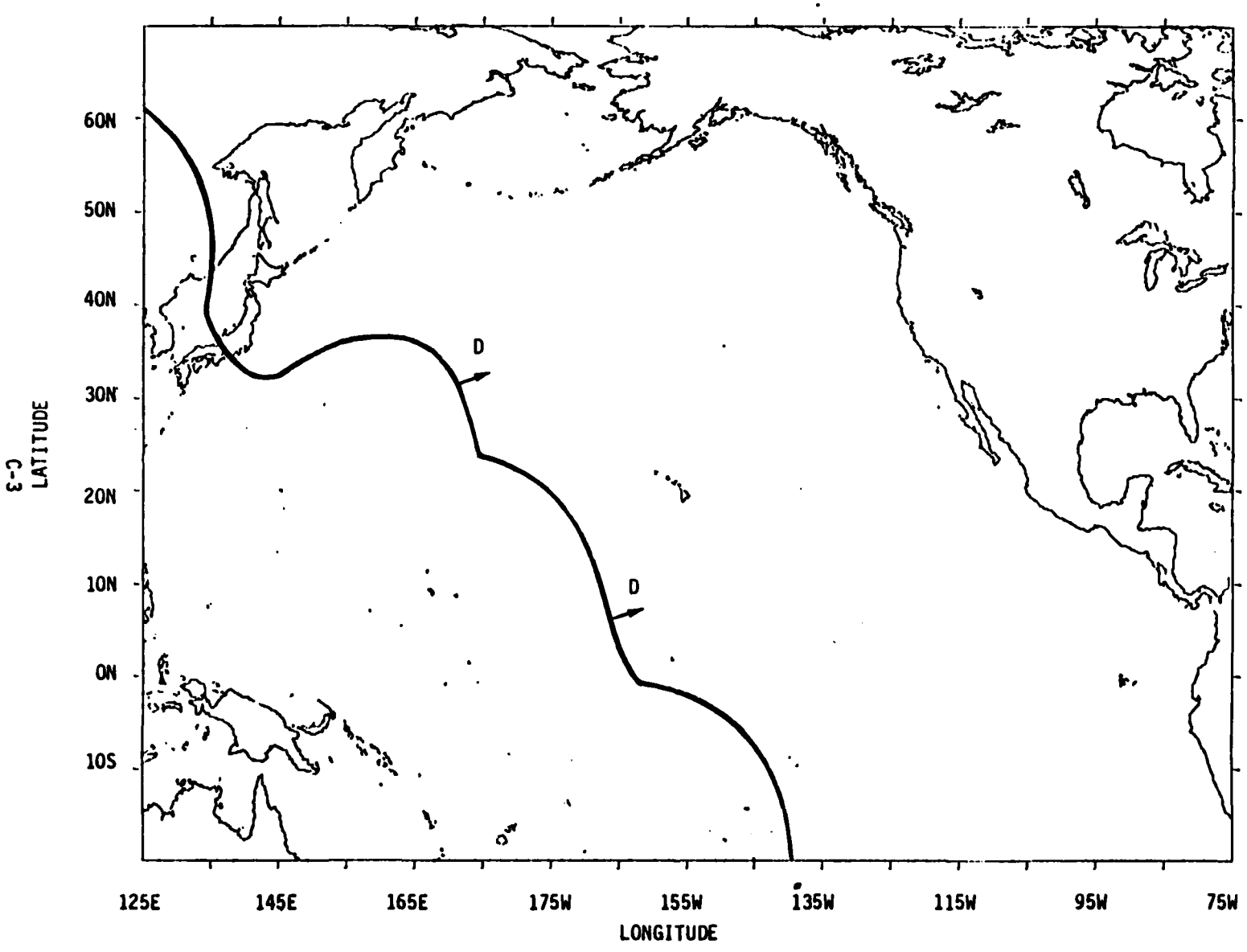

FIGURE C-3. Omega North Dakota Predicted Signal Threshold Boundary (-20dB)

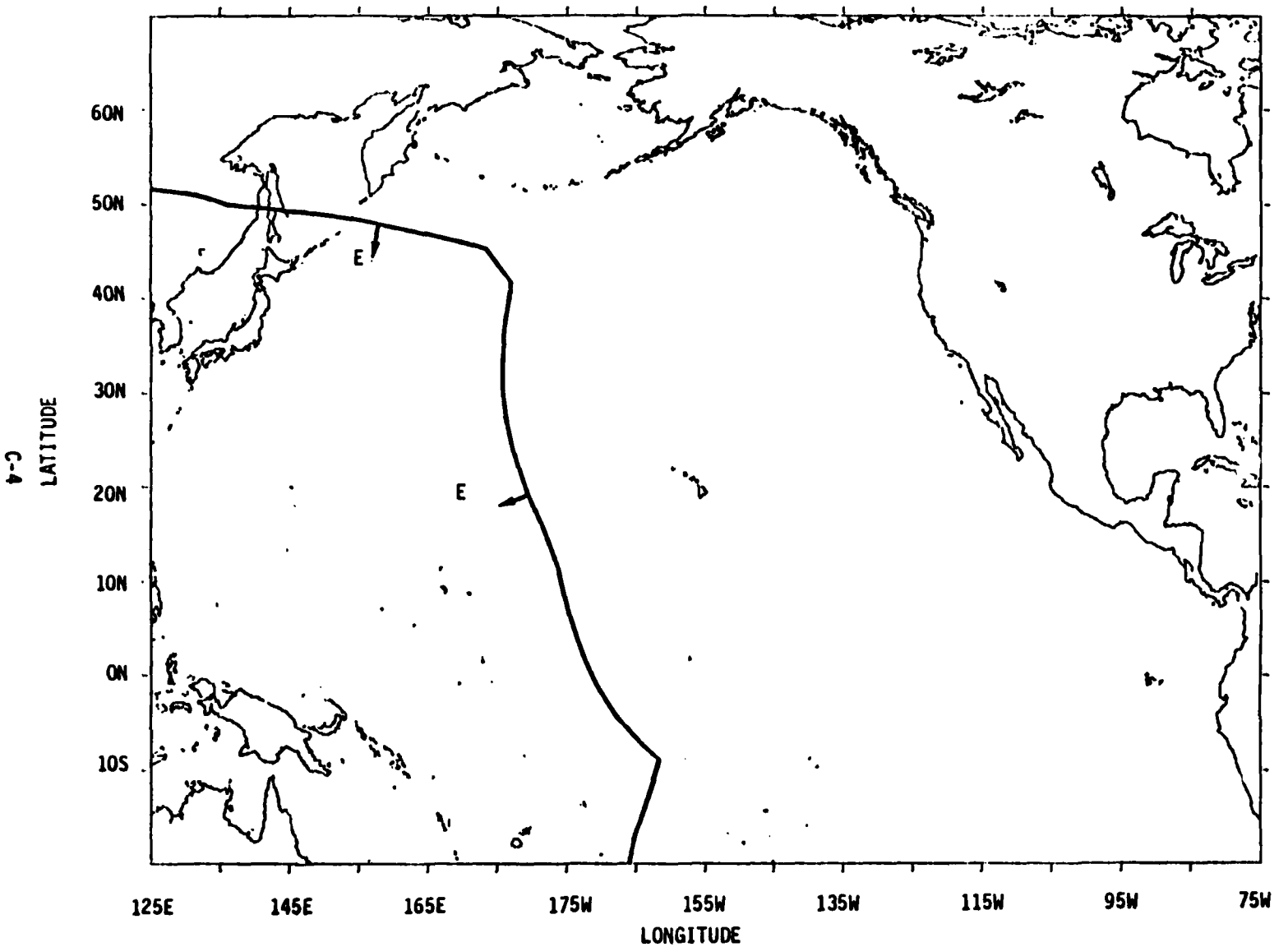

FIGURE C-4. Omega La Reunion Predicted Signal Threshold Boundary (-20dB)

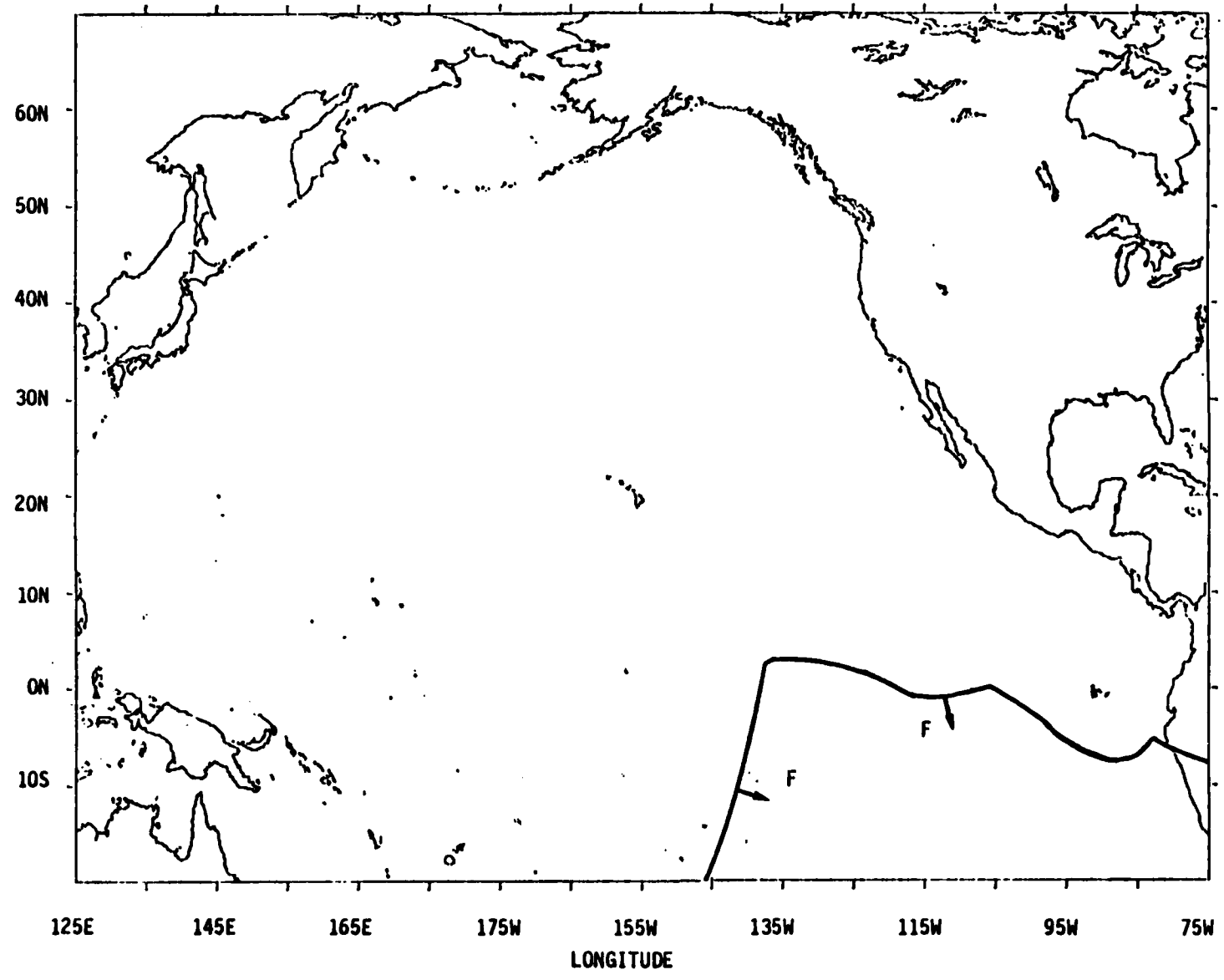

FIGURE C-5. Omega Argentina Predicted Signal Threshold Boundary (-20dB)

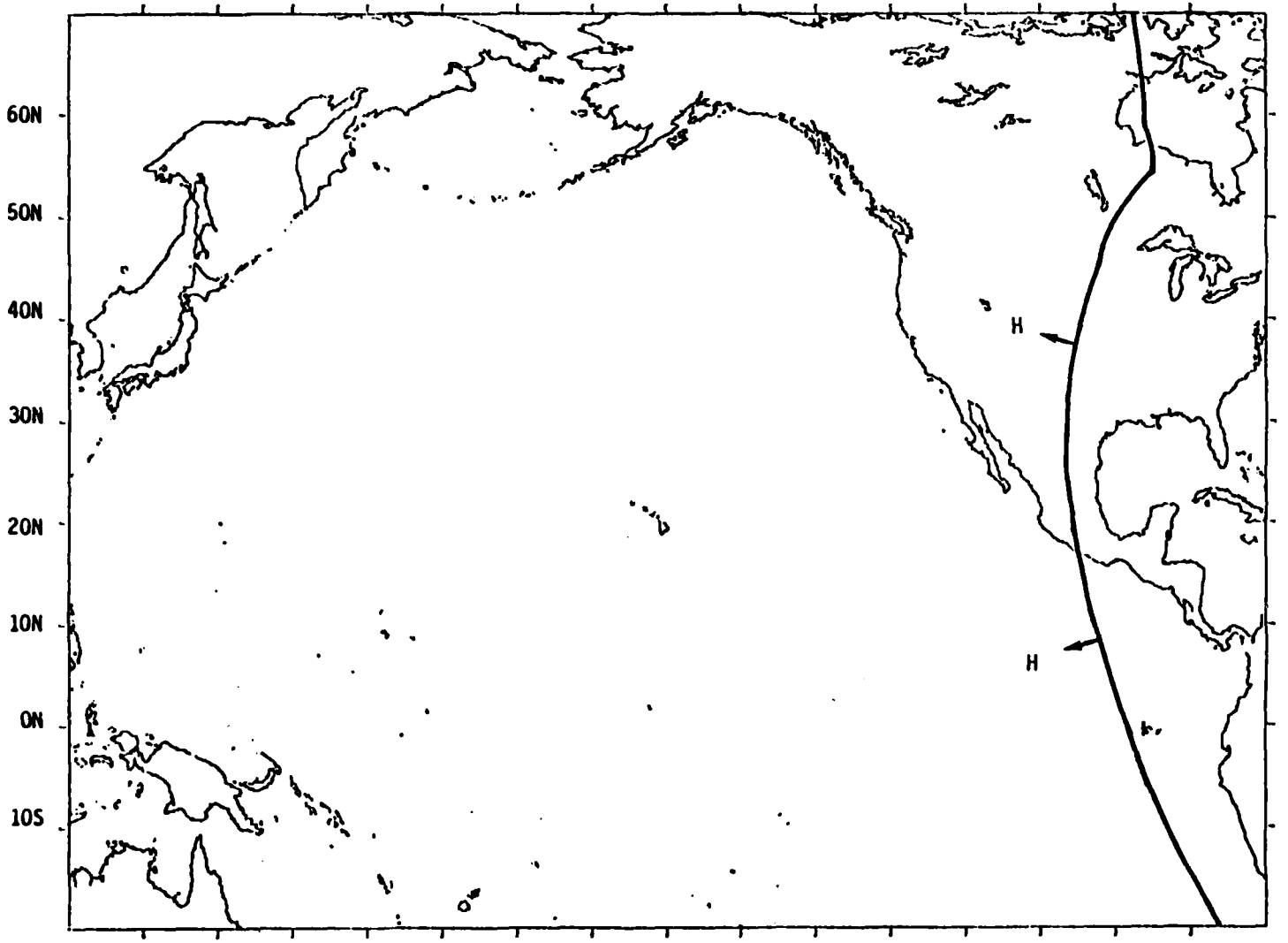

FIGURE C-6. Omega Japan Predicted Signal Threshold Boundary (-20dB)

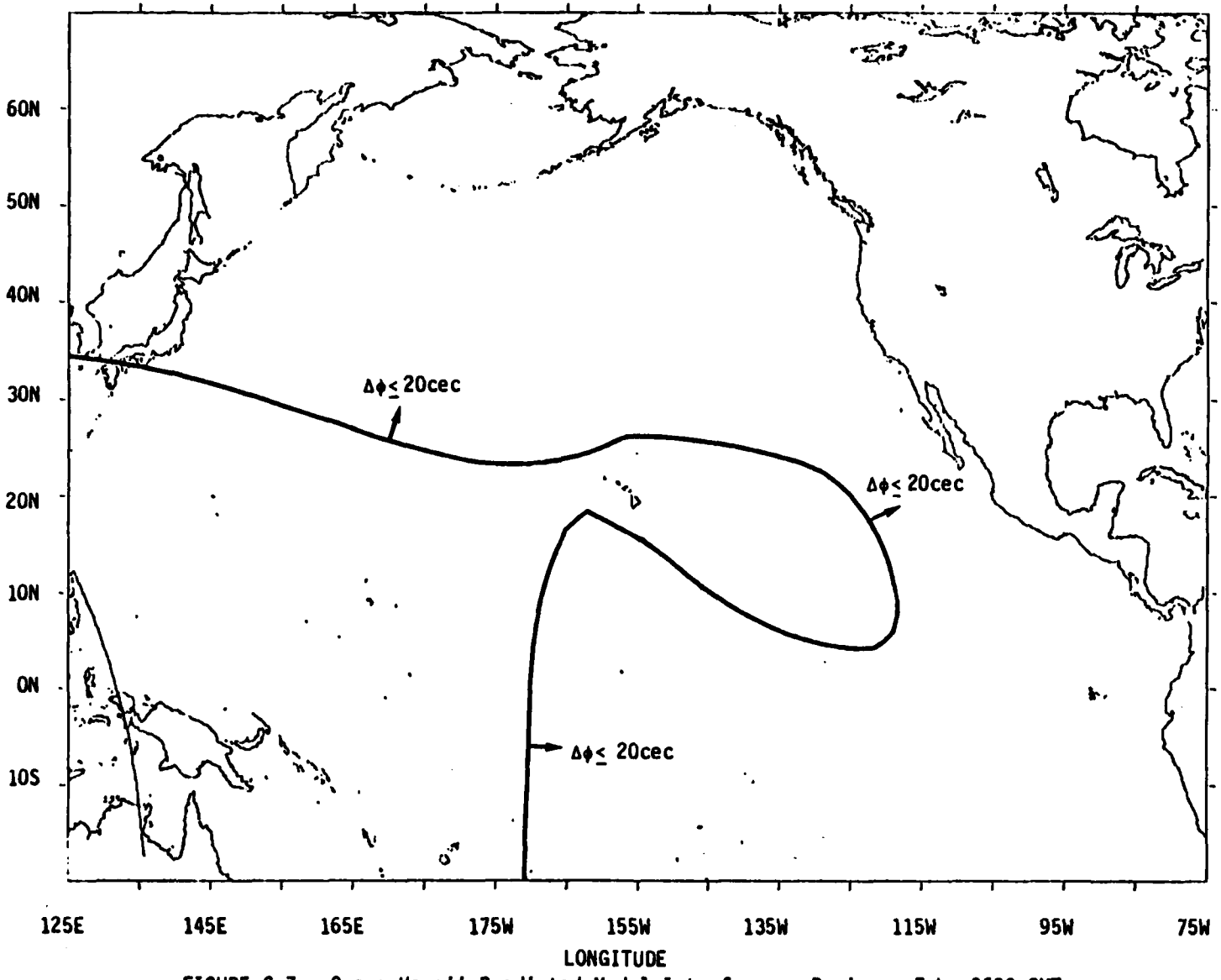

FIGURE C-7. Omega Hawaii Predicted Modal Interference Region - Feb. 0600 GMT

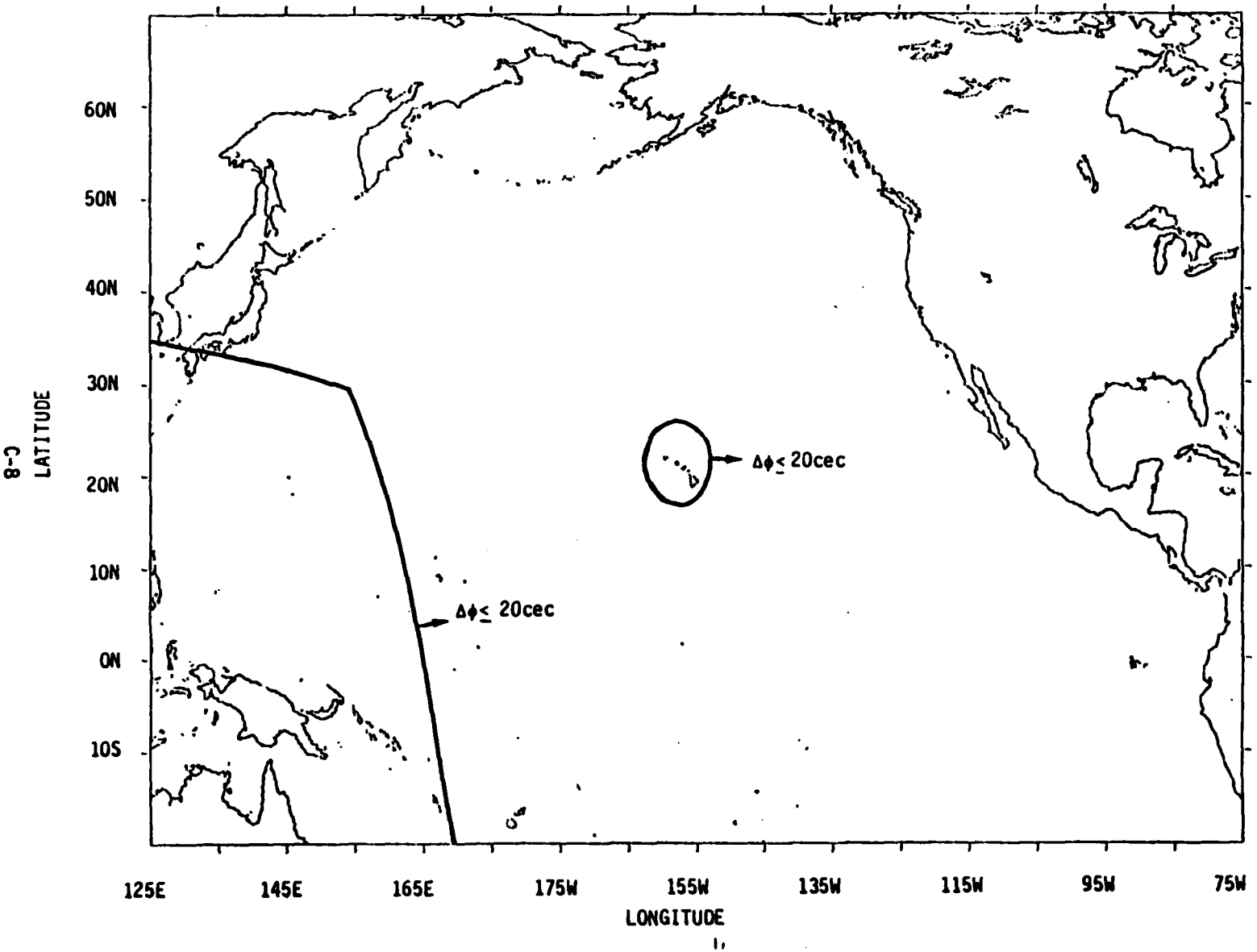

FIGURE C-8. Omega Hawaii Predicted Modal Interference Regions - Aug. 1800 GMT

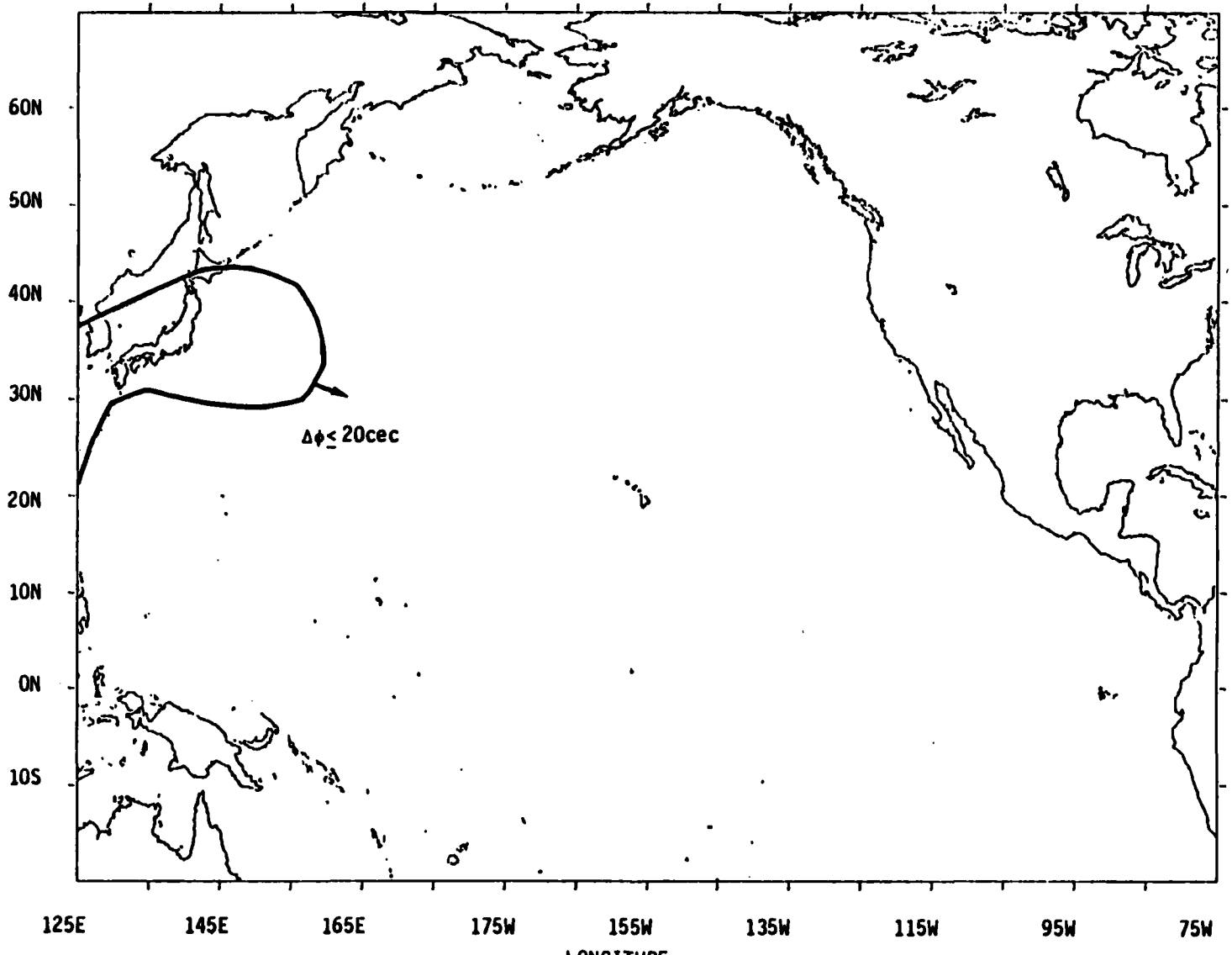

FIGURE C-9. Omega Japan Predicted Modal Interference Region - Feb. 1800 GMT

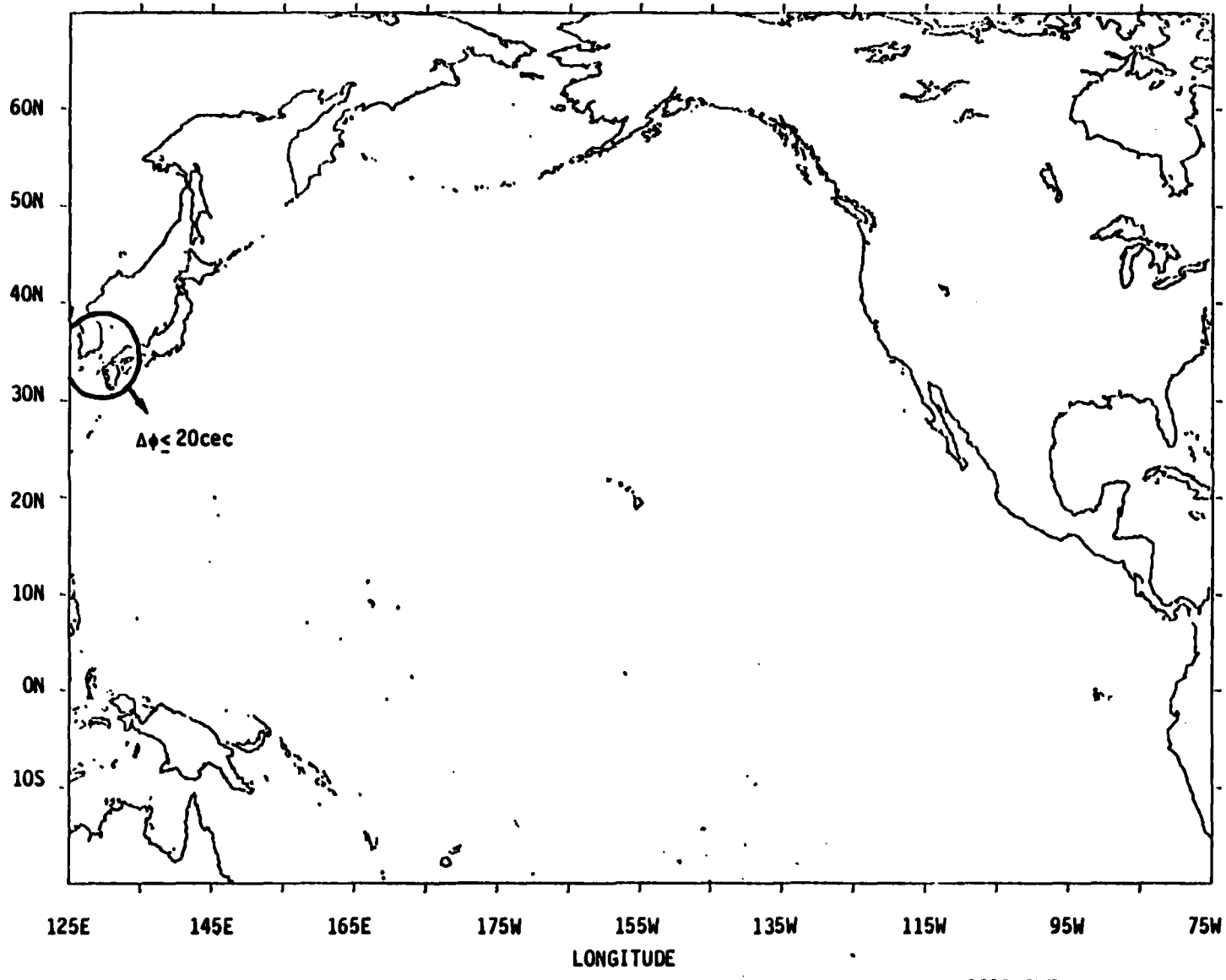

FIGURE C-10. Omega Japan Predicted Modal Interference Region - Aug. 0600 GMT

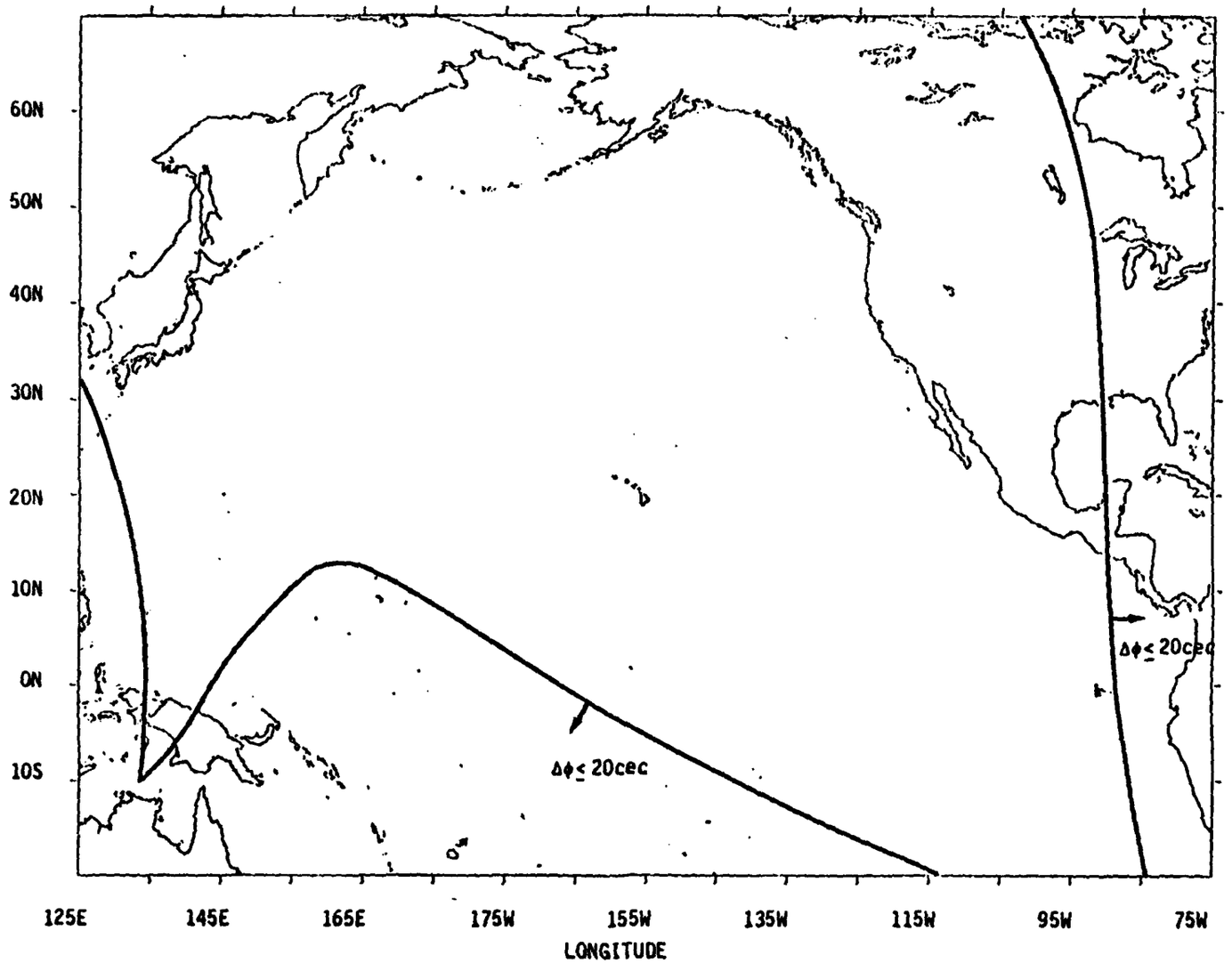

FIGURE C-11. Omega Argentina Predicted Modal Interference Region - Feb. 0600 GMT

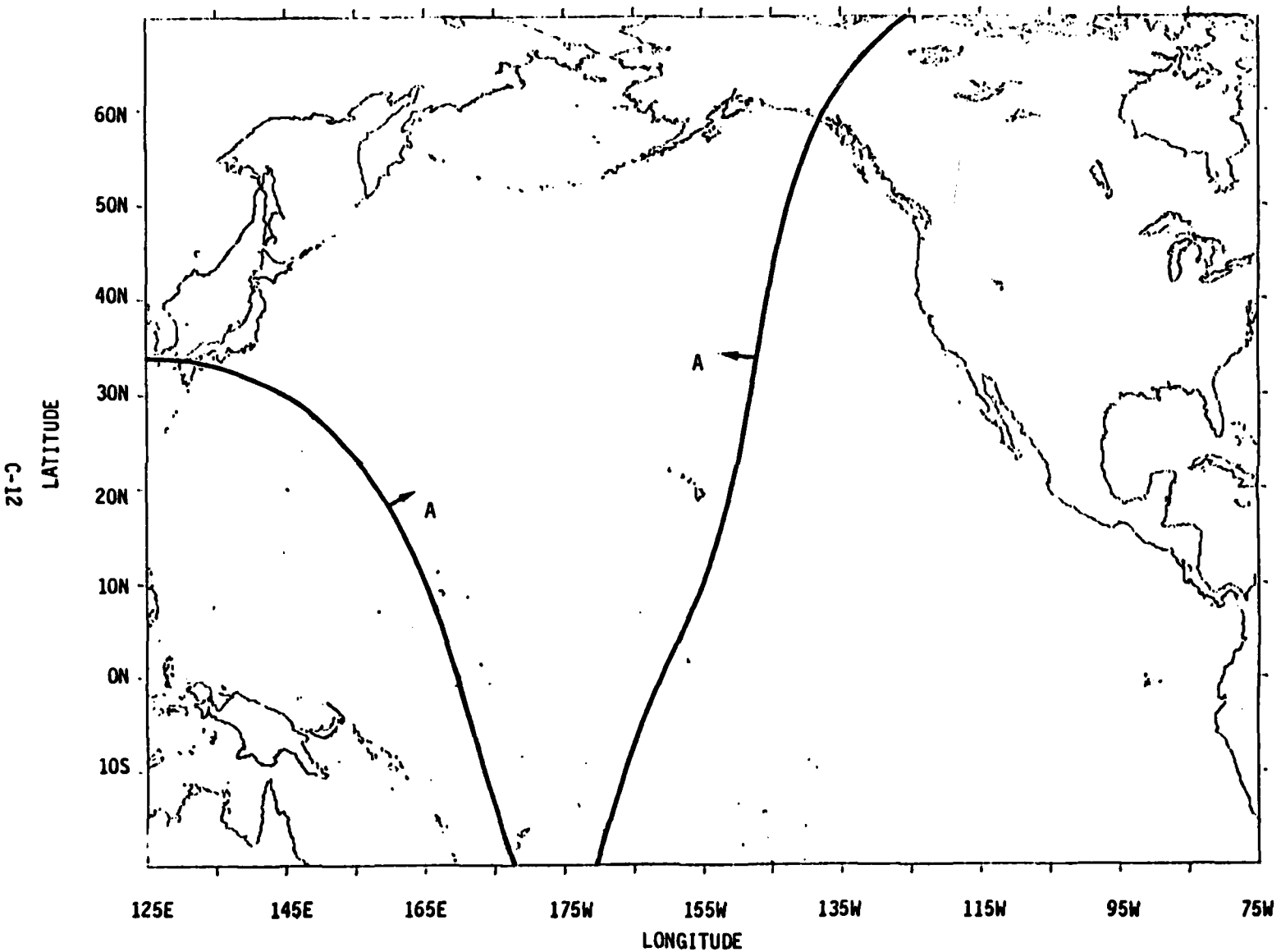

FIGURE C-12. Omega Norway Predicted All-Time Signal Coverage Contour

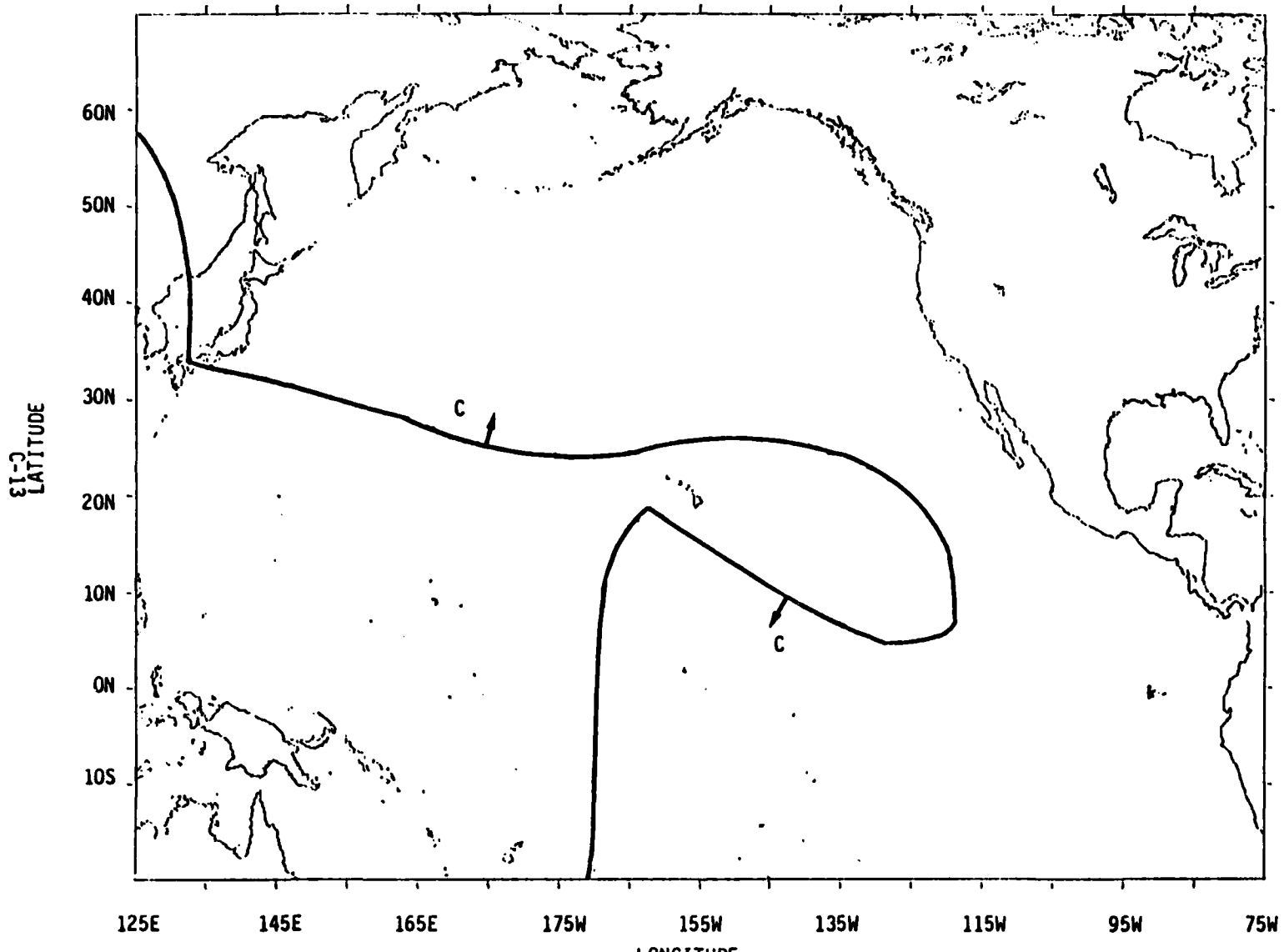

FIGURE C-13. Omega Hawaii Predicted All-Time Signal Coverage Contour

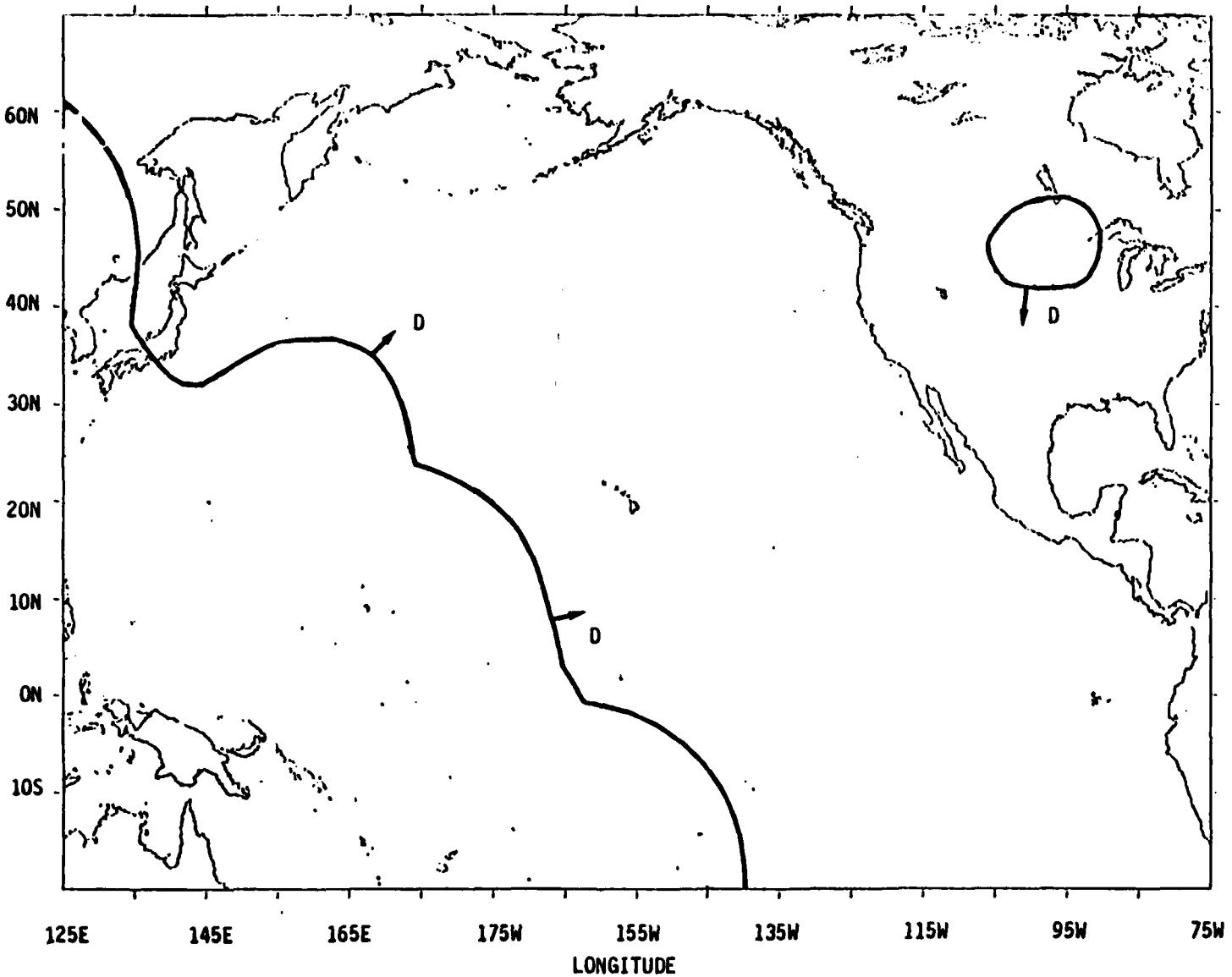

FIGURE C-14. Omega North Dakota Predicted All-Time Signal Coverage Contour

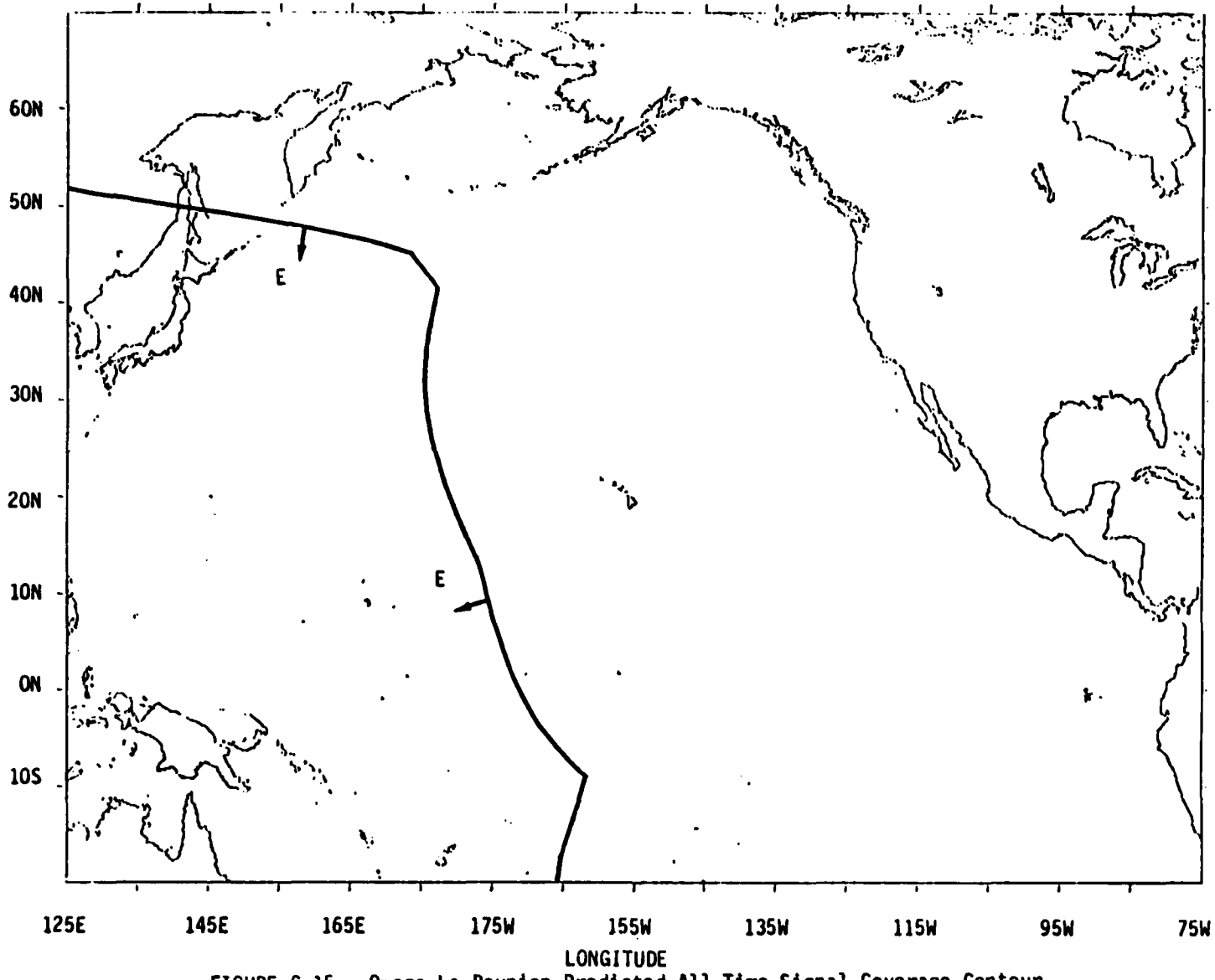

FIGURE C-15. Omega La Reunion Predicted All-Time Signal Coverage Contour

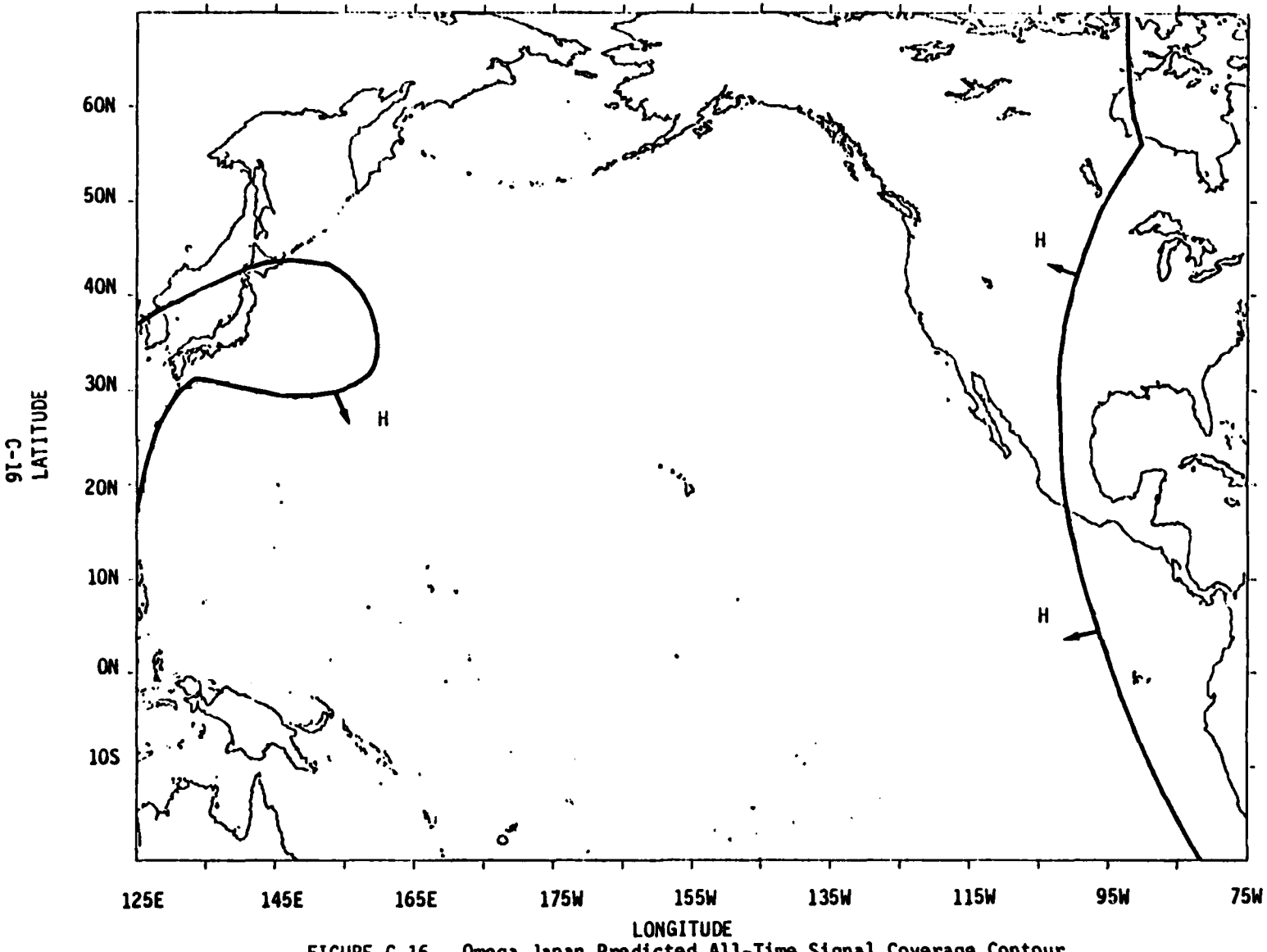

FIGURE C-16. Omega Japan Predicted All-Time Signal Coverage Contour

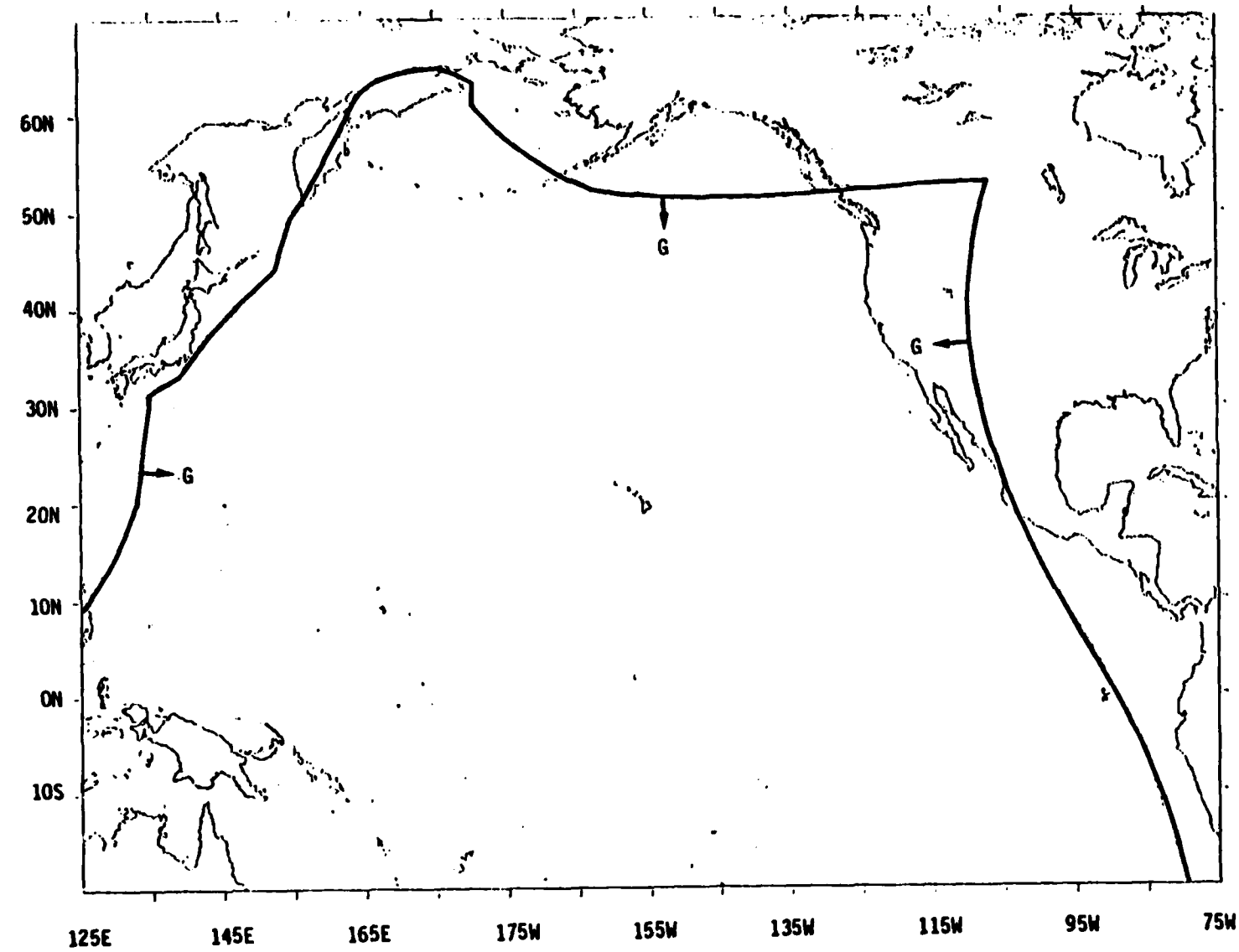

FIGURE C-17. Omega Australia Predicted Signal Threshold Boundary (-20dB) and All-Time Signal Coverage Contour

APPENDIX D: NOSC AIRBORNE AND FIXED MONITOR DATA EXAMPLES

FIGURE D-1. Sample Time Plot Marked With Predicted and Observed Locations of Contour Crossing

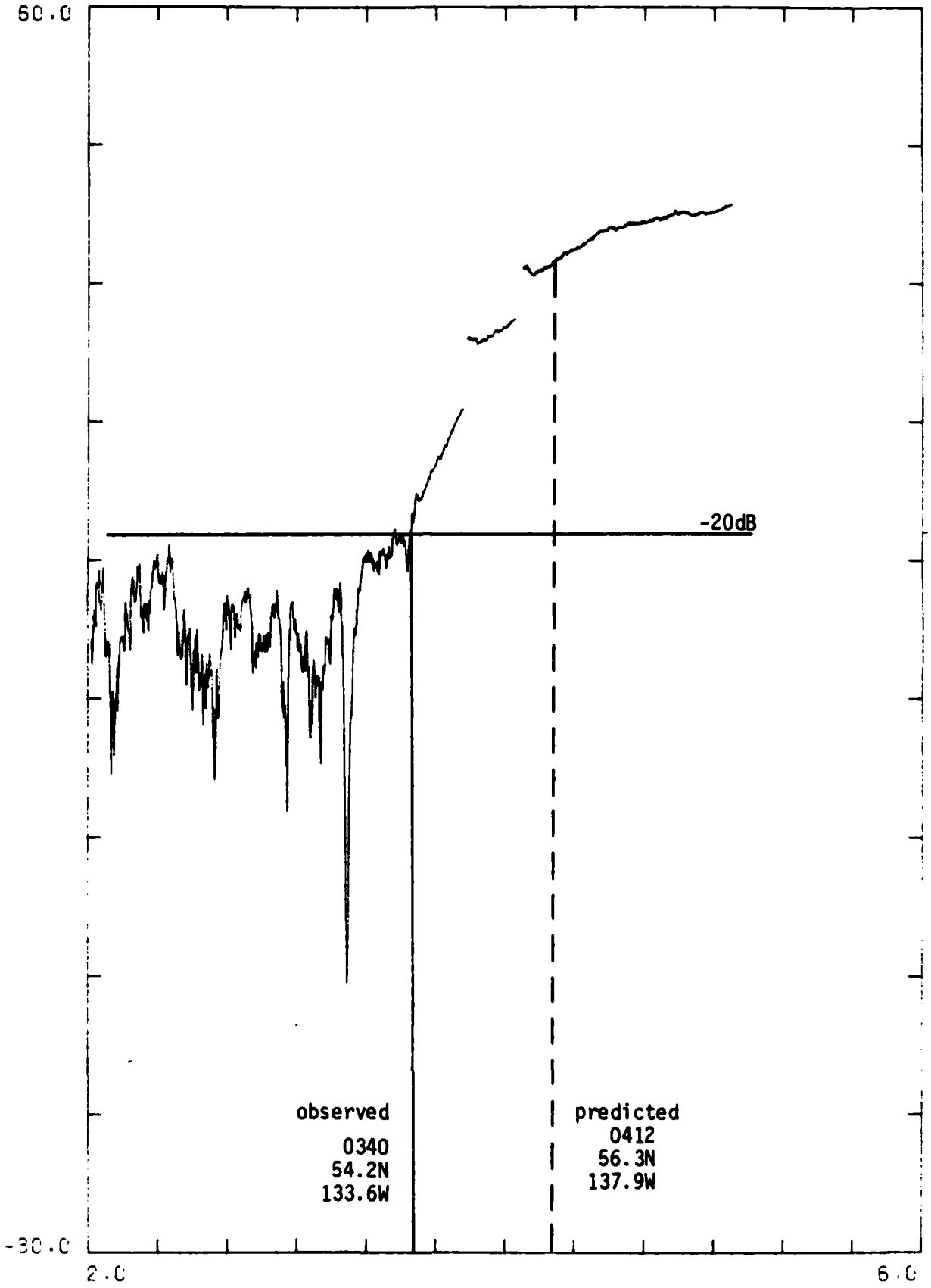

END OF FRAME 1 0 MINUTES

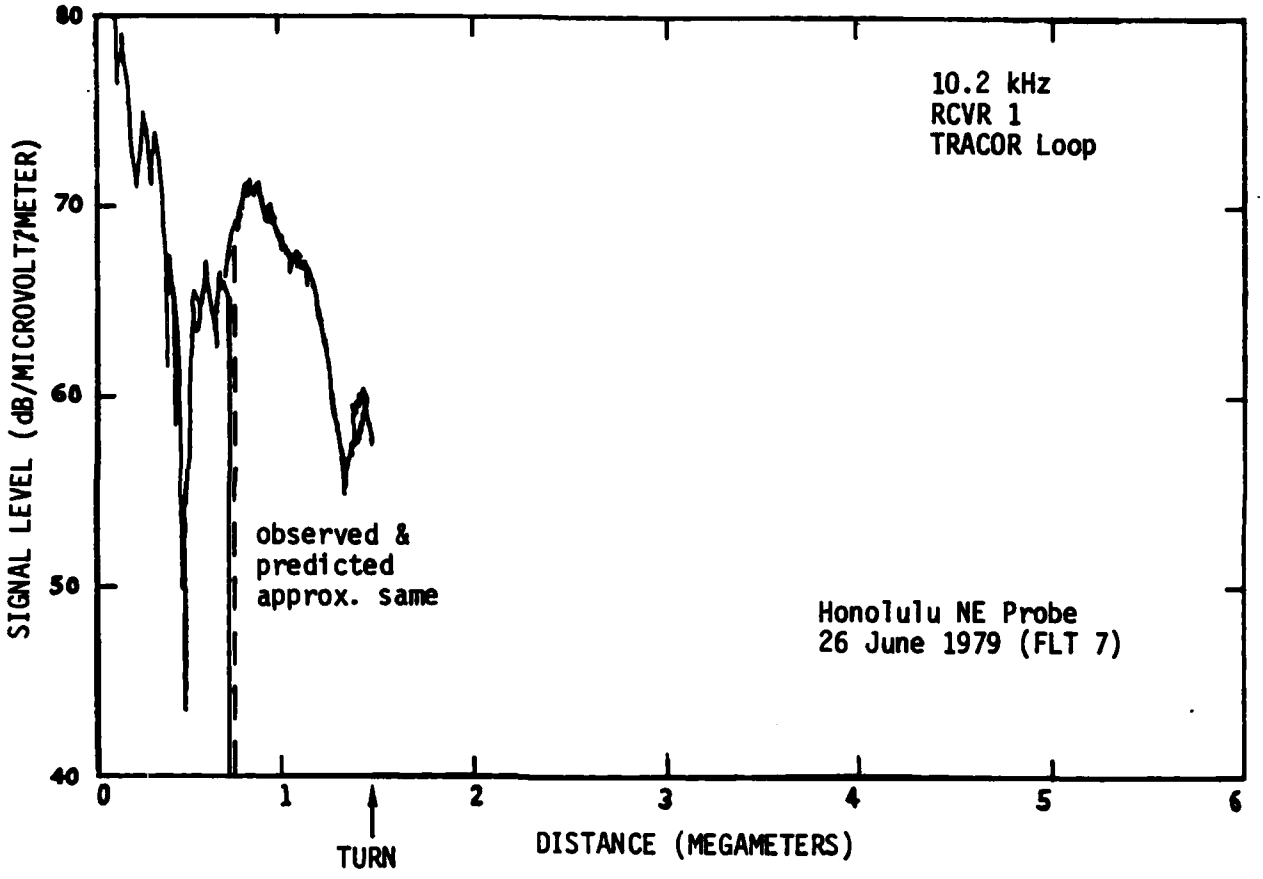

FIGURE D-2. Sample Radial Plot Marked With Predicted and Observed Locations of Contour Crossing

Omega	Flight No.	Route	T-time R-radial Plot Type	Day
NORWAY	7	Hawaii to Hawaii	T	26 Jun 79
	8	Hawaii to Hawaii	T	27 Jun 79
	18	Anchorage to Juneau	T	10 July 79
	29	Seattle to Anchorage	T	2 Oct 79
Hawaii	6	Wake to Honolulu	R	23 Jun 79
	7	Hawaii to Hawaii	R	26 Jun 79
	8	Hawaii to Hawaii	R	27 Jun 79
	9	Honolulu to Midway	R	28 Jun 79
North Dakota	5	Midway to Wake	T&R	22 Jun 79
	22	Fargo to San Diego	T&R	22 Sept 79
La Reunion	6	Wake to Honolulu	T&R	23 Jun 79
Japan	22	Fargo to San Diego	T	22 Sept 79
	23	San Diego to Mexico City	T&R	22 Sept 79

Table D-1. NOSC Test Flights Traversing Predicted All-Time Signal Coverage Boundaries

		Predicted			Observed		
OMEGA	Flight No.	GMT	LAT	LONG	GMT	LAT	LONG
A	7	0820	28.5	149.	0820	28.6	148.6
	8	1300	18.7	152.9	1310	18.	151.7
	18	2330	59.	137.	2355	57.5	131.6
	29	0412	56.3	137.9	0340	54.2	133.6
D	5	0930	26.1	174.2E	0948	24.5	172.3E
	22	0242	42.5	105.	0220	44.4	101.9
H	22	0155	46.3	98.3	0310	40.1	108.4
	23	0112	22.	101.9	0130	20.5	100.

Table D-2. Predicted and Observed Locations of Contour Crossings by NOSC Test Flights

	GMT					
A - Norway	200	600	1000	1400	1800	2200
Adak	-4	-2	-5	-4	-2	-2
Kauai	-15	-15	-8	-10	-13	-12
Wake	-17	-16	-17	-14	-18	-14
San Diego						
Whidbey						
Juneau	--	-12	-8	-7	-8	-13
Anchorage	-2	-2	0	2	3	3
Midway	0	2	4	5	-2	-5
C - Hawaii						
Adak	5	6	6	8	8	7
Kauai						
Wake	1	-2	-2	0	-4	3
San Diego	5	10	11	11	11	3
Whidbey	5	12	14	13	14	6
Juneau	--	6	12	10	9	5
Anchorage	6	6	10	11	10	6
Midway	12	10	9	10	14	17
D - North Dakota						
Adak	-5	-2	2	7	3	4
Kauai	-7	-1	3	-5	-5	-4
Wake	-18	-15	-11	-17	-19	-13
San Diego	5	11	12	11	11	4
Whidbey	7	15	17	15	17	9
Juneau	--	9	13	12	11	6
Anchorage	1	3	3	4	5	1
Midway	2	5	7	3	3	7
E - La Reunion						
Wake	11	9	10	6	4	3
Kauai	-14	-11	-3	-1	-1	-3
H - Japan						
Adak	8	11	7	14	11	9
Kauai	4	5	10	12	5	7
Wake	8	9	9	12	10	12
San Diego	-8	-2	4	3	-2	-10
Whidbey	-6	-1	5	6	2	5
Juneau	--	-4	-2	-6	-2	-5
Anchorage	6	4	6	13	8	5
Midway	7	9	11	14	10	11

Table D-3. Estimated SNR Levels Observed at NOSC Fixed-Sites, Summer 1979

APPENDIX E: AED PLOTS COMPARING SIGNAL COVERAGE/MODAL INTERFERENCE OBSERVED WITH INTEGRATED SATELLITE/OMEGA RECEIVERS AND PREDICTED ALL-TIME COVERAGE CONTOURS

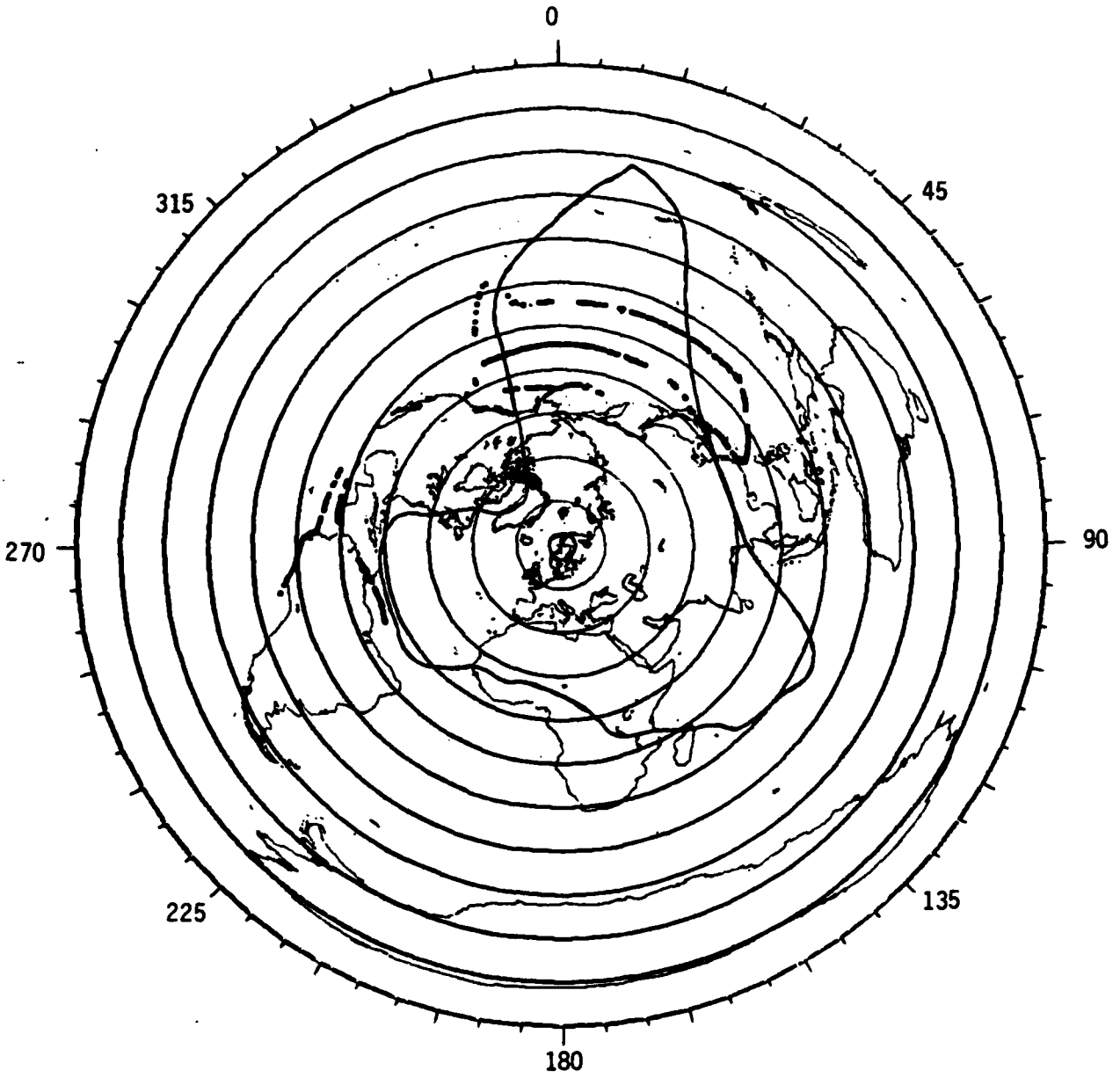

FIGURE E-1. Comparison of Omega Norway Predicted All-time Signal Coverage Contour and Observed Signal Coverage from Integrated Satellite/Omega Data

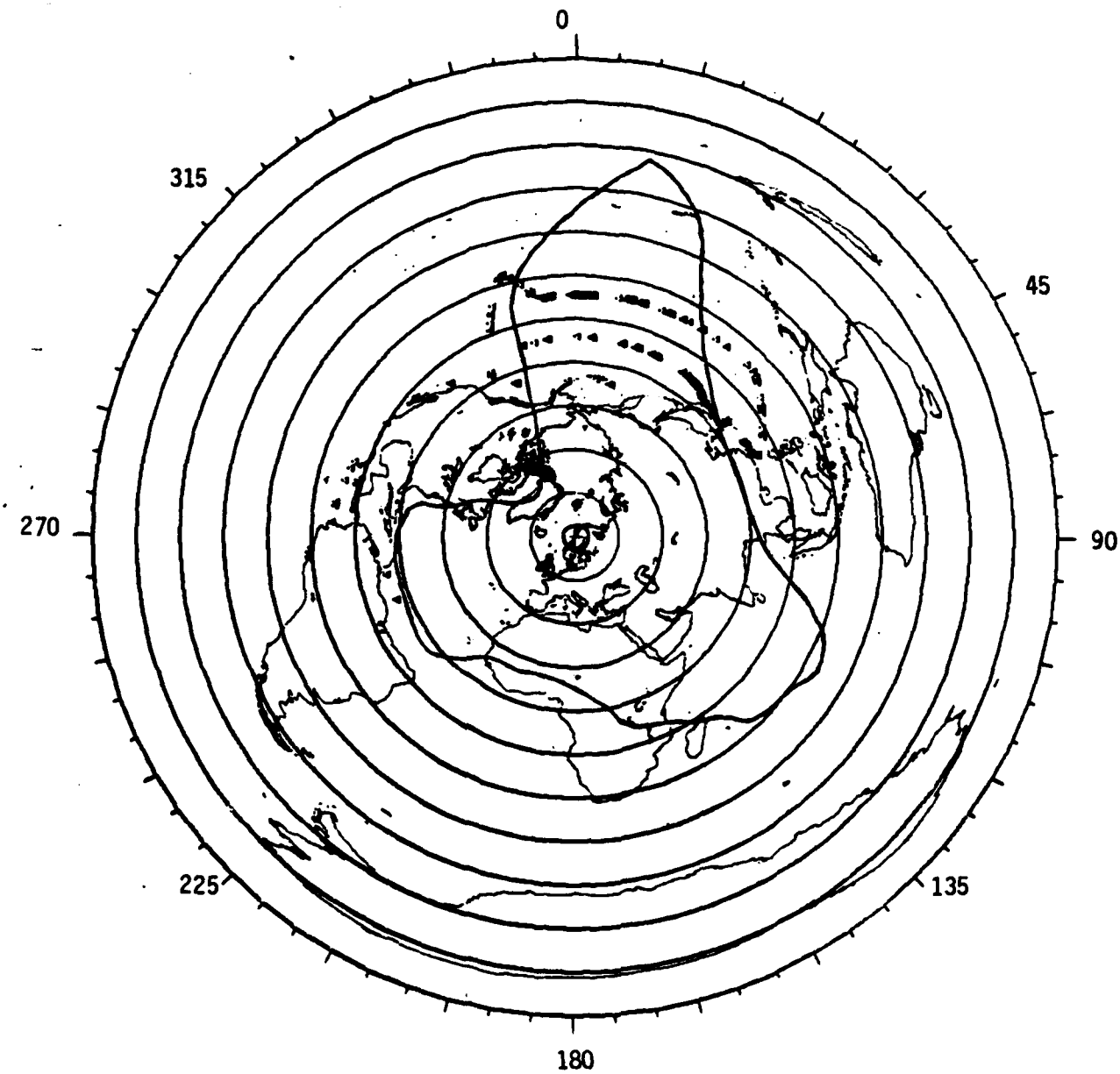

FIGURE E-2. Comparison of Omega Norway Predicted All-time Signal Coverage Contour and Positions of Possible Modal Interference from Integrated Satellite/Omega Data

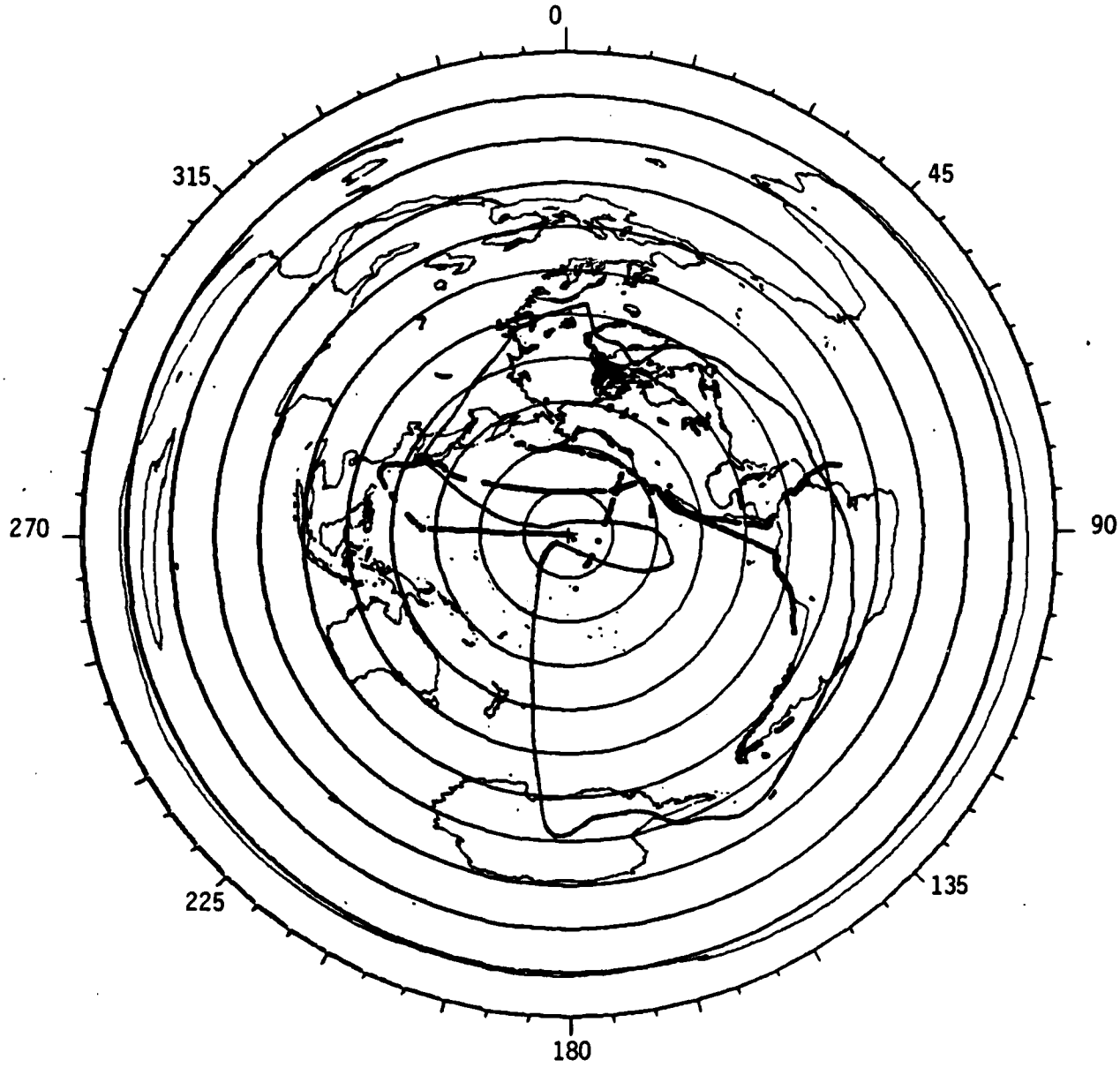

FIGURE E-3. Comparison of Omega Hawaii Predicted All-time Signal Coverage Contour and Observed Signal Coverage from Integrated Satellite/Omega Data

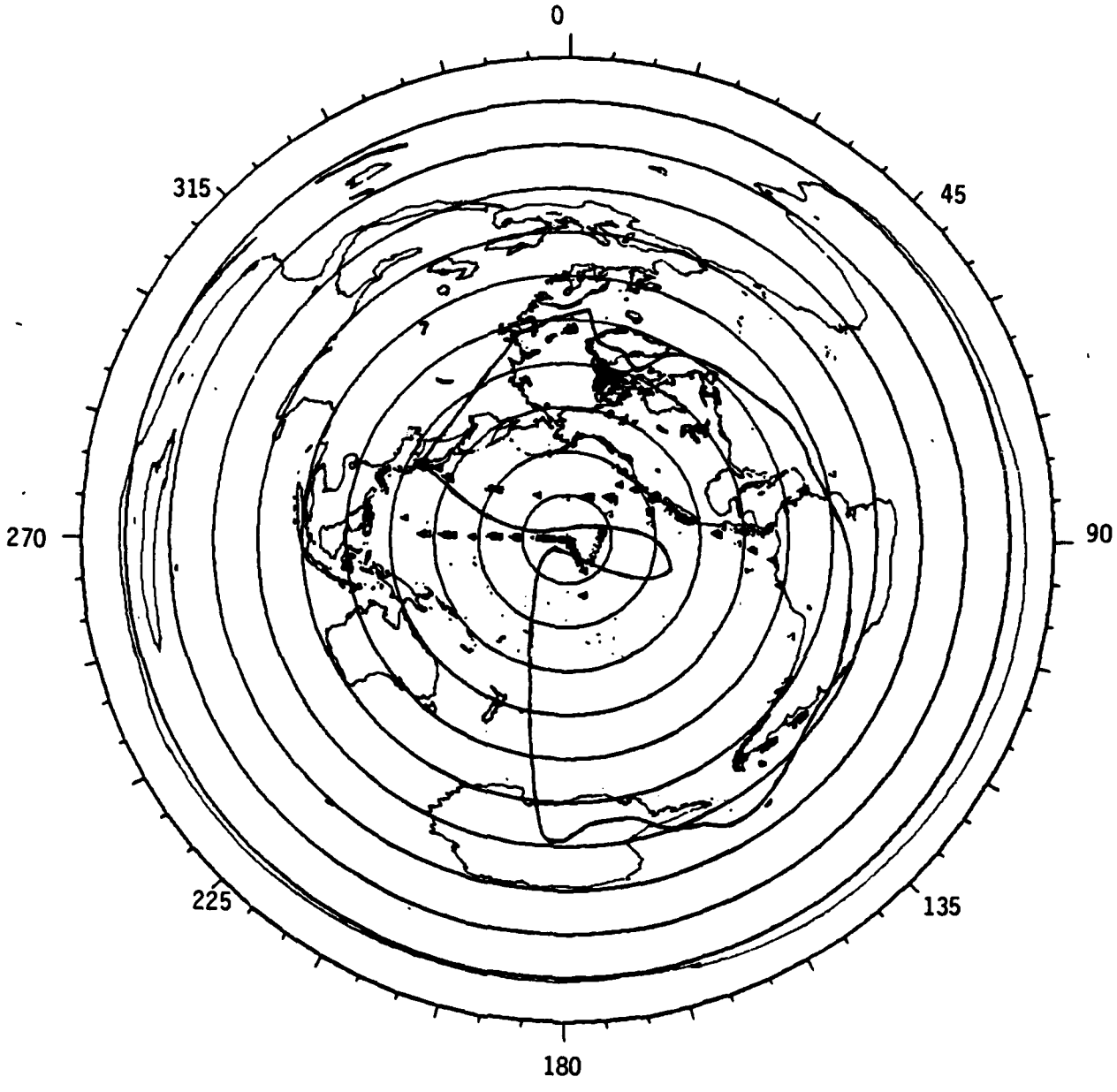

FIGURE E-4. Comparison of Omega Hawaii Predicted All-time Signal Coverage Contour and Positions of Possible Modal Interference from Integrated Satellite/Omega Data

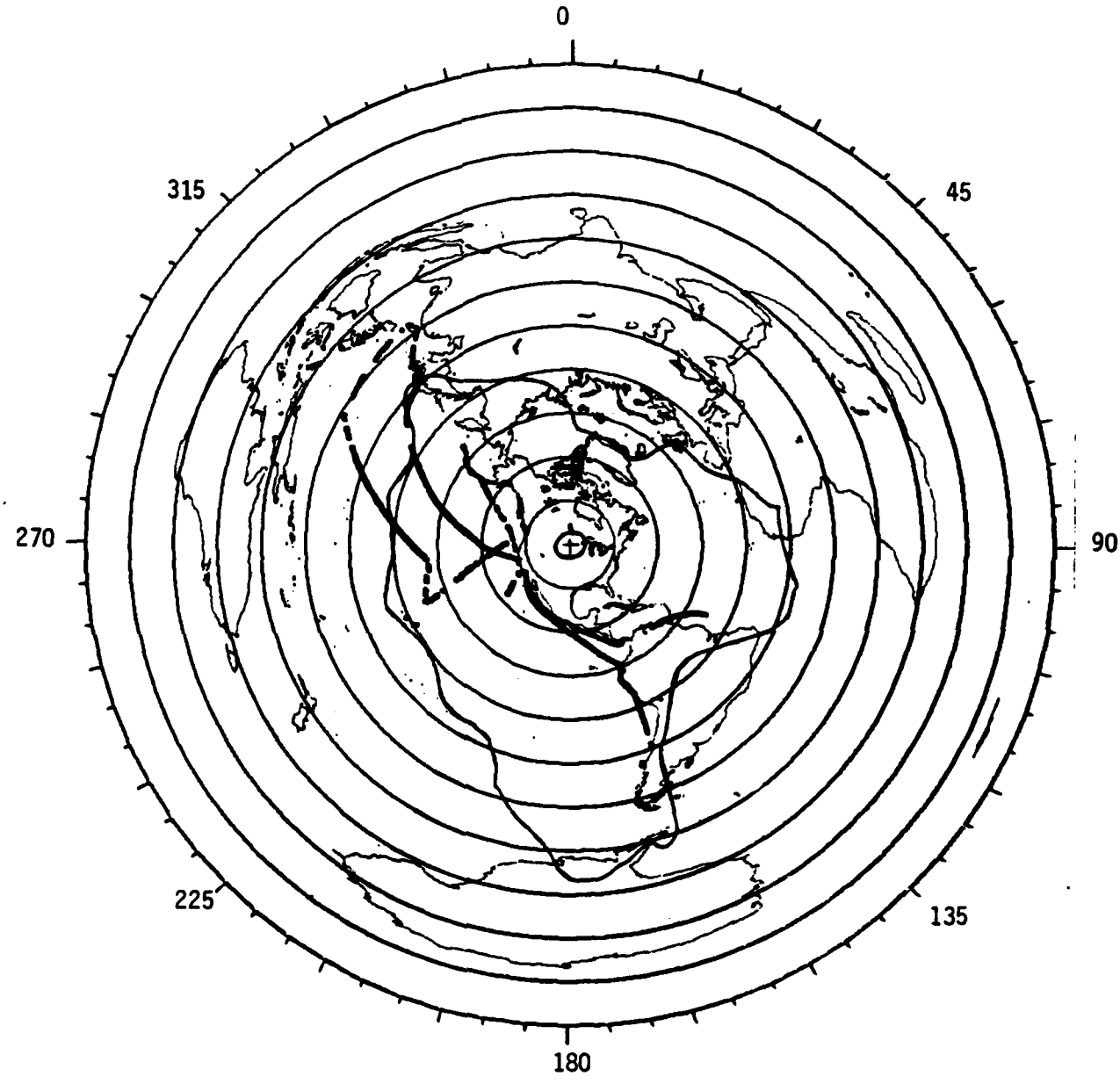

FIGURE E-5. Comparison of Omega North Dakota Predicted All-time Signal Coverage Contour and Observed Signal Coverage from Integrated Satellite/Omega Data

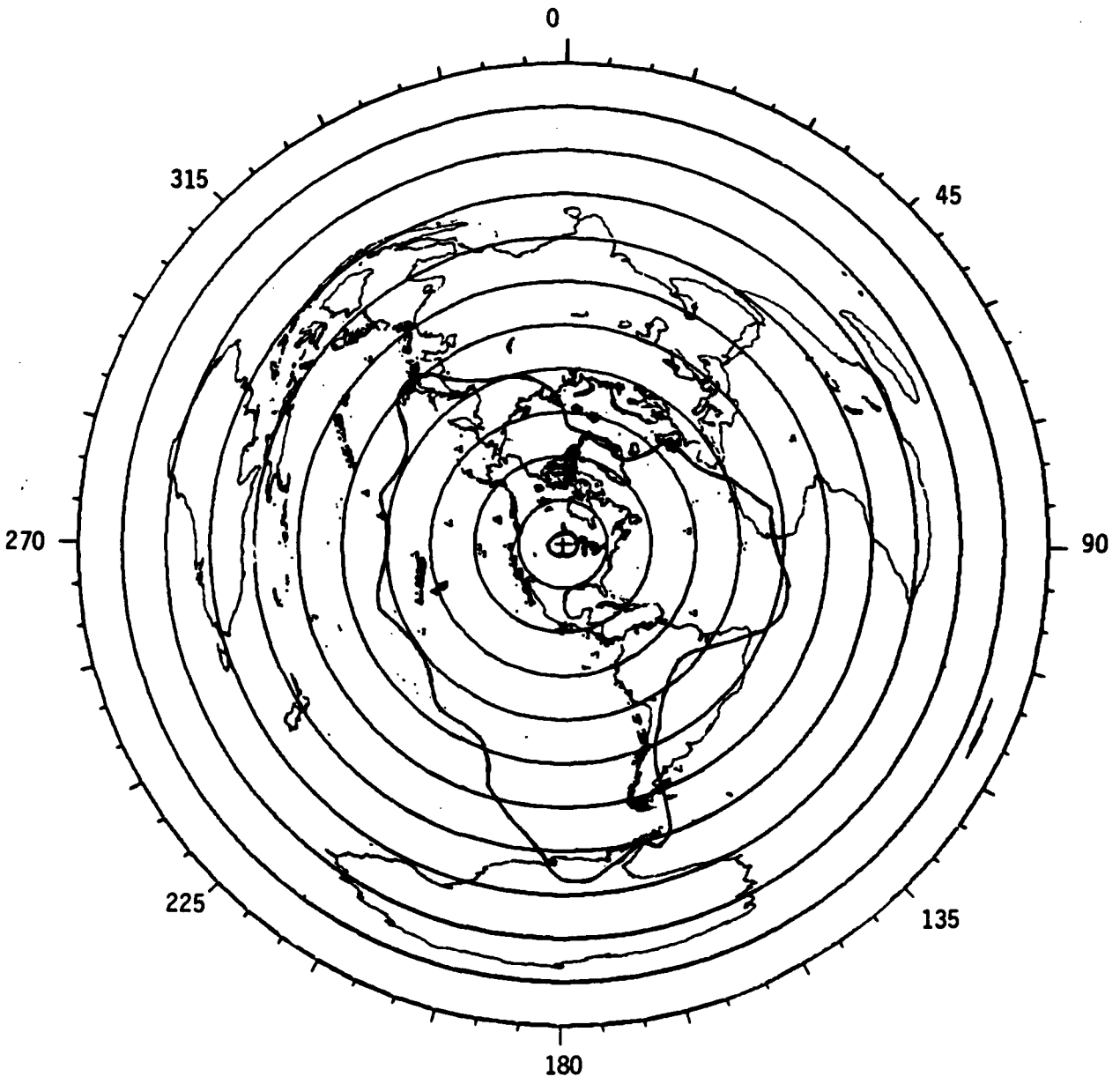

FIGURE E-6. Comparison of Omega North Dakota Predicted All-time Signal Coverage Contour and Positions of Possible Modal Interference from Integrated Satellite/Omega Data

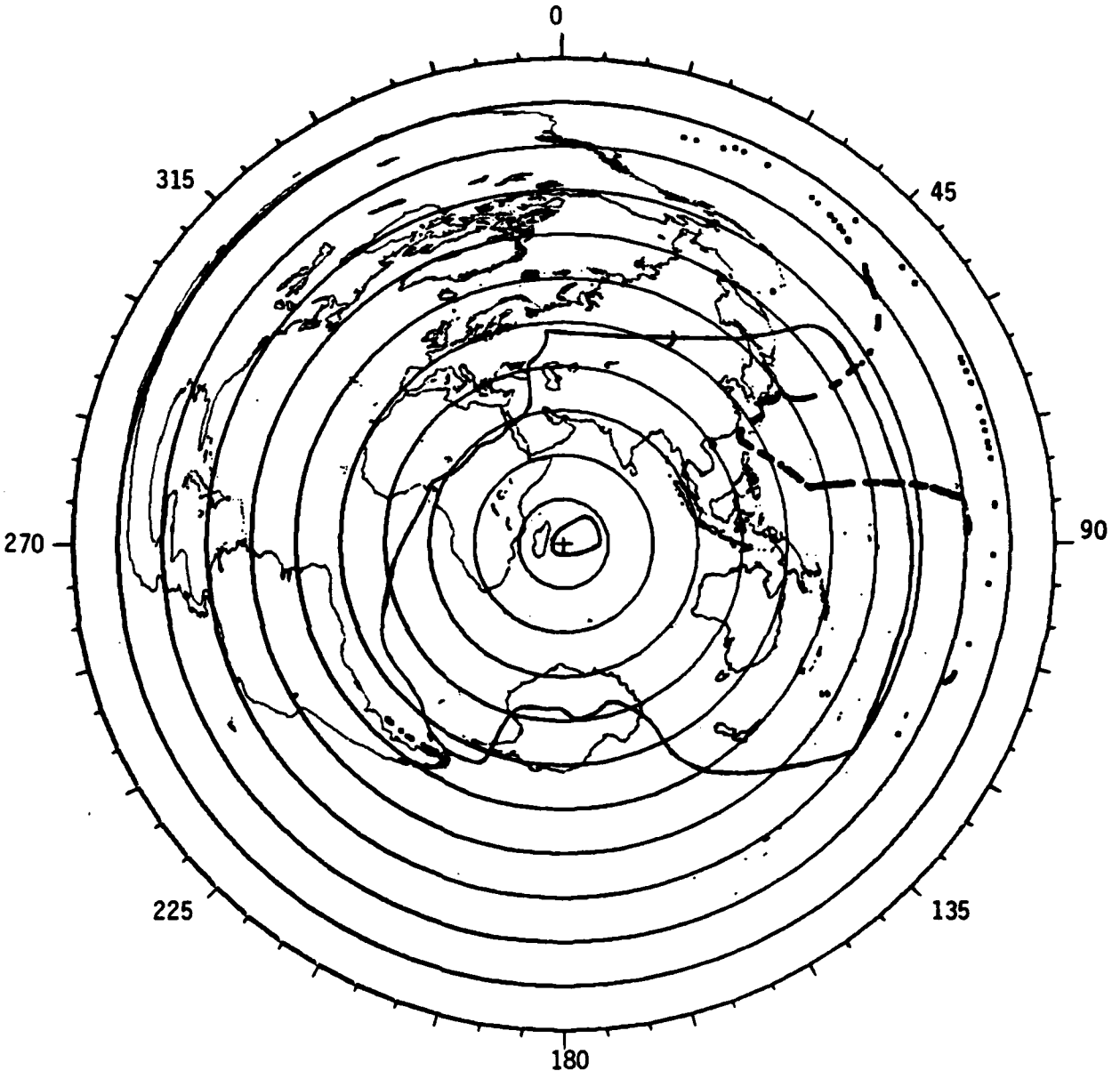

FIGURE E-7. Comparison of Omega La Reunion Predicted All-time Signal Coverage Contour and Observed Signal Coverage from Integrated Satellite/Omega Data

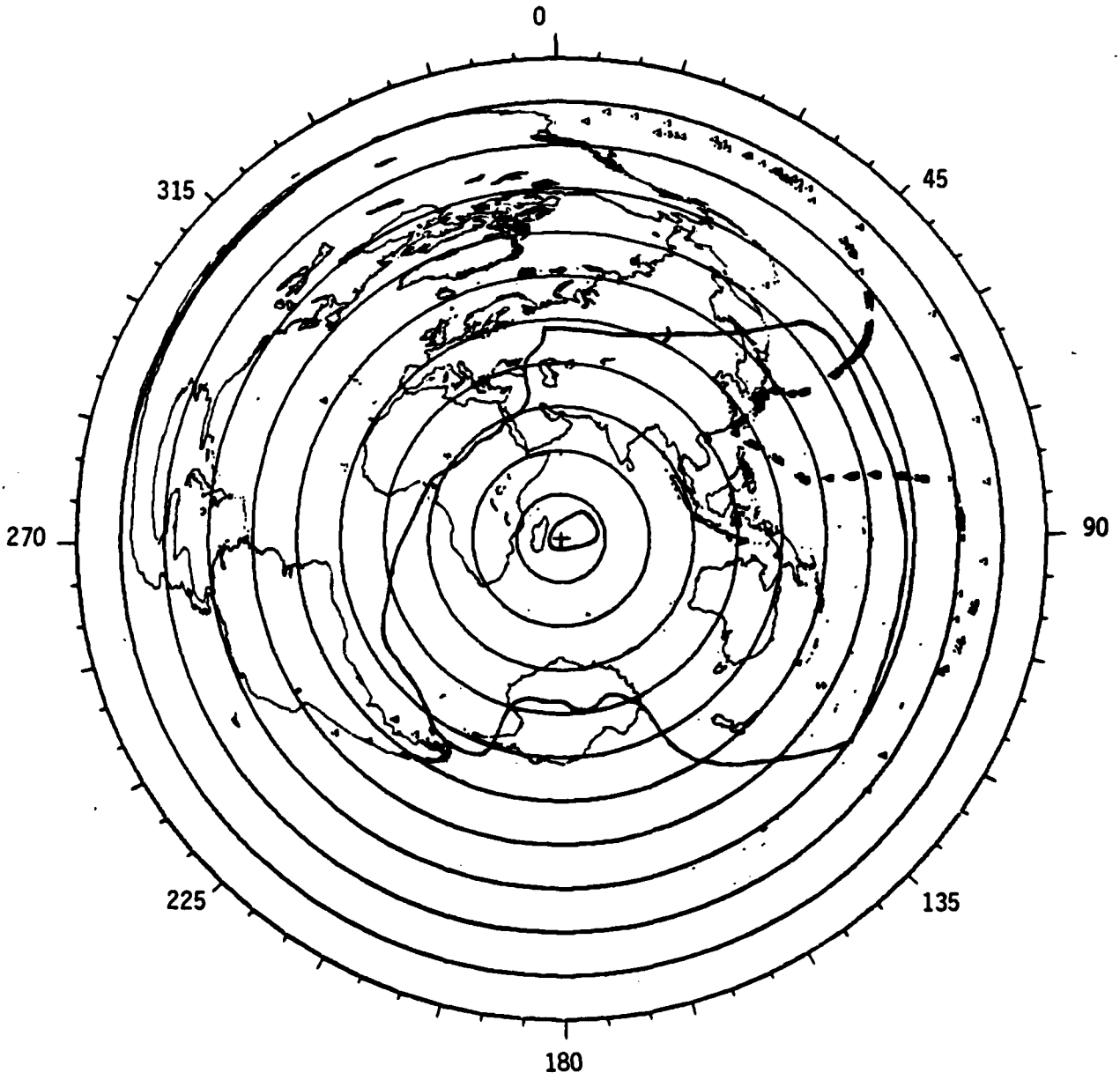

FIGURE E-8. Comparison of Omega La Reunion Predicted All-time Signal Coverage Contour and Positions of Possible Modal Interference from Integrated Satellite/Omega Data

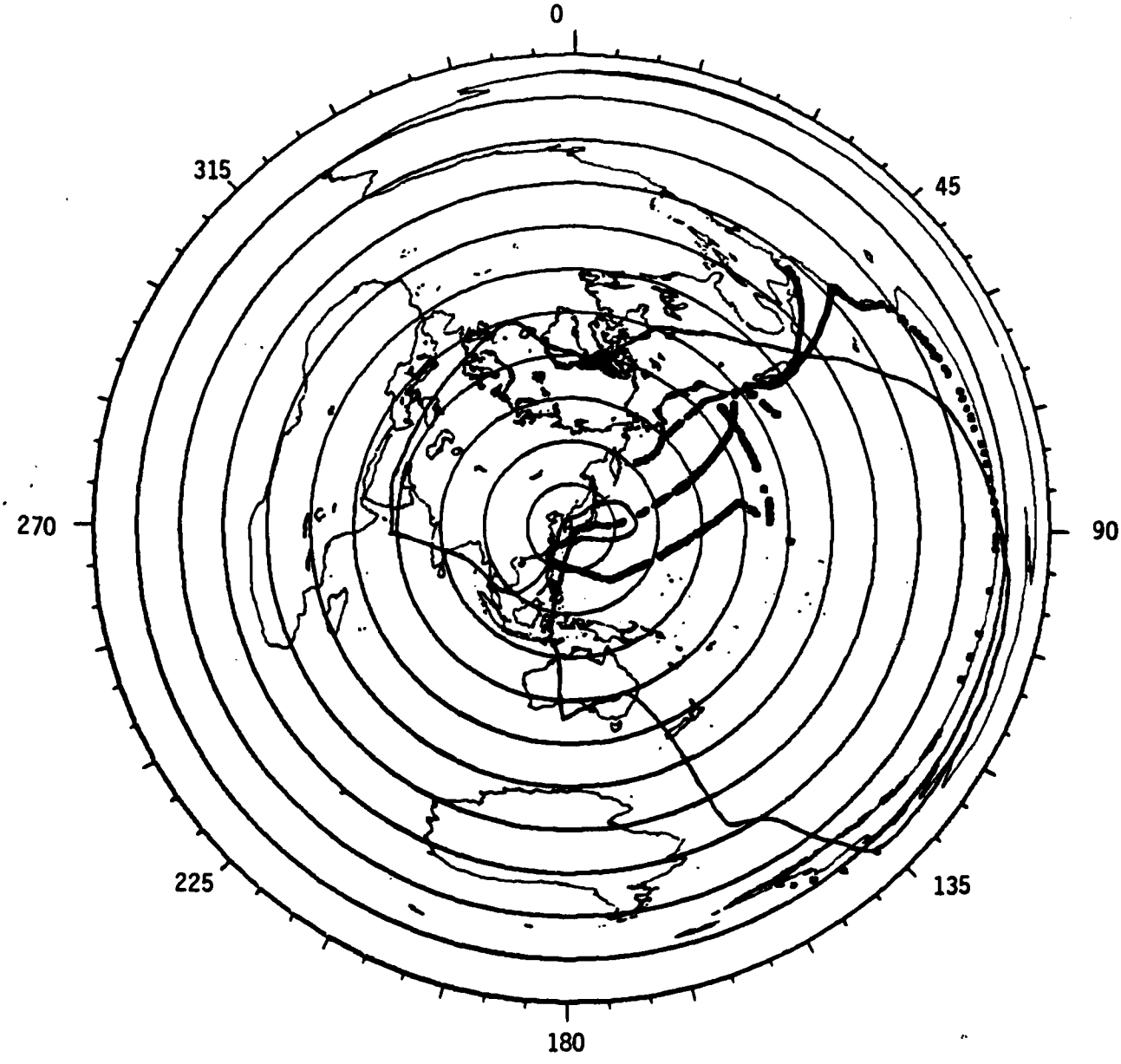

FIGURE E-9. Comparison of Omega Japan Predicted All-time Signal Coverage Contour and Observed Signal Coverage from Integrated Satellite/Omega Data

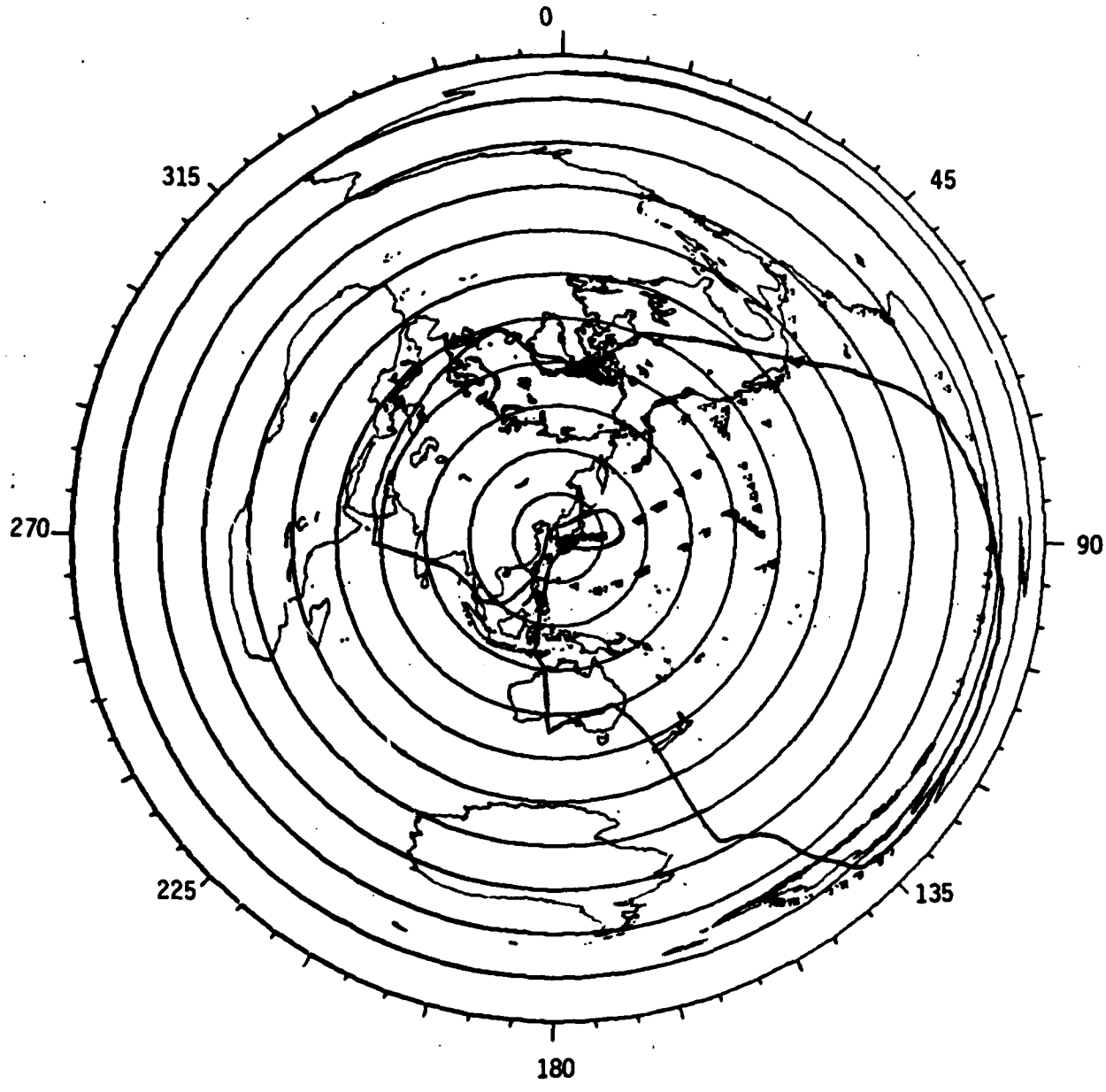

FIGURE E-10. Comparison of Omega Japan Predicted All-time Signal Coverage Contour and Positions of Possible Modal Interference from Integrated Satellite/Omega Data

APPENDIX F: SID-INDUCED NAVIGATIONAL ERRORS IN NORTH PACIFIC

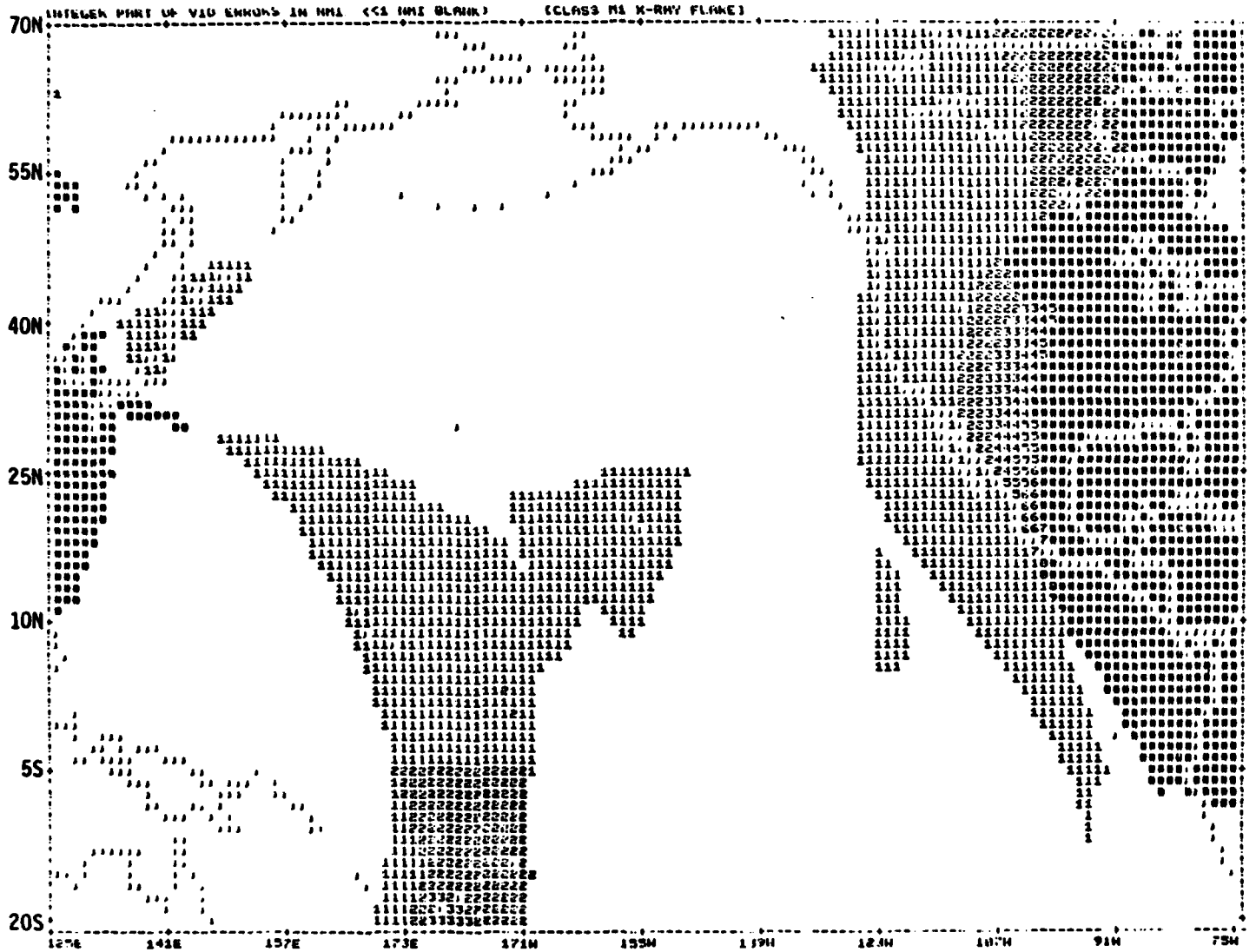

FIGURE F-1. SID-INDUCED ERRORS: LOCAL MIDNIGHT, JUNE 21, CLASS M1 FLARE

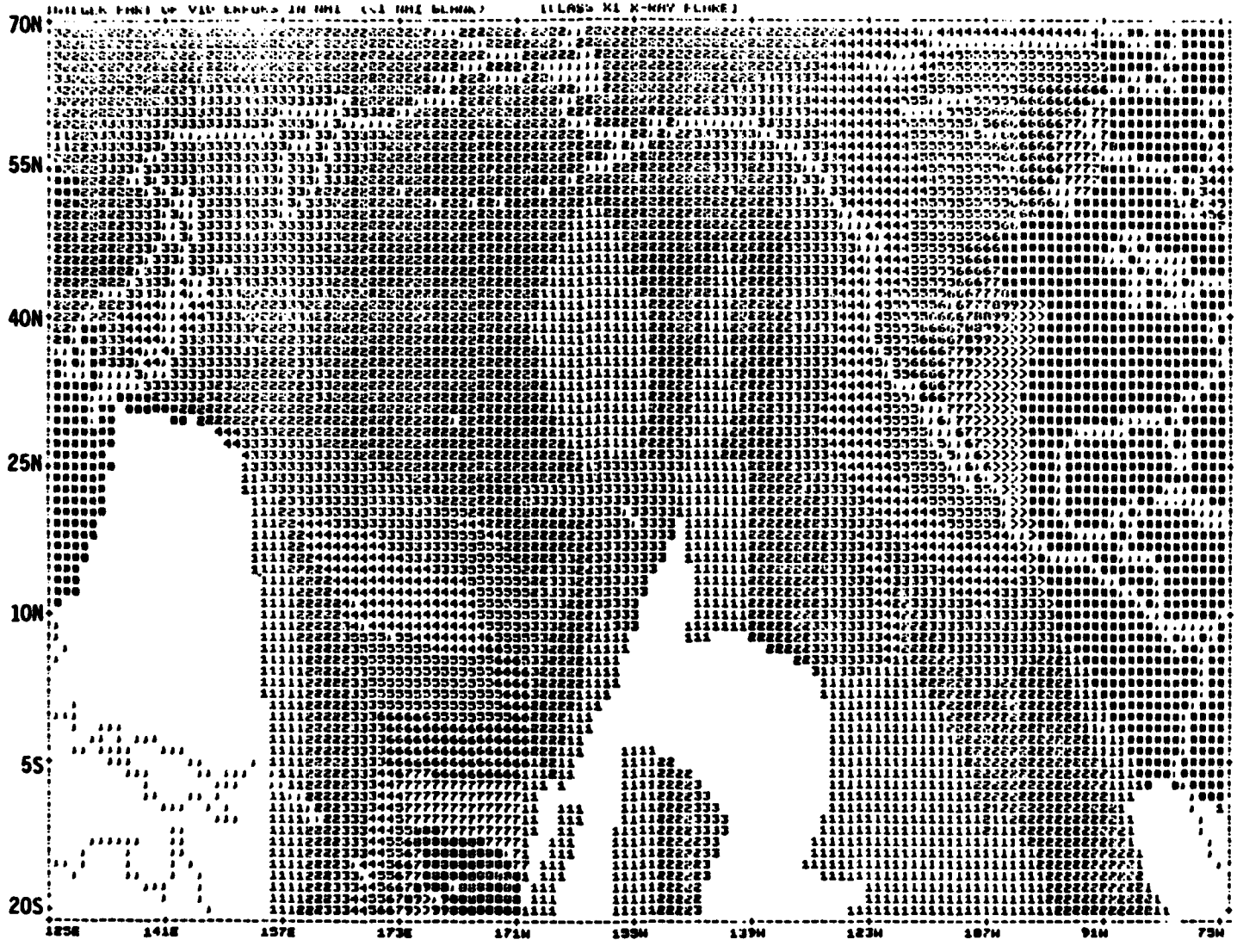

FIGURE F-2. SID-INDUCED ERRORS: LOCAL MIDNIGHT, JUNE 21, CLASS X1 FLARE

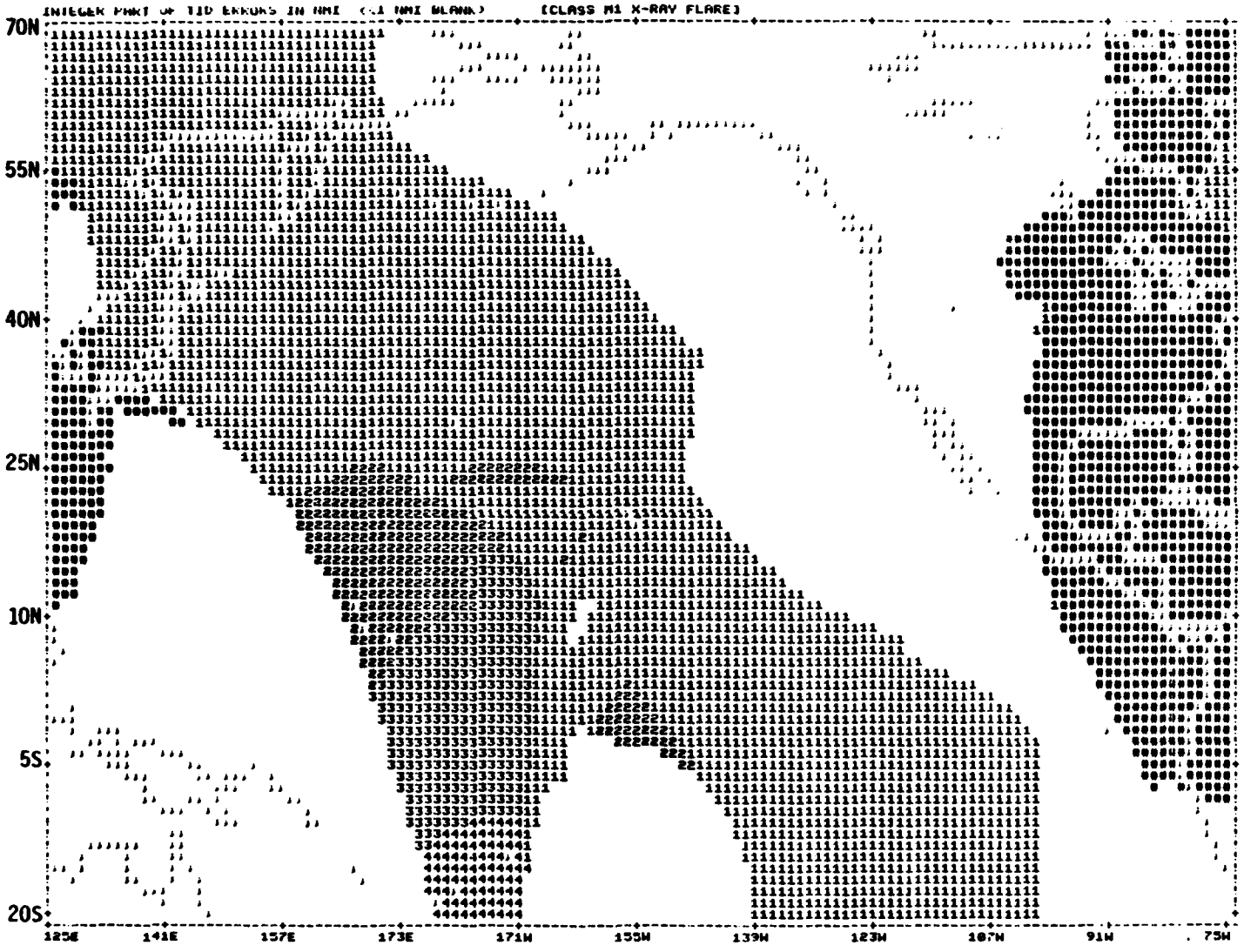

FIGURE F-3. SID-INDUCED ERRORS: 0600 LOCAL TIME, JUNE 21, CLASS M1 FLARE

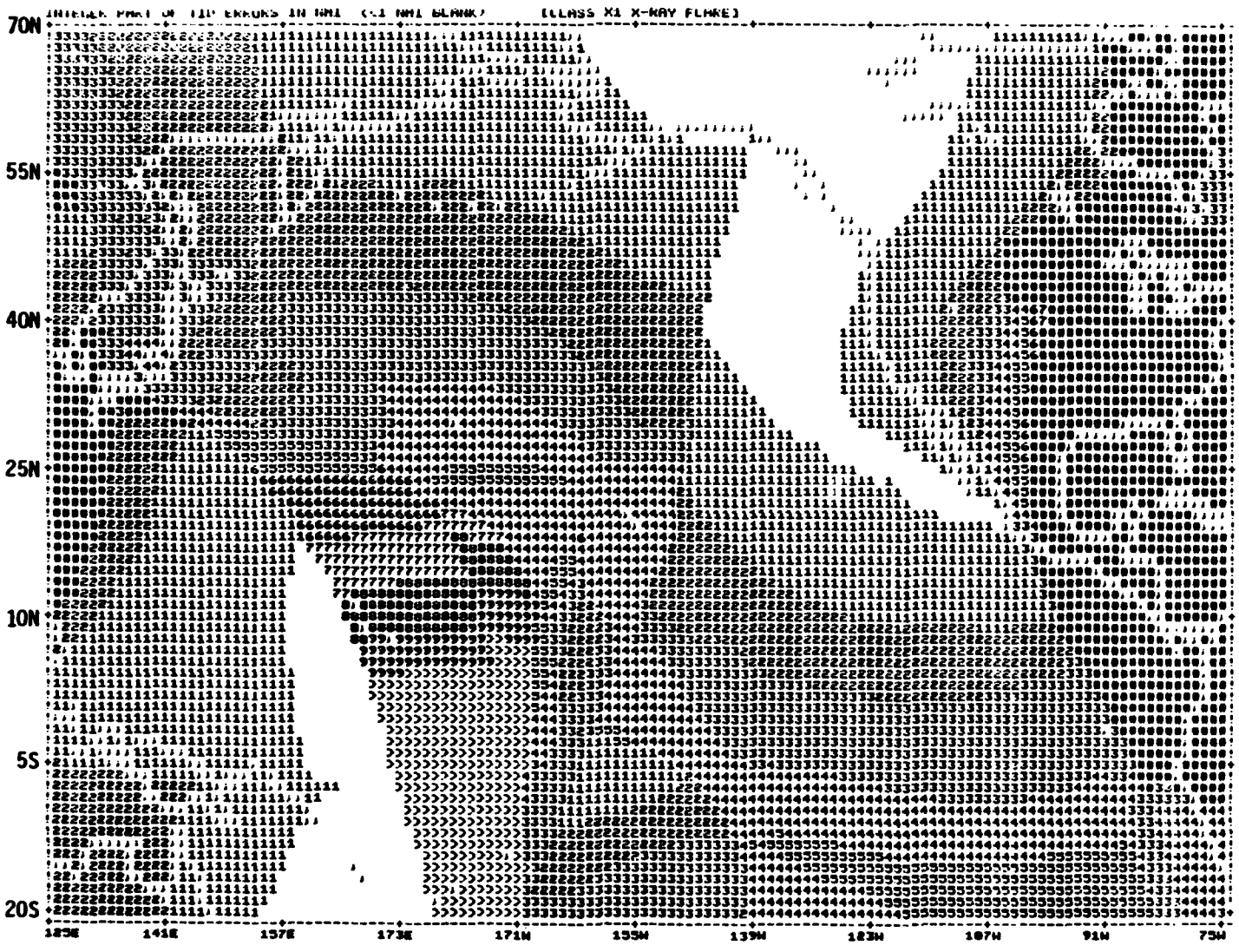

FIGURE F-4. SID-INDUCED ERRORS: 0600 LOCAL TIME, JUNE 21, CLASS X1 FLARE

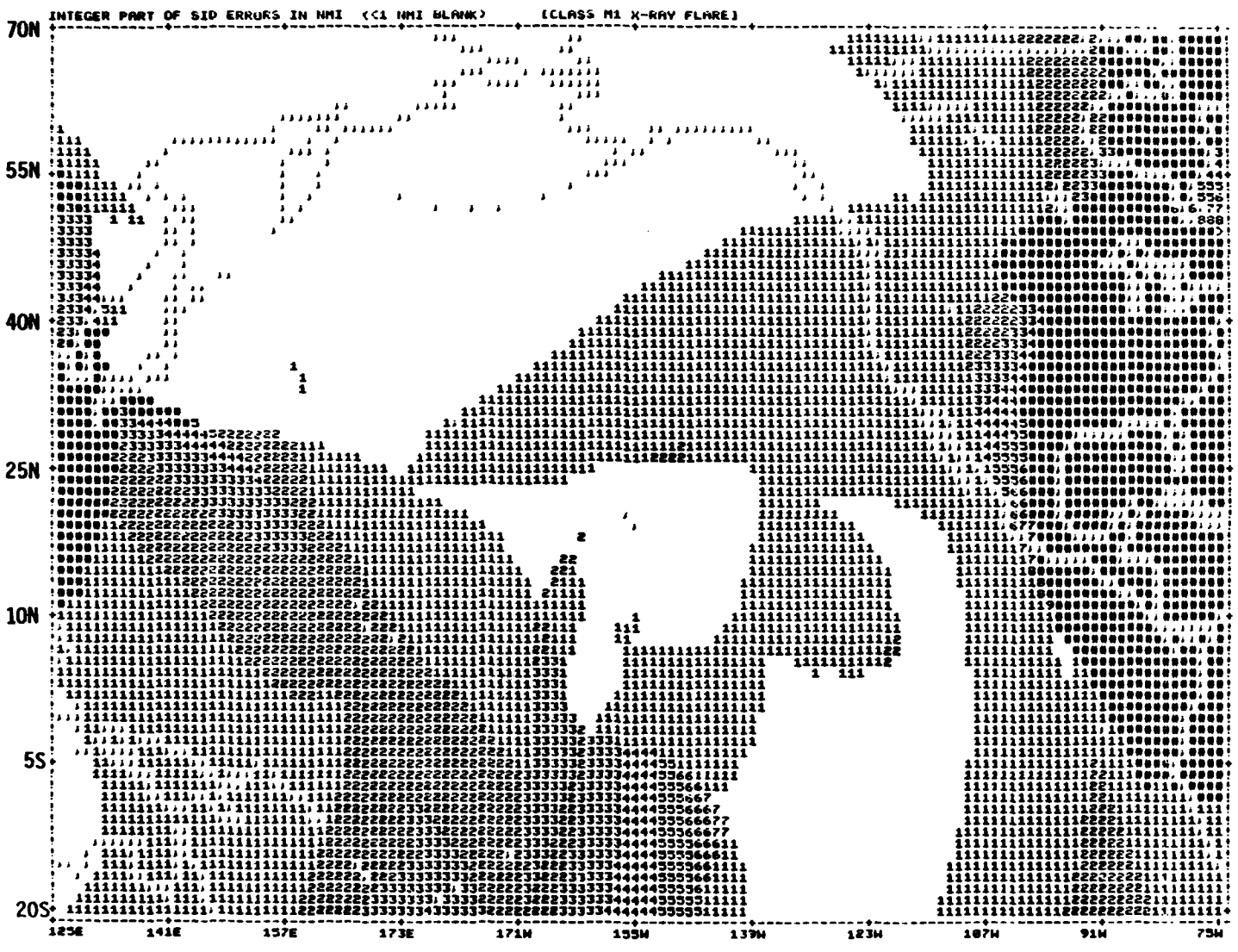

FIGURE F-5. SID-INDUCED ERRORS: LOCAL NOON, JUNE 21, CLASS M1 FLARE

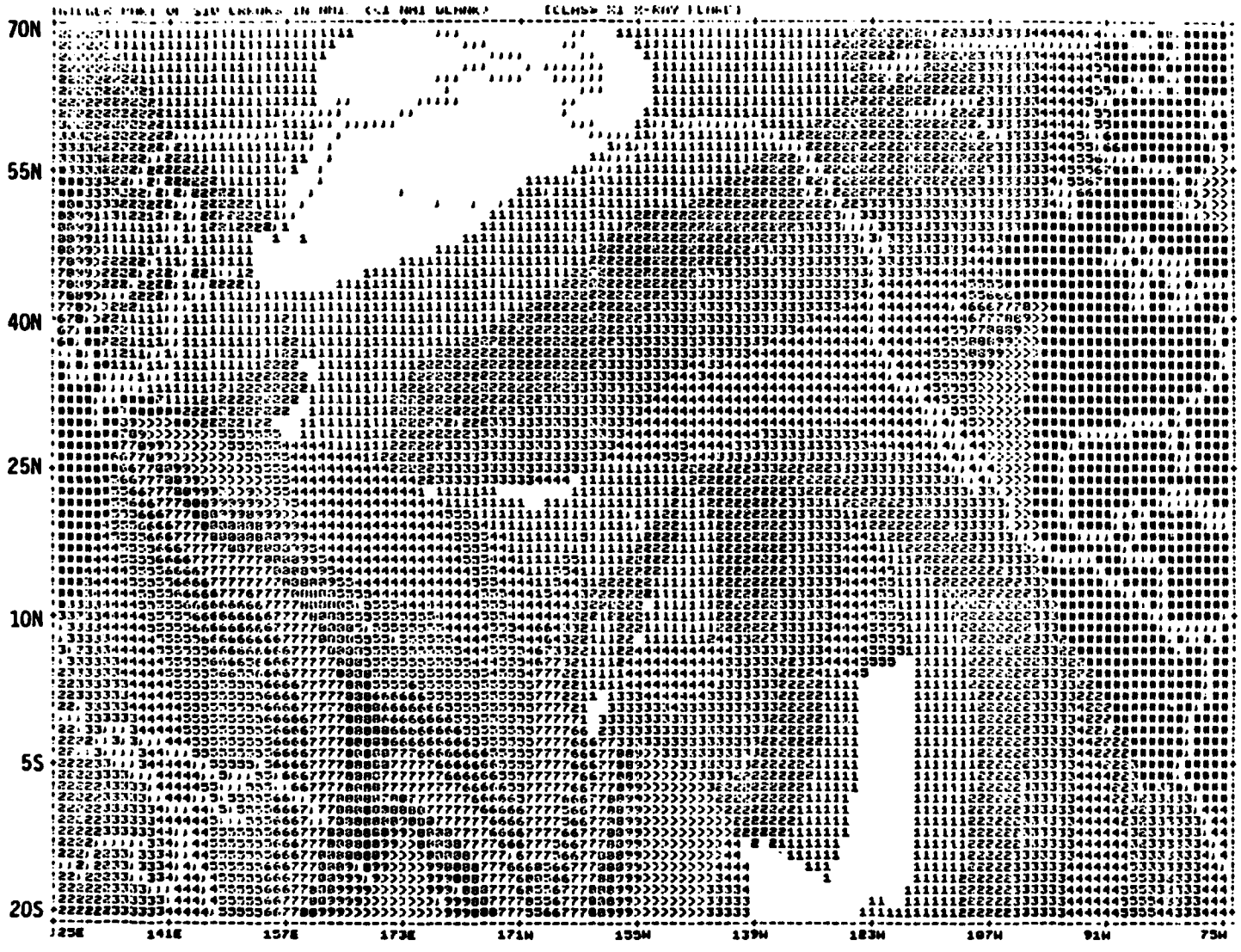

FIGURE F-6. SID-INDUCED ERRORS: LOCAL NOON. JUNE 21, CLASS X1 FLARE

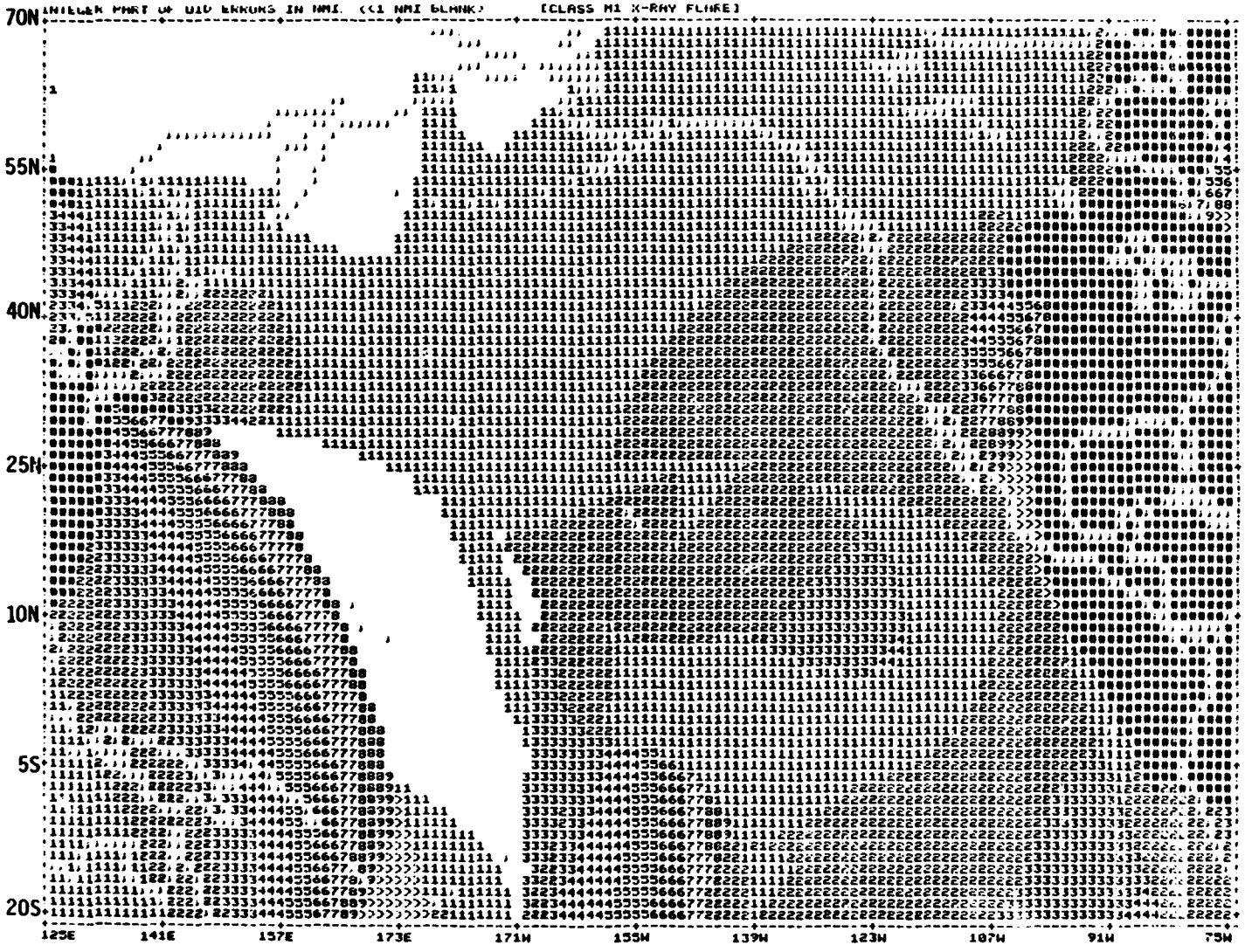

FIGURE F-7: SID-INDUCED ERRORS: 1800 LOCAL TIME, JUNE 21, CLASS M1 FLARE

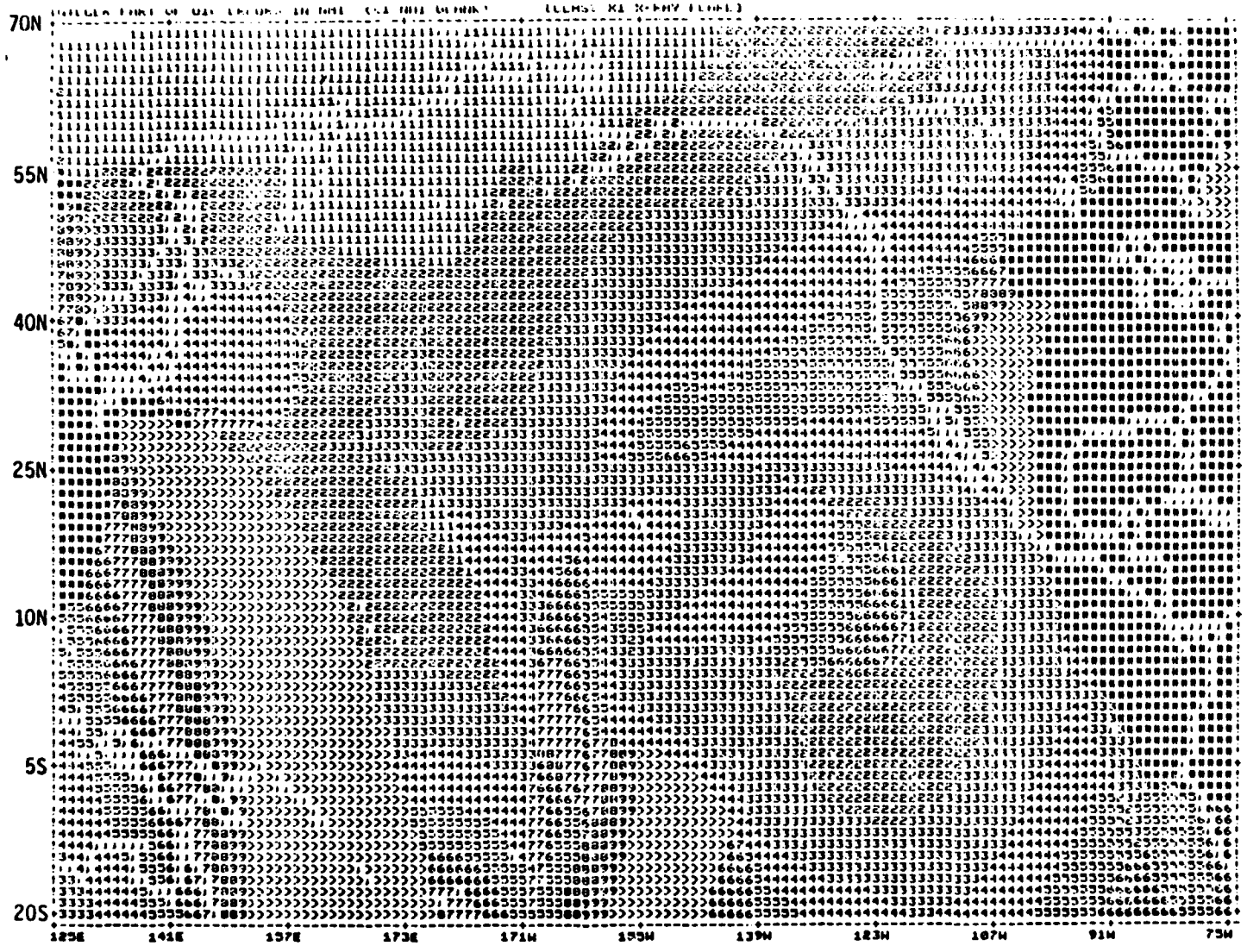

FIGURE F-8: SID-INDUCED ERRORS: 1000 LOCAL TIME, JUNE 21, CLASS X1 FLARE

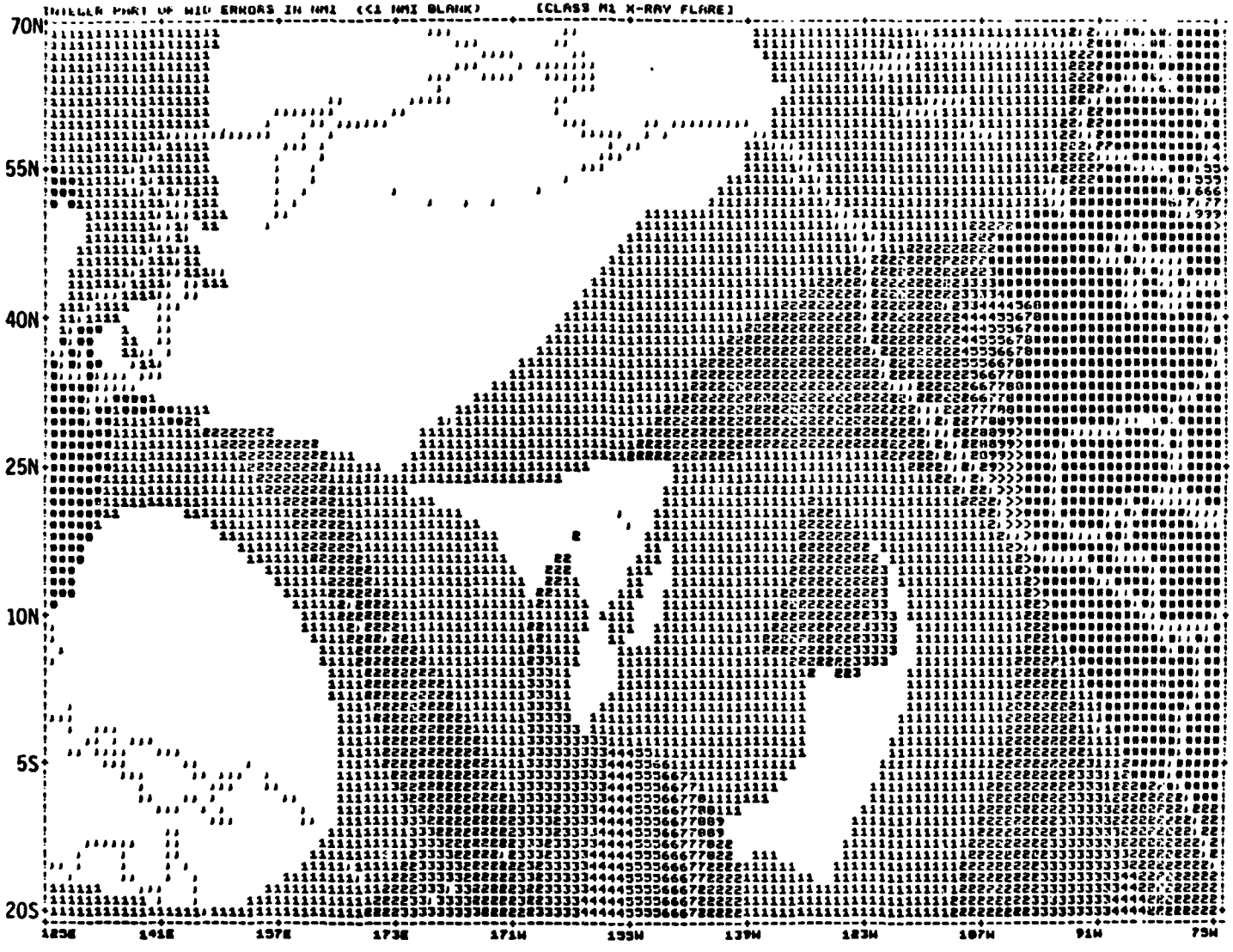

FIGURE F-9: SID-INDUCED ERRORS: 0000Z, JUNE 21, CLASS M1 FLARE

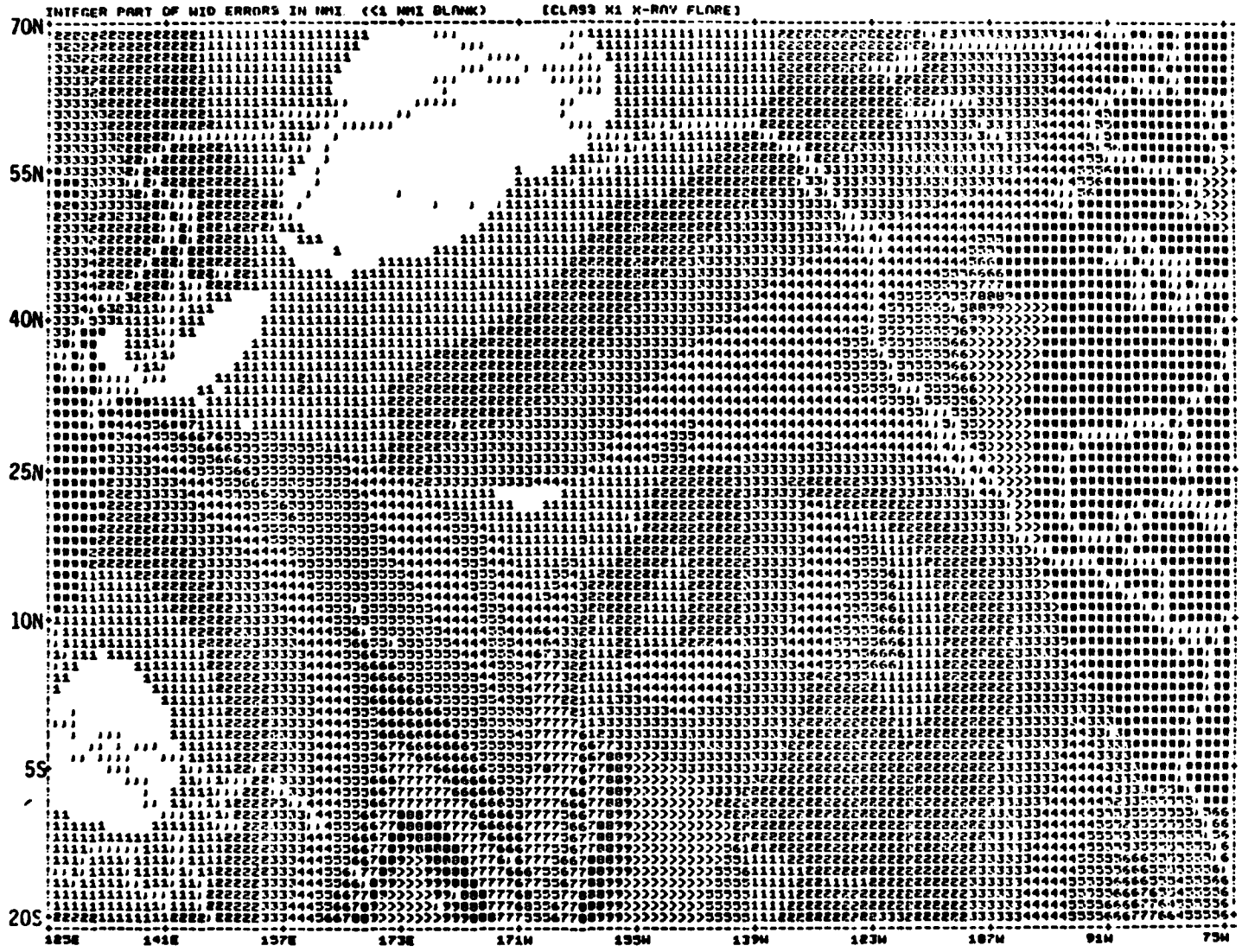

FIGURE F-10: SID-INDUCED ERRORS: 0000Z, JUNE 21, CLASS X1 FLARE

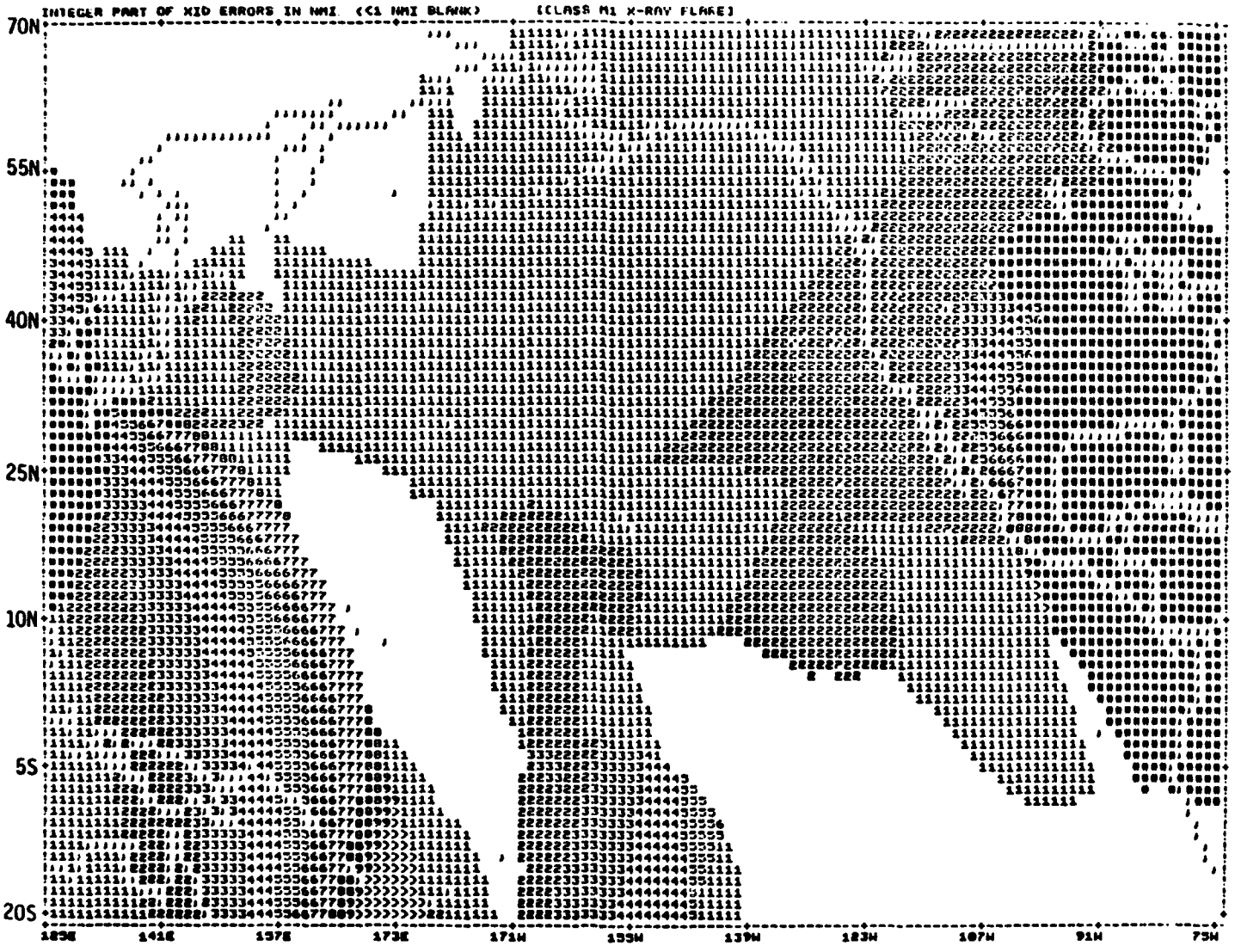

FIGURE F-11: SID-INDUCED ERRORS: 0600Z, JUNE 21, CLASS M1 FLARE

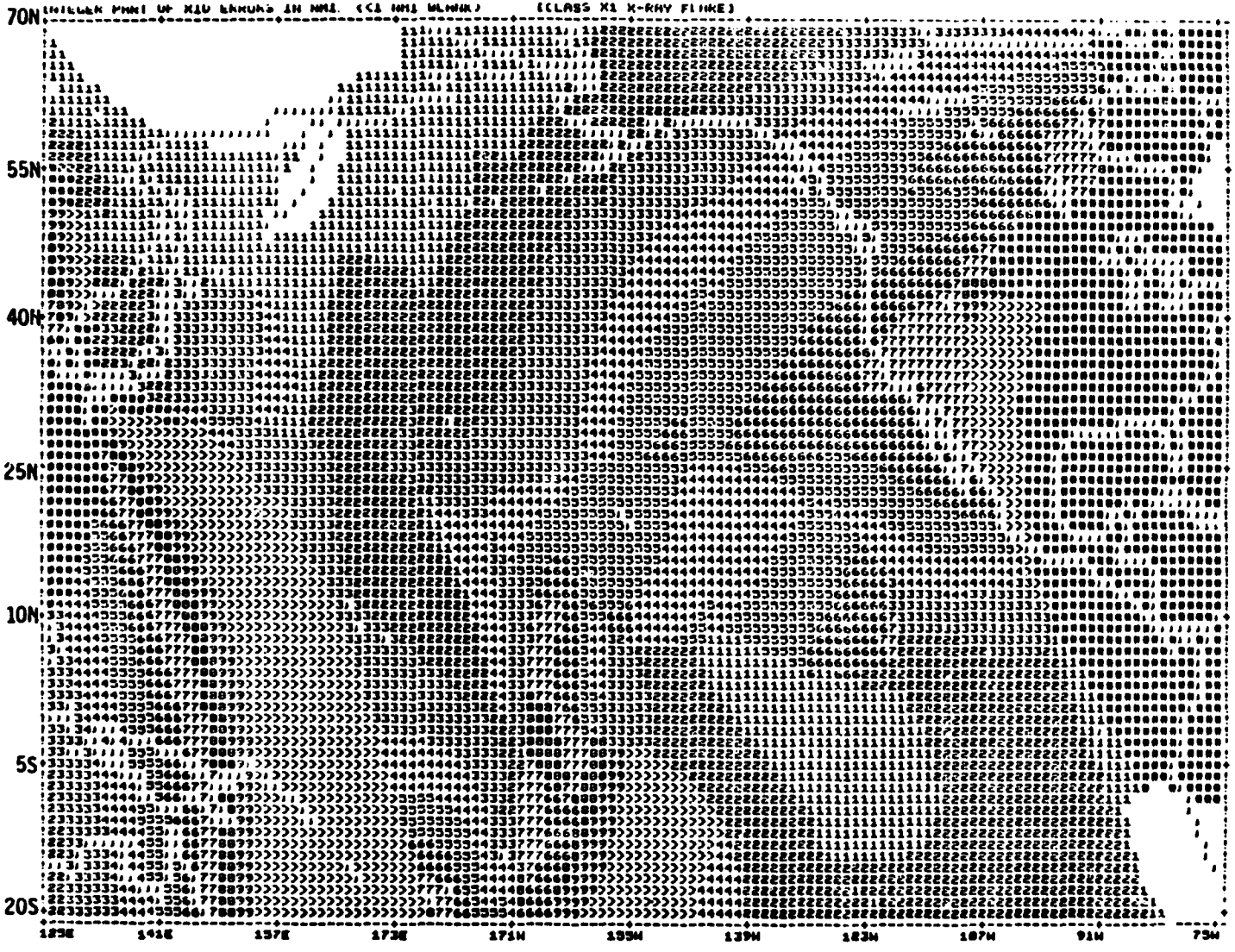

FIGURE F-12: SID-INDUCED ERRORS: 0600Z, JUNE 21, CLASS X1 FLARE